UNIVERSITÀ POLITECNICA DELLE MARCHE

Department of Life and Environmental Sciences

XXXII PhD cycle in Life and Environmental Sciences

Curriculum Biomolecular Sciences (SB)

Potential amphiphilic antibacterial compounds

(DRAFT)

PhD candidate:

Giulia Guerra

Supervisor:

Samuele Rinaldi, PhD

XXXII PhD cycle – 2016/2019

Abstract 1

Pursuing the search for a new class of structurally simple mimics of antimicrobial peptides, we have optimized a short, cheap and high-yielding synthesis of mono-charged amphiphilic *α*-hydrazido acid derivatives. The most active derivatives furnished MICs that are among the best values reported in literature for synthetic amphiphilic membranolytic compounds. They exhibited a broad-spectrum *in vitro* activity against a variety of Gram-positive and Gram-negative bacteria, including two multidrug-resistant strains. In addition, they showed synergistic effects whit tetracycline toward sensitive bacteria, whereas either synergistic effects or indifference were observed for combinations with different first-line antibiotics toward multidrug-resistant strains, depending on the mechanism of action of the conventional antibiotic used. Despite the minimal cationic charge, the best compounds demonstrated to be selective toward bacterial cell membranes over mammalian cell membranes. The relationship between either the antibacterial or the haemolytic activity and the overall lipophilicity furnished an easy way to individuate the best dimensional range for the hydrophobic portions. The importance of a non-disrupted amphiphilicity was also demonstrated. Considering the bioactivity profile and the ease of synthesis, these chemically and proteolytically stable hydrochlorides are suitable for development of a new class of wide-spectrum antibiotics.

Abstract 2

The globally rise of multidrug-resistant Gram-negative bacteria (MDR-GNB) and the lack of new therapeutic options, has recently resumed the interest of colistin, a polycationic, cyclic lipodecapeptide, belonging to polymyxins, which is especially used as “last resort” treatment against “superbugs” pathogens. With a very excellent antibacterial activity against selected Gram-negative bacteria such as *P. aeruginosa*, *A. baumanii* spp., *K. pneumoniae* spp. and *Enterobacter* spp., the clinical utility is however limited, due to its nephrotoxic side effects.

With the aim to administer lower doses of colistin reducing the toxic side effects, the Department of Chemical Biology at HZI (Braunschweig, Germany) developed a novel peptide-colistin construct. It consists of a mixture of five regioisomers where each of its free amino groups of colistin was coupled to the C-terminal of a synthetic peptide. The cleavage of the newly introduced amide group by human elastase neutrophils, releases colistin directly on the surface of bacteria in order to kill them. Thus, exploiting solid phase methodology, we regioselectively prepared the isomers of the colistin construct in order to investigate if all the regioisomers undergo selective cleavage by elastase with the same efficacy and fidelity. Then,

we carried out the antimicrobial assays against a strain of *E. coli* K12, and the results were compared with the activity of regioisomeric mixture.

SUMMARY

1. THE "POST-ANTIBIOTIC ERA": NEED FOR NEW AGENTS

The exponentially rising number of drug and multidrug resistant bacteria, together with the slowing down of the discovery of new antibacterial compounds, is a well-known world public health priority, and non-judicial use or abuse of antibiotics, as well as the widespread use of antimicrobials in livestock,[1] are further favoring the spread of antibiotic resistance.[2]

Some bacteria are naturally resistant to certain classes of antibiotics, due to different mechanisms such as: production of specific enzymes, release of antibacterial agents through a system of efflux pumps, modification of the antibacterial targets and presence of alternative metabolic pathways. Other bacteria may spontaneously develop resistance due to genetic mutations. These genes can also be transferred by conjugation, transduction or transformation to other strains of the same bacterium, or also to different species (Figure 1).

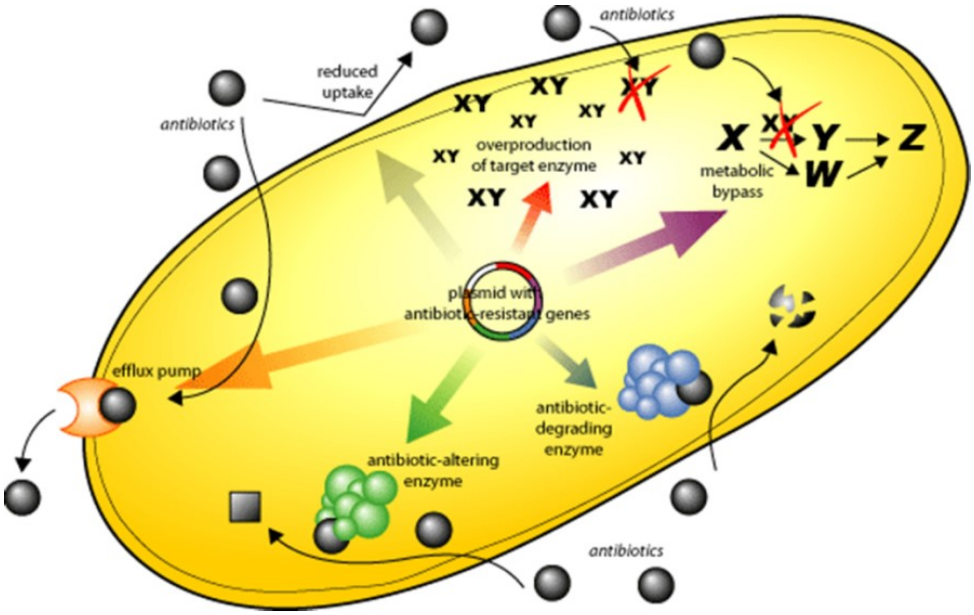

Figure 1. Bacterial resistance mechanisms.

Therefore, mutations and selection, together with the genetic exchange mechanisms, make many bacterial species able to adapt quickly to new antibacterial agents, facilitating the development of drug resistance, as exemplified by the sharp rise in strains of *S. aureus* resistant to methicillin (MRSA), multidrug-resistant *K. pneumoniae* (MDRKP), vancomycin-resistant *Enterococci* (VRE), and multidrug-resistant *E. coli* (MRE) in Europe in 2018 (Figure 2).

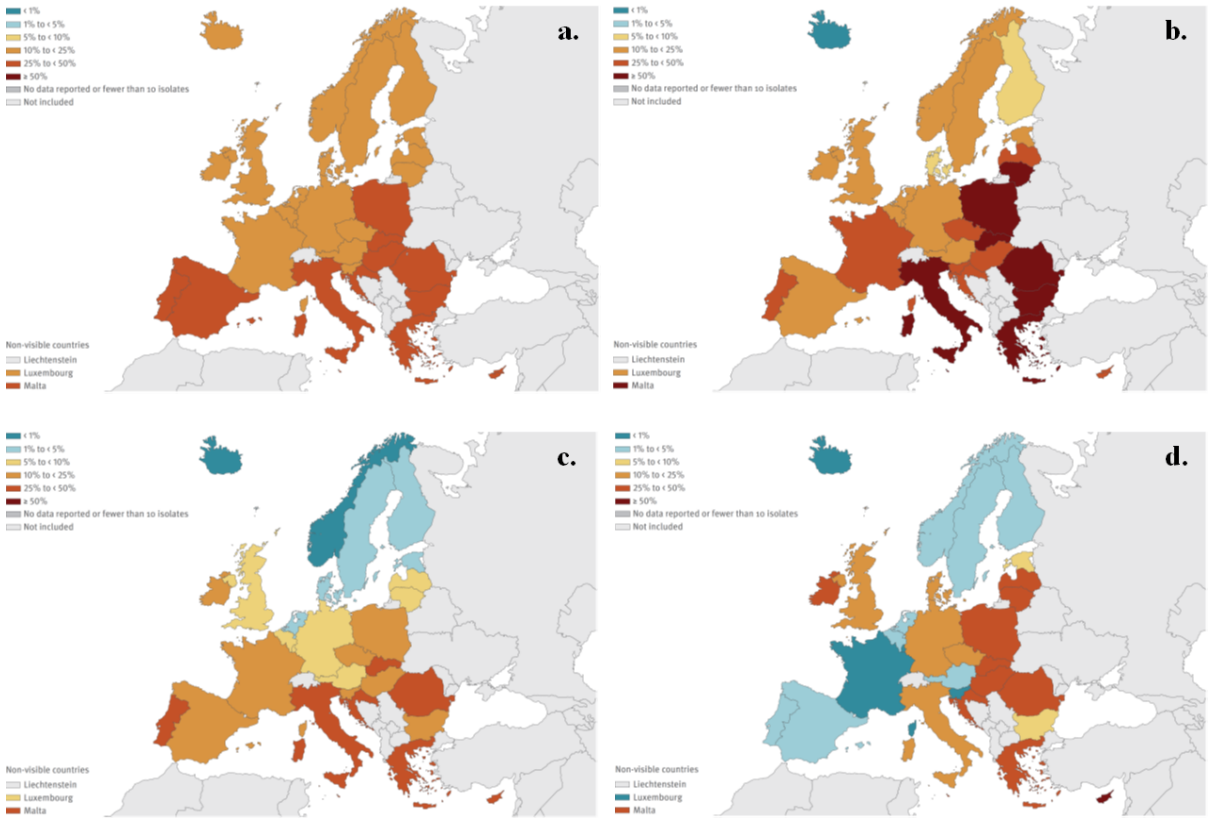

Figure 2. Percentage (%) of invasive isolates with resistance to several drugs by country (EU/EEA countries, 2018). (a) *E. coli* isolates with resistance to aminoglycosides; (b) *K. pneumoniae* isolates with resistance to fluoroquinolones; (c) *S. aureus* isolates with resistance to methicillin (MRSA); (d) *Enterococci* isolates with resistance to vancomycin (VRE). Data from European Centre for Disease Prevention and Control (ECDC).

The emergence of bacterial strains resistant to last-resort antibiotics, widely used in clinical settings, has left few therapeutic options.[3]

Given these premises, it is therefore evident the need to find new classes of antimicrobial agents with new mechanisms of action, or that have as targets bacterial structures or molecules that are difficult to change, making these new drugs much less susceptible to the development of resistance.

2. α-HYDRAZIDO ACID-BASED SMMAMPS

2.1 Introduction

In the search for new classes of antibiotics, the natural cationic antimicrobial peptides (AMPs), also called host defense peptides (HDPs), have been extensively taken into consideration in the last decades.[4] They are the first defense against infections for organisms belonging to all classes of life,[5,6] and their amphiphilic active secondary structure is essential to cause lysis of the bacterial cell membrane, even if occasionally they can also act on intracellular targets.[7,8,9,10] Additionally, in few cases they can also modulate the innate immune response (e.g. human cathelicidin and defensins),[11] and it is usually claimed that, differently from conventional antibiotics, bacteria can hardly develop resistance toward AMPs,[8] due to their peculiar mode of action. However, there are growing reports both on intrinsic resistance, mainly due to membrane modifications, and on the mechanisms by which sensitive bacteria can acquire resistance to AMPs.[11] Another common feature of cationic antimicrobial peptides is their abundance of net positive charges, thus they are moderately selective toward bacterial cells, whose membranes are abundant in anionic lipids, over mammalian cells, which have a high content of uncharged or zwitterionic lipids.[12]

To date, in spite of the above reported advantages, the clinical use of AMPs has been mainly hampered by the differences between in vitro and in vivo efficacy and toxicity. In fact, only polymyxins have been systemically administered since the 1950s,[13] but their use has been strongly limited by the high incidence of nephrotoxicity and neurotoxicity.[14] Aside from polymyxins, no other AMP has yet been approved for therapeutic use, and the vast majority of antimicrobial peptides that are currently in clinical development are for topical use only.[11] In addition, other important drawbacks, such as high cost of manufacture, instability toward proteases and low bioavailability, have further hindered the application of natural AMPs in clinical therapeutics.[5,15] In order to circumvent the above mentioned problems associated with AMPs, several groups have been working on antibacterial cationic species (Figure 1), usually with oligomeric or polymeric structures, which either are inherently amphipathic or spatially segregate the hydrophilic and lipophilic portions only during the interaction with the bacterial membrane. Apart from some rationally designed short α-helices[16,17] and α-peptidic dendrimers,[18,19] most of the oligomeric structures with a number of residues between 5 and 20 units are based on the diverse stable non-natural helices (foldamers) formed in solution by β-

peptides,[20,21,22,23,24,25] oligoureas,[26,27] and α-peptoids.[28,29,30,31] However, foldamers rely mainly on expensive chiral monomers joined together by a multistep solid phase peptide synthesis followed by a demanding purification, which are not suitable for industrial applications. Stable amphipathic conformations also characterize shorter oligomers, such as de novo designed synthetic tripeptides[32,33] and triarylamides (Figure 3).[34,35,36] In all of these cases, the preorganization of monomers is at the basis of inherently stable secondary structures,[21,24,35,36,37] which do not have to spend free energy in order to arrange into an amphiphilic folding when interacting with the phospholipid bilayers of bacterial membranes, thus leading to better antimicrobial activities. Examples of amphipathic antimicrobials based on an extremely rigid backbone can also be found in synthetically-produced cationic steroid antimicrobials (CSAs),[38,39,40,41] as well as in aryl trimers where the facially amphiphilic topology is constitutionally guaranteed by the proper 1,3,5-substitution of aryl scaffolds (Figure 3).[42]

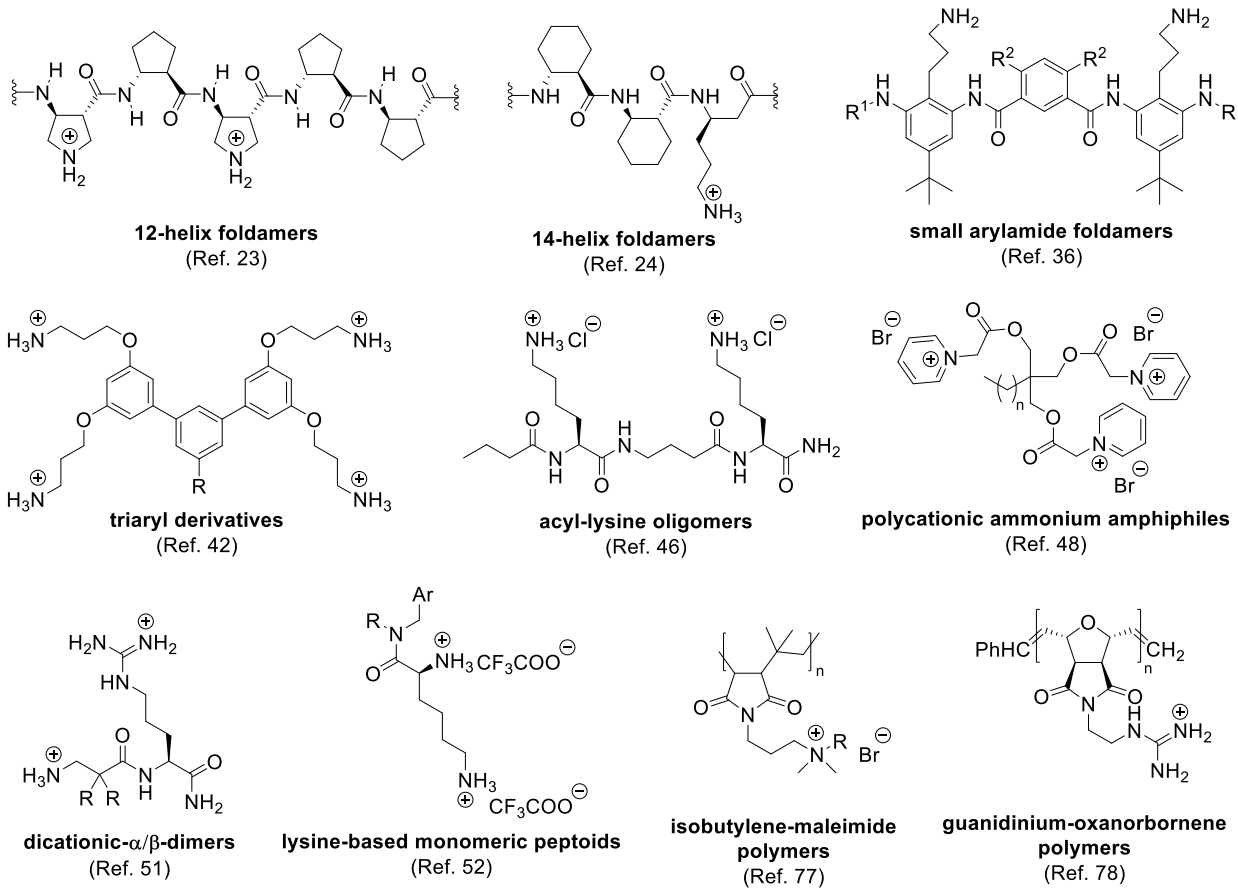

Figure 3. Representative synthetic mimics of antimicrobial peptides.

However, the opposite approach has also been used, thus mimicking AMPs like indolicidin, which is unstructured in aqueous environment, but shows a stable polyproline II-like structure upon interaction with liposomes and is a membrane permeabilizing peptide.[43] In fact, it has been elegantly demonstrated that also synthetic oligomeric species not based on preorganized monomers, thus having much more flexible backbones, may penetrate the bacterial cell wall barrier in an easier way, compared to conformationally rigid antimicrobials. Moreover, due to the great number of rotatable backbone single bonds, they can still easily assume amphiphilic conformations when interacting with phospholipid bilayers, and then have a potent disrupting action on membranes.[44] Noteworthy members of these flexible oligomeric antimicrobials are *α*-AApeptides,[45] which are based on *α*-chiral PNA-like skeletons, acyl-lysine oligomers,[46] in which lysine and amino alkanoic acids alternate in the short hetero-oligomeric backbones, a few dicationic oligo-*α*-peptide analogues with a minimalist design,[47] and various bio-inspired polycationic ammonium amphiphiles (Figure 3).[48,49,50] Interesting examples of apparently unstructured antibacterials with a very small size have been recently reported in literature, such as dicationic *α/β*-amino acid dimers[51] and extremely simple, but still potent, lysine-based monomeric peptoids (Figure 3).[52]

The use of polycationic antimicrobial polymers based on inexpensive monomers, whose active amphipathic conformation is taken only when they interact with microbial membranes, has also been extensively investigated and reviewed on all aspects (Figure 3).[53,54,55] Even if most of them are used for surfaces sanitization and their mechanisms of action not always involve membranes disruption, they can sometimes show better activity and resistance to degradation, together with reduced toxicity and environmental problems, in comparison to smaller counterparts.[55]

Herein we report the synthesis and the in vitro antibacterial and hemolytic activities of small amphiphilic achiral *α*-hydrazido acids. In their design, the hydrophobic portion is composed of both the *N*- and *C*-terminal lipophilic groups, whereas the single charge is furnished by the ammonium ion of the glycine side chain (Figure 4). The *α*-hydrazido acids are mimics of *β*-amino acids and have been chosen because, as we have recently demonstrated, oligomers of their conformationally constrained version are prone to form the peculiar intramolecular hydrogen bond pattern of the hydrazido-turn secondary structure.[56] Thus, this folding could also be assumed by the present non-preorganized acyclic *α*-hydrazido acids, especially upon interaction with phospholipid bilayers, and easily used to segregate polar and charged molecular

portions from the lipophilic moieties. However, albeit these compounds are able to generate the desired amphipathic structure (*vide infra*), the lack of conformational constrictions in their flexible backbone should facilitate the penetration through the bacterial cell wall barrier and give rise to a more potent activity, as demonstrated for amphiphilic compounds of different dimensions.[46,57,58] In order to facilitate both the inexpensive synthesis of target compounds and the deduction of structure-activity relationships at the basis of activity and selectivity, in this initial investigation we devoted our attention only to mono-charged compounds. According to all the previously reported studies, monocationic compounds are likely to be less potent as antimicrobial and less selective toward mammalian cells, so that this choice should also ensure the possibility for easy future improvements, by simply changing the glycine side chain for a multiple charge-bearing fragment.[59]

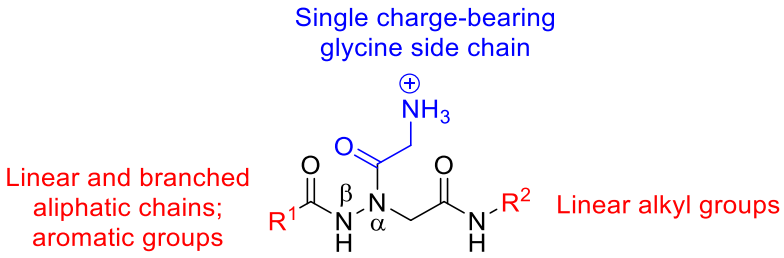

Figure 4. General structure of antibacterial *α*-hydrazido acids, with the common nomenclature for nitrogen atoms in these compounds.

2.2 Results and discussion

2.2.1 Design of the Amphiphilic Lead Structure.

A complete theoretical investigation of the mechanism of action of our *α*-hydrazido acids by means of molecular dynamics simulations was out of the scope of this thesis, but the idea at the basis of the choice of this particular backbone, that is its innate tendency to form amphiphilic structures, was the subject of a high-level density functional theory (DFT) analysis. After a complete conformational search at a lower theory level on a model compound with $R^1 = R^2 =$ Me, all the previously found energy minima were refined using the well-performing hybrid functional ωB97X-D3(0),[60] which includes the long-range dispersion corrections, together with the very large 6-311++g(3df,3pd) basis set, describing the solvent bulk with the integral equation formalism version of polarizable continuum model method (IEF-PCM).[61] The highly predominating conformer of the model compound was then used for constructing selected conformers of an actually used compound, namely **4Cb**, all having the aliphatic chains in the

most stable all-antiperiplanar conformation (see Computational investigation). The theoretical approach indicated that the preferred conformation in water for this monomeric compounds, substituted with a carbonyl at the *N*-terminal and a *N*-alkyl amide at the *C*-terminal, is the same hydrazido-turn assumed by their conformationally constrained oligomeric versions (Figure 5).[56]

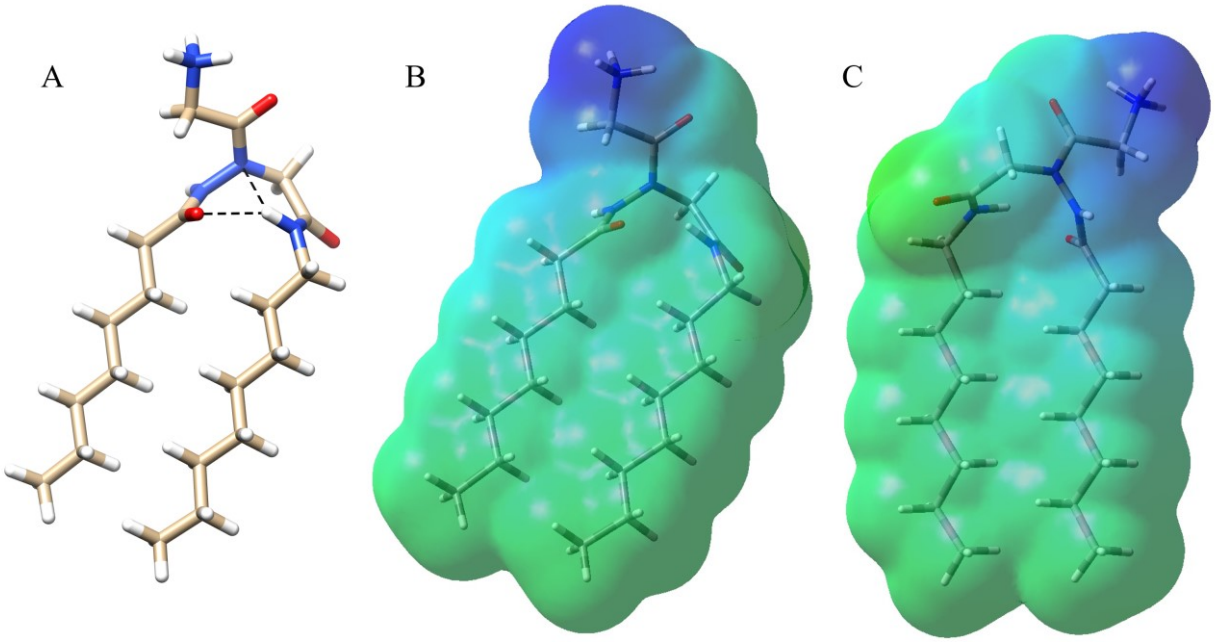

Figure 5. (A) Structure of most stable conformer of ammonium cation $C_7H_{15}CO$-HydrGlyH$^+$-NHC_8H_{17} (**4Cb**, R^1 = *n*-C_7H_{15}, R^2 = *n*-C_8H_{17}), computed at ωB97X-D3(0)/6-311++g(3df,3pd)/IEF-PCM level in water. (B) Front and (C) rear views of electrostatic potential surface (see text for explanations).

The Natural Bond Orbital (NBO)[62,63] analysis pointed out that this structure is mainly stabilized by the C=O···H-N hydrogen bond (2.08 Å), which is characterized by an important covalent contribution and forms an eight-membered pseudocycle, and, to a lesser extent, by the N^{α}···H-N H-bond (2.38 Å), which is instead essentially electrostatic in nature, due to a wrong directionality of donor and acceptor atoms (Table 5 and Table 7 in Computational investigation). The study exploiting the Atoms In Molecules (AIM)[64,65] theory confirmed the existence of a bond critical point associated with a quite strong C=O···H-N hydrogen bond, whereas no critical point was found in the case of N^{α}···H-N interaction, thus describing this latter hydrogen bond as purely electrostatic (Table 6).

Moreover, the theoretical inclusion of solvent bulk effects and van der Waals interactions made the structure having the aliphatic chains almost parallel to each other much more stable, with respect to conformations with R^1 and R^2 pointing in different directions, thus emphasizing the overall amphiphilicity of these ammonium cations. It is easy to see from the electrostatic potential surface in Figure 3 that, in spite of the overall +1 net charge, the only hydrogen atoms belonging to hydrocarbon chains that do not have an almost neutral potential are the ones attached to C-1 in the *N*-terminal octanoyl group (light blue). On the other hand, all the remaining methylene and methyl groups in R^1 and R^2 show the expected neutral potential (light green). Hydrogens on hydrazide C^{α} possess a small positive potential, likely due to both electronwithdrawing neighbors and proximity to ammonium moiety, thus their presence do not cause any substantial interruption in the polar character of the upper/rear part of the molecule.

Apart from the obvious contribution of the charged glycine side chain, within this hydrophilic molecular portion the *C*-terminal carbonyl and the *N*-terminal NH functionalities must play an important role in forming hydrogen bonds with water and charged lipid heads while interacting with phospholipid bilayers. The ability of hydrazide NHs to form quite strong hydrogen bonds is also readily apparent considering that their experimental proton chemical shifts in diluted deuterochloroform solutions range from 7.81 to 8.03 ppm when R^1 = OBn, and reach very high values (8.74-9.87 ppm) when R^1 is a hydrocarbon chain, thus experimentally confirming their high positive charge (see Supporting Information). Calculations of atomic charges of ammonium cation with NBO, AIM, Merz-Singh-Kollman,[66,67] CHelpG,[68] and Hu-Lu-Yang[69] schemes (Figure 16-Figure 20), as well as the computed electrostatic potential and NBO charges taking also into account the chloride anion (Figure 19), plenty confirmed these findings about the segregation of polar/charged and apolar portions. It must be noted here that, from both a computational and an experimental point of view, only inherently very stable structures can display amphipathic conformations in water, whereas the use of organic co-solvents or the presence of liposomes and vesicles greatly facilitates the formation of the amphiphilic secondary structure even for compounds which are substantially unstructured in water or aqueous buffers.[37,70,71] This observations strongly point toward an amphiphilic arrangement of our *α*-hydrazido acid hydrochlorides during the action on phospholipidic bilayers.

2.2.2 Synthesis of compounds

Prompted with the idea of an innate tendency of these conformationally unconstrained compounds to the formation of amphiphilic structures, we undertook a short, inexpensive and high-yielding synthesis of *α*-hydrazido acids hydrochlorides (Scheme 1). First, benzyl carbazate

was reacted with methyl bromoacetate in the presence of *N*,*N*-diisopropylethylamine, obtaining compound **1** in excellent yield. Benzyl carbazate demonstrated to be a poor nucleophile, thus concentrated dichloromethane solutions had to be used in order to obtain reasonable reaction times. Moreover, DIPEA was necessary to avoid the competition in the nucleophilic substitution from less hindered amines, such as triethylamine, which invariably led to unsustainable decreases in yields, due to the substantial formation of the corresponding quaternary ammonium salts with methyl bromoacetate.

Scheme 1. General Synthetic Scheme for the Preparation of Amphiphilic *α*-Hydrazido Acid Derivatives[a]

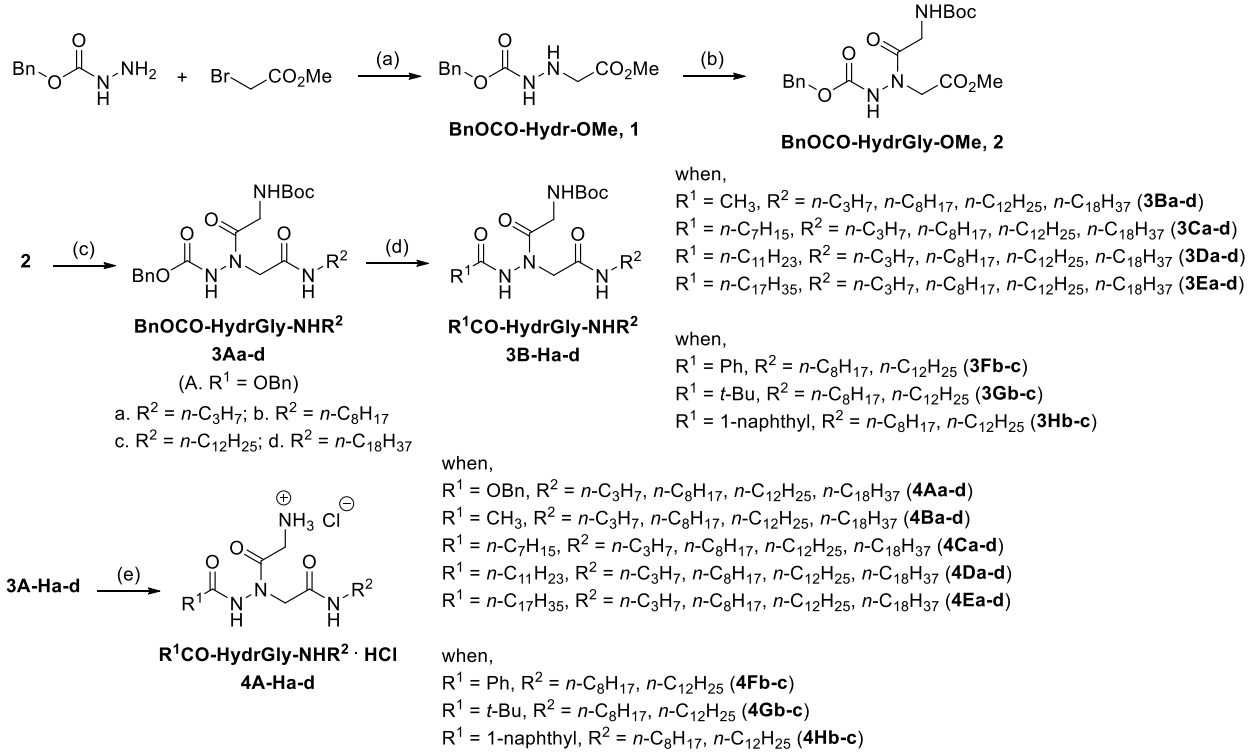

[a] (a) *N*,*N*-diisopropylethylamine (DIPEA), anh. DCM (0.5 mL per mmol of benzyl carbazate), rt, 48 h, 96%; (b) Boc-Gly-OH, 1-ethyl-3-(3-dimethylaminopropyl)carbodiimide hydrochloride (EDCI), anh. DCM (0.5 mL per mmol of **2**), -20 °C, 2 h, 86%; (c) R^2NH_2 (R = alkyl group), anh. MeOH, 7 h at rt for **3Aa**, 18, 24 or 36 h at reflux for **3Ab**, **3Ac**, and **3Ad**, 88-94%; (d) HCO_2H, Pd/C, anh. DCM, rt, 1 h, then pyridine, R^1COCl, anh. DCM, rt, 1 h, 65-95%; (e) Trifluoroacetic acid (TFA)/DCM 1:3, rt, 20 min, chromatographic purification of free amine, then 3 M HCl in anh. MeOH, 68-98%.

Then compound **1** was reacted with Boc-Gly-OH, using EDCI as the coupling agent, obtaining the desired common precursor **2** in very good yield, but even in this case it was necessary to circumvent the scarce reactivity of **1** by using concentrated solutions and also optimizing all the other experimental conditions. After reaction of **2** with the suitable alkyl amines, the first four compounds ready to be deprotected, **3Aa-d** (R^1 = OBn), where successfully synthesized, and the change of R^1 group by means of the carboxybenzyl removal/free hydrazide acylation sequence furnished the remaining compounds **3B-Ha-d** in good to excellent overall yields. Hydrochlorides **4** were then obtained in pure form by Boc removal with trifluoroacetic acid, followed by an easy chromatographic purification of free amines on silica gel and re-salification with hydrochloric acid. It must be pointed out that the achievement of the best possible antibacterial efficacy was out of the scope of this initial evaluation, so a coarse grid approach was voluntarily chosen, and only alkyl chains differing one from another for a large number of methylenic units were chosen. Moreover, when R^1 groups different from linear alkyl chains were taken into account, not all the possible combinations among R^1 and R^2 groups were synthesized and tested. In fact, as correctly reported in Scheme 1, this was done when the *N*-terminal chain, R^1, was the parent carboxybenzyl protecting groups, and for all the alkyl chains R^1 = CH_3-$C_{17}H_{35}$. After this screening, the best performing *C*-terminal chains (R^2 = C_8H_{17}, $C_{12}H_{25}$) were chosen to synthesize selected compounds with R^1 = *t*Bu, Ph, and 1-naphthyl.

2.2.3 Antimicrobial and haemolytic activity

The antibacterial activity was first tested against the following bacterial collection strains (Table 1):

- *Enterococcus faecalis* ATCC 29212 (Gram-positive);
- *Enterococcus faecium* 135562(35C) (Gram-positive);
- *Staphylococcus aureus* ATCC 29123 (Gram-positive);
- *Escherichia coli* ATCC 25922 (Gram-negative);
- *Pseudomonas aeruginosa* ATCC 27853 (Gram-negative)

The minimum inhibitory concentrations (MICs) were evaluated using the broth microdilution method in 96-well microtiter plates, following the CLSI guidelines[72] and using tetracycline as internal control. The results were evaluated after 24 h at 37 °C to allow visible growth of all tested strains. Compounds **4Ae** (R^1 = *n*-$C_{17}H_{35}$, R^2 = *n*-$C_{18}H_{37}$) and **4Hc** (R^1 = 1-naphthyl, R^2 = *n*-$C_{12}H_{25}$) were too insoluble to be tested. In addition, two among the most active compounds were subsequently tested against multidrug-resistant bacteria, namely the linezolid- and

methicillin-resistant *Staphylococcus aureus* AOUC-0915 (LR-MRSA) and the gentamicin- and colistin-resistant *Escherichia coli* 288328 (GR-CREc). Hemolytic activity was also evaluated, according to a reported procedure,[28] using freshly drawn, heparinized human blood diluted with phosphate buffered saline (PBS), pH 7.4. MICs and hemolysis results were reproducible between three independent experimental replicates. These results, as well as the reverse-phase HPLC-derived overall lipophilicity, are reported in Table 1.

From the results in Table 1, many general deductions can be drawn, even if more complete and detailed analyses will be conducted in a graphical way (*vide infra*). First, the hydrochlorides of *α*-hydrazido acids are somewhat more active against Gram-positive bacteria, *E. faecium* being the most sensitive, with respect to Gram-negatives, especially *Pseudomonas aeruginosa*. This observation makes readily apparent that the thick peptidoglycan layer of Gram-positive bacteria cannot prevent the entry of these flexible molecules, even when a large and rigid 1-naphthyl group is present as R^1 (**4Hb**), because of the nano-sized pores in the membrane of Gram-positive bacteria.[73] Moreover, the lower sensitivity of Gram-negatives is common in literature for cationic amphipathic membranolytic compounds, and is usually claimed as mainly caused by the reduced active concentration that can reach and disrupt both the outer and inner membranes of Gram-negative bacteria. This in turn is due to inability to permeabilize their primary barrier for hydrophobic compounds, which is the electrostatic network of negatively charged lipopolysaccharide molecules bound to divalent cations in the outer leaflet.[74] However, as demonstrated for ceragenins, which are cationic amphiphilic derivatives of bile salts, the lower activity toward Gram-negative bacteria could also be due to differences in phospholipid bilayers compositions, especially the high content of phosphatidylethanolamine, a zwitterionic lipid, in Gram-negatives, in comparison to bilayers of Gram-positives, which are usually richer in negatively charged phosphatidylglycerol and cardiolipin.[39] Conversely, the membrane activity of cationic *m*-phenylene ethynylene oligomers was demonstrated to be much more dependent on type and structure of lipids, and then on intrinsic membrane curvature, than on lipid headgroup net charges.[75]

Table 1. In Vitro Antibacterial and Hemolytic Activities of the Compounds

			MIC *vs* drug sensitive bacteria (μg mL^{-1})[a]								
Compd	**R^1**	**R^2**	***E. faecalis***	***E. faecium***	***S. aureus***	***E. coli***	***P. aeruginosa***	**HC_{50} (μg mL^{-1})**	**TI *vs S. aureus* (HC_{50}/MIC)**	**TI *vs E. coli* (HC_{50}/MIC)**	**RP-HPLC retention times (min)[b]**
4Aa	OBn	*n*-C_3H_7	1024	512	512	512	512	775	1.5	1.5	3.4

4Ab	OBn	*n*-C_8H_{17}	128	64	64	64	128	189	3.0	3.0	14.3
4Ac	OBn	*n*-$C_{12}H_{25}$	16	8	8	32	128	86	11	2.7	21.2
4Ad	OBn	*n*-$C_{18}H_{37}$	512	256	512	512	512	243	0.5	0.5	30.9
4Ba	CH_3	*n*-C_3H_7	2048	2048	1024	2048	2048	2700	2.6	1.3	0.3
4Bb	CH_3	*n*-C_8H_{17}	256	128	128	256	256	223	1.7	0.9	9.3
4Bc	CH_3	*n*-$C_{12}H_{25}$	32	32	64	64	64	127	2.0	2.0	17.5
4Bd	CH_3	*n*-$C_{18}H_{37}$	32	32	256	512	512	228	0.9	0.5	28.0
4Ca	*n*-C_7H_{15}	*n*-C_3H_7	1024	1024	1024	1024	2048	433	0.4	0.4	5.2
4Cb	*n*-C_7H_{15}	*n*-C_8H_{17}	32	16	16	16	32	131	8.2	8.2	17.8
4Cc	*n*-C_7H_{15}	*n*-$C_{12}H_{25}$	32	16	64	256	512	367	5.7	1.4	24.0
4Cd	*n*-C_7H_{15}	*n*-$C_{18}H_{37}$	>256	>256	>256	>256	>256	267	<1.0	<1.0	33.1
4Da	*n*-$C_{11}H_{23}$	*n*-C_3H_7	64	64	64	64	64	167	2.6	2.6	16.6
4Db	*n*-$C_{11}H_{23}$	*n*-C_8H_{17}	16	8	64	128	128	486	7.6	3.8	23.5
4Dc	*n*-$C_{11}H_{23}$	*n*-$C_{12}H_{25}$	128	128	>128	>128	>128	438	<3.4	<3.4	29.1
4Dd	*n*-$C_{11}H_{23}$	*n*-$C_{18}H_{37}$	512	512	256	>512	512	364	1.4	<0.7	35.9
4Ea	*n*-$C_{17}H_{35}$	*n*-C_3H_7	32	16	64	512	512	234	3.7	0.5	26.5
4Eb	*n*-$C_{17}H_{35}$	*n*-C_8H_{17}	512	64	128	512	512	200	1.6	0.4	32.2
4Ec	*n*-$C_{17}H_{35}$	*n*-$C_{12}H_{25}$	512	256	256	512	512	124	0.5	0.2	35.8
4Ed	*n*-$C_{17}H_{35}$	*n*-$C_{18}H_{37}$	N.D.[c]	N.D.	N.D.	N.D.	N.D.	N.D.	N.D.	N.D.	41.8
4Fb	Ph	*n*-C_8H_{17}	128	128	128	128	128	368	2.9	2.9	12.3
4Fc	Ph	*n*-$C_{12}H_{25}$	4	4	4	4	64	195	49	49	19.7
4Gb	*t*-Bu	*n*-C_8H_{17}	256	256	512	256	512	775	1.5	3.0	11.7
4Gc	*t*-Bu	*n*-$C_{12}H_{25}$	8	8	4	8	16	394	99	49	19.8
4Hb	1-Naphthyl	*n*-C_8H_{17}	32	16	32	16	64	311	9.7	19	14.4
4Hc	1-Naphthyl	*n*-$C_{12}H_{25}$	N.D.	N.D.	N.D.	N.D.	N.D.	N.D.	N.D.	N.D.	21.6
MSI-78			---	64[d]	8-16[d]	16-32[d]	---	120[e]	7.5-15	3.8-7.5	---

			MIC *vs* multi-drug resistant bacteria (μg mL^{-1})[a]					
			LR-MRSA[f]	**GR-CREc[g]**	**HC_{50} (μg mL^{-1})**	**TI *vs* LR-MRSA (HC_{50}/MIC)**	**TI *vs* GR-CREc (HC_{50}/MIC)**	**HPLC retention times (min)[c]**
4Fc	Ph	*n*-$C_{12}H_{25}$	4	4	195	49	49	19.7
4Gc	*t*-Bu	*n*-$C_{12}H_{25}$	4	8	394	99	49	19.8

[a] Conservative estimates of at least three independent trials. [b] Adjusted retention times, computed as the instrumental retention time minus the hold-up time. [c] N.D. stands for "not determined". [d] Values taken from Ref. 76. [e] Value taken from Ref. 34. [f] Linezolid- and methicillin-resistant *S. aureus* AOUC-0915. [g] Gentamicin- and colistin-resistant *E. coli* 288328.

As expected from the wide dimensional range of substituents used, which in the case of R^1 also encompasses groups with different shapes and electronic features, MICs vary to a very large

extent. As an example, while compound **4Ba** ($R^1 = CH_3$, $R^2 = C_3H_7$) having the shortest chains is almost completely inactive, likely due to a poor interaction with the apolar portions of phospholipid bilayer, compound **4Cb** ($R^1 = n\text{-}C_7H_{15}$, $R^2 = n\text{-}C_8H_{17}$) shows a good activity, and the MIC increases again for too long chains, as for **4Cd** ($R^1 = n\text{-}C_7H_{15}$, $R^2 = n\text{-}C_{18}H_{37}$), **4Dd** ($R^1 = n\text{-}C_{11}H_{23}$, $R^2 = n\text{-}C_{18}H_{37}$), and **4Ec** ($R^1 = n\text{-}C_{17}H_{35}$, $R^2 = n\text{-}C_{12}H_{25}$). Even in this case, the necessity to tune the overall hydrophobicity, avoiding either too small or too large apolar fragments, parallels the findings for amphiphilic antibacterials with different dimensions, such as polymers,[76] foldamers,[23] and small peptoids.[52] The best MICs (**4Fc**, R^1 = Ph, $R^2 = n\text{-}C_{12}H_{25}$, and **4Gc**, $R^1 = t$Bu, $R^2 = n\text{-}C_{12}H_{25}$), are equal to or better than the values for the magainin derivative MSI-78 (pexiganan, MIC = 64 μg mL^{-1} *vs E. faecium*, 8-16 μg mL^{-1} *vs S. aureus*, and 16-32 μg mL^{-1} *vs E. coli*),[77] which is also more hemolytic (HC_{50} = 120 μg mL^{-1}).[34] Despite the lack of any thorough optimization, these extremely simple and mono-charged compounds are competitive toward much more complex and expensive 12- and 14-helix foldamers (best MICs = 3.1-3.2 μg mL^{-1} *vs S. aureus*),[23,24] and polymers (best MICs = 3-12 μg mL^{-1} *vs S. aureus*) (Figure 3),[78,79] even if some of those oligomeric and polymeric antibacterials exhibit marginally better therapeutic indices. Taking into consideration small molecules, *α*-hydrazido acids outperform tricationic tripeptides based on 2,5,7-tri-*tert*-butyl tryptophan in terms of both antimicrobial activity and therapeutic window,[32] whereas only the most effective among tetracationic triaryl derivatives (best MICs = 0.78 μg mL^{-1} *vs S. aureus*, 3.13 μg mL^{-1} *vs E. coli*; best therapeutic indices = 406 *vs S. aureus*, 172 *vs E. coli*)[42] give better overall results (Figure 3). Even some structurally very simple peptoids show a slightly more powerful antimicrobial efficacy (best MICs = 2.2 μg mL^{-1} *vs S. aureus*, 2.9 μg mL^{-1} *vs E. coli*), but despite the double positive charge they are less selective toward erythrocytes and have worst therapeutic indices (best TIs = 34 *vs S. aureus*, 23 *vs E. coli*) (Figure 3).[52] It is worth noting that these *α*-hydrazido acids show identical activities towards two multidrug resistant strains, the linezolid- and methicillin-resistant *S. aureus* AOUC-0915 (LR-MRSA, MICs = 4 μg mL^{-1} for both **4Fc** and **4Gc**) and the gentamicin- and colistin-resistant *E. coli* 288328 (GR-CREc, MICs = 4 μg mL^{-1} for **4Fc** and 8 μg mL^{-1} for **4Gc**, Table 1). This is not surprising for LR-MRSA, whose resistances to methicillin and linezolid rely, respectively, on the presence of PBP2a, a penicillin binding protein with extremely low affinity for all *β*-lactams, except for last-generation cephalosporins,[80] and an rRNA methyltransferase that catalyzes post-transcriptional methylation to the C8 position of nucleotide A2503 in 23S rRNA, causing a decreased binding affinity for linezolid.[81] Thus, the phospholipidic bilayers of LR-MRSA membrane are not

substantially changed in comparison to the drug sensitive counterpart, *S. aureus* ATCC 29213. On the other hand, the conservation of efficacy of these cationic *α*-hydrazido acids toward GR-CREc was not predictable. In fact, whereas the resistance to gentamicin of GR-CREc is due to the *aac(3)-IIa* gene, which causes the covalent modification of gentamicin and lead to a poor binding to the ribosome target,[82] the resistance to colistin is due to the MCR-1 protein, which lead to addition of phosphoethanolamine to lipid A. Consequently, the binding between the less negatively charged lipopolysaccharide (LPS) and the positively charged colistin is much less effective,[83] and the same reduced binding affinity was demonstrated to be at the basis of an intrinsic resistance to cationic AMPs.[84] However, in the present case the possible decrease in electrostatic interaction between the cationic *α*-hydrazido acids and the outer membrane external leaflet, that is the first mandatory step for the following insertion and damaging action on phospholipid bilayers, does not appear to be detrimental for the antimicrobial activity. This observation suggests that these new amphiphilic organic compounds might also be active against other MDR strains with the same compositions of lipid bilayers.

As far as hemolytic activity is concerned, at a first glance it is evident from data Table 1 that the smallest and less active compounds show larger HC_{50} values, while the most active species with medium-sized R^1 and R^2 chains are also more active against red blood cells. However, the two most powerful antibacterial compounds (**4Fc**, R^1 = Ph, R^2 = *n*-$C_{12}H_{25}$, and **4Gc**, R^1 = *t*Bu, R^2 = *n*-$C_{12}H_{25}$) have hemolytic concentrations that are much higher than their MICs, thus leading to substantially better therapeutic indices than all the other compounds, and they have almost null hemolysis computed at concentrations equal to their MICs (Table 2).

Table 2. Hill equation slopes (b) and percent hemolysis of compounds 4A-Ha-d at MICs toward *S. aureus* and *E. coli*.[a]

Compd	Hill slope (b)	Hemolysis at MIC toward *S. aureus* (%)	Hemolysis at MIC toward *E. coli* (%)
4Aa	2.35	28	28
4Ab	8.65	$9\ 10^{-3}$	$9\ 10^{-3}$
4Ac	2.72	3.7	9
4Ad	2.86	89	89
4Ba	3.62	3.0	27
4Bb	14.63	0.04	88
4Bc	2.30	17	17
4Bd	2.50	57	88

4Ca	3.13	94	94
4Cb	2.04	1.4	1.4
4Cc	2.02	2.9	33
4Cd	2.63	>47[b]	>47[b]
4Da	3.49	4.5	4.5
4Db	3.88	0.04	0.6
4Dc	1.47	>14[b]	>14[b]
4Dd	2.08	34	>68[b]
4Ea	4.97	0.2	98
4Eb	5.60	7.3	96
4Ec	4.99	97	99.9
4Ed	N.D.	N.D.	N.D.
4Fb	8.49	1.0	1.0
4Fc	1.28	0.7	0.7
4Gb	9.89	2.2	$2\ 10^{-3}$
4Gc	1.33	0.2	0.6
4Hb	1.64	2.4	0.8
4Hc	N.D.	N.D.	N.D.

[a] Computed by interpolation or extrapolation by using the Hill equation, exploiting HC_{50} and b (Hill slope) values obtained by non-linear regression of experimental data. [b] In cases where the MIC was determined as major than a minimum value, the corresponding percent hemolysis was reported as major than its computed value at the minimum MIC.

In addition, due the wide range of slopes obtained by non-linear regression of experimental hemolysis data by the Hill equation,[85,86] also many less selective compounds with poorer therapeutic indices show extremely low percent hemolysis at MICs (Table 2). Interestingly, contrarily to antibacterial efficacy, the hemolytic activity does not decrease when large *N*- and *C*-terminal substituents are present, and also has a more erratic general behaviour. Both of these characteristics, taken together with the wide dimensional range of substituents considered, are directly involved in the very large interval of therapeutic indices obtained for all bacteria (e.g. from 0.5 to 99 for *S. aureus*), which is unusual for simple compounds of comparable size.[30,32,42,52]

In literature it is common to find that, after a monotonic decrease in MICs up to a certain dimension of a given apolar substituent for a constant size of the other hydrophobic group(s) in the molecule, a further increase in size of that group can lead to a more or less pronounced loss

in antibacterial activity.[29,52] It is easy to find the first structure-activity relationship considering only compounds **4A-Ea-d**, for which all the possible twenty combinations of R^1 (OBn, methyl, heptyl, undecyl, or heptadecyl) and R^2 (propyl, octyl, dodecyl, or octadecyl) were synthesized (Figure 6). Considering for example *E. faecium* in Figure 6 on the left, for the shortest R^1 tail (Me), there is a striking improvement in antibacterial efficacy passing from R^2 = propyl to the octyl, and then the dodecyl and octadecyl chains. On the contrary, for the longest R^1 (*n*-$C_{17}H_{35}$), the best-performing R^2 fragment is the propyl, whereas a continuous increase in MICs is observed as the length of R^2 increases. For all the other R^1, there is a clear decrease of antibacterial potency at both sides of the R^2 that best matches the particular R^1. The same findings, in the right part of *E. faecium* in Figure 6, can be deduced considering how MICs vary according to different R^1 moieties, taking constant R^2 group. Analysing the complete series of graphs for all the bacteria (Figure 6), it is also worth noting that *enterococci* are more sensitive to compounds having *N*- and *C*-terminal chains longer than those required to inhibit growth of *S. aureus*, which in turn is more sensitive to chains longer than those necessary against Gram-negative bacteria. For example, when R^1 = *n*-$C_{11}H_{23}$, the best activities toward *E. faecalis* and *E. faecium* are obtained for R^2 = *n*-C_8H_{17}, while in the case of *S. aureus* R^2 = *n*-C_3H_7 and *n*-C_8H_{17} show the same potency, and for *E. coli* and *P. aeruginosa* the shortest R^2 furnished the lowest MICs (Figure 6).

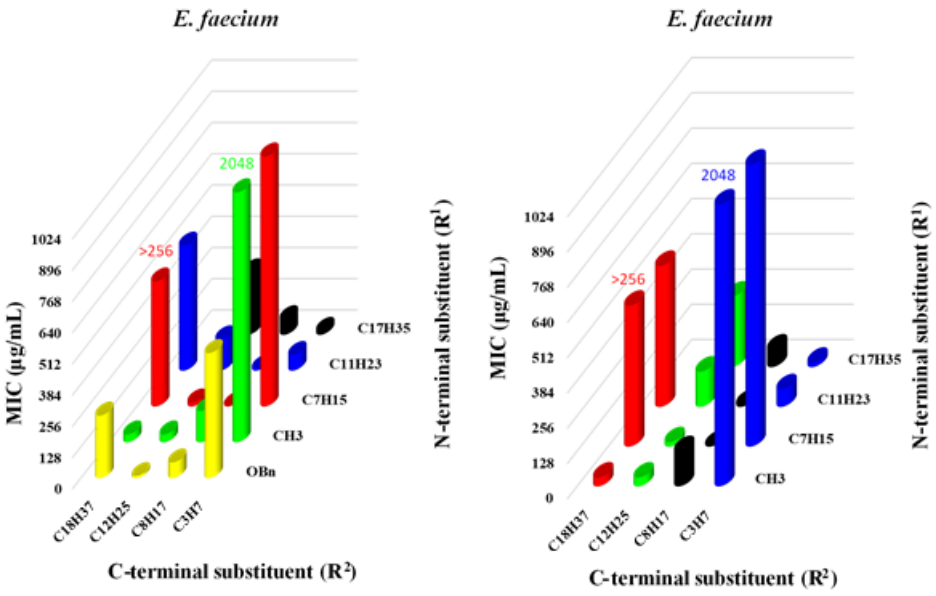

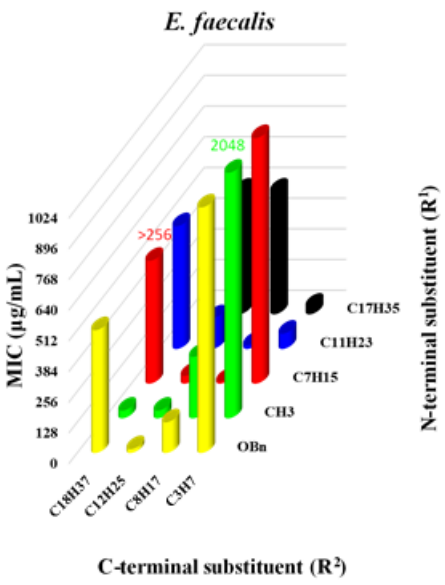
E. faecalis
MIC (μg/mL)
1024
896
768
640
512
384
256
128
0
>256
2048
C18H37
C12H25
C8H17
C3H7
OBn
CH3
C7H15
C11H23
C17H35
N-terminal substituent (R1)
C-terminal substituent (R2)

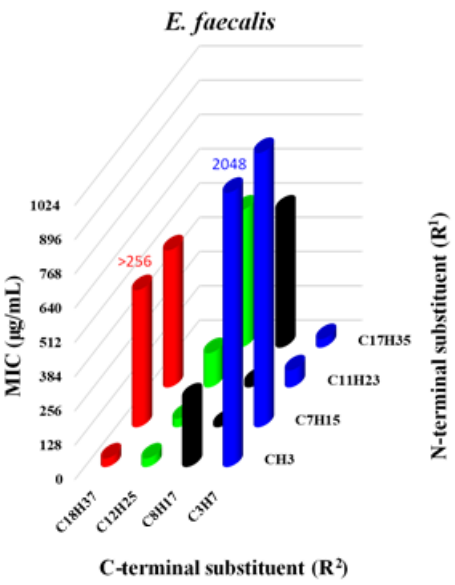
E. faecalis
MIC (μg/mL)
1024
896
768
640
512
384
256
128
0
>256
2048
C18H37
C12H25
C8H17
C3H7
CH3
C7H15
C11H23
C17H35
N-terminal substituent (R1)
C-terminal substituent (R2)

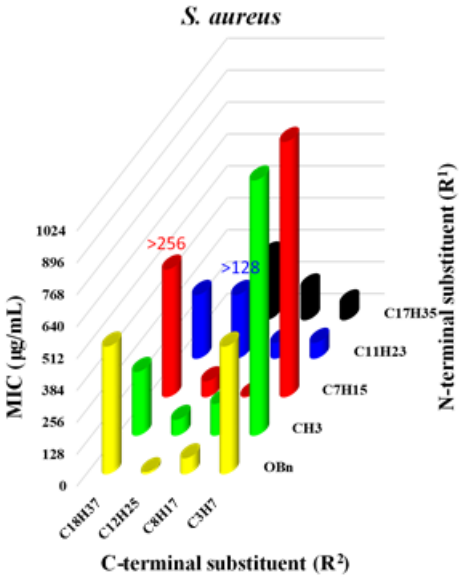
S. aureus
MIC (μg/mL)
1024
896
768
640
512
384
256
128
0
>256
>128
C18H37
C12H25
C8H17
C3H7
OBn
CH3
C7H15
C11H23
C17H35
N-terminal substituent (R1)
C-terminal substituent (R2)

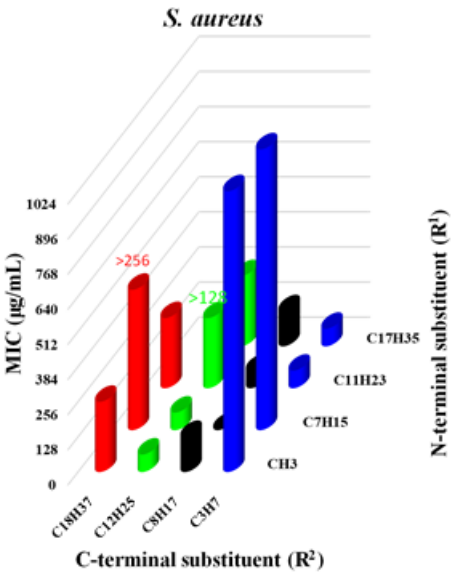
S. aureus
MIC (μg/mL)
1024
896
768
640
512
384
256
128
0
>256
>128
C18H37
C12H25
C8H17
C3H7
CH3
C7H15
C11H23
C17H35
N-terminal substituent (R1)
C-terminal substituent (R2)

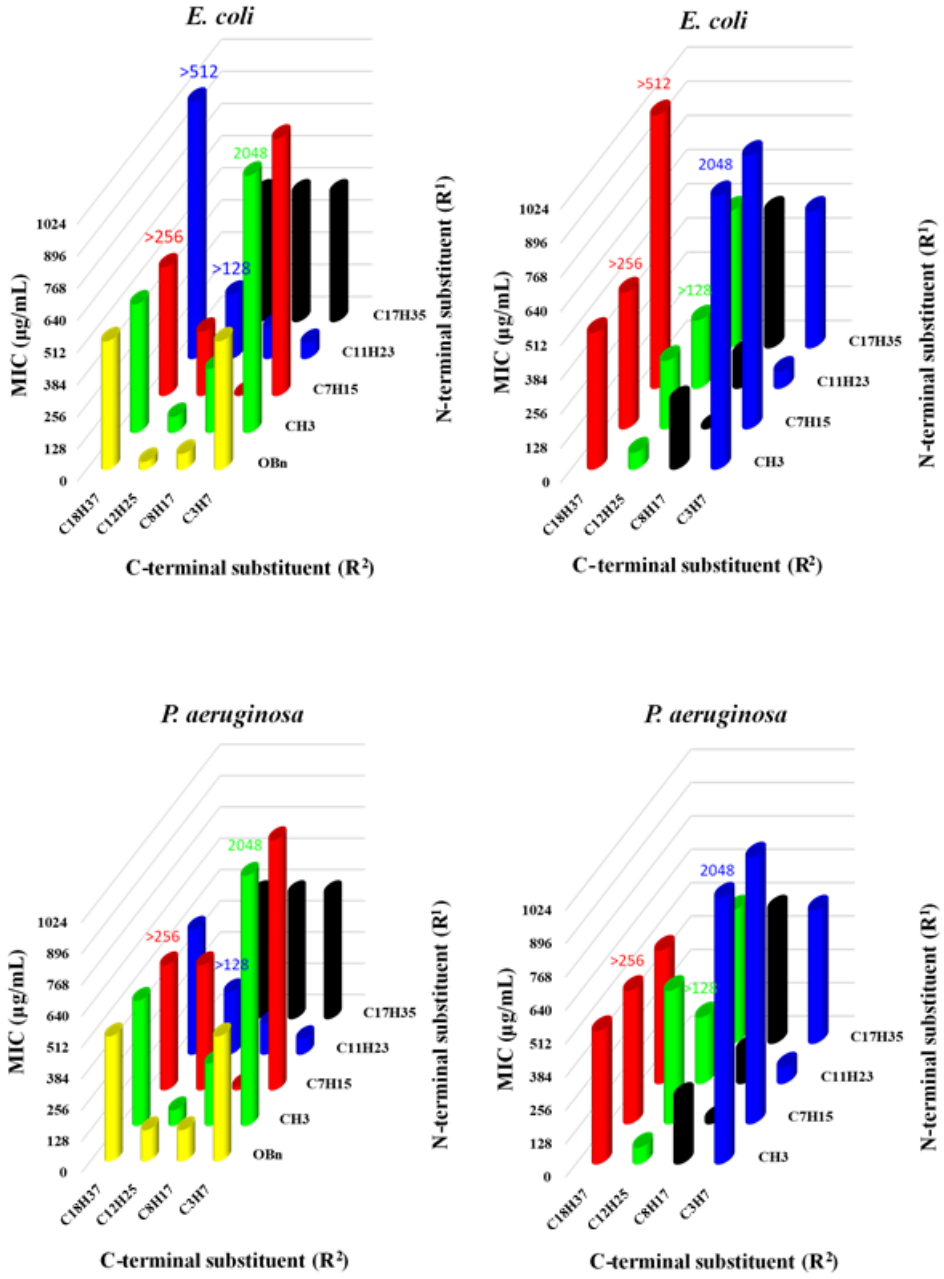

Figure 6. Variation of antimicrobial activity toward *E. faecium, E. faecalis, S. aureus, E. coli, P. aeruginosa* with R^1 and R^2 substituents, for compounds 4A-Ea-d**. On the left: bar graphs colored taking constant R^1 groups, highlighting the dependence of antimicrobial activity on R^2 length. On the right: bar graphs colored taking constant R^2 groups, highlighting the dependence of antimicrobial activity on alkyl R^1 length (compounds** 4Aa-d**, with R^1 = OBn are not reported).**

Figure 6 was useful for comparing homogenous series of compounds with the same type of substituents, but after the initial investigation we introduced *ad hoc* variations in R^1 groups, taking constant the two most active *C*-terminal R^2 groups, the octyl and dodecyl chains (Table 1). A possible way to develop a more general model for antibacterial activity, and also for

hemolytic activity, is to use the reverse-phase HPLC-based (RP-HPLC) overall lipophilicity, in the form of either the retention time[32,42,52,87] or the percentage of less polar eluent at retention time.[29,30]

This kind of structure-activity relationship highlights that, for all the bacteria tested, there is a parabolic trend of MICs toward retention time (Figures 5A and 5B for *S. aureus*, see Figure 6 in additional figures for other bacteria). Of course, due to the fact that MICs determined with the adopted protocol were measured in powers of 2,[72] and that in some cases only minimum theoretical values corresponding to the highest concentration tested were available, coefficient of determination, r^2, indicating a very good parabolic interpolation could not be expected. However, r^2 of 0.88, 0.80, 0.68, 0.76, and 0.63 for *E. faecalis*, *E. faecium*, *S. aureus*, *E. coli*, and *P. aeruginosa*, respectively, still confirm the visual impression that MIC varies with retention time with an approximately parabolic trend and, most important, that overall lipophilicity is by far the main parameter governing the antimicrobial activity for this series of mono-charged compounds differing only by the size, shape and electronic features of apolar portions. Albeit this finding is of obvious practical importance for directing the future synthesis of most active compounds in a more effective way, at the moment a simple interpretation of the observed raise of MICs after the optimal retention time ranges cannot be done. Of course, it is striking that the reason must relies on the differences between the ability of these compounds to simply bind to covalently linked monolayers of linear C18 hydrocarbon chains in a RP-HPLC column, and their capability to be attracted to the external bacterial surface, reach the fluid double layers of differently composed membranes, insert and then weaken or damage them by one or more of the known mechanisms. In fact, while the former clearly appears to be a monotonically raising additive function of van der Waals interactions, the latter is a much more complex phenomenon that encompasses many different molecular movements and interactions. Depending on the particular mechanism, different dispositions of amphiphilic compounds are required for either a regular pores formation, a generalized membrane weakening/permeabilization, or a less ordered membrane dissolution/destruction with a detergent-like effect.[7,10] Thus, it is not obvious that the ability of these compounds to kill bacteria must always increase as the interactions with the apolar stationary phase in a RP-HPLC strengthens, and a further different behavior was observed regarding the relationship between overall lipophilicity and hemolytic activity (see below). In addition, even if overall lipophilicity is strikingly the main parameter for quantitatively describing the growth-inhibiting effect of these amphiphilic compounds, there must also be

secondary variables, such as substituent-specific effects relying on shape and/or electronic features, which can hardly be described at the moment. In fact, for all the bacteria there are some cases in which compounds with very close retention times have different antibacterial activities, as well as cases of compounds with fairly different retention times that show the same MICs (Figure 7 and

Figure 92 in Additional Figures and Tables).

The higher sensitivity of Gram-negative bacteria to shorter alkyl chains than those required for Gram-positives, previously highlighted analyzing complete homogeneous series in Figure 6, can be deduced here in a more comprehensive way taking into consideration the ranges of retention times in which compounds show good antimicrobial efficacy. In fact, retention time ranges where MICs drop below a given value (e.g. ≤64 μg mL^{-1}) in Figure 7 and

Figure 92 (this latter in Additional figures and tables), become narrower and globally shift toward lesser values passing from *E. faecium* (14.3-32.2 minutes), to *E. faecalis* (14.4-28.0 minutes), to *S. aureus* (14.3-26.5 minutes), to *E. coli* (14.3-21.2 minutes), and eventually to *P. aeruginosa* (14.4-19.7 minutes). To the best of our knowledge, in all cases available in literature of RP-HPLC-derived overall lipophilicity measured for cationic antibacterial amphiphiles, such a clear parabolic relationship has never been found, and only a few cases of increases in MICs for large lipophilic chains have been reported so far. However, it must be pointed out that this lack of previously reported similar behaviors could be due to the usually much smaller dimensional span of hydrophobic moieties investigated, especially avoiding combinations of two or more extended apolar substituents, thus generally leading to a monotonic increase in antibacterial activity as the overall lipophilicity increases.[30,32,42,87] Only in one case for peptoid monomers (e.g. from a octyl to a decyl chain),[52] and in two cases for *N*-terminal alkylated oligopeptoids,[29] a sharp decrease of antimicrobial efficacy with extended retention times was evidenced for structurally homogenous backbones bearing too large lipophilic portions.

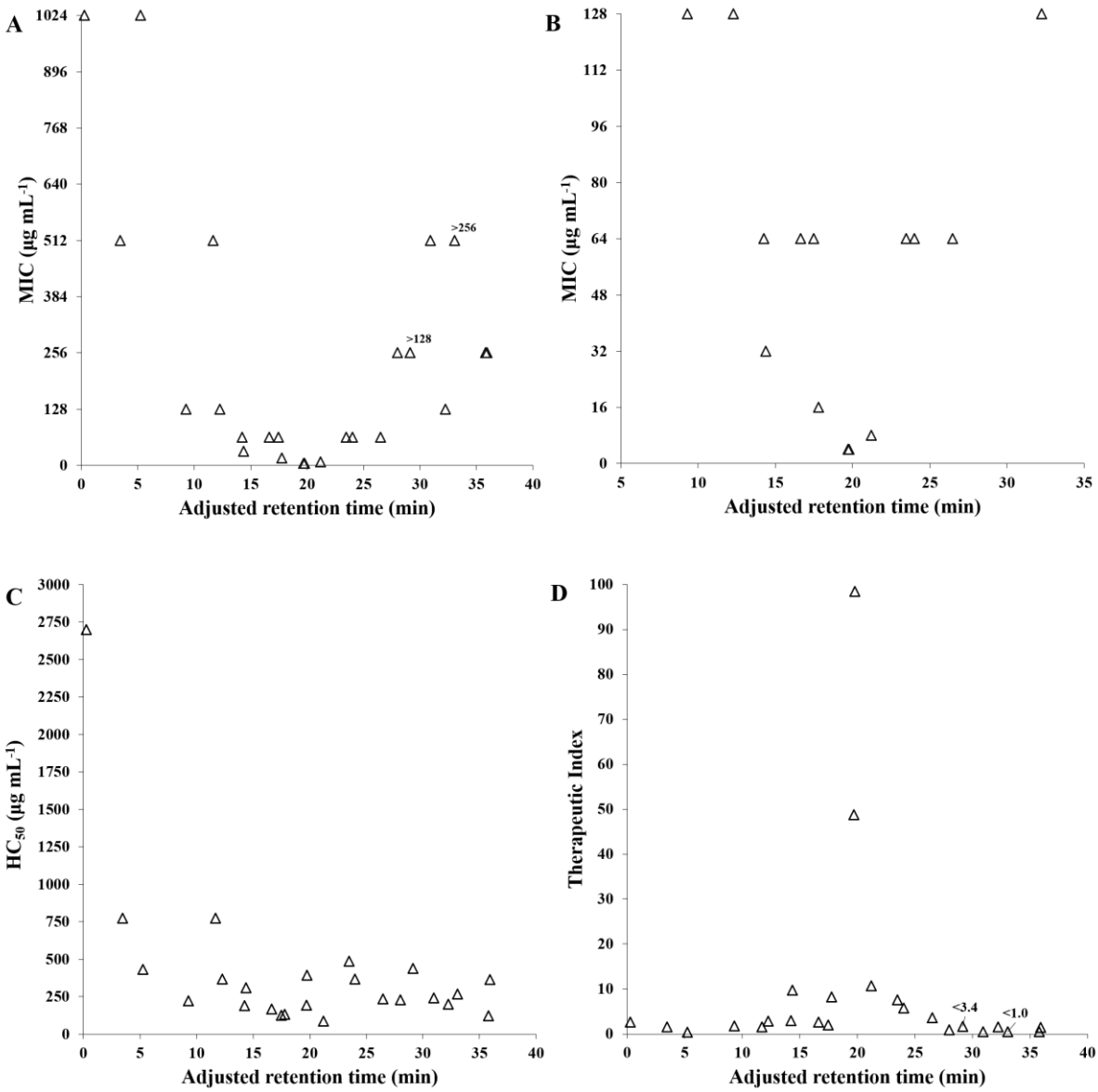

Figure 7. Variation of (A,B) antibacterial activity toward *S. aureus* (two different vertical scales), (C) hemolytic activity, and (D) therapeutic index toward *S. aureus* with adjusted retention time (instrumental retention time minus the hold-up time; Hewlett-Packard Lichrosorb RP 18 column, 5 μm, L × I.D. 200 × 4.6 mm, flow rate = 0.5 mL min^{-1}; elution gradient: from water:2-propanol = 70:30 to water:2-propanol = 10:90 in 40 minutes).

After demonstrating that the variation of minimum inhibitory concentration with retention time might be used as a powerful tool for an antimicrobial activity-directed synthesis of these amphiphilic compounds, the hemolysis-overall lipophilicity relationship was also evaluated (Figure 7C). In contrast to the approximately parabolic trend of minimum inhibitory concentrations, HC_{50} values show a sharp decrease as soon as the overall lipophilicity starts increasing and then, for the remaining range of retention times, they have a quite erratic behavior but without any overall reduction or increase. This difference with respect MICs is

also readily apparent directly analyzing only data for compounds belonging to the complete series with all the combinations of R^1 and R^2 used in the initial investigation (Table 1 and Figure 8).

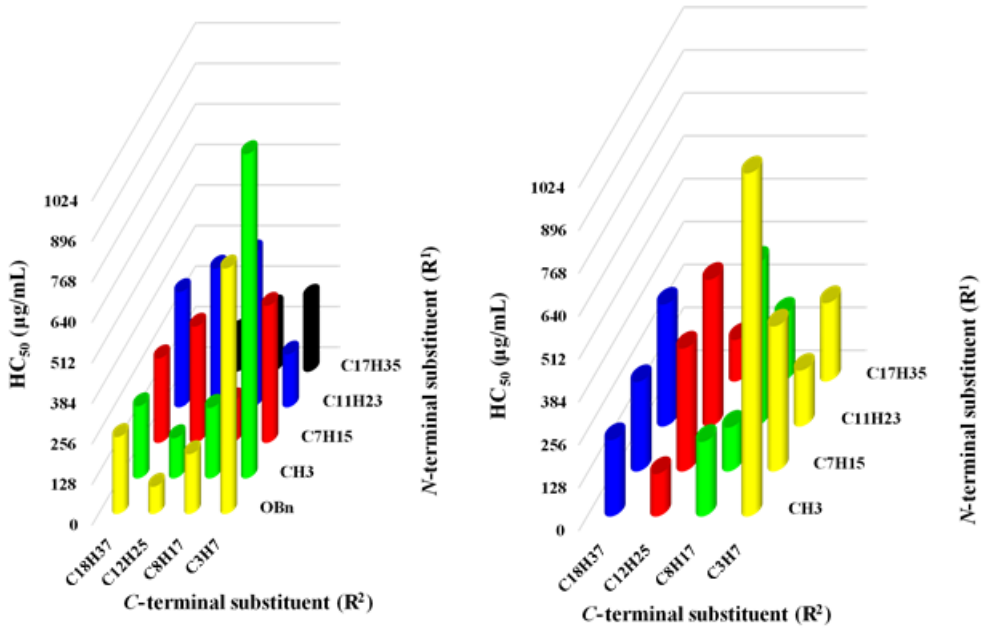

Figure 8. Dependence of HC_{50} on the length of R^1 and R^2 substituents, for compounds whose complete series with all the possible combinations of R^1 and R^2 were synthesized (4A-Ea-d). Left: bar graph colored taking constant R^1 groups, highlighting the dependence of hemolytic activity on R^2 length. Right: bar graph colored taking constant R^2 groups, highlighting the dependence of hemolytic activity on R^1 length (compounds 4Aa-d, with R^1 = OBn, are not reported).

As an example, within the series of compounds **4Ca-d** (R^1 = *n*-C_7H_{15}), **4Da-d** (R^1 = *n*-$C_{11}H_{23}$), and **4Ea-c** (R^1 = *n*-$C_{17}H_{35}$), the variation of hemolytic concentration with R^2 groups is strikingly different from the homogenous trends of MICs toward any of the bacteria tested, as reported for *E. faecium* in Figure 6. The same applies to the dependence of HC_{50} on R^1 groups, taking into consideration compounds having the same R^2 chain (Figure 8), thus confirming a somewhat more unpredictable behavior of hemolytic activity in terms of both the overall lipophilicity and the size of *N*- and *C*-terminal substituents. In addition, there are no other evident variables, such as shape or electronic features, identifying subgroups of clearly more (or less) hemolytic compounds.

Due to the peculiar and extremely different trends of MIC and HC_{50} with respect to retention time, the resulting pointed graphs of computed therapeutic indices (TI = HC_{50}/MIC) as a function of overall lipophilicity are not surprising (Figure 7A for *S. aureus*, Figure 93 for other bacteria in Additional Figures and Tables), and exactly the same behavior has already been

found for analogs of antimicrobial peptide gramicidin S.[88] For all bacteria, compounds having too short or too long retention times invariably show extremely low TIs, thus being completely unsafe. Only within the range of optimal overall lipophilicity, corresponding to the range of moderate to good antimicrobial activity (approximately from 14 to 27 minutes toward *S. aureus*), *α*-hydrazido acids can show a better *in vitro* selectivity, confirming the usefulness of this quantitative evaluation of overall lipophilicity by means of adjusted retention times. Obviously, due to the definition of TI itself, the wider or narrower ranges of best therapeutic indices toward other bacteria must parallel the wider intervals of overall lipophilicity furnishing good antimicrobial activity toward *enterococci*, as well as the narrower intervals toward Gram-negative strains. In addition, based on the general order of sensitivity of bacteria to these compounds reported above (Table 1), TI values for many amphiphilic *α*-hydrazido acids decrease in the order *E. faecium* > *E. faecalis* > *S. aureus* > *E. coli* > *P. aeruginosa*. However, mainly due to the fluctuating behavior of hemolytic activity, even within the optimal range for each bacterium there are some compounds showing a fairly reduced therapeutic window (Figure 7A and Figure 93, Table 1 and Table 12). The two most powerful antibacterials, **4Fc** (R^1 = Ph, R^2 = *n*-$C_{12}H_{25}$) and **4Gc** (R^1 = *t*Bu, R^2 = *n*-$C_{12}H_{25}$), are by far the most selective compounds and have almost identical retention times, thus they appear as a sort of spike in most of the graphs. They also show the same good selectivity when multi-drug resistant bacteria are taken into consideration (Table 1) and, even more remarkably, **4Fc** is the only one having a quite good therapeutic index for *Pseudomonas aeruginosa* (25), toward which all the other compounds show much poorer TIs (<5). The only remarkable exception to their superiority is *α*-hydrazido acid **4Db** (R^1 = *n*-$C_{11}H_{23}$, R^2 = *n*-C_8H_{17}) toward *E. faecium*, whose highest therapeutic index, 61 (Table 12 in Additional Figures and Tables), is caused by both its high activity toward that bacterium and its inherently low hemolytic potency.

2.2.4 Permeabilization of Outer and Inner Membranes

To ascertain beyond doubt the permeabilizing and destabilizing action on bacterial membranes of *α*-hydrazido acid amphiphiles, we slightly modified previously reported procedures[49] and used compound **4Gc** (R^1 = *t*-Bu, R^2 = *n*-$C_{12}H_{25}$) at its MIC as a model system toward both the susceptible (ATCC 25922) and the MDR (GR-CREc, 288328) *E. coli* strains (Figure 9). *N*-phenyl-1-naphthylamine (NPN) was chosen as a fluorescent probe for the outer membrane permeabilization, due to its gain in fluorescence when passing from an aqueous solution to a hydrophobic environment (i.e. the membrane lipid bilayers), whereas propidium iodide (PI)

was chosen as an indicator of inner membrane permeabilization, because its fluorescence is greatly enhanced when it binds to nucleic acids. The fluorescent probes showed a null (NPN) or extremely reduced (PI) uptake in absence of **4Gc**, while rapid increases in normalized fluorescence were observed in both cases by addition of the amphiphile to suspensions containing either the sensitive (Figure 9A) or the MDR strain (Figure 9B), thus plenty confirming the permeabilizing and damaging action of *α*-hydrazido acid hydrochlorides on bacterial membranes.

Even if the raise in normalized fluorescence for the susceptible ATCC collection strain seems to be extremely reduced for both probes in comparison to the gentamicin- and colistin-resistant GR-CREc strain, this is mainly due to substantially different starting points in terms of absolute fluorescence intensity. The computed permeabilization rate constants must therefore be considered in order to effectively compare the behavior of compound **4Gc** toward the two strains. At least with these experimental conditions and for the time considered (10 minutes), the permeabilization of both membranes always demonstrated to follow an exponential raise to maximum (r^2 ≥0.99), and the actual rate constants computed for outer membrane and inner membrane permeabilization are quite close for the two strains.

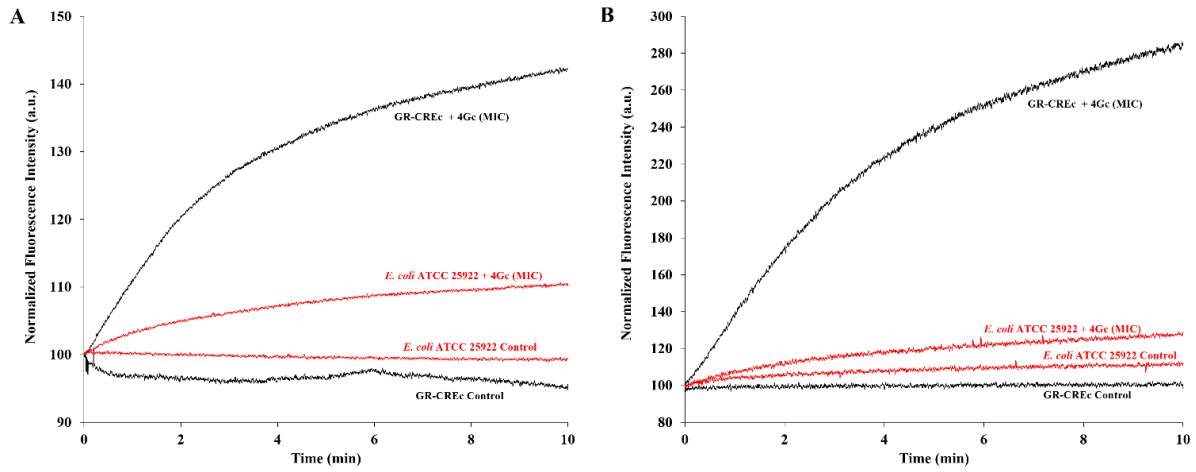

Figure 9. Variation of (A) NPN and (B) PI fluorescence with time, as a measure of outer and inner membrane permeabilization, respectively, caused by compound 4Gc [red: *E. coli* ATCC 25922; black: GR-CREc (*E. coli* 288328)].

Interestingly, the outer membrane permeabilization rate constant measured by NPN uptake for GR-CREc (0.31 min^{-1}) resulted to be about 1.2 times greater than for the sensitive bacterium (0.25 min^{-1}), whereas for the inner membrane permeabilization the rate constant of PI uptake for GR-CREc (0.24 min^{-1}) was about 1.1 times greater than for *E. coli* ATCC 25922 (0.22 min^{-}

[1]). Thus, not only the less negatively charged LPS of GR-CREc was unable to prevent the action of these amphiphiles more effectively than that of susceptible *E. coli*, but it resulted even more permeable to *α*-hydrazido acid hydrochlorides. This is in agreement with the identical MIC values of compounds **4Fc** and **4Gc** obtained against either susceptible or resistant *S. aureus* and *E. coli* strains (Table 1).

2.2.5 Stability Toward Enzymatic and Chemical Degradation

Like any other therapeutic peptide, AMPs suffer from low oral bioavailability due to proteolysis, and their systemic administration is also limited by a very short half-life caused by the rapid degradation by blood plasma enzymes.[89] In spite of the *α*-hydrazido acid skeleton, the sensitivity to proteolytic degradation could not be excluded *a priori*, due to the presence of three different potentially hydrolysable carbonyl-nitrogen bonds, one of which linking the N^{α} atom to a glycine side chain. Thus, the minimum inhibitory concentrations toward *S. aureus* of compounds **4Cb** (R^1 = *n*-C_7H_{15}, R^2 = *n*-C_8H_{17}), **4Fc** (R^1 = Ph, R^2 = *n*-$C_{12}H_{25}$), and **4Gc** (R^1 = *t*-Bu, R^2 = *n*-$C_{12}H_{25}$), were evaluated after preincubation in fresh 50% blood plasma solution for 0, 3 and 6 hours at 37 °C, followed by broth microdilution method in 96-well microtiter plates.[52]

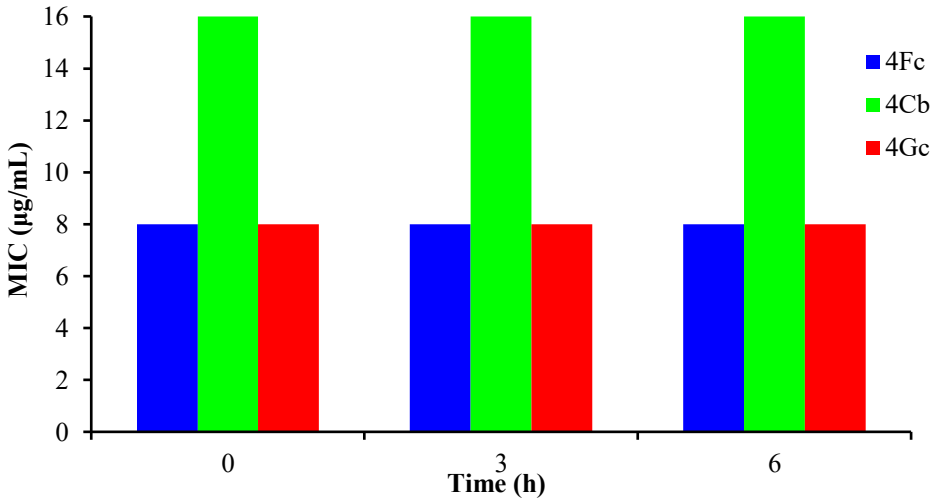

Figure 10. MICs toward *S. aureus* of compounds 4Cb, 4Fc, and 4Gc, after preincubation in 50% plasma solution for 0, 3 and 6 h at 37 °C. Conservative estimates of three trials for each compound. ***Note: in one trial, compounds 4Fc and 4Gc gave both constants MICs of 4 µg/mL.***

Albeit MICs of both compounds **4Fc** and **4Gc** were subjected to a two-fold increase in presence of blood plasma, whereas for **4Cb** no variation was observed, it is very remarkable that all antimicrobial activities remained constant even after 6 hours preincubation (Figure 10)

therefore demonstrating the resistance to proteolytic degradation for physiologically relevant time intervals.

The stability toward chemical degradation in different conditions was also important in view of a potential practical implementation, and some decomposition had already been noted during the initial stage of this work for compounds stored for prolonged periods (>3 months) at -18 °C as free amines. Without re-salification after the chromatographic purification, the main side reaction in diluted conditions was demonstrated to be the transacylation, with transfer of *N*-terminal acyl group to the glycine amine functionality by means of an intramolecular nucleophilic acyl substitution (see synthesis of compound **7** in Experimental). On the other hand, solid free amines intentionally stored at room temperature for more than one month also underwent intermolecular attacks and gave complex mixtures of products. Conversely, solid hydrochlorides demonstrated to be completely stable at -18 °C for at least 6 months. To better evaluate resistance to chemical degradation, samples of compound **4Cb** (R^1 = *n*-C_7H_{15}, R^2 = *n*-C_8H_{17}) as hydrochloride (1 μg mL^{-1}) in PBS (pH = 7.4), pure water, and an aqueous solution mimicking the lowest value for the stomach pH range (1.5), were stored at room temperature for 8 weeks, together with a methanolic solution of the free amine (Figure 11).

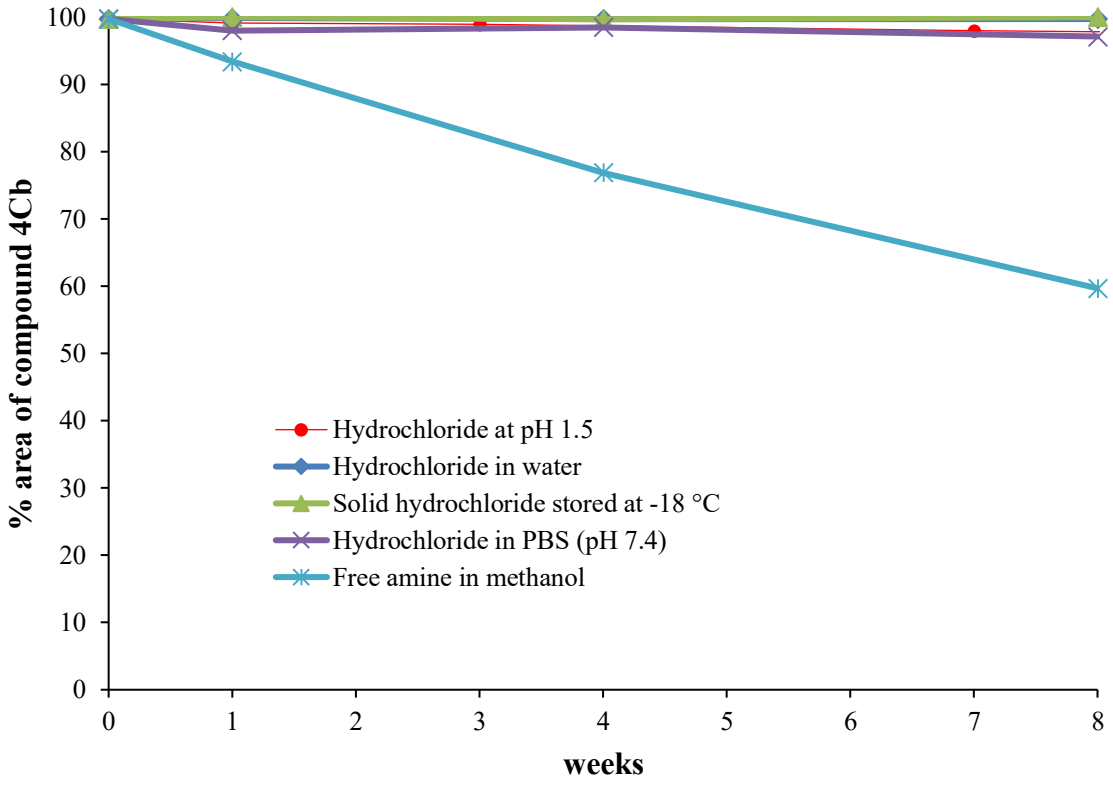

Figure 11. Percent areas of samples of compound 4Cb, stored in different conditions at room temperature, unless otherwise indicated (Hewlett-Packard Lichrosorb RP 18 column, 5 μm, L × I.D. 200 × 4.6 mm, flow rate = 0.5 mL/min; eluent water:2-propanol = 50:50). ***Note: solid hydrochloride demonstrated to be completely stable at -18 °C for at least 6 months.***

Starting with a freshly prepared compound having a 99.7% purity, based on HPLC areas, the hydrochloride in water did not show any decomposition up to the maximum time, whereas only marginal changes were experienced by the samples in PBS and acidic solution (97.1% and 97.2% final purities, respectively). As expected, the methanolic solution of free amine was subjected to a pronounced degradation, with a loss of purity of more than 6% within the first week and about 40% after 8 weeks.

2.2.6 Importance of Hydrazide NH and Non-Disrupted Amphiphilicity

As initially reported, the well-defined amphiphilic character of the preferred conformations and the presence of highly positive hydrazide NH hydrogens should be determining in favoring the destabilizing action on phospholipid bilayers. To verify these hypotheses, the *N*-methylated versions of six selected compounds having a wide range of antimicrobial activities were synthesized (Scheme 2). Starting from **3Ab** (R^1 = OBn, R^2 = *n*-C_8H_{17}) and **3Ac** (R^1 = OBn, R^2 = *n*-$C_{12}H_{25}$), deprotonation with lithium bis(trimethylsilyl)amide followed by reaction with iodomethane directly gave the corresponding *N*-methylated compounds **5Ab** and **5Ac** in very good yields. Compounds **5Bb** (R^1 = CH_3, R^2 = *n*-C_8H_{17}), **5Bc** (R^1 = CH_3, R^2 = *n*-$C_{12}H_{25}$), **5Gb** (R^1 = *t*-Bu, R^2 = *n*-C_8H_{17}), and **5Gc** (R^1 = *t*-Bu, R^2 = *n*-$C_{12}H_{25}$) were then obtained in good overall yields following the same methodology reported above for the corresponding unmethylated compounds, but using a prolonged reaction time when the acylating reagent was pivaloyl chloride. Exploiting the sequence acidic Boc removal/purification of free amine/re-salification, hydrochlorides **6** were eventually obtained in pure form in yields ranging from 75% to 98%.

Scheme 2. Synthetic Scheme for the Preparation of *N*-Methylated *α*-Hydrazido Acid Derivatives[a]

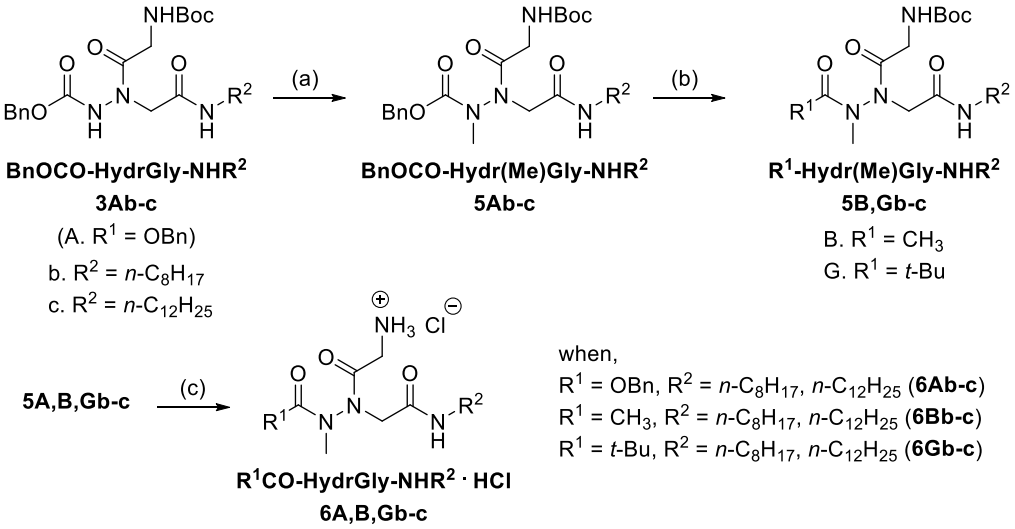

[a] (a) Lithium bis(trimethylsilyl)amide (LHMDS), anh. THF, Ar, 0 °C, 10 min, then methyl iodide, rt, 24 h, **5Ab**: 87% **5Ac**: 90%; (b) HCO_2H, Pd/C, anh. DCM, rt, 1 h, then pyridine, R^1COCl, anh. DCM, rt, 1 h for **5Bb-c**, 20 h for **5Gb-c**, 81-92%; (c) Trifluoroacetic acid (TFA)/DCM 1:3, rt, 20 min, chromatographic purification of free amine, then 3 M HCl in anh. MeOH, 75-98%.

Comparing the antibacterial activities in Table 3 with the MICs of the corresponding unmethylated compounds in Table 1, it is easy to see that in only one case (hydrochlorides **4Ac** and **6Ac** against *E. faecalis*) the *N*-methylated version is the most active, and in few other cases NMe derivatives have the same potency than their parent NH compounds. However, in the vast majority of cases there is a great increase (from two-fold to sixteen-fold) in minimum inhibitory concentrations, and the overall decrease in activity toward Gram-negative bacteria is more pronounced than that against Gram-positives. For all compounds there is also a reduction up to 0.9 minutes in retention times, with respect to their NH counterparts. This decrease in the RP-HPLC measured overall hydrophobicity could be due to the contribution of a low energy conformation with an unconventional C=O···H-C hydrogen bond between the *C*-terminal hydrazide carbonyl and one of the slightly positive *N*-methyl hydrogens, as computationally demonstrated for the model *N*-methylated ammonium cation mAc-Hydr(Me)GlyH^+-NHMe (see Computational investigation). This conformation has a worst directionality of the hydrophobic R^1 and R^2 groups, compared to the hydrazido-turn arrangement, thus probably leading to a poorer interaction with both the C18 hydrocarbon chains of the stationary phase in the HPLC column, and the lipid portions of membrane bilayers.

Table 3. In Vitro Antibacterial Activities of the N-Methylated Compounds

			MIC *vs* drug sensitive bacteria (μg mL^{-1})[a]					RP-HPLC retention times (min)[b]
Compd	**R^1**	**R^2**	***E. faecalis***	***E. faecium***	***S. aureus***	***E. coli***	***P. aeruginosa***	
6Ab	OBn	*n*-C_8H_{17}	128	128	128	128	256	13.8
6Ac	OBn	*n*-$C_{12}H_{25}$	8	8	8	64	512	20.7
6Bb	CH_3	*n*-C_8H_{17}	1024	1024	2048	2048	2048	9.1
6Bc	CH_3	*n*-$C_{12}H_{25}$	32	32	64	128	256	17.1
6Gb	*t*-Bu	*n*-C_8H_{17}	512	512	512	256	512	11.7
6Gc	*t*-Bu	*n*-$C_{12}H_{25}$	16	16	16	64	512	18.9

[a] Conservative estimates of at least three independent trials. [b] Adjusted retention times, computed as the instrumental retention time minus the hold-up time.

Despite the observed reductions in overall lipophilicities, it must be pointed out that retention times for the most active compounds in Table 3 (**6Ac**, **6Bc**, and **6Gc**) are well within the optimal ranges determined for unmethylated hydrochlorides **4**. Thus, overall hydrophobicity still remains the main parameter for describing the antimicrobial activity even in the case of *N*-methylated hydrochlorides, but other concepts must be invoked in order to explain the deleterious effect of such an apparently small structural change. To this end, the two most stable hydrazido-turn conformers of unmethylated (mAc-HydrGlyH$^+$-NHMe) and *N*-methylated (mAc-Hydr(Me)GlyH$^+$-NHMe) model ammonium cations, having two methyls as R^1 and R^2 groups, were analyzed comparing the electrostatic potential surfaces (Figure 12) and the atomic charges of hydrazide NH and NMe functionalities. All the charge calculations schemes confirmed that, despite the electronwithdrawing hydrazide nitrogen, the three hydrogens of the NMe group in the methylated species only have very small positive charges, therefore being essentially hydrophobic in nature, which was experimentally demonstrated for Boc-protected compounds **5** in deuterochloroform (see proton NMR spectra in Figure 53-Figure 58). On the contrary, for the hydrazide NH of unmethylated model compound, high positive charges were invariably obtained, coherently with the initially reported experimental and theoretical findings on compound **4Cb** (R^1 = *n*-C_7H_{15}, R^2 = *n*-C_8H_{17}). In addition, even the possible orbital contribution of methyl hydrogens to H-bonding must be very reduced, as it is easy to deduce comparing the NBO and AIM analyses on the conformation of *N*-methylated mAc-Hydr(Me)GlyH$^+$-NHMe model cation with an intramolecular unconventional C=O···H-C hydrogen bond (Table 9 and Figures 20-22 in Computational investigation), with the one on the hydrazido-turn conformation of unmethylated mAc-HydrGlyH$^+$-NHMe cation (Tables 5 and 6

in Computational investigation). The partial disruption of amphiphilicity in *N*-methylated compounds, due to the substantially lipophilic character of the methyl group on the N^{α} atom, as well as the difference between the atomic charges of NH and NMe groups, are both visually evident from the electrostatic potential surfaces (Figure 12). Even if it is the smallest alkyl group, the methyl on hydrazide nitrogen behaves like a "hydrophobic bulge" in the otherwise polar and charged rear portion, which very likely negatively affects the interaction with phospholipid heads and water molecules during the destabilizing and damaging action on membrane bilayers.

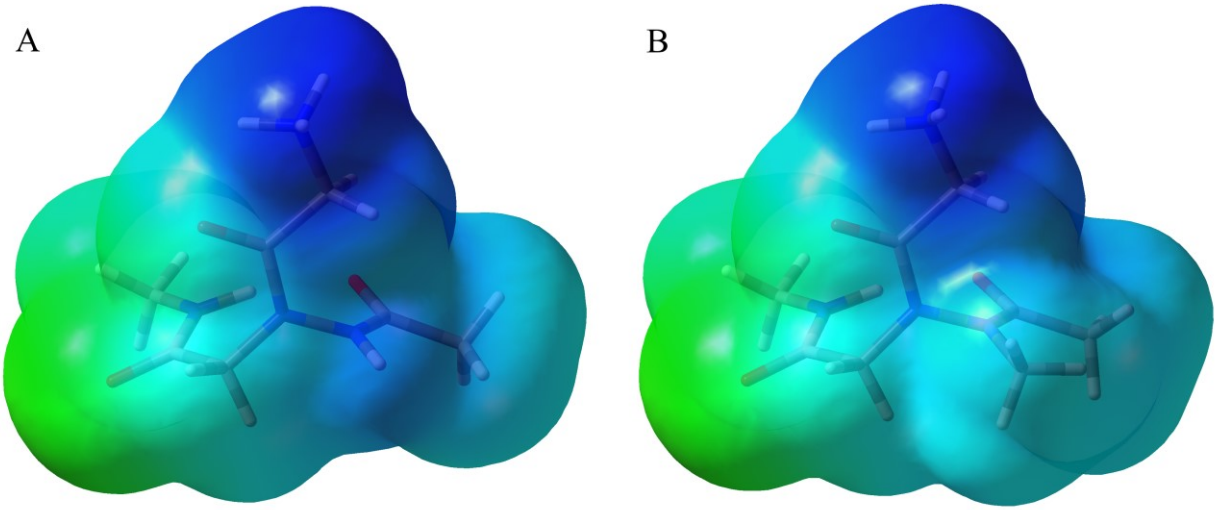

Figure 12. Rear view of electrostatic potential surfaces for the most stable structures of (A) model ammonium cation mAc-HydrGlyH^{+}-NHMe and (B) *N*-methylated model ammonium cation mAc-Hydr(Me)GlyH^{+}-NHMe.

These findings about the decrease of activity induced by a partly disrupted amphiphilic topology are similar and complementary to the results obtained for tetracationic synthetic mimics of antimicrobial peptides with a triaryl backbone and an additional pendant lipophilic group.[42] In both cases, amphiphilicity seems to have a greater importance for the activity against Gram-negative bacteria. In the present case amphiphilicity is ruined by addition of a small lipophilic group in the hydrophilic face, with the concomitant loss of a hydrogen bond-donating functionality, whereas in the case of tetracationic triaryl derivatives the negative effect was obtained by insertion of an amide linker in an otherwise completely hydrophobic region. However, for those triaryl derivatives with facially disrupted amphiphilicity, the almost complete loss of activity against Gram-negative bacteria was ascribed to a much less efficient insertion of the negative curvature-inducing hydrophobic portions, caused by the high content

in phosphatidylethanolamine (PE) of Gram-negatives, which is itself a negative-inducing lipid. On the contrary, for the present *α*-hydrazido acids the lipophilic portions are unchanged with respect their unmethylated versions, whereas the *N*-methylation should reduce the overall ability of the polar and charged groups to act as a positive curvature-inducing components. The correct balance between components inducing both positive and negative curvature was demonstrated to be crucial to induce negative curvature in phospholipid bilayers,[90] which in turn is necessary for the formation of pores in bacterial membranes.[91] Thus, complementary reasons could be at the basis of the more pronounced decrease in antibacterial efficacy toward Gram-negative bacteria for tetracationic triaryl derivatives and *α*-hydrazido acids.

2.2.7 Combinations with First-Line Antibiotics

The synergy of antibiotics and *α*-hydrazido acids against both sensitive and multidrug-resistant strain was evaluated by the checkerboard method, calculating the fractional inhibitory concentrations (FICs) as the MIC of drug A or B in combination divide by the MIC of drug A or B alone, and then the ΣFIC indices, as the sum of FICs. The values of ΣFIC were interpreted as follows: ≤0.5, synergy; >0.5 and <4, indifference; and ≥4, antagonism.[92]

Eight among the most active hydrochlorides were first tested in combination with tetracycline against two representative susceptible strains, namely the Gram-positive *S. aureus* ATCC 29213 and the Gram-negative *E. coli* ATCC 25922, whose MICs for tetracycline alone were determined to be 0.125 and 0.5 μg mL^{-1}, respectively (Table 4). Tetracycline was chosen because of its mechanism of action, which should be at a first glance independent from the membrane activity of *α*-hydrazido acids. The binding of tetracycline to 16S rRNA in the small ribosomal 30S subunit of microbial ribosomes prevents the attachment of aminoacyl-tRNA on the ribosome, therefore inhibiting the initiation of translation. Recent studies have shown that tetracyclines may also bind to 23S rRNA in the large ribosomal 50S subunit.[93]

To our delight, three compounds with a R^2 *C*-terminal dodecyl chain and diverse *N*-terminal groups (R^1 = Me for **4Bc**, Ph for **4Fc**, and *t*-Bu for **4Gc**) furnished a synergistic effect toward *S. aureus*, whereas six hydrochlorides exhibited synergy against *E. coli*. Moreover, the ΣFIC indices for a given pair tetracycline/amphiphilic compound for *E. coli* are always better than or equal to the corresponding value for *S. aureus*, the only exception being compound **4Gc** (R^1 = *t*-Bu, R^2 = *n*-$C_{12}H_{25}$), thus highlighting a globally higher sensitivity of *E. coli* to those combinations. The two compounds whose ΣFICs are greater than 0.5 for *E. coli* still have values very close to the accepted limit of synergy, and this also applies to two cases for *S. aureus*,

whereas only for compound **4Da** (R^1 = *n*-$C_{11}H_{23}$, R^1 = *n*-C_3H_7) toward the Gram-positive bacterium the combination with tetracycline led to an almost perfect additivity (Table 4). Even if at the moment other actions of *α*-hydrazido acids on intracellular targets cannot be completely excluded, these somewhat unexpected results for combinations of molecules acting on completely different bacterial targets can be explained by invoking a substantial increase in cytoplasmic concentrations of tetracycline. This effect should be based on the fact that tetracycline is a hydrophilic antibiotic that uses both a porin-mediated pathway and a direct diffusion through lipid bilayers. As demonstrated for *E. coli*, this influx through the outer membrane lipids is much slower when tetracycline is in the protonated form at a pH under its pKa (7.7), so reducing the overall uptake.[94] Then, at the experimental pH of 7.4, the presence of otherwise subtoxic concentrations of amphiphilic and permeabilizing compounds should increase the influx of tetracycline and ultimately its concentration inside the bacterial cell. In addition, while the outer membrane of Gram-negatives is an effective and selective barrier for many antibiotics, the more permeable cell wall in Gram-positive bacteria is not as efficient in reducing uptake. Therefore, the generally less pronounced synergism observed for combinations *α*-hydrazido acids/tetracycline against *S. aureus* with respect to *E. coli* (Table 4), could easily be explained on the basis of a reduced need for membrane permeabilization by amphiphilic compounds in the former case. In view of a potential practical implementation, another remarkable finding about synergisms is that all the MICs of *α*-hydrazido acids in combinations with tetracycline (Table 4) are much lower than the values in Table 1 for *α*-hydrazido acids alone. Due to the fact that interpolated percent hemolysis at concentrations equal to their MICs were already demonstrated to be very reduced for the best performing compounds in the absence of tetracycline (Table 2), this synergy-based substantial reduction in the amounts of amphiphilic compounds needed to inhibit bacterial growth would lead to substantially null hemolysis. Much higher corresponding therapeutic indices can then be computed for *α*-hydrazido acids in combination with tetracycline. As an example, TIs for compound **4Fc** (R^1 = Ph, R^2 = *n*-$C_{12}H_{25}$) toward the same sensitive strains of *S. aureus* and *E. coli* changed from 49 (Table 1) to 195 in the present case, whereas for **4Gc** (R^1 = *t*-Bu, R^2 = *n*-$C_{12}H_{25}$) the previous TIs for the compound alone were 99 and 49 for *S. aureus* and *E. coli*, respectively (Table 1), and raised to 394 and 197 for the combination with tetracycline.

Table 4. Lowest ΣFIC Indices for Binary Combinations of Selected α-Hydrazido Acids and First-Line Antibiotics Toward Drug Sensitive and Multi-Drug Resistant Strains

			ΣFIC *vs* drug sensitive bacteria ([H]/[T]),[a] for combinations with tetracycline			
Compd	**R^1**	**R^2**	***S. aureus* ATCC 29213[b]**		***E. coli* ATCC 25922[b]**	
4Ab	OBn	*n*-C_8H_{17}	0.53 (2/0.0625)		0.53 (1/0.25)	
4Ac	OBn	*n*-$C_{12}H_{25}$	0.75 (2/0.0625)		0.25 (4/0.0625)	
4Bc	CH_3	*n*-$C_{12}H_{25}$	0.38 (8/0.0313)		0.38 (8/0.125)	
4Cb	*n*-C_7H_{15}	*n*-C_8H_{17}	0.75 (4/0.0625)		0.28 (1/0.0156)	
4Da	*n*-$C_{11}H_{23}$	*n*-C_3H_7	1.02 (1/0.125)		0.63 (8/0.25)	
4Fc	Ph	*n*-$C_{12}H_{25}$	0.50 (1/0.0313)		0.38 (1/0.0625)	
4Gc	*t*-Bu	*n*-$C_{12}H_{25}$	0.38 (1/0.0156)		0.50 (2/0.125)	
4Hb	1-Naphthyl	*n*-C_8H_{17}	0.56 (2/0.0625)		0.50 (4/0.125)	
			ΣFIC *vs* multidrug-resistant bacteria ([H]/[X]),[a] for combinations with the indicated antibiotics			
			LR-MRSA[c]		**GR-CREc[d]**	
			Methicillin[e]	**Linezolid**	**Colistin**	**Gentamicin**
4Fc	Ph	*n*-$C_{12}H_{25}$	0.5<ΣFIC≤0.53 (2/64)	1.03 (0.125/16)	0.31 (1/0.5)	1.25 (1/128)
4Gc	*t*-Bu	*n*-$C_{12}H_{25}$	0.5<ΣFIC≤1.0 (2/1024)	1.03 (0.125/16)	0.28 (2/0.25)	1.50 (4/128)

[a] [H] indicates the concentration of *α*-hydrazido acid in μg mL^{-1}, whereas [T] indicates the concentration of tetracycline in μg mL^{-1}. For multidrug-resistant bacteria, [X] are the concentrations of the indicated antibiotics in μg mL^{-1}. [b] MICs of tetracycline: 0.125 μg mL^{-1} for *S. aureus* ATCC 29213, 0.5 μg mL^{-1} for *E. coli* ATCC 25922. [c] Linezolid- and methicillin-resistant *S. aureus* AOUC-0915. MICs: 16 μg mL^{-1} for linezolid, >1024 μg mL^{-1} for methicillin. [d] Gentamicin- and colistin-resistant *E. coli* 288328. MICs: 128 μg mL^{-1} for gentamicin, 8 μg mL^{-1} for colistin. [e] The exact MIC for methicillin could not be obtained, thus the upper and lower limits in reported ranges were calculated using the minimum possible value (2048 μg mL^{-1}) and an infinite value, respectively, for the actual methicillin MIC.

In the study on combinations of the two most active amphiphilic *α*-hydrazido acids, **4Fc** (R^1 = Ph, R^2 = *n*-$C_{12}H_{25}$) and **4Gc** (R^1 = *t*-Bu, R^2 = *n*-$C_{12}H_{25}$), and first-line antibiotics against multidrug-resistant bacteria, two already widely characterized isolates were used. The linezolid- and methicillin-resistant *Staphylococcus aureus* AOUC-0915 (LR-MRSA) carries both the *mecA* gene, responsible to methicillin resistance, and the *cfr* gene, responsible to linezolid resistance.[95] The gentamicin- and colistin-resistant *Escherichia coli* 288328 (GR-CREc) possesses the *mcr-1* gene, responsible for colistin resistance,[96] and the *aac(3)-IIa* gene, responsible for gentamicin resistance.[97] Susceptibility tests indicated that LR-MRSA had MICs to methicillin and linezolid of >1024 μg mL^{-1} and 16 μg mL^{-1}, respectively, whereas for GR-CREc the MICs to gentamicin and colistin were of 128 μg mL^{-1} and 8 μg mL^{-1}, respectively (Table 4). Furthermore, LR-MRSA had MICs for compounds **4Fc** and **4Gc** corresponding to 4 μg mL^{-1}, while GR-CREc had a MIC for compound **4Fc** of 4 μg mL^{-1} and 8 μg mL^{-1} for compound **4Gc**. Thus, as reported above, the good activity of **4Fc** and **4Gc** against the two MDR clinical isolates is the same observed toward the corresponding sensitive strains *E. coli*

ATCC 25922 and *S. aureus* ATCC 29213 (Table 1), and suggests that these new amphiphilic organic compounds might also be active against other MDR strains with the same compositions of lipid bilayers.

The checkerboard assays for multidrug-resistant bacteria exhibited synergism only against GR-CREc strain, when colistin was combined with either **4Fc** (R^1 = Ph, R^2 = *n*-$C_{12}H_{25}$) or **4Gc** (R^1 = *t*-Bu, R^2 = *n*-$C_{12}H_{25}$). All the other combinations were indifferent, even if for **4Fc** against LR-MRSA the range of possible values of ΣFIC for combinations with methicillin is certainly very close to 0.5. No antagonism was observed (Table 4). In order to make deductions, it is mandatory to analyze case by case both the mechanisms of action of the different antibiotics and the modifications in MDR strains with respect to their sensitive counterparts.

Colistin belongs to the family of polymyxins, which are cationic polypeptides with broad-spectrum activity against Gram-negative bacteria, especially several species of the family *Enterobacteriaceae*. The target of colistin is the outer membrane of Gram-negative bacteria, because of an electrostatic interaction occurring between the many positively charged ammonium functions of diaminobutyric acid residues of colistin and the phosphate groups of the negatively charged lipid A of lipopolysaccharide (LPS), displacing divalent cations. The LPS is therefore destabilized, consequently increasing the permeability of the bacterial membrane, leading to leakage of the cytoplasmic content and ultimately causing cell death.[98] The MCR-1 protein, encoded by *mcr-1* gene in colistin-resistant strains, is a member of the phosphoethanolamine transferase enzyme family, and its acquisition lead to addition of phosphoethanolamine to lipid A. Consequently, the binding between the more cationic LPS and colistin is less effective,[83] as witnessed by the change in MIC of colistin alone from the accepted range for sensitive *E. coli* ATCC 25922 strain (0.5-2 μg mL^{-1})[72] to 8 μg mL^{-1} for GR-CREc. In our study, checkerboard experiments showed that compounds **4Fc** (R^1 = Ph, R^2 = *n*-$C_{12}H_{25}$) and **4Gc** (R^1 = *t*-Bu, R^2 = *n*-$C_{12}H_{25}$) have a powerful synergistic interaction with colistin against GR-CREc, despite the presence of the *mcr-1* gene, leading to MICs of colistin in combination of 0.25-0.5 μg mL^{-1} (Table 4). It is quite unlikely that amphiphilic *α*-hydrazido acids increase the binding of colistin to lipid A, thus recovering the original ability of colistin itself of destabilizing the outer membrane. On the other hand, the residual outer membrane destabilizing action of colistin, together with the concomitant destabilization of underlying phospholipid bilayers elicited by amphiphilic *α*-hydrazido acids, still can promote a combined and synergistic potent disrupting action on membranes, leading to lysis and cell death. Similar synergisms have already been reported for colistin/AMPs combinations.[99,100]

Methicillin, as the other *β*-lactams, disrupts cell-wall synthesis by inhibiting transpeptidase activity of penicillin-binding proteins (PBPs) that cross-link the nascent peptidoglycan. The mechanism of methicillin resistance relies on acquisition of the chromosomal cassette mec (*SCCmec*) containing *mecA*, which encodes PBP2a, a transpeptidase with extremely low affinity for all *β*-lactams, except for last-generation cephalosporins.[80] In fact, MIC of methicillin alone dramatically raises from 0.5-2 μg mL^{-1} for *S. aureus* ATCC 29213[72] to >1024 μg mL^{-1} for LR-MRSA. Even if the computed intervals for the possible actual values of ΣFICs are out of the commonly accepted range for synergistic effects (Table 4), the ≥32-fold increase in methicillin activity (MIC = 64 μg mL^{-1}) in combination with 2 μg mL^{-1} of hydrochloride **4Fc** (R^1 = Ph, R^2 = *n*-$C_{12}H_{25}$), leading to $0.5<\Sigma FIC\leq 0.53$, must be emphasized. This remarkable increment in methicillin activity when in combination with **4Fc**, and to a much more reduced extent with **4Gc** (R^1 = *t*-Bu, R^2 = *n*-$C_{12}H_{25}$), is not safely explainable at the moment. Of course, since the PBP2a protein is stably localized in the cell membrane, an increase in cytoplasmic methicillin concentration cannot be invoked as in the previous case of tetracycline, but possible reasons based on the action of *α*-hydrazido acids on membrane phospholipids and/or directly on PBP2a can be putatively adduced. The deep investigation on the resistance of PBP2a to most *β*-lactams, but not to the recent 5th generation cephalosporins ceftaroline and ceftobiprole, led to the discovery that older *β*-lactams does not acylate serine S403 in the active site of PBP2a, which is responsible for transpeptidase activity. Both the dissociation constants and the rates of acylation are highly unfavorable, and X-ray structures showed that active site is completely inaccessible to older *β*-lactams, but ceftaroline and ceftobiprole can access it by allosteric regulation. The presence of ammonium functionalities in ceftaroline and ceftobiprole is essential to bind to allosteric site, and the consequent cascade of conformational changes, involving a complex network of salt bridges, enables the active site opening and ultimately its acylation by a second molecule of *β*-lactam.[101] Possible conformational variations of PBP2a induced by environmental changes of lipid disposition around the protein, associated to the action of amphiphilic *α*-hydrazido acids on bilayers, could be part of the observed increase in methicillin activity. However, if they were the only cause, a comparable effect should be detected for **4Fc** and **4Gc**, which had always previously demonstrated very similar actions on bacterial and erythrocyte membranes, as well as almost identical interactions with the apolar stationary phase of RP-HPLC column. In our opinion, the striking difference between the capabilities of the two *α*-hydrazido acid hydrochlorides to promote a partial recovery in methicillin activity might be explained with a mechanism involving a more specific interaction with either the allosteric site or the salt bridges network of PBP2a. In this case the glycine

ammonium functionality, which is identical in **4Fc** (R^1 = Ph, R^2 = *n*-$C_{12}H_{25}$) and **4Gc** (R^1 = *t*-Bu, R^2 = *n*-$C_{12}H_{25}$), cannot account for the completely different outcomes. Likely some π-stacking or cation-π interaction of the aromatic *N*-terminal group in **4Fc** (R^1 = Ph) with one or more residues of PBP2a, which would be stronger than the simple van der Waals interactions of the aliphatic and almost spherical *tert*-butyl fragment in **4Gc**, could be at the basis of the experimental results.

The indifferences showed by combinations of *α*-hydrazido acids with linezolid against LR-MRSA, and with gentamicin against GR-CREc (Table 4), can be explained in both cases with the lack of an increased accumulation of first-line antibiotic when in combination with our amphiphilic compounds, even if the supposed mechanistic reasons are different. Linezolid, the first member of oxazolidinones, was introduced into clinical use for treatment of complicated infections by MDR Gram-positive pathogens. It inhibits protein synthesis by binding to the peptidyl transferase centre of the bacterial ribosome. When present, the gene *cfr* encodes an rRNA methyltransferase that catalyzes post-transcriptional methylation to the C8 position of nucleotide A2503 in 23S rRNA. The result of this modification at the ribosomal binding site is co-resistance to oxazolidinones, phenicols, lincosamides, pleuromutilins and streptogramin A, due to a decreased binding affinity.[81] In particular, MIC for linezolid raises from 1-4 μg mL^{-1} for *S. aureus* ATCC 29213[72] to 16 μg mL^{-1} for *S. aureus* AOUC-0915 (LR-MRSA), then the MDR strain maintains some susceptibility, contrarily to the previous case of methicillin. Aminoglycosides as gentamicin play an important role in treating serious Gram-negative infections, and are often used as part of combination therapy with cell wall biosynthesis inhibition agents, such as *β*-lactams. *aac(3)-IIa* gene, one of the most common resistance genes found in Gram-negative isolates, causes the covalent modification of aminoglycoside molecules, resulting in poor binding to the ribosome target and thus leading to resistance to this antibiotics.[97] For gentamicin, the resistant *E. coli* 288328 (GR-CREc) strain has only a very reduced sensitivity to the antibiotic (MIC = 128 μg mL^{-1}), compared to the susceptible strain *E. coli* ATCC 25922 (MIC = 0.25-1 μg mL^{-1}).[72] The best ΣFIC indices and their related single-drug concentrations reported in Table 4 for combinations of *α*-hydrazido acids with linezolid and gentamicin indicate that, in those cases, the bacteriostatic activity is mainly due to the conventional antibiotics, whose concentrations necessary to inhibit bacterial growth in combination are the same as for the antibiotics alone. However, it must also be pointed out that slightly greater ΣFICs, not reported in Table 4, were obtained for concentrations of compounds **4Fc** and **4Gc** equal to their MICs for the *α*-hydrazido acids alone, together with subtoxic concentrations of linezolid or gentamicin. It must be concluded that, differently from the

previously reported synergies for combinations *α*-hydrazido acids/tetracycline against susceptible strains of *S. aureus* and *E. coli*, for linezolid and gentamicin toward the corresponding resistant strains the presence of amphiphilic permeabilizing compounds acting on lipid membranes is not able to substantially increase their cytoplasmic active concentrations. In fact, to the best of our knowledge, a decreased linezolid uptake has never been reported for any *S. aureus* strain, as it occurred instead for an *in vitro*-selected linezolid-resistant *Staphylococcus epidermidis* mutant.[82] Therefore a considerable increase in linezolid active cytoplasmic concentration, when used with *α*-hydrazido acids, was not expected, in agreement with the experimental findings that strongly point toward completely independent mechanisms of action. In the case of gentamicin, it was demonstrated that this hydrophilic molecule can hardly pass through porin channels due to its molecular size, as previously supposed, but its polycationic structure is necessary for the uptake by many different strains of *E. coli*. In fact, the uptake follows a self-promoted pathway involving disruption, by gentamicin itself, of Mg^{2+} bridges between LPS molecules in the outer membrane.[102] In addition, mutations in LPS phosphates of *E. coli* were shown to strongly decrease this self-promoted uptake and cause an increase in MIC to gentamicin.[103] Thus, the observed indifference for *α*-hydrazido acids/gentamicin combinations against GR-CREc strain, which has a modified LPS, is in agreement with the expected inability of monocationic *α*-hydrazido acids to favorably interact with the modified LPS and consequently increase the influx of gentamicin through the outer membrane.

2.3 Conclusions

Starting from the idea that an *α*-hydrazido acid skeleton with suitable derivatizations has an inherent propensity to the formation of the hydrazido-turn motif, simple mono-charged amphiphilic derivatives were first computationally analyzed and then easily synthesized. A short, cheap and high-yielding synthesis furnished a number of these novel mimics of antimicrobial peptides, which were submitted to biological assays. The most active amphiphilic *α*-hydrazido acids exhibited a broad-spectrum *in vitro* activity against a variety of Gram-positive and Gram-negative bacteria, which did not change when multidrug resistant strains were employed. Structure-activity relationships demonstrated that the overall lipophilicity is the main parameter governing the bacteriostatic activity and the selectivity with respect hemolysis, whereas the change of a hydrazide NH in favor of a methyl group caused both the loss of a good hydrogen bond donor and the partial disruption of amphiphilicity, thus reducing the antibacterial activity. Either synergism or indifference was observed for combinations with

first-line antibiotics toward both sensitive and multidrug-resistant strains, which were analyzed case by case on the basis of the bacterial target, the possible mechanistic interdependence, and the mechanism of resistance to the conventional antibiotic. Considering that the results reported here were obtained without performing any optimization in the search for the best bioactivity profile, we believe that these chemically and proteolitically stable *α*-hydrazido acids are promising lead compounds for the development of a new class of wide-spectrum antibiotics. Further studies are ongoing to precisely define the mechanism of action and evaluate the effect of di- and tricationic side chains, as well as different *N*- and *C*-terminal substituents, in order to find safer and more active compounds.

2.4 Experimental

2.4.1 General methods and materials for the biological evaluations of products

General Important Notes.

All the hydrochlorides of *α*-hydrazido acids are surfactants, and their tendency to form foams very negatively affected the first preliminary evaluations of MICs and HC_{50}s. This was especially true for more concentrated solutions, and was ascertained to be related to the speed of withdrawal and, to a lesser extent, of the addition, causing evident dispersion and unreliability of results. These observations also applied to withdrawal and addition of 0.2 vol % Triton X-100. As an example, when both the withdrawal and the addition of nominal values of 150 μL of 0.2 vol % Triton X-100 solution with a Gilson P200 pipette were conducted employing about 0.5-1 seconds, the weights of solutions actually transferred into the vials for five trials were much less than expected and not constant (126.9±12.5 mg, mean±standard error), as determined with an analytical balance. On the contrary, employing about three seconds for both the withdrawal and the addition steps, the reliability and reproducibility of weights greatly improved (150.3±2.3 mg). To make much more reliable and reproducible the results, a time of at least three seconds was always used in definitive assays for all the withdrawal and addition steps. For the same reasons, the clear and homogeneous stock solutions were not vortexed immediately before the experiments. Another variable that is usually underestimated, that is the rigorous mixing in each well during the serial dilutions, was ascertained to be a secondary factor of error during the preliminary trials.

2.4.2 General Procedure For The Evaluation Of Minimum Inhibitory Concentrations.

All tested compounds were dissolved in sterile water at the maximum possible concentration. Bacterial strains were grown for 6 hours in Brain Heart Infusion (BHI) broth and diluted in Mueller-Hinton II (MHII) broth (Oxoid spa, Milan, Italy) to give a final concentration of 1×10^6 cfu/mL. Serial dilutions of the tested compounds in MHII broth were prepared in 96-well microtiter plate (Cellstar, Greiner bio-one, Kremsmünster, Austria) (50 µL per well) and 50 µL of diluted bacterial suspension were added into each well. The wells with bacteria alone were used as positive growth control wells. Tetracycline was used as internal control, starting from a 1024 µg/mL stock solution made from a freshly prepared 10000 µg/mL solution. The plate was aerobically incubated at 37 °C for 24 hours. All tests were performed in triplicate. The MICs were defined as the lowest concentrations of compounds inhibiting visible growth after 24 hours of incubation.

2.4.3 General Procedure For The Evaluation Of Hemolytic Concentrations.

Hemolysis experiments were performed with a slight modification of a reported procedure.[28] 4 mL of freshly drawn heparinized human blood were diluted with 25 mL of phosphate buffered saline (PBS) pH 7.4, centrifuged at 1000 g for 10 minutes and resuspended in 25 mL of PBS for three times. After washing, the pellet was resuspended in PBS to ~20 vol % and, in a 96-well microtiter plates, 100 µL of erythrocyte suspension were added to 100 µL of different concentrations of the tested compounds (1:2 serial dilutions in PBS) and incubated for 1 hour at 37 °C. The negative and positive controls were 100 µL of PBS and 100 µL of 0.2 vol % Triton X-100, respectively. After incubation, each well was supplemented with 150 µL of PBS and the plate centrifuged at 1.200 g for 15 minutes. The supernatant was diluted 1:60 (5 µl of supernatant in 295 µl of PBS), transferred in a new plate, and its absorbance at a wavelength of 350 nm (A_{350}) was measured using the Synergy HT microplate reader spectrophotometer (BioTek, Winooski, VT, USA). The percent hemolysis was determined as follows: $[(A - A_0)/(A_{\text{total}} - A_0)] \times 100$, where A is the absorbance of the test well, A_0 is the absorbance of the negative control, and A_{total} is the absorbance of the positive control. Evaluation of HC_{50} and b slope were carried out by nonlinear regression of the four-parameter logistic model of Hill,[78] in all cases were 100% hemolysis was reached in the experiments conducted using stock solutions of the tested compounds at the maximum possible concentration. For compounds for which the 100% hemolysis could not be obtained, the three-parameter logistic model of Hill with the constrain of 100% hemolysis as the final value was used. The errors of the experiments were always less than 10%. The mean values of three replicates were reported for HC_{50} and b slope.

2.4.4 General Procedure For Checkerboard Assays.

Checkerboard assays were performed with a slight modification of a reported procedure.[31] Bacterial inoculations and stock solutions of *α*-hydrazido acids were carried out as previously described in the General Procedure For The Evaluation Of Minimum Inhibitory Concentrations. For *α*-hydrazido acids having MICs for the compound alone of 32 or 64 μg/mL, stock solutions with a concentration of 256 μg/mL were used, whereas in all the other cases the concentration of the stock solution was 64 μg/mL. Stock solutions for tetracycline, linezolid, colistin, and gentamicin, had 32- or 64-fold concentrations with respect to the MIC of antibiotic alone. Stock solution for methicillin had a concentration of 2048 μg/mL. The minimum inhibitory concentrations for tetracycline, methicillin, linezolid, colistin, gentamicin (Sigma-Aldrich, St Louis, MO, USA), and for *α*-hydrazido acids alone were determined by the broth microdilution procedure previously reported. Briefly, each well of the microtiter plate was inoculated with 50 μL of MHII broth. Then, 50 μL of stock solution in water of the suitable *α*-hydrazido acid were added to each well of the first row and twofold serially diluted in the vertical direction. Subsequently, 50 μL of stock solution in MHII broth of the suitable first-line antibiotic were added to each well of the last column and twofold serially diluted 1:2 leftward in the horizontal direction. Finally, 50 μL of bacterial suspension were added to every well of the plate, then the plates were incubated at 37 °C for 24 hours. Each experiment was performed in triplicate. The fractional inhibitory concentrations (FICs) were calculated as the MIC of a drug in combination divided by the MIC of the same drug alone, and then the ΣFIC indices as the sum of FICs. The values of ΣFIC were interpreted as follows: ≤0.5, synergy; >0.5 and <4, indifference; ≥4, antagonism.

2.4.5 General Procedure For The Evaluation Of Antibacterial Activity In Plasma.

S. aureus ATCC 29213 was grown for 6 h in brain heart infusion (BHI) broth and diluted in Mueller Hinton II broth (Oxoid spa, Milan, Italy) to give a final concentration of 1×10^6 cfu/mL. Fresh human blood cells were centrifuged at 3000 rpm for 5 minutes to separate the plasma from the red blood cells. Three aliquots for each tested compound were dissolved in water at a concentration of 512 μg/mL and diluted twofold in the plasma to reach the final concentration of 256 μg/mL. The aliquots were preincubated at 37 °C for 0, 3, and 6 hours, and then used to perform MIC assays according to the broth microdilution method in 96-well microtiter plates. The stability of the compounds into the plasma was considered positive in absence of any change of their MIC values among the trials at different preincubation times. The results are reported in Figure 10.

*2.4.6 General Procedure For The Evaluation Of Chemical Stability Of Compound **4Cb***

Four 1 mg/mL solutions of compound **4Cb** (free amine in methanol, hydrochloride dissolved in water, PBS, and water at pH 1.5 prepared using phosphoric acid) were stored at room temperature up to 8 weeks (temperature ranging from 20 to 25 °C). Suitable aliquots were taken and analyzed at the times reported in Figure 11. The fifth sample, that is the solid hydrochloride stored at -18 °C, was analyzed taking a small amount of compound (about 1 mg) and dissolving it in methanol. Percent areas of different samples of compound **4Cb** as a function of time were taken on a reverse-phase Hewlett-Packard Lichrosorb RP 18 column, 5 μm, L × I.D. 200 × 4.6 mm, with a flow rate 0.5 mL/min and water:2-propanol = 50:50, both containing 0.1% of trifluoroacetic acid, as the eluent. Elution was continued up to 1 hour. Areas of spikes at the hold-up time were not considered for integration.

2.4.7 General material and method for the synthetic part

Melting points were obtained on an Electrothermal apparatus IA 9000 and are uncorrected. Melting points for hydrochlorides were not taken, due to decomposition at about 100 °C for all compounds, which was caused by loss of hydrogen chloride. ^{1}H and ^{13}C NMR spectra were determined at 25 °C on a Varian MR400 spectrometer, at 400 and 100 MHz for ^{1}H and ^{13}C, respectively, in $CDCl_3$ unless otherwise reported. Chemical shifts are reported in ppm relative to residual solvent signals (δ = 7.26 and 77.16 ppm for ^{1}H and ^{13}C NMR, respectively), and coupling constants (*J*) are given in Hz. Identity of hydrochlorides **4** and **6** was confirmed by elemental analyses performed in triplicates with a Thermo Scientific FLASH 2000 Elemental Analyzer. RP-HPLC analyses were performed with a Hewlett-Packard 1100 chromatograph equipped with a diode-array detector (λ = 210 nm) and a Lichrosorb RP18 5 μm column, L × I.D. 200 × 4.6 mm, using a constant flow rate of 0.5 mL/min. Water:2-propanol mixtures were used as eluents, both solvents containing 0.1% v/v of TFA. The hydrochlorides were dissolved in a water:2-propanol 70:30 mixture (0.5-1 mg/mL) and submitted to a gradient elution from water:2-propanol 70:30 to water:2-propanol 10:90 in 40 min (gradient +1.5% 2-propanol/min), followed by additional 20 min with water:2-propanol 10:90. After return to the initial eluent composition, the column was re-conditioned for at least 20 min before the following analysis. Adjusted retention times, t'_R, are reported as the instrumental retention time, t_R, minus the hold-up time, t_M, which was determined to be 4.7 min for a flow rate of 0.5 mL/min. With the exception of compound **4Ba**, which was used as crude product with 95% purity, all the freshly synthesized hydrochlorides **4** and **6** were always determined to have >95% purity by integration of HPLC areas, excluding spikes at the hold-up time. LCMS electrospray ionization mass spectra were obtained with a Finnigan Navigator LC/MS single-quadrupole mass spectrometer,

cone voltage 25 V and capillary voltage 3.5 kV, injecting samples dissolved in methanol. Column chromatography was performed using Kieselgel 60 Merck (230-400 mesh ASTM). All the starting compounds were reagent grade and used without further purification. Ethyl acetate and cyclohexane used for chromatographic purifications were distilled at reduced pressure, using a rotary evaporator. Dichloromethane, methanol and dimethylformamide were distilled from calcium hydride, sodium, and phosphorus pentoxide, respectively, under an argon atmosphere. TLC analysis was performed with sheets of silica gel Fluka TLC-PET, using exposure to UV light and immersion in aqueous $KMnO_4$, followed by heating and by possible immersion in H_2SO_4 9 M. Retention factors (R_f) are reported, for a given eluent, as the ratio of the distance moved by the solute to that moved by the solvent. In the case of hydrochlorides **4** and **6**, the R_f factors are referred to free amines.

2.4.8 Synthesis and characterizations of the compounds

*Synthesis Of Benzyl 2-(2-methoxy-2-oxoethyl)hydrazine-1-carboxylate, Cbz-Hydr-OMe, (**1**).* To a solution of benzyl carbazate (105 mmol, 17.45 g) and methyl bromoacetate (100 mmol, 9.76 mL) in anhydrous DCM (50 mL) at room temperature under inert atmosphere, DIPEA (105 mmol, 18.34 ml) was added. The reaction was stirred for 48 hours. After evaporation under vacuum, the residue was extracted using a mixture of cyclohexane/ethyl acetate 1:1 (400 mL) as the organic phase and water (100 mL). The organic phase was washed with HCl 1 M (2 × 10 mL) and water (10 mL), then the aqueous phases were sequentially extracted with additional 400 mL of cyclohexane/AcOEt 1:1. The second organic phase was washed with HCl 1 M (2 × 10 mL) and water (10 mL), then the reunited organic phases were dried over anhydrous sodium sulphate. After evaporation under vacuum, the crude product was purified by flash chromatography on silica gel (cyclohexane/AcOEt), obtaining the pure product **1** as a colorless oil in a 96% yield (96 mmol, 22.87 g).

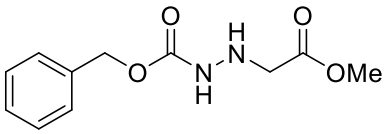

R_f = 0.32 (cyclohexane/AcOEt = 1:1). ^{1}H NMR (400 MHz, $CDCl_3$): δ 3.69 (s, 2H), 3.72 (s, 3H), 5.13 (s, 2H), 6.93 (bs, 1NH), 7.31 (bs, 1NH), 7.34 (s, 5ArH) ppm. ^{13}C NMR (100 MHz, $CDCl_3$): δ 52.2, 52.6, 67.4, 128.4, 128.5, 128.7, 135.9, 156.9, 171.5 ppm. LCMS: *m/z* = 239.1 $[M+H]^+$, 261.1 $[M+Na]^+$.

*Synthesis Of Benzyl 2-((tert-Butoxycarbonyl)glycyl)-2-(2-methoxy-2-oxoethyl)hydrazine-1-carboxylate, Cbz-HydrGly-OMe, (**2**).*

To a solution of compound **1** (45 mmol, 10.72 g) in dry DCM (22.5 mL) under inert atmosphere, Boc-Gly-OH (58.5 mmol, 10.04 g) was added and the reaction mixture was thermostated at -20 °C. EDCI (67.5 mmol, 12.94 g) was added and the mixture was stirred vigorously at -20 °C for 1 hour, then the reaction mixture was diluted with AcOEt (400 mL) and water (50 mL). After separation, the organic phase was sequentially washed with HCl 1 M (3 × 10 mL) and saturated solution of Na_2CO_3 (3 × 10 mL). The aqueous phases were sequentially extracted with AcOEt (250 mL) and the organic phase was washed with HCl 1 M (3 × 5 mL) and water (50 mL). The combined organic phases were dried over anhydrous Na_2SO_4, the solvent was evaporated under reduced pressure and the residue was purified by silica gel chromatography (cyclohexane/AcOEt mixtures as eluents) to give the pure compound **2** as a colorless low-melting wax in 86% yield (38.7 mmol, 15.30 g).

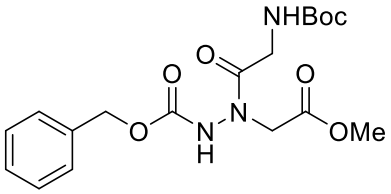

R_f = 0.50 (cyclohexane/AcOEt = 1:1). ^{1}H NMR (400 MHz, $CDCl_3$): δ 1.44 (s, 9H), 3.64 (bs, 1H), 3.73 (s, 3H), 4.09 (bs, 2H), 5.06 (bs, 1H), 5.17 (s, 2H), 5.25 (bs, 1NH), 7.30-7.51 (m, 5ArH+1NH) ppm. ^{13}C NMR (100 MHz, $CDCl_3$): δ 28.4, 42.0, 48.5, 52.6, 68.5, 80.0, 128.5, 128.8, 135.0, 154.8, 155.9, 169.4, 171.9 ppm. LCMS: *m/z* = 396.2 $[M+H]^+$, 418.2 $[M+Na]^+$.

General Procedure For The Synthesis Of C-terminal Derivatives.

Note: the representative procedure is referred to 1 mmol of starting compound.

To a solution of compound **2** (1 mmol) in dry MeOH (2 mL) under inert atmosphere, the suitable amine was added (3 eq. for propylamine and 1.5 eq. for octylamine, dodecylamine and octadecylamine). The reaction was stirred for 7 hours at room temperature for the synthesis of compound **3Aa**, and refluxed for 18, 24 and 36 hours for the syntheses of compounds **3Ab**, **3Ac**, and **3Ad**, respectively. Thus, the volatile species were removed under vacuum and the residue was submitted for three times to the dissolution in few milliliters of anhydrous dichloromethane, followed by in vacuo evaporation. The residue was purified by silica gel chromatography (cyclohexane/AcOEt mixtures as eluents) to give the corresponding pure compound.

Benzyl 2-((*tert*-butoxycarbonyl)glycyl)-2-(2-oxo-2-(propylamino)ethyl)hydrazine-1-carboxylate, Cbz-HydrGly-NHC$_3$H$_7$, (3Aa).

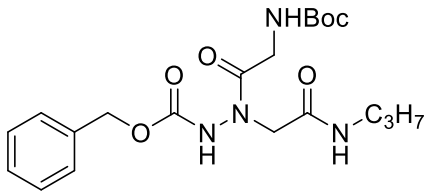

Starting from **2** (2.00 mmol, 791 mg) and following the general procedure, compound **3Aa** was obtained in 94% yield (1.88 mmol, 794 mg) as a white amorphous solid. R_f = 0.55 (cyclohexane/AcOEt 2:8). m.p. = 49-50 °C. ^{1}H NMR (400 MHz, $CDCl_3$): δ 0.89 (t, J = 7.4 Hz, 3H), 1.42 (s, 9H), 1.45-1.54 (m, 2H), 3.14-3.20 (m, 2H), 3.75-4.51 (m, 4H), 5.17 (s, 2H), 5.24 (bs, 1NH), 6.77 (bs, 1NH), 7.32-7.40 (m, 5ArH), 7.97 (bs, 1NH) ppm. ^{13}C NMR (100 MHz, $CDCl_3$): δ 11.4, 22.5, 28.4, 41.4, 41.9, 52.9, 68.4, 80.0, 128.4, 128.7, 135.1, 156.1, 156.2, 167.9, 172.3 ppm. LCMS: *m/z* = 423.2 $[M+H]^+$, 445.2 $[M+Na]^+$.

Benzyl 2-((*tert*-butoxycarbonyl)glycyl)-2-(2-(octylamino)-2-oxoethyl)hydrazine-1-carboxylate, Cbz-HydrGly-NHC$_8$H$_{17}$, (3Ab).

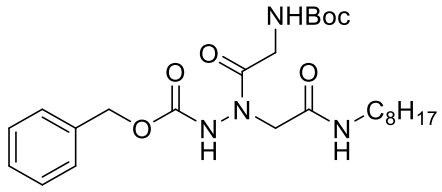

Starting from **2** (5.00 mmol, 1.98 g) and following the general procedure, compound **3Ab** was obtained in 88% yield (4.41 mmol, 2.17 g) as a white waxy solid. R_f = 0.60 (cyclohexane/AcOEt 2:8). m.p. = 74-76 °C. ^{1}H NMR (400 MHz, $CDCl_3$): δ 0.87 (t, J = 7.0 Hz, 3H), 1.26 (bs, 10H), 1.42 (s, 9H), 1.46 (bs, 2H), 3.12-3.26 (m, 2H), 3.75-4.47 (m, 4H), 5.17 (s, 2H), 5.25 (bs, 1NH), 6.77 (bs, 1NH), 7.32-7.38 (m, 5ArH), 8.02 (bs, 1NH) ppm. ^{13}C NMR (100 MHz, $CDCl_3$): δ 14.1, 22.7, 26.9, 28.4, 29.26, 29.29, 31.9, 39.7, 41.88, 41.90, 52.9, 68.4, 79.9, 128.4, 128.68, 128.72, 135.1, 156.0, 156.2, 167.7, 172.2 ppm. LCMS: *m/z* = 493.3 $[M+H]^+$, 515.3 $[M+Na]^+$.

Benzyl 2-((*tert*-butoxycarbonyl)glycyl)-2-(2-(dodecylamino)-2-oxoethyl)hydrazine-1-carboxylate, Cbz-HydrGly-NHC$_{12}$H$_{25}$, (3Ac).

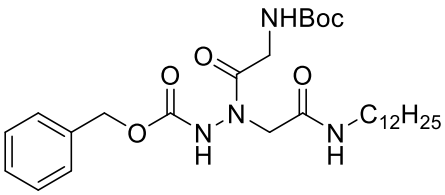

Starting from **2** (5.00 mmol, 1.98 g) and following the general procedure, compound **3Ac** was obtained in 88% yield (4.39 mmol, 2.41 g) as a white amorphous solid. R_f = 0.43 (cyclohexane/AcOEt = 2:8). m.p. = 76-78 °C. ^{1}H NMR (400 MHz, $CDCl_3$): δ 0.87 (t, J = 7.0

Hz, 3H), 1.25 (bs, 18H), 1.42 (s, 9H), 1.45 (bs, 2H), 3.14-3.24 (m, 2H), 3.74-4.46 (m, 4H), 5.17 (s, 2H), 5.25 (bs, 1NH), 6.73 (bs, 1NH), 7.29-7.39 (m, 5ArH), 8.01 (bs, 1NH) ppm. ^{13}C NMR (100 MHz, $CDCl_3$): δ 14.1, 22.8, 27.0, 28.4, 29.3, 29.4, 29.5, 29.67, 29.73, 29.76, 32.0, 39.8, 41.9, 52.8, 68.5, 80.0, 128.4, 128.7, 128.8, 135.1, 156.04, 156.07, 167.7, 172.2 ppm. LCMS: *m/z* = 549.4 $[M+H]^+$, 571.4 $[M+Na]^+$.

Benzyl 2-((*tert*-butoxycarbonyl)glycyl)-2-(2-(octadecylamino)-2-oxoethyl)hydrazine-1-carboxylate, Cbz-HydrGly-NHC$_{18}$H$_{37}$, (3Ad).

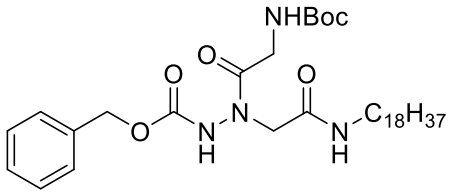

Starting from **2** (5.00 mmol, 1.98 g) and following the general procedure, the compound **3Ad** was obtained in 90% yield (4.50 mmol, 2.85 g) as a white waxy solid. R_f = 0.63 (cyclohexane:AcOEt 2:8). m.p. = 84-86 °C. ^{1}H NMR (400 MHz, $CDCl_3$): δ 0.88 (t, *J* = 7.0 Hz, 3H), 1.25 (bs, 30H), 1.43 (s, 9H), 1.47 (bs, 2H), 3.15-3.25 (m, 2H), 3.74-4.56 (m, 4H), 5.18 (s, 2H), 5.23 (bs, 1NH), 6.61 (bs, 1NH), 7.32-7.40 (m, 5ArH), 7.81 (bs, 1NH) ppm. ^{13}C NMR (100 MHz, $CDCl_3$): δ 14.1, 22.7, 27.0, 28.3, 29.2, 29.36, 29.40, 29.6, 29.70, 29.75, 32.0, 39.7, 41.9, 53.0, 68.3, 79.9, 128.3, 128.6, 128.7, 135.1, 156.1, 156.3, 167.8, 172.2 ppm. LCMS: *m/z* = 655.5 $[M+Na]^+$.

General procedure for the synthesis of the N-terminal derivatives.

Note: representative procedure referred to 1 mmol of starting compound; the actual amounts of starting compounds used in the reactions are reported below.

To a solution of compound **3Aa-d** (1 mmol) dissolved in dry DCM (2 mL) under inert atmosphere at room temperature, Pd/C (100 mg) and formic acid (76 µL, 2 mmol) were sequentially added and the mixture was stirred for 1 hour. The volatile species were removed under vacuum at room temperature, then DCM (20 mL) was added and the reaction mixture was filtered through Celite, washing with DCM (3 × 10 mL). The organic phase was washed with a saturated solution of Na_2CO_3 (5 mL), then the aqueous phase was newly extracted with DCM (25 mL) and, after separation, the second organic phase was washed with a saturated solution of Na_2CO_3 (5 mL). The combined organic phases were dried over anhydrous Na_2SO_4, the solvent was evaporated under vacuum at room temperature and the free hydrazide intermediate was directly submitted to the following acylation reaction. The free hydrazide was dissolved in dry DCM (5 mL) under inert atmosphere, then pyridine (121 µL) was added,

followed by dropwise addition of the suitable acyl chloride (1.1 eq). The solution was stirred for 1 hour, then all the volatile species were removed in vacuo at room temperature and the residue was diluted with AcOEt (30 mL) and water (5 mL). After separation, the organic phase was washed with HCl 1 M (2 × 3 mL), saturated aqueous sodium carbonate (5 mL) and water (5 mL). The aqueous phases were sequentially extracted with additional 30 mL of ethyl acetate, then the second organic phase was washed with HCl 1 M (2 × 3 mL), saturated aqueous sodium carbonate (5 mL) and water (5 mL). The combined organic phases were dried over anhydrous sodium sulfate and evaporated under vacuum, then the crude product was purified by column chromatography on silica gel (cyclohexane/AcOEt mixtures as eluents), to give the pure compound.

***tert*-Butyl (2-(2-acetyl-1-(2-oxo-2-(propylamino)ethyl)hydrazinyl-2-oxoethyl)carbamate, CH_3CO-HydrGly-NHC_3H_7, (3Ba)**.

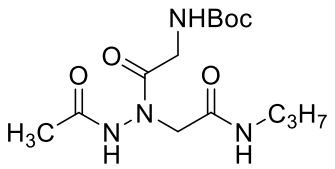

Starting from **3Aa** (265 µmol, 117 mg) and following the general procedure, compound **3Ba** was obtained in 65% yield (172 µmol, 56.8 mg) as a white waxy solid. R_f = 0.23 (AcOEt:MeOH 95:5). m.p. = 138-140 °C. ^{1}H NMR (400 MHz, $CDCl_3$): δ 0.92 (t, J = 7.4 Hz, 3H), 1.43 (s, 9H), 1.51-1.60 (m, 2H), 2.09 (s, 3H), 3.22 (q, J = 6.6 Hz, 2H), 4.00 (bs, 2H), 4.23 (bs, 2H), 5.28 (bs, 1NH), 7.63 (bs, 1NH), 9.32 (bs, 1NH) ppm. ^{13}C NMR (100 MHz, $CDCl_3$): δ 11.5, 20.8, 22.6, 28.5, 41.6, 41.8, 53.8, 80.2, 156.2, 168.3, 171.1, 171.7 ppm. LCMS: m/z = 331.2 $[M+H]^+$, 353.2 $[M+Na]^+$.

***tert*-Butyl (2-(2-acetyl-1-(2-(octylamino)-2-oxoethyl)hydrazinyl)-2-oxoethyl)carbamate, CH_3CO-HydrGly-NHC_8H_{17}, (3Bb).**

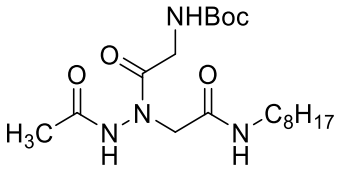

Starting from **3Ab** (1.10 mmol, 542 mg) and following the general procedure, compound **3Bb** was obtained in 95% yield (1.05 mmol, 419 mg) as a colorless pitchy compound. R_f = 0.22 (AcOEt). ^{1}H NMR (400 MHz, $CDCl_3$): δ 0.87 (t, J = 7.0 Hz, 3H), 1.24-1.32 (m, 10H), 1.43 (s, 9H), 1.48-1.55 (m, 2H), 2.09 (s, 3H), 3.24 (q, J = 6.6 Hz, 2H), 3.99 (bs, 2H), 4.23 (bs, 2H), 5.28 (bs, 1NH), 7.60 (bs, 1NH), 9.31 (bs, 1NH) ppm. ^{13}C NMR (100 MHz, $CDCl_3$): δ 14.2, 20.8,

22.8, 27.0, 28.5, 29.2, 29.3, 31.9, 40.0, 54.0, 80.2, 156.2, 168.3, 171.0, 171.6 ppm. LCMS: *m/z* = 401.4 $[M+H]^+$, 423.4 $[M+Na]^+$.

***tert*-Butyl (2-(2-acetyl-1-(2-(dodecylamino)-2-oxoethyl)hydrazinyl)-2-oxoethyl)carbamate, CH_3CO-HydrGly-$NHC_{12}H_{25}$, (3Bc).**

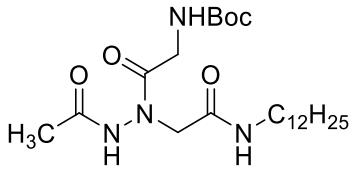

Starting from **3Ac** (1.15 mmol, 631 mg) and following the general procedure, compound **3Bc** was obtained in 88% yield (1.01 mmol, 462 mg) as a white waxy solid. R_f = 0.14 (AcOEt). m.p. = 58-60 °C. ^{1}H NMR (400 MHz, $CDCl_3$): δ 0.88 (t, *J* = 7.0 Hz, 3H), 1.25 (s, 18H), 1.43 (s, 9H), 1.46-1.56 (m, 2H), 2.08 (s, 3H), 3.22 (q, *J* = 6.6 Hz, 2H), 3.99 (bs, 2H), 4.17 (bs, 2H), 5.30 (bs, 1NH), 7.62 (bs, 1NH), 9.46 (bs, 1NH) ppm. ^{13}C NMR (100 MHz, $CDCl_3$): δ 14.2, 20.8, 22.8, 27.0, 28.5, 29.3, 29.4, 29.5, 29.68, 29.74, 29.76, 29.79, 32.0, 39.9, 41.8, 53.9, 80.1, 156.2, 168.2, 171.1, 171.7 ppm. LCMS: *m/z* = 457.4 $[M+H]^+$, 479.4 $[M+Na]^+$.

***tert*-Butyl (2-(2-acetyl-1-(2-(octadecylamino)-2-oxoethyl)hydrazinyl)-2-oxoethyl)carbamate, CH_3CO-HydrGly-$NHC_{18}H_{37}$, (3Bd).**

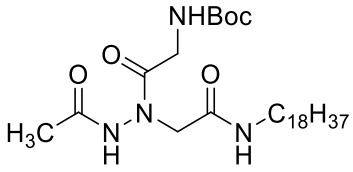

Starting from **3Ad** (1.00 mmol, 633 mg) and following the general procedure, compound **3Bd** was obtained in 91% yield (0.91 mmol, 492 mg) as a white waxy solid. R_f = 0.32 (AcOEt). m.p. = 77-79 °C. ^{1}H NMR (400 MHz, $CDCl_3$): δ 0.88 (t, *J* = 7.0 Hz, 3H), 1.25 (s, 30H), 1.43 (s, 9H), 1.47-1.55 (m, 2H), 2.09 (s, 3H), 3.24 (q, *J* = 6.6 Hz, 2H), 3.98 (bs, 2H), 4.23 (bs, 2H), 5.28 (bs, 1NH), 7.54 (bs, 1NH), 9.27 (bs, 1NH) ppm. ^{13}C NMR (100 MHz, $CDCl_3$): δ 14.2, 20.8, 22.8, 27.1, 28.5, 29.3, 29.4, 29.5, 29.70, 29.77, 29.83, 32.0, 39.9, 41.8, 53.9, 80.1, 156.2, 168.2, 171.1, 171.7 ppm. LCMS: *m/z* = 541.5 $[M+H]^+$, 563.5 $[M+Na]^+$.

***tert*-Butyl (2-(2-octanoyl-1-(2-oxo-2-(propylamino)ethyl)hydrazinyl)-2-oxoethyl)carbamate, $C_7H_{15}CO$-HydrGly-NHC_3H_7, (3Ca).**

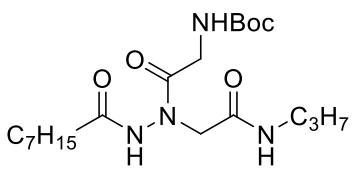

Starting from **3Aa** (1.00 mmol, 423 mg) and following the general procedure, compound **3Ca** was obtained in 90% yield (0.901 mmol, 373 mg) as a white waxy solid. R_f = 0.4 (cyclohexane/AcOEt 2:8). m.p. = 76-78°C. ^{1}H NMR (400 MHz, $CDCl_3$): δ 0.88 (t, *J* = 7.0 Hz, 3H), 0.90 (t, *J* = 7.4 Hz, 3H), 1.22-1.37 (m, 8H), 1.43 (s, 9H), 1.48-1.57 (m, 2H), 1.63-1.70 (m, 2H), 2.24-2.30 (m, 2H), 3.19 (q, *J* = 6.6 Hz, 2H), 3.70-4.30 (m, 2H), 4.12 (bs, 2H), 5.30 (bs, 1NH), 7.71 (bs, 1NH), 9.37 (bs, 1NH) ppm. ^{13}C NMR (100 MHz, $CDCl_3$): δ 11.4, 14.0, 22.4, 22.6, 25.1, 28.3, 28.9, 29.2, 31.6, 33.8, 41.3, 41.7, 54.1, 79.7, 156.1, 168.2, 171.7, 174.3 ppm. LCMS: *m/z* = 414.3 $[M+H]^+$, 436.3 $[M+Na]^+$.

***tert*-Butyl (2-(2-octanoyl-1-(2-(octylamino)-2-oxoethyl)hydrazinyl)-2-oxoethyl)carbamate, $C_7H_{15}CO$-HydrGly-NHC_8H_{17}, (3Cb).**

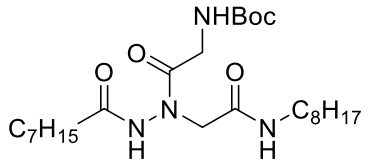

Starting from **3Ab** (0.899 mmol, 443 mg) and following the general procedure, compound **3Cb** was obtained in 88% yield (0.790 mmol, 383 mg) as a white waxy solid. R_f = 0.47 (AcOEt). m.p. = 77-79 °C. ^{1}H NMR (400 MHz, $CDCl_3$): δ 0.86-0.89 (m, 6H), 1.21-1.36 (m, 18H), 1.43 (s, 9H), 1.47-1.54 (m, 2H), 1.61-1.72 (m, 2H), 2.25 (t, *J* = 7.4 Hz, 2H), 3.22 (q, *J* = 6.6 Hz, 2H), 3.54-4.45 (m, 2H), 4.18 (bs, 2H), 5.25 (bs, 1NH), 7.12 (bs, 1NH), 8.74 (bs, 1NH) ppm. ^{13}C NMR (100 MHz, $CDCl_3$): δ 14.1, 14.2, 22.7, 22.8, 25.2, 27.0, 28.4, 29.0, 29.27, 29.34, 31.7, 31.9, 34.0, 39.8, 41.7, 54.1, 80.0, 156.2, 168.2, 171.7, 174.3 ppm. LCMS: *m/z* = 485.4 $[M+H]^+$, 507.4 $[M+Na]^+$.

***tert*-Butyl (2-(1-(2-(dodecylamino)-2-oxoethyl)-2-octanoylhydrazinyl)-2-oxoethyl)carbamate, $C_7H_{15}CO$-HydrGly-$NHC_{12}H_{25}$, (3Cc).**

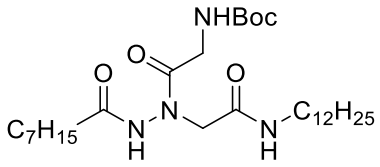

Starting from **3Ac** (390 μmol, 214 mg) and following the general procedure, compound **3Cc** was obtained in 83% yield (324 μmol, 175 mg) as a white amorphous solid. R_f = 0.35 (AcOEt). m.p. = 81-83 °C. ^{1}H NMR (400 MHz, $CDCl_3$): δ 0.86-0.89 (m, 6H), 1.21-1.38 (m, 26H), 1.43 (s, 9H), 1.47-1.59 (m, 2H), 1.62-1.73 (m, 2H), 2.24-2.33 (m, 2H), 3.20-3.31 (m, 2H), 3.63-4.50 (m, 2H), 4.23 (bs, 2H), 5.26 (bs, 1NH), 7.56 (bs, 1NH), 9.03 (bs, 1NH) ppm. ^{13}C NMR (100 MHz, $CDCl_3$): δ 14.17, 14.24, 22.7, 22.8, 25.2, 27.1, 28.5, 29.1, 29.3, 29.36, 29.44, 29.5, 29.7,

29.78, 29.80, 31.8, 32.0, 34.0, 39.9, 41.8, 54.1, 80.0, 156.1, 168.2, 171.7, 174.3 ppm. LCMS: *m/z* = 541.5 $[M+H]^+$,563.5 $[M+Na]^+$.

***tert*-Butyl (2-(1-(2-(octadecylamino)-2-oxoethyl)-2-octanoylhydrazinyl)-2-oxoethyl)carbamate, $C_7H_{15}CO$-HydrGly-$NHC_{18}H_{37}$, (3Cd).**

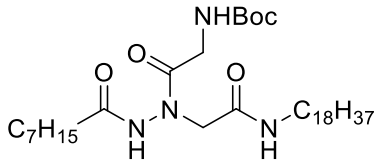

Starting from **3Ad** (525 μmol, 332 mg) and following the general procedure, compound **3Cd** was obtained in 83% yield (437 μmol, 273 mg) as a white amorphous solid. R_f = 0.75 (AcOEt). m.p. = 83-85 °C. ^{1}H NMR (400 MHz, $CDCl_3$): δ 0.86-0.89 (m, 6H), 1.22-1.36 (m, 38H), 1.43 (s, 9H), 1.48-1.59 (m, 2H), 1.63-1.73 (m, 2H), 2.25-2.35 (m, 2H), 3.22-3.31 (m, 2H), 3.70-4.48 (m, 2H), 4.27 (bs, 2H), 5.26 (bs, 1NH), 7.58 (bs, 1NH), 9.02 (bs, 1NH) ppm. ^{13}C NMR (100 MHz, $CDCl_3$): δ 14.18, 14.24, 22.7, 22.8, 25.2, 27.1, 28.5, 29.1, 29.3, 29.36, 29.44, 29.48, 29.73, 29.79, 29.84, 31.8, 32.1, 34.0, 39.9, 41.8, 54.0, 80.0, 156.1, 168.2, 171.7, 174.2 ppm. LCMS: *m/z* = 625.5 $[M+H]^+$, 647.5 $[M+Na]^+$.

***tert*-Butyl (2-(2-dodecanoyl-1-(2-oxo-2-(propylamino)ethyl)hydrazinyl)-2-oxoethyl)carbamate, $C_{11}H_{23}CO$-HydrGly-NHC_3H_7, (3Da).**

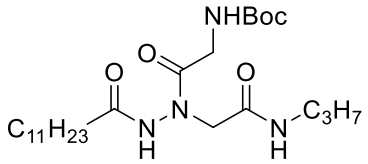

Starting from **3Aa** (954 μmol, 403 mg) and following the general procedure, compound **3Da** was obtained in 94% yield (897 μmol, 422 mg) as a white amorphous solid. R_f = 0.33 (cyclohexane/AcOEt 2:8). m.p. = 69-71 °C. ^{1}H NMR (400 MHz, $CDCl_3$): δ 0.88 (t, *J* = 7.0 Hz, 3H), 0.90 (t, *J* = 7.4 Hz, 3H), 1.20-1.38 (m, 16H), 1.43 (s, 9H), 1.46-1.58 (m, 2H), 1.60-1.72 (m, 2H), 2.27 (t, *J* = 7.4 Hz, 2H), 3.14-3.24 (m, 2H), 3.60-4.30 (m, 4H), 5.31 (bs, 1NH), 7.79 (bs, 1NH), 9.48 (bs, 1NH) ppm. ^{13}C NMR (100 MHz, $CDCl_3$): δ 11.4, 14.2, 22.5, 22.7, 25.2, 28.4, 29.35, 29.38, 29.5, 29.66, 29.67, 32.0, 33.9, 41.4, 41.7, 54.3, 79.8, 156.1, 168.3, 171.8, 174.3 ppm. LCMS: *m/z* = 471.4 $[M+H]^+$, 493.4 $[M+Na]^+$.

***tert*-Butyl (2-(2-dodecanoyl-1-(2-(octylamino)-2-oxoethyl)hydrazinyl)-2-oxoethyl)carbamate, $C_{11}H_{23}CO$-HydrGly-NHC_8H_{17}, (3Db).**

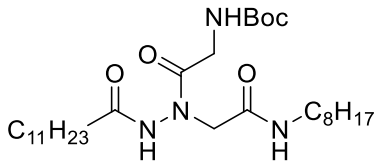

Starting from **3Ab** (627 μmol, 309 mg) and following the general procedure, compound **3Db** was obtained in 88% yield (553 μmol, 299 mg) as a white amorphous solid. R_f = 0.38 (cyclohexane:AcOEt 2:8). m.p. = 67-69 °C. ^{1}H NMR (400 MHz, $CDCl_3$): δ 0.86-0.89 (m, 6H), 1.19-1.38 (m, 26H), 1.43 (s, 9H), 1.45-1.54 (m, 2H), 1.59-1.73 (m, 2H), 2.24-2.28 (m, 2H), 3.21 (q, *J* = 6.2 Hz, 2H), 3.62-4.33 (m, 2H), 4.15 (bs, 2H), 5.27 (bs, 1NH), 7.52 (bs, 1NH), 9.19 (bs, 1NH) ppm. ^{13}C NMR (100 MHz, $CDCl_3$): δ 14.20, 14.22, 22.76, 22.79, 25.2, 27.0, 28.5, 29.29, 29.35, 29.36, 29.42, 29.46, 29.6, 29.7, 29.8, 31.9, 32.0, 34.0, 39.9, 41.8, 54.0, 80.0, 156.2, 168.2, 171.7, 174.2 ppm. LCMS: *m/z* = 541.3 $[M+H]^+$, 563.3 $[M+Na]^+$.

***tert*-Butyl (2-(2-dodecanoyl-1-(2-(dodecylamino)-2-oxoethyl)hydrazinyl)-2-oxoethyl)carbamate, $C_{11}H_{23}$CO-HydrGly-NH-$C_{12}H_{25}$, (3Dc).**

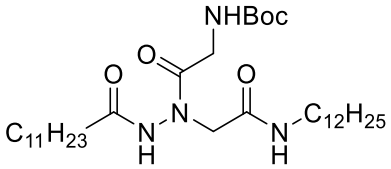

Starting from **3Ac** (600 μmol, 329 mg) and following the general procedure, compound **3Dc** was obtained in 86% yield (516 μmol, 308 mg) as a white amorphous solid. R_f = 0.44 (AcOEt). m.p. = 63-65 °C. ^{1}H NMR (400 MHz, $CDCl_3$): δ 0.86-0.89 (m, 6H), 1.19-1.38 (m, 34H), 1.43 (s, 9H), 1.46-1.55 (m, 2H), 1.60-1.70 (m, 2H), 2.26 (t, *J* = 7.4 Hz, 2H), 3.21 (q, *J* = 6.2 Hz, 2H), 3.59-4.35 (m, 2H), 4.15 (bs, 2H), 5.27 (bs, 1NH), 7.50 (bs, 1NH), 9.16 (bs, 1NH) ppm. ^{13}C NMR (100 MHz, $CDCl_3$): δ 14.2, 22.8, 25.3, 27.1, 28.5, 29.3, 29.45, 29.48, 29.50, 29.6, 29.73, 29.76, 29.79, 29.82, 32.1, 34.0, 39.9, 41.8, 54.0, 80.0, 156.2, 168.2, 171.7, 174.2 ppm. LCMS: *m/z* = 597.6 $[M+H]^+$, 619.6 $[M+Na]^+$.

***tert*-Butyl (2-(2-dodecanoyl-1-(2-(octadecylamino)-2-oxoethyl)hydrazinyl)-2-oxoetyl)carbamate, $C_{11}H_{23}$CO-HydrGly-NH$C_{18}H_{35}$, (3Dd).**

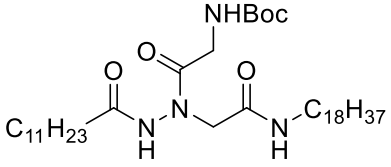

Starting from **3Ad** (341 μmol, 216 mg) and following the general procedure, compound **3Dd** was obtained in 70% yield (238 μmol, 162 mg) as a white amorphous solid. R_f = 0.32 (AcOEt).

m.p. = 45-47 °C. ^{1}H NMR (400 MHz, $CDCl_3$): δ 0.86-0.89 (m, 6H), 1.20-1.37 (m, 46H), 1.43 (s, 9H), 1.46-1.54 (m, 2H), 1.59-1.72 (m, 2H), 2.26 (t, *J* = 7.4 Hz, 2H), 3.18-3.23 (m, 2H), 3.62-4.30 (m, 2H), 4.12 (bs, 2H), 5.29 (bs, 1NH), 7.62 (bs, 1NH), 9.30 (bs, 1NH) ppm. ^{13}C NMR (100 MHz, $CDCl_3$): δ 14.2, 22.8, 25.2, 27.1, 28.5, 29.3, 29.45, 29.48, 29.6, 29.75, 29.78, 29.80, 29.83, 32.0, 34.0, 39.9, 41.8, 54.2, 79.9, 156.2, 168.2, 171.7, 174.3 ppm. LCMS: *m/z* = 658.6 $[M+H]^+$, 680.6 $[M+Na]^+$.

***tert*-Butyl (2-oxo-2-(1-(2-oxo-2-(propylamino)ethyl)-2-stearoylhydrazinyl)ethyl)carbamate, $C_{17}H_{35}$CO-HydrGly-NHC_8H_{17}, (3Ea).**

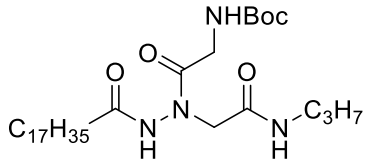

Starting from **3Aa** (265 μmol, 112 mg) and following the general procedure, compound **3Ea** was obtained in 70% yield (186 μmol, 103 mg) as a white amorphous solid. R_f = 0.42 (AcOEt). m.p. = 63-65 °C. ^{1}H NMR (400 MHz, $CDCl_3$): δ 0.88 (t, *J* = 7.0 Hz, 3H), 0.92 (t, *J* = 7.4 Hz, 3H), 1.20-1.38 (m, 28H), 1.43 (s, 9H), 1.51-1.60 (m, 2H), 1.62-1.73 (m, 2H), 2.29 (t, *J* = 7.4 Hz, 2H), 3.23 (q, *J* = 6.6 Hz, 2H), 3.96 (bs, 2H), 4.22 (bs, 2H) 5.28 (bs, 1NH), 7.78 (bs, 1NH), 9.25 (bs, 1NH) ppm. ^{13}C NMR (100 MHz, $CDCl_3$): δ 11.5, 14.2, 22.6, 22.8, 25.3, 28.5, 29.40, 29.43, 29.47, 29.6, 29.78, 29.82, 32.0, 34.0, 41.5, 41.8, 54.2, 80.0, 156.2, 168.3, 171.8, 174.3 ppm. LCMS: *m/z* = 532.4 $[M+H]^+$, 554.4 $[M+Na]^+$.

***tert*-Butyl (2-(1-(2-(octylamino)-2-oxoethyl)-2-stearoylhydrazinyl)-2-oxoethyl)carbamate, $C_{17}H_{35}$CO-HydrGly-NHC_8H_{17}, (3Eb).**

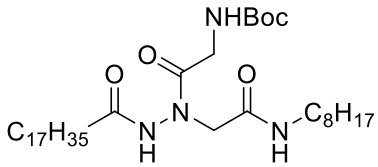

Starting from **3Ab** (451 μmol, 222 mg) and following the general procedure, compound **3Eb** was obtained in 86% yield (389 μmol, 243 mg) as a white amorphous solid. R_f = 0.52 (cyclohexane:AcOEt 3:7). m.p. = 125-127 °C. ^{1}H NMR (400 MHz, $CDCl_3$): δ 0.86-0.89 (m, 6H), 1.18-1.38 (m, 38H), 1.43 (s, 9H), 1.45-1.54 (m, 2H), 1.58-1.72 (m, 2H), 2.25-2.29 (m, 2H), 3.18-3.23 (m, 2H), 3.64-4.40 (m, 2H), 4.12 (bs, 2H), 5.31 (bs, 1NH), 7.73 (bs, 1NH), 9.45 (bs, 1NH) ppm. ^{13}C NMR (100 MHz, $CDCl_3$): δ 14.2, 22.76, 22.80, 25.2, 27.0, 28.5, 29.30, 29.36, 29.44, 29.47, 29.6, 29.78, 29.83, 31.95, 32.04, 34.0, 39.9, 41.8, 54.1, 80.0, 156.2, 168.2, 171.7, 174.2 ppm. LCMS: *m/z* = 625.6 $[M+H]^+$, 647.6 $[M+Na]^+$.

***tert*-Butyl (2-(1-(2-(dodecylamino)-2-oxoethyl)-2-stearoylhydrazinyl)-2-oxoethyl)carbamate, $C_{17}H_{35}CO$-HydrGly-$NHC_{12}H_{25}$, (3Ec).**

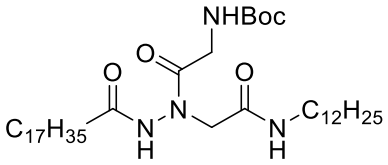

Starting from **3Ac** (304 μmol, 167 mg) and following the general procedure, compound **3Ec** was obtained in 80% yield (242 μmol, 165 mg) as a white amorphous solid. R_f = 0.46 (cyclohexane:AcOEt 2:8). m.p. = 60-63 °C. ^{1}H NMR (400 MHz, $CDCl_3$): δ 0.86-0.89 (m, 6H), 1.18-1.38 (m, 46H), 1.43 (s, 9H), 1.45-1.54 (m, 2H), 1.59-1.72 (m, 2H), 2.21-2.35 (m, 2H), 3.16-3.28 (m, 2H), 3.64-4.36 (m, 2H), 4.16 (bs, 2H), 5.29 (bs, 1NH), 7.69 (bs, 1NH), 9.34 (bs, 1NH) ppm. ^{13}C NMR (100 MHz, $CDCl_3$): δ 14.2, 22.8, 25.3, 27.1, 28.5, 29.3, 29.45, 29.49, 29.6, 29.7, 29.79, 29.85, 32.1, 34.0, 39.9, 41.8, 53.9, 80.0, 156.2, 168.2, 171.7, 174.2 ppm. LCMS: *m/z* = 658.6 $[M+H]^+$, 680.6 $[M+Na]^+$.

***tert*-Butyl (2-(1-(2-(octadecylamino)-2-oxoethyl)-2-stearoylhydrazinyl)-2-oxoethyl)carbamate, $C_{17}H_{35}CO$-HydrGly-$NHC_{18}H_{37}$, (3Ed).**

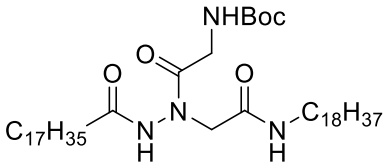

Starting from **3Ad** (348 μmol, 220 mg) and following the general procedure, compound **3Ed** was obtained in 80% yield (278 μmol, 213 mg) as a white waxy solid. R_f = 0.82 (AcOEt). m.p. = 89-90 °C. ^{1}H NMR (400 MHz, $CDCl_3$): δ 0.86-0.89 (m, 6H), 1.19-1.37 (m, 46H), 1.43 (s, 9H), 1.45-1.56 (m, 2H), 1.59-1.72 (m, 2H), 2.21-2.35 (m, 2H), 3.21 (q, *J* = 6.4 Hz, 2H), 3.56-4.40 (m, 2H), 4.16 (s, 2H), 5.29 (bs, 1NH), 7.62 (bs, 1NH), 9.31 (bs, 1NH) ppm. ^{13}C NMR (100 MHz, $CDCl_3$): δ 14.2, 22.8, 25.3, 27.1, 28.5, 29.3, 29.45, 29.51, 29.65, 29.75, 29.81, 29.87, 32.1, 34.1, 39.9, 41.8, 53.8, 80.1, 156.2, 168.2, 171.7, 174.1 ppm. LCMS: *m/z* = 787.8 $[M+Na]^+$.

***tert*-Butyl (2-(2-benzoyl-1-(2-(octylamino)-2-oxoethyl)hydrazinyl)-2-oxoethyl)carbamate, *t*BuCO-HydrGly-NHC_8H_{17}, (3Fb).**

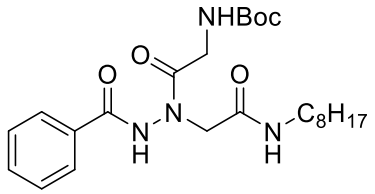

Starting from **3Ab** (899 μmol, 443 mg) and following the general procedure, compound **3Fb** was obtained in 92% yield (828 μmol, 383 mg) as a white amorphous solid. R_f = 0.16 (AcOEt). m.p. = 128-130 °C. ^{1}H NMR (400 MHz, $CDCl_3$): δ 0.87 (t, *J* = 7.0 Hz, 3H), 1.19-1.34 (m, 10H), 1.41 (s, 9H), 1.46-1.57 (m, 2H), 3.21-3.29 (m, 2H), 3.68-4.56 (m, 2H), 4.32 (bs, 2H), 5.29 (bs, 1NH), 7.23 (bs, 1NH), 7.48 (t, *J* = 7.4 Hz, 2ArH), 7.60 (t, *J* = 7.4 Hz, 1ArH), 7.88 (d, *J* = 7.4 Hz, 2ArH), 9.67 (bs, 1NH) ppm. ^{13}C NMR (100 MHz, $CDCl_3$): δ 14.2, 22.8, 27.1, 28.4, 29.30, 29.33, 29.36, 31.9, 39.9, 41.9, 54.2, 80.0, 128.0, 128.9, 130.7, 133.2, 156.2, 167.7, 168.3, 172.1 ppm. LCMS: *m/z* = 463.3 $[M+H]^+$, 485.3 $[M+Na]^+$.

***tert*-Butyl (2-(2-benzoyl-1-(2-(dodecylamino)-2-oxoethyl)hydrazinyl)-2-oxoethyl)carbamate, PhCO-HydrGly-NHC$_{12}$H$_{25}$, (3Fc).**

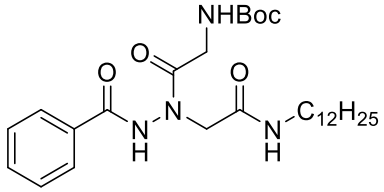

Starting from **3Ac** (425 μmol, 233 mg) and following the general procedure, compound **3Fc** was obtained in 85% yield (361 μmol, 187 mg) as a white amorphous solid. R_f = 0.56 (AcOEt). m.p. = 123-125 °C. ^{1}H NMR (400 MHz, $CDCl_3$): δ 0.87 (t, *J* = 7.0 Hz, 3H), 1.21-1.31 (m, 18H), 1.40 (s, 9H), 1.46-1.56 (m, 2H), 3.21-3.26 (m, 2H), 3.71-4.47 (m, 2H), 4.29 (bs, 2H), 5.31 (bs, 1NH), 7.48 (t, *J* = 7.4 Hz, 2ArH + 1NH), 7.59 (t, *J* = 7.4 Hz, 1ArH), 7.89 (d, *J* = 7.4 Hz, 2ArH), 9.87 (bs, 1NH) ppm. ^{13}C NMR (100 MHz, $CDCl_3$): δ 14.2, 22.8, 27.1, 28.4, 29.3, 29.4, 29.5, 29.70, 29.76, 29.79, 32.0, 40.0, 41.9, 54.2, 80.0, 128.0, 128.9, 130.7, 133.2, 156.2, 167.7, 168.4, 172.1 ppm. LCMS: *m/z* = 519.4 $[M+H]^+$, 541.4 $[M+Na]^+$.

***tert*-Butyl (2-(1-(2-(octylamino)-2-oxoethyl)-2-pivaloylhydrazinyl)-2-oxoethyl)carbamate, *t*BuCO-HydrGly-NHC$_8$H$_{17}$, (3Gb).**

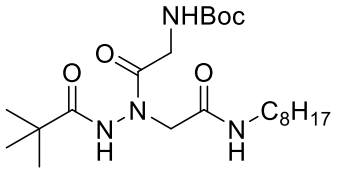

Starting from **3Ab** (510 μmol, 251 mg) and following the general procedure, compound **3Gb** was obtained in 89% yield (454 μmol, 201 mg) as a colorless pitchy compound. R_f = 0.22 (cyclohexane:AcOEt 3:7). m.p. = 121-123 °C. ^{1}H NMR (400 MHz, $CDCl_3$): δ 0.87 (t, *J* = 7.0 Hz, 3H), 1.20-1.31 (m, 19H), 1.42 (s, 9H), 1.44-1.54 (m, 2H), 3.15-3.27 (m, 2H), 3.73 (bs, 1H), 4.10 (bs, 3H), 5.31 (bs, 1NH), 7.75 (bs, 1NH), 9.36 (bs, 1NH) ppm. ^{13}C NMR (100 MHz,

$CDCl_3$): δ 14.2, 22.7, 27.0, 27.2, 28.5, 29.3, 31.9, 38.4, 39.8, 41.7, 54.1, 79.9, 156.1, 168.2, 171.8, 179.1 ppm. LCMS: *m/z* = 443.3 $[M+H]^+$, 465.2 $[M+Na]^+$.

***tert*-Butyl (2-(1-(2-(dodecylamino)-2-oxoethyl)-2-pivaloylhydrazinyl)-2-oxoethyl)carbamate, *t*BuCO-HydrGly-NHC$_{12}$H$_{25}$, (3Gc).**

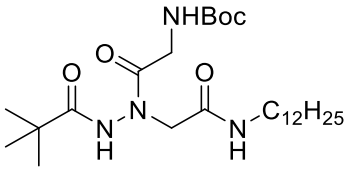

Starting from **3Ac** (672 μmol, 369 mg) and following the general procedure, compound **3Gc** was obtained in 90% yield (606 μmol, 302 mg) as a colorless waxy solid. R_f = 0.49 (AcOEt). m.p. = 115-117 °C. ^{1}H NMR (400 MHz, $CDCl_3$): δ 0.88 (t, *J* = 7.0 Hz, 3H), 1.20-1.33 (m, 27H), 1.43 (s, 9H), 1.46-1.55 (m, 2H), 3.20-3.30 (m, 2H), 3.5-4.37 (m, 4H), 5.26 (bs, 1NH), 7.50 (bs, 1NH), 9.09 (bs, 1NH) ppm. ^{13}C NMR (100 MHz, $CDCl_3$): δ 14.2, 22.7, 27.0, 27.1, 28.4, 29.2, 29.36, 29.40, 29.6, 29.7, 32.0, 38.3, 39.7, 41.6, 54.5, 79.6, 156.0, 168.2, 171.9, 179.2 ppm. LCMS: *m/z* = 499.4 $[M+H]^+$, 521.4 $[M+Na]^+$.

***tert*-Butyl (2-(2-(2-naphtoyl)-1-(2-(octylamino)-2-oxoethyl)hydrazinyl)-2-oxoethyl)carbamate, 1-naphthylCO-HydrGly-NHC$_8$H$_{17}$, (3Hb).**

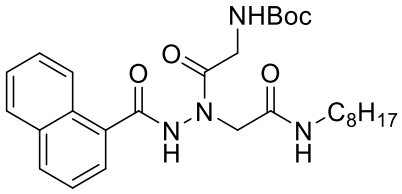

Starting from **3Ab** (400 μmol, 197 mg) and following the general procedure, compound **3Hb** was obtained in 91% yield (365 μmol, 187 mg) as a white amorphous solid. R_f = 0.28 (cyclohexane/AcOEt 3:7). m.p. = 186-188 °C. ^{1}H NMR (400 MHz, $CDCl_3$): δ 0.84-0.90 (m, 3H), 1.17-1.33 (m, 10H), 1.41 (s, 9H), 1.46-1.57 (m, 2H), 3.21-3.26 (m, 2H), 3.92-4.95 (m, 2H), 4.41 (bs, 2H), 5.31 (bs, 1NH), 7.23 (bs, 1NH), 7.49 (t, *J* = 7.4 Hz, 1ArH), 7.54-7.61 (m, 2ArH), 7.77 (d, *J* = 6.2 Hz, 1ArH), 7.89 (d, *J* = 8.6 Hz, 1ArH), 8.01 (d, *J* = 8.2 Hz, 1ArH), 8.34 (d, *J* = 8.2 Hz, 1ArH), 9.33 (bs, 1NH) ppm. ^{13}C NMR (100 MHz, DMSO-d_6): δ 13.9, 22.1, 26.4, 28.2, 28.6, 28.7, 29.0, 31.2, 38.6, 41.1, 51.1, 78.0, 124.80, 124.84, 126.48, 126.53, 127.2, 128.5, 129.8, 130.5, 131.3, 133.2, 155.8, 166.9, 167.8, 170.9 ppm. LCMS: *m/z* = 503.3 $[M+H]^+$, 525.3 $[M+Na]^+$.

***tert*-Butyl (2-(2-(2-naphthoyl)-1-(2-(dodecylamino)-2-oxoethyl)hydrazinyl)-2-oxoethyl)carbamate, 1-naphthylCO-HydrGly-NHC$_{12}$H$_{25}$, (3Hc).**

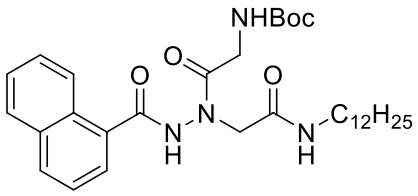

Starting from **3Ac** (322 μmol, 177 mg) and following the general procedure, compound **3Hc** was obtained in 87% yield (280 μmol, 159 mg) as a white waxy solid. R_f = 0.40 (DCM/MeOH 95:5). m.p. = 178-180 °C. ^{1}H NMR (400 MHz, $CDCl_3$): δ 0.86-0.89 (m, 3H), 1.18-1.35 (m, 18H), 1.41 (s, 9H), 1.46-1.56 (m, 2H), 3.18-3.28 (m, 2H), 3.91-4.56 (m, 2H), 4.41 (bs, 2H), 5.32 (bs, 1NH), 7.41 (bs, 1NH), 7.40 (t, *J* = 7.4 Hz, 1ArH), 7.54-7.60 (m, 2ArH), 7.77 (d, *J* = 6.3 Hz, 1ArH), 7.89 (d, *J* = 7.4 Hz, 1ArH), 8.00 (d, *J* = 8.2 Hz, 1ArH), 8.35 (d, *J* = 8.2 Hz, 1ArH), 9.49 (bs, 1NH) ppm. ^{13}C NMR (100 MHz, DMSO-*d*$_6$): δ 13.9, 22.0, 26.3, 28.2, 28.66, 28.73, 28.90, 28.95, 29.00, 31.2, 38.6, 41.1, 51.0, 78.0, 124.8, 126.44, 126.47, 127.2, 128.4, 129.8, 130.5, 131.2, 133.1, 155.8, 166.8, 167.8, 170.9 ppm. LCMS: *m/z* = 569.5 $[M+H]^+$, 591.5 $[M+Na]^+$.

General procedure for the synthesis of hydrochlorides 4.

Note: representative procedures are referred to 1 mmol of starting compound; the actual amounts of starting compounds used in the reactions are reported below.

Compound **4Ba**, due to very high solubility in water, was not submitted to the extractive procedure and was used as crude product, after azeotropic removal of TFA, in biological assays. The suitable compound was dissolved in dry DCM (3 mL), then TFA (1 mL) was added and the reaction was stirred at room temperature for 30 minutes. All the volatile species were removed at reduced pressure at room temperature, then traces of TFA were azeotropically removed by addition of DCM (1-2 mL) to the residue and further evaporation under vacuum (procedure repeated three times). The residue was diluted with DCM (10 mL) and a saturated solution of Na_2CO_3 (3 mL), then the phases were separated and the aqueous one was newly extracted with DCM (10 mL). After separation, the second organic phase was washed with a saturated solution of Na_2CO_3 (3 mL). The combined organic phases were dried over anhydrous Na_2SO_4, the solvent was evaporated under vacuum at room temperature and the residue was purified by flash chromatography on silica gel, using the suitable mixtures of distilled DCM and distilled MeOH as the eluents. After concentration at reduced pressure and room temperature, the pure free amine was dissolved in dry DCM (3 mL), 3 M HCl in dry methanol (0.35 mL) was added and the mixture was evaporated under vacuum at room temperature, obtaining the desired pure hydrochlorides. Occasionally, if very careful smelling indicated that

an excess HCl was still present, the residue was dissolved again in dry DCM (1-2 mL) and evaporated under vacuum.

2-(2-((Benzyloxy)carbonyl)-1-(2-oxo-2-(propylamino)ethyl)hydrazinyl)-2-oxoethan-1-aminium chloride, BnOCO-HydrGly-NHC$_3$H$_7$ · HCl, (4Aa).

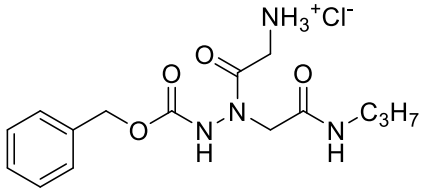

Starting from **3Aa** (263 μmol, 111 mg) and following the general procedure, compound **4Aa** was obtained in 98% yield (257 μmol, 92.2 mg) as a colorless waxy solid. R_f = 0.38 (free amine, DCM/MeOH 9:1). ^{1}H NMR (400 MHz, DMSO-*d*$_6$): δ 0.84 (t, *J* = 7.4 Hz, 3H), 1.36-1.45 (m, 2H), 3.03 (q, *J* = 7.0 Hz, 2H), 3.56-4.65 (m, 4H), 5.15 (s, 2H), 7.33-7.41 (m, 5ArH), 8.01-8.18 (m, 4NH), 10.19 (bs, 1NH) ppm. t'$_R$ = 3.45 min (%2-propanol = 35.17%). HPLC purity: 98.2%. LCMS: *m/z* = 323.2 [M-Cl]$^+$, 345.2 [M-HCl+Na]$^+$. Elemental analysis: Anal. Calcd for $C_{15}H_{23}ClN_4O_4$: C, 50.21; H, 6.46; N, 15.61. Found: C, 50.08; H, 6.48; N, 15.59.

2-(2-((Benzyloxy)carbonyl)-1-(2-(octylamino)-2-oxoethyl)hydrazinyl)-2-oxoethan-1-aminium chloride, BnOCO-HydrGly-NH-C$_8$H$_{17}$ · HCl, (4Ab).

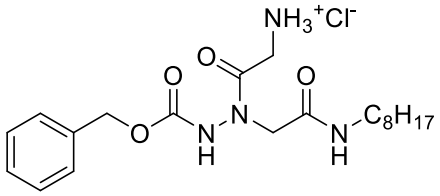

Starting from **3Ab** (355 μmol, 175 mg) and following the general procedure, compound **4Ab** was obtained in 90% yield (320 μmol, 137 mg) as a colorless waxy solid. R_f = 0.31 (free amine, DCM/MeOH 95:5). ^{1}H NMR (400 MHz, DMSO-*d*$_6$): δ 0.85 (t, *J* = 7.0 Hz, 3H), 1.24 (s, 10H), 1.34-1.43 (m, 2H), 3.05 (q, *J* = 6.6 Hz, 2H), 3.56-4.64 (m, 4H), 5.15 (s, 2H), 7.32-7.41 (m, 5ArH), 8.01 (t, *J* = 5.4 Hz, 1NH), 8.09-8.17 (m, 3NH), 10.19 (bs, 1NH) ppm. t'$_\mathbf{R}$ = 3.45 min (%2-propanol = 51.38%). HPLC purity: 99.1%. LCMS: *m/z* = 393.3 [M-Cl]$^+$, 415.2 [M-HCl+Na]$^+$. Elemental analysis: Anal. Calcd for $C_{20}H_{33}ClN_4O_4$: C, 56.00; H, 7.75; N, 13.06. Found: C, 56.13; H, 7.77; N, 13.04.

2-(2-((Benzyloxy)carbonyl)-1-(2-(octylamino)-2-oxoethyl)hydrazinyl)-2-oxoethan-1-aminium chloride, BnOCO-HydrGly-NHC$_{12}$H$_{25}$ · HCl, (4Ac).

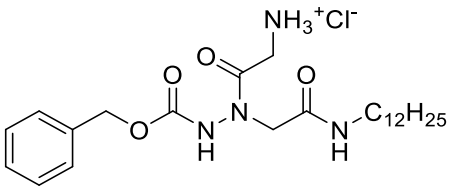

Starting from **3Ac** (155 μmol, 85.2 mg) and following the general procedure, compound **4Ac** was obtained in 88% yield (136 μmol, 66.1 mg) as a colorless waxy solid. R_f = 0.37 (free amine, DCM:MeOH 9:1). ^{1}H NMR (400 MHz, DMSO-d_6): δ 0.85 (t, J = 7.0 Hz, 3H), 1.24 (s, 18H), 1.34-1.42 (m, 2H), 3.05 (q, J = 6.6 Hz, 2H), 3.37-4.60 (m, 4H), 5.15 (s, 2H), 7.32-7.41 (m, 5ArH), 8.01 (t, J = 5.6 Hz, 1NH), 8.06-8.17 (m, 3NH), 10.17 (bs, 1NH) ppm. t'$_R$ = 21.21 min (%2-propanol = 61.82%). HPLC purity: 97.1%. LCMS: m/z = 449.3 $[M\text{-}Cl]^+$, 471.3 $[M\text{-}HCl+Na]^+$. Elemental analysis: Anal. Calcd for $C_{24}H_{41}ClN_4O_4$: C, 59.43; H, 8.52; N, 11.55. Found: C, 59.40; H, 8.53; N, 11.55.

2-(2-((Benzyloxy)carbonyl)-1-(2-(octadecylamino)-2-oxoethyl)hydrazinyl)-2-oxoethan-1-aminium chloride, BnOCO-HydrGly-NHC$_{18}$H$_{37}$ · HCl, (4Ad).

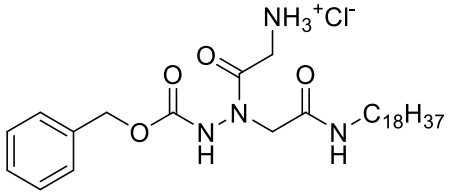

Starting from **3Ad** (152 μmol, 96.2 mg) and following the general procedure, compound **4Ad** was obtained in 82% yield (125 μmol, 71.0 mg) as a white waxy solid. R_f = 0.16 (free amine, DCM:MeOH 95:5). ^{1}H NMR (400 MHz, DMSO-d_6): δ 0.85 (t, J = 7.0 Hz, 3H), 1.23 (s, 30H), 1.33-1.43 (m, 2H), 3.05 (q, J = 6.5 Hz, 2H), 3.59-4.60 (m, 4H), 5.15 (s, 2H), 7.32-7.41 (m, 5ArH), 8.01 (t, J = 5.5 Hz, 1NH), 8.10-8.20 (m, 3NH), 10.19 (bs, 1NH) ppm. t'$_R$ = 30.94 min (%2-propanol = 76.41%). HPLC purity: 97.2%. LCMS: m/z = 533.4 $[M\text{-}Cl]^+$, 555.4 $[M\text{-}HCl+Na]^+$. Elemental analysis: Anal. Calcd for $C_{30}H_{53}ClN_4O_4$: C, 63.30; H, 9.39; N, 9.84. Found: C, 63.25; H, 9.42; N, 9.85.

2-(2-Acetyl-1-(2-oxo-2-(propylamino)ethyl)hydrazinyl)-2-oxoethanaminium 2,2,2-trifluoroacetate, CH$_3$CO-HydrGly-NHC$_3$H$_7$ · CF$_3$CO$_2$H, (4Ba).

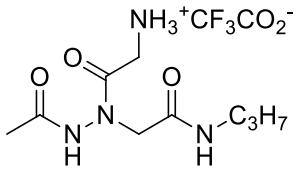

Starting from **3Ba** (275 μmol, 90.8 mg), compound **4Ba** was obtained as crude trifluoroacetate product in 95% yield (95.7 mg of crude product, corresponding to about 261 μmol, 90.0 mg, of pure product considering the HPLC purity, 95%) as a pale yellow oil, through evaporation under vacuum of the volatile species after reaction with TFA/DCM. R_f = 0.15 (free amine, DCM:MeOH = 8:2). ^{1}H NMR (400 MHz, DMSO-*d*$_6$): δ 0.84 (t, *J* = 7.4 Hz, 3H), 1.37-1.46 (m, 2H), 1.92 (s, 3H), 3.04 (q, *J* = 6.5 Hz, 2H), 3.48-4.77 (m, 4H), 7.98-8.24 (m, 4NH), 10.59 (s, 1NH) ppm. t'$_R$ = 0.26 min (%2-propanol = 30.39%). HPLC purity: 95.1%. LCMS: *m/z* 231.2 [M-$CF_3CO_2^-$]$^+$, 253.1 [M-CF_3CO_2H+Na]$^+$. Elemental analysis: Anal. Calcd for $C_{11}H_{19}F_3N_4O_5$: C, 38.37; H, 5.56; N, 16.27. Found: C, 38.39; H, 5.58; N, 16.25.

2-(2-Acetyl-1-(2-(octylamino)-2-oxoethyl)hydrazinyl)-2-oxoethan-1-aminium chloride, CH_3CO-HydrGly-NHC_8H_{17} · HCl, (4Bb).

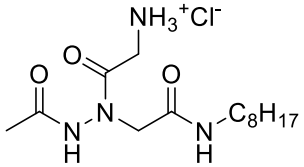

Starting from **3Bb** (357 μmol, 143 mg) and following the general procedure, compound **4Bb** was obtained in 68% yield (242 μmol, 81.6 mg) as a white waxy solid. R_f = 0.13 (free amine, DCM:MeOH 9:1). ^{1}H NMR (400 MHz, DMSO-*d*$_6$): δ 0.86 (t, *J* = 6.8 Hz, 3H), 1.24 (s, 10H), 1.34-1.44 (m, 2H), 1.92 (s, 3H), 3.06 (q, *J* = 6.4 Hz, 2H), 3.43-4.88 (m, 4H), 8.02-8.24 (m, 4NH), 10.60 (s, 1NH) ppm. t'$_\mathbf{R}$ = 9.29 min (%2-propanol = 43.94%). HPLC purity: 96.0%. LCMS: *m/z* = 301.2 [M-Cl]$^+$, 323.2 [M-HCl+Na]$^+$. Elemental analysis: Anal. Calcd for $C_{14}H_{29}ClN_4O_3$: C, 49.92; H, 8.68; N, 16.63. Found: C, 49.89; H, 8.69; N, 16.66.

2-(2-Acetyl-1-(2-(dodecylamino)-2-oxoethyl)hydrazinyl)-2-oxoethan-1-aminium chloride, CH_3CO-HydrGly-$NHC_{12}H_{25}$ · HCl, (4Bc).

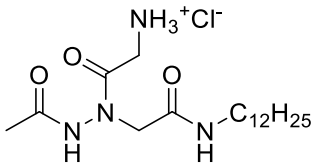

Starting from **3Bc** (175 μmol, 79.8 mg) and following the general procedure, compound **4Bc** was obtained in 70% yield (123 μmol, 48.5 mg) as a white waxy solid. R_f = 0.42 (free amine, DCM:MeOH 7:3). ^{1}H NMR (400 MHz, DMSO-*d*$_6$): δ 0.85 (t, *J* = 6.8 Hz, 3H), 1.24 (s, 18H), 1.34-1.44 (m, 2H), 1.92 (s, 3H), 3.06 (q, *J* = 6.4 Hz, 2H), 3.41-4.72 (m, 4H), 8.03-8.24 (m, 4NH), 10.62 (s, 1NH) ppm. t'$_\mathbf{R}$ = 17.47 min (%2-propanol = 56.21%). HPLC purity: 99.6%.

LCMS: *m/z* = 357.3 $[M\text{-}Cl]^+$, 379.3 $[M\text{-}HCl+Na]^+$. Elemental analysis: Anal. Calcd for $C_{18}H_{37}ClN_4O_3$: C, 55.02; H, 9.49; N, 14.26. Found: C, 54.80; H, 9.50; N, 14.29.

2-(2-Acetyl-1-(2-(octadecylamino)-2-oxoethyl)hydrazinyl)-2-oxoethan-1-aminium chloride, CH_3CO-HydrGly-$NHC_{18}H_{37}$ · HCl, (4Bd).

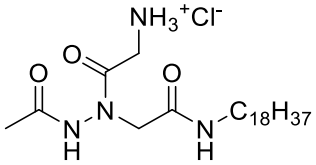

Starting from **3Bd** (262 μmol, 142 mg) and following the general procedure, compound **4Bd** was obtained in 89% yield (233 μmol, 111 mg) as a white waxy solid. R_f = 0.29 (free amine, DCM:MeOH 85:15). ^{1}H NMR (400 MHz, DMSO-d_6): δ 0.85 (t, J = 6.8 Hz, 3H), 1.23 (s, 30H), 1.34-1.43 (m, 2H), 1.91 (s, 3H), 3.05 (q, J = 6.4 Hz, 2H), 3.39-4.73 (m, 4H), 8.03-8.25 (m, 4NH), 10.64 (s, 1NH) ppm. t'$_\mathbf{R}$ = 27.99 min (%2-propanol = 71.99%). HPLC purity: 99.1%. LCMS: *m/z* = 441.4 $[M\text{-}Cl]^+$, 463.3 $[M\text{-}HCl+Na]^+$. Elemental analysis: Anal. Calcd for $C_{24}H_{49}ClN_4O_3$: C, 60.42; H, 10.35; N, 11.74. Found: C, 60.39; H, 10.31; N, 11.77.

2-(2-Octanoyl-1-(2-oxo-2-(propylamino)ethyl)hydrazinyl)-2-oxoethan-1-aminium chloride, $C_7H_{15}CO$-HydrGly-NHC_3H_7 · HCl, (4Ca).

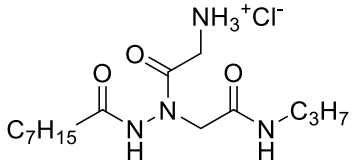

Starting from **3Ca** (192 μmol, 79.5 mg) and following the general procedure, compound **4Ca** was obtained in 95% yield (182 μmol, 64.0 mg) as a white waxy solid. R_f = 0.47 (free amine, DCM:MeOH 8:2). ^{1}H NMR (400 MHz, DMSO-d_6): δ 0.82-0.87 (m, 6H), 1.24 (s, 8H), 1.36-1.45 (m, 2H), 1.47-1.57 (m, 2H), 2.13-2.21 (m, 2H), 3.01-3.06 (m, 2H), 3.39-4.68 (m, 4H), 7.97-8.29 (m, 4NH), 10.63 (s, 1NH) ppm. t'$_\mathbf{R}$ = 5.24 min (%2-propanol = 37.86%). HPLC purity: 97.0%. LCMS: *m/z* = 315.2 $[M\text{-}Cl]^+$, 337.2 $[M\text{-}HCl+Na]^+$. Elemental analysis: Anal. Calcd for $C_{15}H_{31}ClN_4O_3$: C, 51.35; H, 8.91; N, 15.97. Found: C, 51.46; H, 8.89; N, 15.91.

2-(2-Octanoyl-1-(2-(octylamino)-2-oxoethyl)hydrazinyl)-2-oxoethan-1-aminium chloride, $C_7H_{15}CO$-HydrGly-NHC_8H_{17} · HCl, (4Cb).

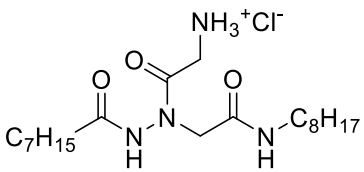

Starting from **3Cb** (192 μmol, 93.2 mg) and following the general procedure, compound **4Cb** was obtained in 87% yield (167 μmol, 70.4 mg) as a white waxy solid. R_f = 0.28 (free amine, DCM:MeOH 1:1).). ^{1}H NMR (400 MHz, DMSO-*d*$_6$): δ 0.84-0.87 (m, 6H), 1.19-1.29 (m, 18H), 1.35-1.41 (m, 2H), 1.48-1.56 (m, 2H), 2.11-2.19 (m, 2H), 2.99-3.14 (m, 2H), 3.40-4.62 (m, 4H), 7.98-8.25 (m, 4NH), 10.58 (s, 1NH) ppm. t'$_R$ = 17.78 min (%2-propanol = 56.67%). HPLC purity: 98.2%. LCMS: *m/z* = 385.3 $[M\text{-}Cl]^+$, 407.3 $[M\text{-}HCl+Na]^+$. Elemental analysis: Anal. Calcd for $C_{20}H_{41}ClN_4O_3$: C, 57.06; H, 9.82; N, 13.31. Found: C, 57.00; H, 9.84; N, 13.35.

2-(1-(2-(Dodecylamino)-2-oxoethyl)-2-octanoylhydrazinyl)-2-oxoethan-1-aminium chloride, C_7H_{15}CO-HydrGly-NH$C_{12}H_{25}$ · HCl, (4Cc).

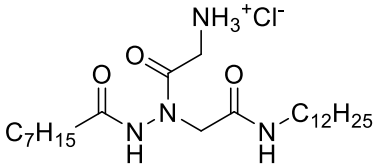

Starting from **3Cc** (135 μmol, 73.1 mg) and following the general procedure, compound **4Cc** was obtained in 84% yield (113 μmol, 53.8 mg) as a white waxy solid. R_f = 0.06 (free amine, DCM:MeOH 9:1). ^{1}H NMR (400 MHz, DMSO-*d*$_6$): δ 0.84-0.87 (m, 6H), 1.19-1.31 (m, 26H), 1.34-1.44 (m, 2H), 1.46-1.57 (m, 2H), 2.11-2.19 (m, 2H), 2.99-3.13 (m, 2H), 3.37-4.65 (m, 4H), 7.91-8.24 (m, 4NH), 10.59 (s, 1NH) ppm. t'$_R$ = 24.01 min (%2-propanol = 66.02%). HPLC purity: 98.7%. LCMS: *m/z* = 441.4 $[M\text{-}Cl]^+$, 463.3 $[M\text{-}HCl+Na]^+$. Elemental analysis: Anal. Calcd for $C_{24}H_{49}ClN_4O_3$: C, 60.42; H, 10.35; N, 11.74. Found: C, 60.28; H, 10.32; N, 11.72.

2-(1-(2-(Octadecylamino)-2-oxoethyl)-2-octanoylhydrazinyl)-2-oxoethan-1-aminium chloride, C_7H_{15}CO-HydrGly-NH$C_{18}H_{37}$ · HCl, (4Cd).

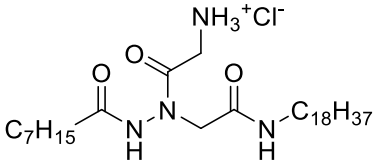

Starting from **3Cd** (174 μmol, 108.8 mg) and following the general procedure, compound **4Cd** was obtained in 81% yield (141 μmol, 79.2 mg) as a white waxy solid. R_f = 0.09 (free amine, DCM:MeOH 95:5). ^{1}H NMR (400 MHz, DMSO-*d*$_6$): δ 0.84-0.88 (m, 6H), 1.23 (s, 38H), 1.34-1.42 (m, 2H), 1.47-1.56 (m, 2H), 2.11-2.19 (m, 2H), 2.98-3.14 (m, 2H), 3.27-4.66 (m, 4H), 7.97-8.14 (m, 4NH), 10.57 (s, 1NH) ppm. t'$_R$ = 33.05 min (%2-propanol = 79.58%). HPLC purity: 97.1%. LCMS: *m/z* = 525.5 $[M\text{-}Cl]^+$, 547.4 $[M\text{-}HCl+Na]^+$. Elemental analysis: Anal. Calcd for $C_{30}H_{61}ClN_4O_3$: C, 64.20; H, 10.95; N, 9.98. Found: C, 64.23; H, 10.99; N, 9.97.

2-(2-dodecanoyl-1-(2-oxo-2-(propylamino)ethyl)hydrazinyl)-2-oxoethan-1-aminium chloride, $C_{11}H_{23}CO$-HydrGly-NHC_3H_7 · HCl, (4Da).

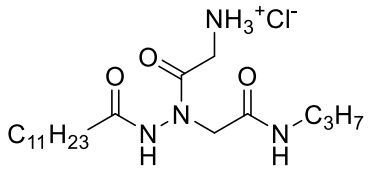

Starting from **3Da** (157 μmol, 73.8 mg) and following the general procedure, compound **4Da** was obtained in 84% yield (132 μmol, 53.8 mg) as a white waxy solid. R_f = 0.40 (free amine, AcOEt:MeOH 8:2). ^{1}H NMR (400 MHz, DMSO-*d*$_6$): δ 0.82-0.87 (m, 6H), 1.24 (s, 8H), 1.36-1.46 (m, 2H), 1.47-1.57 (m, 2H), 2.17 (t, *J* = 7.4 Hz, 2H), 3.01-3.06 (m, 2H), 3.32-4.75 (m, 4H), 8.00-8.27 (m, 4NH), 10.60 (s, 1NH) ppm. t'$_R$ = 16.63 min (%2-propanol = 54.95%). HPLC purity: 97.3%. LCMS: *m/z* = 371.3, $[M\text{-}Cl]^+$, 393.3 $[M\text{-}HCl+Na]^+$. Elemental analysis: Anal. Calcd for $C_{19}H_{39}ClN_4O_3$: C, 56.07; H, 9.66; N, 13.77. Found: C, 56.12; H, 9.69; N, 13.76.

2-(2-Dodecanoyl-1-(2-(octylamino)-2-oxoethyl)hydrazinyl)-2-oxoethan-1-aminium chloride, $C_{11}H_{23}CO$-HydrGly-NHC_8H_{17} · HCl, (4Db).

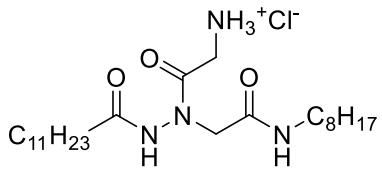

Starting from **3Dd** (169 μmol, 91.5 mg) and following the general procedure, compound **4Db** was obtained in 89% yield (150 μmol, 71.8 mg) as a white waxy solid. R_f = 0.08 (free amine, DCM:MeOH 9:1). ^{1}H NMR (400 MHz, DMSO-*d*$_6$): δ 0.84-0.87 (m, 6H), 1.18-1.29 (m, 26H), 1.34-1.43 (m, 2H), 1.46-1.56 (m, 2H), 2.11-2.20 (m, 2H), 3.00-3.12 (m, 2H), 3.32-4.79 (m, 4H), 7.98-8.24 (m, 4NH), 10.59 (s, 1NH) ppm. t'$_R$ = 23.46 min (%2-propanol = 65.19%). HPLC purity: 97.4%. LCMS: *m/z* = 441.4 $[M\text{-}Cl]^+$, 463.4 $[M\text{-}HCl+Na]^+$. Elemental analysis: Anal. Calcd for $C_{24}H_{49}ClN_4O_3$: C, 60.42; H, 10.35; N, 11.74. Found: C, 60.46; H, 10.33; N, 11.72.

2-(2-Dodecanoyl-1-(2-(dodecylamino)-2-oxoethyl)hydrazinyl)-2-oxoethan-1-aminium chloride, $C_{11}H_{23}CO$-HydrGly-$NHC_{12}H_{25}$ · HCl, (4Dc).

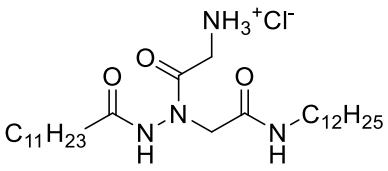

Starting from **3Dc** (253 μmol, 151 mg) and following the general procedure, compound **4Dc** was obtained in 82% yield (207 μmol, 111 mg) as a colorless waxy solid. R_f = 0.11 (free amine,

DCM:MeOH 9:1). ^{1}H NMR (400 MHz, DMSO-d_6): δ 0.84-0.87 (m, 6H), 1.24 (s, 34H), 1.33-1.43 (m, 2H), 1.46-1.56 (m, 2H), 2.11-2.20 (m, 2H), 2.94-3.16 (m, 2H), 3.36-4.69 (m, 4H), 7.99-8.17 (m, 4NH), 10.59 (s, 1NH) ppm. t'$_\mathbf{R}$ = 29.14 min (%2-propanol = 73.71%). HPLC purity: 97.2%. LCMS: *m/z* = 497.4 $[M\text{-}Cl]^+$, 519.5 $[M\text{-}HCl+Na]^+$. Elemental analysis: Anal. Calcd for $C_{28}H_{57}ClN_4O_3$: C, 63.07; H, 10.77; N, 10.51. Found: C, 62.92; H, 10.77; N, 10.53.

2-(2-Dodecanoyl-1-(2-(octadecylamino)-2-oxoethyl)hydrazinyl)-2-oxoethanaminium chloride, $C_{11}H_{23}$CO-HydrGly-NH$C_{18}H_{37}$ · HCl, (4Dd).

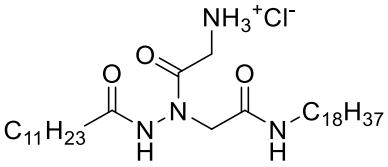

Starting from **3Dd** (110 μmol, 74.8 mg) and following the general procedure, compound **4Dd** was obtained in 97% yield (107 μmol, 66.3 mg) as a colorless waxy solid. R_f = 0.10 (free amine, DCM:MeOH 9:1). ^{1}H NMR (400 MHz, DMSO-d_6): δ 0.84-0.87 (m, 6H), 1.19-1.29 (s, 46H), 1.34-1.43 (m, 2H), 1.46-1.56 (m, 2H), 2.11-2.20 (m, 2H), 2.96-3.16 (m, 2H), 3.36-4.67 (m, 4H), 8.00-8.23 (m, 4NH), 10.57 (s, 1NH) ppm. t'$_\mathbf{R}$ = 35.93 min (%2-propanol = 83.90%). HPLC purity: 98.2%. LCMS: *m/z* = 581.6 $[M\text{-}Cl]^+$, 603.5 $[M\text{-}HCl+Na]^+$. Elemental analysis: Anal. Calcd for $C_{34}H_{69}ClN_4O_3$: C, 66.14; H, 11.27; N, 9.07. Found: C, 66.06; H, 11.25; N, 9.08.

2-oxo-2-(1-(2-oxo-2-(propylamino)ethyl)-2-stearoylhydrazinyl)ethanaminium chloride, $C_{17}H_{35}$CO-HydrGly-NHC_3H_7 · HCl, (4Ea).

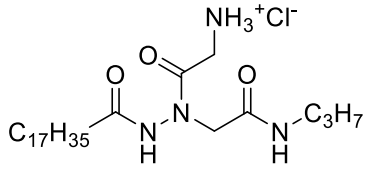

Starting from **3Ea** (81.3 μmol, 45.1 mg) and following the general procedure, compound **4Ea** was obtained in 96% yield (77.0 μmol, 37.8 mg) as a white waxy solid. R_f = 0.1 (free amine, DCM:MeOH 9:1). ^{1}H NMR (400 MHz, DMSO-d_6): δ 0.82-0.87 (m, 6H), 1.23 (s, 28H), 1.37-1.46 (m, 2H), 1.46-1.57 (m, 2H), 2.11-2.19 (m, 2H), 3.04 (q, *J* = 6.3 Hz, 2H), 3.39-4.68 (m, 4H), 8.01-8.26 (m, 4NH), 10.59 (s, 1NH) ppm. t'$_\mathbf{R}$ = 26.49 min (%2-propanol = 69.74%). HPLC purity: 95.8%. LCMS: *m/z* = 455.4 $[M\text{-}Cl]^+$, 477.4 $[M\text{-}HCl+Na]^+$. Elemental analysis: Anal. Calcd for $C_{25}H_{51}ClN_4O_3$: C, 61.14; H, 10.47; N, 11.41. Found: C, 60.94; H, 10.46; N, 11.37.

2-(1-(2-(Octylamino)-2-oxoethyl)-2-stearoylhydrazinyl)-2-oxoethan-1-aminium chloride, $C_{17}H_{35}$CO-HydrGly-NHC_8H_{17} · HCl, (4Eb).

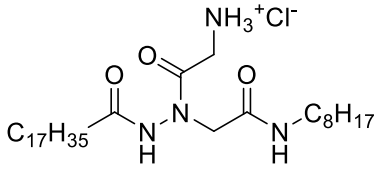

Starting from **3Eb** (81.9 μmol, 51.2 mg) and following the general procedure, compound **4Eb** was obtained in 80% yield (65.9 μmol, 37.0 mg) as a white waxy solid. R_f = 0.35 (free amine, DCM:MeOH 9:1). ^{1}H NMR (400 MHz, DMSO-*d*$_6$): δ 0.83-0.87 (m, 6H), 1.23 (s, 38H), 1.33-1.43 (m, 2H), 1.45-1.56 (m, 2H), 2.11-2.19 (m, 2H), 2.96-3.14 (m, 2H), 3.40-4.62 (m, 4H), 8.00-8.26 (m, 4NH), 10.61 (s, 1NH) ppm. t'$_R$ = 32.24 min (%2-propanol = 78.36%). HPLC purity: 96.3%. LCMS: *m/z* = 525.5 $[M\text{-}Cl]^+$, 547.4 $[M\text{-}HCl+Na]^+$. Elemental analysis: Anal. Calcd for $C_{30}H_{61}ClN_4O_3$: C, 64.20; H, 10.95; N, 9.98. Found: C, 64.44; H, 10.93; N, 9.96.

2-(1-(2-(Dodecylamino)-2-oxoethyl)-2-stearoylhydrazinyl)-2-oxoethanamium chloride, $C_{17}H_{35}$CO-HydrGly-NH$C_{12}H_{25}$ · HCl, (4Ec).

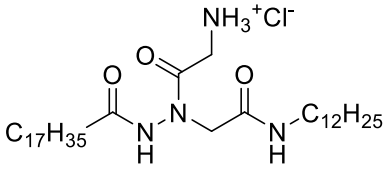

Starting from **3Ec** (44.0 μmol, 30.0 mg) and following the general procedure, compound **4Ec** was obtained in 85% yield (37.3 μmol, 23.0 mg) as a colorless pitchy compound. R_f = 0.09 (free amine, DCM:MeOH 95:5). ^{1}H NMR (400 MHz, DMSO-*d*$_6$): δ 0.83-0.87 (m, 6H), 1.23 (s, 46H), 1.33-1.43 (m, 2H), 1.45-1.56 (m, 2H), 2.11-2.19 (m, 2H), 2.93-3.19 (m, 2H), 3.41-4.67 (m, 4H), 7.99-8.26 (m, 4NH), 10.60 (s, 1NH) ppm. t'$_R$ = 35.81 min (%2-propanol = 83.72%). HPLC purity: 99.5%. LCMS: *m/z* = 581.5 $[M\text{-}Cl]^+$, 603.5 $[M\text{-}HCl+Na]^+$. Elemental analysis: Anal. Calcd for $C_{34}H_{69}ClN_4O_3$: C, 66.14; H, 11.27; N, 9.07. Found: C, 66.25; H, 11.24; N, 9.04.

2-(1-(2-(Octadecylamino)-2-oxoethyl)-2-stearoylhydrazinyl)-2-oxoethan-1-aminium, $C_{17}H_{35}$CO-HydrGly-NH$C_{18}H_{37}$ · HCl, (4Ed).

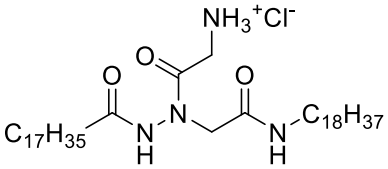

Starting from **3Ed** (141 μmol, 108 mg) and following the general procedure, compound **4Ed** was obtained in 82% yield (116 μmol, 81.4 mg) as a white waxy solid. R_f = 0.40 (free amine, DCM:MeOH 9:1). ^{1}H NMR (400 MHz, DMSO-*d*$_6$): δ 0.84 (s, 6H), 1.10-1.53 (m, 62H), 2.08-2.22 (m, 2H), 2.92-3.24 (m, 2H), 3.42-4.66 (m, 4H), 7.97-8.26 (m, 4NH), 10.58 (s, 1NH) ppm.

t'$_{\mathbf{R}}$ = 41.78 min (%2-propanol = 92.67%). HPLC purity: 98.5%. LCMS: *m/z* = 665.6 $[M\text{-}Cl]^+$, 687.6 $[M\text{-}HCl+Na]^+$. Elemental analysis: Anal. Calcd for $C_{40}H_{81}ClN_4O_3$: C, 68.48; H, 11.64; N, 7.99. Found: C, 68.43; H, 11.67; N, 8.02.

2-(2-Benzoyl-1-(2-(octylamino)-2-oxoethyl)hydrazinyl)-2-oxoethan-1-aminium chloride, PhCO-HydrGly-NHC$_8$H$_{17}$ · HCl, (4Fb).

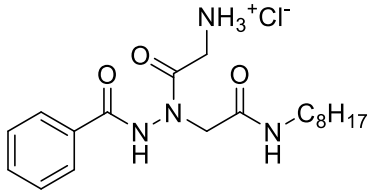

Starting from **3Fb** (183 μmol, 84.7 mg) and following the general procedure, compound **4Fb** was obtained in 97% yield (178 μmol, 71.0 mg) as a colorless waxy solid. R_f = 0.12 (free amine, DCM:MeOH 9:1). ^{1}H NMR (400 MHz, DMSO-d_6): δ 0.84 (t, *J* = 6.8 Hz, 3H), 1.16-1.28 (m, 10H), 1.33-1.43 (m, 2H), 3.00-3.14 (m, 2H), 3.25-4.70 (m, 4H), 7.50-7.55 (m, 2ArH), 7.62-7.66 (m, 1ArH), 7.87-7.92 (m, 2ArH), 8.04-8.26 (m, 4NH), 11.19 (s, 1NH) ppm. t'$_{\mathbf{R}}$ = 12.27 min (%2-propanol = 48.41%). HPLC purity: 100%. LCMS: *m/z* = 363.2 $[M\text{-}Cl]^+$, 385.2 $[M\text{-}HCl+Na]^+$. Elemental analysis: Anal. Calcd for $C_{19}H_{31}ClN_4O_3$: C, 57.20; H, 7.83; N, 14.04. Found: C, 57.24; H, 7.85; N, 14.00.

2-(2-Benzoyl-1-(2-(dodecylamino)-2-oxoethyl)hydrazinyl)-2-oxoethan-1-aminium chloride, PhCO-HydrGly-NHC$_{12}$H$_{25}$ · HCl, (4Fc).

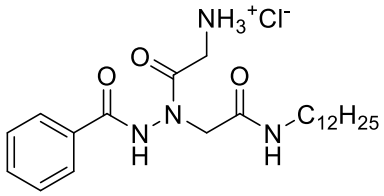

Starting from **3Fc** (183 μmol, 94.9 mg) and following the general procedure, compound **4Fc** was obtained in 89% yield (163 μmol, 74.2 mg) as a colorless waxy solid. R_f = 0.12 (free amine, DCM:MeOH 9:1). ^{1}H NMR (400 MHz, DMSO-d_6): δ 0.85 (t, *J* = 6.8 Hz, 3H), 1.15-1.29 (m, 18H), 1.33-1.43 (m, 2H), 3.00-3.14 (m, 2H), 3.47-4.87 (m, 4H), 7.48-7.55 (m, 2ArH), 7.60-7.66 (m, 1ArH), 7.87-7.92 (m, 2ArH), 8.06-8.27 (m, 4NH), 11.2 (s, 1NH) ppm. t'$_{\mathbf{R}}$ = 19.70 min (%2-propanol = 59.55%). HPLC purity: 98.9%. LCMS: *m/z* = 419.3 $[M\text{-}Cl]^+$, 441.3 $[M\text{-}HCl+Na]^+$. Elemental analysis: Anal. Calcd for $C_{23}H_{39}ClN_4O_3$: C, 60.71; H, 8.64; N, 12.31. Found: C, 60.70; H, 8.61; N, 12.36.

2-(1-(2-(Octylamino)-2-oxoethyl)-2-pivaloylhydrazinyl)-2-oxoethan-1-aminium chloride, *t*-BuCO-HydrGly-NHC$_8$H$_{17}$ · HCl, (4Gb).

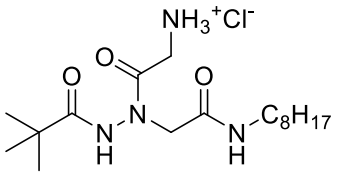

Starting from **3Gb** (255 μmol, 113 mg) and following the general procedure, compound **4Gb** was obtained in 96% yield (245 μmol, 92.9 mg) as a colorless pitchy compound. R_f = 0.49 (free amine, DCM:MeOH 8:2). ^{1}H NMR (400 MHz, DMSO-d_6): δ 0.85 (t, J = 6.8 Hz, 3H), 1.15 (s, 9H), 1.19-1.29 (m, 10H), 1.33-1.43 (m, 2H), 3.00 (bs, 1H), 3.11 (bs, 1H), 3.37-3.50 (m, 1H), 3.60-3.75 (m, 1H), 3.82-3.98 (m, 1H), 4.41-4.56 (m, 1H), 8.02-8.28 (m, 4NH), 10.37 (s, 1NH) ppm. t'$_R$ = 11.69 min (%2-propanol = 47.54%). HPLC purity: 98.1%. LCMS: m/z = 343.3 [M-Cl]$^+$, 365.3 [M-HCl+Na]$^+$. Elemental analysis: Anal. Calcd for $C_{17}H_{35}ClN_4O_3$: C, 53.88; H, 9.31; N, 14.79. Found: C, 53.93; H, 9.30; N, 14.83.

2-(1-(2-(Dodecylamino)-2-oxoethyl)-2-pivaloylhydrazinyl)-2-oxoethan-1-aminium chloride, *t*-BuCO-HydrGly-NHC$_{12}$H$_{25}$ · HCl, (4Gc).

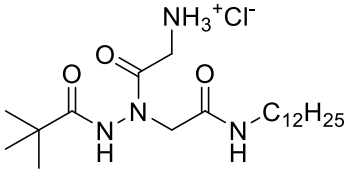

Starting from **3Gb** (222 μmol, 111 mg) and following the general procedure, compound **4Gc** was obtained in 94% yield (208 μmol, 90.5 mg) as a colorless waxy solid. R_f = 0.07 (free amine, DCM:MeOH 9:1). ^{1}H NMR (400 MHz, DMSO-d_6): δ 0.85 (t, J = 6.8 Hz, 3H), 1.15 (s, 9H), 1.19-1.30 (m, 18H), 1.33-1.43 (m, 2H), 2.92-3.19 (m, 2H), 3.37-3.51 (m, 1H), 3.61-3.73 (m, 1H), 3.82-3.95 (m, 1H), 4.42-4.54 (m, 1H), 8.00-8.27 (m, 4NH), 10.35 (s, 1NH) ppm. t'$_R$ = 19.77 min (%2-propanol = 59.66%). HPLC purity: 98.9%. LCMS: m/z = 399.3 [M-Cl]$^+$, 421.3 [M-HCl+Na]$^+$. Elemental analysis: Anal. Calcd for $C_{21}H_{43}ClN_4O_3$: C, 57.98; H, 9.96; N, 12.88. Found: C, 58.04; H, 9.98; N, 12.90.

2-(2-(1-Naphtoyl)-1-(2-(octylamino)-2-oxoethyl)hydrazinyl)-2-oxoethan-1-aminium chloride, 1-NaphtylCO-HydrGly-NHC$_8$H$_{17}$ · HCl, (4Hb).

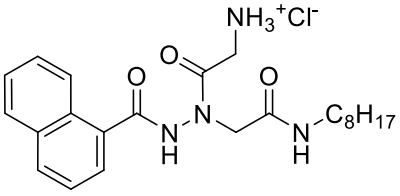

Starting from **3Hb** (246 μmol, 126 mg) and following the general procedure, compound **4Hb** was obtained in 88% yield (216 μmol, 96.8 mg) as a colorless pitchy compound. R_f = 0.48 (free amine, DCM:MeOH 8:2). ^{1}H NMR (400 MHz, DMSO-d_6): δ 0.88 (t, J = 6.8 Hz, 3H), 1.17-1.34 (m, 10H), 1.39-1.48 (m, 2H), 3.00-3.25 (m, 2H), 3.78-4.91 (m, 4H), 7.58-7.67 (m, 3ArH), 7.78-7.80 (m, 1ArH), 8.03-8.08 (m, 1ArH), 8.15-8.21 (m, 4NH), 8.22-8.38 (m, 2ArH), 11.30 (s, 1NH) ppm. t'$_R$ = 14.37 min (%2-propanol = 51.56%). HPLC purity: 98.0%. LCMS: *m/z* = 413.3 $[M\text{-}Cl]^+$, 435.2 $[M\text{-}HCl+Na]^+$. Elemental analysis: Anal. Calcd for $C_{23}H_{33}ClN_4O_3$: C, 61.53; H, 7.41; N, 12.48. Found: C, 61.48; H, 7.39; N, 12.47.

2-(2-(1-Naphtoyl)-1-(2-(dodecylamino)-2-oxoethyl)hydrazinyl)-2-oxoethan-1-aminium chloride, 1-NaphtylCO-HydrGly-NHC$_{12}$H$_{25}$ · HCl, (4Hc).

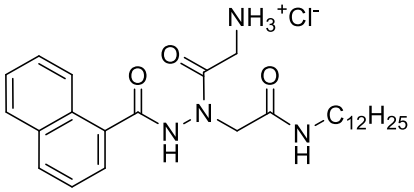

Starting from **3Hc** (190 μmol, 108 mg) and following the general procedure, compound **4Hc** was obtained in 79% yield (150 μmol, 75.8 mg) as a colorless pitchy compound. R_f = 0.37 (free amine, DCM:MeOH 8:2). ^{1}H NMR (400 MHz, DMSO-d_6): δ 0.84 (t, J = 6.8 Hz, 3H), 1.19-1.27 (m, 18H), 1.36-1.45 (m, 2H), 2.98-3.20 (m, 2H), 3.79-4.85 (m, 4H), 7.55-7.63 (m, 3ArH), 7.75-7.77 (m, 1ArH), 7.99-8.05 (m, 1ArH), 8.12-8.19 (m, 4NH), 8.21-8.34 (m, 2ArH), 11.27 (s, 1NH) ppm. t'$_R$ = 21.60 min (%2-propanol = 62.40%). HPLC purity: 98.8%. LCMS: *m/z* = 469.3 $[M\text{-}Cl]^+$, 491.3 $[M\text{-}HCl+Na]^+$. Elemental analysis: Anal. Calcd for $C_{27}H_{41}ClN_4O_3$: C, 64.20; H, 8.18; N, 11.09. Found: C, 64.29; H, 8.21; N, 11.05.

General Procedure For The Synthesis Of Compounds 5Ab And 5Ac.

Note: representative procedure referred to 1 mmol of starting compound.

To a solution of compound **3Ab** or **3Ac** dissolved in dry THF (5 mL) under inert atmosphere at 0 °C, LHMDS 1.0 M in THF (1.01 mL, 1.01 mmol) and CH_3I (65.4 μL, 1.05 mmol) were sequentially added. The mixture was stirred at 0 °C for 10 min and subsequently at room

temperature for 2 h, then HCl 1 M (1.05 mL) was added. The volatile species were removed under vacuum at room temperature. The residue was diluted with AcOEt (50 mL) and water (20 mL), then the phases were separated and the organic layer was washed with additional water (5 mL). The aqueous phases were newly extracted with 50 mL di AcOEt, then the second organic phase was washed with 5 mL water. The combined organic phases were dried over anhydrous Na_2SO_4, the solvent was evaporated under vacuum and the residue was purified by flash chromatography on silica gel (DCM/MeOH mixtures as eluents), obtaining the pure compound.

Benzyl 2-(2-((*t*-butoxycarbonyl)glycyl)-1-methyl-2-(2-(octylamino)-2-oxoethyl)hydrazinecarboxylate, BnOCO-Hydr(Me)Gly-NHC$_8$H$_{17}$, (5Ab).

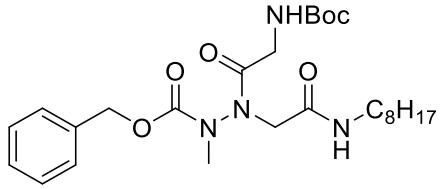

Starting from **2Ab** (3.00 mmol, 1.48 g) and following the general procedure, compound **5Ab** was obtained in 87% yield (2.61 mmol, 1.32 g) as a colorless pitchy compound. R_f = 0.33 (DCM:MeOH 95:5). ^{1}H NMR (400 MHz, $CDCl_3$): δ 0.87 (t, *J* = 6.6 Hz, 3H), 1.20-1.33 (m, 10H), 1.44 (s, 9H), 1.41-1.50 (m, 2H), 3.12-3.26 (m, 2H), 3.24 (s, 3H), 3.65-4.43 (m, 4H), 5.14-5.23 (m, 3H), 7.30-7.42 (m, 5ArH+1NH) ppm. ^{13}C NMR (100 MHz, $CDCl_3$): δ 14.2, 22.7, 27.0, 28.4, 29.3, 31.9, 36.6, 39.7, 41.8, 51.8, 69.4, 80.1, 128.4, 128.9, 135.0, 155.9, 167.1, 171.5 ppm. LCMS: *m/z* = 507.3 $[M+H]^+$, 529.3 $[M+Na]^+$.

Benzyl 2-(2-((*t*-butoxycarbonyl)glycyl)-2-(2-(dodecylamino)-2-oxoethyl)-1-methylhydrazinecarboxilate, BnOCO-Hydr(Me)Gly-NHC$_{12}$H$_{25}$, (5Ac).

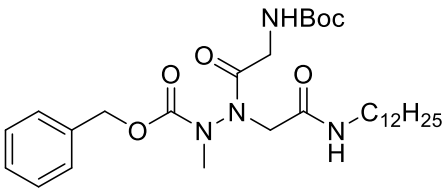

Starting from **2Ac** (3.01 mmol, 1.65 g) and following the general procedure, compound **5Ac** was obtained in 90% yield (2.72 mmol, 1.53 g) as a white amorphous solid. R_f = 0.12 (cyclohexane:AcOEt 1:1). m.p. = 74-76 °C. ^{1}H NMR (400 MHz, $CDCl_3$): δ 0.87 (t, *J* = 6.6 Hz, 3H), 1.18-1.34 (m, 18H), 1.44 (s, 11H), 3.11-3.29 (m, 2H), 3.24 (s, 3H), 3.68-4.39 (m, 4H), 5.14-5.23 (m, 3H), 7.28-7.47 (m, 5ArH+1NH) ppm. ^{13}C NMR (100 MHz, $CDCl_3$): δ 14.2, 22.7,

26.9, 28.4, 29.3, 29.4, 29.63, 29.67, 29.69, 29.71, 32.0, 36.5, 39.7, 41.8, 51.7, 69.4, 80.0, 128.3, 128.8, 135.0, 155.9, 167.0, 171.5 ppm. LCMS: *m/z* = 563.4 $[M+H]^+$, 585.3 $[M+Na]^+$.

General Procedure For The Synthesis Of Compounds 5Bb, 5Bc, 5Gb, And 5Gc.

Note: representative procedure referred to 1 mmol of starting compound.

To a solution of compound **5Ab** or **5Ac** dissolved in dry DCM (2 mL) under inert atmosphere at room temperature, Pd/C (100 mg) and formic acid (76 µL, 2 mmol) were sequentially added and the mixture was stirred for 1 hour. The volatile species were removed under vacuum at room temperature, then DCM (20 mL) was added and the reaction mixture was filtered through Celite, washing with DCM (3 × 10 mL). The organic phase was washed with a saturated solution of Na_2CO_3 (5 mL), then the aqueous phase was newly extracted with DCM (25 mL) and, after separation, the second organic phase was washed with a saturated solution of Na_2CO_3 (5 mL). The combined organic phases were dried over anhydrous Na_2SO_4, the solvent was evaporated under vacuum at room temperature and the free hydrazide intermediate was directly submitted to the following acylation reaction or stored at -18 °C. To a solution of the suitable free hydrazide intermediate in dry DCM (5 mL) under inert atmosphere at room temperature, pyridine (121 µL, 1.5 mmol, for the synthesis of **5Bb** and **5Bc**; 145 µL, 1.8 mmol, for the synthesis of **5Gb** and **5Gc**) was added, followed by dropwise addition of the suitable acyl chloride (acetyl chloride, 78.5 µL, 1.1 mmol, for the synthesis of **5Bb** and **5Bc**; pivaloyl chloride, 185 µL, 1.5 mmol, for the synthesis of **5Gb** and **5Gc**). The solution was stirred at room temperature for 1 h (**5Bb** and **5Bc**) or 20 h (**5Gb** and **5Gc**), then all the volatile species were removed in vacuo at room temperature and the residue was diluted with AcOEt (30 mL) and water (5 mL). After separation, the organic phase was washed with HCl 1 M (2 × 3 mL), saturated aqueous sodium carbonate (5 mL) and water (5 mL). The aqueous phases were sequentially extracted with additional 30 mL of ethyl acetate, then the second organic phase was washed with HCl 1 M (2 × 3 mL), saturated aqueous sodium carbonate (5 mL) and water (5 mL). The combined organic phases were dried over anhydrous sodium sulfate and evaporated under vacuum, then the crude product was purified by column chromatography on silica gel (cyclohexane/AcOEt mixtures as eluents), to give the pure compound.

***t*-Butyl (2-(2-acetyl-2-methyl-1-(2-(octilamino)-2-oxoethyl)hydrazinyl)-2-oxoethyl)carbamate, CH_3CO-Hydr(Me)Gly-NHC_8H_{17}, (5Bb).**

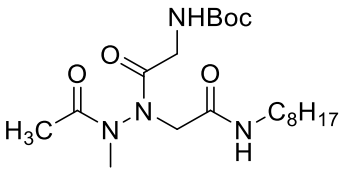

Starting from **5Ab** (505 μmol, 256 mg) and following the general procedure, compound **5Bb** was obtained in 87% yield (439 μmol, 182 mg) as a colorless pitchy compound. R_f = 0.10 (cyclohexane:AcOEt 2:8). ^{1}H NMR (400 MHz, $CDCl_3$, three conformers in a 64:28:8 ratio): δ 0.85-0.88 (m, 3H), 1.19-1.34 (m, 10H), 1.43 (s, 9H), 1.45-1.55 (m, 2H), 2.08 (s, 3H, 28%), 2.19 (s, 3H, 64%+8%), 3.17-3.24 (m, 2H + 3H, 28%+8%), 3.35 (s, 3H, 64%), 3.68 (dd, *J* = 3.5 Hz, 17.6 Hz, 1H, 64%+8%), 3.73 (d, *J* = 15.6 Hz, 1H, 28%), 3.85 (d, *J* = 16.8 Hz, 1H, 64%), 3.89-3.94 (m, 1H, 8%, + 2H, 28%), 4.05 (dd, *J* = 6.2 Hz, 17.6 Hz, 1H, 64%+8%), 4.25 (d, *J* = 18.0 Hz, 1H, 8%), 4.31 (d, *J* = 16.8 Hz, 1H, 64%), 4.48 (d, *J* = 15.6 Hz, 1H, 28%), 5.19 (bs, 1NH, 28%), 5.23 (bs, 1NH, 64%+8%), 6.28 (bs, 1NH, 28%), 7.63 (bs, 1NH, 64%), 8.73 (bs, 1NH, 8%) ppm. ^{13}C NMR (100 MHz, $CDCl_3$, three conformers in a 64:28:8 ratio, only the major conformer is given): δ 14.1, 21.6, 22.7, 26.9, 28.4, 29.2, 31.8, 38.1, 39.7, 41.6, 51.7, 80.1, 155.9, 167.1, 170.7, 171.0 ppm. LCMS: *m/z* = 415.3 $[M+H]^+$, 437.3 $[M+Na]^+$.

***t*-Butyl (2-(2-acetyl-1-(2-(dodecylamino)-2-oxoethyl)-2-methylhydrazinyl)-2-oxoethyl)carbamate, CH_3CO-Hydr(Me)Gly-$NHC_{12}H_{25}$, (5Bc).**

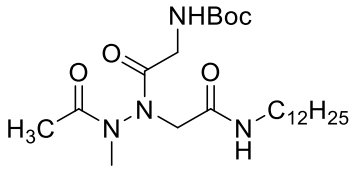

Starting from **5Ac** (547 μmol, 308 mg) and following the general procedure, compound **5Bc** was obtained in 86% yield (470 μmol, 221 mg) as a colorless pitchy compound. R_f = 0.29 (AcOEt). ^{1}H NMR (400 MHz, $CDCl_3$, three conformers in a 62:31:7 ratio): δ 0.87 (t, *J* = 6.8 Hz, 3H), 1.20-1.35 (m, 18H), 1.44 (s, 9H), 1.45-1.55 (m, 2H), 2.09 (s, 3H, 31%), 2.20 (s, 3H, 62%+7%), 3.17-3.24 (m, 2H + 3H, 31%+7%), 3.35 (s, 3H, 62%), 3.66-3.75 (m, 1H, 62%+7%, + 1H, 31%), 3.85 (d, *J* = 16.8 Hz, 1H, 62%), 3.87-3.94 (m, 1H, 7%, + 2H, 31%), 4.05 (dd, *J* = 4.6 Hz, 17.6 Hz, 1H, 62%+7%), 4.25 (d, *J* = 18.0 Hz, 1H, 7%), 4.33 (d, *J* = 16.8 Hz, 1H, 62%), 4.48 (d, *J* = 15.2 Hz, 1H, 31%), 5.17 (bs, 1NH, 31%), 5.21 (bs, 1NH, 62%+7%), 6.23 (bs, 1NH, 31%), 7.65 (bs, 1NH, 62%), 8.74 (bs, 1NH, 7%) ppm. ^{13}C NMR (100 MHz, $CDCl_3$, three conformers in a 62:31:7 ratio, only the major conformer is given): δ 14.2, 21.6, 22.8, 27.0, 28.4, 29.3, 29.4, 29.5, 29.66, 29.70, 29.75, 32.0, 38.2, 39.8, 41.6, 51.7, 80.2, 156.0, 167.1, 170.9, 170.9 ppm. LCMS: *m/z* = 471.4 $[M+H]^+$, 493.3 $[M+Na]^+$.

***t*-Butyl (2-(2-methyl-1-(2-(octylamino)-2-oxoethyl)-2-pivaloylhydrazinyl)-2-oxoethyl)carbamate, *t*BuCO-Hydr(Me)Gly-NHC$_8$H$_{17}$, (5Gb).**

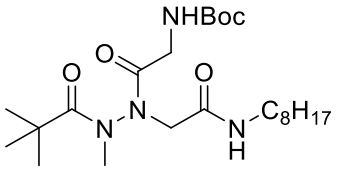

Starting from **5Ab** (419 μmol, 212 mg) and following the general procedure, compound **5Gb** was obtained in 81% yield (339 μmol, 155 mg) as a colorless pitchy compound. R_f = 0.12 (cyclohexane:AcOEt 2:8). ^{1}H NMR (400 MHz, $CDCl_3$, two conformers in a 90:10 ratio, all the assignable signals are given): δ 0.84-0.87 (m, 3H), 1.17-1.30 (m, 10H), 1.31 (s, 9H), 1.42 (s, 9H), 1.44-1.52 (m, 2H), 3.12-3.26 (m, 2H), 3.30 (s, 3H, 10%), 3.45 (s, 3H, 90%), 3.57 (dd, *J* = 3.5 Hz, 17.6 Hz, 1H), 3.95 (d, *J* = 16.8 Hz, 1H), 4.00 (dd, *J* = 6.3 Hz, 17.6 Hz, 1H), 4.16 (d, *J* = 16.8 Hz, 1H), 4.99 (bs, 1NH, 10%), 5.23 (bs, 1NH, 90%), 7.56 (bs, 1NH, 90%), 8.73 (bs, 1NH, 10%) ppm. ^{13}C NMR (100 MHz, $CDCl_3$, two conformers in a 90:10 ratio, only the major conformer is given): δ 14.2, 22.7, 27.0, 27.5, 28.4, 29.34, 29.36, 31.9, 38.7, 39.7, 41.5, 52.2, 80.1, 156.0, 167.3, 171.1, 178.0 ppm. LCMS: *m/z* = 457.3 $[M+H]^+$, 479.3 $[M+Na]^+$.

***t*-Butyl (2-(1-(2-(dodecylamino)-2-oxoethyl)-2-methyl-2-pivaloylhydrazinyl)-2-oxoethyl)carbamate, *t*BuCO-Hydr(Me)Gly-NHC$_{12}$H$_{25}$, (5Gc).**

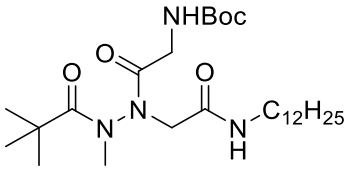

Starting from **5Ac** (604 μmol, 340 mg) and following the general procedure, compound **5Gc** was obtained in 92% yield (550 μmol, 282 mg) as a colorless pitchy compound. R_f = 0.50 (AcOEt). ^{1}H NMR (400 MHz, $CDCl_3$): δ 0.87 (t, *J* = 6.8 Hz, 3H), 1.19-1.29 (m, 18H), 1.33 (s, 9H), 1.43 (s, 9H), 1.44-1.54 (m, 2H), 3.13-3.29 (m, 2H), 3.46 (s, 3H), 3.58 (dd, *J* = 3.1 Hz, 17.6 Hz, 1H), 3.95 (d, *J* = 16.4 Hz, 1H), 4.02 (dd, *J* = 6.0 Hz, 17.6 Hz, 1H), 4.19 (d, *J* = 16.4 Hz, 1H), 5.21 (bs, 1NH), 7.54 (bs, 1NH) ppm. ^{13}C NMR (100 MHz, $CDCl_3$): δ 14.3, 22.8, 27.0, 27.56, 27.61, 28.5, 29.40, 29.45, 29.49, 29.7, 29.8, 32.1, 38.7, 39.7, 41.5, 52.2, 80.3, 156.0, 167.3, 171.1, 177.9 ppm. LCMS: *m/z* = 513.4 $[M+H]^+$, 535.4 $[M+Na]^+$.

General Procedure For The Synthesis Of N-methyl Hydrazide Hydrochlorides 6.

*The procedure is the same previously reported for the synthesis of hydrochlorides **4**.*

2-(2-((Benzyloxy)carbonyl)-2-methyl-1-(2-(octilamino)-2-oxoethyl)hydrazinyl)-2-oxoethanaminium chloride, BnOCO-Hydr(Me)Gly-NHC$_8$H$_{17}$ · HCl, (6Ab).

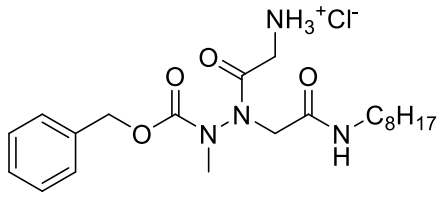

Starting from **5Ab** (201 μmol, 102 mg) and following the general procedure, compound **6Ab** was obtained in 82% yield (165 μmol, 73.1 mg) as a colorless pitchy compound. R_f = 0.13 (free amine, DCM:MeOH 95:5). ^{1}H NMR (400 MHz, DMSO-*d*$_6$, mixture of conformers): δ 0.85 (t, *J* = 7.0 Hz, 3H), 1.24 (s, 10H), 1.32-1.46 (m, 2H), 3.02-3.15 (m, 2H), 3.21 (s, 3H), 3.48-3.73 (m, 1H), 3.78-4.15 (m, 2H), 4.40-4.52 (m, 1H), 5.00-5.26 (m, 2H), 7.27-7.43 (m, 5ArH), 8.05 (t, *J* = 5.5 Hz, 1NH), 8.10-8.33 (m, 4NH) ppm. t'$_R$ = 13.77 min (%2-propanol = 50.66%). HPLC purity: 96.4%. LCMS: *m/z* = 407.3 [M-Cl]$^+$, 429.2 [M-HCl+Na]$^+$. Elemental analysis: Anal. Calcd for $C_{21}H_{35}ClN_4O_4$: C, 56.94; H, 7.96; N, 12.65. Found: C, 57.02; H, 7.99; N, 12.64.

2-(2-((Benzyloxy)carbonyl)-1-(2-(dodecylamino)-2-oxoethyl)-2-methylhydrazinyl)-2-oxoethanaminium chloride, BnOCO-HydrGly(Me)-NH-C$_{12}$H$_{25}$ · HCl, (6Ac).

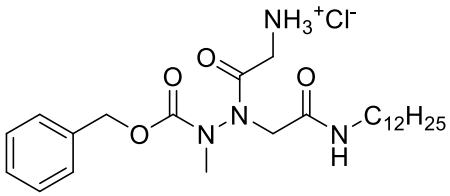

Starting from **5Ac** (200 μmol, 112.8 mg) and following the general procedure, compound **6Ac** was obtained in 97% yield (194 μmol, 96.7 mg) as a colorless waxy solid. R_f = 0.72 (free amine, DCM:MeOH 8:2). ^{1}H NMR (400 MHz, DMSO-*d*$_6$, mixture of conformers): δ 0.85 (t, *J* = 7.0 Hz, 3H), 1.23 (s, 18H), 1.32-1.44 (m, 2H), 2.98-3.15 (m, 2H), 3.21 (s, 3H), 3.48-3.74 (m, 1H), 3.83-4.13 (m, 2H), 4.43-4.52 (m, 1H), 5.00-5.20 (m, 2H), 7.30-7.41 (m, 5ArH), 8.04 (t, *J* = 5.5 Hz, 1NH), 8.08-8.30 (m, 4NH) ppm. t'$_R$ = 20.66 min (%2-propanol = 60.99%). HPLC purity: 99.4%. LCMS: *m/z* = 463.3 [M-Cl]$^+$, 485.3 [M-HCl+Na]$^+$. Elemental analysis: Anal. Calcd for $C_{25}H_{43}ClN_4O_4$: C, 60.16; H, 8.68; N, 11.23. Found: C, 60.11; H, 8.69; N, 11.25.

2-(2-Acetyl-2-methyl-1-(2-(octylamino)-2-oxoethyl)hydrazinyl)-2-oxoethanaminium chloride, CH$_3$CO-HydrGly(Me)-NHC$_8$H$_{17}$ · HCl, (6Bb).

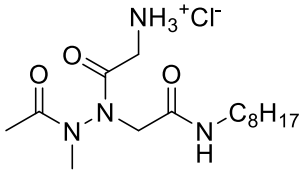

Starting from **5Bb** (80.1 μmol, 33.2 mg) and following the general procedure, compound **6Bb** was obtained in 75% yield (60.4 μmol, 21.1 mg) as a colorless pitchy compound. R_f = 0.16 (free amine, DCM:MeOH 9:1). ^{1}H NMR (400 MHz, DMSO-*d*$_6$, mixture of 3 major conformers in about 1:1:1 ratio and a minor conformer): δ 0.86 (t, *J* = 6.8 Hz, 3H), 1.24 (s, 10H), 1.34-1.46 (m, 2H), 1.88 (s, 3H, major conf.), 2.02 (s, 3H, major conf.), 2.07 (s, 3H, minor conf.), 2.10 (s, 3H, major conf.), 2.90 (s, 3H, major conf.), 3.02-3.16 (m, 2H), 3.10 (s, 3H, major conf.), 3.16 (s, 3H, minor conf.), 3.31 (s, 3H, major conf.), 3.40-3.51 (m, 2H, major conf.), 3.70 (d, *J* = 16.4 Hz, 1H, major conf.), 3.74-3.94 (m, 1H+1H two major conf. and minor conf.), 4.00 (d, *J* = 16.0 Hz, 1H, major conf.), 4.12 (d, *J* = 17.2 Hz, 1H, major conf.+minor conf.), 4.41 (d, *J* = 16.4 Hz, 1H, major conf.), 4.42 (d, *J* = 16.0 Hz, 1H, major conf.), 4.49 (d, *J* = 17.2 Hz, 1H, major conf.), 8.05-8.39 (m, 4NH) ppm. t'$_R$ = 9.11 min (%2-propanol = 43.67%). HPLC purity: 98.6%. LCMS: *m/z* = 315.3 $[M\text{-}Cl]^+$, 337.2 $[M\text{-}HCl+Na]^+$. Elemental analysis: Anal. Calcd for $C_{15}H_{31}ClN_4O_3$: C, 51.35; H, 8.91; N, 15.97. Found: C, 51.49; H, 8.88; N, 15.94.

2-(2-Acetyl-1-(2-(dodecylamino)-2-oxoethyl)-2-methylhydrazinyl)-2-oxoethanaminium chloride, CH_3CO-HydrGly(Me)-$NHC_{12}H_{25}$ · HCl, (6Bc).

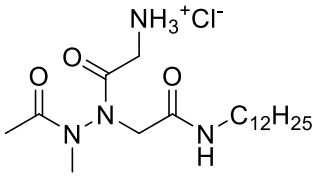

Starting from **5Bc** (83.1 μmol, 39.1 mg) and following the general procedure, compound **6Bc** was obtained in 78% yield (64.6 μmol, 26.3 mg) as a colorless pitchy compound. R_f = 0.42 (free amine, DCM:MeOH 8:2). ^{1}H NMR (400 MHz, DMSO-*d*$_6$, mixture of 3 major conformers in about 1:1:1 ratio and a minor conformer): δ 0.85 (t, *J* = 6.8 Hz, 3H), 1.24 (s, 18H), 1.33-1.44 (m, 2H), 1.88 (s, 3H, major conf.), 2.01 (s, 3H, major conf.), 2.07 (s, 3H, minor conf.), 2.10 (s, 3H, major conf.), 2.90 (s, 3H, major conf.), 3.01-3.15 (m, 2H), 3.10 (s, 3H, major conf.), 3.16 (s, 3H, minor conf.), 3.31 (s, 3H, major conf.), 3.70 (d, *J* = 16.4 Hz, 1H, major conf.), 3.74-3.95 (m, 1H+1H two major conf. and minor conf.), 4.00 (d, *J* = 16.0 Hz, 1H, major conf.), 4.11 (d, *J* = 17.2 Hz, 1H, major conf.+minor conf.), 4.41 (d, *J* = 16.4 Hz, 1H, major conf.), 4.42 (d, *J* = 16.0 Hz, 1H, major conf.), 4.48 (d, *J* = 17.2 Hz, 1H, major conf.), 8.03-8.34 (m, 4NH) ppm. t'$_R$ = 17.05 min (%2-propanol = 55.58%). HPLC purity: 97.4%. LCMS: *m/z* = 371.3 $[M\text{-}Cl]^+$, 393.3

[M-HCl+Na]$^+$. Elemental analysis: Anal. Calcd for $C_{19}H_{39}ClN_4O_3$: C, 56.07; H, 9.66; N, 13.77. Found: C, 56.02; H, 9.66; N, 13.82.

2-(2-Methyl-1-(2-(octylamino)-2-oxoethyl)-2-pivaloylhydrazinyl)-2-oxoethanaminium chloride, *t*-BuCO-HydrGly(Me)-NHC$_8$H$_{17}$ · HCl, (6Gb).

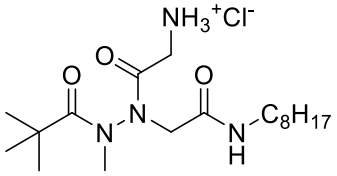

Starting from **5Gb** (180 μmol, 82.3 mg) and following the general procedure, compound **6Gb** was obtained in 98% yield (176 μmol, 69.2 mg) as a colorless pitchy compound. R_f = 0.40 (free amine, DCM:MeOH 8:2). ^{1}H NMR (400 MHz, DMSO-*d*$_6$, two conformers in about 7:3 ratio): δ 0.85 (t, *J* = 7.0 Hz, 3H), 1.12 (s, 9H, minor conf.), 1.23 (s, 9H, major conf.), 1.24 (s, 10H), 1.34-1.46 (m, 2H), 2.86-3.21 (m, 2H+2H, minor conformer), 3.39 (bs, 3H, minor conf.), 3.43 (s, 3H, major conf.), 3.66 (d, *J* = 16.4 Hz, 1H, major conf.), 3.88-4.13 (m, 2H, major conf., + 1H, minor conf.), 4.46 (d, *J* = 16.4 Hz, 1H, major conf.), 4.58-4.77 (m, 1H, minor conf.), 8.10 (t, *J* = 5.6 Hz, 3NH, minor conf.), 8.14 (bs, 3NH, major conf.), 8.28 (bs, 1NH, major conf.), 8.38 (t, *J* = 5.2 Hz, 1NH, minor conf.) ppm. t'$_R$ = 11.66 min (%2-propanol = 47.49%). HPLC purity: 95.3%. LCMS: *m/z* = 357.3 [M-Cl]$^+$, 379.3 [M-HCl+Na]$^+$. Elemental analysis: Anal. Calcd for $C_{18}H_{37}ClN_4O_3$: C, 55.02; H, 9.49; N, 14.26. Found: C, 55.10; H, 9.50; N, 14.26.

2-(1-(2-(Dodecylamino)-2-oxoethyl)-2-methyl-2-pivaloylhydrazinyl)-2-oxoethanaminium chloride, *t*-BuCO-HydrGly(Me)-NHC$_{12}$H$_{25}$ · HCl, (6Gc).

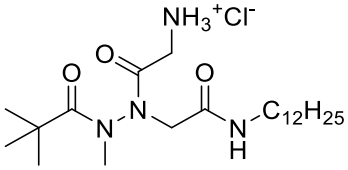

Starting from **5Gc** (185 μmol, 94.9 mg) and following the general procedure, compound **6Gc** was obtained in 98% yield (181 μmol, 81.4 mg) as a colorless waxy solid. R_f = 0.53 (free amine, DCM:MeOH 8:2). ^{1}H NMR (400 MHz, DMSO-*d*$_6$, two conformers in about 7:3 ratio): δ 0.85 (t, *J* = 7.0 Hz, 3H), 1.14 (s, 9H, minor conf.), 1.23 (s, 9H, major conf.), 1.24 (s, 18H), 1.34-1.45 (m, 2H), 2.98-3.21 (m, 2H+2H, minor conformer), 3.40 (bs, 3H, minor conf.), 3.43 (s, 3H, major conf.), 3.66 (d, *J* = 16.4 Hz, 1H, major conf.), 3.81-4.27 (m, 2H, major conf., + 1H, minor conf.), 4.46 (d, *J* = 16.4 Hz, 1H, major conf.), 4.57-4.71 (m, 1H, minor conf.), 8.09 (t, *J* = 5.2 Hz, 3NH), 8.24 (bs, 1NH, major conf.), 8.34-8.37 (m, 1NH, minor conf.) ppm. t'$_R$ = 18.93 min

(%2-propanol = 58.40%). HPLC purity: 98.8%. LCMS: *m/z* = 413.3 $[M\text{-}Cl]^+$, 435.4 $[M\text{-}HCl+Na]^+$. Elemental analysis: Anal. Calcd for $C_{22}H_{45}ClN_4O_3$: C, 58.84; H, 10.10; N, 12.48. Found: C, 58.78; H, 10.09; N, 12.53.

***N*-(2-(1-(2-(octylamino)-2-oxoethyl)hydrazinyl)-2-oxoethyl)octanamide, (transoctanoylated compound, 7)**

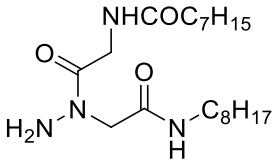

The free amine of compound **4Cb** (70.5 μmol, 27.1 mg), prepared as described in the general procedure for the synthesis of hydrochlorides, was dissolved in dry methanol (27 mL) and refluxed for 30 h. The solvent was evaporated under reduced pressure and the residue was purified by silica gel chromatography (DCM/MeOH) to give the pure compound **7** as a white amorphous solid in 62% yield (43.7 μmol, 16.8 mg).

R_f = 0.27 (DCM/MeOH = 9:1). m.p. = 140-142 °C. ^{1}H NMR (400 MHz, DMSO-d_6, two conformers in about 60:40 ratio): δ 0.84-0.87 (m, 6H), 1.24 (bs, 18H), 1.32-1.52 (m, 4H), 1.96-2.01 (m, 2H), 3.01-3.06 (m, 2H), 3.67 (d, J = 5.8 Hz, 2H), 7.79 (t, J = 5.4 Hz, 1NH, 60%), 8.09 (t, J = 5.6 Hz, 1NH, 40%), 8.20 (t, J = 5.8 Hz, 1NH) ppm. ^{13}C NMR (100 MHz, DMSO-d_6, two conformers in about 60:40 ratio, only the major conformer is given): δ 13.95, 13.97, 25.1, 26.4, 28.4, 28.5, 28.67, 28.74, 29.1, 31.2, 31.3, 33.4, 38.6, 41.9, 54.3, 168.4, 170.0, 171.7 ppm. LCMS: *m/z* = 385.3 $[M+H]^+$, 407.3 $[M+Na]^+$.

2.4.9 Computational investigation

Model ammonium cation mAc-HydrGlyH$^+$-NHMe

The most common approach to the theoretical investigation of the conformational behavior of peptides and their mimics, especially in a biological environment, is related to the use of a prolonged molecular dynamics (MD) simulation with a well parametrized molecular mechanics force field making use of reliable atomic charges. In the present case, the simulation should have been carried out on a system made of a large number of hydrazido acid hydrochlorides, immersed in a phospholipid bilayer and surrounded by water molecules. However, after the good-level preliminary density functional theory (DFT) investigation in water reported below, it has been readily evident that a molecular mechanics force field would not have been able to describe exactly the peculiar atomic arrangement of the hydrazide moiety, especially the large changes in pyramidalization of the N-terminal hydrazidic nitrogen as a function of the two

possible dispositions of the C=O belonging to the glycine side chain. This phenomenon was further emphasized by the results of the following high-level DFT calculations (see Figure 13). In fact, the best force fields available in GROMACS[104] (AMBER,[105] CHARMM,[106] and GROMOS[107]) were not able to give conformer geometries and energy differences sufficiently similar to those deriving from high-level DFT calculations in water, thus we preferred to avoid the usual approach based on a MD simulation.

All the calculations aimed to evaluate the inherent propensity to the formation of amphiphilic structure of the hydrochlorides under investigation were performed on a model ammonium cation (mAc-HydrGlyH$^+$-NHMe), and then on a limited subset of structures of an ammonium cation actually used in experiments (Octanoyl-HydrGlyH$^+$-NHOctyl), with the Gaussian 16 Revision B.01 suite of programs (Gaussian, Inc., Pittsburgh, PA, USA),[108] exploiting the following methodology:

1. Preliminary investigation: more than 50 different initial conformations of model ammonium cation mAc-HydrGlyH$^+$-NHMe were submitted to geometry optimization and frequency calculation using the Becke's three-parameter exchange functional in conjunction with the Lee-Yang-Parr correlation functional (B3LYP),[109,110] and the solvent bulk was described using the integral equation formalism version of polarizable continuum model method (IEF-PCM).[61] For all the atoms, the 6-311G+(2d,p) basis set was used. 26 different conformers were localized, whose Gibbs relative free energies and Boltzmann-weighted populations at equilibrium are reported in Table 5. A brief description of indicators used in structures' names is as follows (see Figure 13 for a better understanding):
   1.1. The "ap" and "sp" indicators refer, respectively, to the antiperiplanar and synperiplanar dispositions of glycine carbonyl with respect to N-N hydrazidic bond.
   1.2. "Cycle-X", where X is a number, indicates an X-membered hydrogen bonded pseudocycle between a generic H-bond donor and a generic H-bond acceptor. In the case of "Cycle-6" structures, the additional indicator "intraresidue" refers to the fact that both the H-bond donor and acceptor belong to the α-hydrazido acid residue, while in all the other cases one of them belongs to either the N- or C-terminal substituent.
   1.3. "Hydrazido-turn" refers to the bifurcated hydrogen bond in which the C-terminal amide NH is the H-bond donor and both the N-terminal CO and the hydrazidic N$^\alpha$ lone pair are the two H-bond acceptors, thus forming an 8-memberd pseudocycle with an enclosed 5-membered pseudocycle.[56]
   1.4. When the ammonium cation in the glycine moiety is in its most stable arrangement - that is with a hydrogen bond with the glycine carbonyl oxygen - no indicator is added

to the names, and the corresponding distances are not shown in Figure 13. On the contrary, when the NH_3^+ group is hydrogen bonded to other hydrogen bond acceptors, the corresponding indicators are added to conformers' names (e.g.: "ammonium_H-bonded-Ac" and "ammonium_H-bonded-CO" indicate that NH_3^+ is bonded, respectively, to the CO of the N-terminal acetyl group and to the CO of the hydrazido acid fragment) and the corresponding distances are reported in Figure 13.

1.5. "NO-H-bond" names are used for conformers in which there are no other hydrogen bonds except that between NH_3^+ and glycine carbonyl.

1.6. When different ordinal numbers are added to names (e.g.: Cycle-7_1 and Cycle-7_2, or NO-H-bond_sp_1 and NO-H-bond_sp_2), they indicate different conformers of the same type.

2. Refining: It has been often rigorously demonstrated, even recently,[111] that the popular B3LYP functional is almost always outperformed by many newer functionals when it is mandatory to properly take into account non-covalent interactions, especially inter- or intramolecular hydrogen bonding. Within this context, we decided to refine B3LYP geometries and energies with a well-performing hybrid functional with long-range dispersion corrections. We exploited the ωB97X-D3(0) functional,[60] using the new parameters for the DFT-D3(0) Grimme's dispersion correction with zero dumping,[112] which give improved accuracy with respect to the original DFT-D3(0) parameters,[113] with the very large 6-311++g(3df,3pd) basis set. Note 1: due to the fact that ωB97X-D3(0) functional is not directly available in Gaussian 16, the improved parameters for DFT-D3(0) empirical correction had to be added to ωB97X (s_6=1.0, $s_{r,6}$=1.281, and s_8=1.0)[112] using the keyword "empiricaldispersion(GD3)" and IOPs (iop(3/174=1000000,3/175=1000000,3/176=1281000) (see Gaussian 16 IOPs reference, overlay 3, http://gaussian.com/overlay3/). Note 2: when we tried to use the usual way to compute frequencies after the optimization ("opt freq" in link 0 section) with this functional and D3 parameters added with IOPs, the scf energy at the beginning of the frequency calculation was different from that at the end of optimization process. This was due to the fact that empirical dispersion correction was no more considered in the frequency calculation step, so leading to a wrong free energy, and the same thing did not happen with B3LYP functional and also in a single trial with DSD-PBEP86-D3(BJ) functional, where the D3 correction is built-in by default. Thus, it was necessary to circumvent this issue by putting the "freq" keyword in a separate link1 section. Below are reported examples of wrong and right ways to perform frequency calculations within this context.

Wrong:

%chk= Cycle-5_ap.chk
%mem=24GB
%nprocshared=6
# opt freq wB97X/6-311++g(3df,3pd) empiricaldispersion(GD3)
iop(3/174=1000000,3/175=1000000,3/176=1281000) scrf=(iefpcm,solvent=water)
nosymm geom=connectivity

Cycle-5_ap
1 1
(Geometry and connectivity sections)
……..

Right:

# opt wB97X/6-311++g(3df,3pd) empiricaldispersion(GD3)
iop(3/174=1000000,3/175=1000000,3/176=1281000) scrf=(iefpcm,solvent=water)
nosymm geom=connectivity

Cycle-5_ap
1 1
(Geometry and connectivity sections)
……..
--Link1--
%chk= Cycle-5_ap.chk
%mem=24GB
%nprocshared=6
freq wB97X/6-311++g(3df,3pd) empiricaldispersion(GD3)
iop(3/174=1000000,3/175=1000000,3/176=1281000) scrf=check
guess=tcheck geom=allcheck genchk nosymm test

3. The Boltzmann-weighted populations of conformers in solution were evaluated using free energy differences (Table 5), as previously reported.[114]

4. The Natural Bond Orbital (NBO)[115,63] and Atoms In Molecules (AIM)[116,65] analyses were carried out on the most important conformers, together with the calculation of atomic charges and electrostatic potential surfaces. Moreover, due to the fact that the performances of atomic charge calculation schemes vary depending on the system/task,[117,118,119,120,121,122] results from Merz-Singh-Kollman,[66,67] CHelpG,[68] and Hu-Lu-Yang[69] schemes were also reported for comparison.
5. Starting from the most stable conformer of model ammonium cation mAc-HydrGlyH$^+$-NHMe at ωB97X-D3(0)/6-311++G(3df,3pd)/PCM(water) level, 9 conformers of a representative actually used hydrochloride, Octanoyl-HydrGlyH$^+$-NHOctyl (compound **4Cb** in main text), were built adding the lipophilic chains in all the possible combinations in place of one of the three hydrogens in both N- and C-terminal methyl groups. For simplicity, the chains were always built with an all-antiperiplanar arrangement. After minimization at ωB97X-D3(0)/6-311+G(2d,p)/PCM(water) level, the NBO and AIM analyses and the calculation of electrostatic potential surfaces were also carried out, together with the computation of Merz-Singh-Kollman, CHelpG, and Hu-Lu-Yang charges.
6. Starting from the nine conformers lying within 3 kcal/mol from the global minimum at ωB97X-D3(0)/6-311++G(3df,3pd)/PCM(water) level of the model ammonium cation, the corresponding N-methylated structures (i.e. conformers of model ammonium cation mAc-Hydr(Me)GlyH$^+$-NHMe) were built and minimized at the same theory level. The results are reported in Figure 22 and Table 10. The NBO and AIM analysis and the calculation of electrostatic potential surfaces were also carried out.

Hydrazido-turn_ap

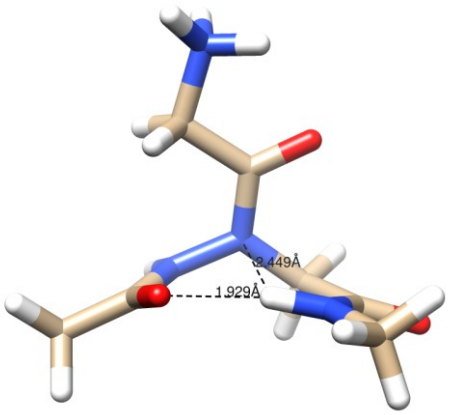

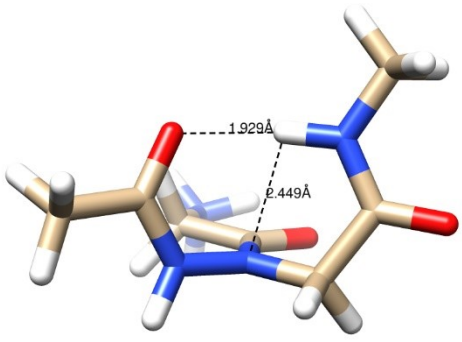

Cycle-6_intraresidue_ap

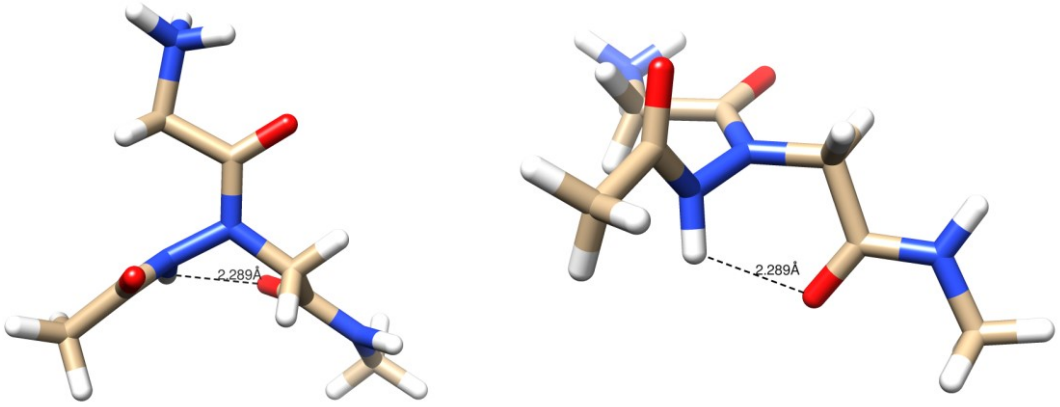

Hydrazido-turn_ap_ammonium_H-bonded-Ac

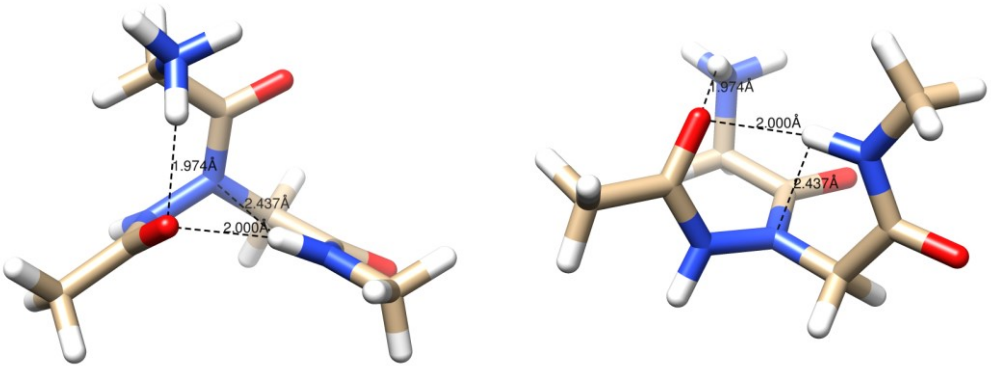

Cycle-6_intraresidue_ap_ammonium_H-bonded-Ac

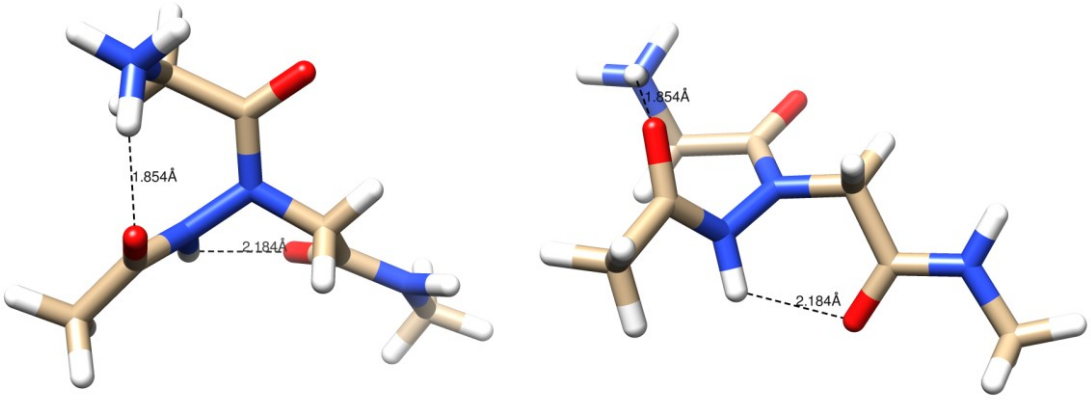

Cycle-5_ap

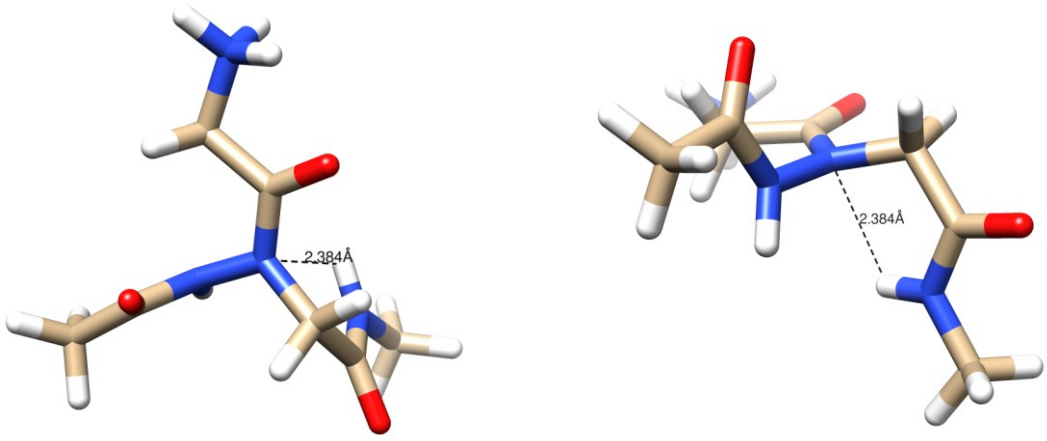

Hydrazido-turn_sp

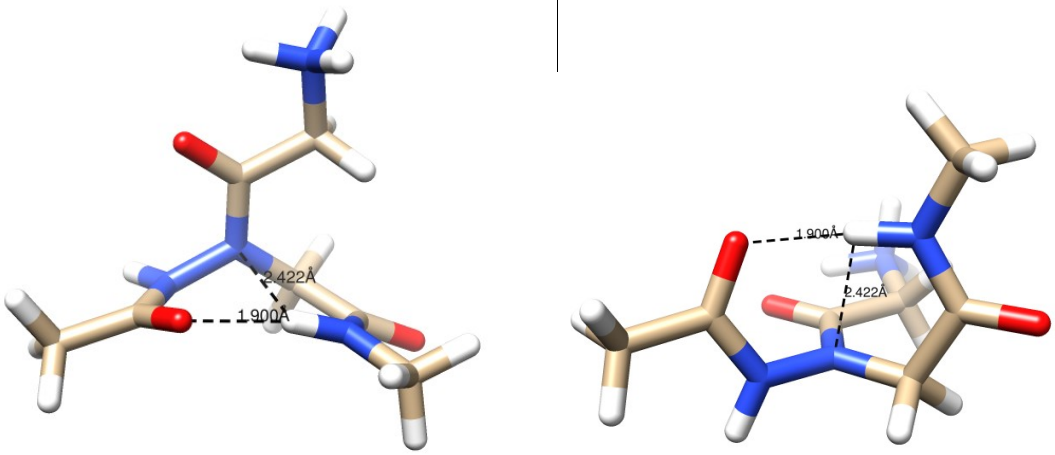

Cycle-7_2

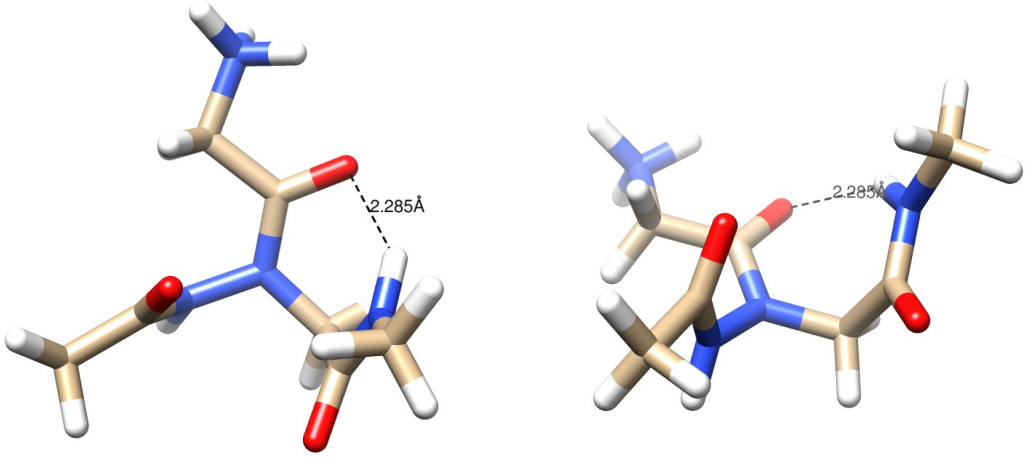

Cycle-7_1

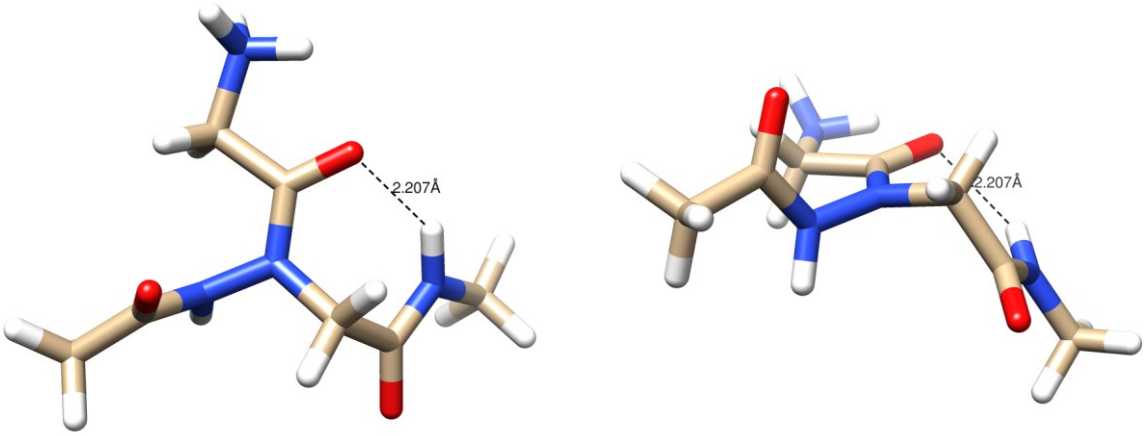

Cycle-6_intraresidue_sp

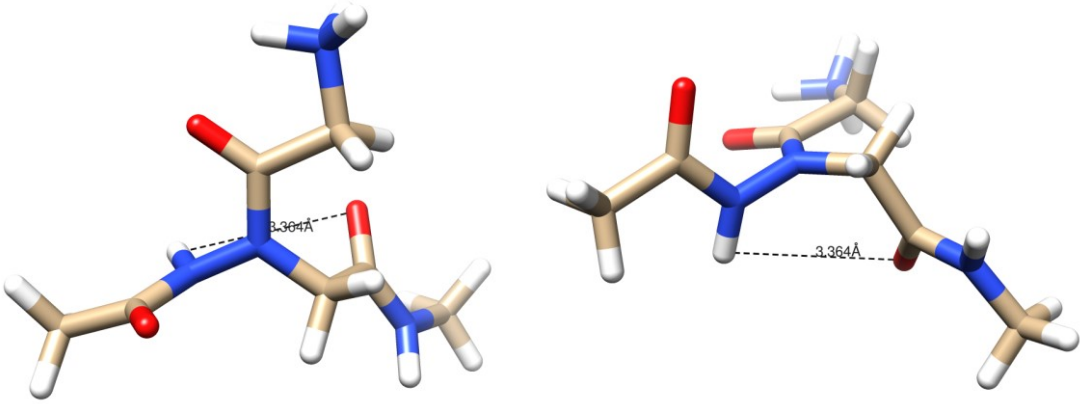

Sp_ammonium_H-bonded-CO_2

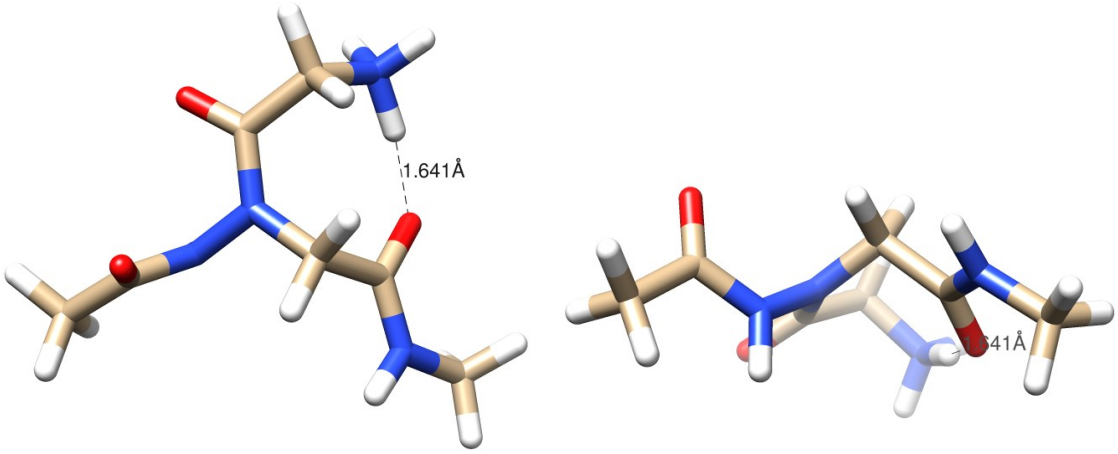

Sp_ammonium_H-bonded-CO

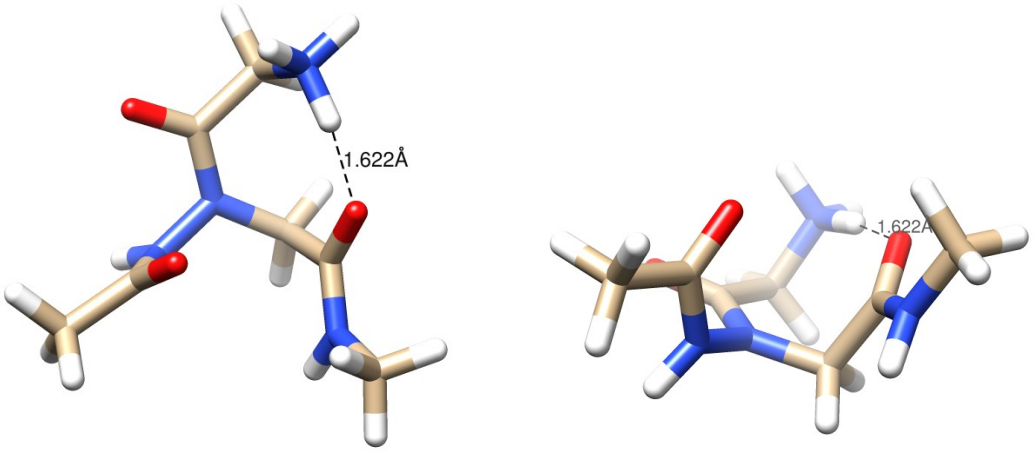

Cycle-7_2_ammonium_H-bonded-Ac

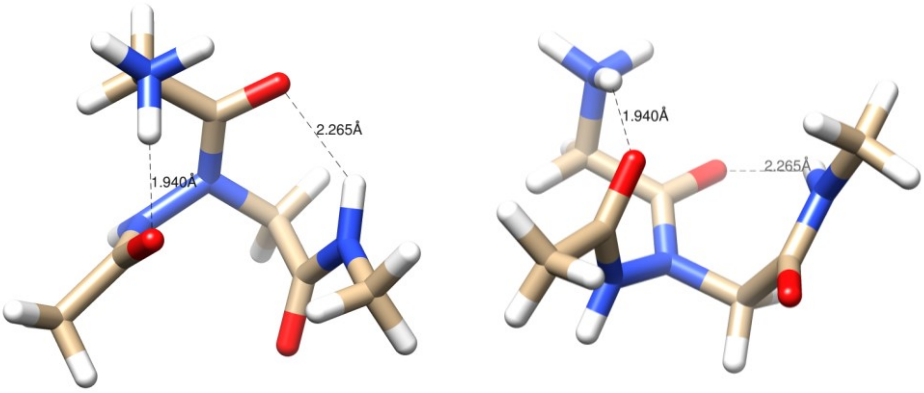

NO-H-bond_ap_1

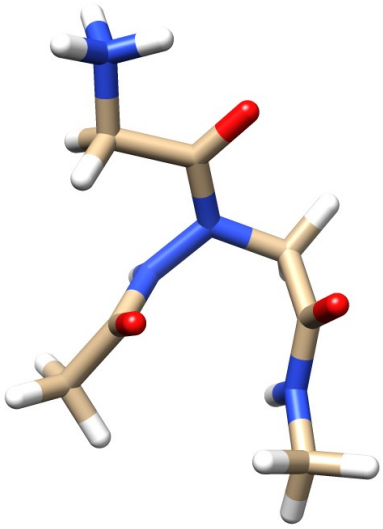

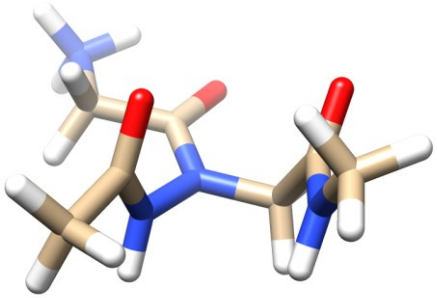

Cycle-5_ap_ammonium_H-bonded-Ac

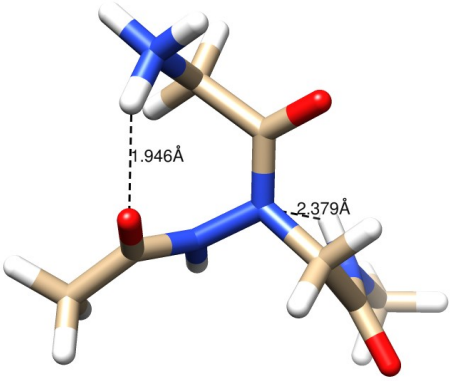

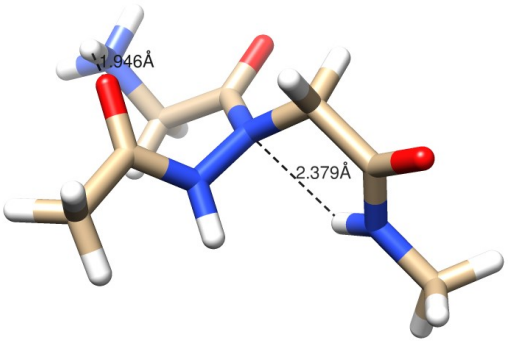

NO-H-bond_ap_2

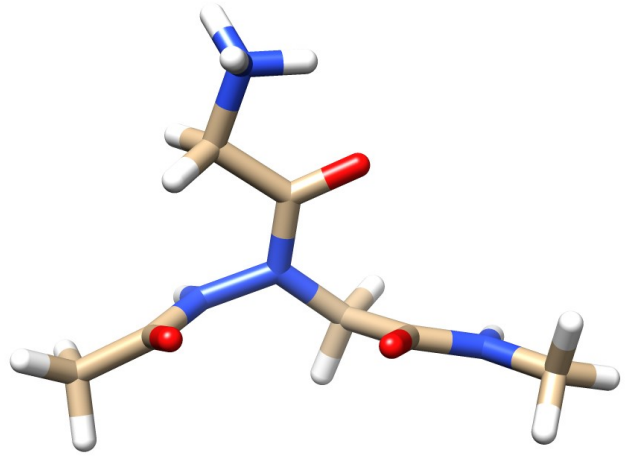

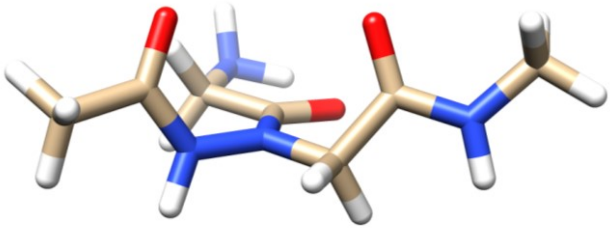

Ap_ammonium_H-bonded-Ac_1

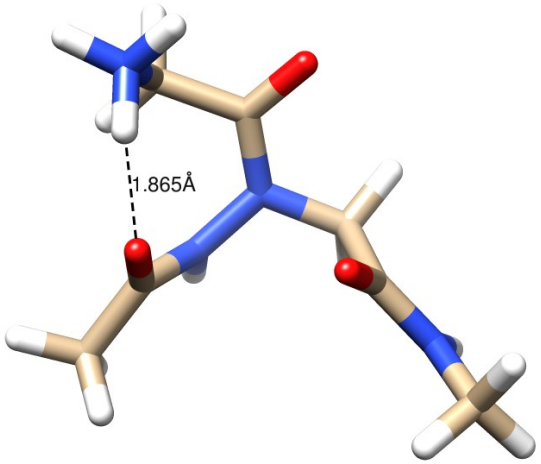

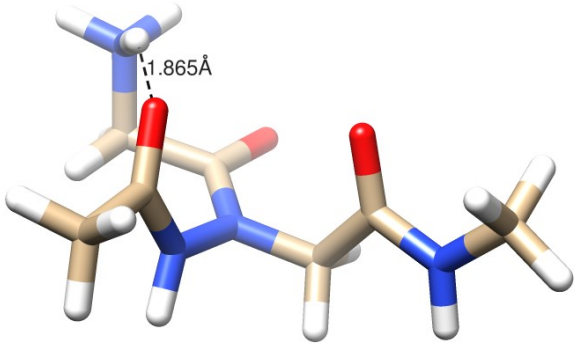

Ap_ammonium_H-bonded-Ac_2

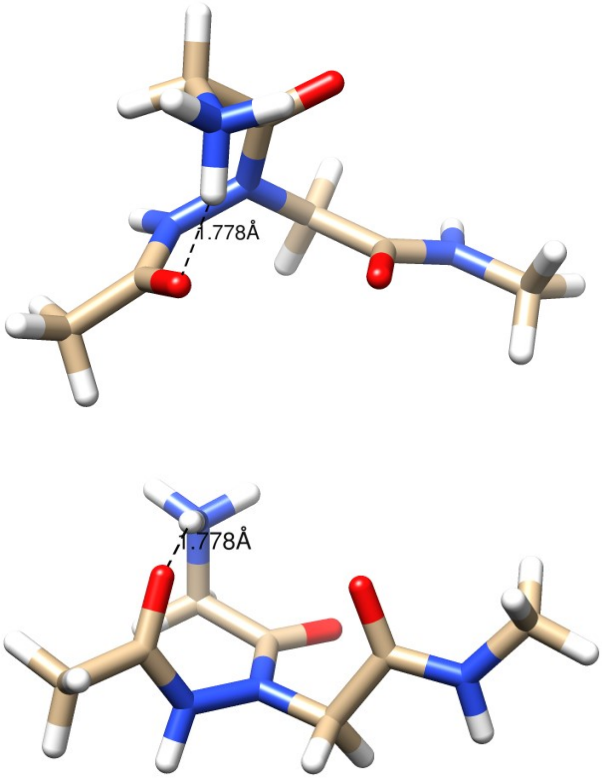

NO-H-bond_sp_1

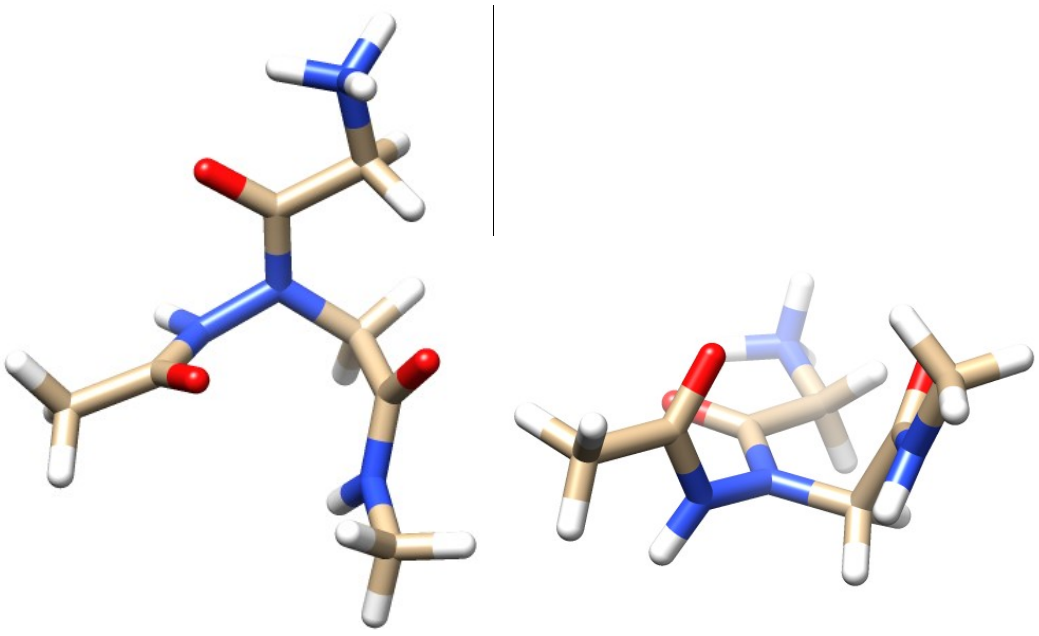

Cycle-7_1_ammonium_H-bonded-Ac

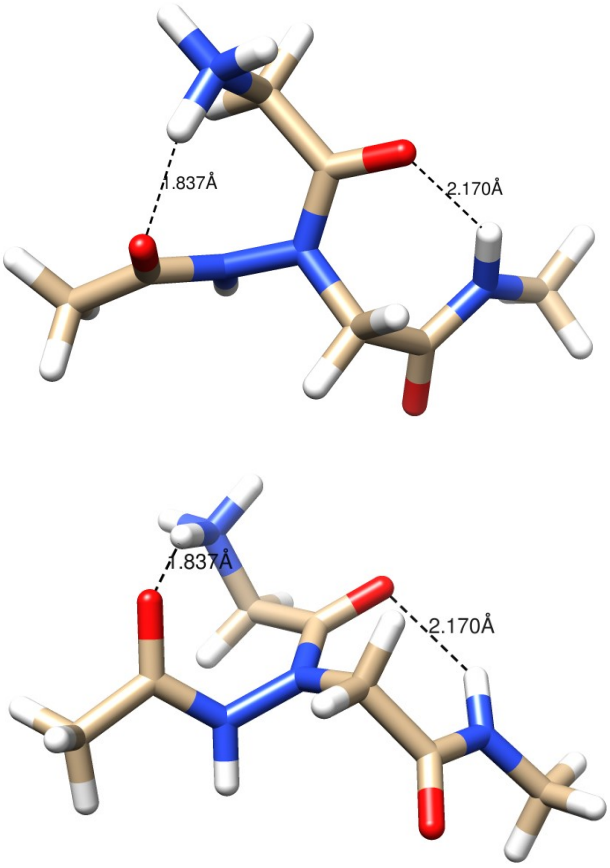

Cycle-6_intraresidue_ap_ammonium_H-bonded-beta-N

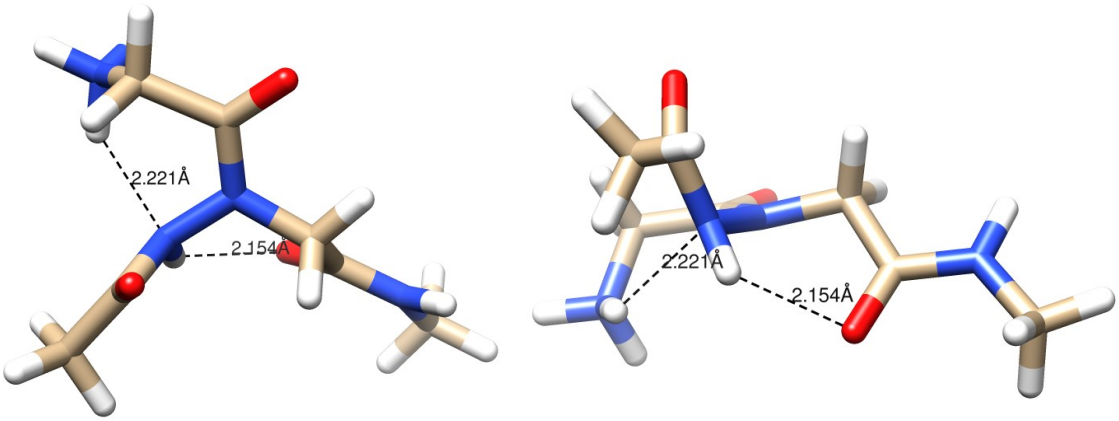

Cycle-5_sp

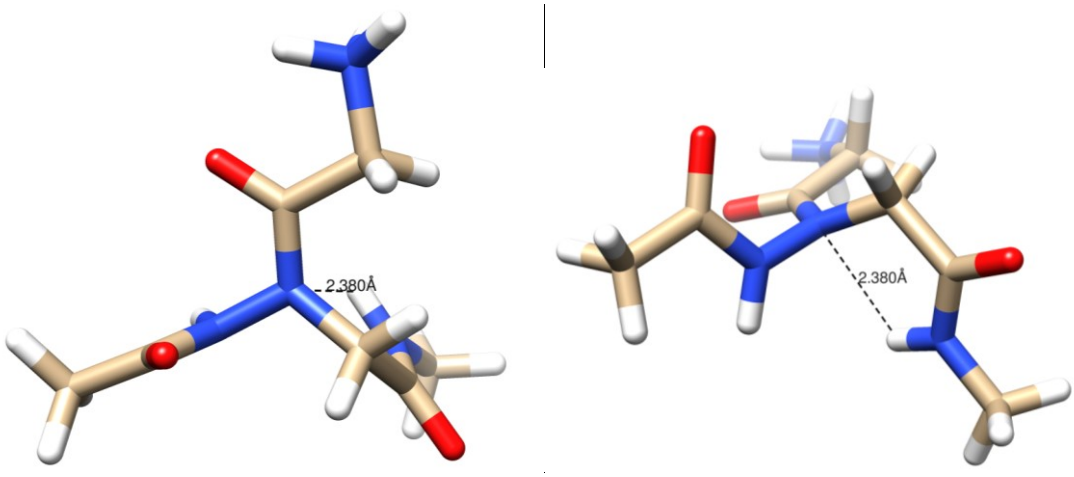

Cycle-6_intraresidue_sp_ammonium_H-bonded-beta-N

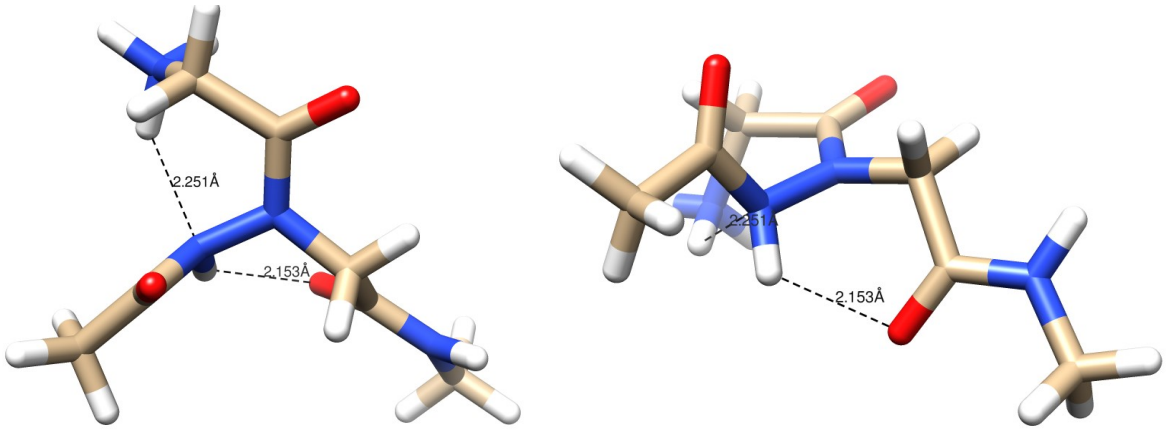

Hydrazido-turn_ap_ammonium_H-bonded-beta-N

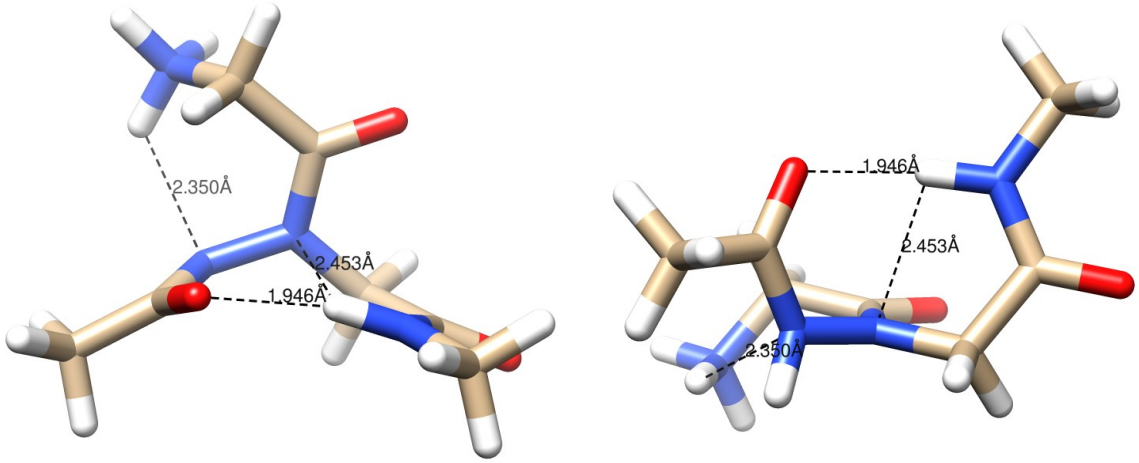

Cycle-7_2_ammonium_H-bonded-beta-N

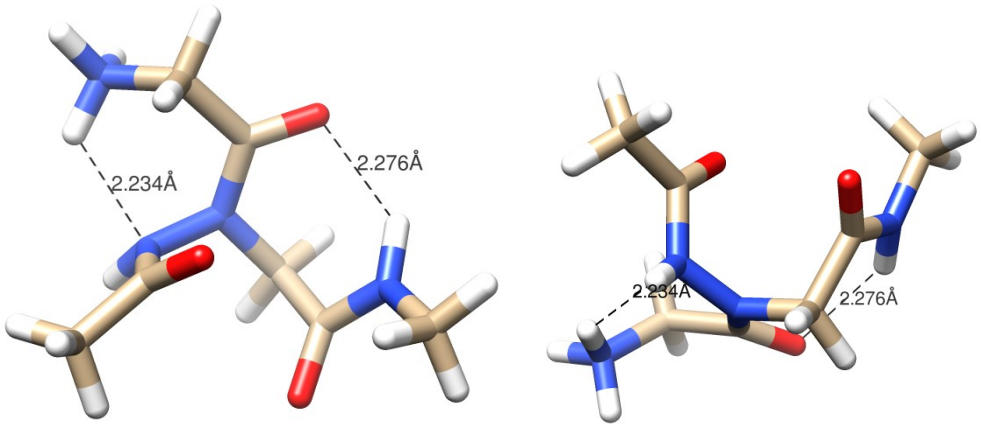

NO-H-bond_sp_2

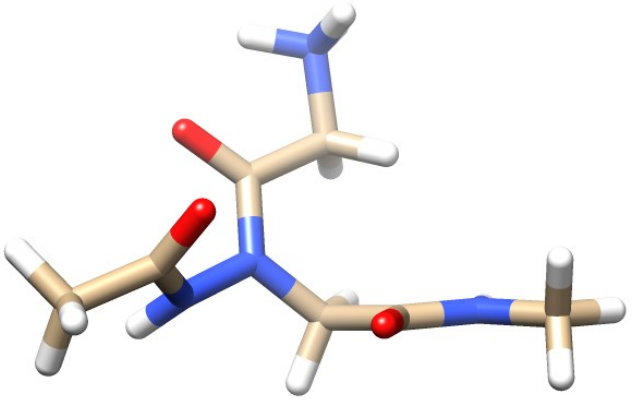

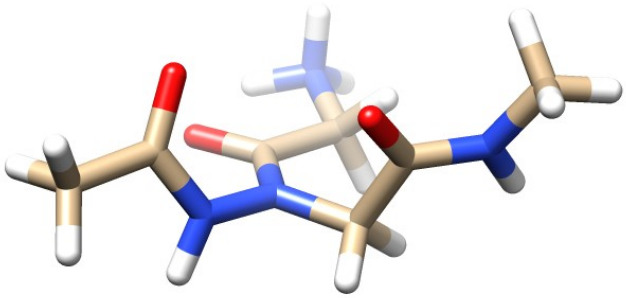

Cycle-7_1_ammonium_H-bonded-beta-N

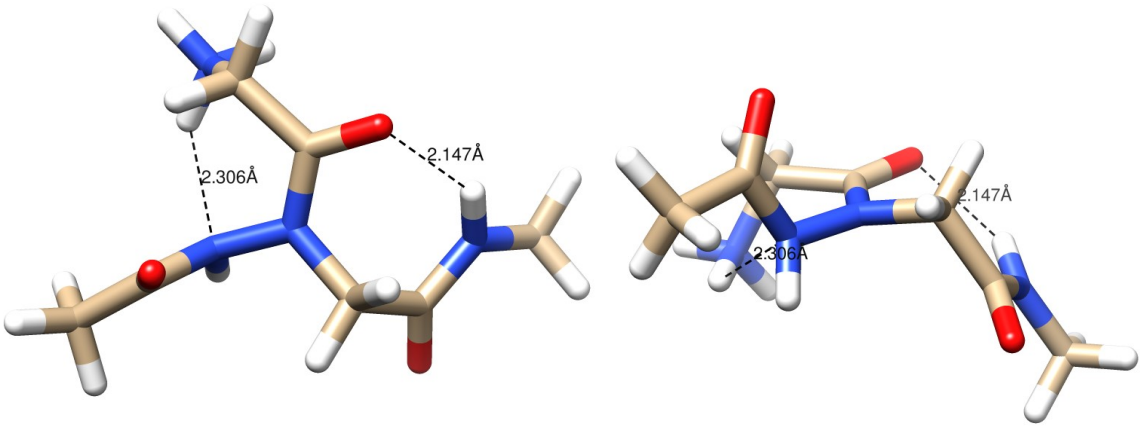

Figure 13. Structures of all the conformers of model ammonium cation mAc-HydrGlyH$^+$-NHMe computed at ωB97X-D3(0)/6-311++G(3df,3pd)/PCM level in water, in order of decreasing stability as reported in Table 5. Two different views are shown for every conformer.

(a)

Cycle-6_intraresidue_ap Hydrazido-turn_ap

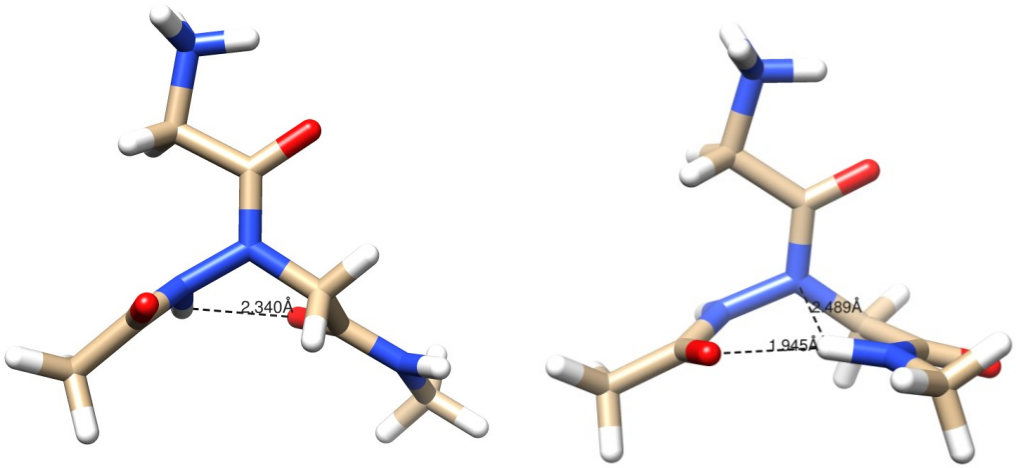

0.00 1.49

(b)

Hydrazido-turn_ap Cycle-6_intraresidue_ap

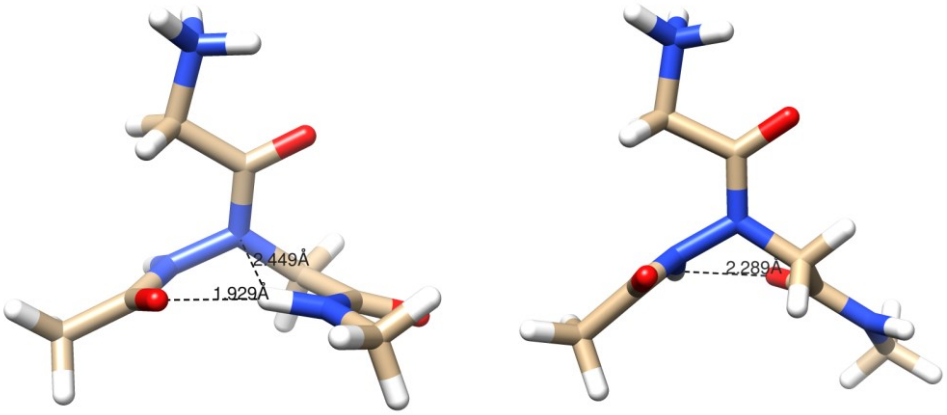

0.00 0.53

Figure 14. Comparison of structures and relative free energies (kcal/mol) for the two most stable conformers of model ammonium cation mAc-HydrGlyH$^+$-NHMe, Hydrazido-turn_ap and Cycle-6_intraresidue_ap, computed at (a) B3LYP/6-311+G(2d,d)/PCM and (b) ωB97X-D3(0)/6-311++G(3df,3pd)/PCM levels in water.

Table 5. Relative free energies and Boltzmann-weighted populations for the conformers of model ammonium cation mAc-HydrGlyH$^+$-NHMe at B3LYP/6-311+G(2d,p)/PCM and ωB97X-D3(0)/6-311++G(3df,3pd)/PCM levels in water.

B3LYP/6-311+G(2d,p)/PCM		
CONFORMER	ΔG_{298} (kcal/mol)[a]	% molar fraction
Cycle-6_intraresidue_ap	0.00	82.841
Hydrazido-turn_ap	1.49	6.737
Cycle-6_intraresidue_ap_ammonium_H-bonded-Ac	1.85	3.633
Cycle-5_ap	2.08	2.484
Cycle-6_intraresidue_sp	2.27	1.806
Cycle-7_1	2.86	0.667
Cycle-7_2	3.09	0.449
NO-H-bond_ap_1	3.18	0.390
NO-H-bond_ap_2	3.21	0.369
Sp_ammonium_H-bonded-CO_2	3.36	0.287
Hydrazido-turn_sp	3.80	0.136
Hydrazido-turn_ap_ammonium_H-bonded-Ac	4.16	0.074
Sp_ammonium_H-bonded-CO	4.53	0.040
NO-H-bond_sp_1	4.84	0.023
Cycle-5_ap_ammonium_H-bonded-Ac	5.01	0.018
Cycle-5_sp	5.30	0.011
Ap_ammonium_H-bonded-Ac_1	5.38	9.420e-3
Cycle-6_intraresidue_ap_ammonium_H-bonded-beta-N	5.46	8.243e-3
Cycle-7_2_ammonium_H-bonded-Ac	5.55	7.115e-3

Cycle-7_1_ammonium_H-bonded-Ac	5.69	5.559e-3
Ap_ammonium_H-bonded-Ac_2	5.91	3.825e-3
Cycle-6_intraresidue_sp_ammonium_H-bonded-beta-N	6.18	2.431e-3
Hydrazido-turn_ap_ammonium_H-bonded-beta-N	7.74	1.763e-4
NO-H-bond_sp_2	7.97	1.186e-4
Cycle-7_1_ammonium_H-bonded-beta-N	8.68	3.619e-5
Cycle-7_2_ammonium_H-bonded-beta-N	9.74	6.028e-6
ωB97X-D3(0)/6-311++G(3df,3pd)/PCM		
CONFORMER	ΔG_{298} (kcal/mol)[a]	% molar fraction
Hydrazido-turn_ap	0.00	64.926
Cycle-6_intraresidue_ap	0.53	26.556
Hydrazido-turn_ap_ammonium_H-bonded-Ac	1.87	2.782
Cycle-6_intraresidue_ap_ammonium_H-bonded-Ac	2.27	1.405
Cycle-5_ap	2.57	0.842
Hydrazido-turn_sp	2.71	0.665
Cycle-7_2	2.80	0.573
Cycle-7_1	2.86	0.521
Cycle-6_intraresidue_sp	2.89	0.490
Sp_ammonium_H-bonded-CO_2	3.01	0.405
Sp_ammonium_H-bonded-CO	3.19	0.297
Cycle-7_2_ammonium_H-bonded-Ac	3.50	0.177
NO-H-bond_ap_1	3.67	0.131
Cycle-5_ap_ammonium_H-bonded-Ac	3.90	0.089
NO-H-bond_ap_2	4.51	0.032
Ap_ammonium_H-bonded-Ac_1	4.54	0.031
Ap_ammonium_H-bonded-Ac_2	4.69	0.024
NO-H-bond_sp_1	4.74	0.022
Cycle-7_1_ammonium_H-bonded-Ac	5.06	0.013
Cycle-6_intraresidue_ap_ammonium_H-bonded-beta-N	5.17	0.010
Cycle-5_sp	5.67	4.565e-3
Cycle-6_intraresidue_sp_ammonium_H-bonded-beta-N	5.79	3713e-3
Hydrazido-turn_ap_ammonium_H-bonded-beta-N	6.83	6.378e-4
Cycle-7_2_ammonium_H-bonded-beta-N	8.40	4.525e-5
NO-H-bond_sp_2	8.89	1.989e-5
Cycle-7_1_ammonium_H-bonded-beta-N	8.95	1.783e-5

[a] Relative free energy at room temperature in water with respect to the most stable conformer.

Table 6. Length of N-H bonds involved in hydrogen bonding in Hydrazido-turn_ap and Cycle-6_intraresidue_ap conformers, together with the lengthening relative to NO-H-bond conformers (structures minimized at ωB97X-D3(0)/6-311++G(3df,3pd)/PCM level in water; length and lengthening of N-H involved in the different hydrogen bonds are reported in italics).

Conformers	C-terminal amide N-H	Hydrazide N^{β}-H

	(Length in Å; Δ_{N-H} in Å)[a]	(Length in Å; Δ_{N-H} in Å)[a]
Hydrazido-turn_ap	*1.01349; +0.00875*	1.00771; -0.00018
Hydrazido-turn_sp	*1.01585; +0.01111*	1.00838; +0.00050
Cycle-6_intraresidue_ap	1.00528; +0.00054	*1.01036; +0.00248*
NO-H-bond_ap_1	1.00469; -0.00005	1.00806; +0.00018
NO-H-bond_ap_2	1.00459; -0.00015	1.00743; -0.00046
NO-H-bond_sp_1	1.00484; +0.00010	1.00743; -0.00046
NO-H-bond_sp_2	1.00485; +0.00011	1.00862; +0.00074

[a] Δ_{N-H} = (Length of indicated N-H - average length of indicated N-H in the four NO-H-bond conformers).

Table 7. NBO analysis on Hydrazido-turn_ap and Cycle-6_intraresidue_ap and NO-H-bond_ap_1 conformers of model ammonium cation mAc-HydrGlyH$^+$-NHMe: second-order perturbation energies ($E^{(2)}$, in kcal/mol) for the interaction between σ^*_{NH} antibonds and the n_O and $n_{N\alpha}$ lone pairs ($n_O \rightarrow \sigma^*_{NH}$ and $n_{N\alpha} \rightarrow \sigma^*_{NH}$), and NBO charges on atoms involved in the hydrogen bonds (ωB97X-D3(0)/6-311++G(3df,3pd)/PCM level in water; the energy difference E(j)-E(i) and the overlap integrals F(i,j) between the donor and acceptor orbitals are also reported in parentheses; charges for NO-H-bond_ap_1 are shown for comparison; charges of atoms involved in the different hydrogen bonds are reported in italics).[a]

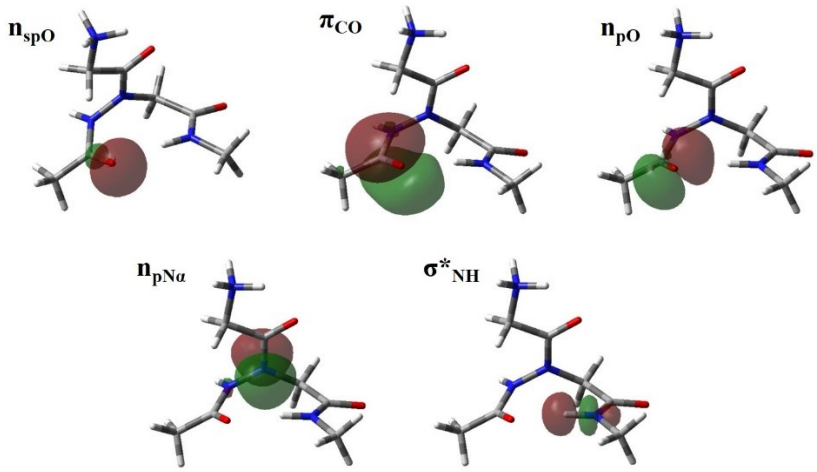

	Conformers		
	Hydrazido-turn_ap	Cycle-6_intraresidue_ap	NO-H-bond_ap_1
$n_{spO} \rightarrow \sigma^*_{NH}$	4.51 (1.37, 0.070)	0.51 (1.33; 0.023)	-
$n_{pO} \rightarrow \sigma^*_{NH}$	7.35 (0.94; 0.076)	1.04 (0.88; 0.028)	-
$\pi_{CO} \rightarrow \sigma^*_{NH}$	0.65 (1.15; 0.025)	0.21 (1.01; 0.013)	-
$n_{pN\alpha} \rightarrow \sigma^*_{NH}$	0.30 (0.93; 0.016)	-	-
Charge on $H_{amideNH}$	*0.430*	0.411	0.410
Charge on $O_{amideCO}$	-0.718	*-0.713*	-0.697
Charge on $H_{hydrazideNH}$	0.424	*0.430*	0.421
Charge on $N^{\alpha}_{hydrazideN\alpha}$	*-0.317*	-0.300	-0.304

Charge on $O_{acetylCO}$	*-0.687*	-0.673	-0.667

[a] See the figure for the correspondence between names and shapes of natural bond orbitals implied. Only orbitals of Hydrazido-turn_ap conformers have been shown as examples.

Hydrazido-turn_ap

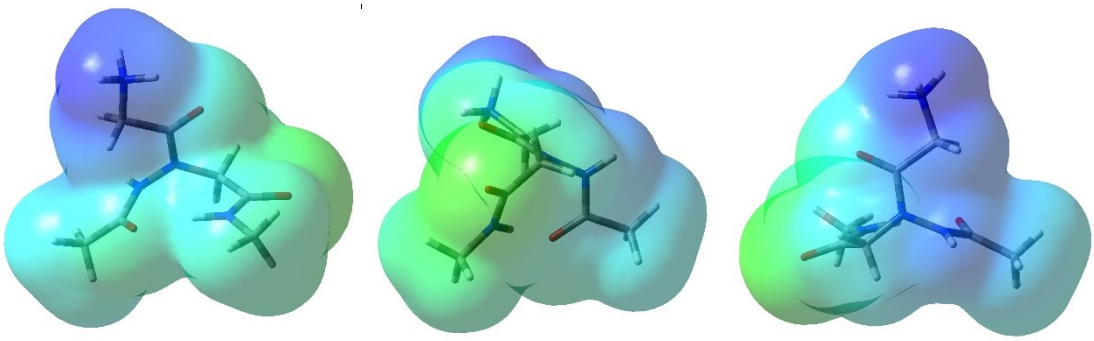

Cycle-6_intraresidue_ap

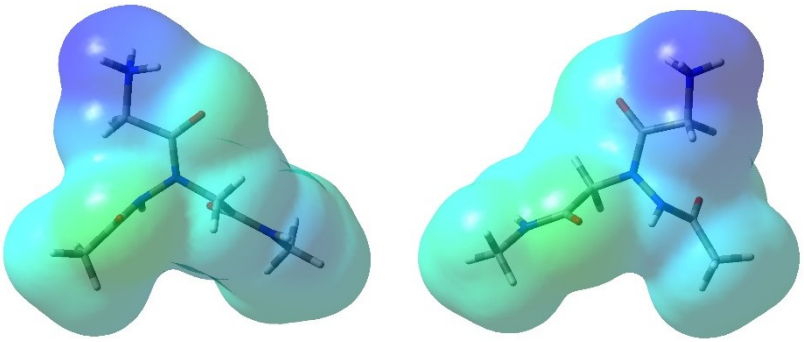

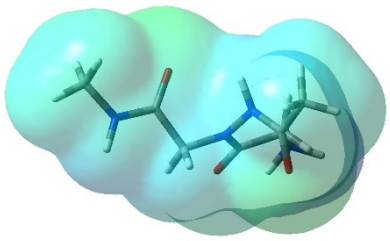

Figure 15. Comparison of electrostatic potential surfaces for the two most stable conformers of model ammonium cation mAc-HydrGlyH$^+$-NHMe, Hydrazido-turn_ap and Cycle-6_intraresidue_ap, computed at ωB97X-D3(0)/6-311++G(3df,3pd)/PCM level in water (three different views for every conformer; density = 0.0004).

Table 8. AIM analysis of Bond Critical Points (BCP) related to intramolecular hydrogen bonds, together with relevant atomic charges of atoms involved, for Hydrazido-turn_ap, Cycle-6_intraresidue_ap and NO-H-bond_ap_1 conformers of model ammonium cation

mAc-HydrGlyH$^+$-NHMe, minimized at ωB97X-D3(0)/6-311++G(3df,3pd)/PCM level in water (charges for NO-H-bond_ap_1 are shown for comparison; charges of atoms involved in the different hydrogen bonds are reported in italics).

Hydrazido-turn_ap Cycle-6_intraresidue_ap NO-H-bond_ap_1

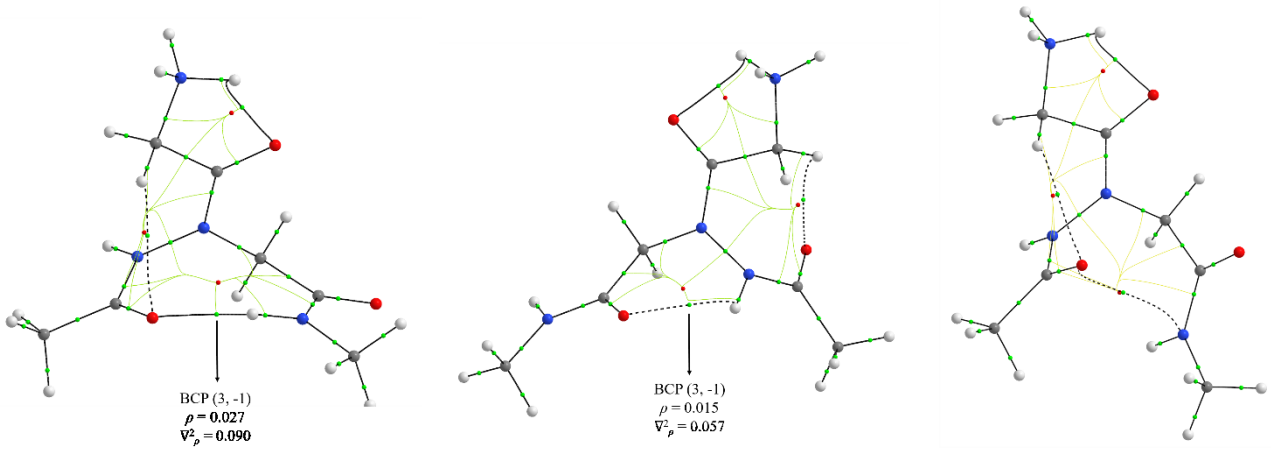

	Conformers		
	Hydrazido-turn_ap	Cycle-6_intraresidue_ap	NO-H-bond_ap_1
Charge on $H_{amideNH}$	*0.459*	0.417	0.414
Charge on $O_{amideCO}$	-1.267	*-1.255*	-1.254
Charge on $H_{hydrazideNH}$	0.446	*0.452*	0.439
Charge on $N^{\alpha}{}_{hydrazideN\alpha}$	*-0.826*	-0.831	-0.813
Charge on $O_{acetylCO}$	*-1.249*	-1.248	-1.222

Some deductions could be easily inferred from the computational investigation (Table 5, Table 7, Figure 13, Figure 14):

1. At both theory levels, the two most stable conformers contribute to the overall population for more than 89%. Moreover, generally all the conformers having hydrogen bond patterns different from those involving (a) the C-terminal amide NH as H-bond donor, and both the N-terminal carbonyl and the hydrazide N^{α} as acceptors (Hydrazido-turns), or (b) the hydrazide $N^{\alpha}H$ as H-bond donor and the hydrazido acid CO as acceptor (intraresidue Cycle-6 structures), are fairly less stable.
2. At the highest theory level (ωB97X-D3(0)/6-311++G(3df,3pd)/PCM in water), the two inherently amphiphilic conformations Hydrazido-turn_ap and Cycle-6_intraresidue_ap are by far the most stable and abundant species in solution. At the lowest level (B3LYP/6-311+G(2d,p)/PCM), Cycle-6_intraresidue_ap is highly predominating,

whereas the populations of Hydrazido-turn_ap and Cycle-6_intraresidue_ap_ammonium_H-bonded-Ac, this latter having a less clear separation of polar and apolar portions, are much lower and comparable.

3. All the structures having the ammonium cation that forms a 5-membered hydrogen bonded pseudocycle with the glycine carbonyl oxygen are more stable than structures having the ammonium cation bonded to other hydrogen bond acceptors (compare every structure_name with the corresponding structure_name_ammonium_H-bonded-Ac, structure_name_ammonium_H-bonded-beta-N, and structure_name_ammonium_H-bonded-CO).
4. All the "ap" structures, where the glycine carbonyl is antiperiplanar to N-N hydrazidic bond, are much more stable with respect to the corresponding "sp" structures, where the glycine carbonyl is antiperiplanar to N-N bond. Moreover, in "sp" structures the N^{β} hydrazidic nitrogen always shows a pronounced pyramidalization.
5. There are no structures devoid of hydrogen bonds. In fact, even in the case of structures of type "NO-H-bond", these names refer to conformers in which there are no other hydrogen bonds except that between $-NH_3^+$ and glycine carbonyl (point 1.5 in the methodological description).
6. The lengths of N-H involved in hydrogen bonding in Hydrazido-turn (ap and sp) and Cycle-6_intraresidue_ap conformers (Table 6) confirm the expected substantial lengthening[123] with respect the same bonds in NO-H-bond conformers. Moreover, the N-H lengthening in C-terminal amide NH of Hydrazido-turn conformers is much larger than the lengthening of hydrazide N^{β}-H in Cycle-6_intraresidue_ap, thus indicating a stronger H-bond in the former case.
7. The NBO analysis of Hydrazido-turn_ap and Cycle-6_intraresidue_ap conformers confirmed that, in both cases, there is a covalent portion in the intramolecular hydrogen bonds. However, the overall covalent contribution deriving from the donation of carbonyl oxygen lone pairs to N-H antibond ($n_{spO} \rightarrow \sigma^*_{NH}$ and $n_{pO} \rightarrow \sigma^*_{NH}$ contributions) and, at a very reduced extend, from the donation of carbonyl π electrons to the same σ^*_{NH} in Hydrazido-turn_ap is much larger than the sum of $n_{spO} \rightarrow \sigma^*_{NH}$ and $n_{pO} \rightarrow \sigma^*_{NH}$ contributions in Cycle-6_intraresidue_ap (Table 7), as expected due to better directionality. This is plenty confirmed by the substantially larger integral overlaps for both the oxygen lone pairs in Hydrazido-turn_ap. On the other hand, the additional stabilization due to 5-membered hydrogen bonded pseudocycle in hydrazido-turn is much smaller and is predominantly only electrostatic in nature (charge on N = -

0.317 e, charge on H = +0.430 e, distance = 2.449 Å), the orbital contribution being very low. As far as the electrostatic contribution is concerned, its stabilization seems to slightly favor the 8-membered pseudocycle in hydrazido-turn conformation (charge on O = -0.687 e, charge on H = +0.430 e, distance = 1.929 Å), compared to the 6-membered pseudocycle in Cycle-6_intraresidue_ap conformation (charge on O = -0.713 e, charge on H = +0.430 e, distance = 2.289 Å), where the larger interatomic distance counterbalance in excess the otherwise favorable more negative charge onto the oxygen. Thus, both the electrostatic and orbital contribution computed with NBO analysis point toward a stronger H-bond in the case of Hydrazido-turn_ap, with respect to Cycle-6_intraresidue_ap.

8. The analyses of atomic charges using the Merz-Singh-Kollman, CHelpG, and Hu-Lu-Yang schemes, not reported here, gave different values for the atoms involved in H-bonds, as expected, but did not change qualitatively the scenario depicted by NBO and AIM results.
9. The AIM analysis (Table 8) also pointed out that, for both Hydrazido-turn_ap and Cycle-6_intraresidue_ap conformers, there are Bond Critical Points (BCP) with the correct positioning and with values of electron density (ρ) and Laplacian of electron density (∇^2_ρ) perfectly consistent with the ranges for hydrogen bonds (ρ = 0.002-0.040 au; ∇^2_ρ = 0.024-0.139 au).[124] In addition, both parameters confirm that the hydrogen bond forming an 8-membered pseudocycle in Hydrazido-turn_ap (ρ = 0.027 au; ∇^2_ρ = 0.090 au) is substantially stronger than the one forming a 6-membered pseudocycle in Cycle-6_intraresidue_ap (ρ = 0.015 au; ∇^2_ρ = 0.057 au). From a purely electrostatic point of view, the AIM analysis led to the same deductions reported in the previous point about the stronger H-bond in the case of Hydrazido-turn_ap than for Cycle-6_intraresidue_ap.
10. From the calculation of DFT-derived electrostatic potential surfaces (Figure 15), it is easy to see that the rear portion in Hydrazido-turn_ap conformer is almost completely hydrophilic, the only slightly less polar zone consisting of the hydrazide methylene group, whose hydrogens bears a small positive charge, according to NBO analysis. On the other hand, the same analysis showed that the hydrogens of the two methyl groups in the N-terminal acetyl moiety and in the C-terminal amide also have very small positive charges (0.21-0.23 e), as expected due to their proximity to electronwithdrawing groups. Thus, according to NBO analysis, the presence of real lipophilic portions seems to be not so clear in the model compound used here. *However,*

(i) in the hydrochlorides used in experiments, the actual R^1 and R^2 groups (N- and C-terminal chains, respectively) have much longer hydrocarbon chains, and (ii) the NBO scheme for atomic charges calculation assign similar values also to standard aliphatic hydrogens. This is demonstrated theoretically for a compound with much longer N- and C-terminal chains, the experimentally used ammonium compound Octanoyl-HydrGlyH$^+$-NHOctyl, in the next section, so that even in the case of the model ammonium cation the preferred conformers must be considered amphiphilic.

Ammonium cation Octanoyl-HydrGlyH$^+$-NHOctyl

Here are reported the salient data and deductions for the most stable Hydrazido-turn_ap conformer of Octanoyl-HydrGlyH$^+$-NHOctyl with all-antiperiplanar arrangement of hydrocarbon N- and C-terminal chains, computed at ωB97X-D3(0)/6-311++g(3df,3pd)/IEF-PCM(water) level. All the other conformers are less stable for at least 1.99 kcal/mol.

Table 9. NBO analysis of the most stable all-antiperiplanar conformer of ammonium cation Octanoyl-HydrGlyH$^+$-NHOctyl with intramolecular Hydrazido-turn_ap arrangement, computed at ωB97X-D3(0)/6-311++g(3df,3pd)/PCM level in water: second-order perturbation energies ($E^{(2)}$, in kcal/mol) for the interaction between σ^*_{NH} antibonds and the n_O and $n_{N\alpha}$ lone pairs ($n_O \rightarrow \sigma^*_{NH}$ and $n_{N\alpha} \rightarrow \sigma^*_{NH}$; the energy difference E(j)-E(i) and the overlap integrals F(i,j) between the donor and acceptor orbitals are also reported in parentheses).[a]

	$E^{(2)}$ (kcal/mol)
$n_{spO} \rightarrow \sigma^*_{NH}$	1.87 (1.35, 0.045)
$n_{pO} \rightarrow \sigma^*_{NH}$	3.37 (0.91; 0.051)
$\pi_{CO} \rightarrow \sigma^*_{NH}$	0.88 (1.05; 0.027)
$n_{pN\alpha} \rightarrow \sigma^*_{NH}$	0.48 (0.91; 0.020)

[a] See the figures in Table 7 for the correspondence between names and shapes of natural bond orbitals implied.

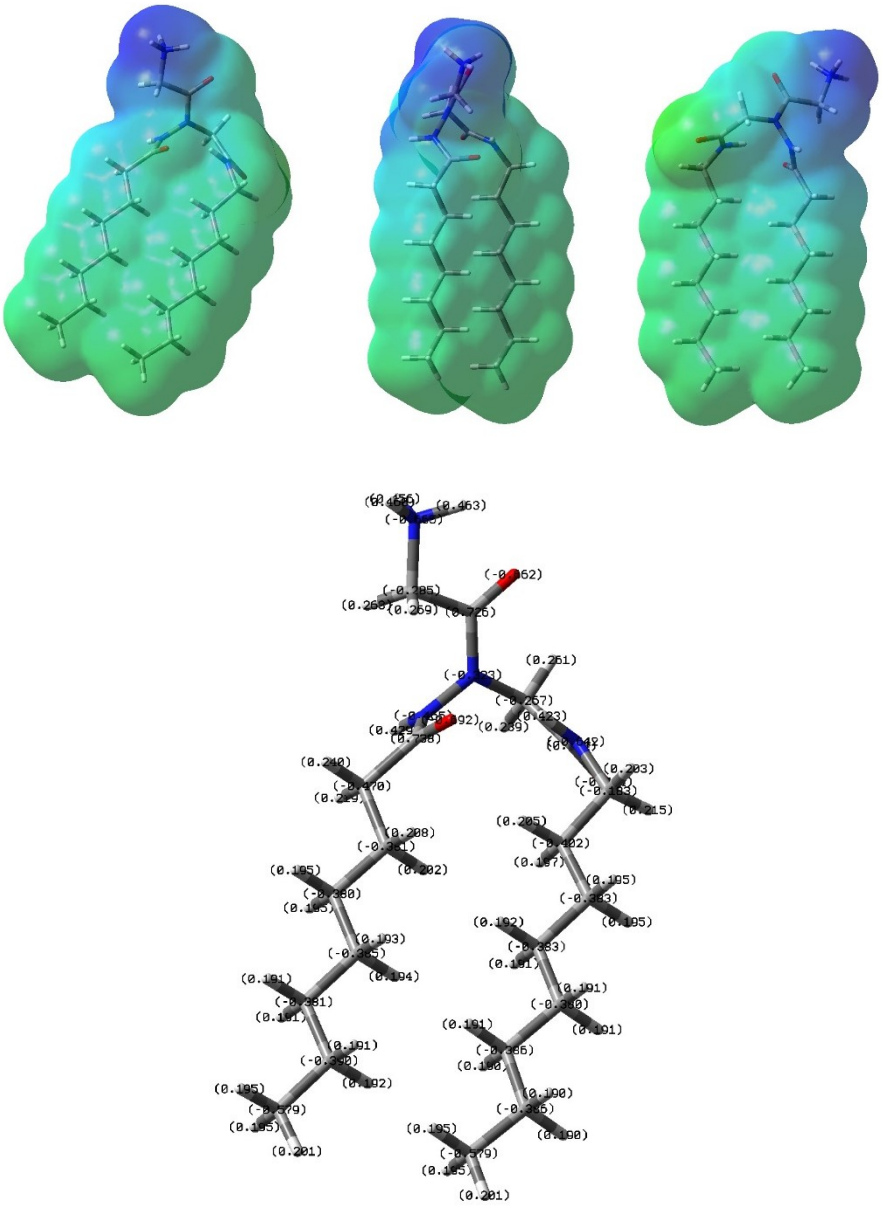

Figure 16. Electrostatic potential surface (density = 0.0004, three different views) and NBO charges for the most stable all-antiperiplanar conformer of ammonium cation Octanoyl-HydrGlyH$^+$-NHOctyl with intramolecular Hydrazido-turn_ap arrangement, computed at ωB97X-D3(0)/6-311++g(3df,3pd)/PCM level in water.

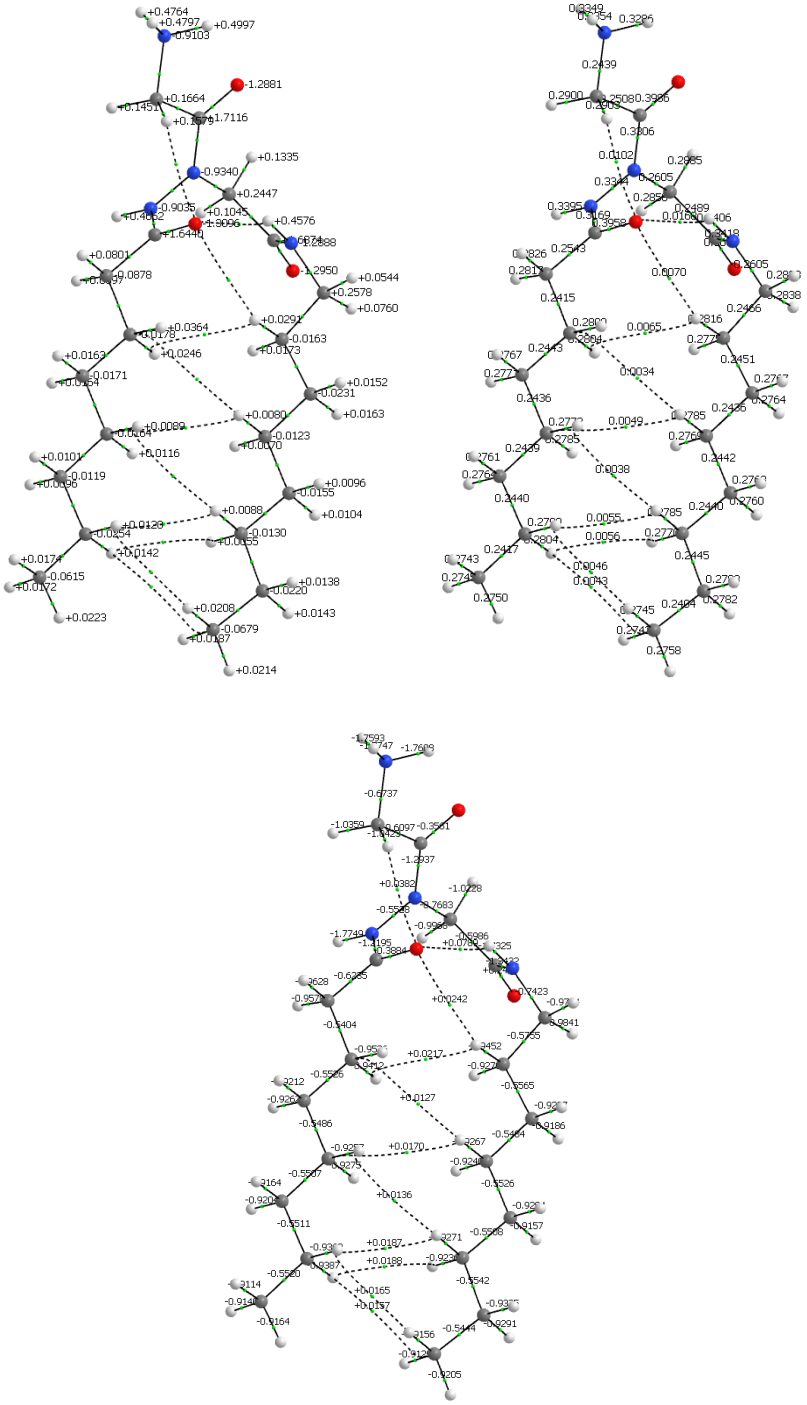

Figure 17. (Left) AIM charges, (middle) ρ, and (right) $\nabla^2\rho$ for the most stable all-antiperiplanar conformer of ammonium cation Octanoyl-HydrGlyH$^+$-NHOctyl with intramolecular Hydrazido-turn_ap arrangement, computed at ωB97X-D3(0)/6-311++g(3df,3pd)/PCM level in water. Bond critical points are reported in green.

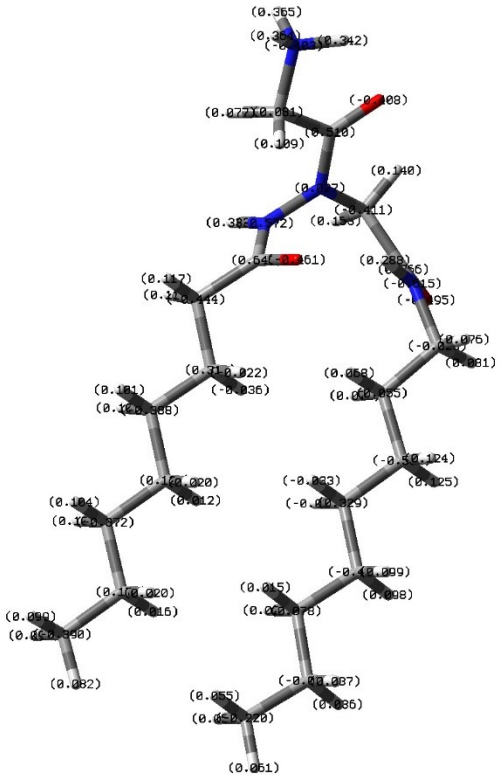

Figure 18. Merz-Singh-Kollman charges for the most stable all-antiperiplanar conformer of ammonium cation Octanoyl-HydrGlyH$^+$-NHOctyl with intramolecular Hydrazido-turn_ap arrangement, computed at ωB97X-D3(0)/6-311++g(3df,3pd)/PCM level in water.

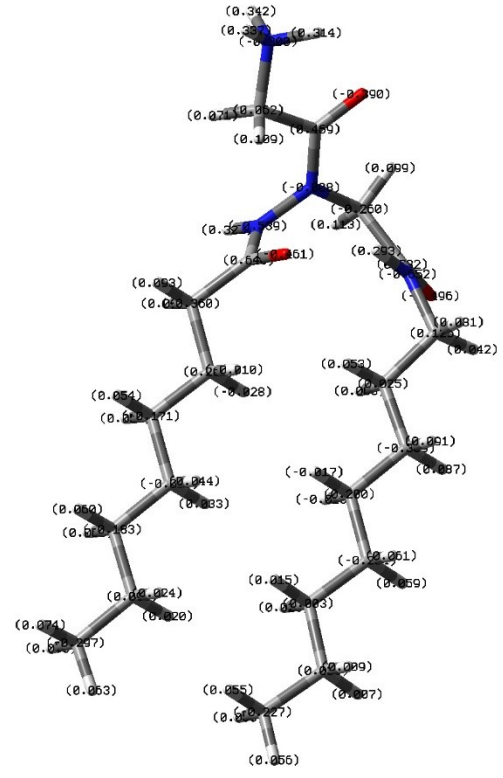

Figure 19. CHelpG charges for the most stable all-antiperiplanar conformer of ammonium cation Octanoyl-HydrGlyH$^+$-NHOctyl with intramolecular Hydrazido-turn_ap arrangement, computed at ωB97X-D3(0)/6-311++g(3df,3pd)/PCM level in water.

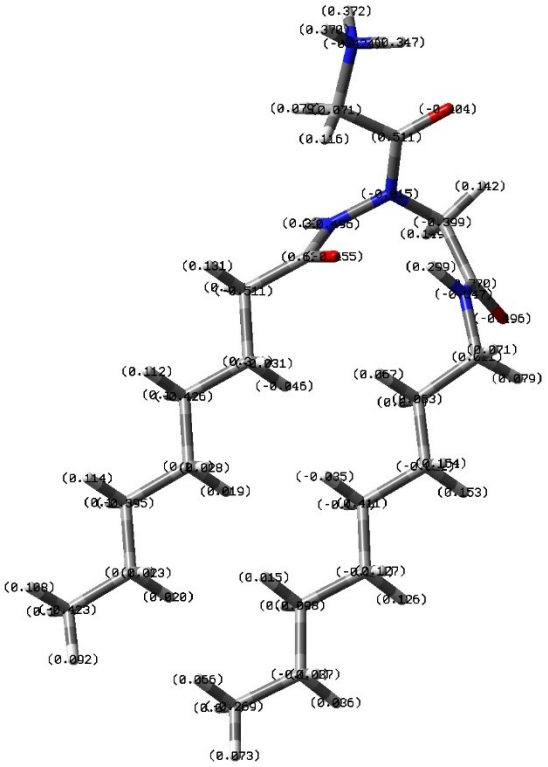

Figure 20. Hu-Lu-Yang charges for the most stable all-antiperiplanar conformer of ammonium cation Octanoyl-HydrGlyH$^+$-NHOctyl with intramolecular Hydrazido-turn_ap arrangement, computed at ωB97X-D3(0)/6-311++g(3df,3pd)/PCM level in water.

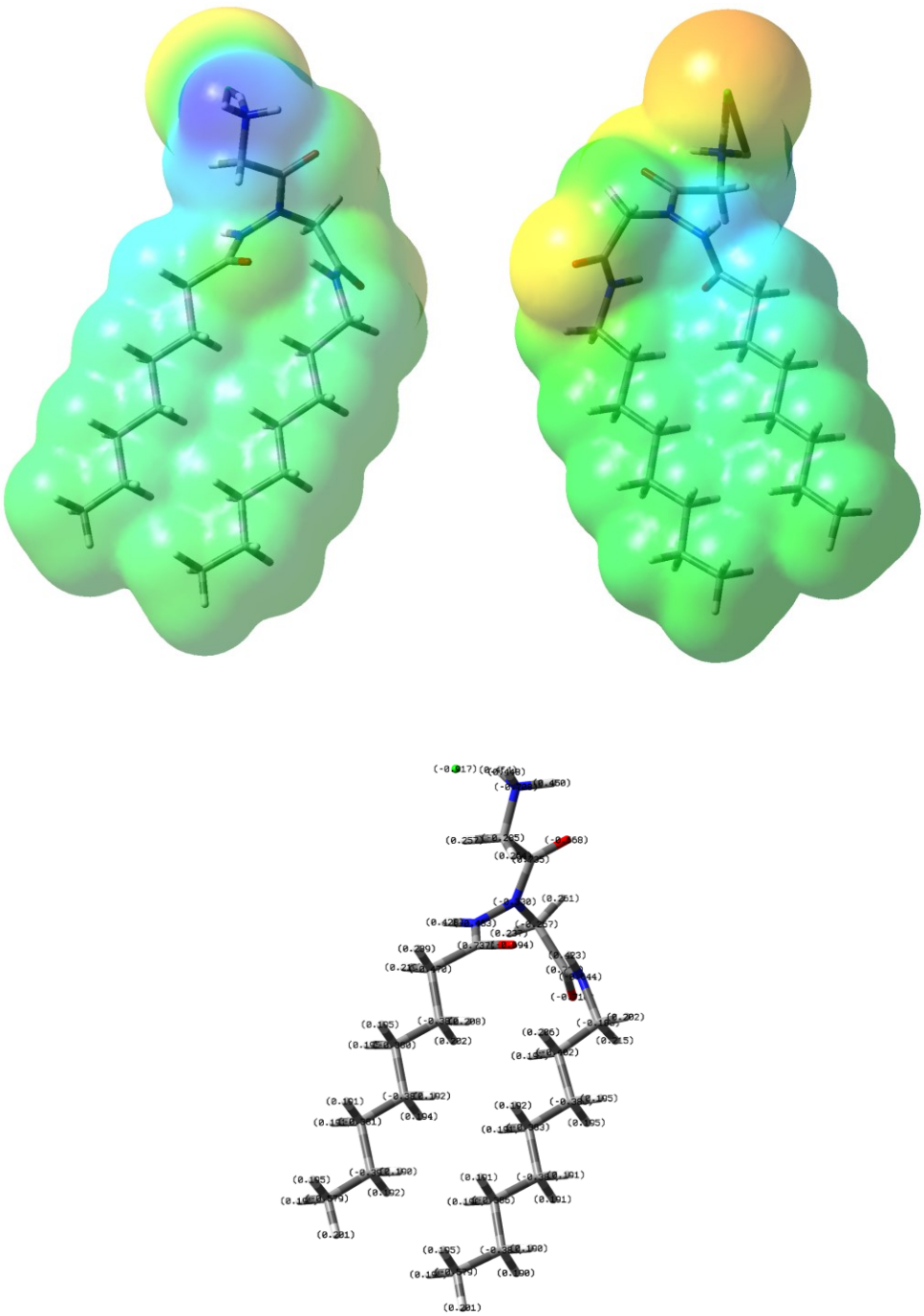

Figure 21. Electrostatic potential surface (density = 0.0004, two different views) and NBO charges for the most stable all-antiperiplanar conformer of ammonium cation with a chloride counterion, Octanoyl-HydrGly-NHOctyl · HCl, with intramolecular Hydrazido-turn_ap arrangement, computed at ωB97X-D3(0)/6-311++g(3df,3pd)/PCM level in water.

Deductions:

1. In the most stable conformer of Octanoyl-HydrGlyH$^+$-NHOctyl the peculiar hydrazido-turn secondary structure is distorted in comparison to the model compound (compare Figure 13 and Figure 16), whereas all the other conformers show a hydrazido-turn structure almost identical to that of model ammonium cation. This is very likely due to the extended contact surface between the two lipophilic chains, which is present only in this conformer and gives rise to large van der Waals interactions. Moreover, the IEF-PCM model for the solvent should also be able to take into account, at least partly, the diminished disruption of hydrogen bond net in the surrounding water, that is less hydrophobic effect. The AIM analysis (Figure 17) also explicitly assigns many bond critical points to hydrogen-hydrogen bonds along the lipophilic chains, the values of ρ and ∇^2_ρ being in agreement with very weak bonds. So, hydrophobic effect and dispersion forces counterbalance in excess the less favorable geometry in hydrogen bonds involved in the formation of hydrazido-turn structure, which becomes evident from the reduced donor-acceptor interactions in Table 9, in comparison to those in Table 7 for the model ammonium cation, which in turn arose from reduced orbital overlaps, especially for carbonyl oxygen lone pairs.
2. The analysis of electrostatic potential surface for the most stable Hydrazido-turn_ap conformer of compound Octanoyl-HydrGlyH$^+$-NHOctyl (Figure 16), as well as the atomic charges obtained with NBO (Figure 16), AIM (Figure 17), Merz-Singh-Kollman (Figure 18), CHelpG (Figure 19), and Hu-Lu-Yang (Figure 20) schemes, respectively, always confirms the almost perfect amphiphilicity of this conformation. Note: as in the case of model ammonium cation, the NBO scheme for atomic charge computation assigns the highest positive values to all hydrogens in aliphatic chains, with respect all the other schemes.

N-methylated model ammonium cation mAc-Hydr(Me)GlyH$^+$-NHMe

The analysis on the N-methylated model ammonium cation, mAc-Hydr(Me)GlyH$^+$-NHMe, was conducted by building and minimizing at the highest level the N-Me versions of the 9 conformers of the N-H parent compound, mAc-HydrGlyH$^+$-NHMe, lying within 3 kcal/mol from the global minimum at ωB97X-D3(0)/6-311++G(3df,3pd)/PCM(water) level (Table 5, and Figure 13).

Hydrazido-turn_ap_Me

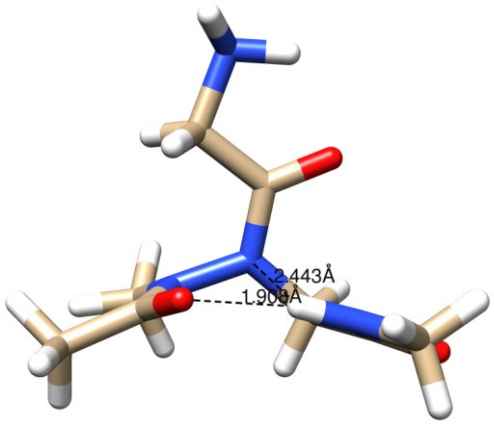

Unconv-H-bond_deriving_from_Cycle-6_intraresidue_ap_Me

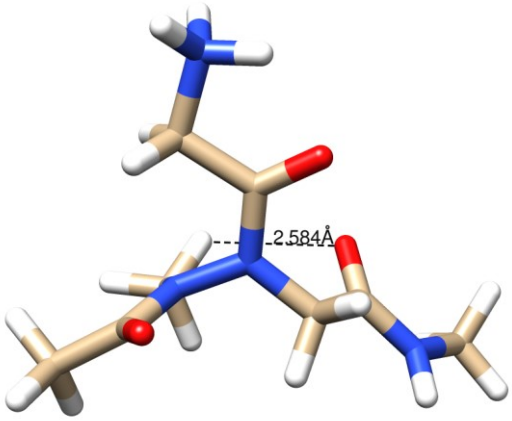

Cycle-7_1_Me

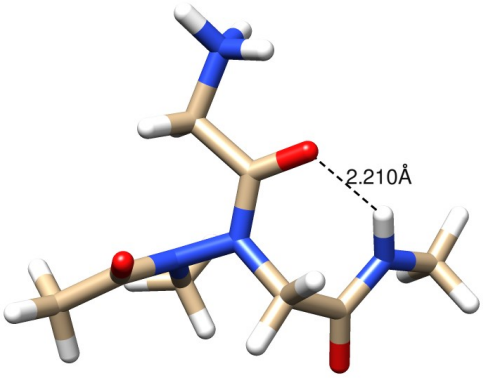

Cycle-5_ap_Me

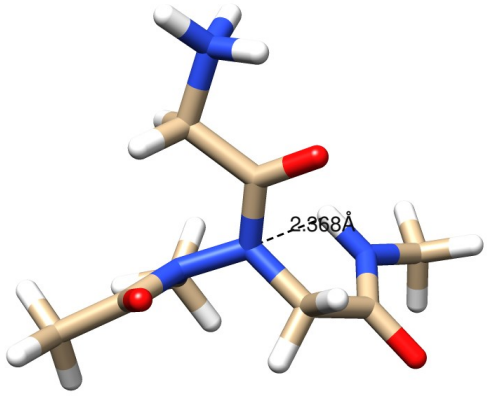

Hydrazido-turn_ap_ammonium_H-bonded-Ac_Me

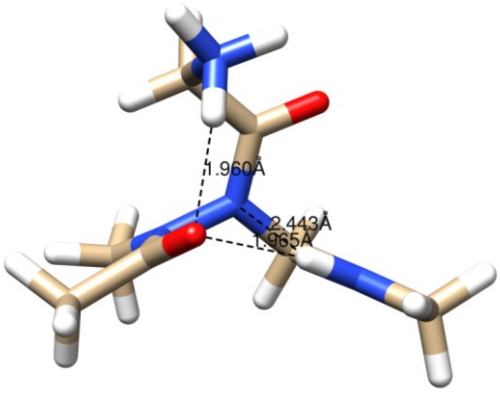

Hydrazido-turn_sp_Me

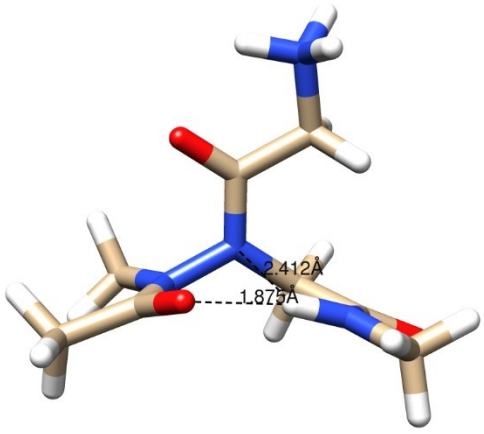

Cycle-7_2_Me

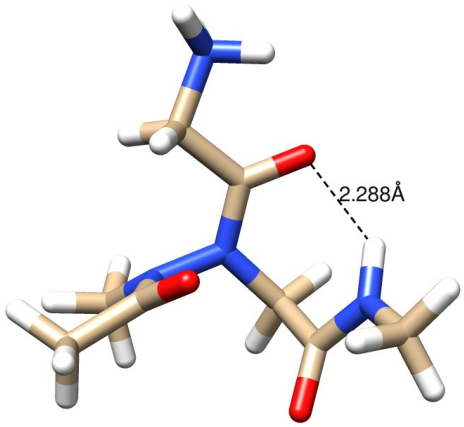

Unconv-H-bond_deriving_from_Cycle-6_intraresidue_sp_Me

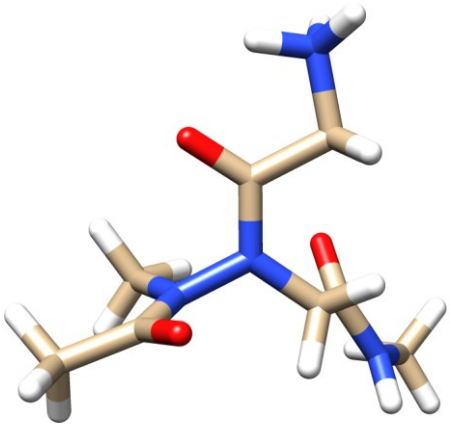

Unconv-H-bond_deriving_from_Cycle-6_intraresidue_ap_ammonium_H-bonded-Ac_Me

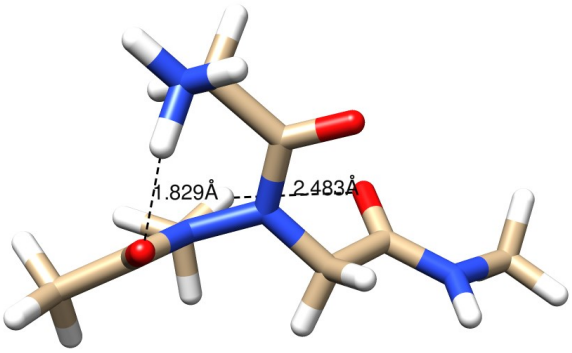

Figure 22. Structures of all the conformers of model N-Me ammonium cation mAc-Hydr(Me)GlyH$^+$-NHMe computed at ωB97X-D3(0)/6-311++G(3df,3pd)/PCM level in water, in order of decreasing stability as reported in Table 10.

Table 10. Relative free energies and Boltzmann-weighted populations for the conformers of model N-Me ammonium cation mAc-Hydr(Me)GlyH$^+$-NHMe at ωB97X-D3(0)/6-311++G(3df,3pd)/PCM level in water.[a]

ωB97X-D3(0)/6-311++G(3df,3pd)/PCM		
CONFORMER	ΔG_{298} (kcal/mol)[b]	% molar fraction
Hydrazido-turn_ap_Me	0.00	47.687
Unconv-H-bond_deriving_from_Cycle-6_intraresidue_ap_Me[c]	0.13	38.338
Cycle-7_1_Me	1.23	5.949
Cycle-5_ap_Me	1.66	2.914
Hydrazido-turn_ap_ammonium_H-bonded-Ac_Me	1.70	2.682
Hydrazido-turn_sp_Me	2.07	1.453
Cycle-7_2_Me	2.88	0.366
Unconv-H-bond_deriving_from_Cycle-6_intraresidue_sp_Me[c]	2.88	0.366
Unconv-H-bond_deriving_from_Cycle-6_intraresidue_ap_ammonium_H-bonded-Ac_Me[c]	3.12	0.244

[a] Only the N-methylated structures derived from the conformers of parent compound mAc-HydrGlyH$^+$-NHMe lying within 3 kcal/mol from the global minimum have been minimized for mAc-Hydr(Me)GlyH$^+$-NHMe. [b] Relative free energy at room temperature in water with respect to the most stable conformer. [c] The geometry of this N-methylated conformer is very similar to that of the parent N-H conformer.

Table 11. NBO analysis on conformers Hydrazido-turn_ap_Me and Unconv-H-bond_deriving_from_Cycle-6_intraresidue_ap_Me of N-methylated model ammonium cation mAc-Hydr(Me)GlyH$^+$-NHMe: second-order perturbation energies ($E^{(2)}$, in kcal/mol) for the interaction between σ^*_{NH} antibonds and the n_O and $n_{N\alpha}$ lone pairs ($n_O \rightarrow \sigma^*_{NH}$ and $n_{N\alpha} \rightarrow \sigma^*_{NH}$) in Hydrazido-turn_ap and for the interaction between the n_O lone pairs of hydrazide C-terminal carbonyl oxygen and the σ^*_{CH} antibond of the nearest hydrogen ($n_O \rightarrow \sigma^*_{CH}$), together with NBO charges on atoms involved in hydrogen bonds (ωB97X-D3(0)/6-311++G(3df,3pd)/PCM level in water; the energy difference E(j)-E(i) and the overlap integrals F(i,j) between the donor and acceptor orbitals are also reported in parentheses; charges of atoms involved in the different hydrogen bonds are reported in italics).

	Conformers	
	Hydrazido-turn_ap_Me	Unconv-H-bond_deriving_from_Cycle-6_intraresidue_ap_Me
$n_{spO} \rightarrow \sigma^*_{NH}$	5.09 (1.37, 0.075)	-
$n_{pO} \rightarrow \sigma^*_{NH}$	7.42 (0.94, 0.076)	-
$\pi_{CO} \rightarrow \sigma^*_{NH}$	0.83 (1.09; 0.027)	-
$n_{pN\alpha} \rightarrow \sigma^*_{NH}$	0.27 (0.93; 0.015)	-
$n_{spO} \rightarrow \sigma^*_{CH}$	-	0.13 (1.33, 0.012)

$n_{pO} \rightarrow \sigma^*_{CH}$	-	0.23 (0.88, 0.013)
$\pi_{CO} \rightarrow \sigma^*_{CH}$	-	-
$n_{pN\alpha} \rightarrow \sigma^*_{CH}$	-	-
Charge on $H_{amideNH}$	*0.432*	0.410
Charge on H_{Me} near to $O_{amideCO}$	-	*0.230*
Charge on $O_{amideCO}$	-0.718	*-0.700*
Charge on $N^{\alpha}_{hydrazideN\alpha}$	*-0.306*	-0.289
Charge on $O_{acetylCO}$	*-0.688*	-0.672

Hydrazido-turn_ap_Me

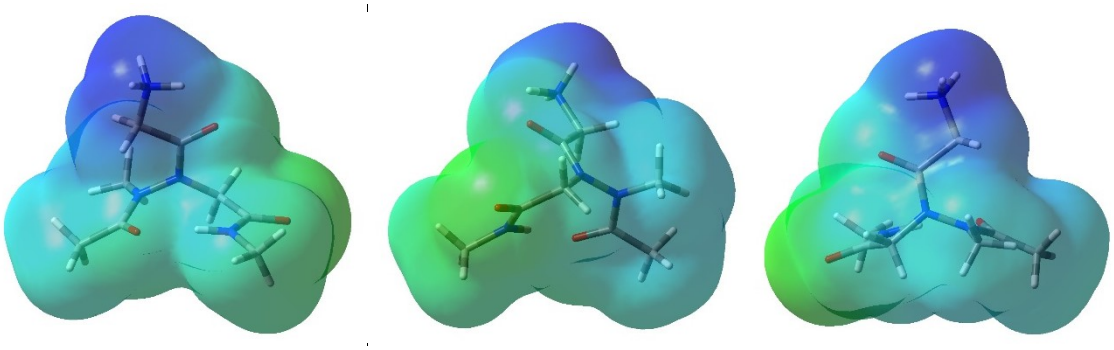

Unconv-H-bond_deriving_from_Cycle-6_intraresidue_ap_Me

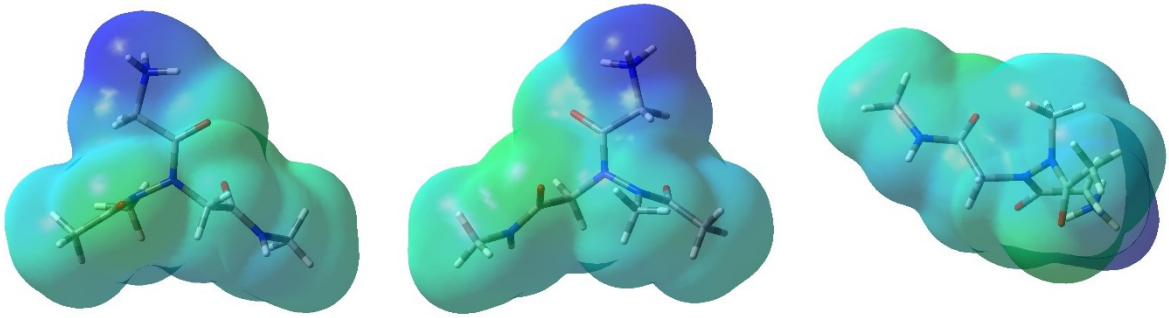

Figure 23. Comparison of electrostatic potential surfaces for the two most stable conformers of model N-Me ammonium cation mAc-Hydr(Me)GlyH$^+$-NHMe, Hydrazido-turn_ap_Me and Unconv-H-bond_deriving_from_Cycle-6_intraresidue_ap_Me, computed at ωB97X-D3(0)/6-311++G(3df,3pd)/PCM level in water (three different views for every conformer; density = 0.0004).

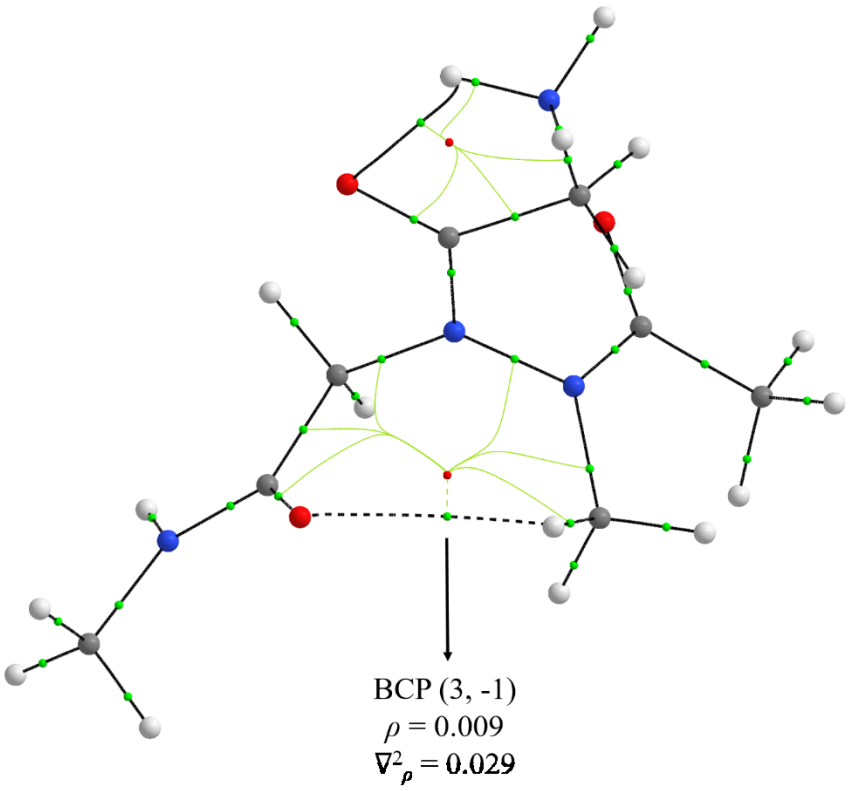

Figure 24. AIM analysis of Unconv-H-bond_deriving_from_Cycle-6_intraresidue_ap_Me conformer of model N-Me ammonium cation mAc-Hydr(Me)GlyH$^+$-NHMe, Hydrazido-turn_ap_Me and, computed at ωB97X-D3(0)/6-311++G(3df,3pd)/PCM level in water.

The deductions from data in Table 10, Table 11, and structures in Figure 22, Figure 23 and Figure 24, are as follows:

1. The two most stable conformers of mAc-Hydr(Me)GlyH$^+$-NHMe are the same computed for the unmethylated version (Table 10 and Figure 22). In fact, despite the lack of a classical hydrogen bond in the N-Me conformer deriving from the parent Cycle-6_intraresidue_ap structure, named Unconv-H-bond_deriving_from_Cycle-6_intraresidue_ap_Me, this conformer has an arrangement very similar to the parent unmethylated conformer and is almost isoenergetic with Hydrazido-turn_ap_Me (+0.13 kcal/mol, Table 10), whereas between the two unmethylated parent conformers there is a much larger energy difference (+0.53 kcal/mol, Table 5). The overall population of Hydrazido-turn_ap_Me and Unconv-H-bond_deriving_from_Cycle-6_intraresidue_ap_Me conformers is about 86%. All the other conformers are substantially less stable.

2. As for the parent unmethylated structures, all the conformers having the ammonium cation that forms a 5-membered hydrogen bonded pseudocycle with the glycine carbonyl oxygen are more stable than structures having the ammonium cation bonded to other hydrogen bond acceptors.
3. As for the parent unmethylated structures, the "ap" structures are much more stable with respect to the corresponding "sp" structures.
4. As for the parent unmethylated structures, there are no structures devoid of hydrogen bonds. In fact, in spite of the "NO-H-Bond" name, even in those structures there is at least the hydrogen bond involving the glycine carbonyl and the ammonium functionality.
5. The most interesting finding is about the methylated versions of conformers forming a 6-membered intraresidual hydrogen bonded pseudocycle (see for example Unconv-H-bond_deriving_from_Cycle-6_intraresidue_ap_Me conformer, Figure 22 and Figure 23). In these cases, only slight geometric variations were observed in most of the molecular skeleton, but there is a substantial difference in the rotations around the C^{α}-N^{α} and C^{α}-C(=O) bonds. The overall result is a hydrazide carbonyl that does not point toward hydrazide N-Me with the geometric parameters suitable for a conventional H-bond, as occurred in the N-H parent conformer (Figure 13 and Figure 15), likely due to the necessity to relief an otherwise strongly destabilizing steric interaction. However, the presence of a weak unconventional hydrogen bond can be easily evidenced (see below).
6. The NBO analysis of the N-Me version of Hydrazido-turn_ap_Me conformer (Table 11) gave results very close to those of its unmethylated counterpart (Table 7). On the contrary, for the N-Me conformer deriving from Cycle-6_intraresidue_ap, that is Unconv-H-bond_deriving_from_Cycle-6_intraresidue_ap_Me, only two very weak donor-acceptor interactions $n_O \rightarrow \sigma^*_{CH}$ could be individuated, which describe the unconventional 7-membered H-bond. This was not unexpected, and is very likely due to the wrong directionality in the donor-acceptor arrangement, leading to very low overlap integrals (Table 11). Moreover, the NBO atomic charges in Table 11 confirm that, in this case, at the best only a small electrostatic hydrogen bond could be postulated. In addition, it should be noted that there is almost no elongation of C-H bond, the difference with the other C-H bond in the N-Me group which does not experience delocalization of N lone pair on σ^*_{CH} being only +0.00031 Å. Even if these

unconventional hydrogen bonds are usually quite weak, they have been recently demonstrated to be sometimes important (see Ref. 9 and references cited therein).

7. The comparison of electrostatic potential surfaces for the parent unmethylated conformers (Figure 15) and their N-Me counterparts (Figure 23), highlights in both cases a partial "disruption of amphiphilicity"[42] for both predominating N-methylated conformers, but especially for Hydrazido-turn_ap_Me. This is due to the substitution of a highly positively charged N-H hydrogen (+0.43 e), which can be a very good hydrogen bond donor for the interaction with water in the hydrophilic portion from both the electrostatic and orbital points of view (see NBO analysis in previous paragraph), with a N-Me group, whose hydrogens are much less positively charged (NBO charges: +0.20-0.23 e; all the other charge schemes evidence almost null charges) and could interact with water only with a very weak donor-acceptor orbital interaction, as reported in the previous point for the intramolecular case in conformer Unconv-H-bond_deriving_from_Cycle-6_intraresidue_ap_Me.
8. The AIM analysis of Unconv-H-bond_deriving_from_Cycle-6_intraresidue_ap_Me conformer (Figure 24) shows the bond critical point corresponding to the weak unconventional C=O···H-C hydrogen bond, forming a 7-membered pseudocycle, already evidenced by NBO analysis. In fact, both the values of electron density and its Laplacian at BCP (ρ = 0.009 au; ∇^2_ρ = 0.029 au), albeit much lower than the corresponding values in the most stable intramolecularly H-bonded unmethylated conformers, are coherent with a weak hydrogen bond involving this kind of donor/acceptor couple.[124]

2.4.10 ^{1}H and ^{13}C NMR Spectra

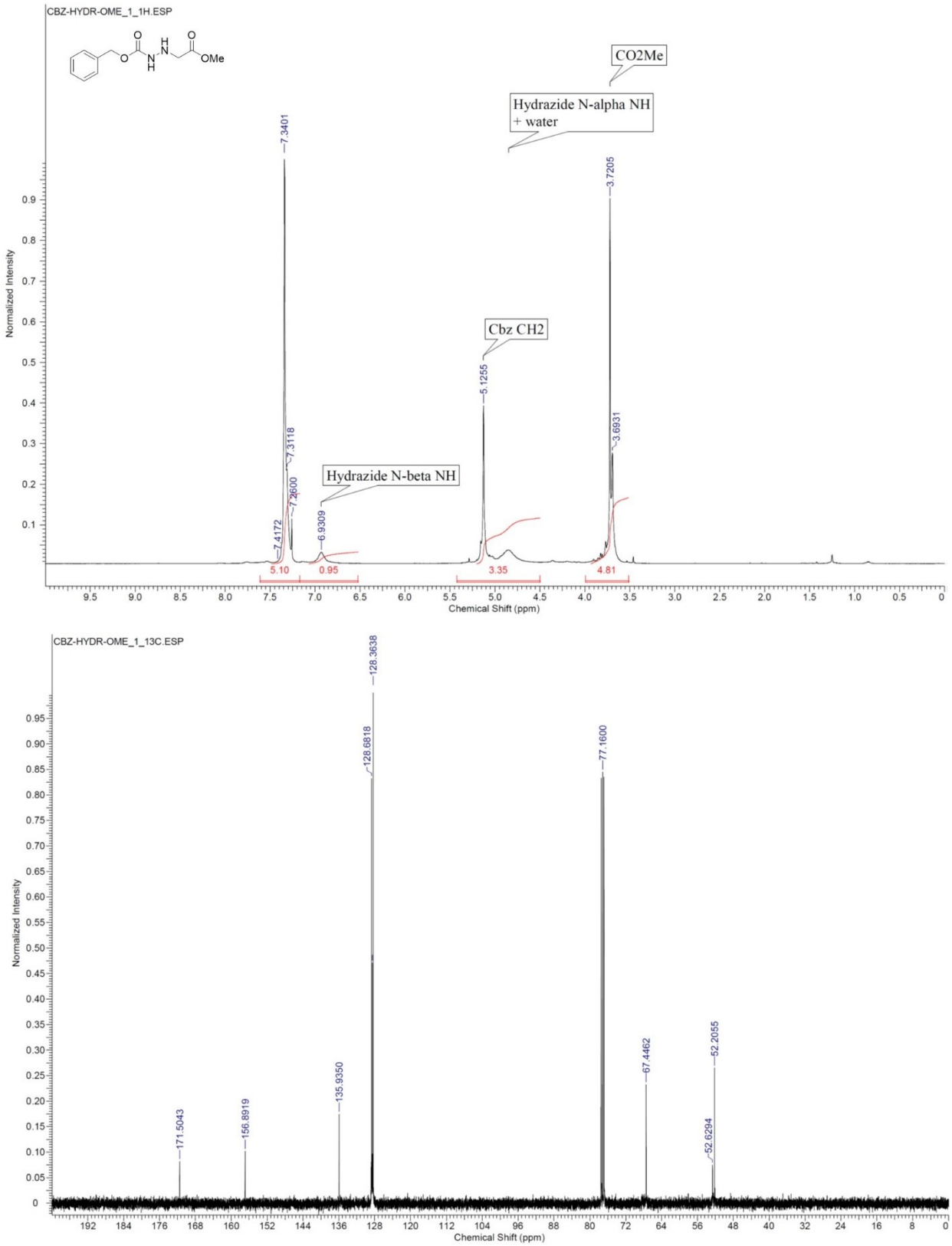

Figure 25. ^{1}H and ^{13}C NMR spectra in $CDCl_3$ of compound 1, Cbz-Hydr-OMe.

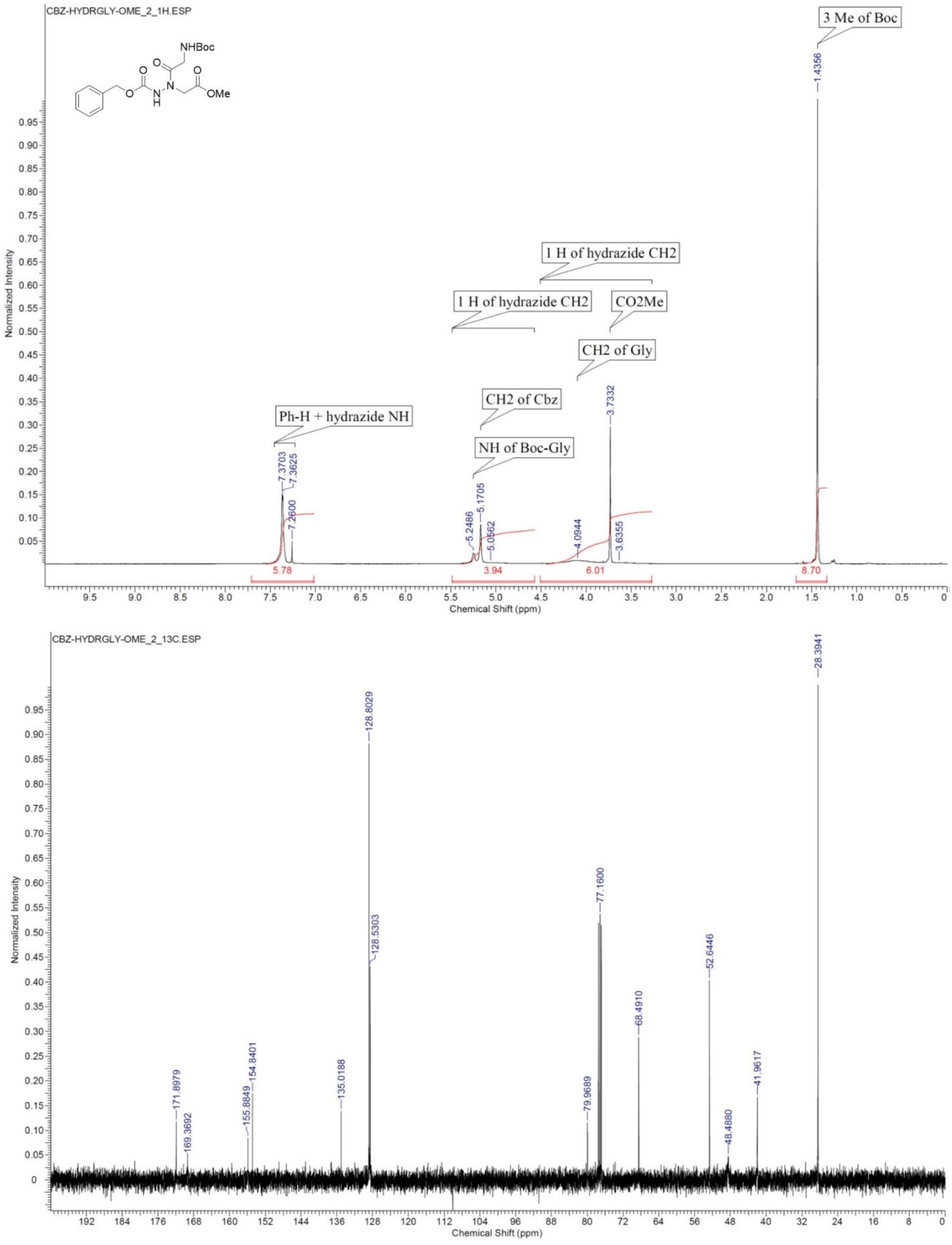

Figure 26. ^{1}H and ^{13}C NMR spectra in $CDCl_3$ of compound 2, Cbz-HydrGly-OMe.

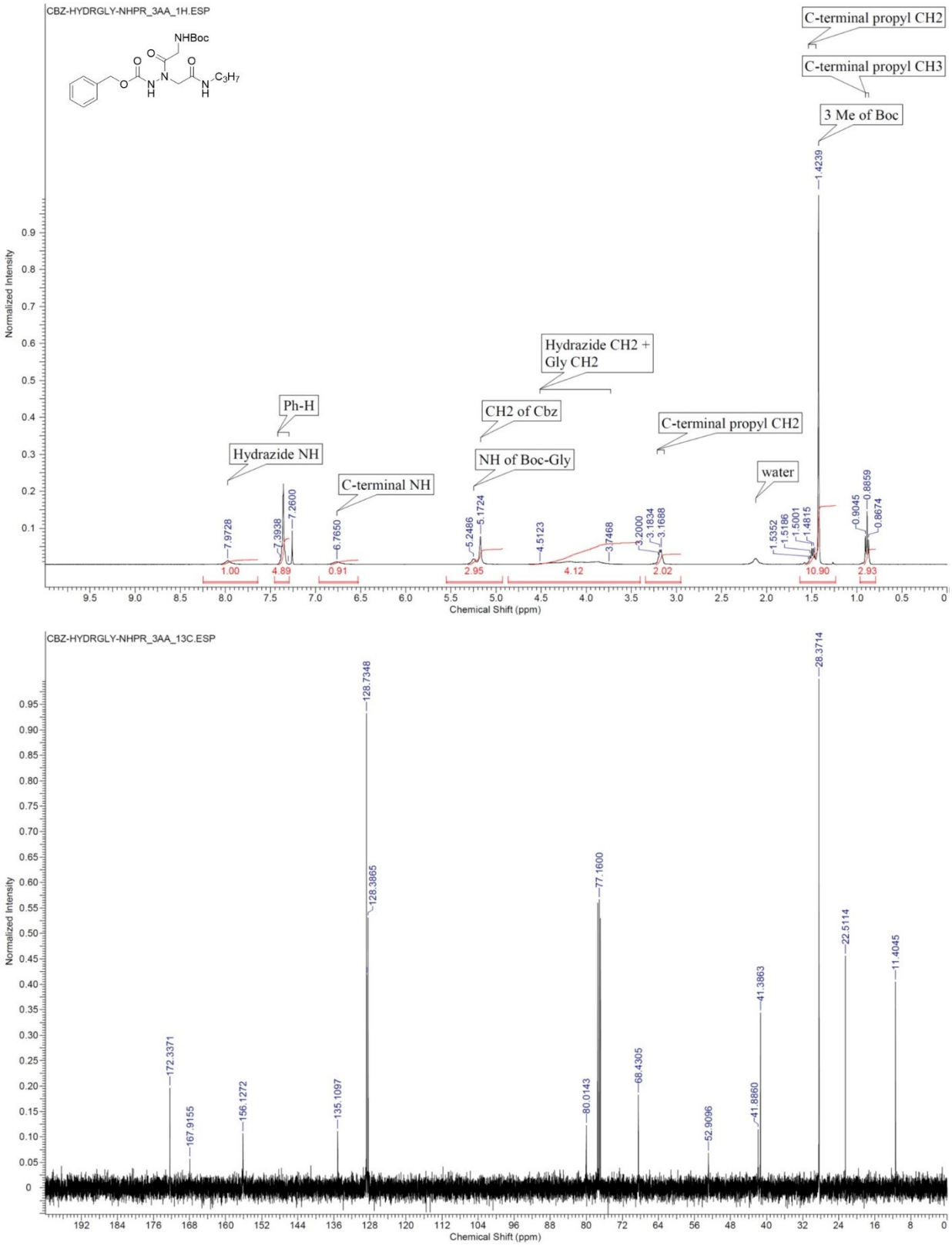

Figure 27. ^{1}H and ^{13}C NMR spectra in $CDCl_3$ of compound 3Aa, Cbz-HydrGly-NHC_3H_7.

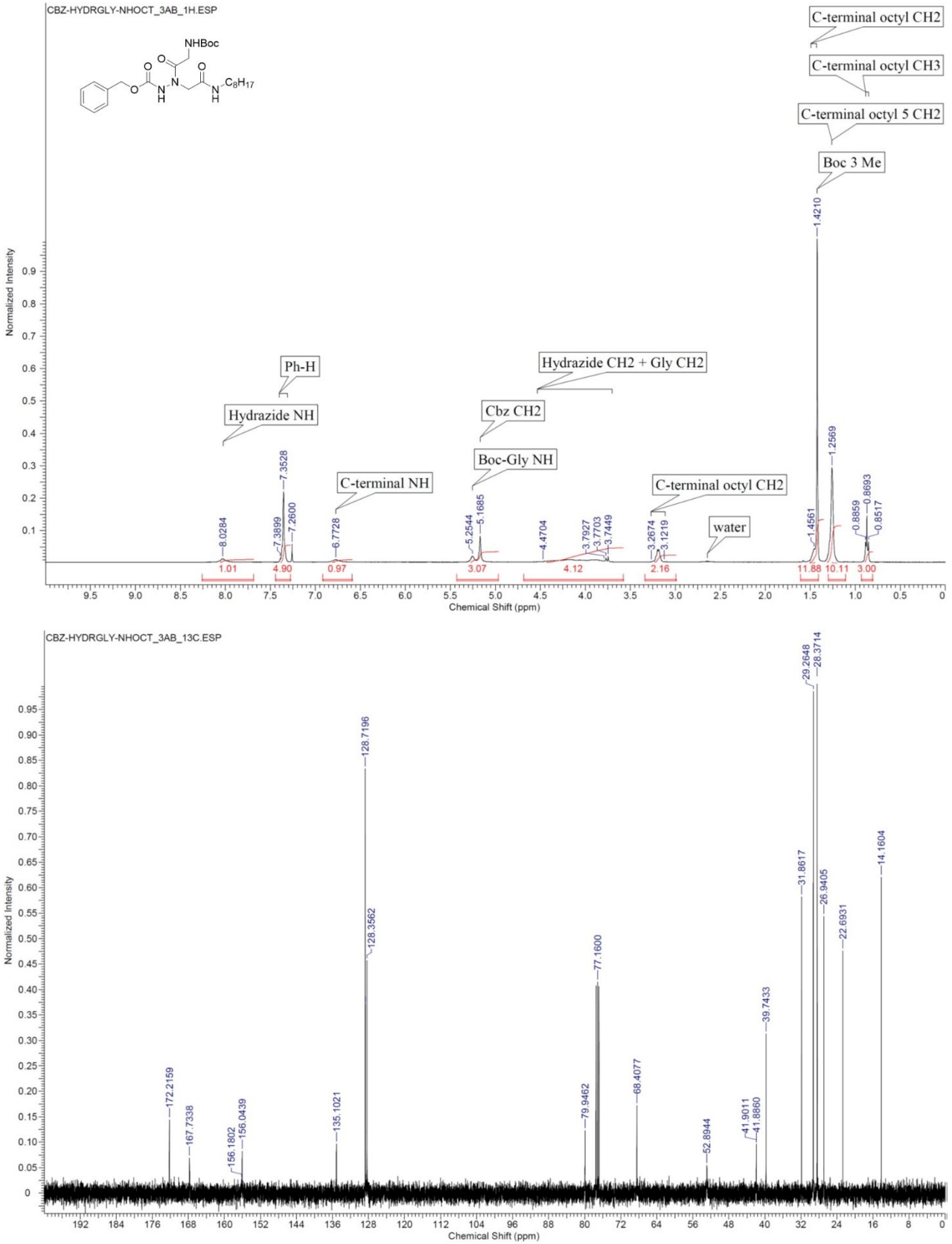

Figure 28. ^{1}H and ^{13}C NMR spectra in $CDCl_3$ of compound 3Ab, Cbz-HydrGly-NHC_8H_{17}.

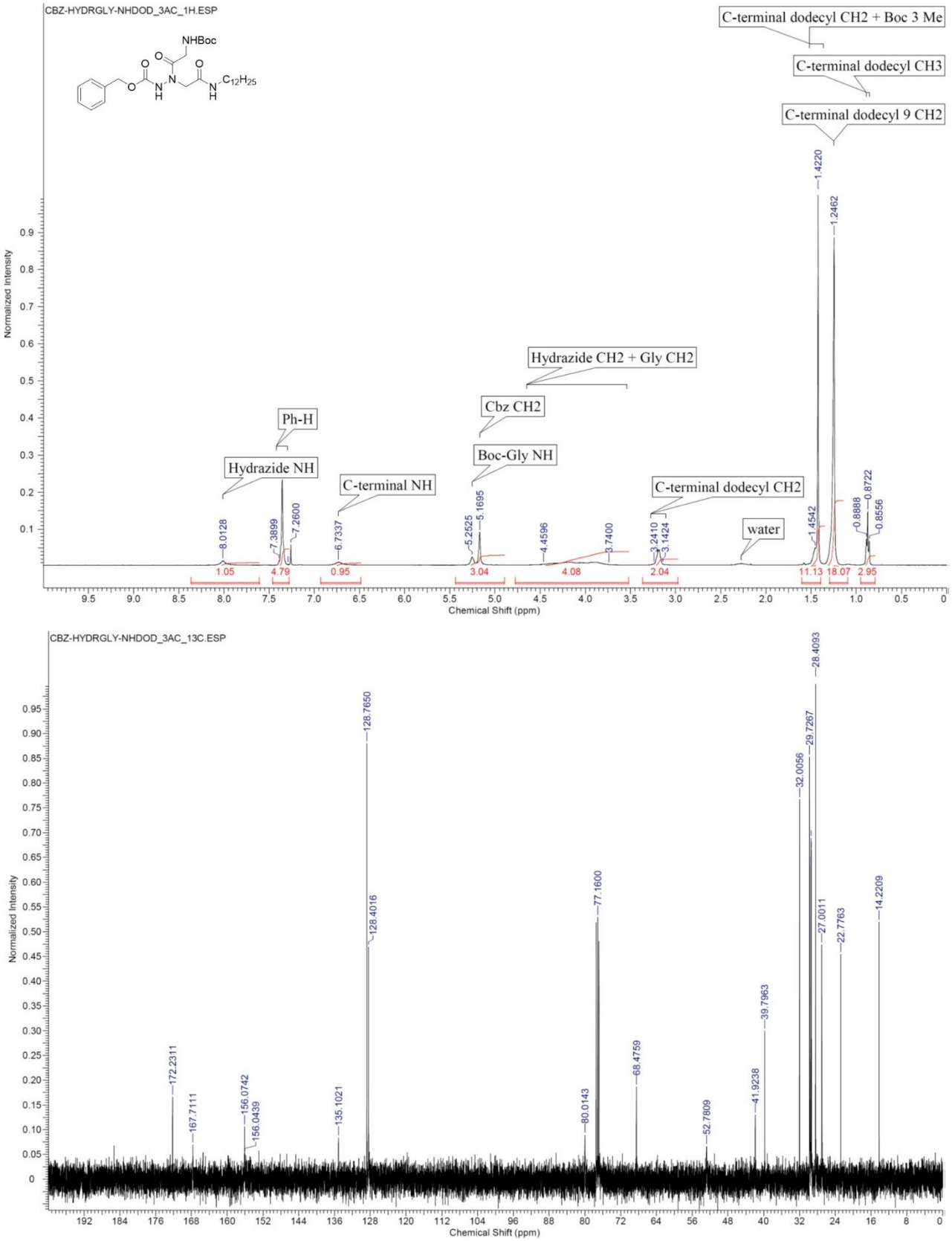

Figure 29. ^{1}H and ^{13}C NMR spectra in $CDCl_3$ of compound 3Ac, Cbz-HydrGly-$NHC_{12}H_{25}$.

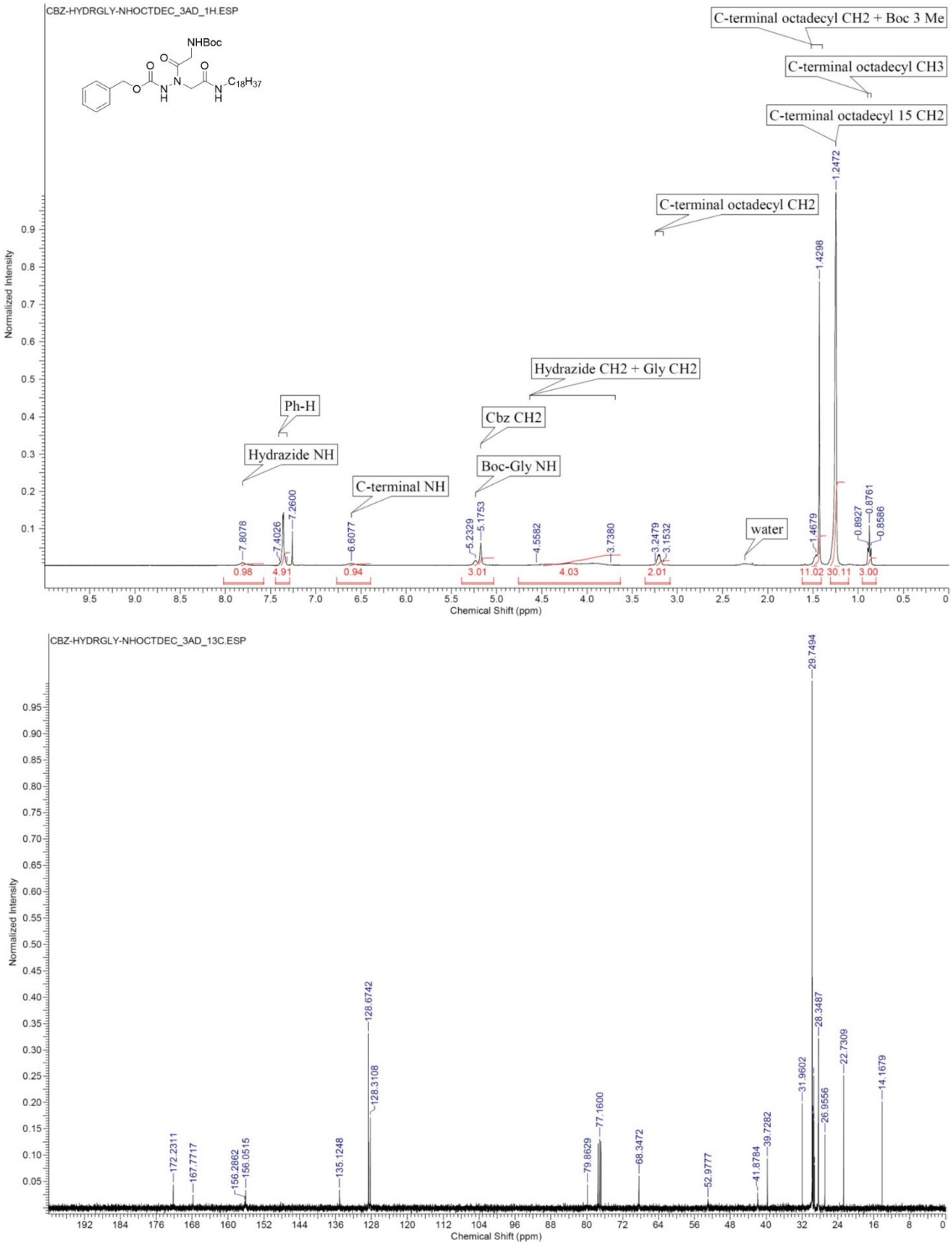

Figure 30. ^{1}H and ^{13}C NMR spectra in $CDCl_3$ of compound 3Ad, Cbz-HydrGly-$NHC_{18}H_{37}$.

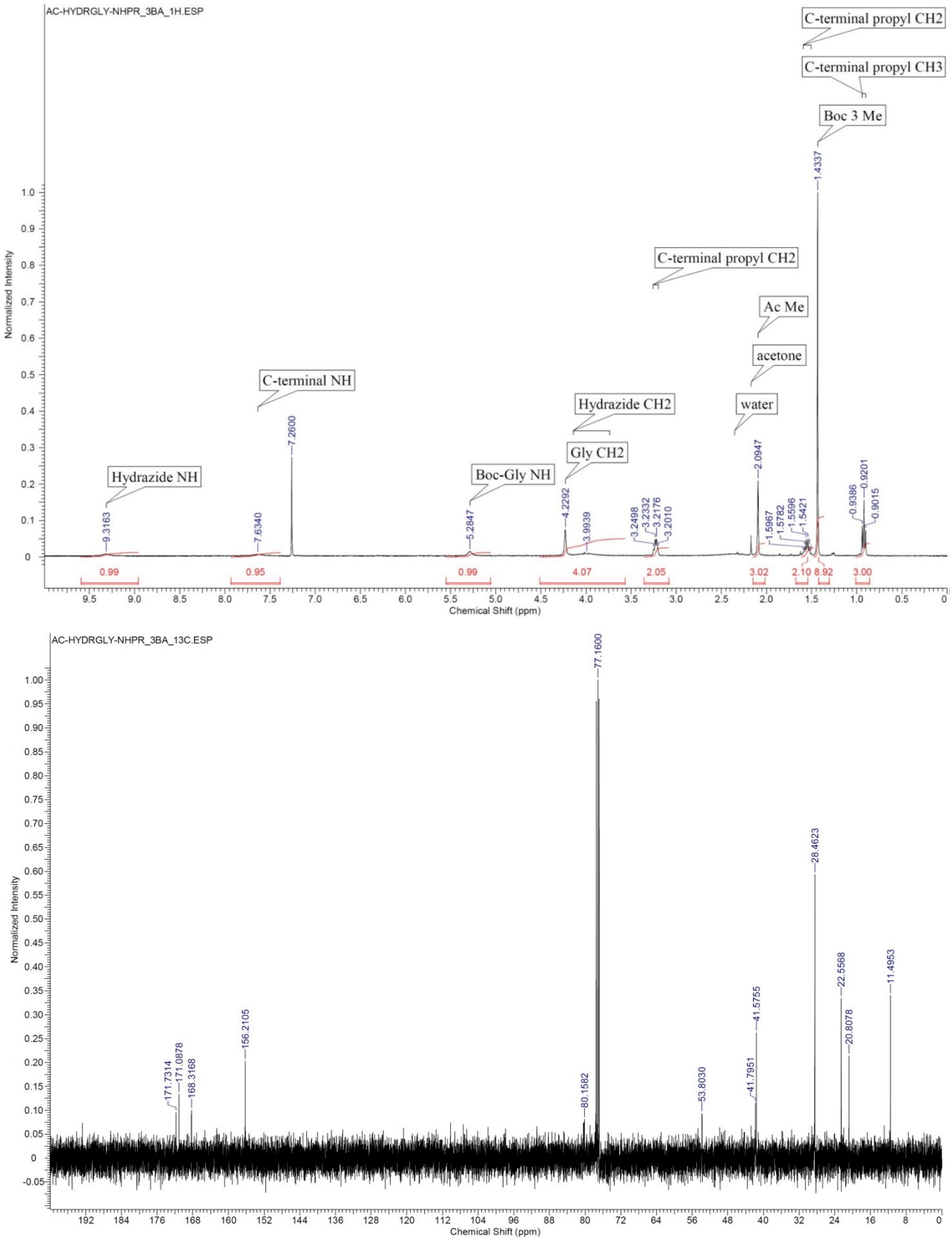

Figure 31. ^{1}H and ^{13}C NMR spectra in $CDCl_3$ of compound 3Ba, CH_3CO-HydrGly-NHC_3H_7.

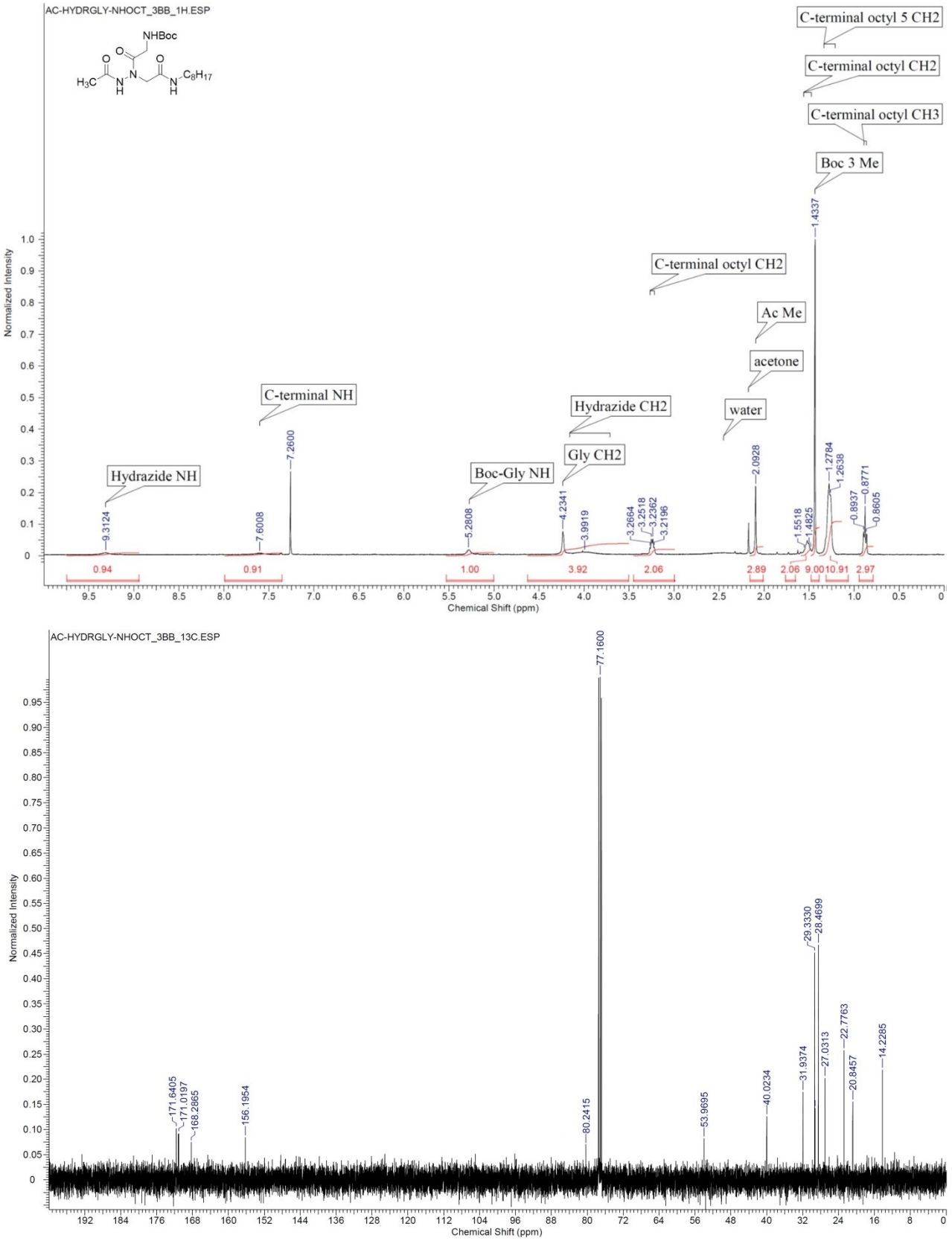

Figure 32. ^{1}H and ^{13}C NMR spectra in $CDCl_3$ of compound 3Bb, CH_3CO-HydrGly-NHC_8H_{17}.

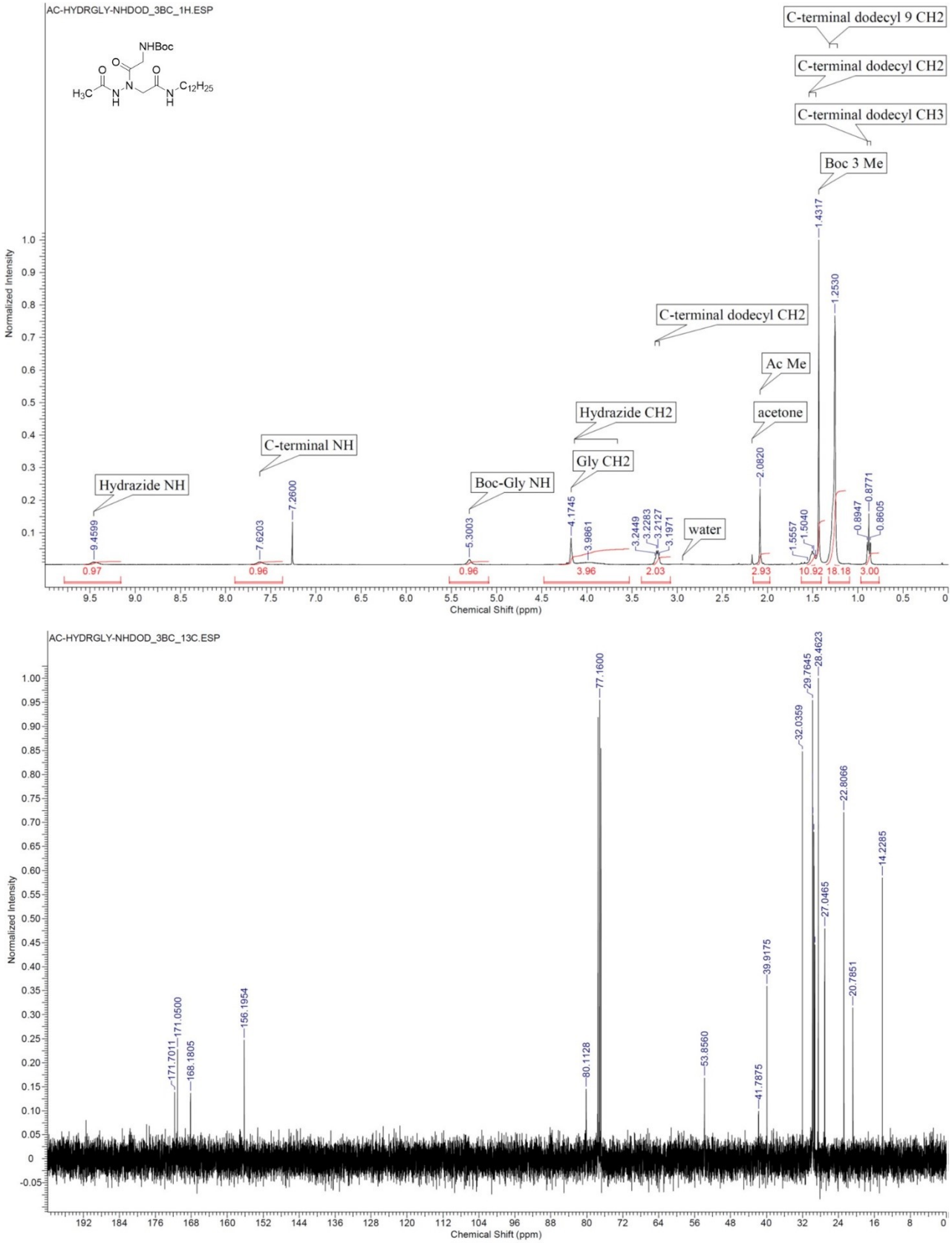

Figure 33. ^{1}H and ^{13}C NMR spectra in $CDCl_3$ of compound 3Bc, CH_3CO-HydrGly-$NHC_{12}H_{25}$.

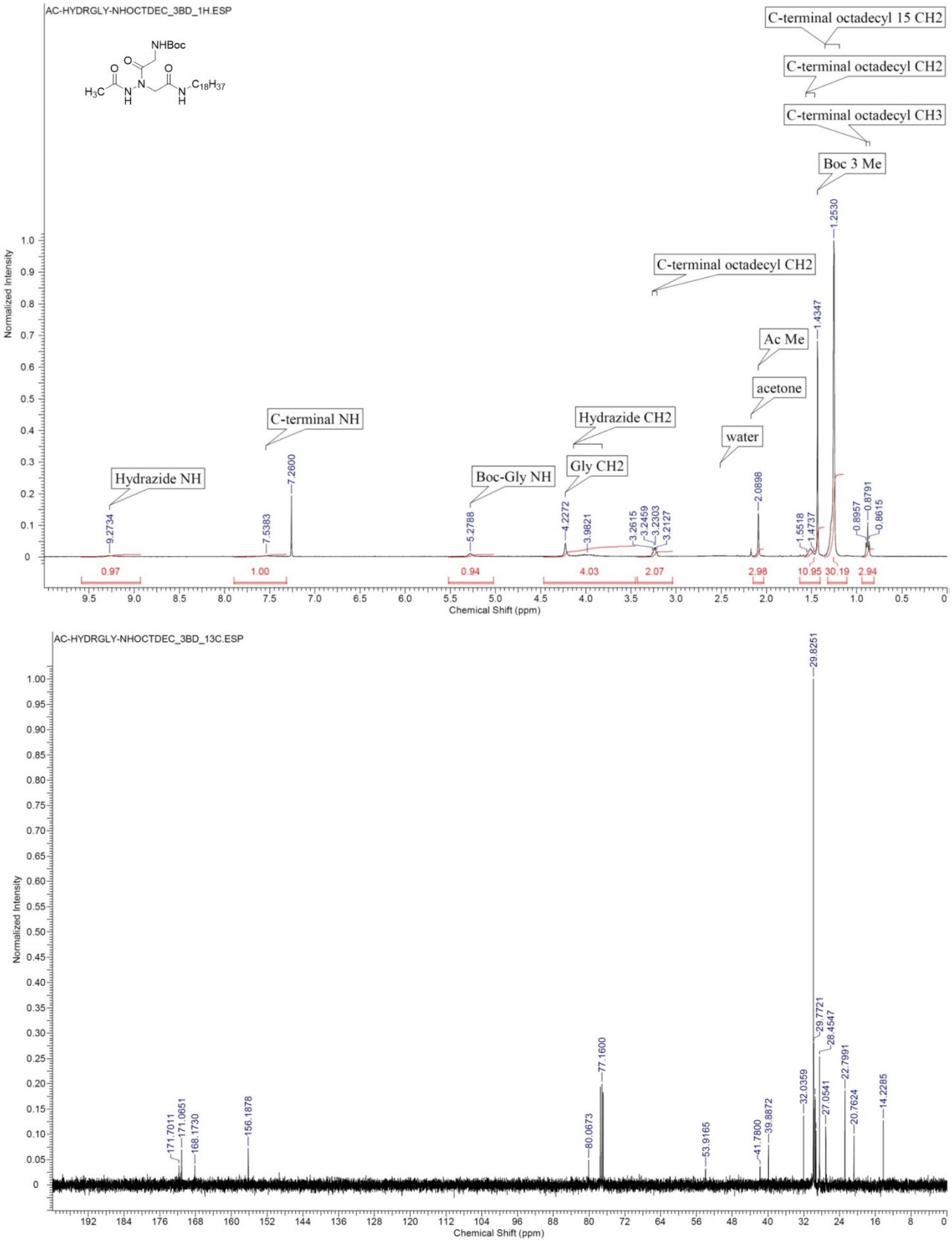

Figure 34. ^{1}H and ^{13}C NMR spectra in $CDCl_3$ of compound 3Bd, CH_3CO-HydrGly-$NHC_{18}H_{37}$.

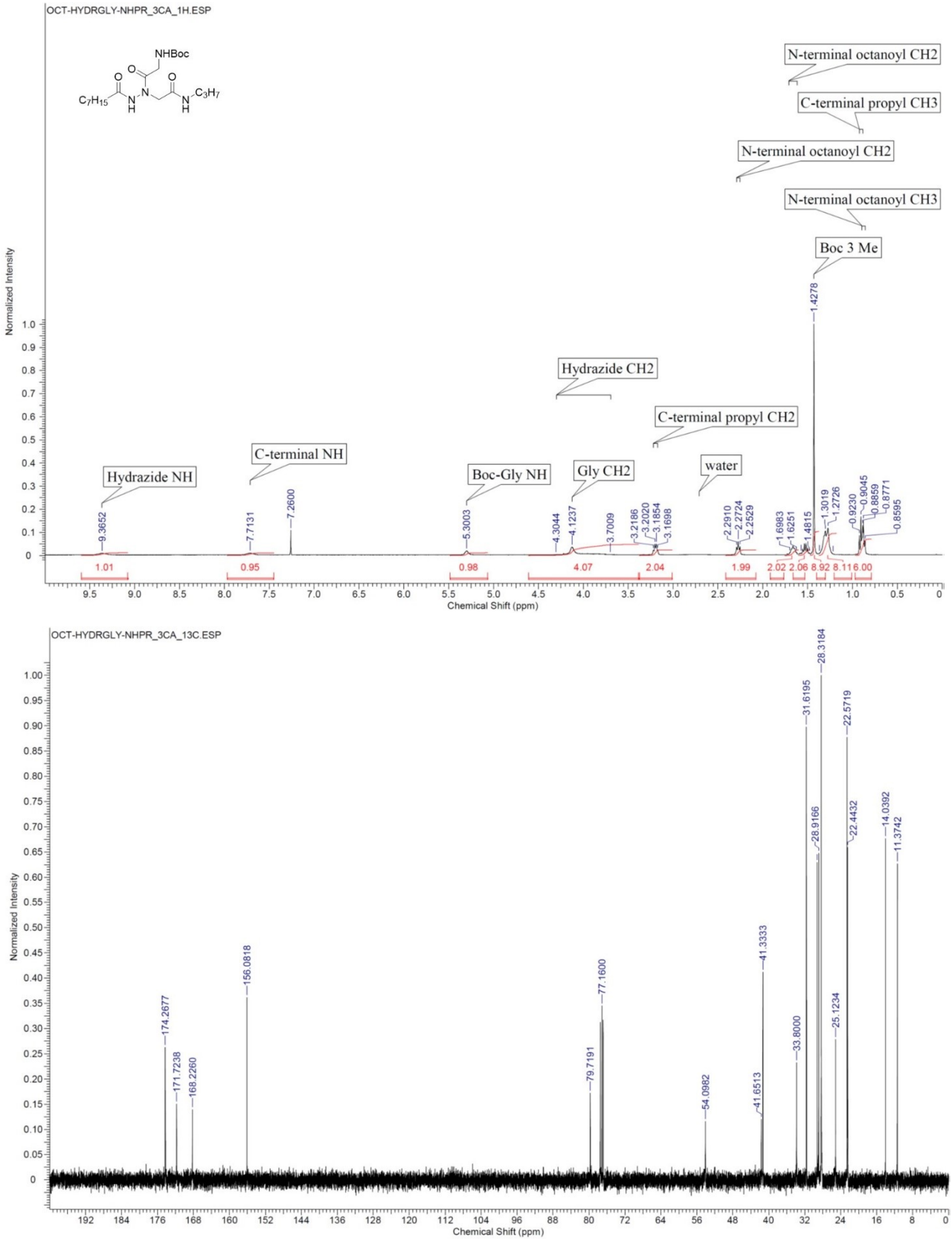

Figure 35. ^{1}H and ^{13}C NMR spectra in $CDCl_3$ of compound 3Ca, $C_7H_{15}CO$-HydrGly-NHC_3H_7.

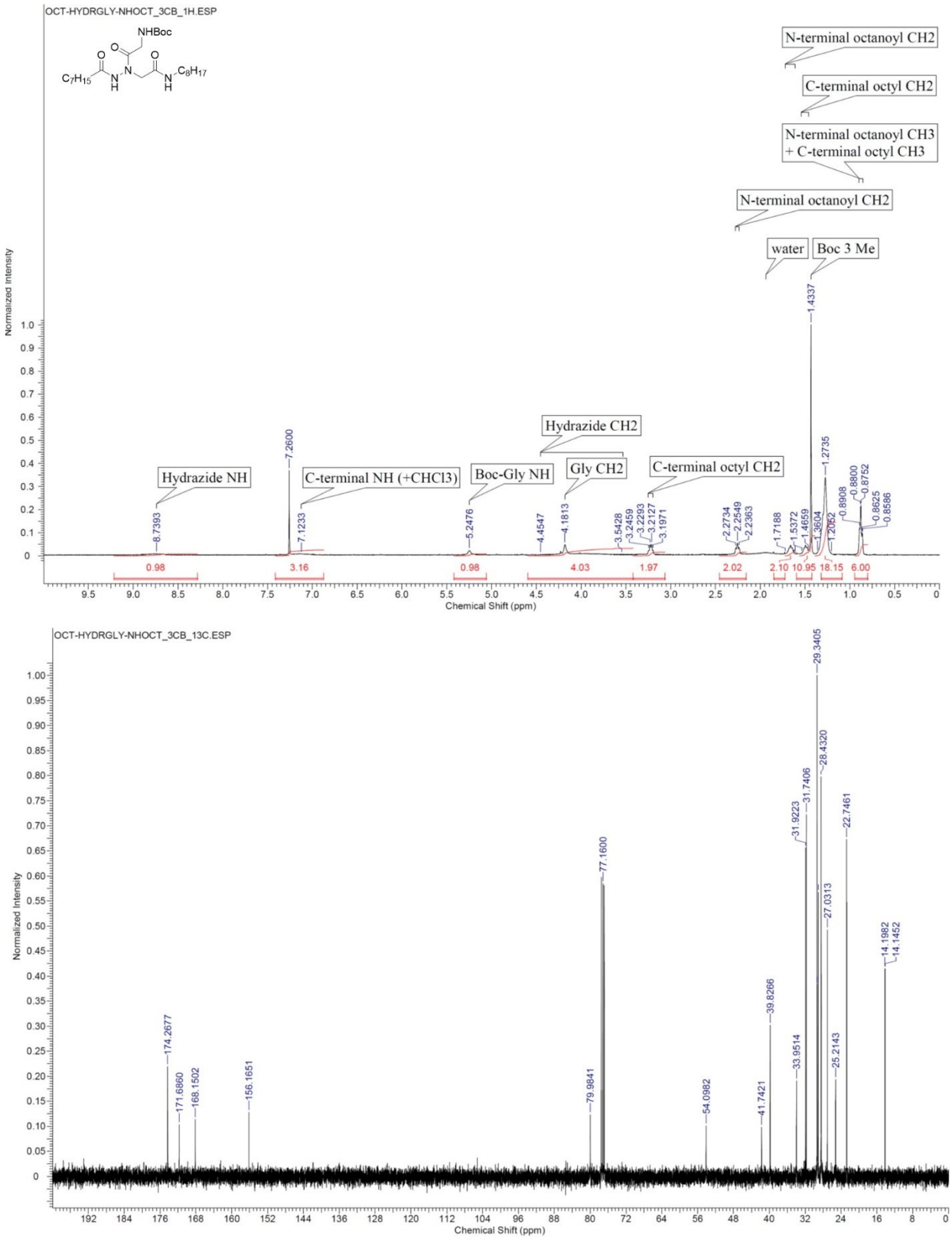

Figure 36. ^{1}H and ^{13}C NMR spectra in $CDCl_3$ of compound 3Cb, $C_7H_{15}CO$-HydrGly-NHC_8H_{17}.

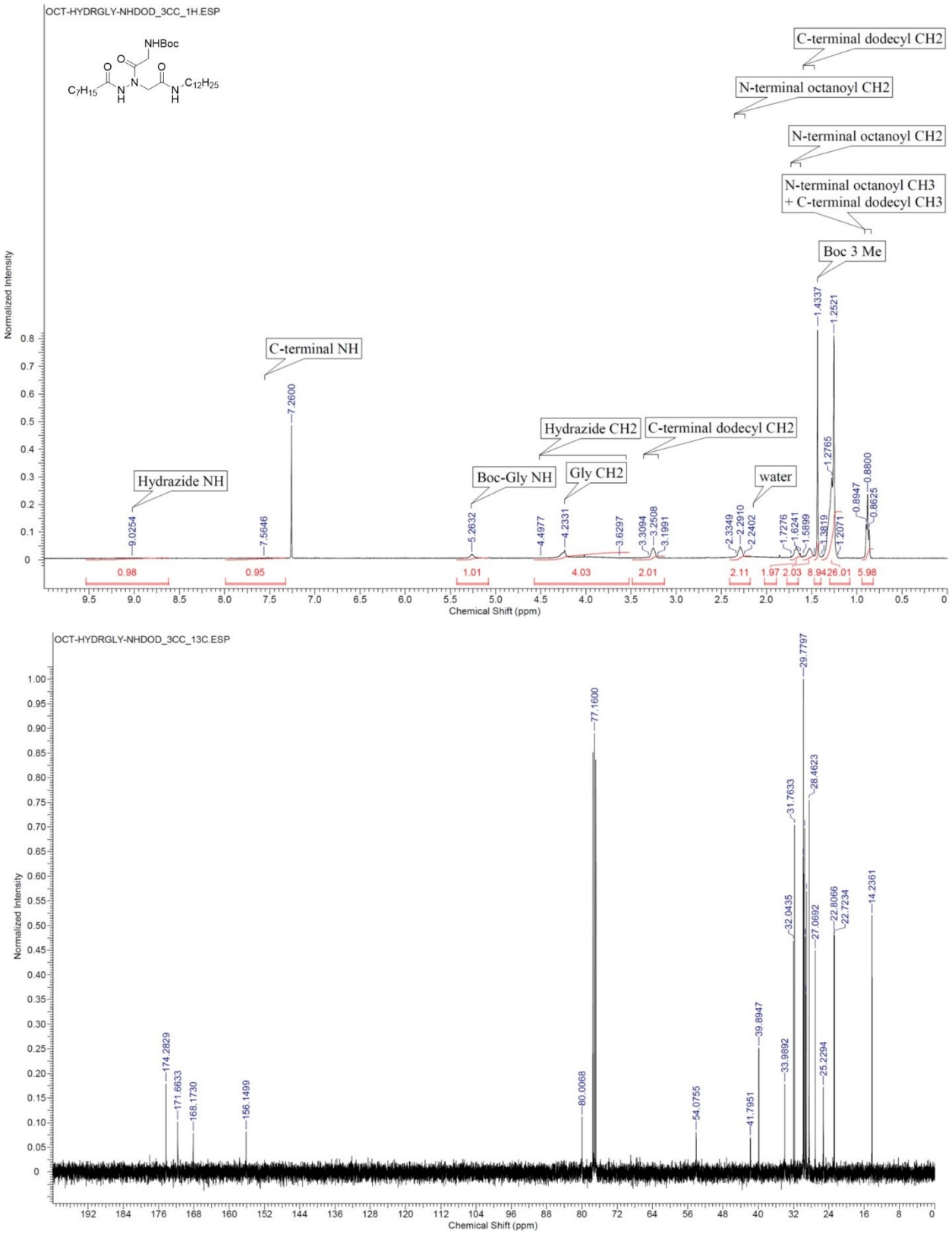

Figure 37. ^{1}H and ^{13}C NMR spectra in $CDCl_3$ of compound 3Cc, $C_7H_{15}CO$-HydrGly-$NHC_{12}H_{25}$.

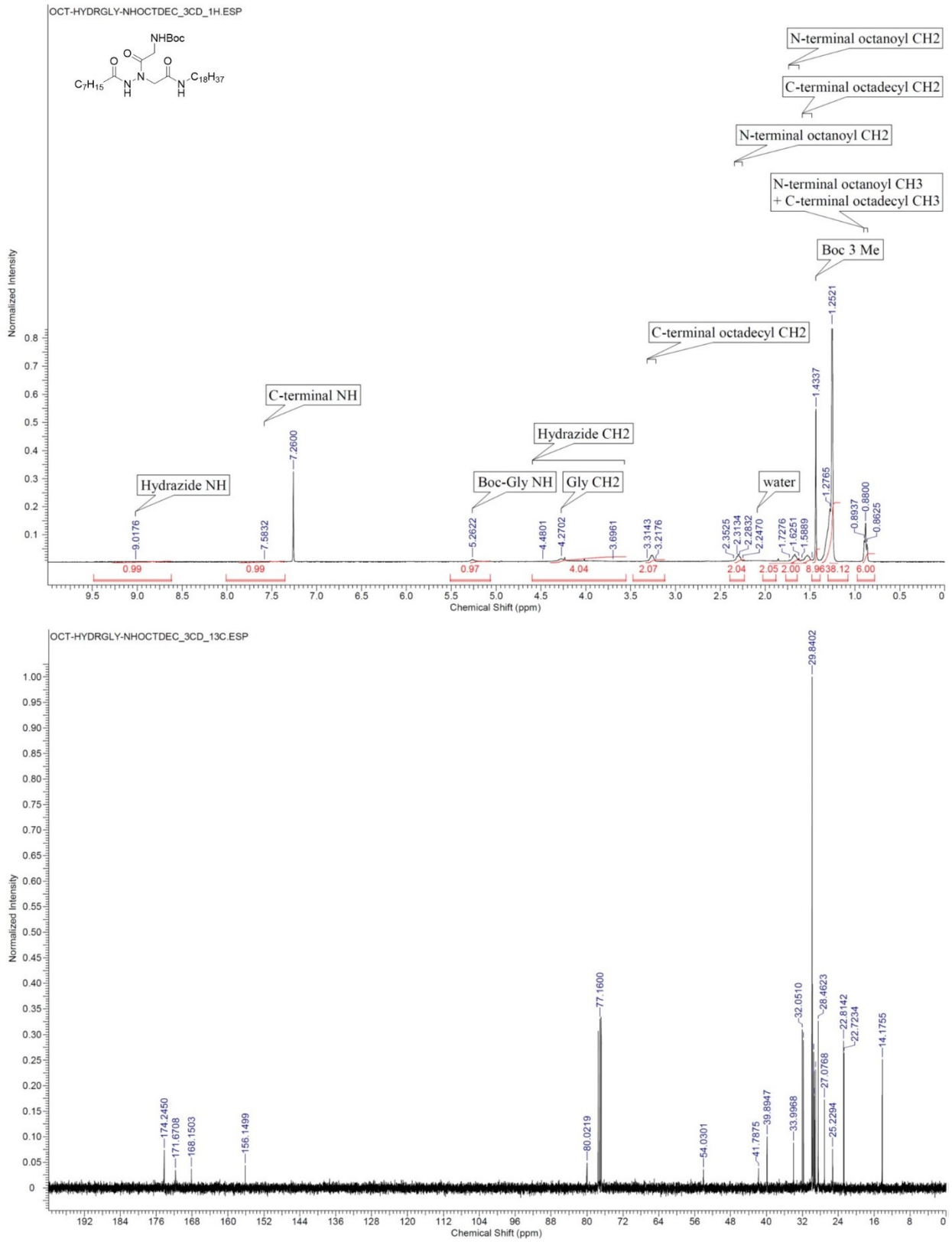

Figure 38. ^{1}H and ^{13}C NMR spectra in $CDCl_3$ of compound 3Cd, $C_7H_{15}CO$-HydrGly-$NHC_{18}H_{37}$.

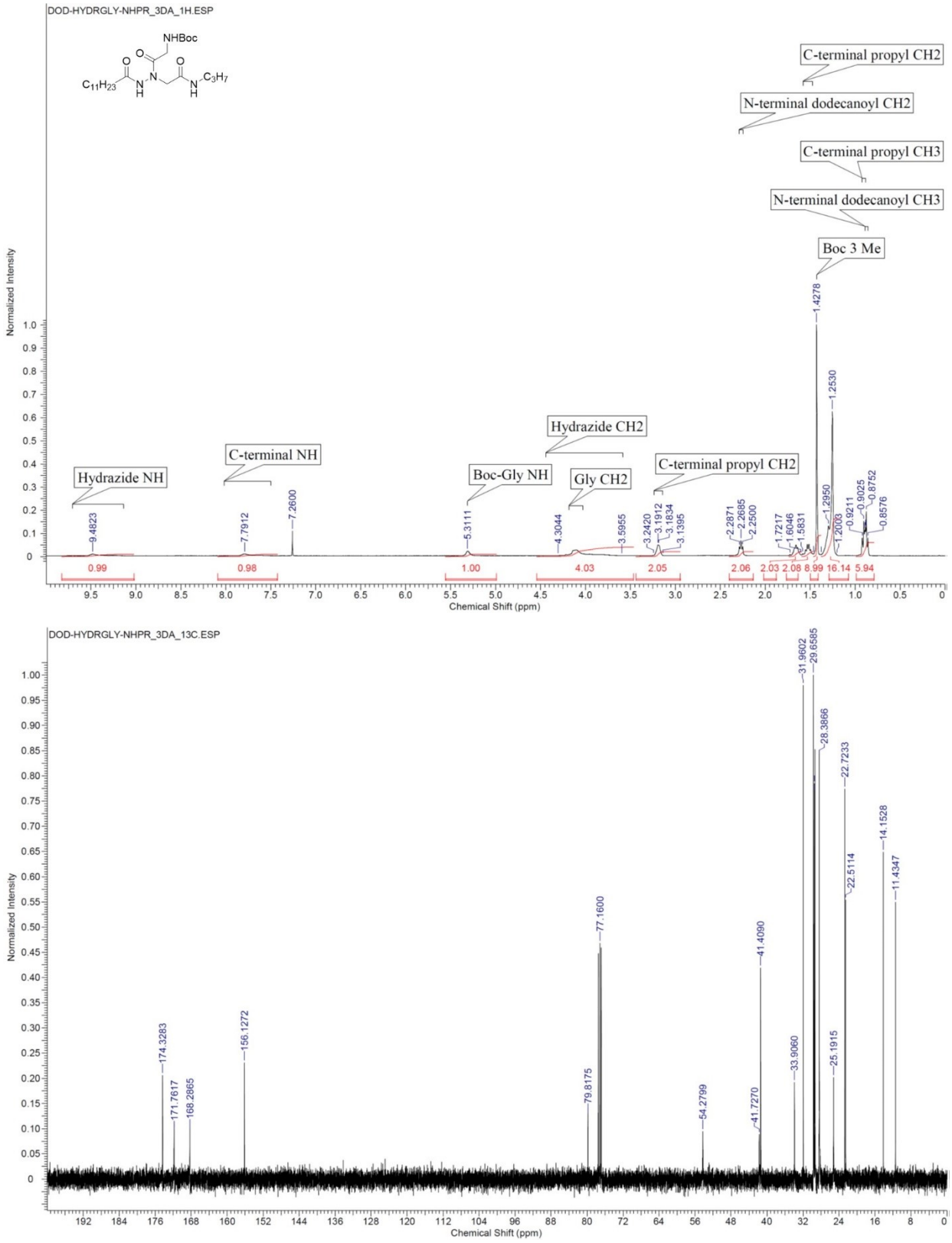

Figure 39. ^{1}H and ^{13}C NMR spectra in $CDCl_3$ of compound 3Da, $C_{11}H_{23}CO$-HydrGly-NHC_3H_7.

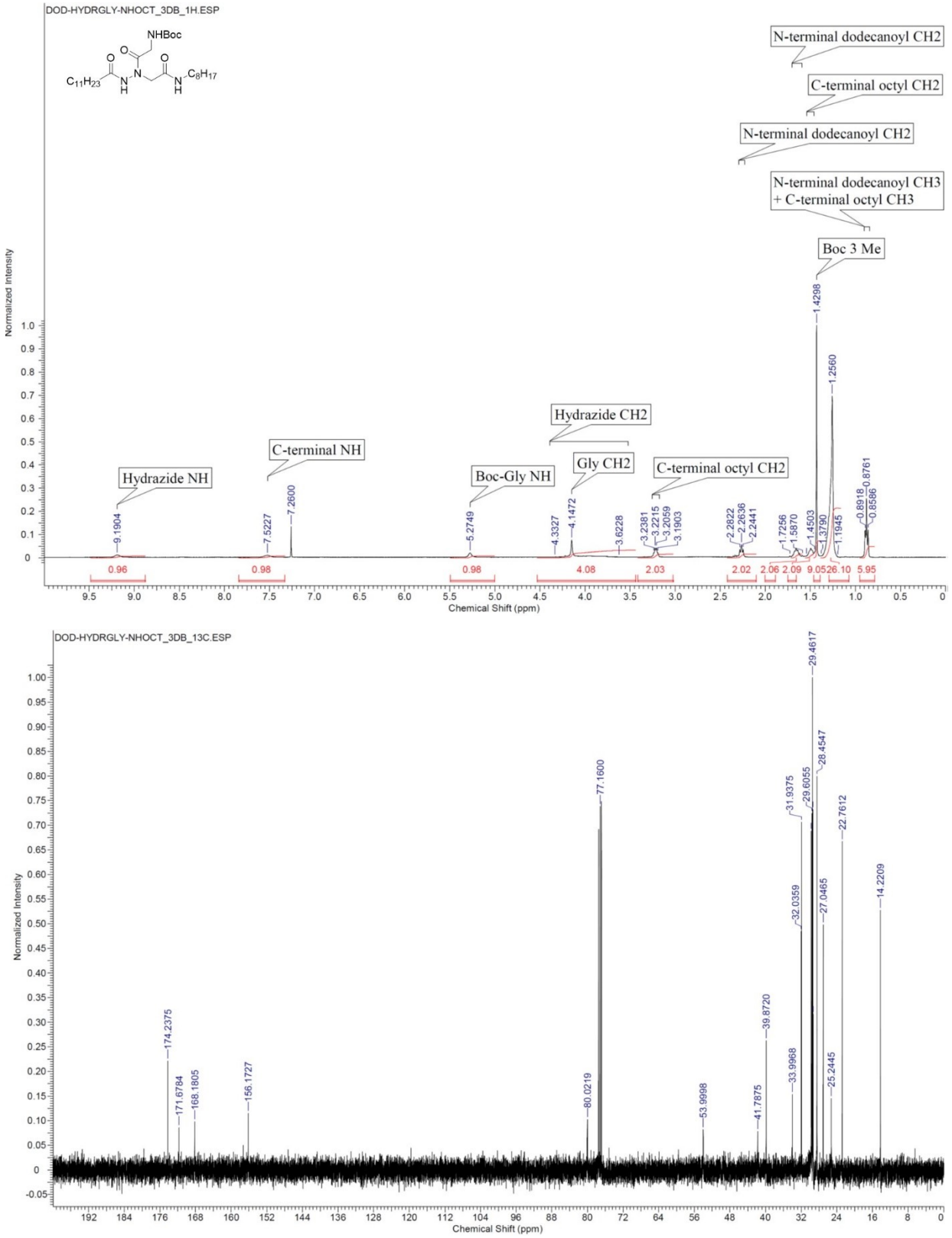

Figure 40. ^{1}H and ^{13}C NMR spectra in $CDCl_3$ of compound 3Db, $C_{11}H_{23}CO$-HydrGly-NHC_8H_{17}.

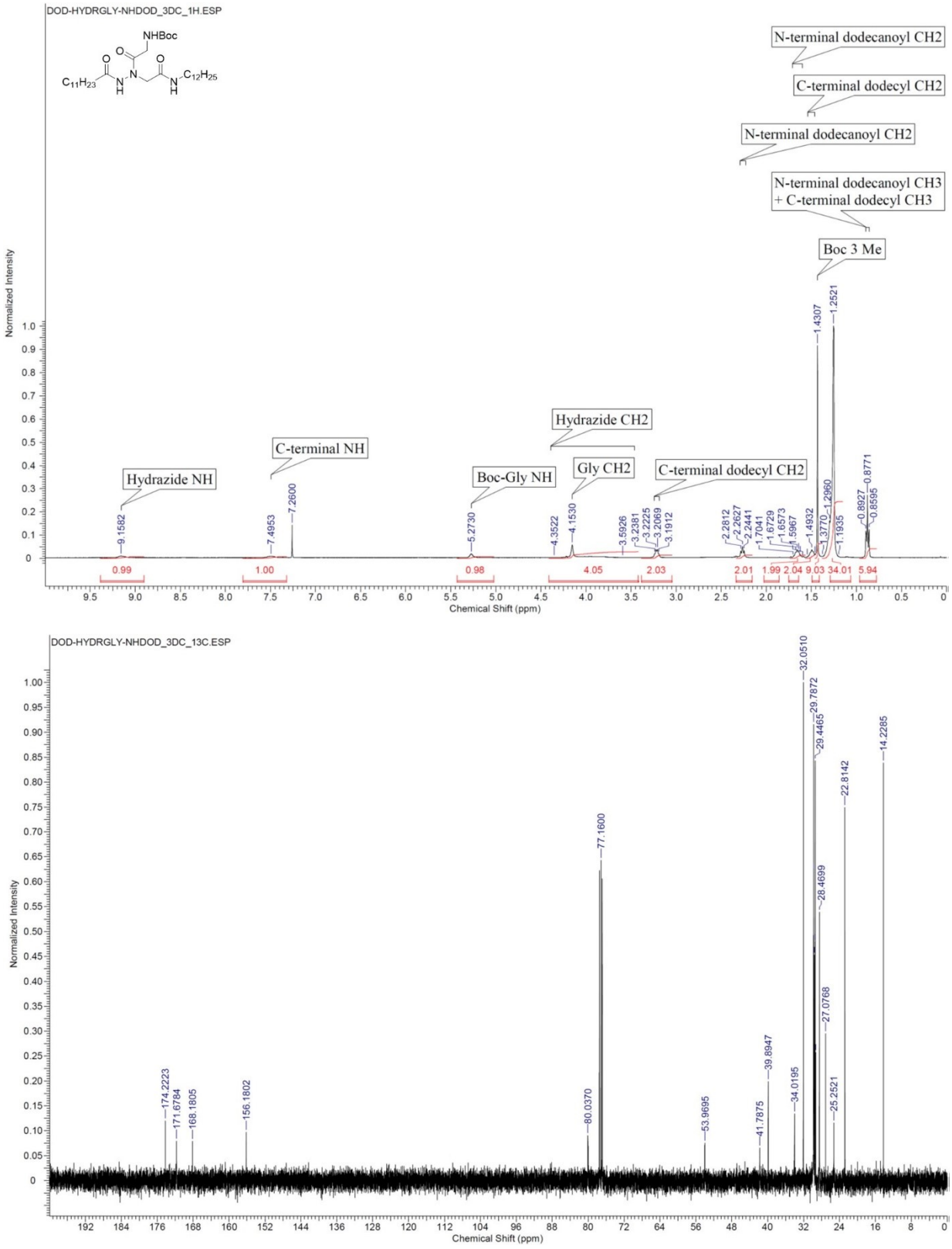

Figure 41. ^{1}H and ^{13}C NMR spectra in $CDCl_3$ of compound 3Dc, $C_{11}H_{23}CO$-HydrGly-$NHC_{12}H_{25}$.

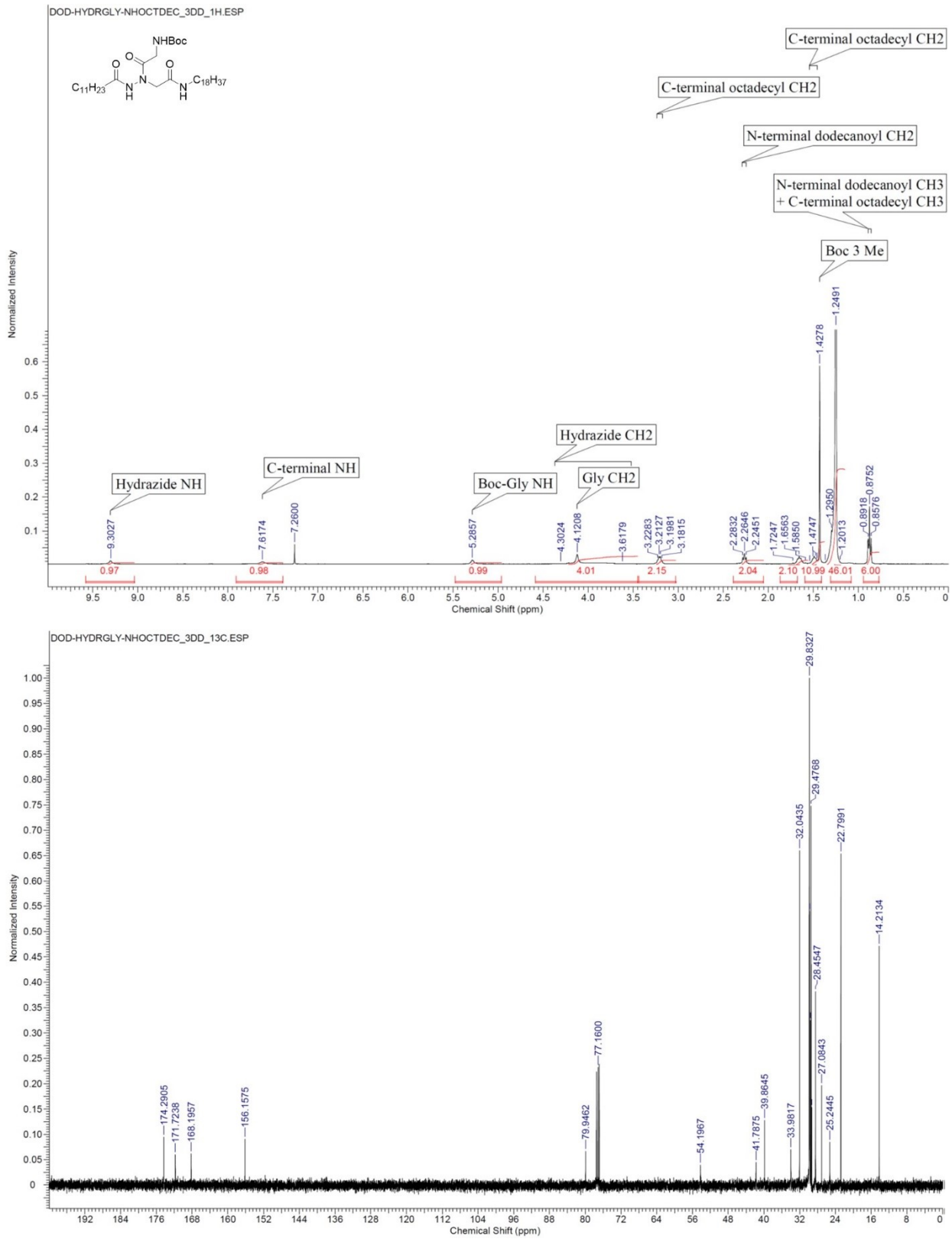

Figure 42. ^{1}H and ^{13}C NMR spectra in $CDCl_3$ of compound 3Dd, $C_{11}H_{23}CO$-HydrGly-$NHC_{18}H_{37}$.

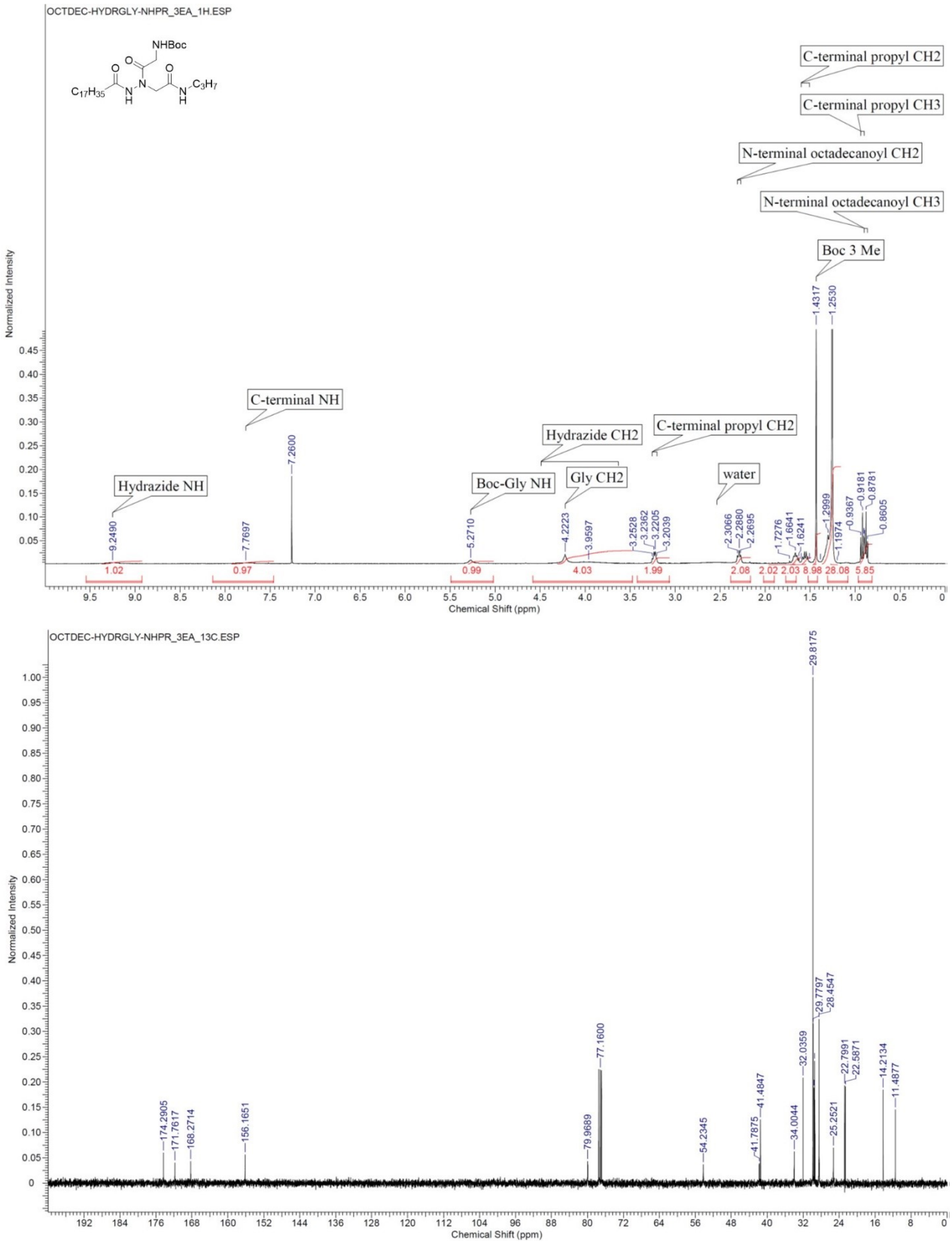

Figure 43. ^{1}H and ^{13}C NMR spectra in $CDCl_3$ of compound 3Ea, $C_{17}H_{35}CO$-HydrGly-NHC_3H_7.

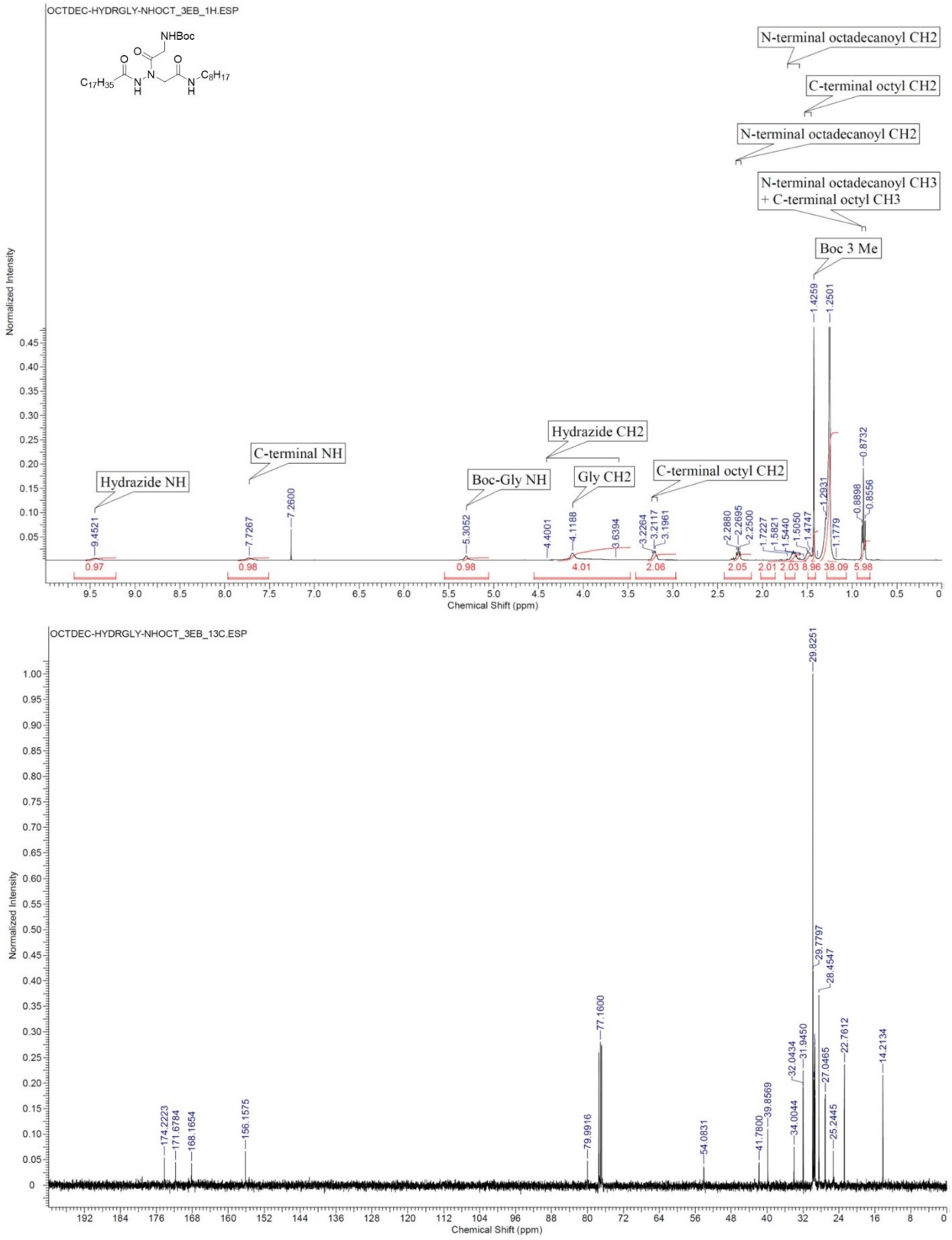

Figure 44. ^{1}H and ^{13}C NMR spectra in $CDCl_3$ of compound 3Eb, $C_{17}H_{35}CO$-HydrGly-NHC_8H_{17}.

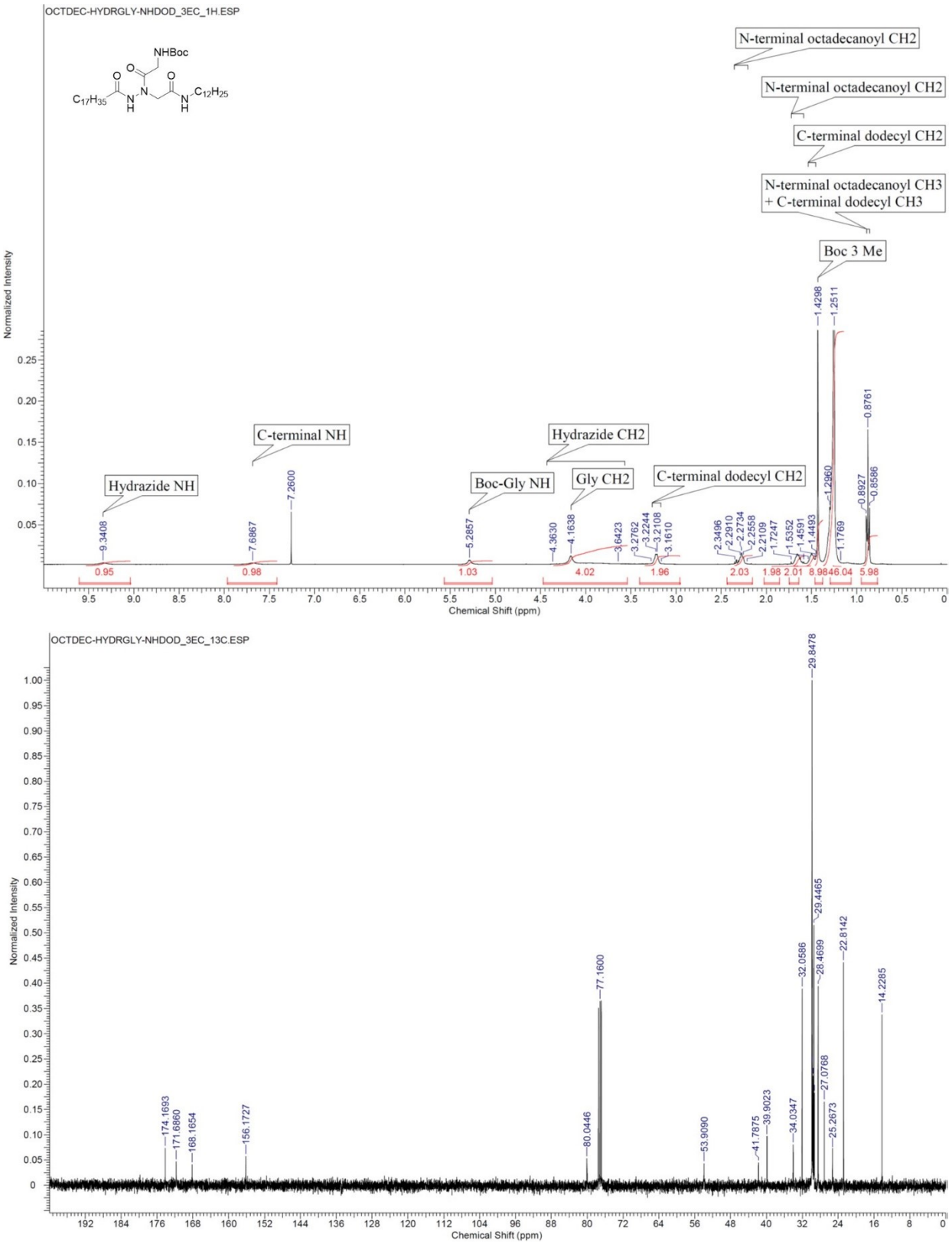

Figure 45. ^{1}H and ^{13}C NMR spectra in $CDCl_3$ of compound 3Ec, $C_{17}H_{35}CO$-HydrGly-$NHC_{12}H_{25}$.

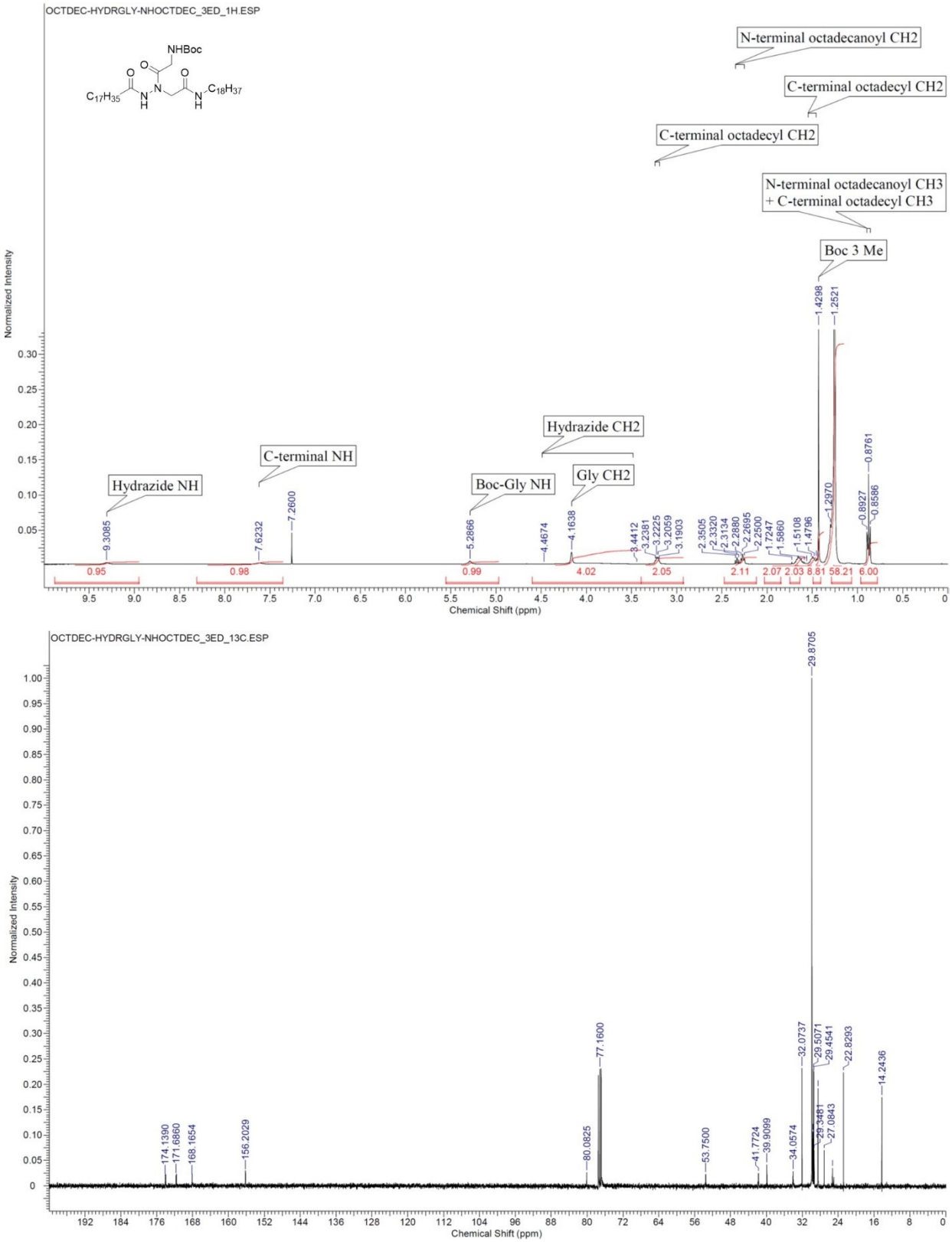

Figure 46. ^{1}H and ^{13}C NMR spectra in $CDCl_3$ of compound 3Ed, $C_{17}H_{35}CO$-HydrGly-$NHC_{18}H_{37}$.

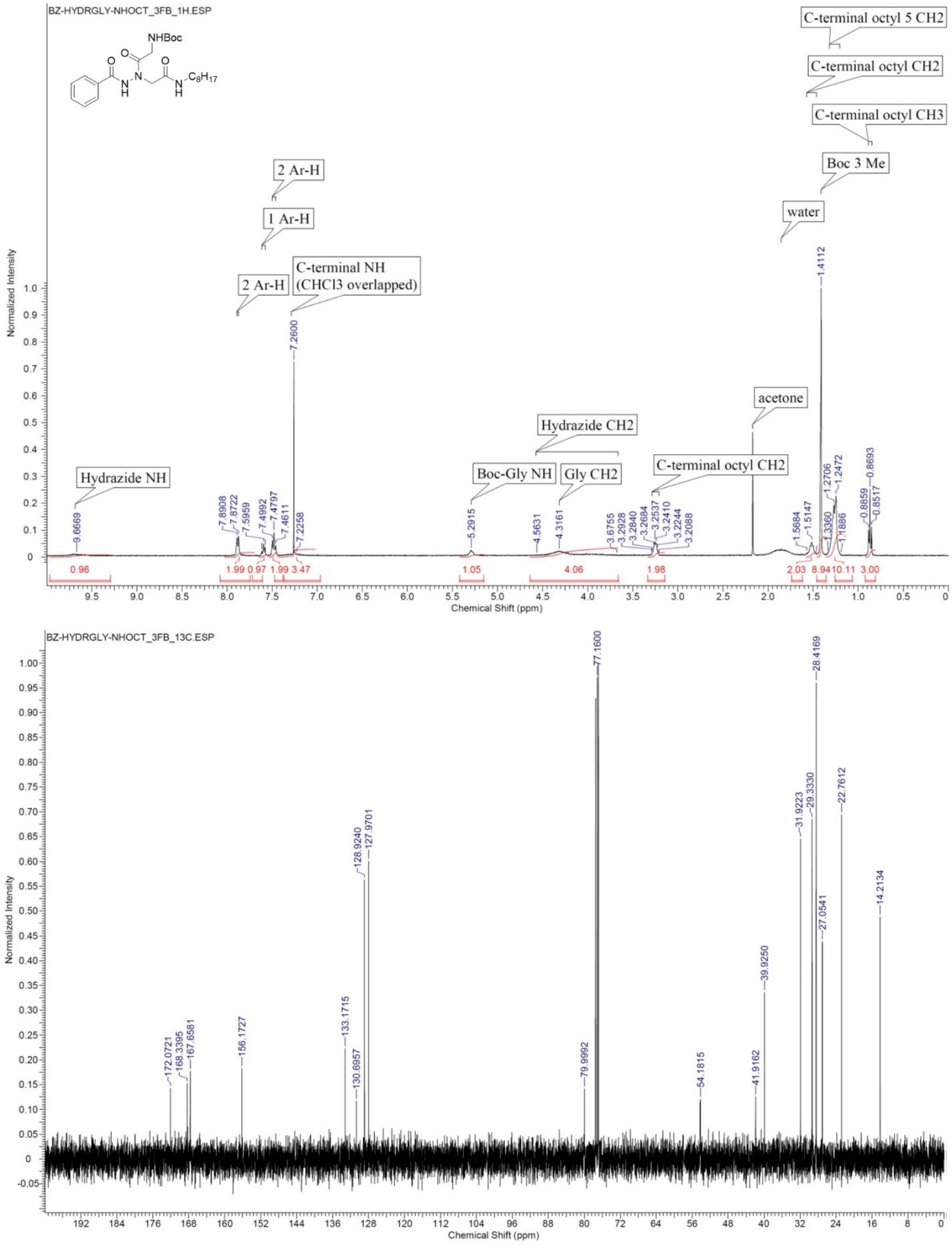

Figure 47. ^{1}H and ^{13}C NMR spectra in $CDCl_3$ of compound 3Fb, PhCO-HydrGly-NHC_8H_{17}.

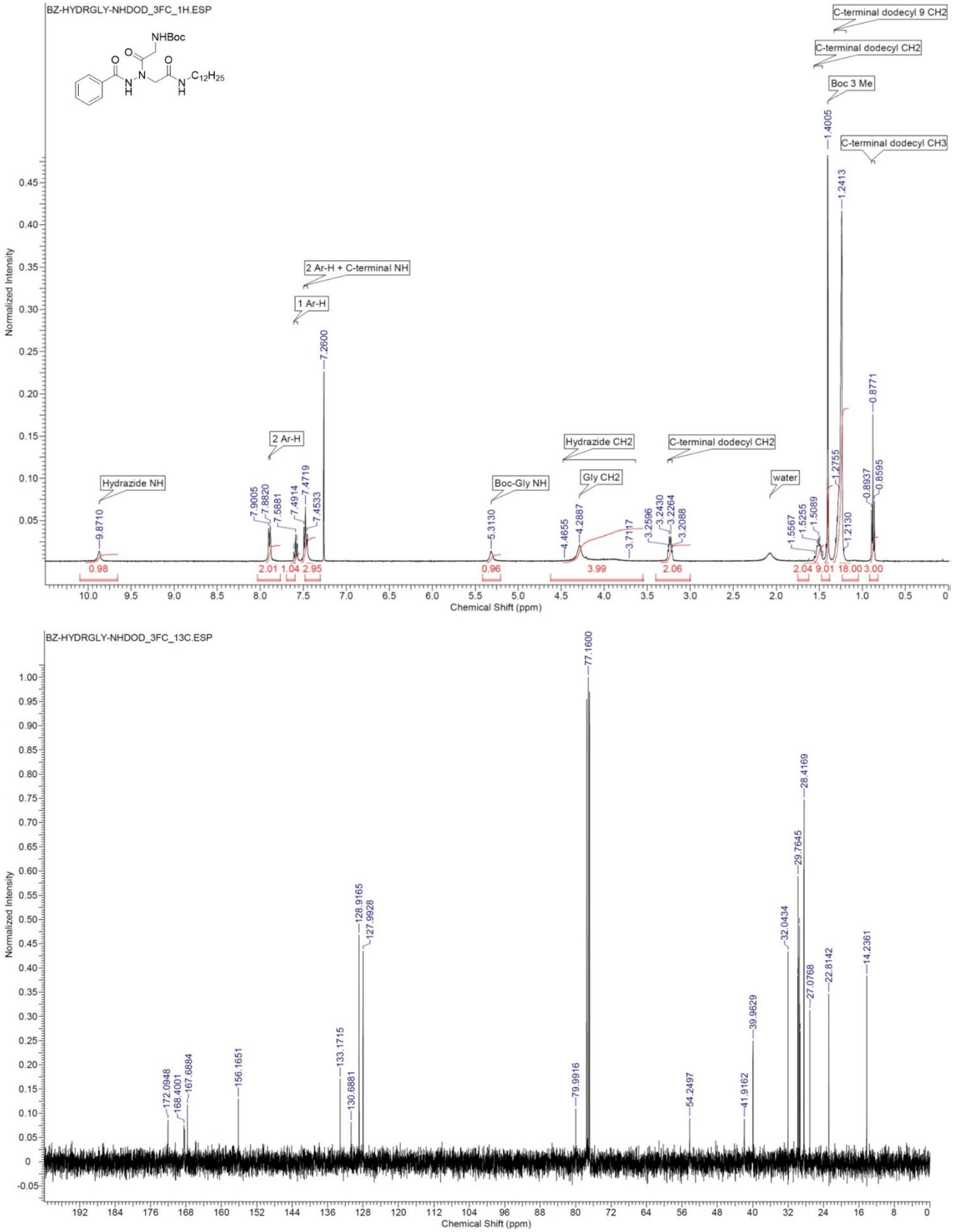

Figure 48. ^{1}H and ^{13}C NMR spectra in $CDCl_3$ of compound 3Fc, PhCO-HydrGly-$NHC_{12}H_{25}$.

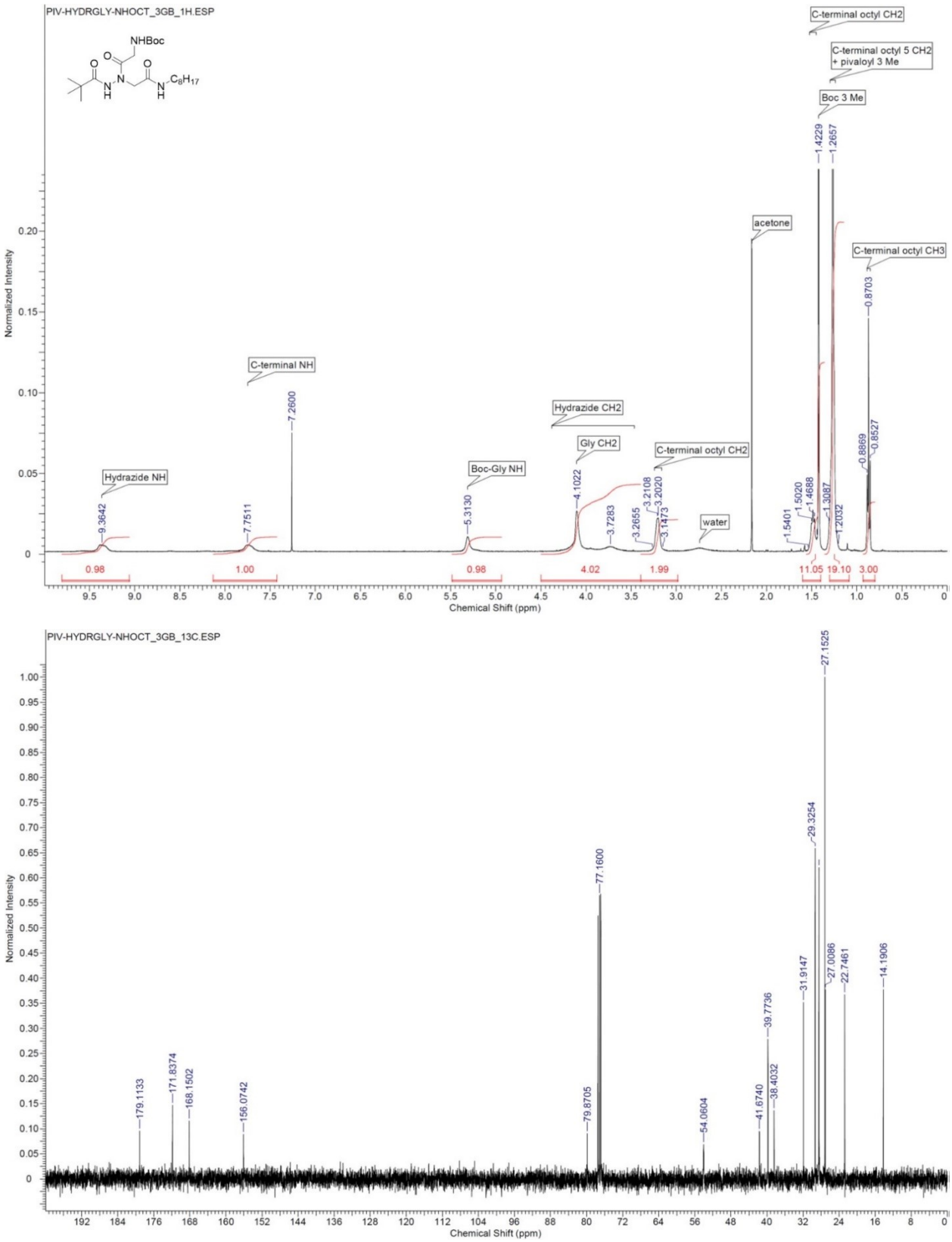

Figure 49. ^{1}H and ^{13}C NMR spectra in $CDCl_3$ of compound 3Gb, *t*BuCO-HydrGly-NHC_8H_{17}.

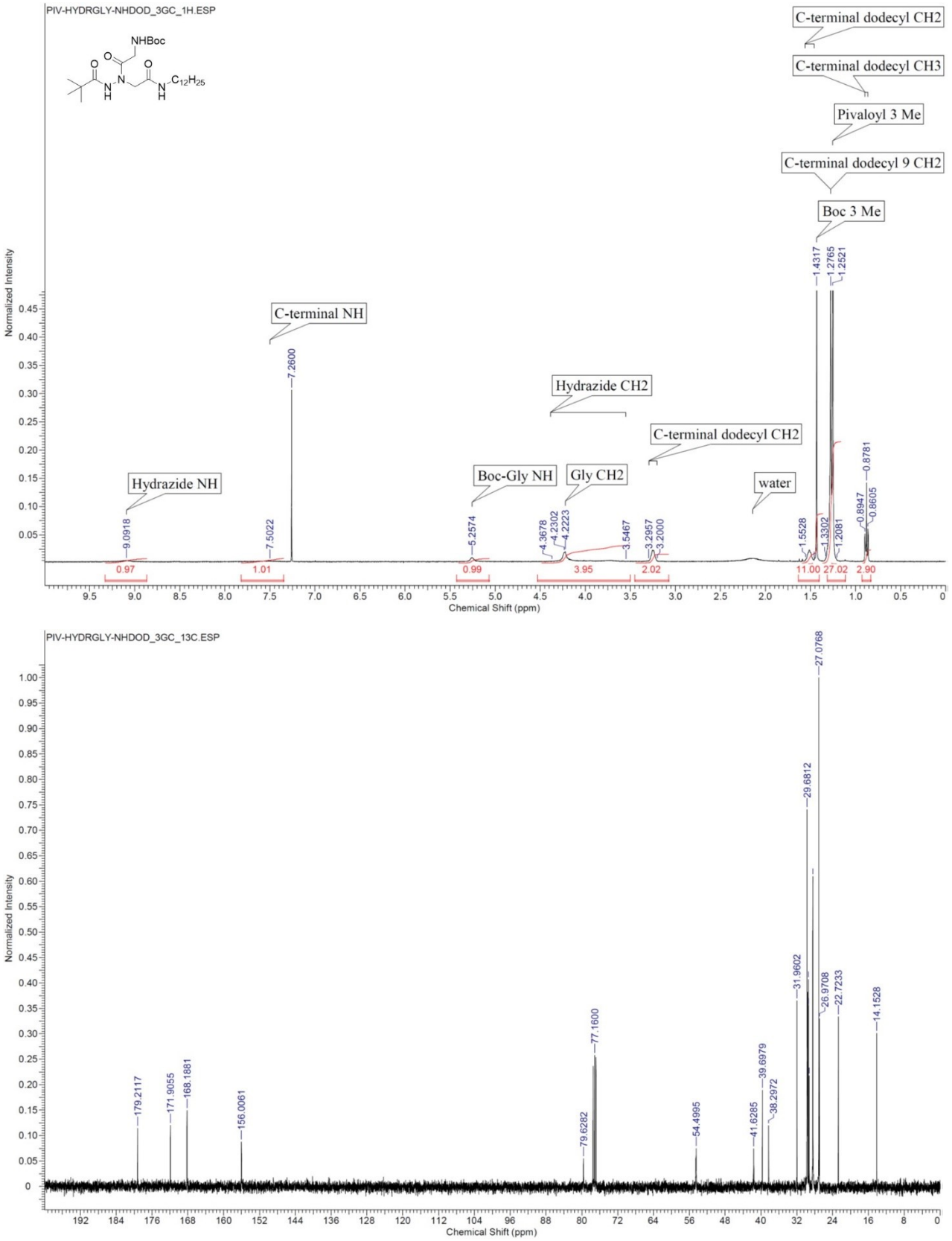

Figure 50. ^{1}H and ^{13}C NMR spectra in $CDCl_3$ of compound 3Gc, *t*BuCO-HydrGly-$NHC_{12}H_{25}$.

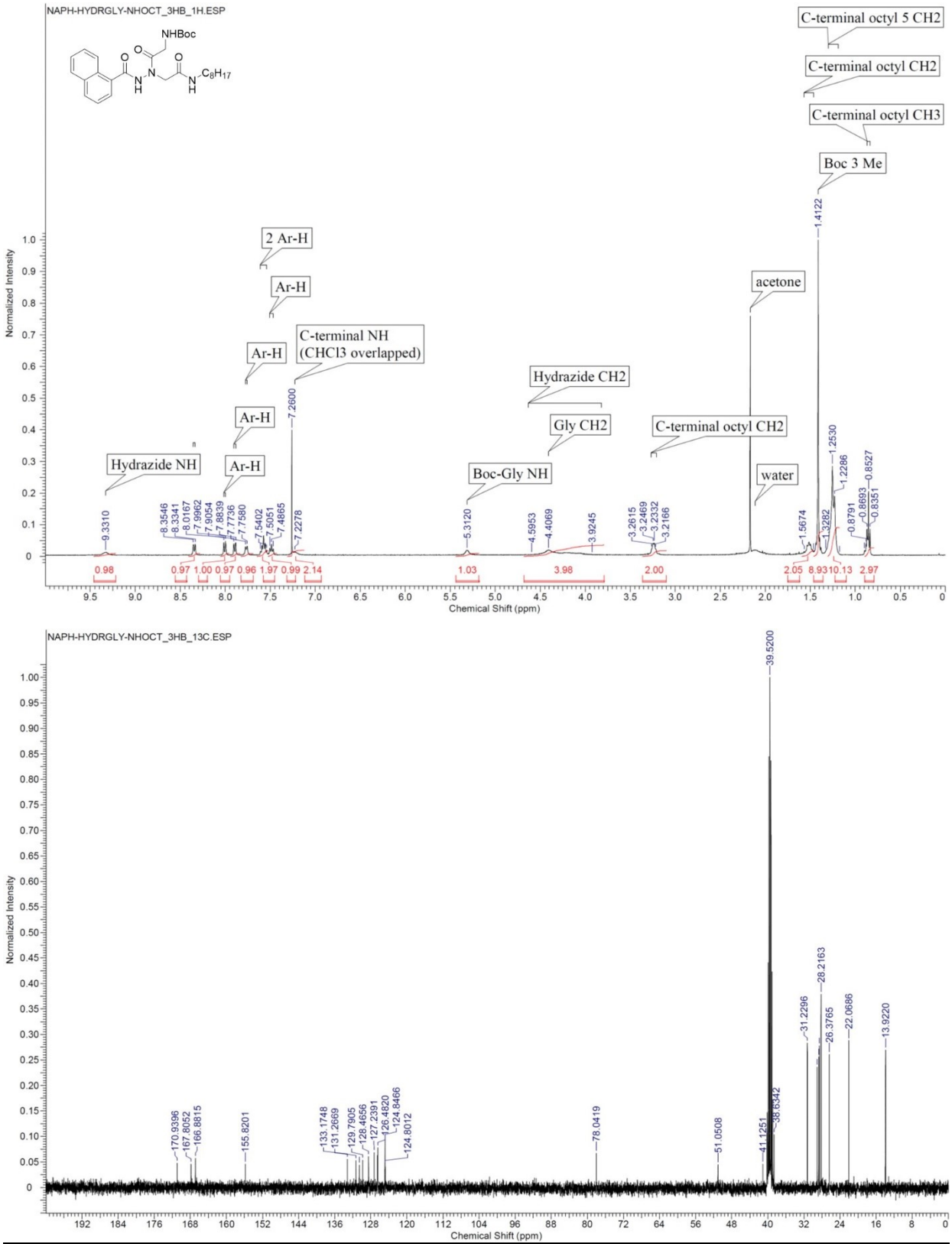

Figure 51. ^{1}H spectrum in $CDCl_3$ and ^{13}C NMR spectrum in DMSO-d_6 of compound 3Hb, 1-naphthylCO-HydrGly-NHC$_8$H$_{17}$.

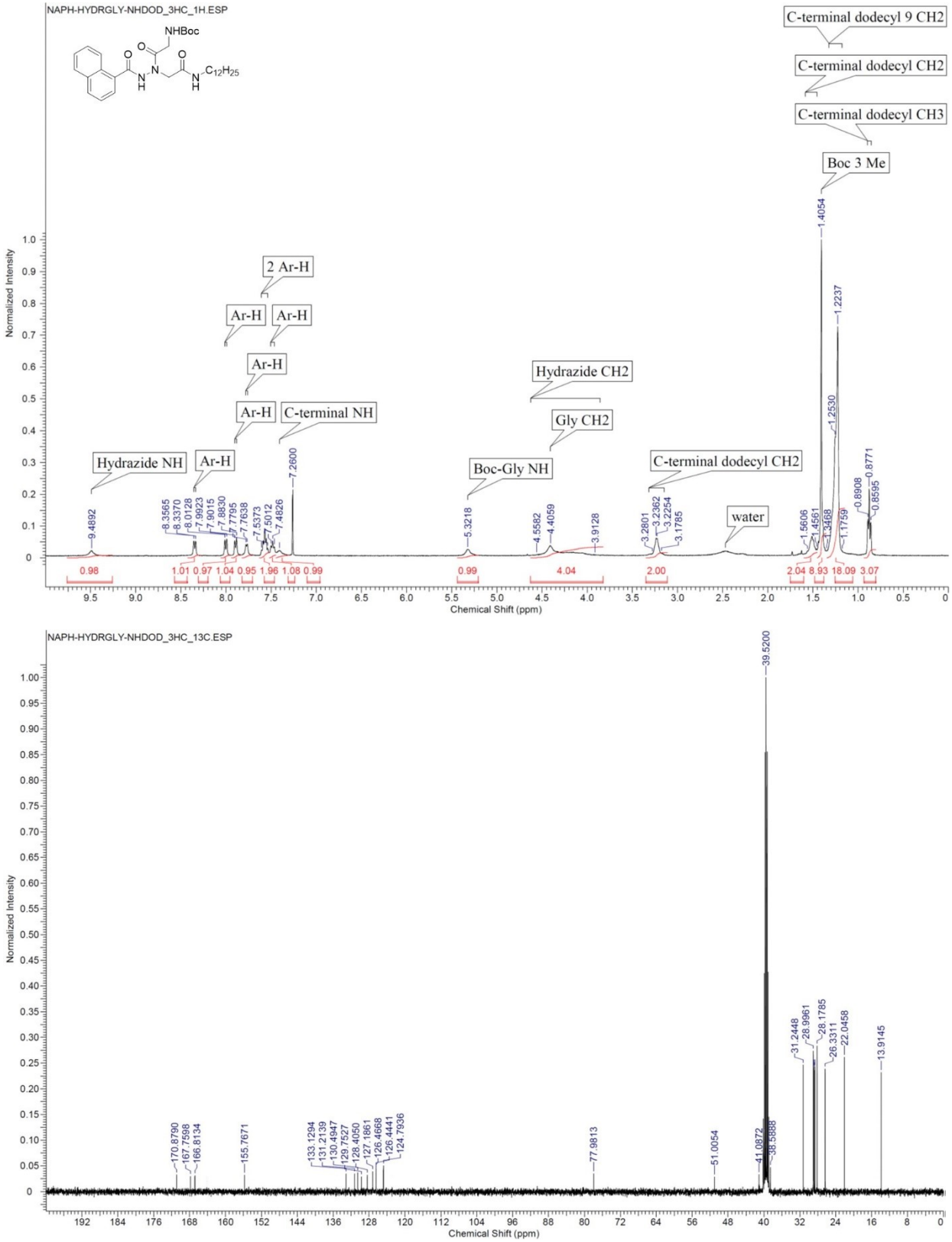

Figure 52. ^{1}H spectrum in $CDCl_3$ and ^{13}C NMR spectrum in DMSO-d_6 of compound 3Hc, 1-naphthylCO-HydrGly-NHC$_{12}$H$_{25}$.

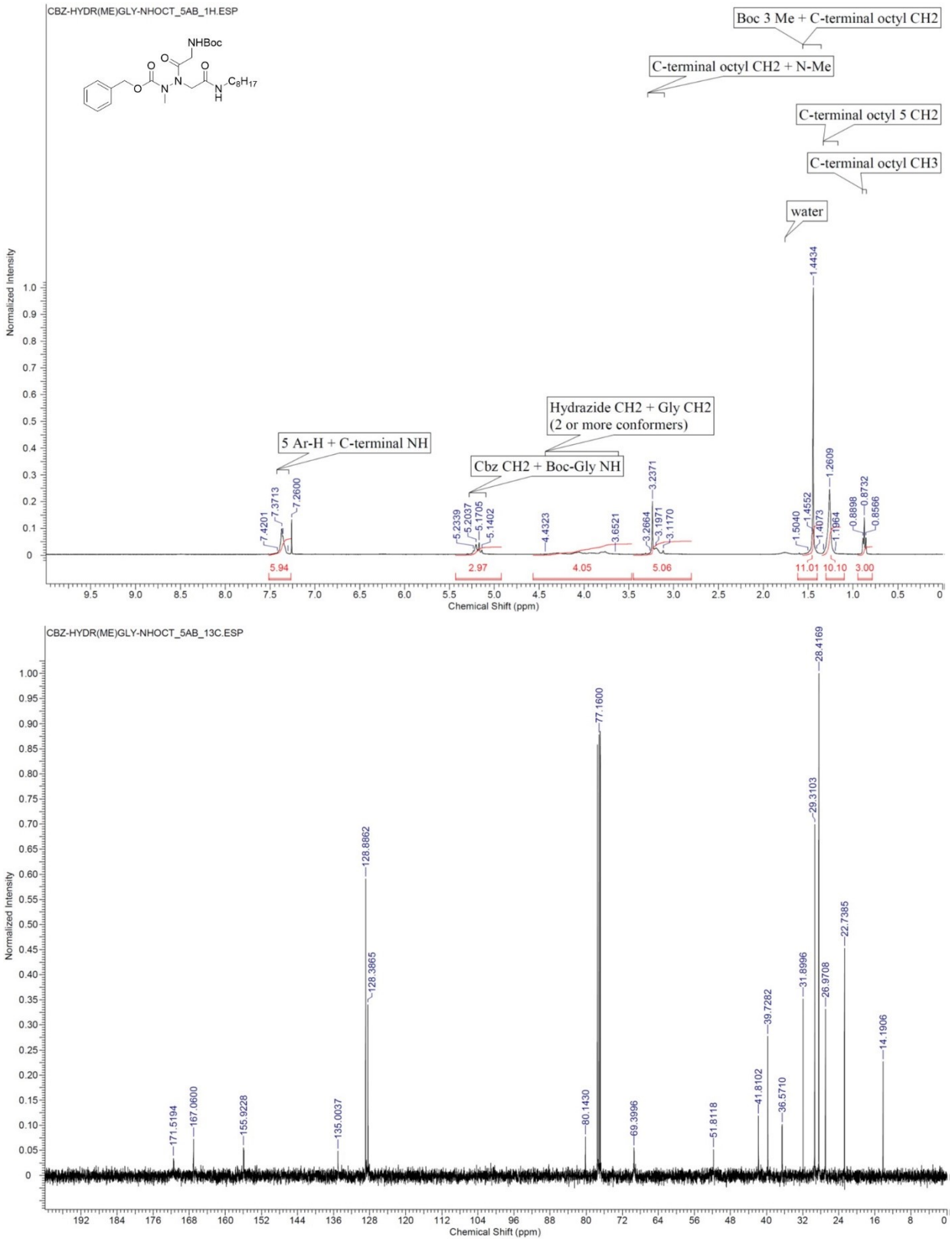

Figure 53. ^{1}H and ^{13}C NMR spectra in $CDCl_3$ of compound 5Ab, Cbz-Hydr(Me)Gly-NH C_8H_{17}.

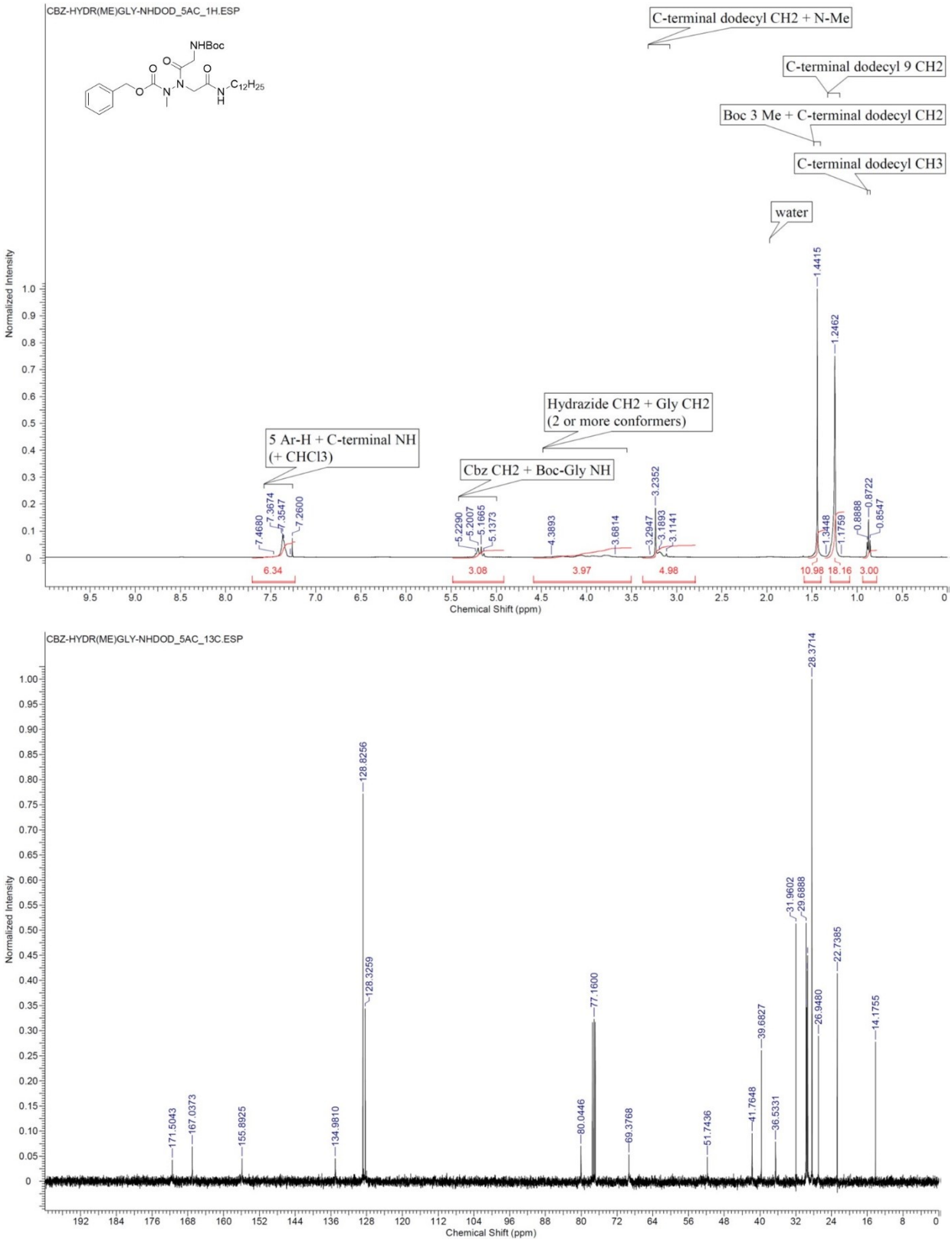

Figure 54. ^{1}H and ^{13}C NMR spectra in $CDCl_3$ of compound 5Ac, Cbz-Hydr(Me)Gly-NH $C_{12}H_{25}$.

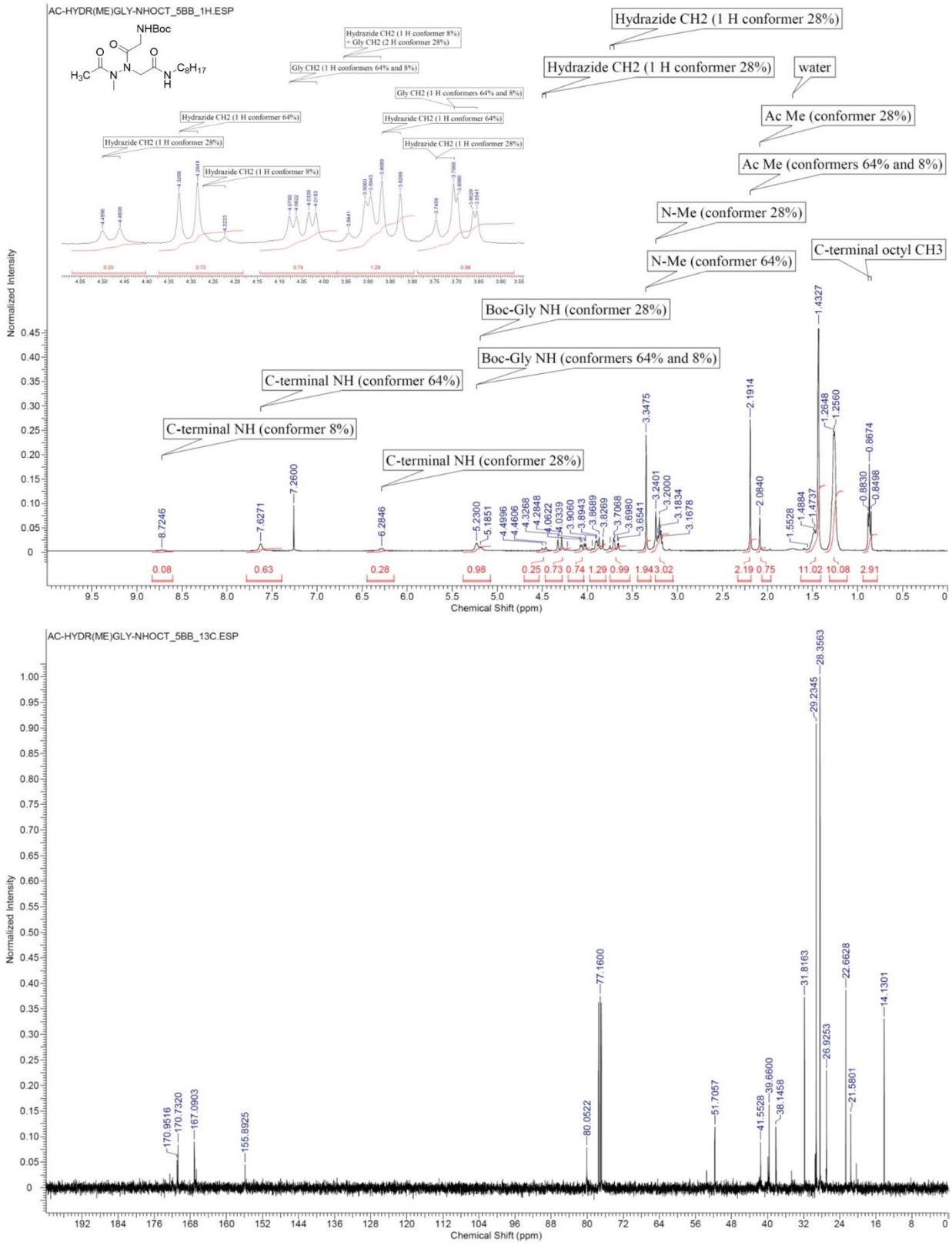

Figure 55. ^{1}H and ^{13}C NMR spectra in $CDCl_3$ of compound 5Bb, CH_3CO-Hydr(Me)Gly-NH C_8H_{17}.

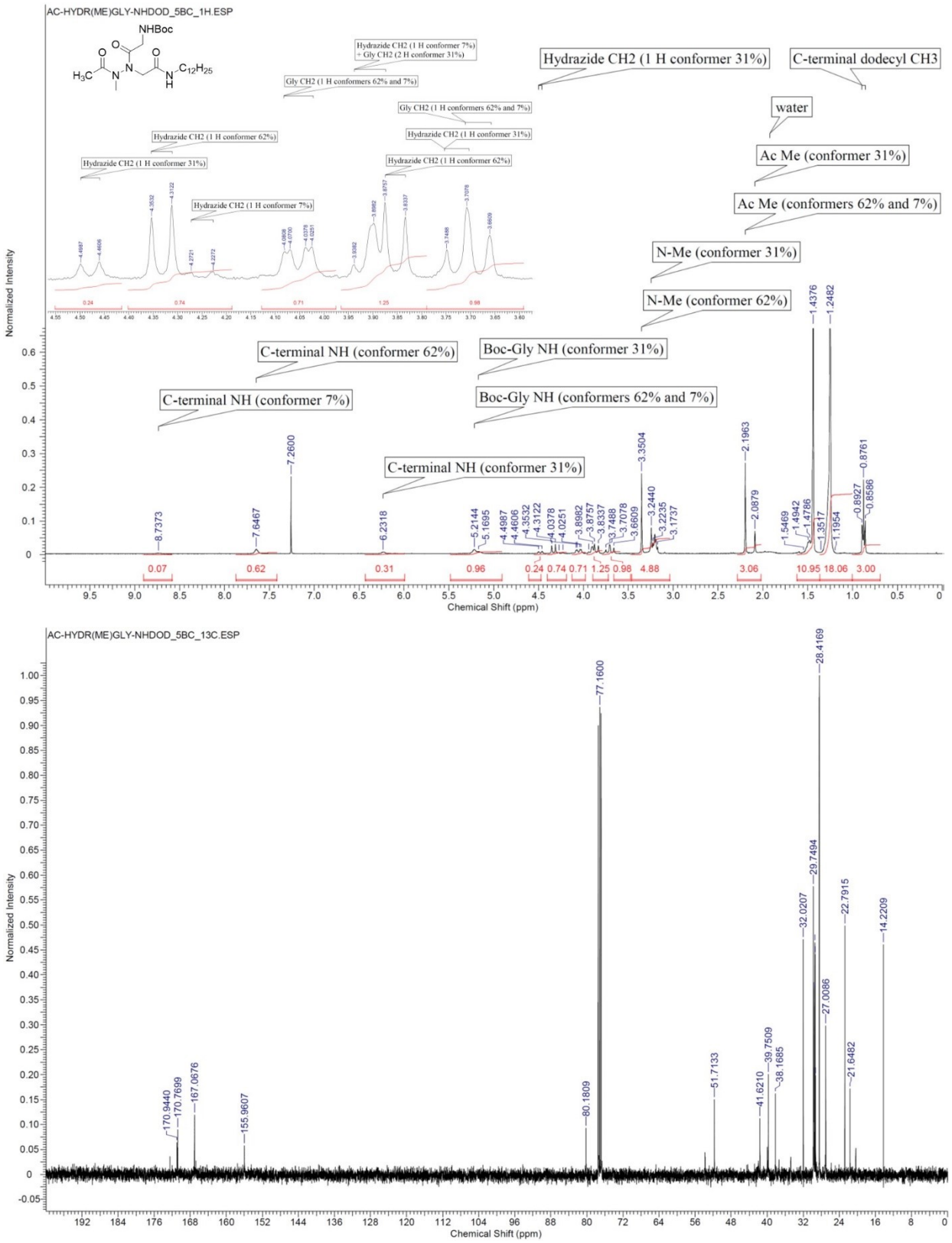

Figure 56. ^{1}H and ^{13}C NMR spectra in $CDCl_3$ of compound 5Bc, CH_3CO-Hydr(Me)Gly-NH $C_{12}H_{25}$.

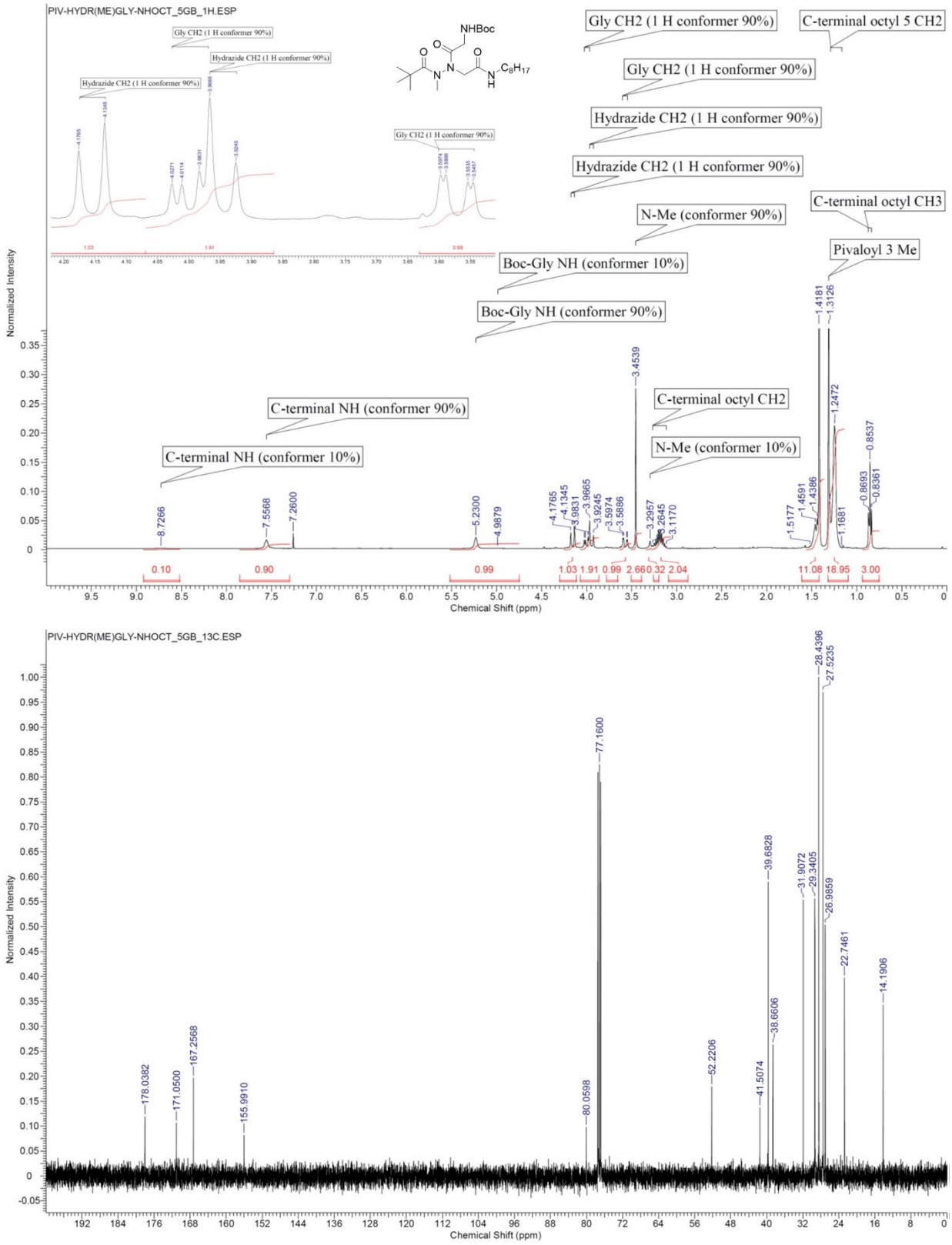

Figure 57. ^{1}H and ^{13}C NMR spectra in $CDCl_3$ of compound 5Gb, *t*BuCO-Hydr(Me)Gly-NH C_8H_{17}.

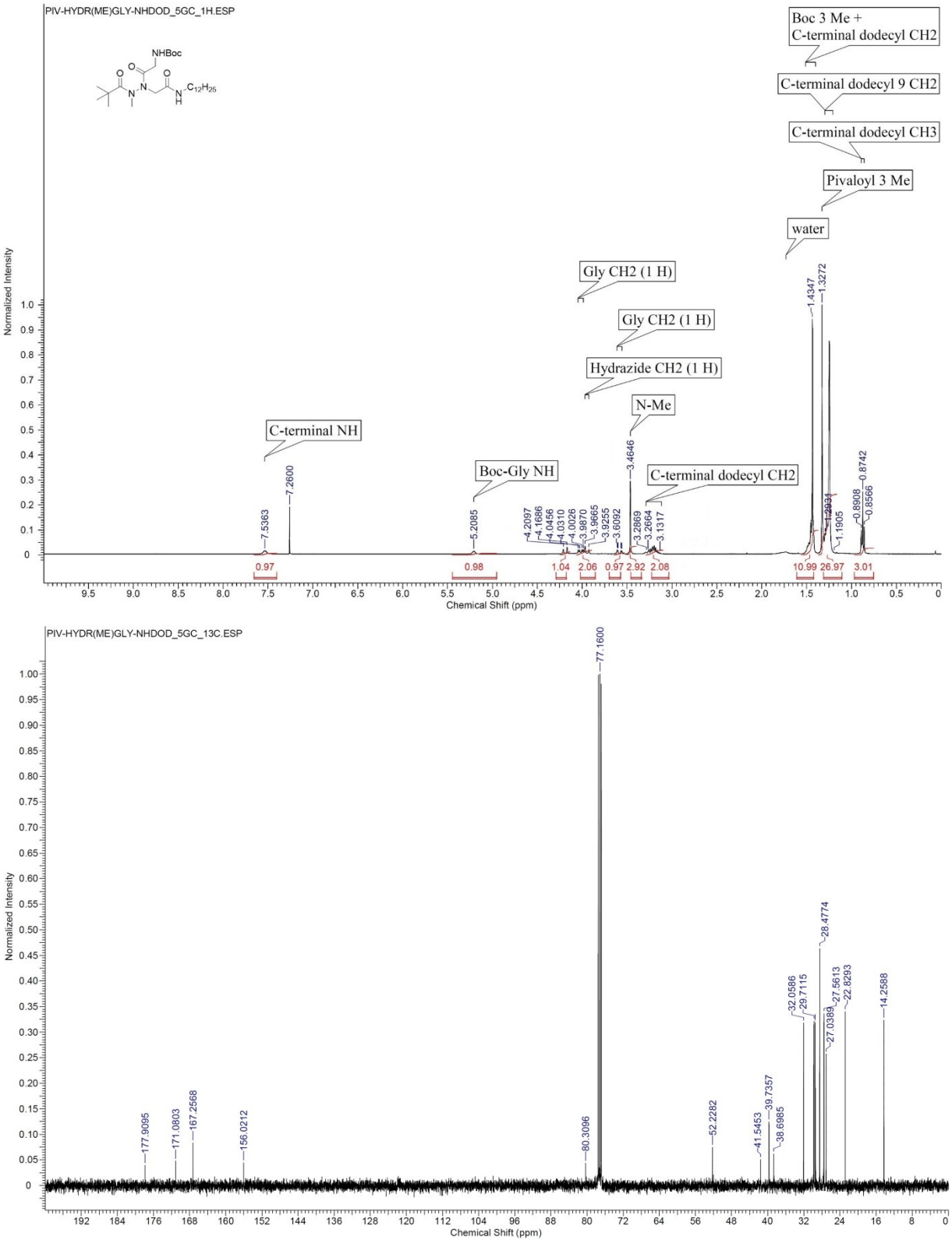

Figure 58. ^{1}H and ^{13}C NMR spectra in $CDCl_3$ of compound 5Gc, *t*BuCO-Hydr(Me)Gly-NH $C_{12}H_{25}$.

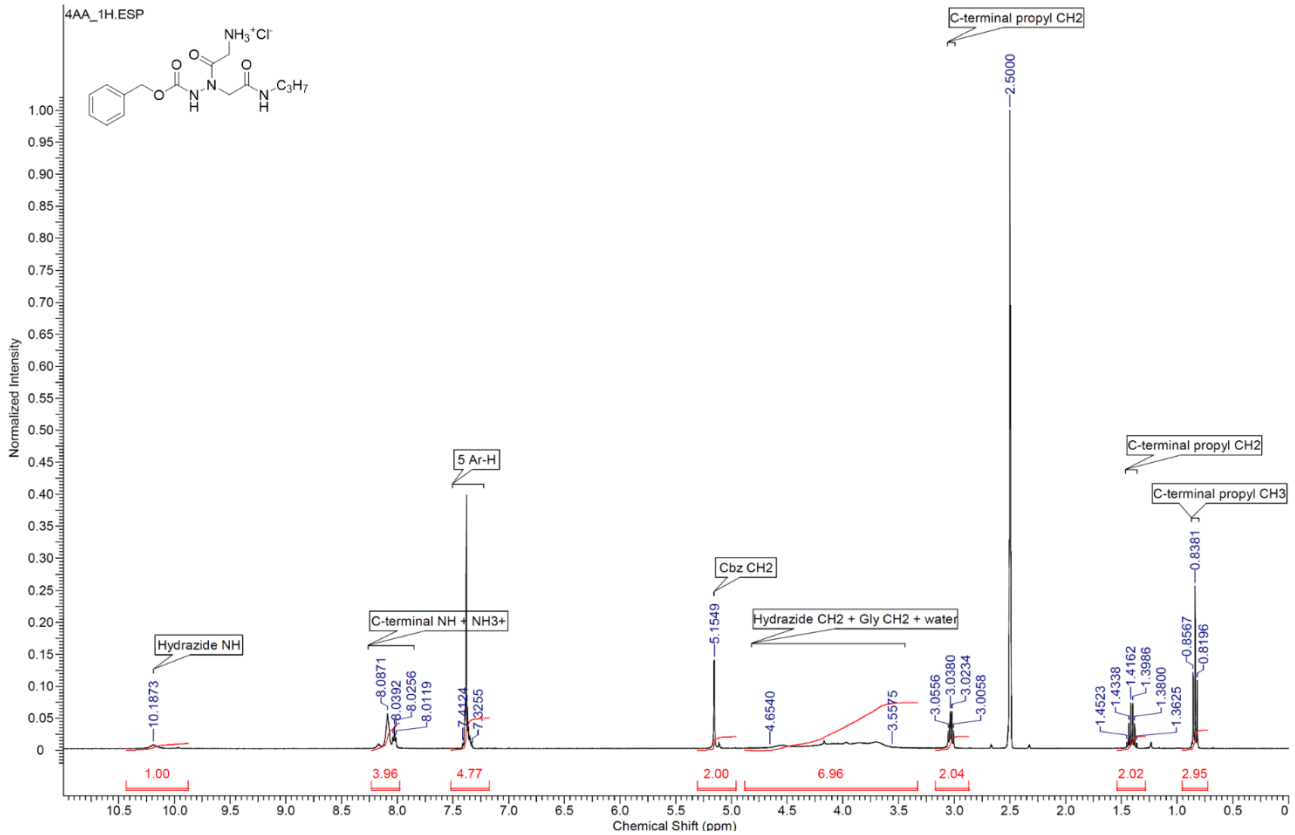

Figure 59. ^{1}H spectrum in DMSO-d_6 of compound 4Aa, Cbz-HydrGly-NHC$_3$H$_7$·HCl.

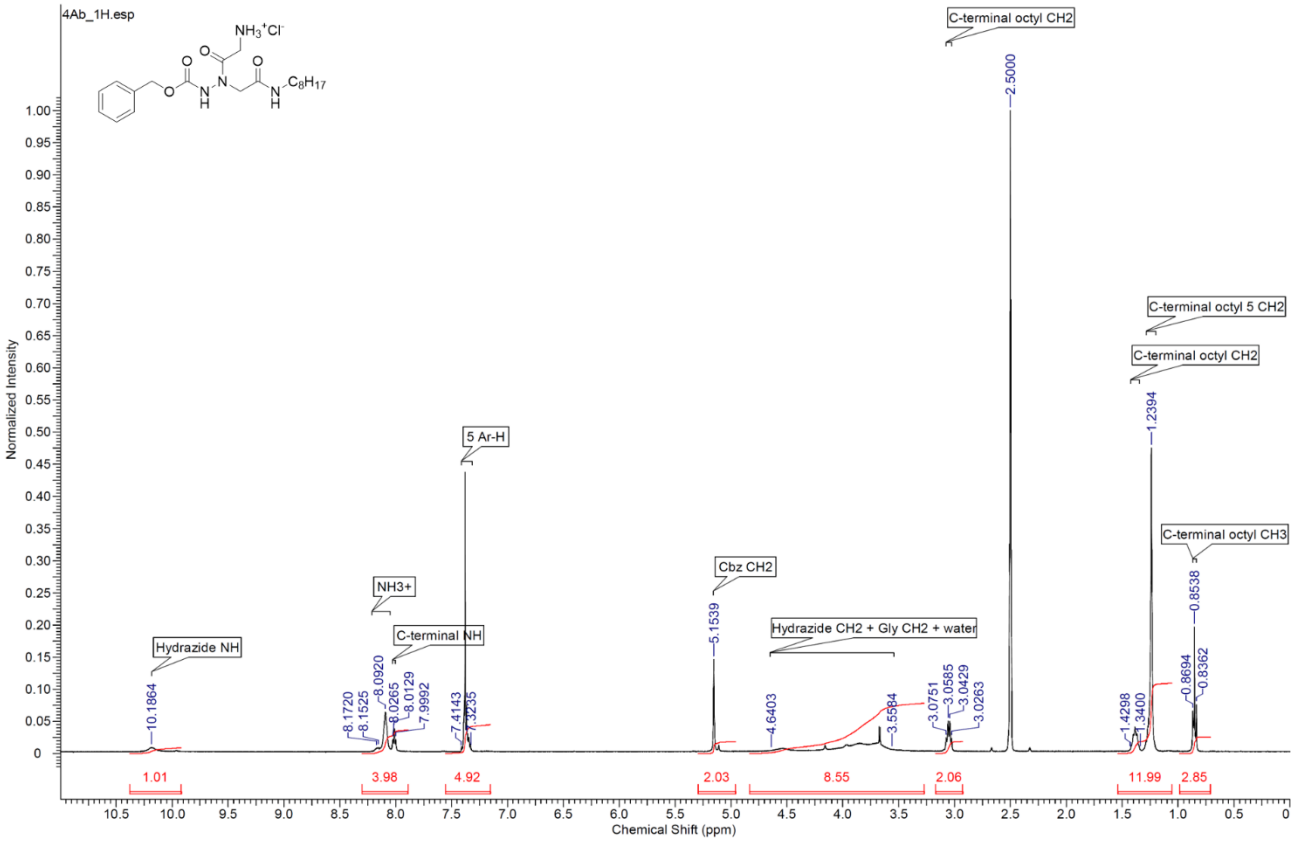

Figure 60. ^{1}H spectrum in DMSO-d_6 of compound 4Ab, Cbz-HydrGly-NHC$_8$H$_{17}$·HCl.

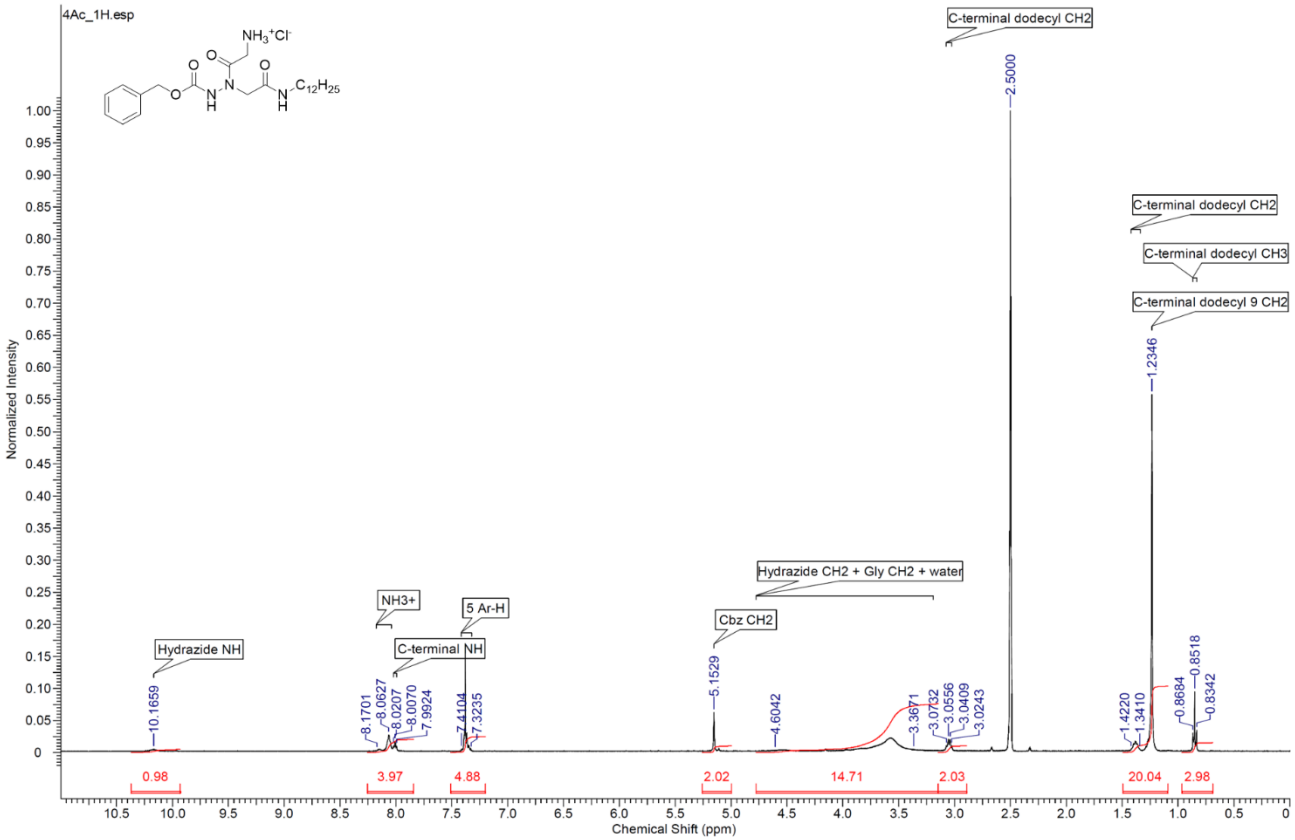

Figure 61. ^{1}H spectrum in DMSO-*d*$_6$ of compound 4Ac, Cbz-HydrGly-NHC$_{12}$H$_{25}$·HCl.

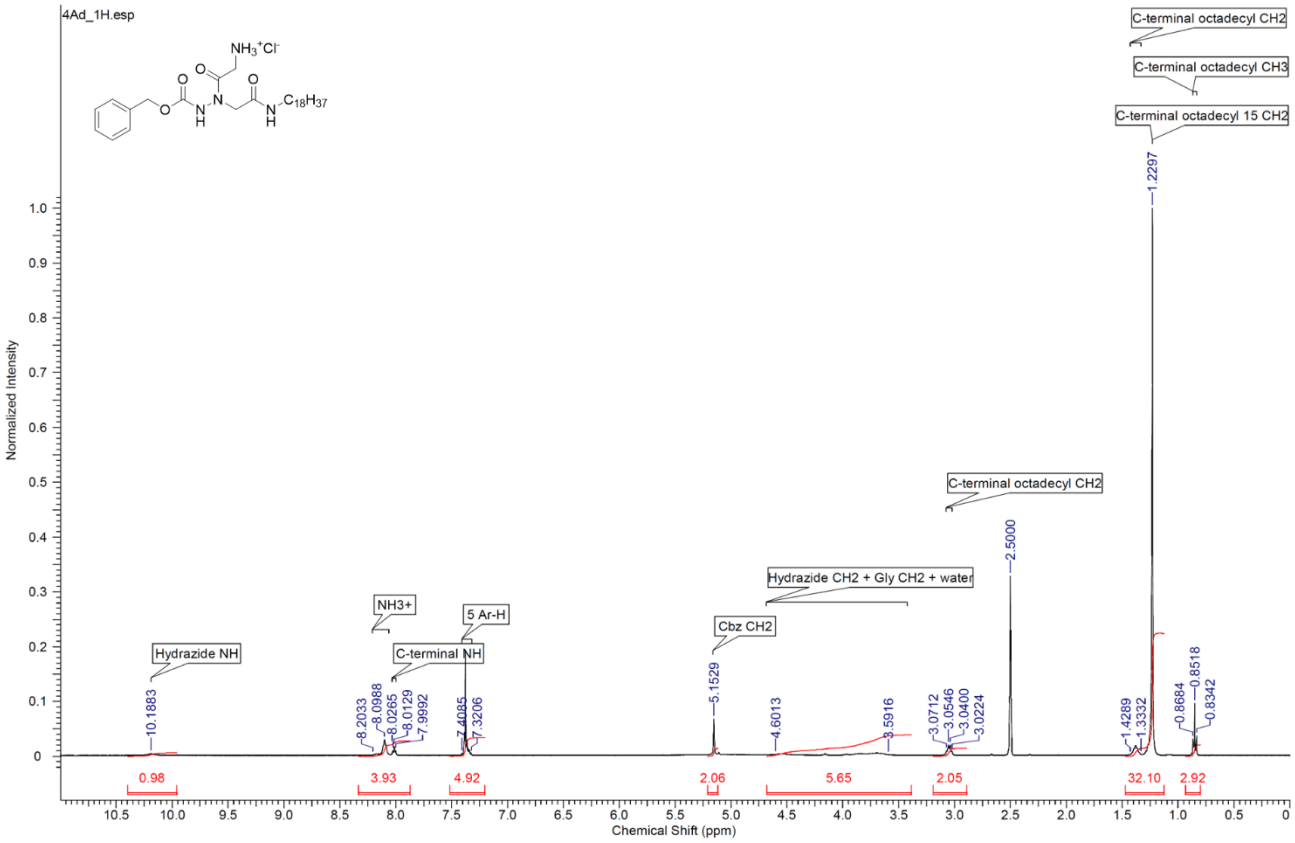

Figure 62. ^{1}H spectrum in DMSO-*d*$_6$ of compound 4Ad, Cbz-HydrGly-NHC$_{18}$H$_{37}$·HCl.

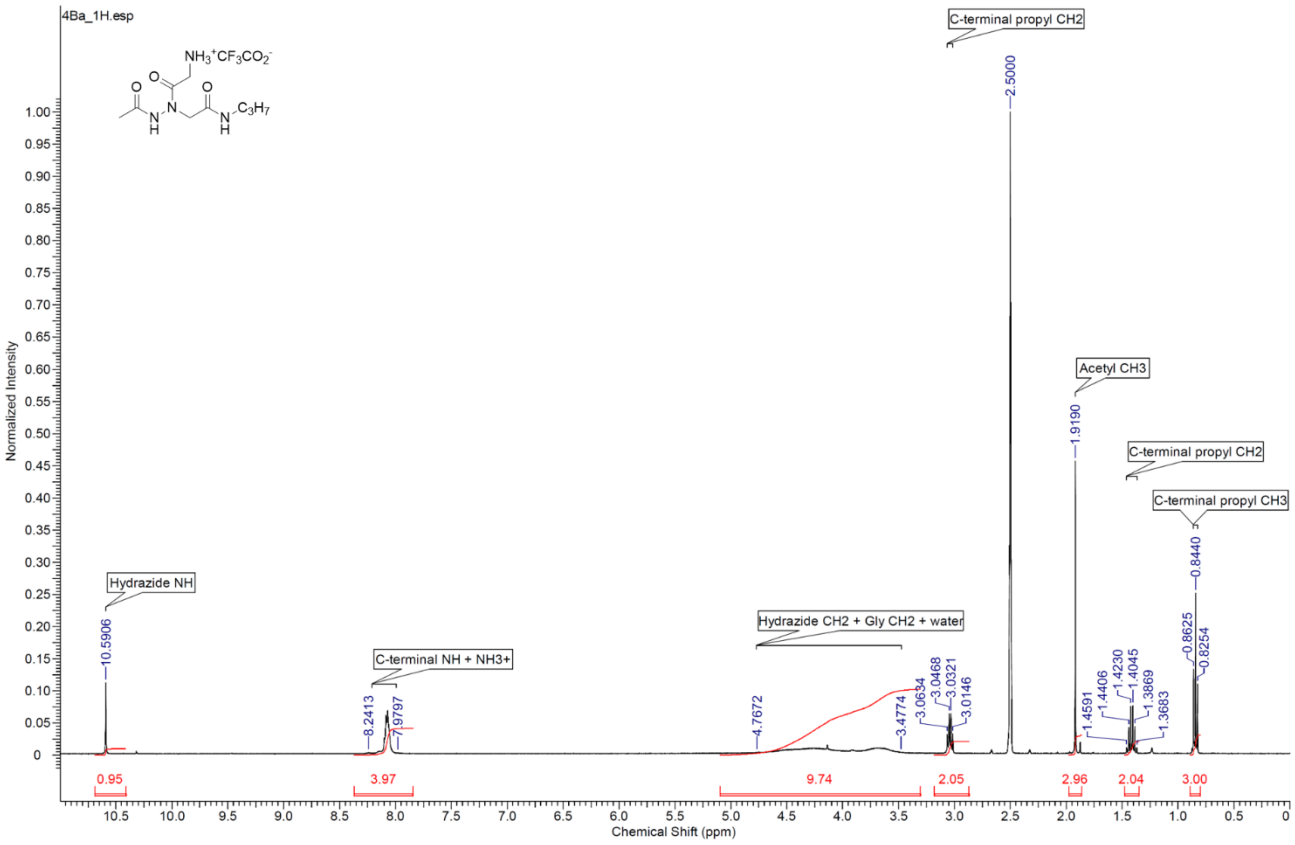

Figure 63. ^{1}H spectrum in DMSO-d_6 of compound 4Ba, Ac-HydrGly-NHC$_3$H$_7$·HCl.

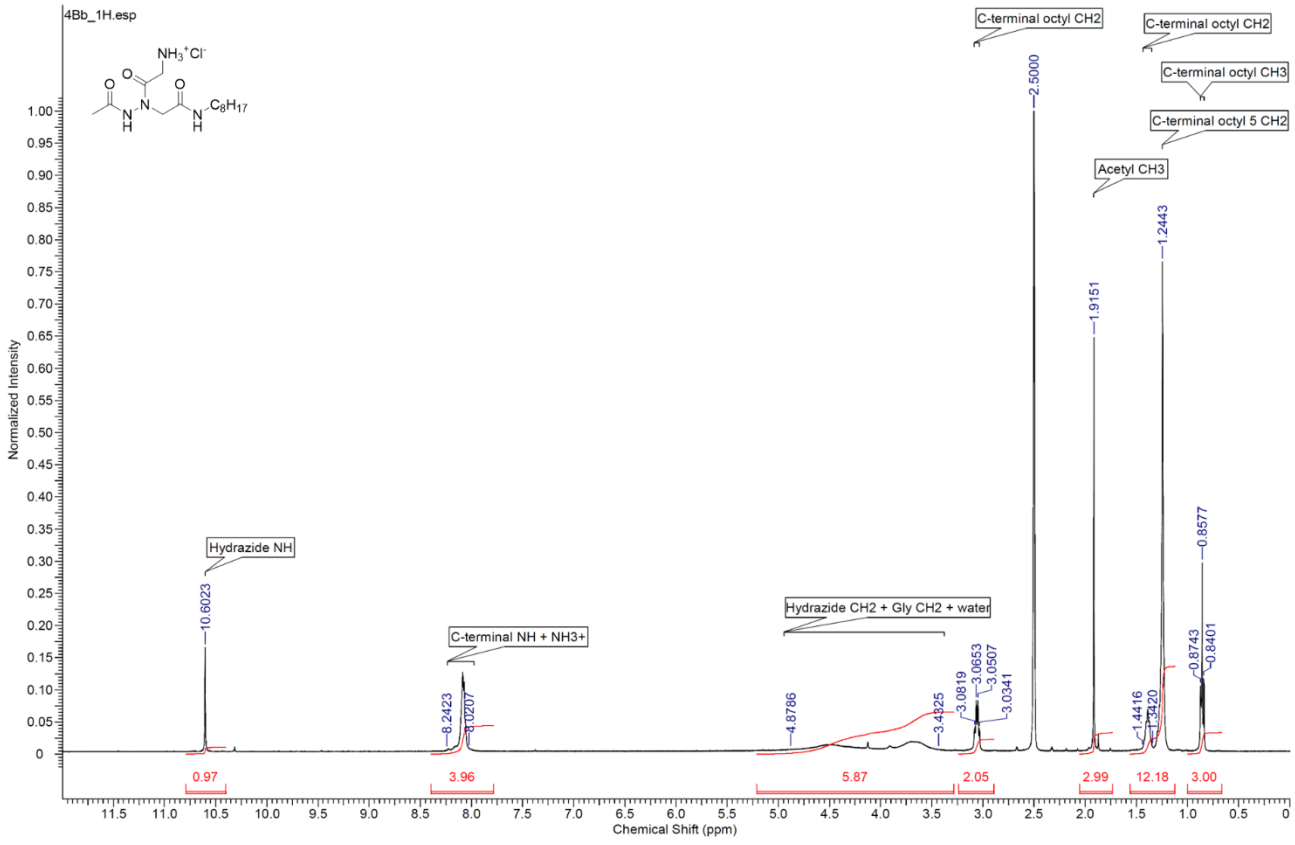

Figure 64. ^{1}H spectrum in DMSO-*d*$_6$ of compound 4Bb, Ac-HydrGly-NHC$_8$H$_{17}$·HCl.

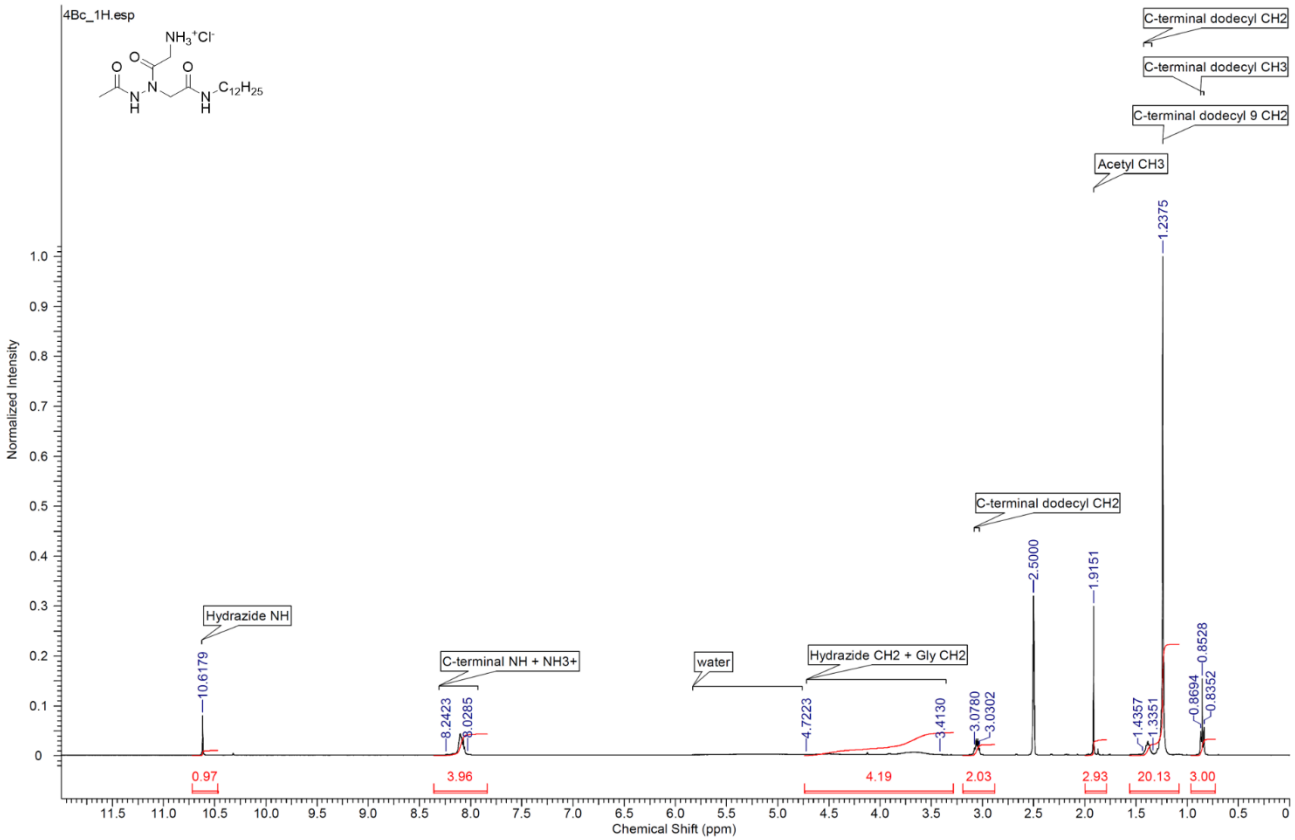

Figure 65. ^{1}H spectrum in DMSO-*d*$_6$ of compound 4Bc, Ac-HydrGly-NHC$_{12}$H$_{25}$·HCl.

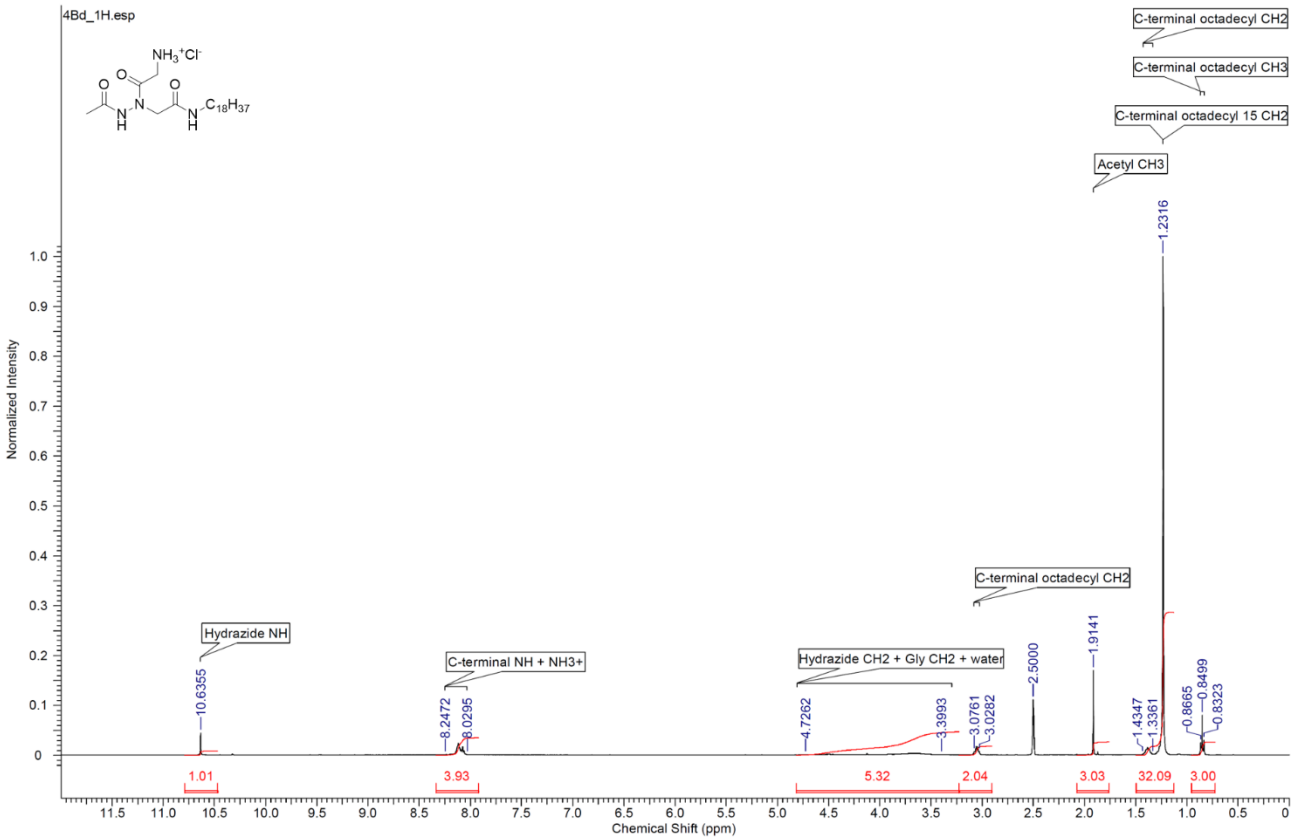

Figure 66. ^{1}H spectrum in DMSO-*d*$_6$ of compound 4Bd, Ac-HydrGly-NHC$_{18}$H$_{37}$·HCl.

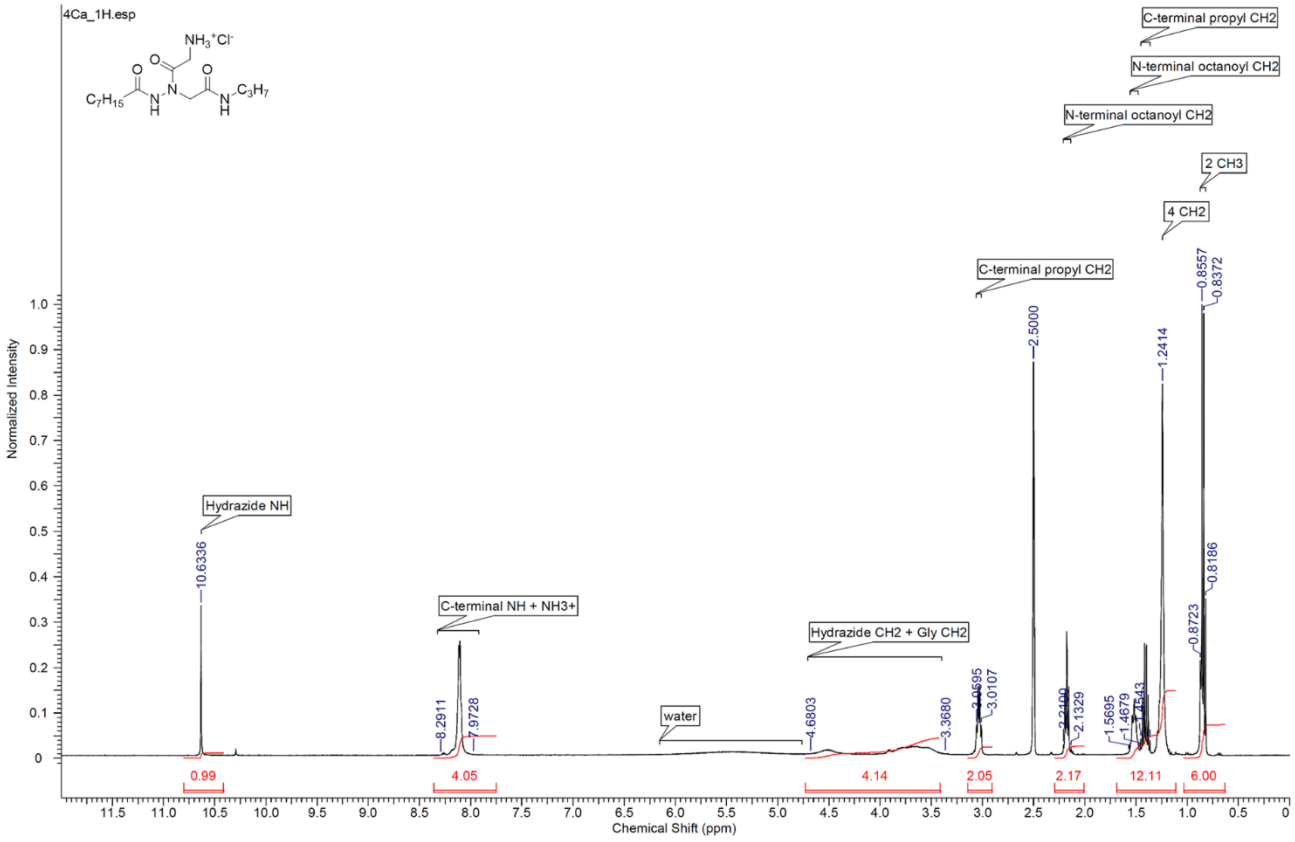

Figure 67. ^{1}H spectrum in DMSO-*d*$_6$ of compound 4Ca, C_7H_{15}CO-HydrGly-NHC_3H_7·HCl.

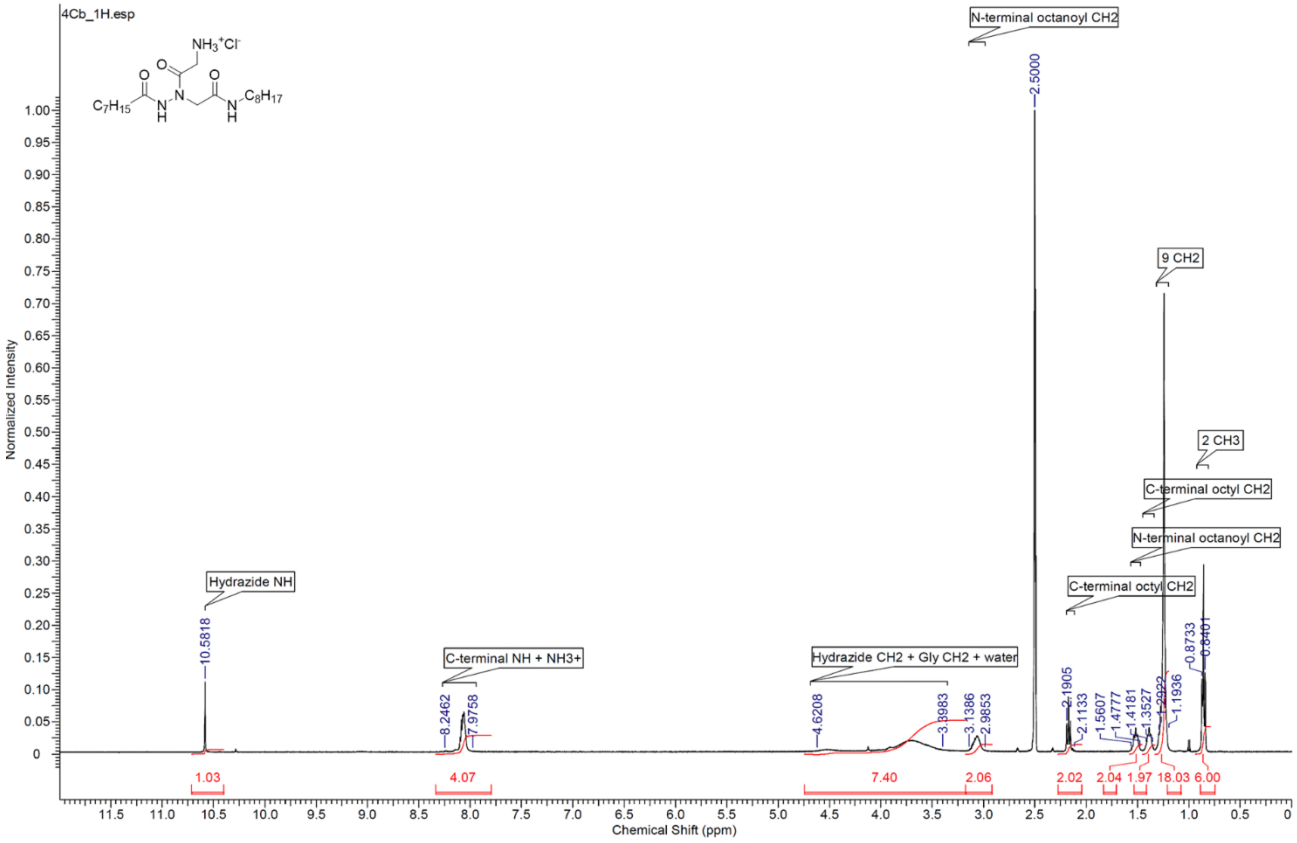

Figure 68. ^{1}H spectrum in DMSO-*d*$_6$ of compound 4Cb, C_7H_{15}CO-HydrGly-NHC_8H_{17}·HCl.

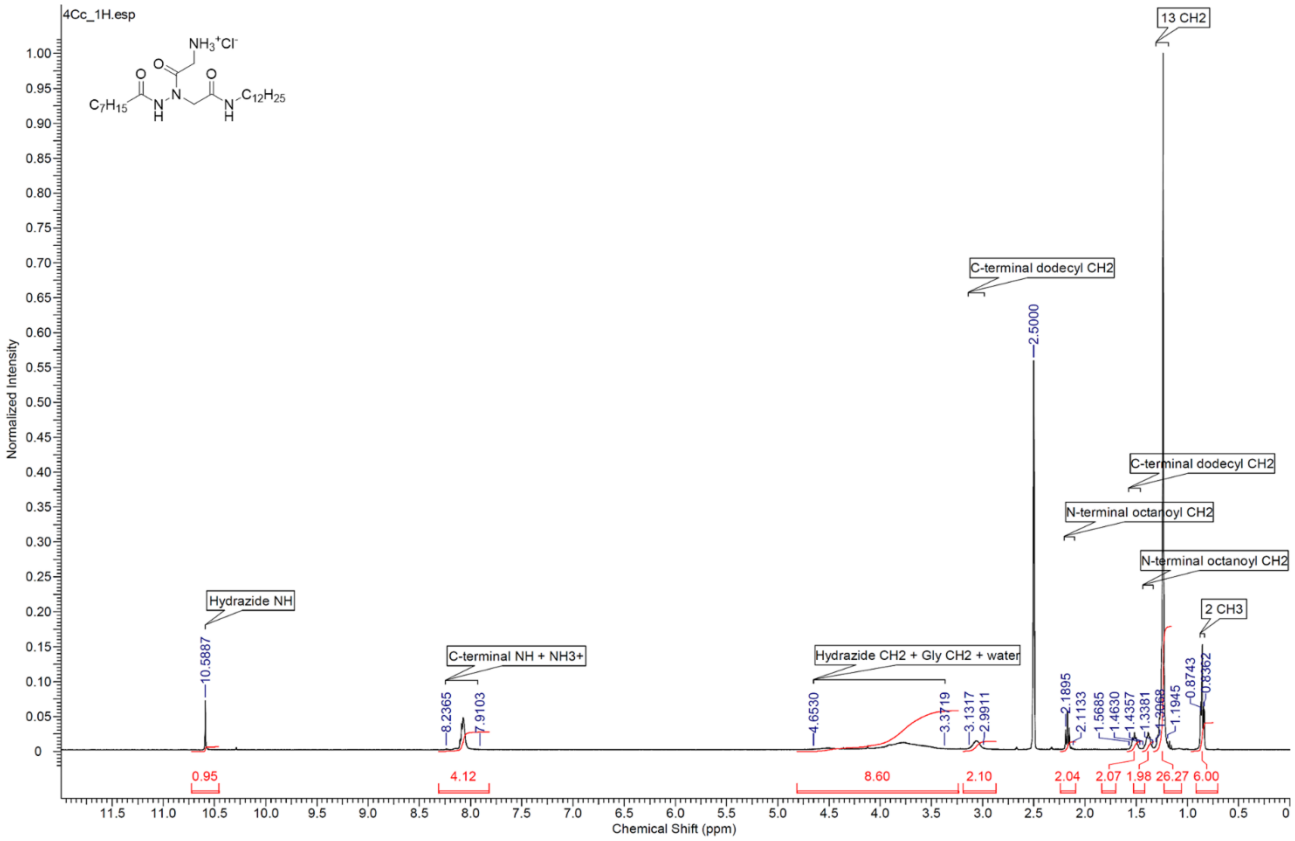

Figure 69. ^{1}H spectrum in DMSO-d_6 of compound 4Cc, C_7H_{15}CO-HydrGly-NH$C_{12}H_{25}$·HCl.

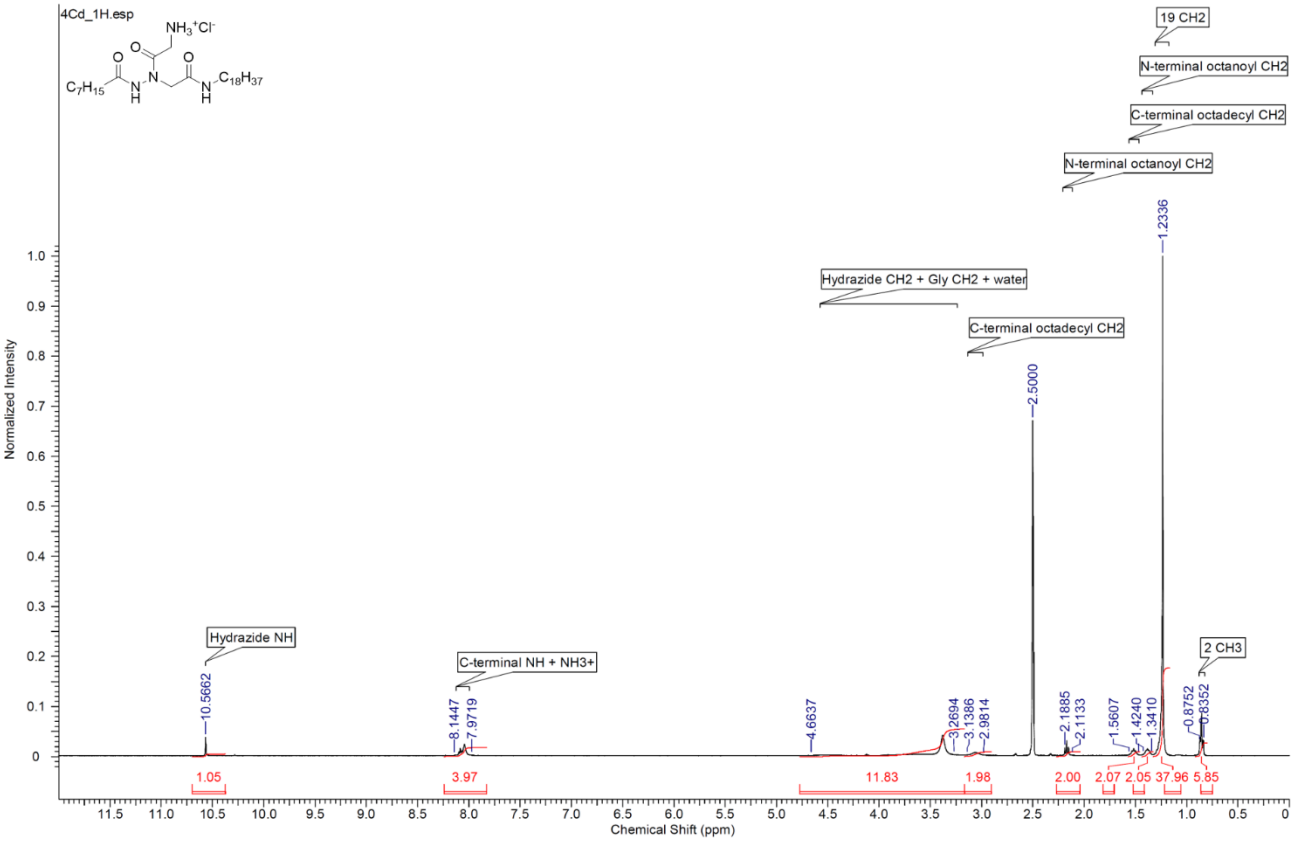

Figure 70. ^{1}H spectrum in DMSO-*d*$_6$ of compound 4Cd, $C_7H_{15}CO$-HydrGly-$NHC_{18}H_{37}$·HCl.

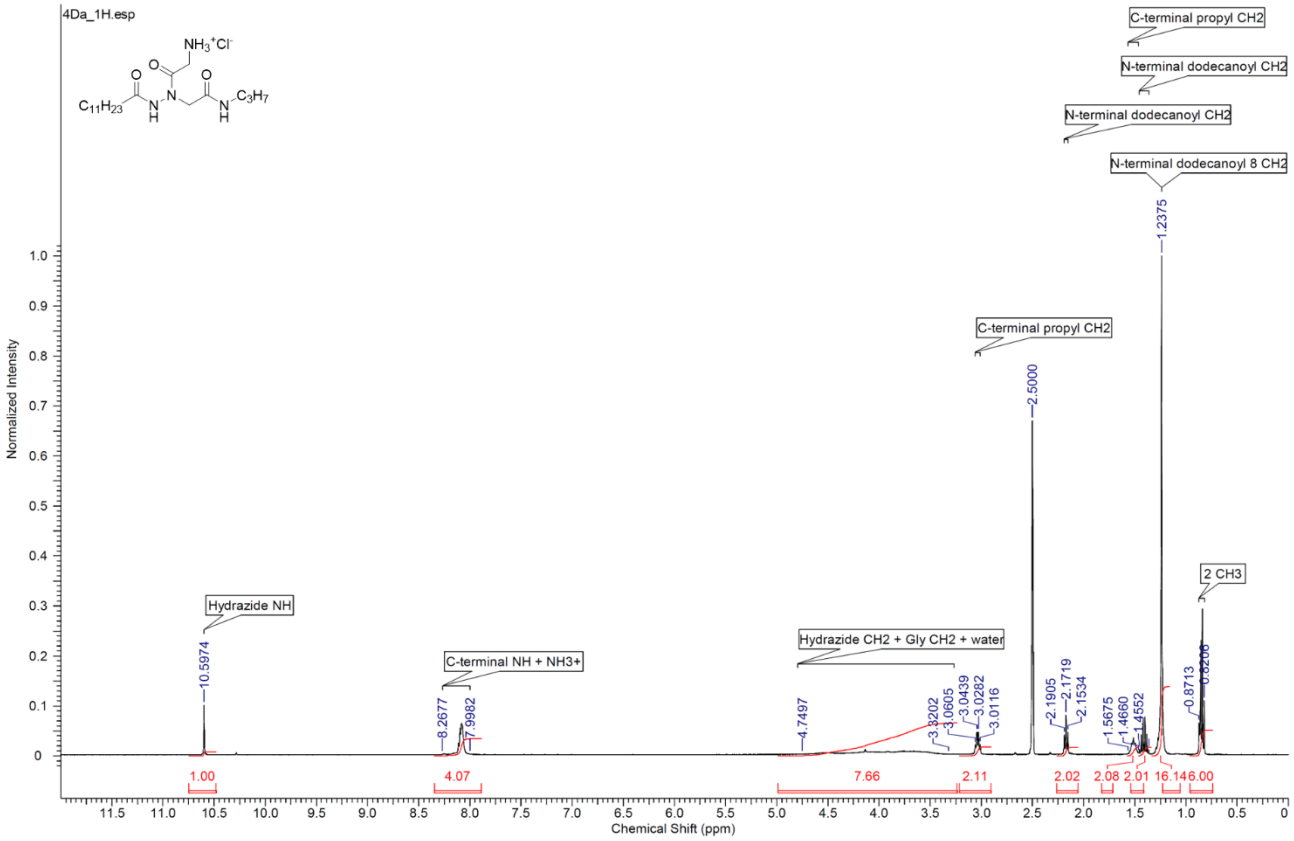

Figure 71. ^{1}H spectrum in DMSO-*d*$_6$ of compound 4Da, $C_{11}H_{23}CO$-HydrGly-NHC_3H_7·HCl.

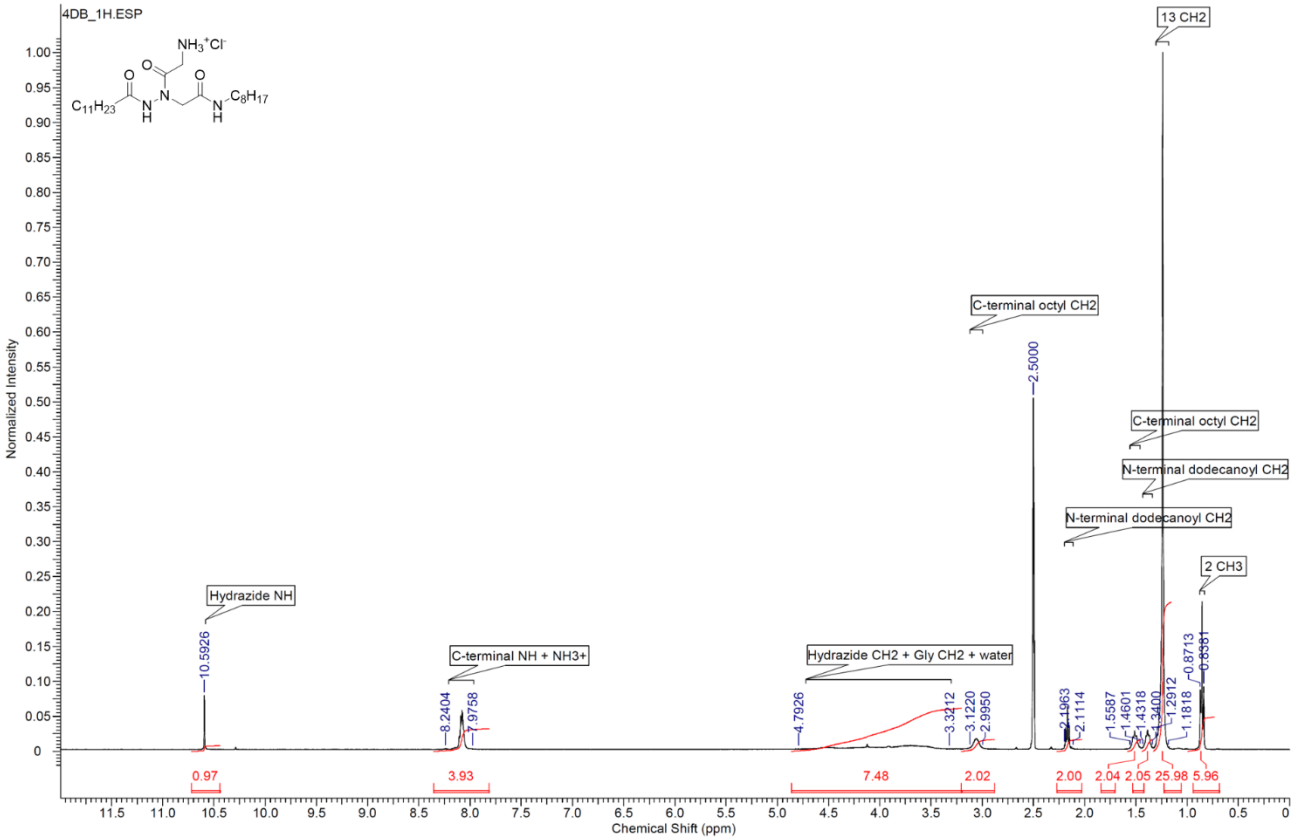

Figure 72. ^{1}H spectrum in DMSO-*d*$_6$ of compound 4Db, $C_{11}H_{23}CO$-HydrGly-NHC_8H_{17}·HCl.

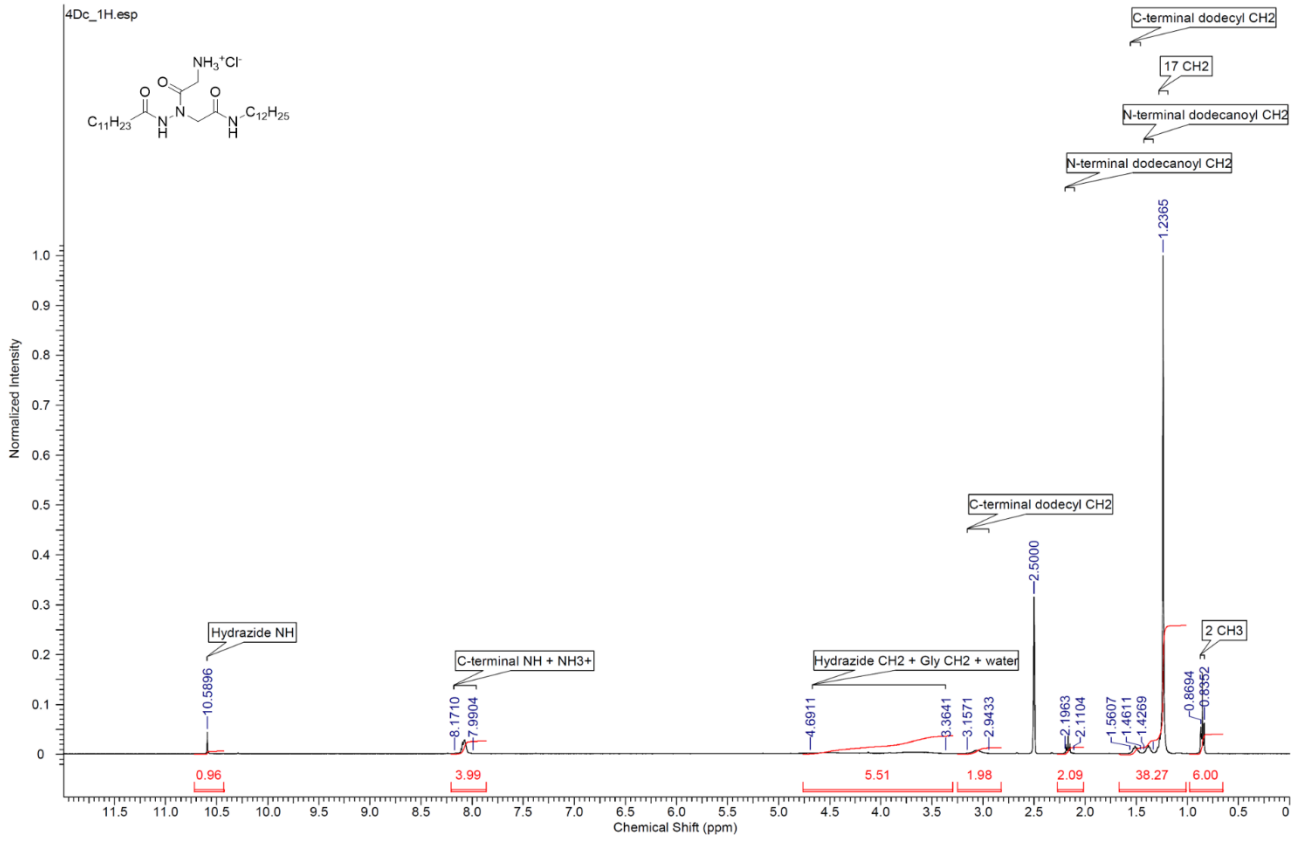

Figure 73. ^{1}H spectrum in DMSO-*d*$_6$ of compound 4Dc, $C_{11}H_{23}CO$-HydrGly-$NHC_{12}H_{25}$·HCl.

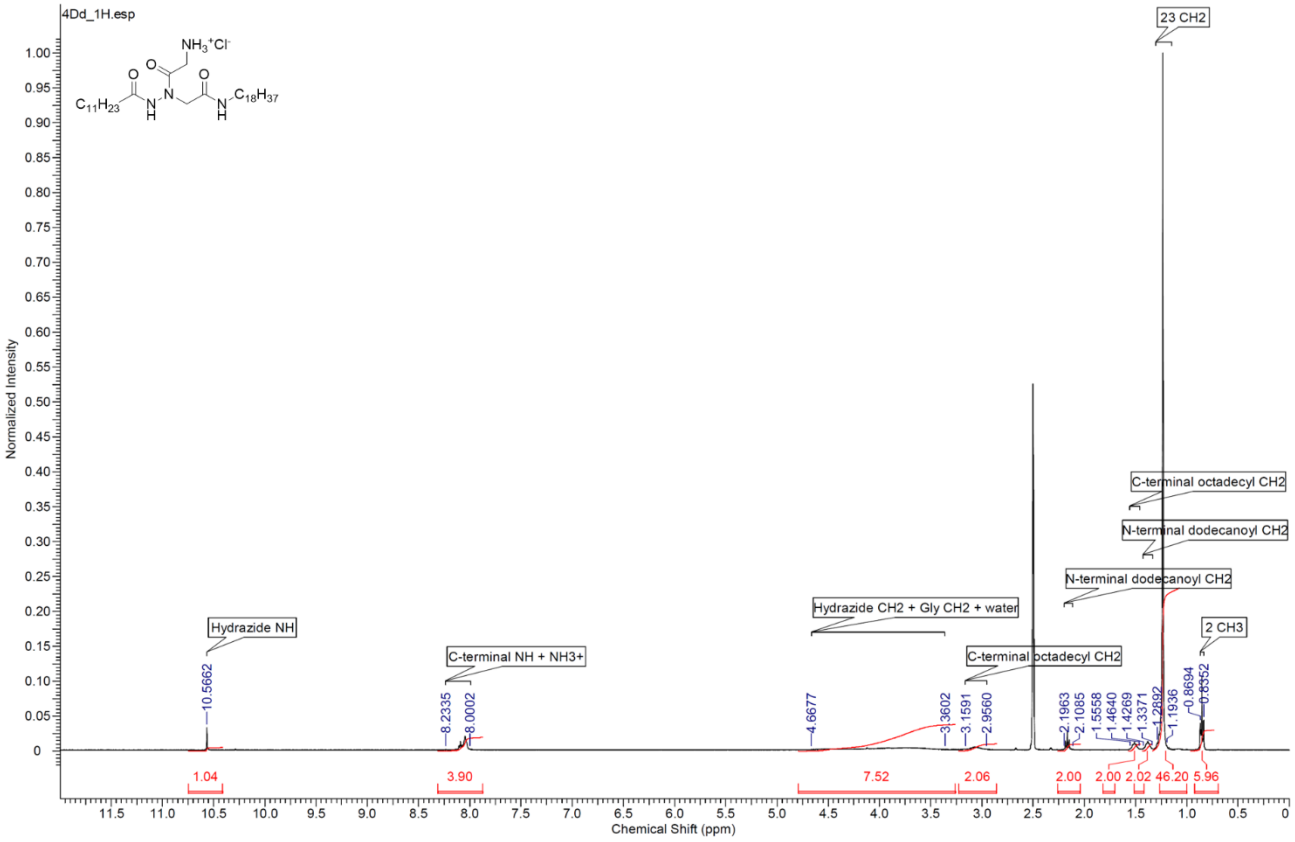

Figure 74. ^{1}H spectrum in DMSO-*d*$_6$ of compound 4Dd, $C_{11}H_{23}CO$-HydrGly-$NHC_{18}H_{37}$·HCl.

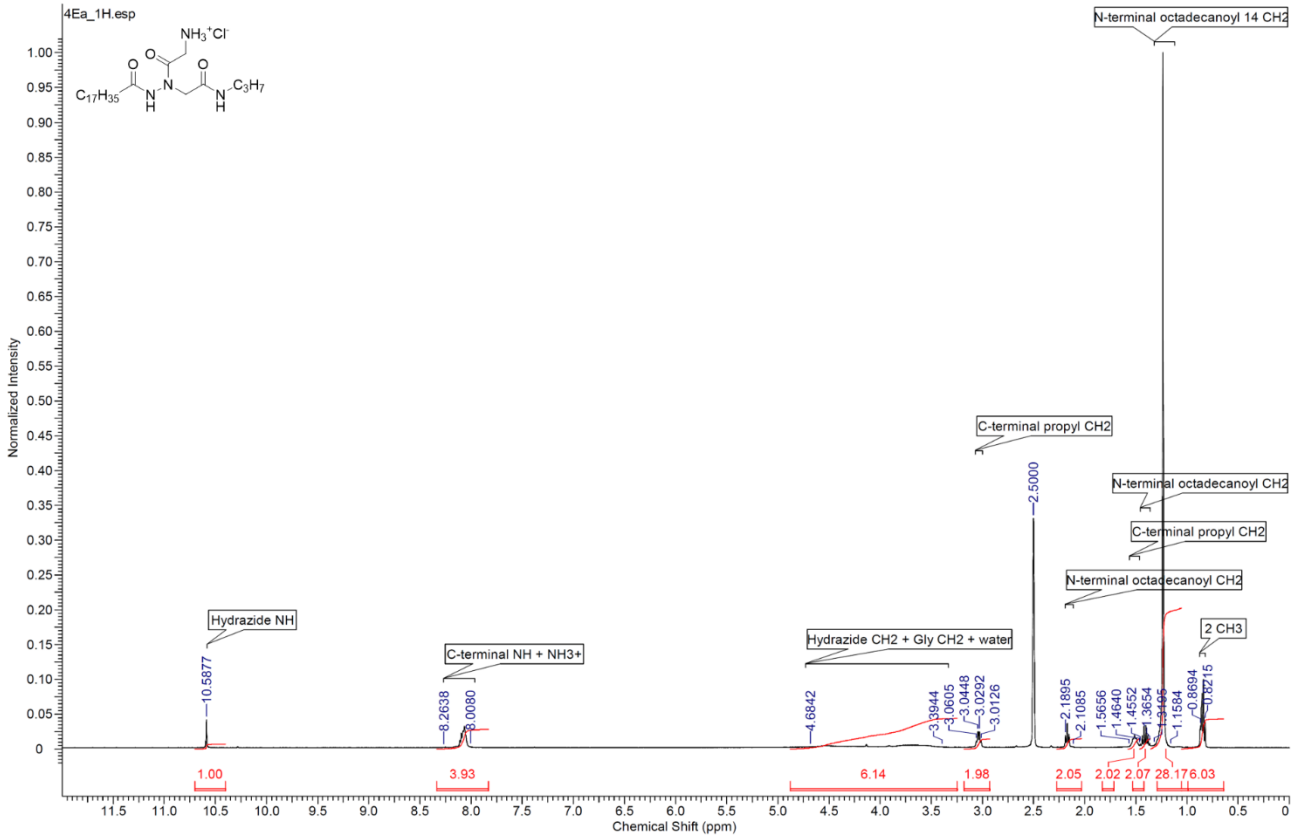

Figure 75. ^{1}H spectrum in DMSO-*d*$_6$ of compound 4Ea, $C_{17}H_{35}CO$-HydrGly-NHC_3H_7·HCl.

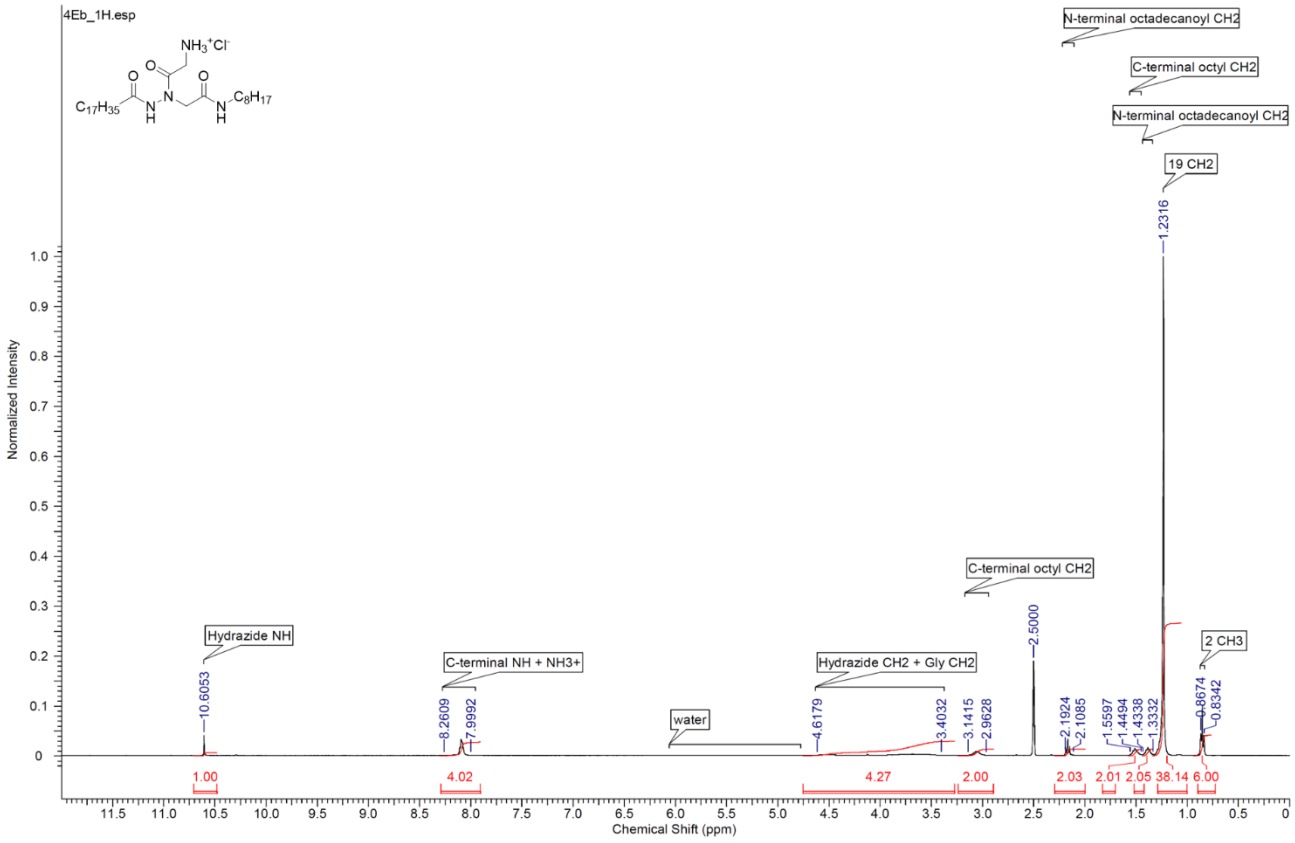

Figure 76. ^{1}H spectrum in DMSO-*d*$_6$ of compound 4Eb, $C_{17}H_{35}CO$-HydrGly-NHC_8H_{17}·HCl.

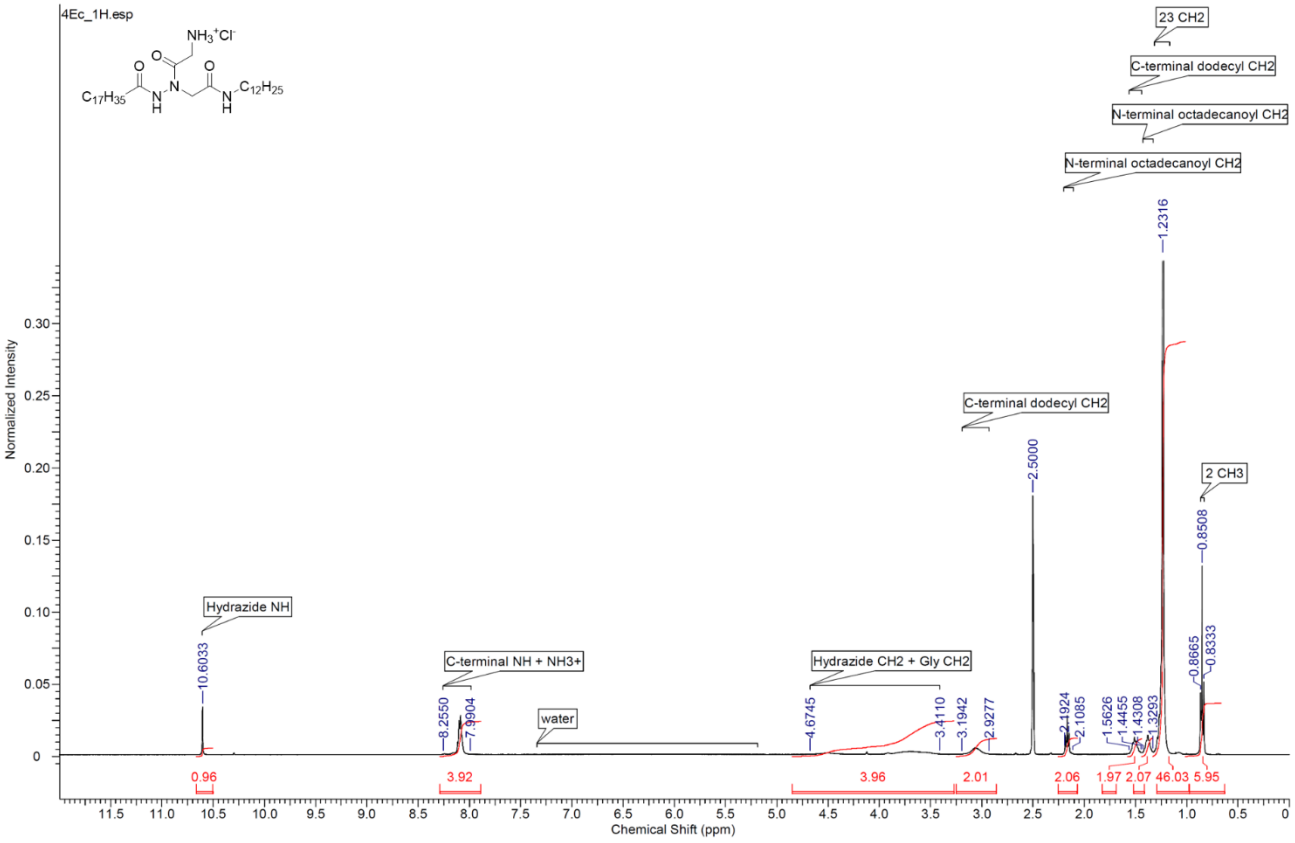

Figure 77. ^{1}H spectrum in DMSO-*d*$_6$ of compound 4Ec, $C_{17}H_{35}CO$-HydrGly-$NHC_{12}H_{25}$·HCl.

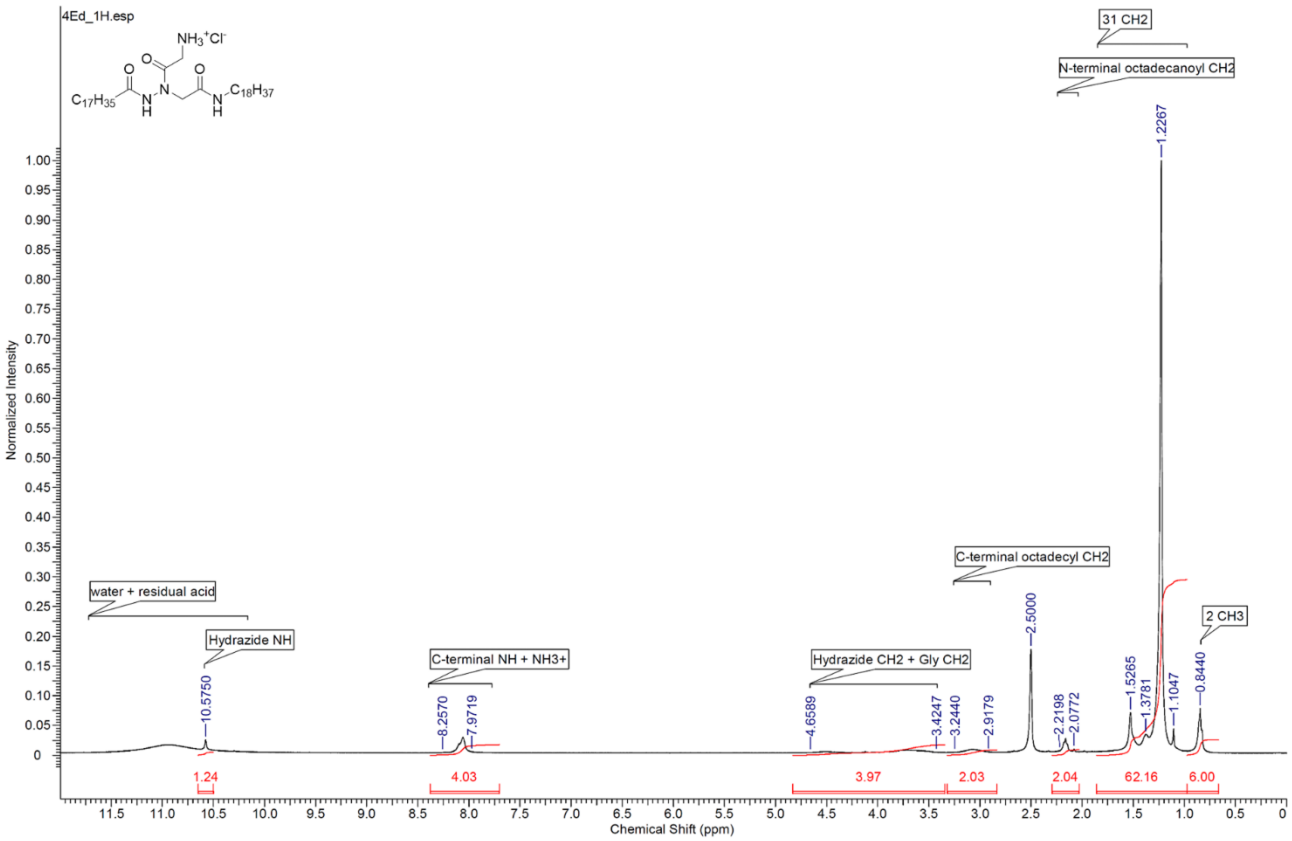

Figure 78. ^{1}H spectrum in DMSO-*d*$_6$ of compound 4Ed, $C_{17}H_{35}CO$-HydrGly-$NHC_{18}H_{37}$·HCl.

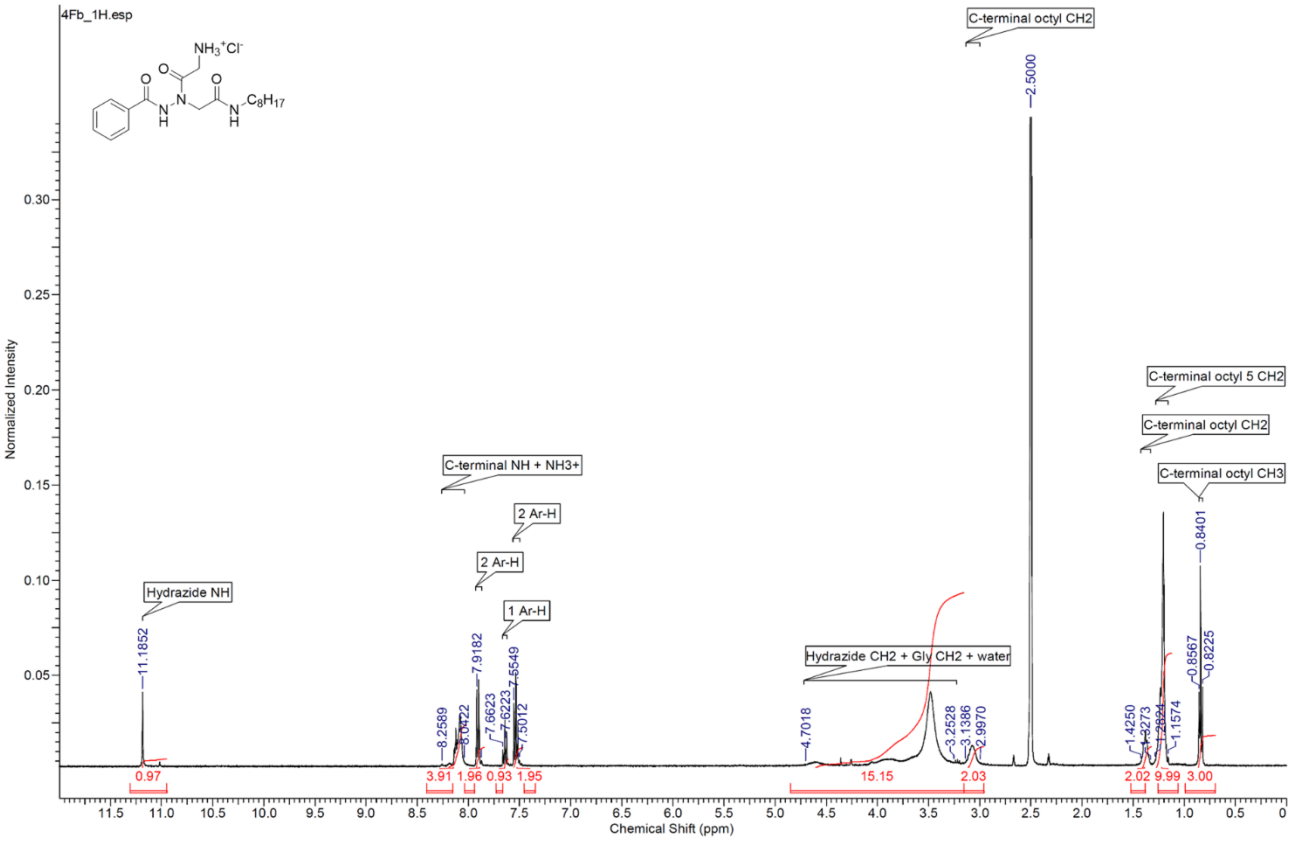

Figure 79. ^{1}H spectrum in DMSO-*d*$_6$ of compound 4Fb, PhCO-HydrGly-NHC_8H_{17}·HCl.

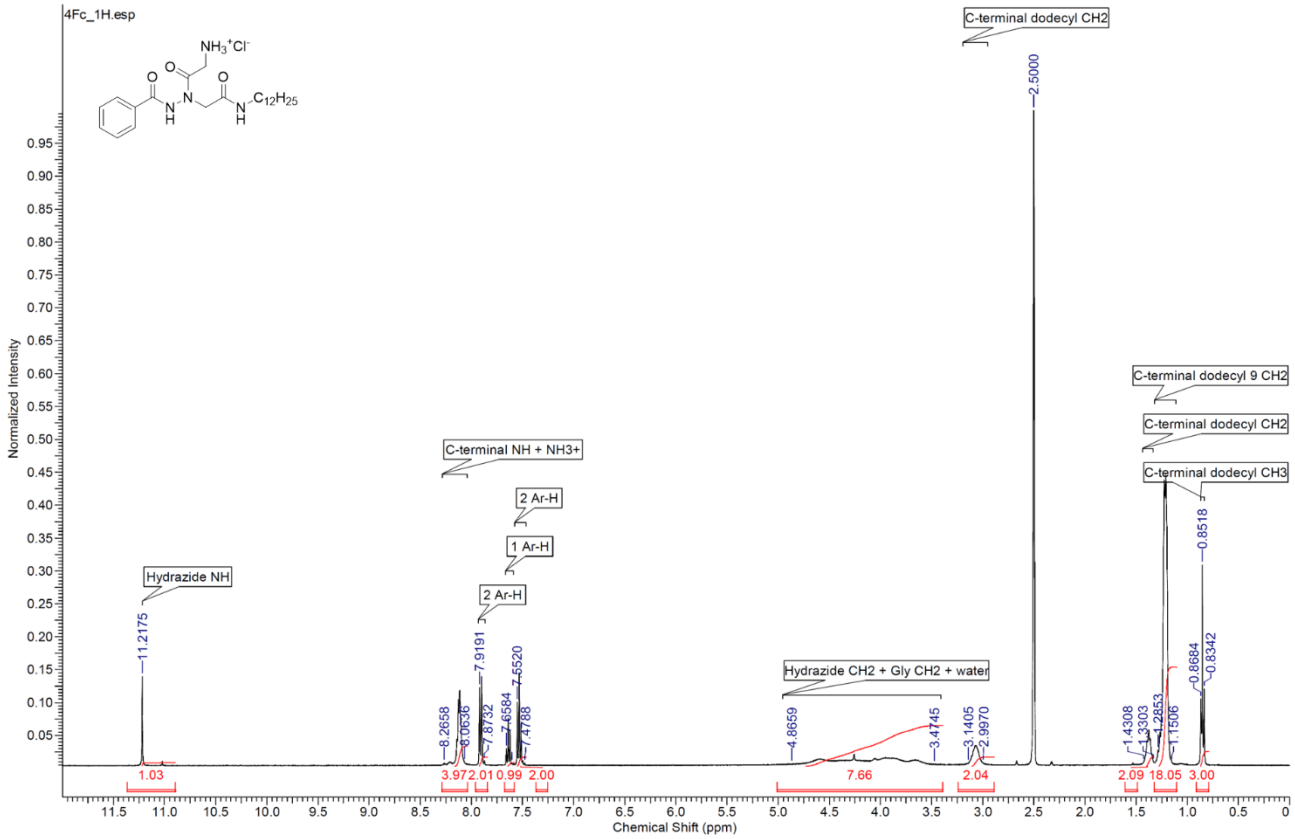

Figure 80. ^{1}H spectrum in DMSO-d_6 of compound 4Fc, PhCO-HydrGly-NHC$_{12}$H$_{25}$·HCl.

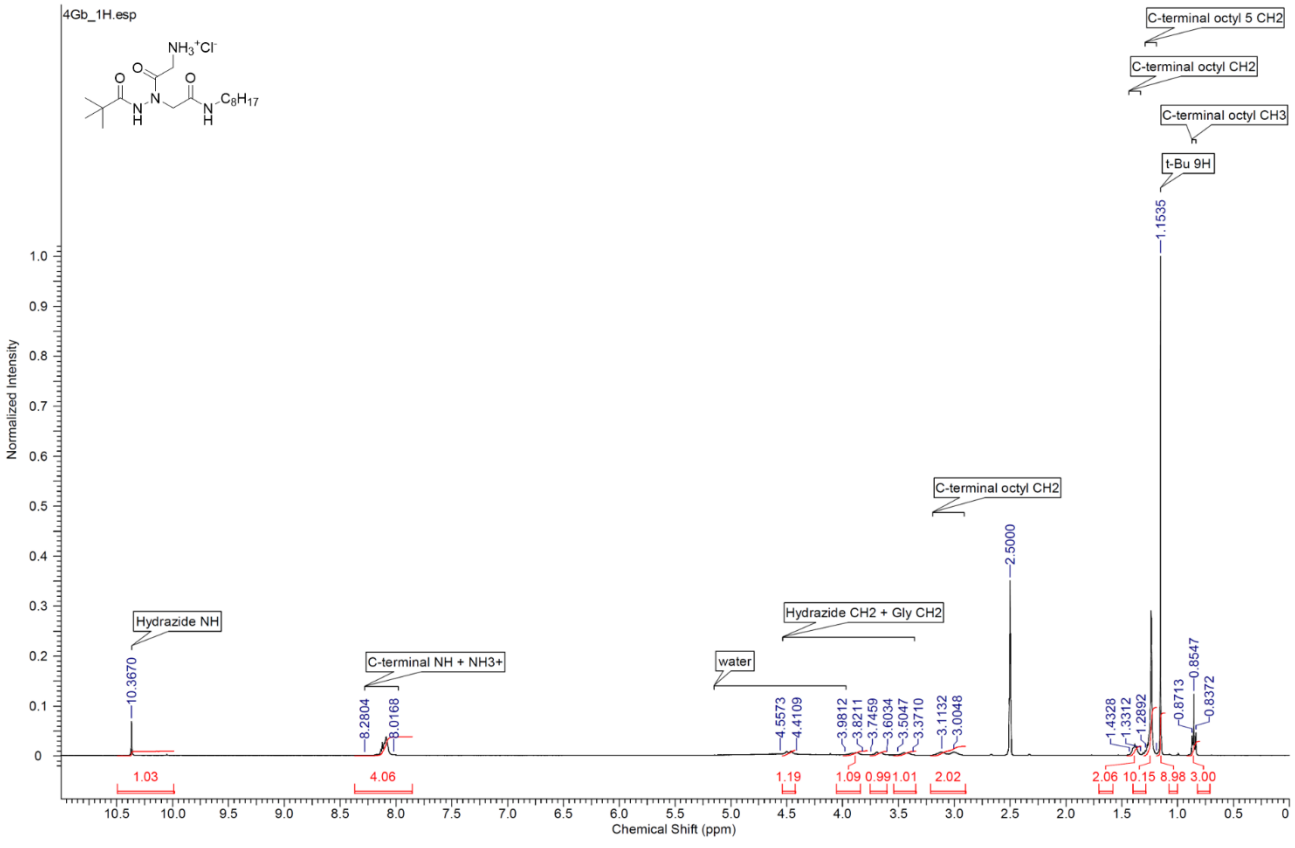

Figure 81. ^{1}H spectrum in DMSO-d_6 of compound 4Gb, *t*BuCO-HydrGly-NHC$_8$H$_{17}$·HCl.

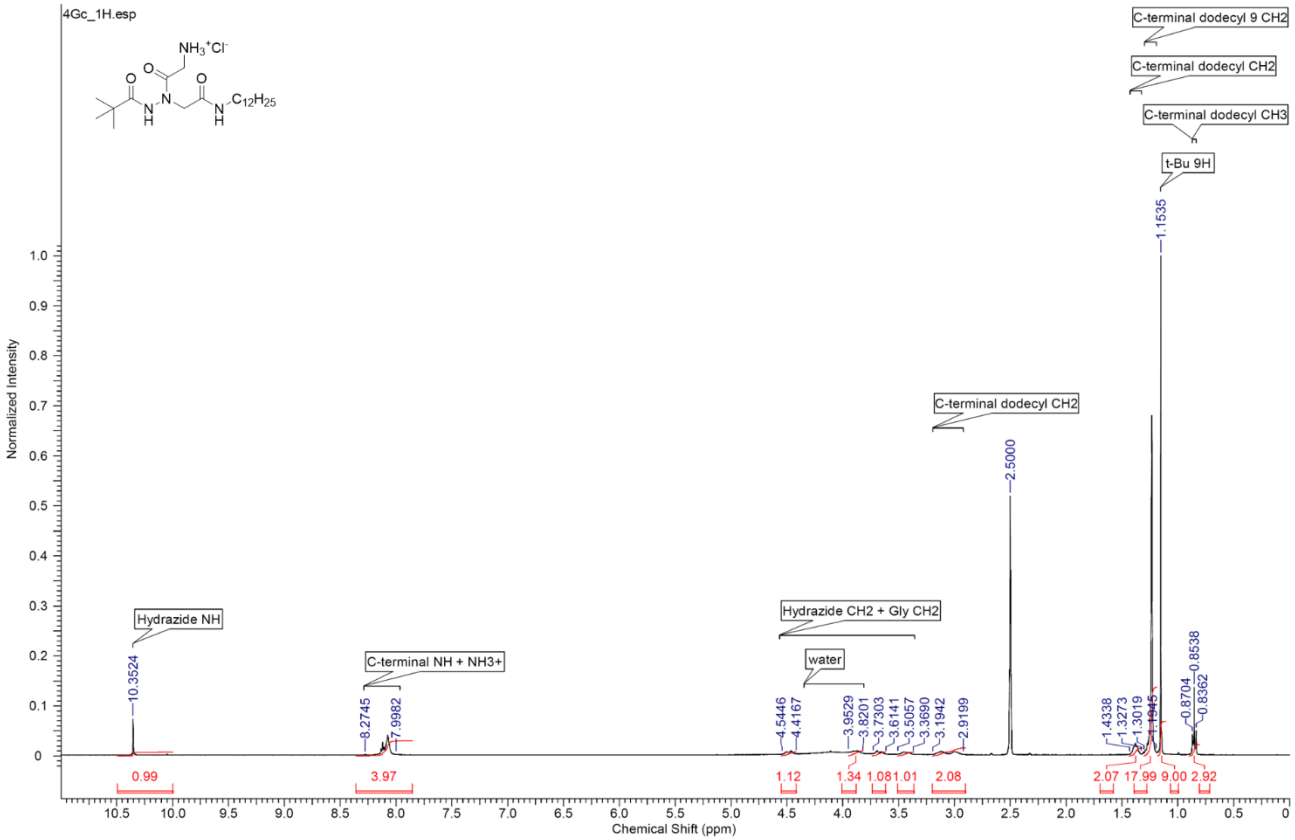

Figure 82. ^{1}H spectrum in DMSO-d_6 of compound 4Gc, *t*BuCO-HydrGly-NHC$_{12}$H$_{25}$·HCl.

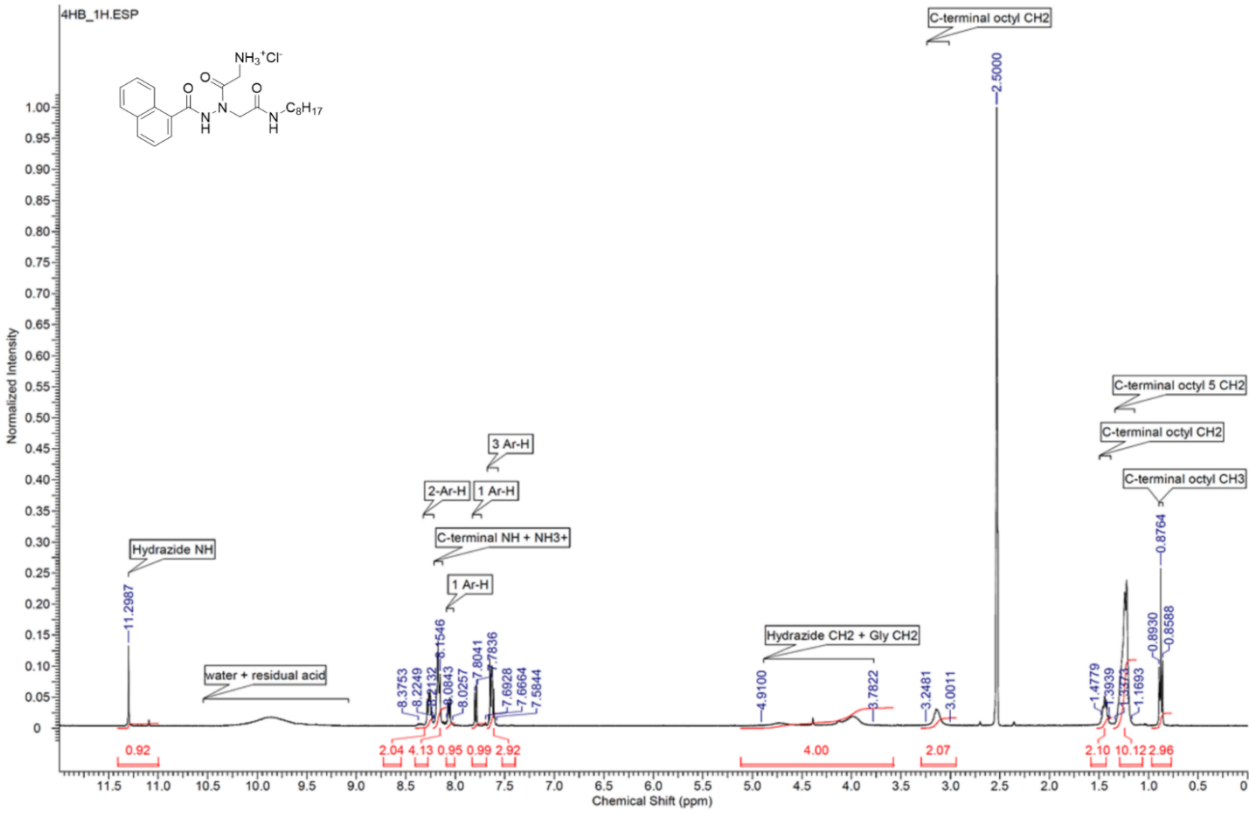

Figure 83. ^{1}H spectrum in DMSO-*d*$_6$ of compound 4Hb, 1-naphthylCO-HydrGly-NHC$_8$H$_{17}$·HCl.

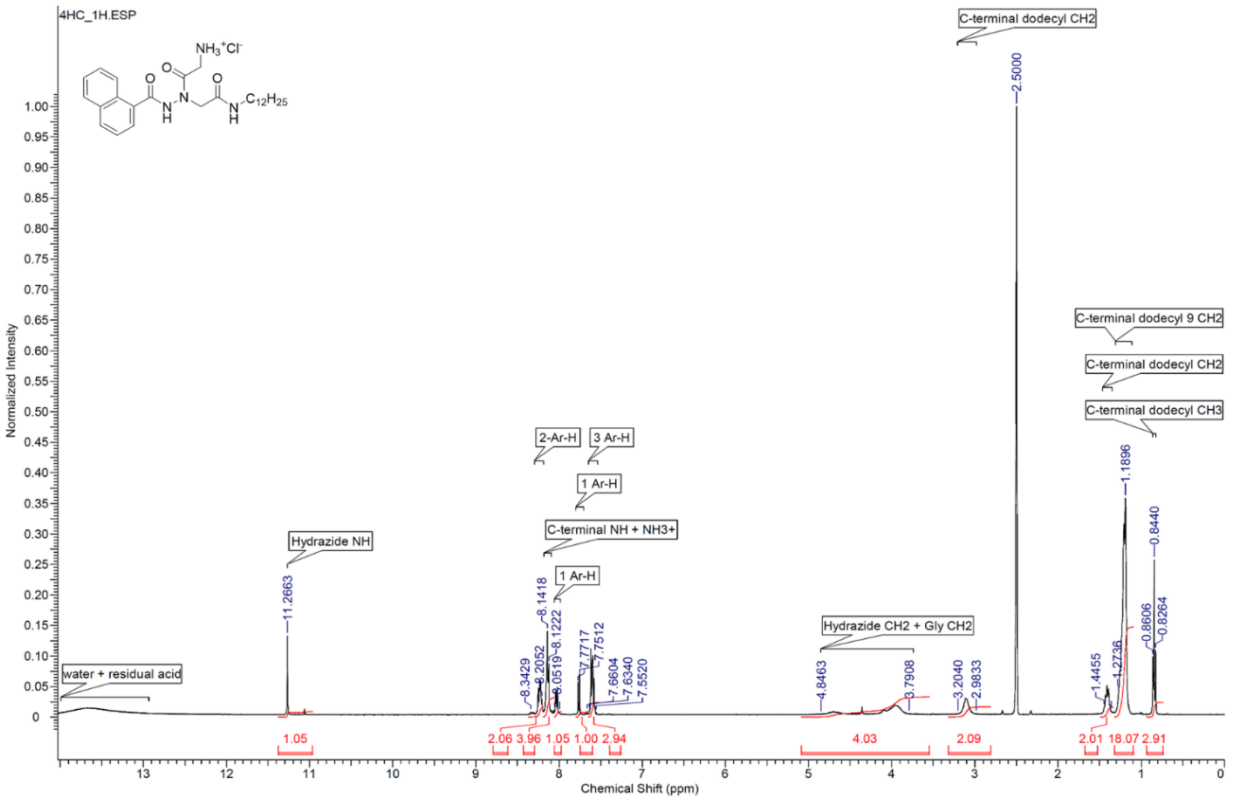

Figure 84. ^{1}H spectrum in DMSO-*d*$_6$ of compound 4Hc, 1-naphthylCO-HydrGly-NHC$_{12}$H$_{25}$·HCl.

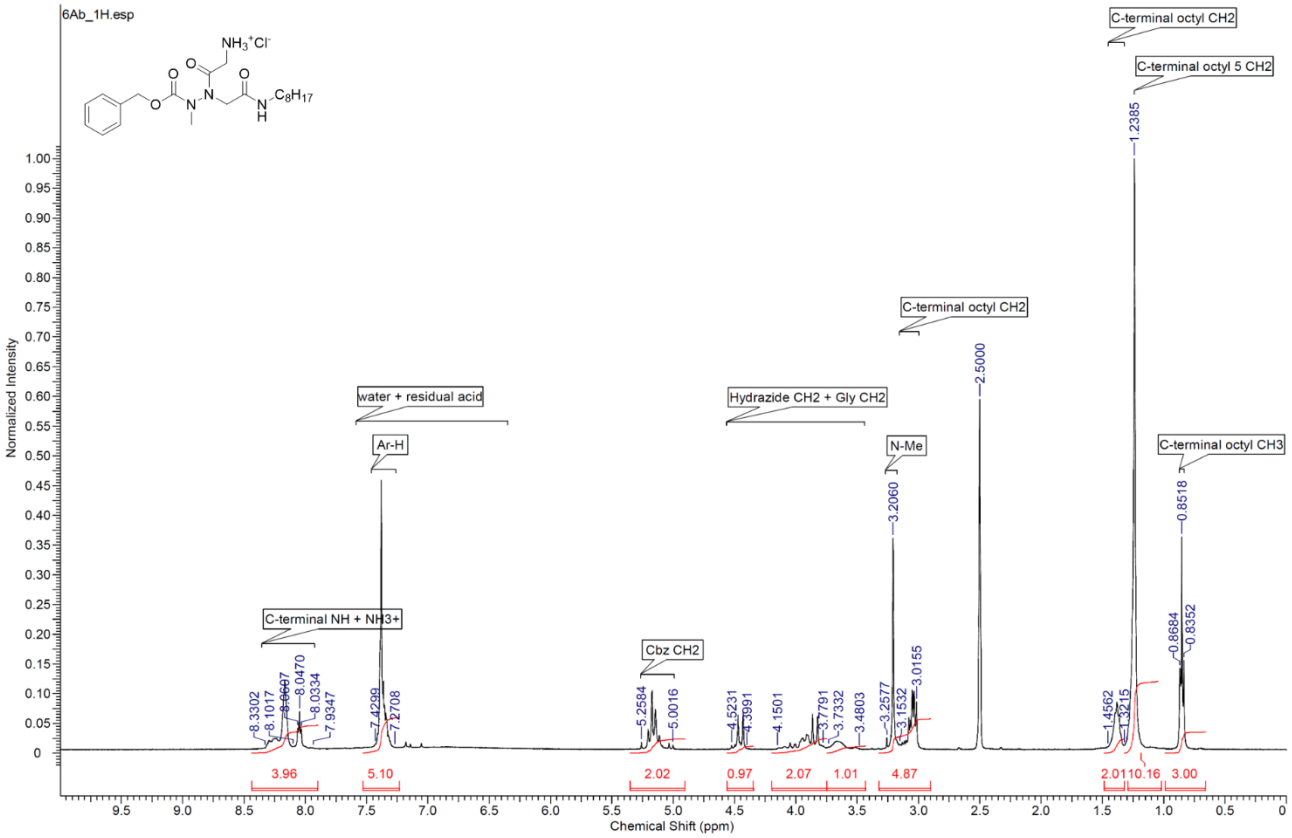

Figure 85. ^{1}H spectrum in DMSO-*d*$_6$ of compound 6Ab, Cbz-Hydr(Me)Gly-NHC$_8$H$_{17}$·HCl.

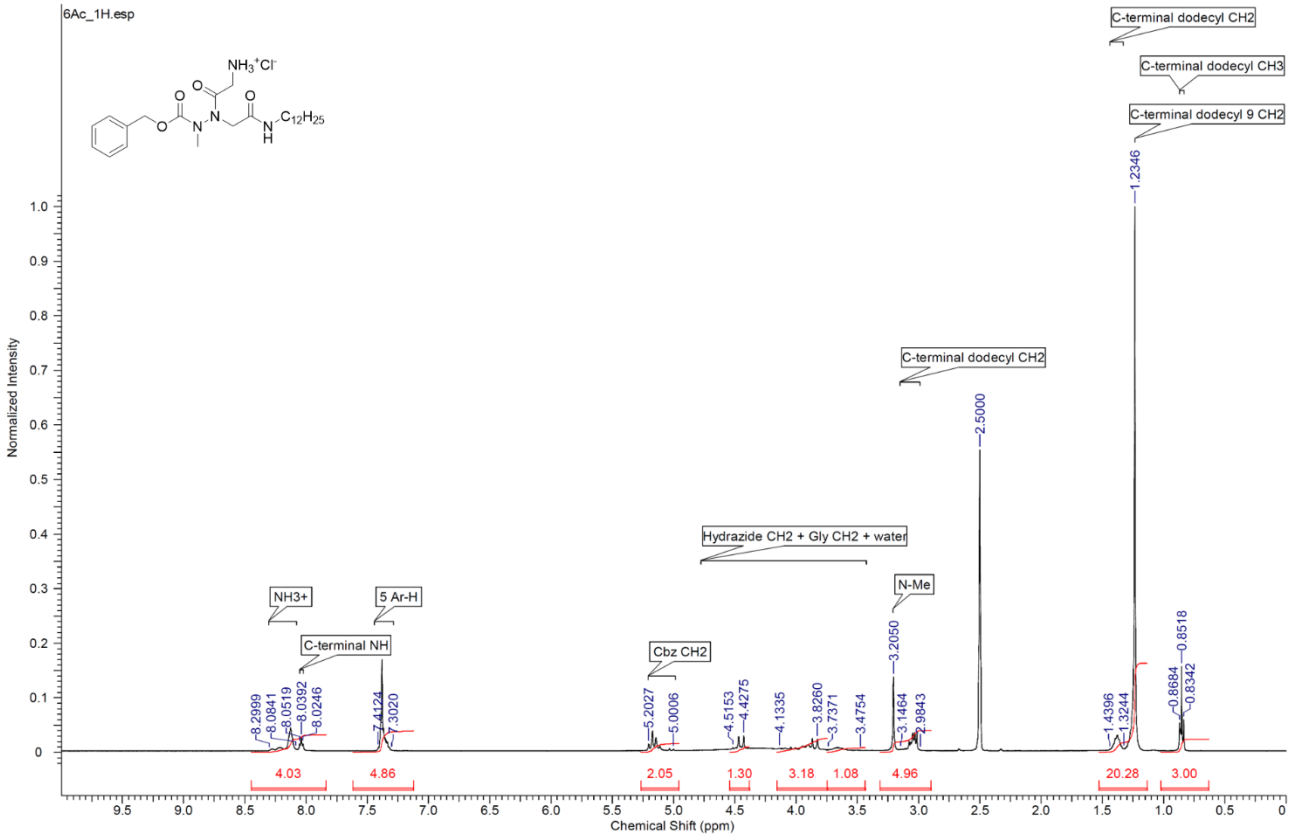

Figure 86. ^{1}H spectrum in DMSO-*d*$_6$ of compound 6Ac, Cbz-Hydr(Me)Gly-NHC$_{12}$H$_{25}$·HCl.

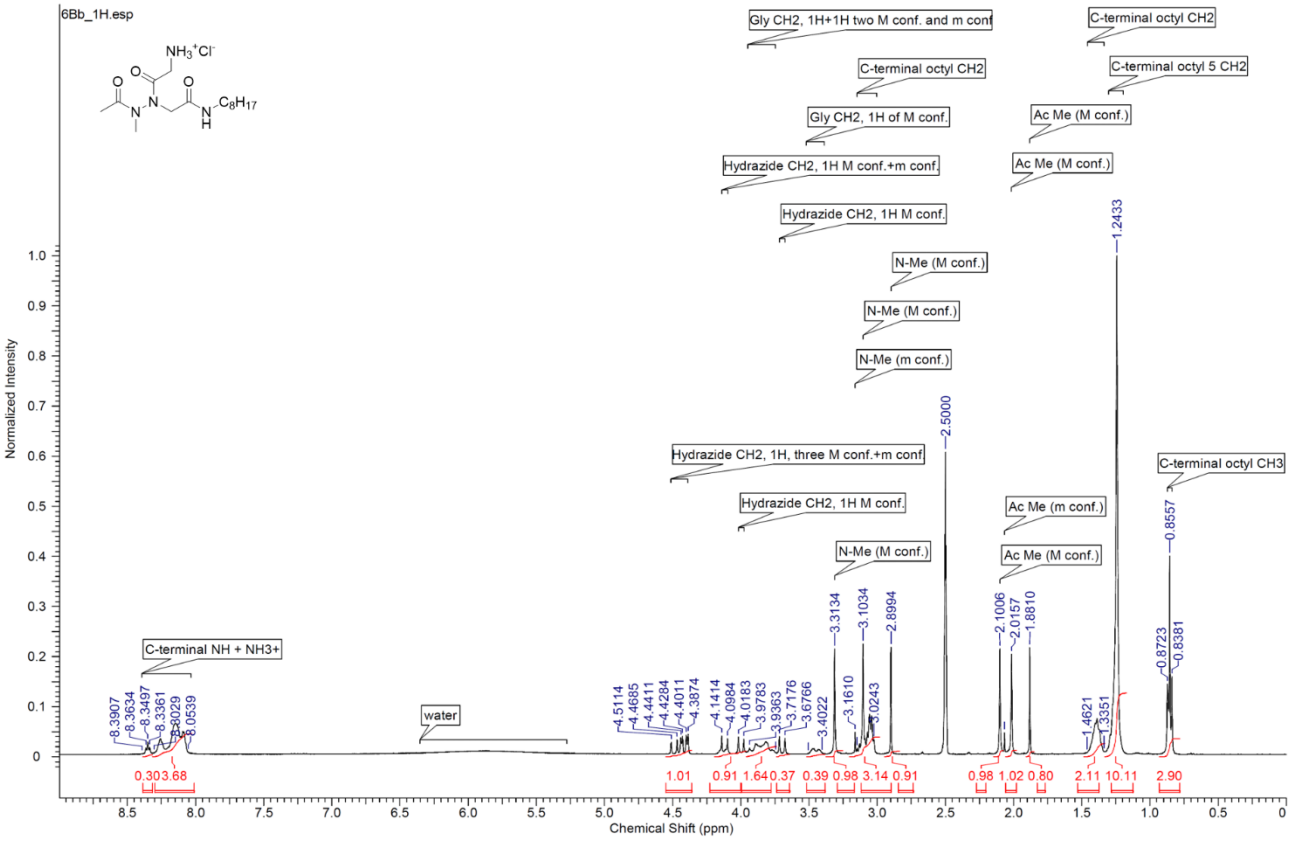

Figure 87. ^{1}H spectrum in DMSO-*d*$_6$ of compound 6Bb, Ac-Hydr(Me)Gly-NHC$_8$H$_{17}$·HCl.

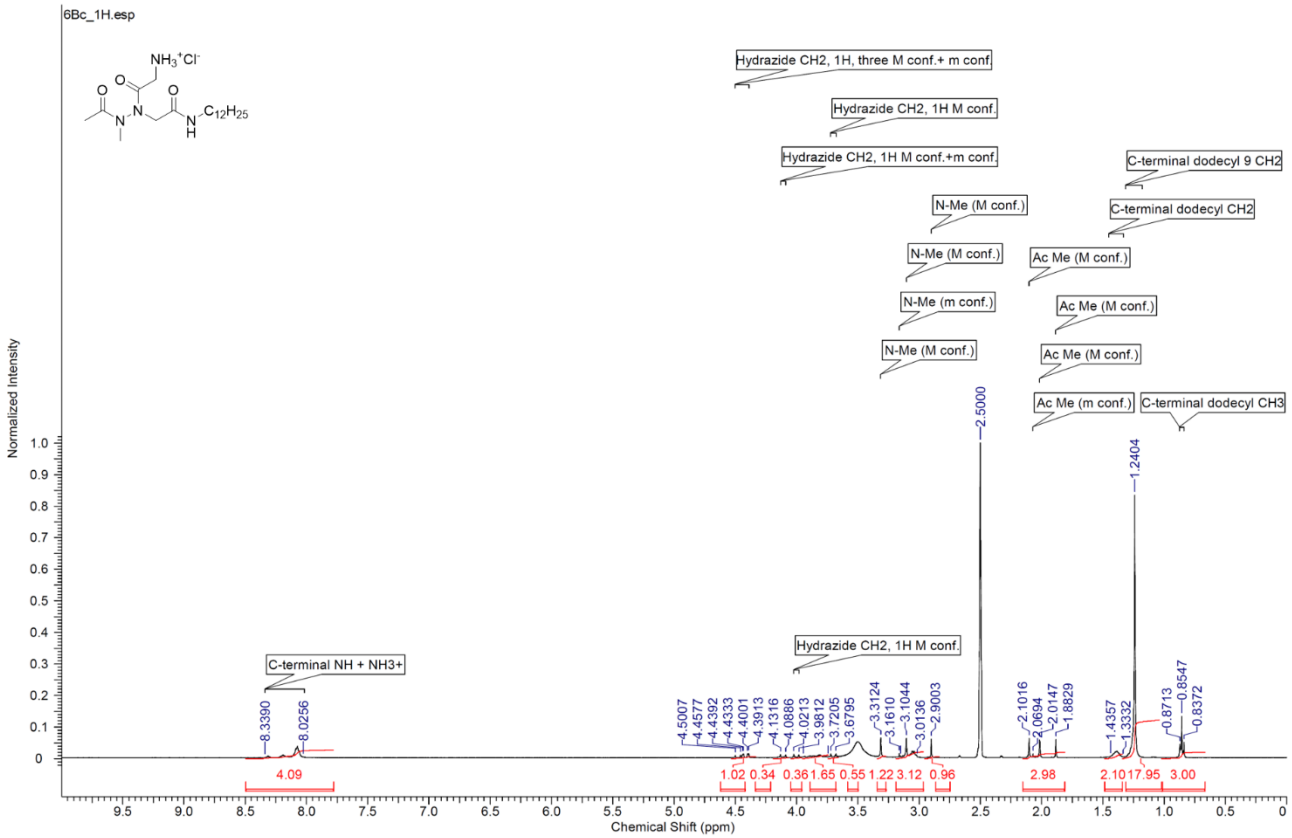

Figure 88. ^{1}H spectrum in DMSO-d_6 of compound 6Bc, Ac-Hydr(Me)Gly-$NHC_{12}H_{25}$·HCl.

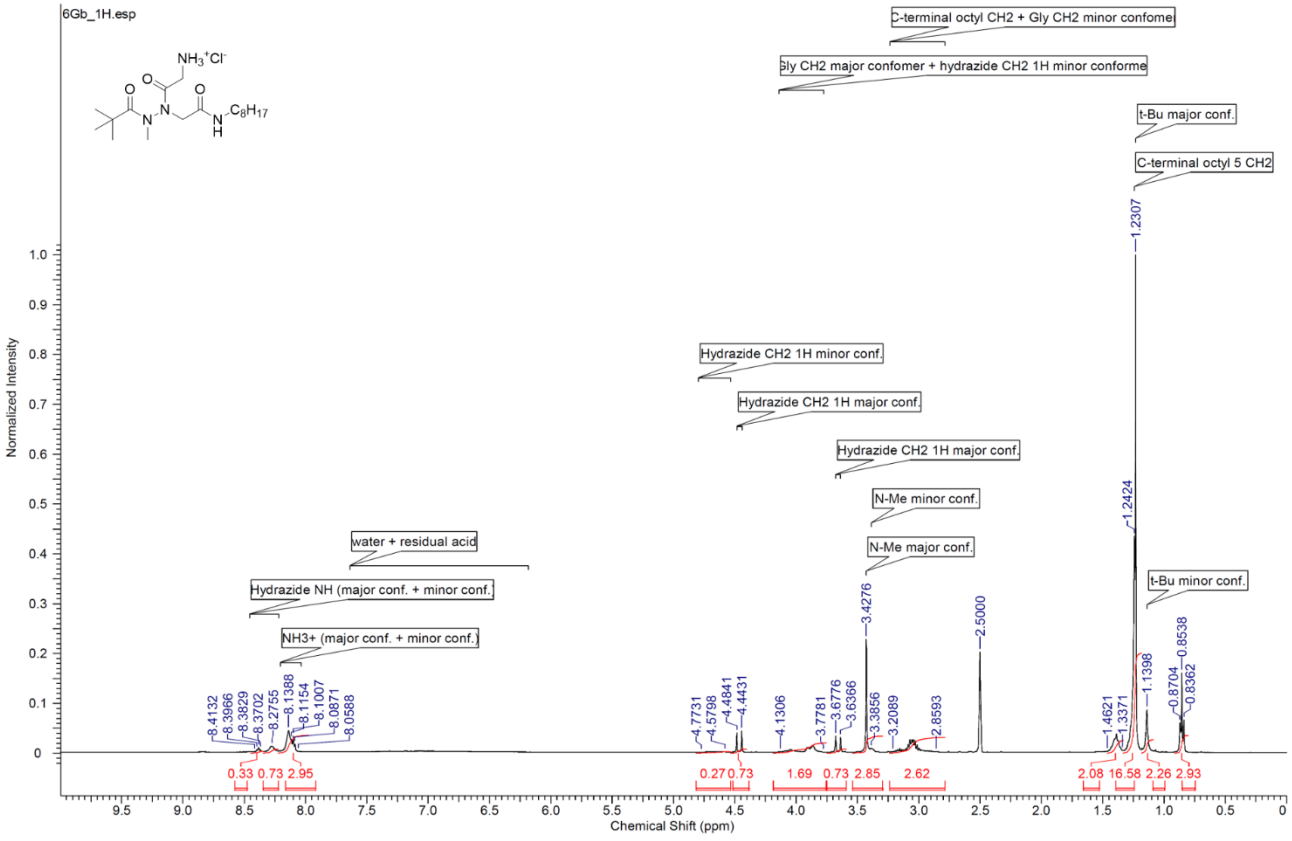

Figure 89. ^{1}H spectrum in DMSO-*d*$_6$ of compound 6Gb, *t*BuCO-Hydr(Me)Gly-NHC$_8$H$_{17}$·HCl.

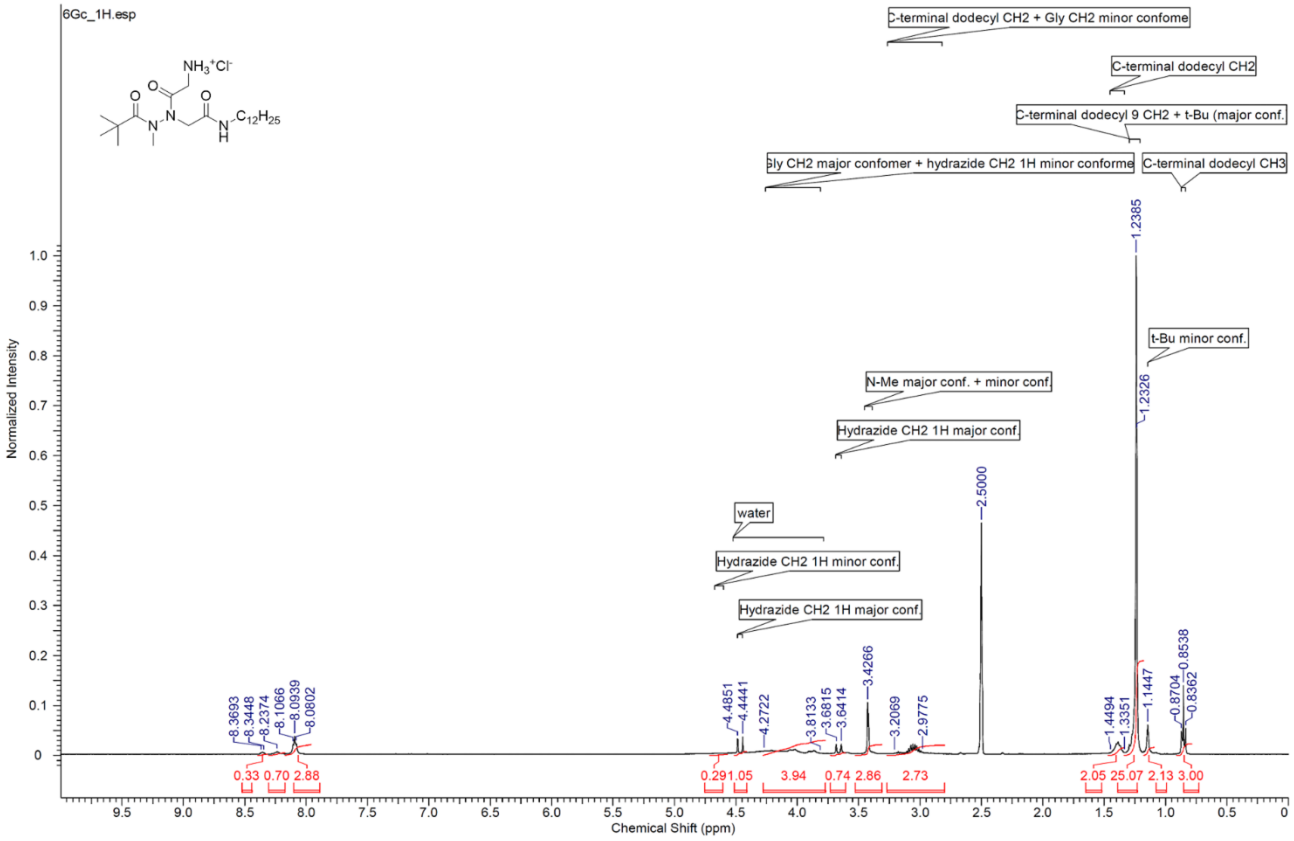

Figure 90. ^{1}H spectrum in DMSO-*d*$_6$ of compound 6Gc, *t*BuCO-Hydr(Me)Gly-NHC$_{12}$H$_{25}$·HCl.

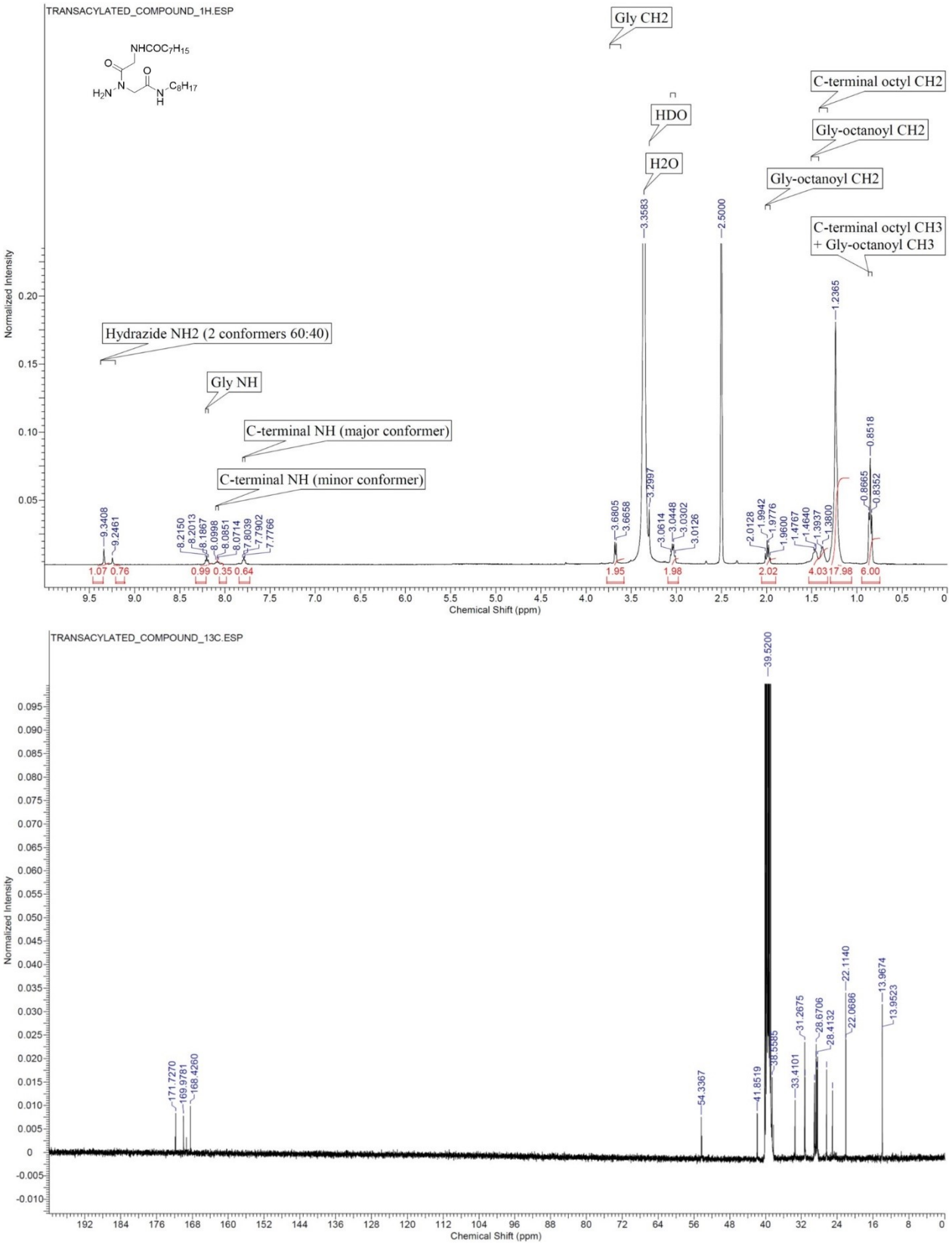

Figure 91. ^{1}H and ^{13}C NMR spectra in DMSO-d_6 of transacylated compound S1.

2.4.11 Additional Figures

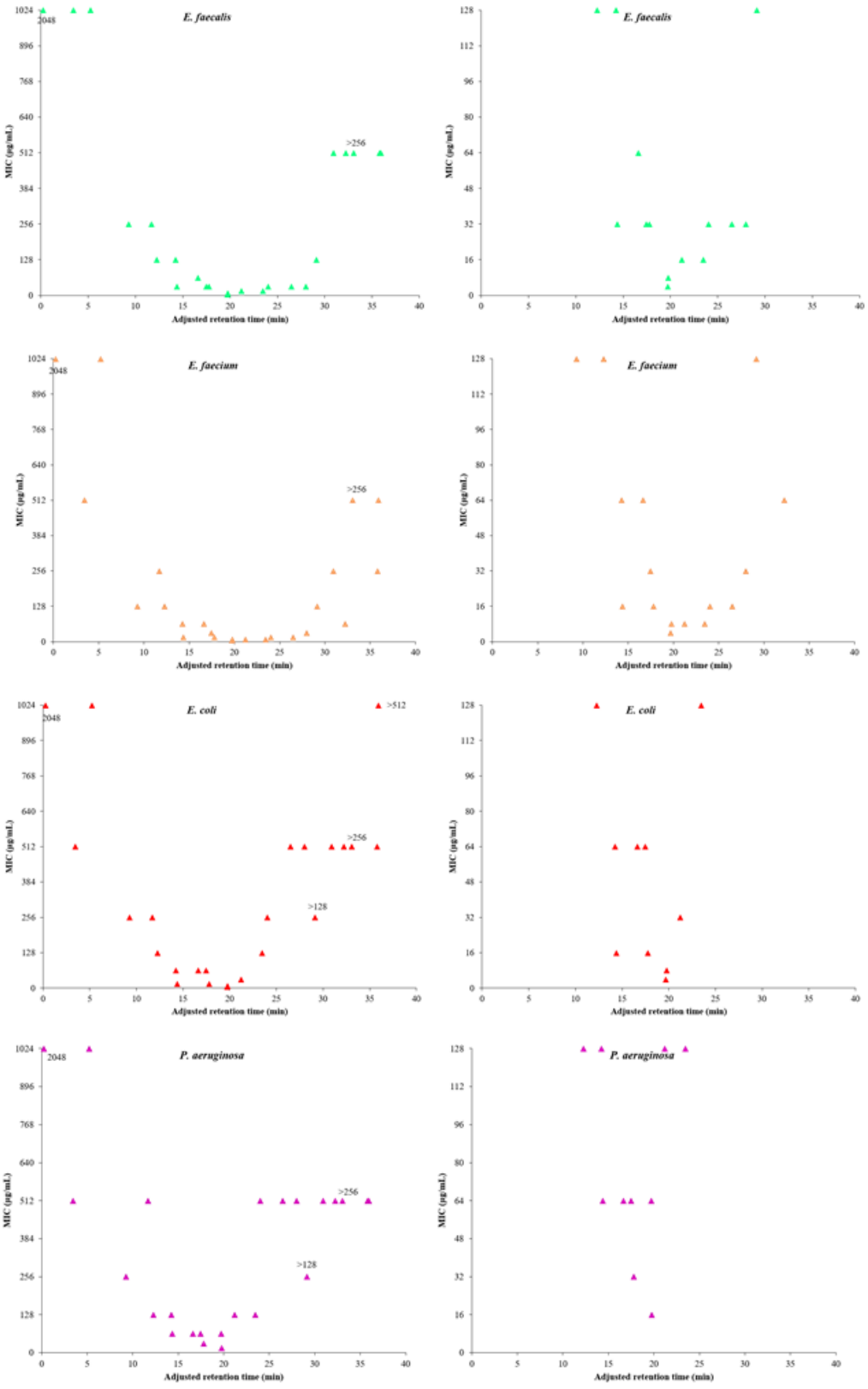

Figure 92. MICs toward different bacteria *vs* adjusted retention times. Left: vertical scale up to 1024 µg/mL. Right: vertical scale up to 128 µg/mL. (Hewlett-Packard Lichrosorb RP 18 column, 5 µm, L × I.D. 200 × 4.6 mm, flow rate = 0.5 mL/min; elution gradient: from water:2-propanol = 70:30 to water:2-propanol = 10:90 in 40 minutes). MICs with the writing ">value" near the triangle are reported as their minimum possible theoretical value, 2 × value, while MICs with experimental values >1024 µg/mL have been shown at 1024 µg/mL with the exact value reported near the triangle.

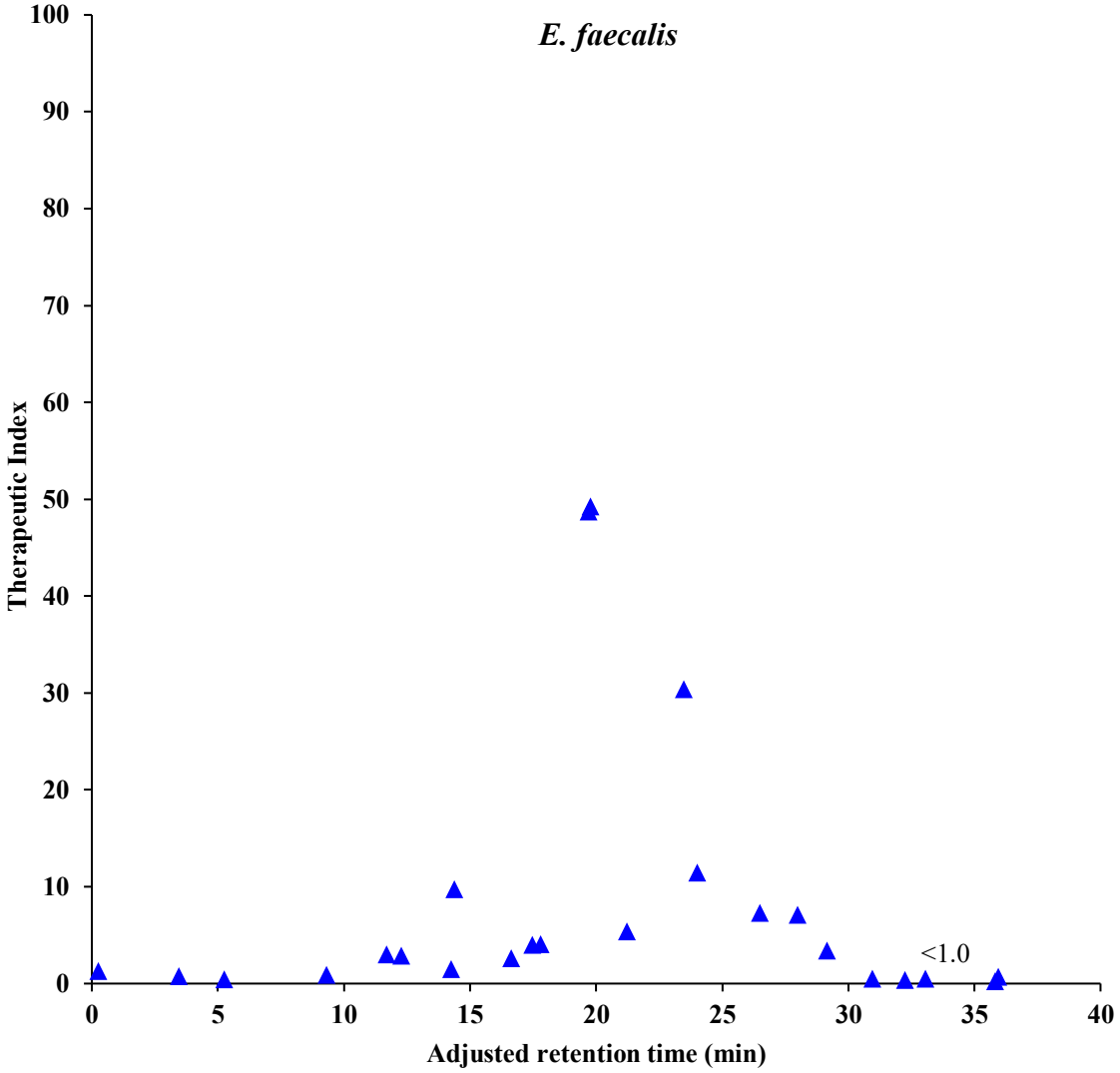

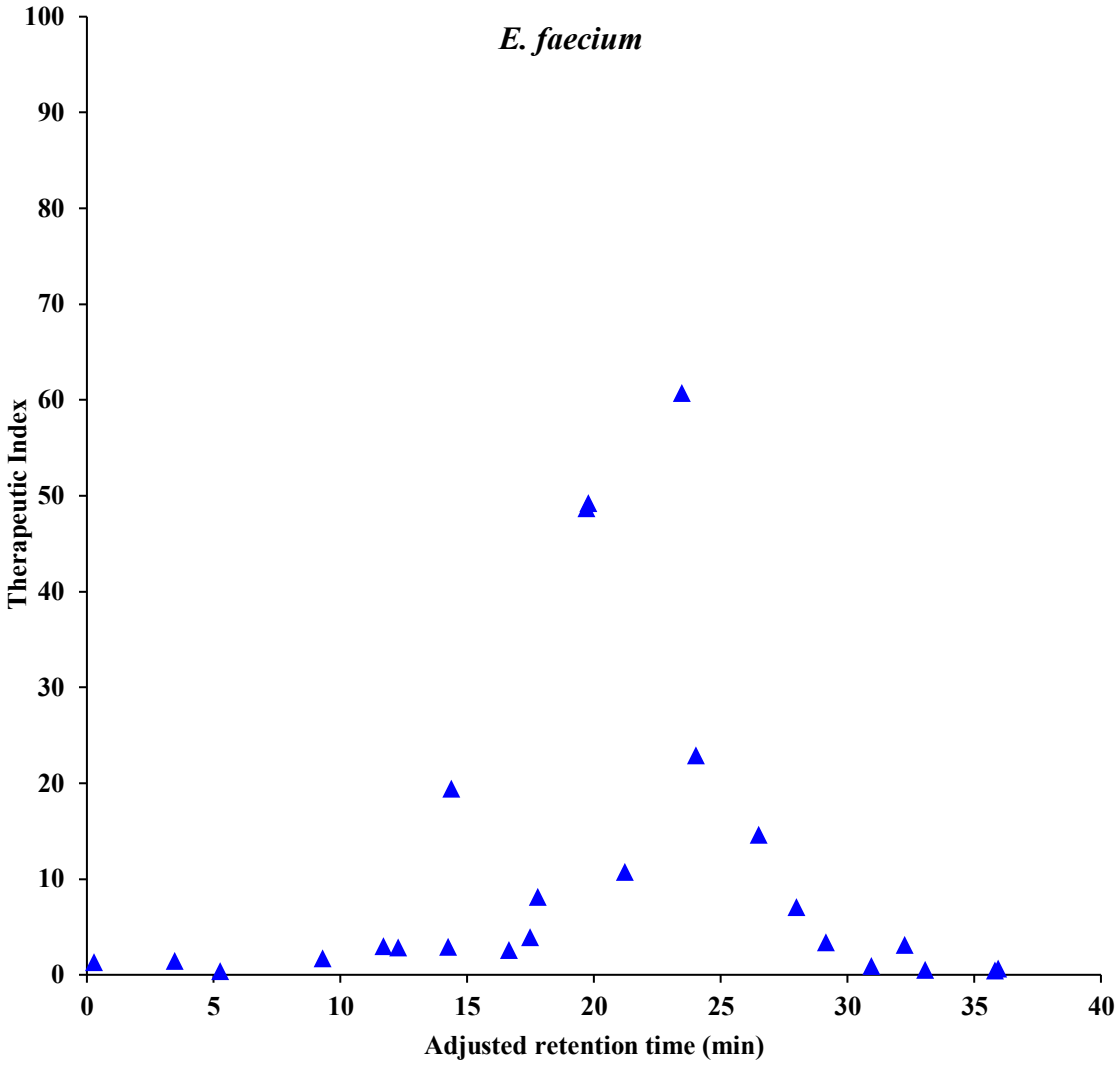
E. faecium
Therapeutic Index
Adjusted retention time (min)
0
10
20
30
40
50
60
70
80
90
100
0
5
10
15
20
25
30
35
40

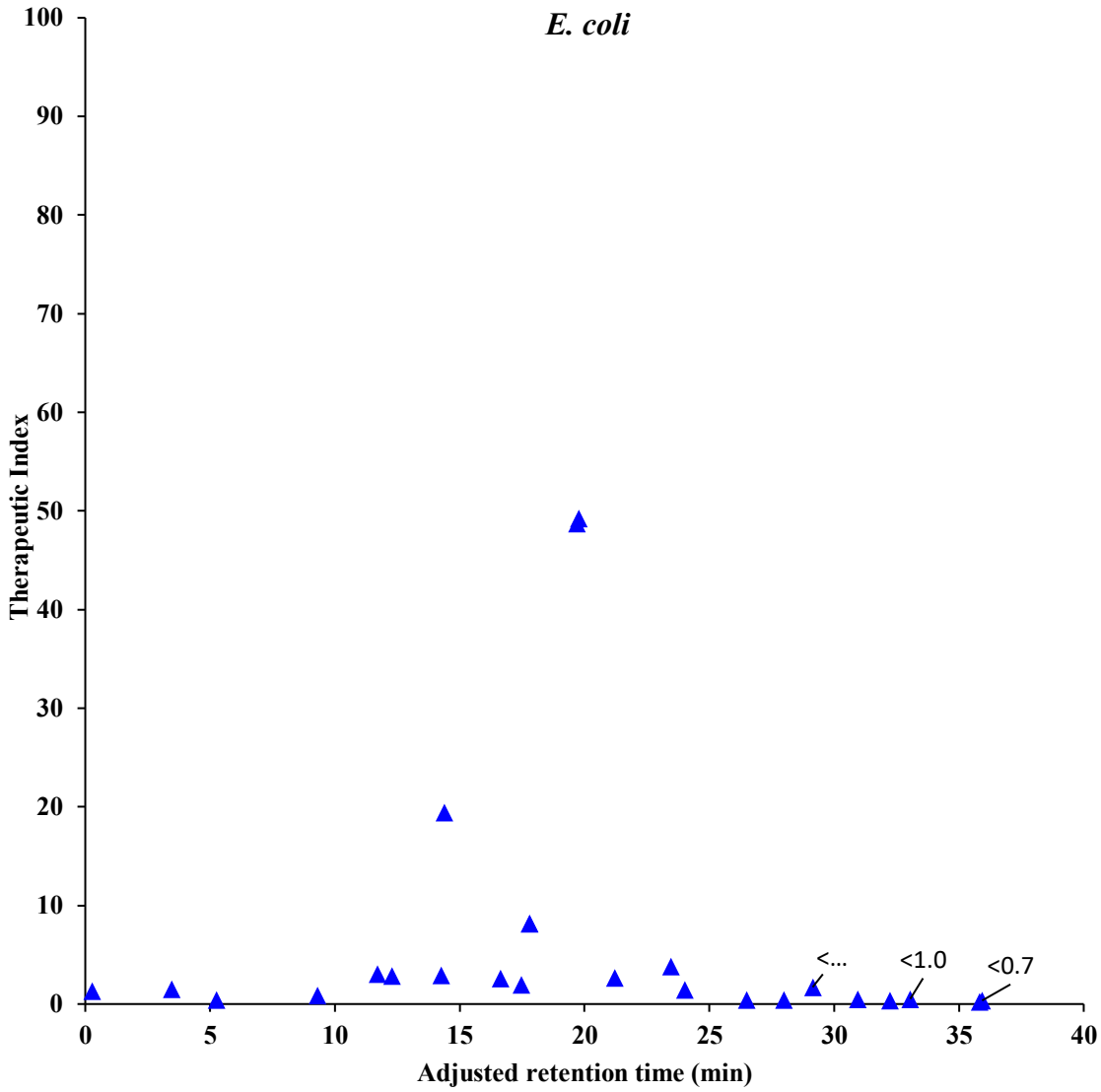
E. coli
Therapeutic Index
Adjusted retention time (min)
100
90
80
70
60
50
40
30
20
10
0
0
5
10
15
20
25
30
35
40
<...
<1.0
<0.7

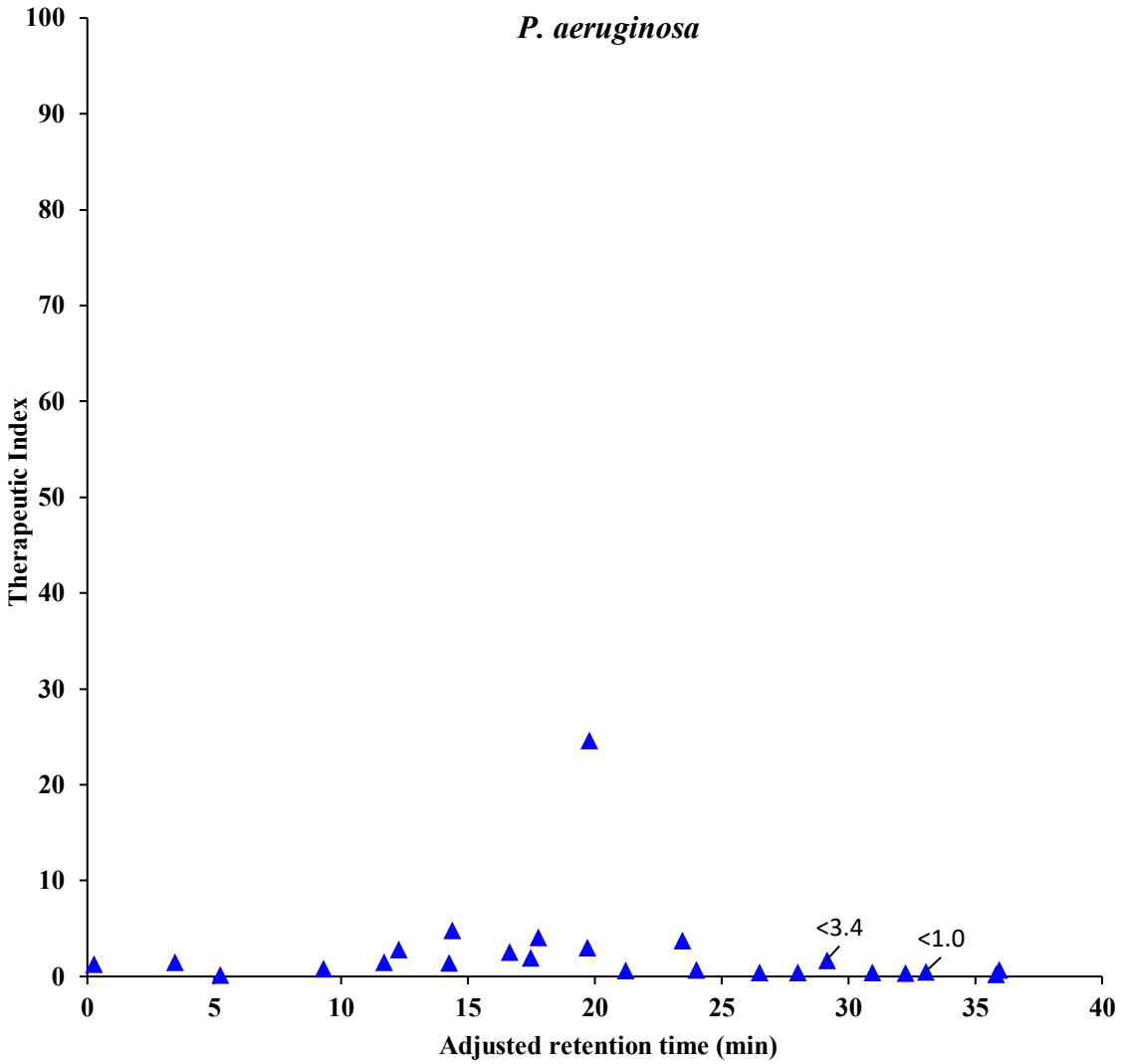

Figure 93. Therapeutic index toward different bacteria *vs* adjusted retention times (Hewlett-Packard Lichrosorb RP 18 column, 5 µm, L × I.D. 200 × 4.6 mm, flow rate = 0.5 mL/min; elution gradient: from water:2-propanol = 70:30 to water:2-propanol = 10:90 in 40 minutes). TIs with the writing "<value" near the triangle are reported as their maximum possible theoretical value, value/2.

Table 12. Therapeutic indices of compounds 4A-Ha-d toward *E. faecalis*, *E. faecium*, and *P. aeruginosa*.

Compd	R^1	R^2	TI *vs E. faecalis* (HC_{50}/MIC)	TI *vs E. faecium* (HC_{50}/MIC)	TI *vs P. aeruginosa* (HC_{50}/MIC)
4Aa	OBn	C_3H_7	0.8	1.5	1.5
4Ab	OBn	C_8H_{17}	1.5	3.0	1.5
4Ac	OBn	$C_{12}H_{25}$	5.4	11	0.7
4Ad	OBn	$C_{18}H_{37}$	0.5	0.9	0.5
4Ba	CH_3	C_3H_7	1.3	1.3	1.3
4Bb	CH_3	C_8H_{17}	0.9	1.7	0.9

4Bc	CH_3	$C_{12}H_{25}$	4.0	4.0	2.0
4Bd	CH_3	$C_{18}H_{37}$	7.1	7.1	0.4
4Ca	C_7H_{15}	C_3H_7	0.4	0.4	0.2
4Cb	C_7H_{15}	C_8H_{17}	4.1	8.2	4.1
4Cc	C_7H_{15}	$C_{12}H_{25}$	11	23	0.7
4Cd	C_7H_{15}	$C_{18}H_{37}$	<1.0	<1.0	<1.0
4Da	$C_{11}H_{23}$	C_3H_7	2.6	2.6	2.6
4Db	$C_{11}H_{23}$	C_8H_{17}	30	61	3.8
4Dc	$C_{11}H_{23}$	$C_{12}H_{25}$	3.4	3.4	<3.4
4Dd	$C_{11}H_{23}$	$C_{18}H_{37}$	0.7	0.7	0.7
4Ea	$C_{17}H_{35}$	C_3H_7	7.3	15	0.5
4Eb	$C_{17}H_{35}$	C_8H_{17}	0.5	4.2	0.5
4Ec	$C_{17}H_{35}$	$C_{12}H_{25}$	0.2	0.5	0.2
4Ed	$C_{17}H_{35}$	$C_{18}H_{37}$	N.D.	N.D.	N.D.
4Fb	Ph	C_8H_{17}	2.9	2.9	2.9
4Fc	Ph	$C_{12}H_{25}$	49	49	3.0
4Gb	*t*-Bu	C_8H_{17}	3.0	3.0	1.5
4Gc	*t*-Bu	$C_{12}H_{25}$	49	49	25
4Hb	1-Naphthyl	C_8H_{17}	9.7	19	4.9
4Hc	1-Naphthyl	$C_{12}H_{25}$	N.D.	N.D.	N.D.

3. TOTAL SYNTHESIS OF FIVE POSITIONAL ISOMERS OF COLISTIN CONJUGATED WITH PEPTIDES TARGETING BACTERIAL INFECTIONS

3.1 Introduction

3.1.1 The comeback of polymyxins in the need of "forgotten" antibiotics.

In the globally contest of antibiotic resistance, the rise of multidrug-resistant Gram-negative bacteria (MDR-GNB) has particularly become a more serious menace to face[125].

Among them, the so-called "pan resistant" belonging to *P. aeruginosa*, *A. baumanii* strains, require more attention to treat in the public health care, since they are resistant to all the "good" antibiotics.[126] The increasing of nosocomial and community-acquired infections caused by these "superbugs" [127] has not properly balanced by the discovery of new agents against them for over two decades, so that the resume of the "forgotten" antibiotics, in the clinical application, seems to be a valid alternative to respond to this crisis[128].

During the last few years, there has been a resurgence of interest about polymyxins, an old class of polycationic, cyclic lipodecapeptides[129], active against selected Gram-negative bacteria such as *P. aeruginosa*, *A. baumanii* spp., *K. pneumoniae* spp. and *Enterobacter* spp[130].

Currently, only polymyxin B and especially colistin (also known as polymyxin E) are been used in the clinical practice and actually defined as the "last line" treatment for MDR-GNB infections, such as *P. aeruginosa*, *A. baumanii*, *K. pneumoniae* and *E. coli*, when other treatment options are limited[131].

Polymyxins in general were discovered in 1947 and consist of five chemically different polypeptides (polymyxins from A to E) produced by a strain of *Bacillus polymyxa*, a Gram-positive soil bacterium.[132]

Colistin was discovered by Koyama in 1949[133] and is a secondary metabolite nonribosomally synthesised by a strain of *Bacillus polymyxa* subspecies *colistinus.*[134]

The chemical structure of colistin consists of a tail tripeptide moiety with two positively charged amino group and a hydrophobic fatty acid tail, that is 6-methylheptanoyl (this is only the fatty acid of colistin B, in colistin A and further variants it is different), linked to a cyclic heptapeptide ring bearing three positively charged amine groups. The amino acid components in this molecule are D-leucine, L-leucine, L-threonine and L-α-γ-diaminobutyric acid (L-Dab).[135] Thus, Colistin is an amphipathic molecule where the hydrophobicity arises from the fatty acid moiety and the hydrophilicity from the five charged L-Dab in the ring (Figure 94).[136]

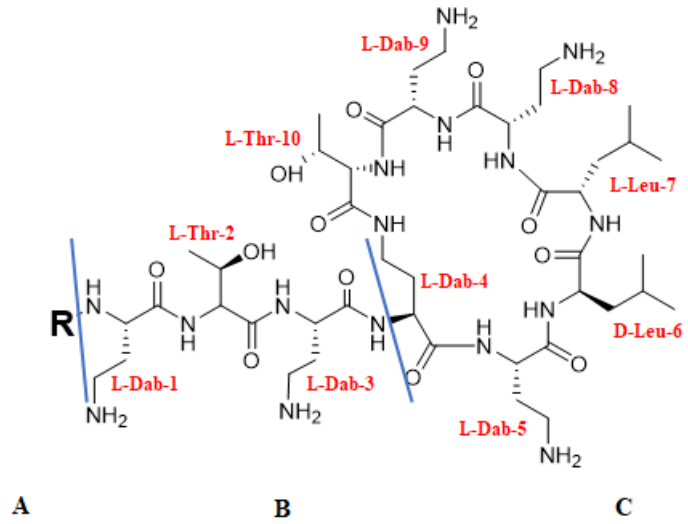

Figure 94. The chemical structure of colistin is composed of three parts: (A) hydrophobic fatty acid tail, (B) linear tripeptide segment, (C) hydrophilic heptapeptide ring. Arabic numeration indicates the position of the amino acid in the molecule. R indicates the fatty acid arm. R6: D-Phe in polymyxin B.

The commercial preparation of colistin, obtained from fermentation, is a complex mixture of closely related polypeptides, where colistin A and B (also known as polymyxin E1 and E2, respectively) are the major components[137], whose ratio depends on the different pharmaceutical preparations available. The only difference, between them, concerns the fatty acid arm at the N-terminal of the molecules: 6-methyloctanoyl group for colistin A and 6-methylheptanoyl group for colistin B (Figure 95).

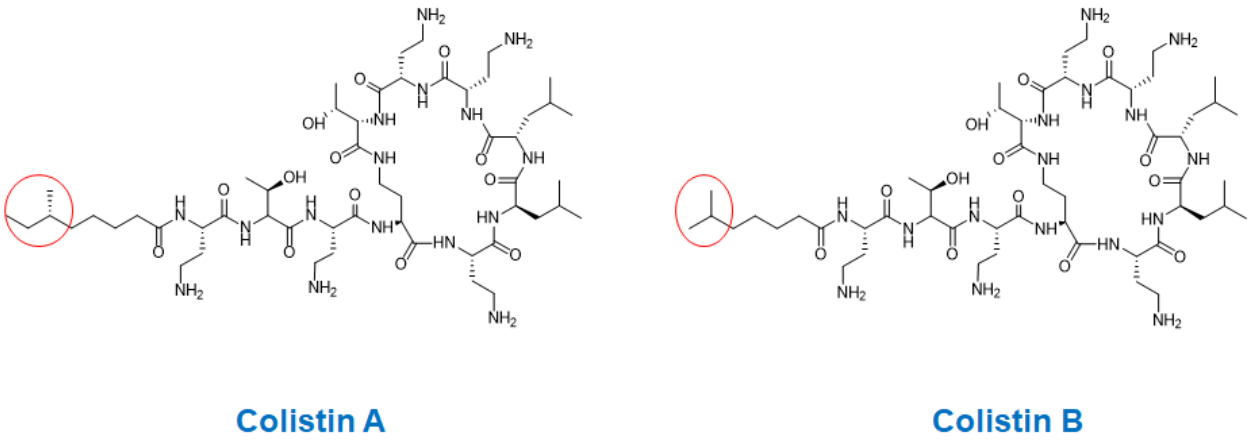

Figure 95. Chemical structure of colistin A and B.

Commercially, this mixture of structural isomers of colistin is available in two different formulations: as sodium salt of the prodrug colistin methanesulfonate, also called colistimethate (CMS) for parenteral use, and colistin sulfate for oral and topic use (Figure 96).[138]

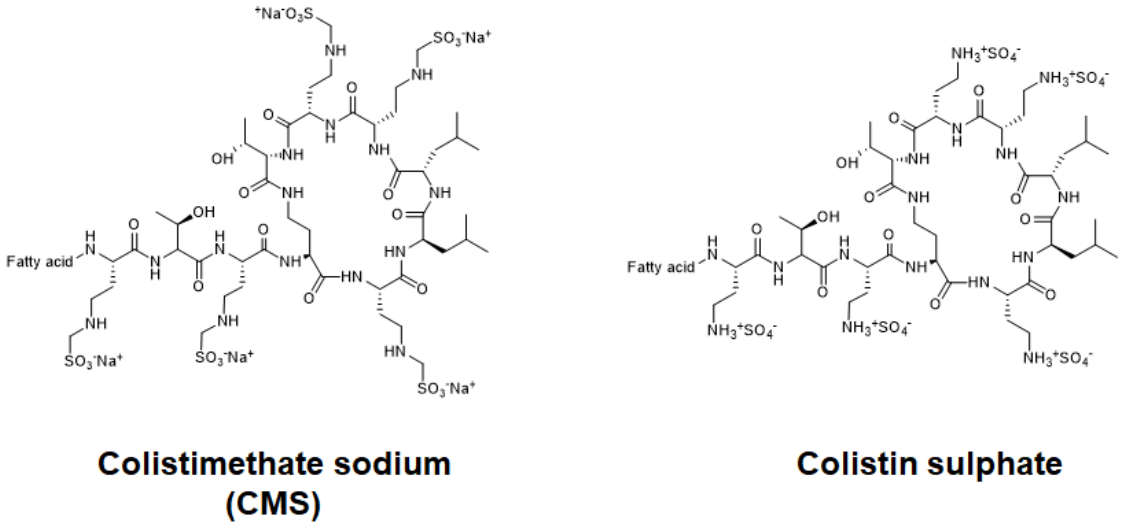

Figure 96. The two commercial formulations of colistin isomeric mixture.

Polymyxin B and colistin are bactericidal and their target of action is the LPS membrane, only present in Gram-negative bacteria. Thus, against Gram-positive bacteria these compounds are typically ineffective. It is assumed that the positively charged Dab residues initially interact on the outer leaf of the outer membrane by first binding the negatively charged lipid A phosphates of lipopolysaccharide.[139] Although it is not entirely clear what exactly happens, experimental modelling suggests that this electrostatic interaction promotes the exchange of phospholipids between the inner and outer membranes, leading to a weakening of the tightly packed lipid fatty acid chains, so resulting in osmotic imbalance and leading to lytic cell death.[139]

After the discovery, colistin was used in clinical medicine initially in Japan and then in Europe in the 1960s but was withdrawn in the 1970s due to its neurotoxic, but mainly nephrotoxic side effects. Clinicians swapped to less toxic alternatives,[140] as novel aminoglycosides (gentamycin) and second and third-generation cephalosporins became available in that period.[141]

Because of the large molecular weight and the electronic feature (polyanionic for CMS and polycationic for colistin) at physiologic pH, colistin and CMS passes through physiologic membranes poorly, so that after systemic administration, their distribution is primarily restrained in the extracellular spaces.[142] The nephrotoxicity of colistin (and CMS as well) is given by an intensive tubular reabsorption, due to low renal clearance, so that most of the

filtered colistin is retained in the body.[143] Diaminobutyric acids (Dabs) and the fatty acid arm are the main components of colistin that cause an acute tubular necrosis, similarly to the mechanism of antibacterial activity.[144] The mechanism of nephrotoxicity has not been comprehensively elucidated, indeed, through an intensive increase of permeability of tubular epithelial cell membrane, leading to water, cations and anions influx, so resulting into cell swelling and lysis. [144]

Currently the intravenous formulation is only restricted as savage therapy to treat patients with severe infections caused by MDR-GNB.[137]

The need to re-introduce again the "old and forgotten" polymyxins B and colistin, together with the need to reduce their toxicity, is the driving force in the last 20 years, to develop new polymyxins-based compounds, in order to fight the more and more worrisome war in the contest of MDR-GNB.

Within the development of new polymyxin derivatives, the clearest observed thing was that the activity of these compounds runs concurrently with the toxicity: more active compounds are, in general, also more toxic.[145] With the aim of designing a new generation of polymyxins, retaining the activity but decreasing toxicity, many researchers kept in mind the relationship between the chemical structure and the antibacterial activity.

First of all, the amphipathicity, the cationic distribution and the fatty acid arm are essential features to their activity.[139] Earlier studies revealed that substitution or modifications from positive to negative charge of the side chains of Dab residues in the ring, resulted in a complete loss of antibacterial activity. [139] Indeed, the Dab amino acids in the lactam ring are needed for the bactericidal activity, the Dab in position 5 being the most important residue.[146] On the other hand, D-Leu, L-Leu and Dab residues in position 1 and 3 are not indispensable for the antimicrobial activity.[146] In addition, modifications to Nα-acyl chains suggested that the optimal chain length ranges from seven and nine carbons.[146]

Among the first colistin derivatives there was PMBN**,** also known as PMB nonapeptide. This compound is essentially polymyxin B without the fatty acid arm and the first Dab residue, obtained by enzymatic treatment of PMB with ficin (Figure 97).[147] Even if PMBN itself is not bactericidal, it keeps the capacity of permeabilizing the outer membrane of Gram-negative bacteria at low concentration, so making bacteria vulnerable to the action of other lipophilic drugs to use in combination with it.[148] Moreover, PMBN is 100 times less toxic than PMB in a eukaryotic cytotoxicity assay, and other studies revealed the less nephrotoxicity potential.[149]

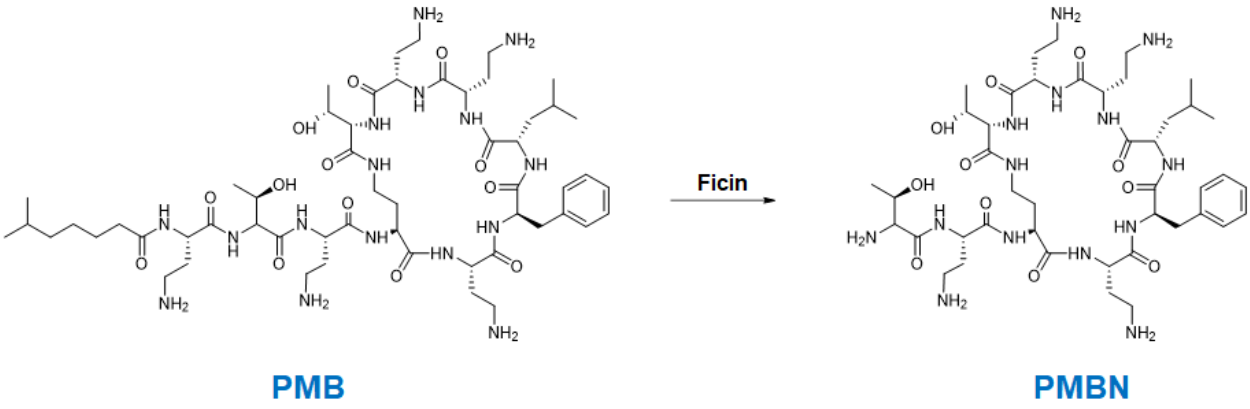

Figure 97. Chemical structure of polymyxin B nonapeptide derivatized by ficin treatment from PMB.

Subsequently, the Vaara group[150] extended their studies synthesizing other polymyxin derivatives, which are in general characterized by the same cyclic core of polymyxin B and carrying out changes in the linear lipopeptide region, so having only three positive charges in total (Figure 98).

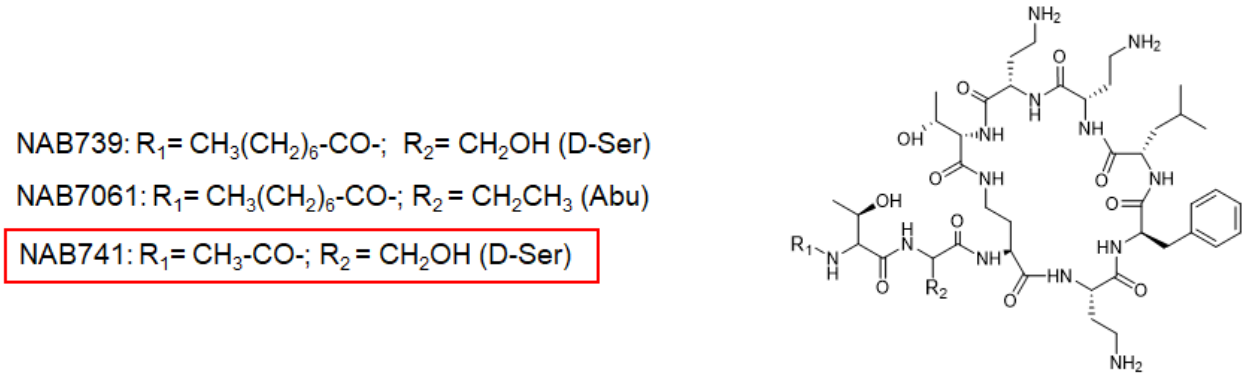

Figure 98. Series of northern antibiotics nonapeptides; in the red box the most promising NAB741.

Most notably, the compound NAB741 (Figure 98), having acetyl-threonyl-D-serinyl as linear tail, displayed low intrinsic antimicrobial activity, still retaining the ability to permeabilizing the OM as PMBN; moreover, is less toxic than its corresponding PMB or colistin with 4000 fold higher renal clearance.[150]

From these studies, it is evident that the Vaara group postulates that the toxicity of polymyxins is influenced by the high number of positive charges and the lipophilic tail of the fatty acid arm.

Cubist Pharmaceutical in collaboration with BioSource Pharm, developed CB-182,804, which essentially differs from PMB by the substitution of the acyl chain with a 2-chlorophenyl urea unit (Figure 99).[151]

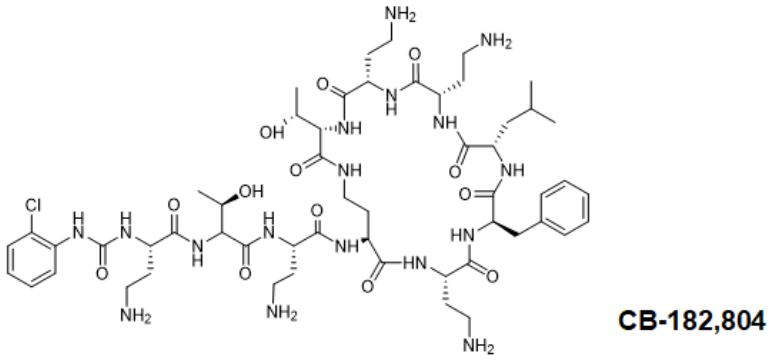

Figure 99. CB-182,804 PMB derivate.

The antibacterial activity was exploited against a wide range of Gram-negative bacteria, and in general the MIC values differ from PMB only for one dilution (2 x) potency. The nephrotoxicity appeared to be lower, but no significant changes were highlighted in terms of renal cells necrosis than PMB, so, after phase I clinical trial, it was phased out.[152]

Magee *et al*.[153] developed a variety of analogues working for Pfizer, replacing the fatty acid with a series of different biaryl moieties and the Dab in position 3 with Dap.[153]

Amongst them, the compound 5x (Figure 100) showed higher activity and reduced toxicity against hRPTEC cell line.

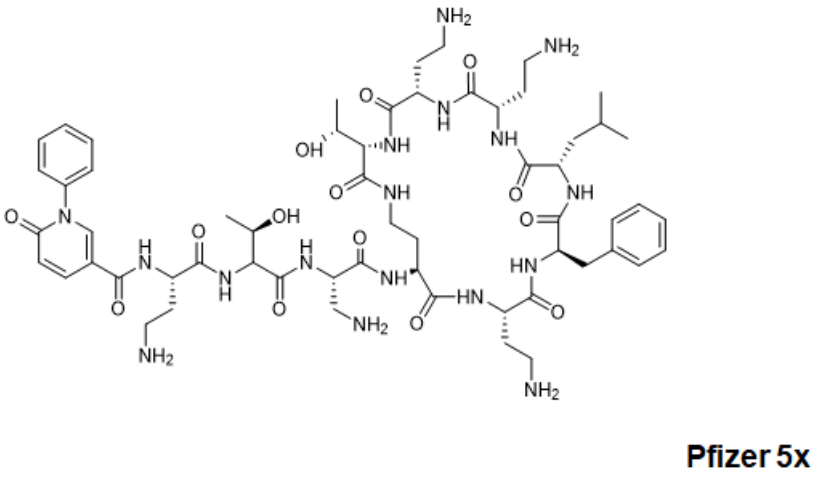

Figure 100. Pfizer 5x.

However, the seven-days toxicology in dogs study evidenced no significant safety margin with respect to PMB, so preclinical investigation was not followed up.[153] The most important thing highlighted from the authors of this study was the necessity to improve the toxicity test *in vitro*, able to predict the nephrotoxicity in preclinical models.[153]

With the same strategy of Pfizer 5x, Cantab reported a series of PMB nonapeptide analogues, with different aminoacyl moieties at the N-terminal, and, in just one case, changed the Dab in position 3 to Dap (Figure 101).[145]

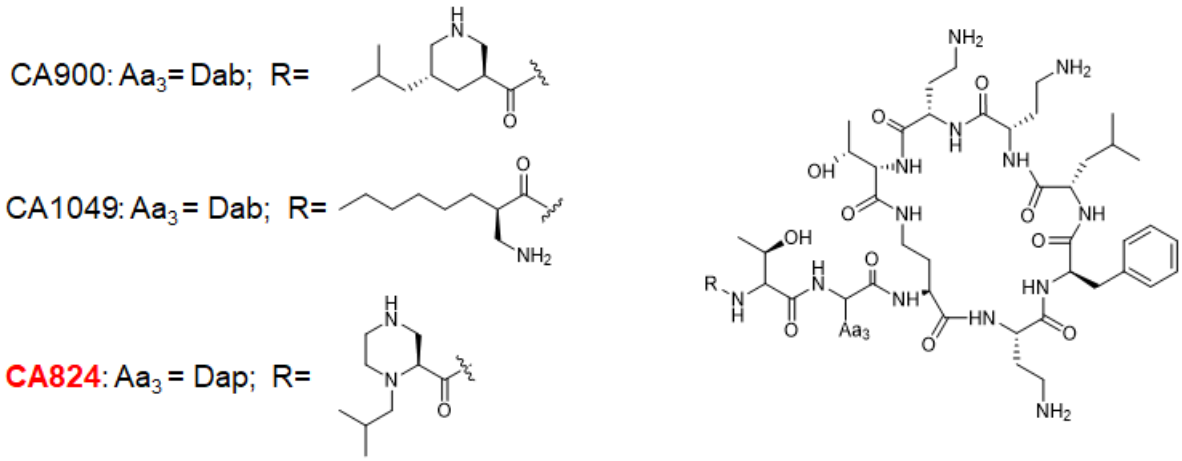

Figure 101. Cantab nonapeptide derivatives; in red the compound CA824 proceeding in the first clinical phase.

In general, only three derivatives showed MIC values similar or slightly better than PMB against selected Gram-negative bacteria, and less cytotoxic in HK-2 cell culture. CA824 (Figure 101) is in preclinical and clinical phases of development.[145]

3.2 Previous work on a special peptide-colistin construct developed in the Department of Chemical Biology at HZI

With these previous understandings, Dr. Tegge, working in the Department of Chemical Biology at HZI, developed a novel peptide-colistin construct, with the aim to administer lower doses of colistin and reduced toxic side effects. It consists of a mixture of five regioisomers where each of the free amino groups of colistin was coupled to the C-terminal of a synthetic peptide.

This latter consists of a linking peptide, that provides a specific site of cleavage for the enzyme human neutrophil elastase (HNE) and a targeting peptide, having high and specific affinity for the membrane of bacteria (Figure 102).

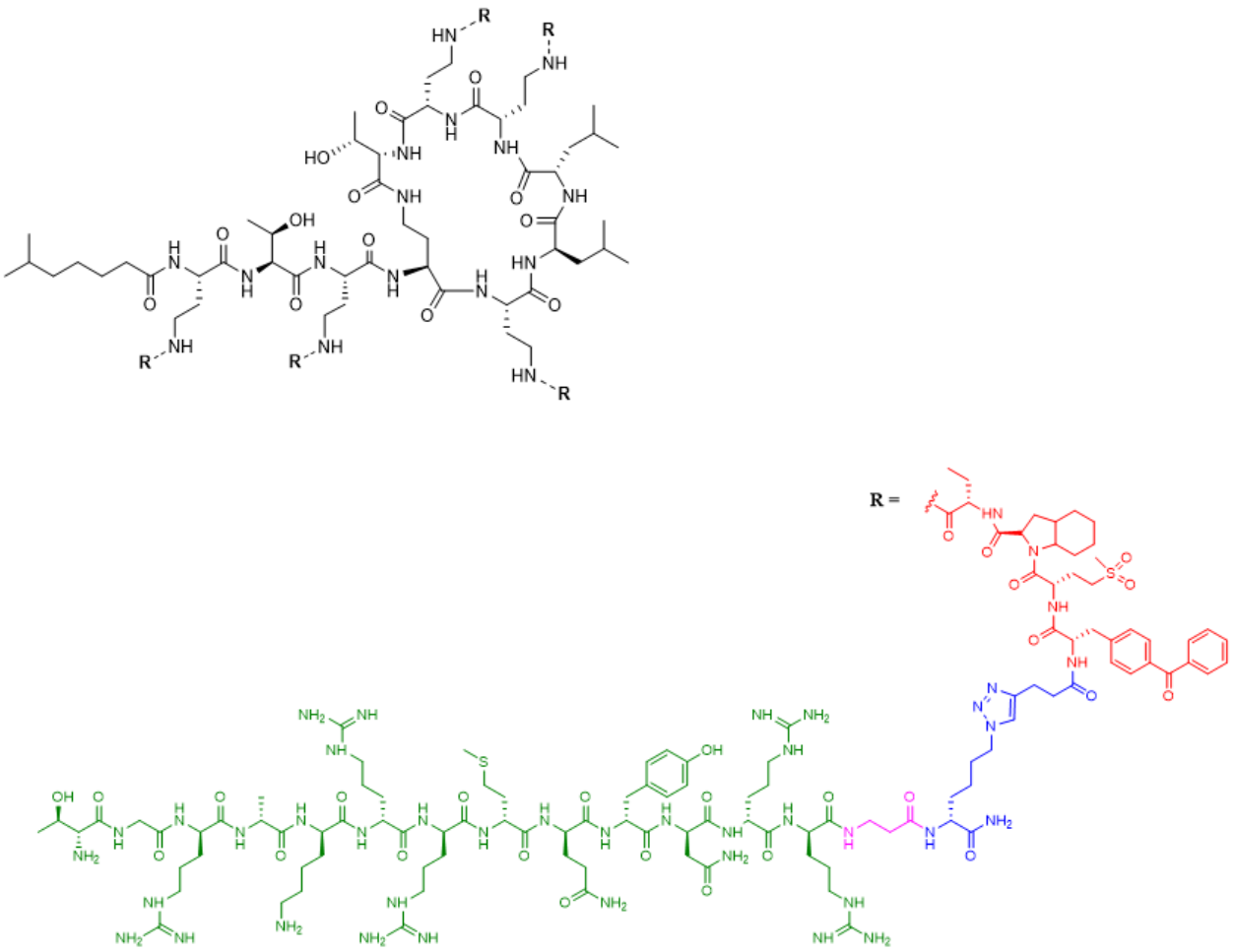

Figure 102. Structure of peptide-colistin construct regioisomers mixture: the R group is attached once to each of the 5 free amino side chains of colistin and the so resulting regioisomers are in an unknown ratio.

In case of infection with multi-resistant Gram-negative bacteria, neutrophils are recruited as the first response to the site of infection and are activated. The cleavage of the newly introduced amide group by human elastase released by activated neutrophils, liberates native colistin directly on the surface of bacteria in order to kill them.

This semisynthetic colistin derivative was obtained by two sequential reactions: a peptide coupling followed by a click reaction, starting from colistin B, obtained as TFA salt after

preparative HPLC purification from the commercially available mixture with colistin A and other isomers.

The nonselective amidation was carried out between the linking peptide and each of the free amino groups of colistin, leading to a mixture of five positional isomers. This cleavage linker consists of a hybrid natural and unnatural amino acid sequence, which is Bpa-Met(O_2)-Oic-Abu,[154] extended with pentynoic acid bonded at its N-terminal, furnishing the triple bond needed for the subsequent click reaction (Figure 103).

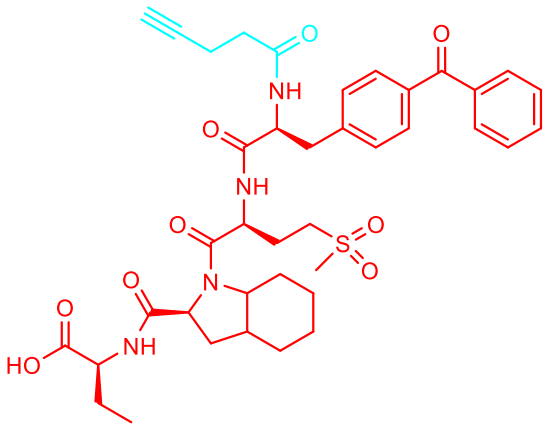

Figure 103. Structure of elastase substrate in red, plus pentynoic acid at C-terminal, in light blue.

This tetrapeptide sequence has been proven to be hydrolysed 7000-times faster by HNE than the commonly used commercial peptide Ala-Ala-Pro-Val in the investigations of another group.[154]

The targeting peptide used was the synthetic cationic human antimicrobial peptide ubiquicidin$_{29\text{-}41}$ (Ubi$_{29\text{-}41}$), having 13 amino acids with the sequence TGRAKRRMQYNRR. This sequence is a fragment of the 6.7 kDa (59 amino acids) linear cationic antimicrobial peptide ubiquicidine, first discovered in cytosolic extracts of murine macrophages.[155] Ubi$_{29\text{-}41}$ binds to the negatively charged Gram-negative bacteria membrane through its cationic amino acids, whilst minimal binding to mammalian cells membrane has been reported.[156]

So far, radio- or fluorescently-labelled Ubi$_{29\text{-}41}$, was used in radiopharmaceuticals for bacterial infection imaging.[157] However, due to proteolytic degradation *in vivo*, several Ubi$_{29\text{-}41}$ derivates were actually synthesized for bacteria detection *in situ*.[158] So that, Ubi$_{29\text{-}41}$ used in the peptide-colistin construct was assembled by solid phase using completely D-amino acids, extending at C-terminal with β-alanine as spacer and azido-lysine needed for the click reaction (Figure 104).

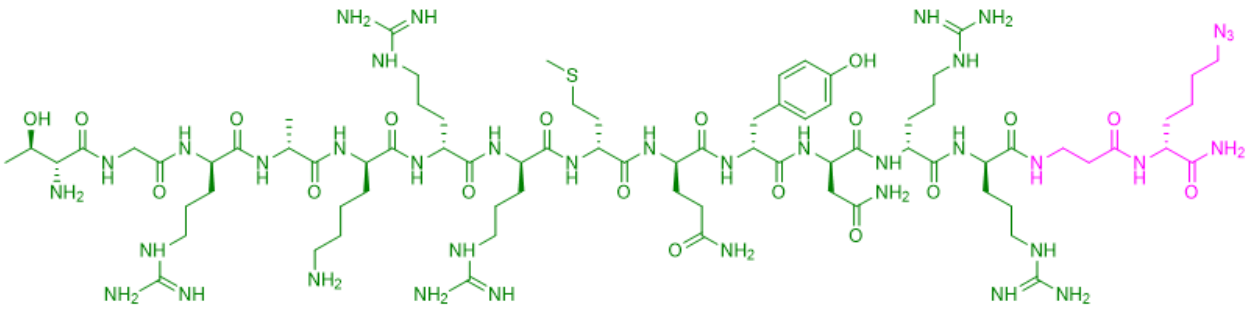

Figure 104. Structure of Ubi$_{29-41}$ highlighted in green, extended at C-terminal with β-alanine and azido-lysine both highlighted in pink.

This latter was used for the final click reaction with the triple bond of the pentynoic acid of the cleavage sequence, leading to the mixture of the five regioisomers. This mixture was used as such, dissolving in milli-Q water, and the *in vitro* antibacterial activity against two strains of *E. coli* K12 and DSM 1116, was evaluated without and with the adding of elastase HNE (10 mU/mL). Then, after incubation of 20 hours at 37 °C in a wet chamber, the results (in μM), obtained measuring the OD_{600} by using a spectrophotometer, are reported in the Table 13.

Table 13. In vitro antibacterial activity of the regioisomers mixture against sensitive *E. coli* strains with or without elastase.

	Bacteria without elastase (μM)[a]		Bacteria with elastase (μM)[a]	
COMPOUND	***E. coli* K12**	***E. coli* DSM 1116**	***E. coli* K12**	***E. coli* DSM 1116**
Peptide-colistin construct mixture	4	8	0.125	0.125
Colistin B	0.063	0.063	-	-

[a] Conservative estimates of at least three independent trials.

The activity of the mixture against the two strains of *E. coli* when elastase was not added was much lower than after addition of HNE. On the contrary, the addition of HNE leads to the release of native colistin, able to perform its antibacterial action, having MIC values similar to plain colistin B, which was used as positive control. Since the activity of the prodrug version of colistin is retained when transformed into the active drug, these results are encouraging for further toxicity assay, which is the major challenge. One major drawback of the investigations

at this stage was the fact, that a mixture of positional isomers was used and not the defined structures. This makes the deduction of differences in the fidelity and specific activity of the individual structures impossible. In view of a possible further development of the compound(s) as a drug for human medicine it seemed highly desirable to carry out total chemical syntheses of the individual isomers in order to elucidate their different activities and toxicities, respectively to find out if those are present.

3.3 My Ph.D. work at HZI

3.3.1 The aim: total synthesis of the five positional isomers of the peptide-colistin construct; overview of the synthetic strategies.

The main aim of this work was to investigate if all the regioisomers undergo selective cleavage by elastase with the same efficacy and fidelity. Then, we carried out the antimicrobial assays against the strain of *E. coli* K12, and the results were compared with the activity of the regioisomeric mixture.

Thus, my work of Ph.D. at HZI was based on total synthesis, by solid phase, of the five regioisomers of the colistin construct.

Each of the residues in the colistin sequence was numerated according the literature (Figure 105).[136]

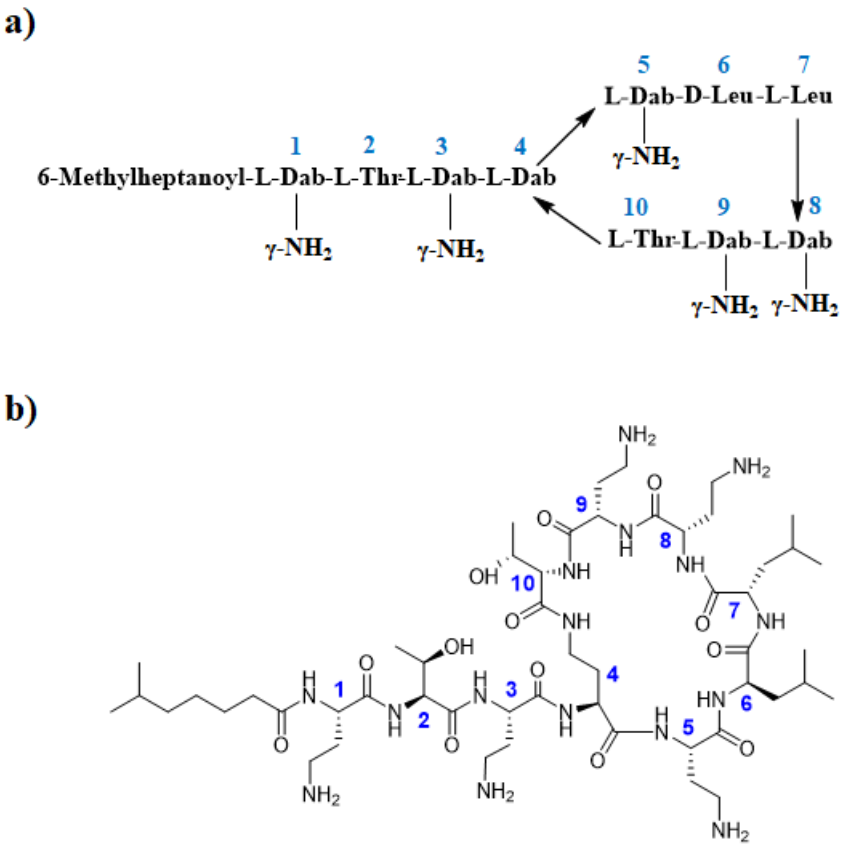

Figure 105. a) Colistin with the amino acid residues in the form of three-letter abbreviations, numbered according to the common numeration system (in blue); b) chemical representation of the structure.

The five isomers synthesised differ from the position of the peptide construct attached individually at the γ-amino side chain of the L-2,4-diaminobutyric acid (Dab) in positions 1, 3, 5, 8 and 9. The first three positions (5, 8 and 9) are named intracyclic residues, while the last two (1 and 3) are the extracyclic ones.

For the synthesis of the three intracyclic isomers (5, 8 and 9), was used the same synthetic strategy, which is different from the scheme of synthesis used for the two extracyclic isomers (1 and 3).

More in detail, Figure 106 reports the strategy adopted for the total synthesis of colistin having the peptide construct assembled on the side chain of the intracyclic Dab residues (compounds **23**, **24** and **25**- see in paragraph *Synthesis and biological activity of the compounds*).

Solid phase peptide synthesis (SPPS) on 2-chlorotrityl chloride (CTC resin) was used, utilizing the Fmoc/tBu protocol.

All the side chain amino groups of Dab were protected as tert-butyloxycarbonyl (**Boc**), the side chain hydroxy group of Thr as tert-butyloxy (**tBu**), while the γ-amino group of the Dab involved

in cyclization as 1-(4,4-dimethyl-2,6-dioxocyclohex-1-ylidene)ethyl (**Dde**). The Boc and tBu protecting groups are orthogonal to Dde.

After the attachment of the Fmoc-protected Thr onto the 2-CTC resin, the stepwise assembling of the colistin isomers was carried out by sequential deprotection/coupling methodology, so obtaining the linear peptides, bearing the elastase sequence on the amino side chain of Dab in positions 9, 8 and 5 (numbering the residues starting from the Thr attached onto the resin).

The subsequent steps were removal of Dde protecting group at the amino side chain of the Dab residue involved in cyclization (which corresponds to position 4) and cleavage of the three isomers from the resin, followed by in solution cyclization and global deprotection of Boc and tBu groups.

Finally, by click reaction, the triple bond of the 4-pentynoyl moiety of the three peptides underwent cycloaddition to the azido group of the ubiquicidin derivative affording the final isomers.

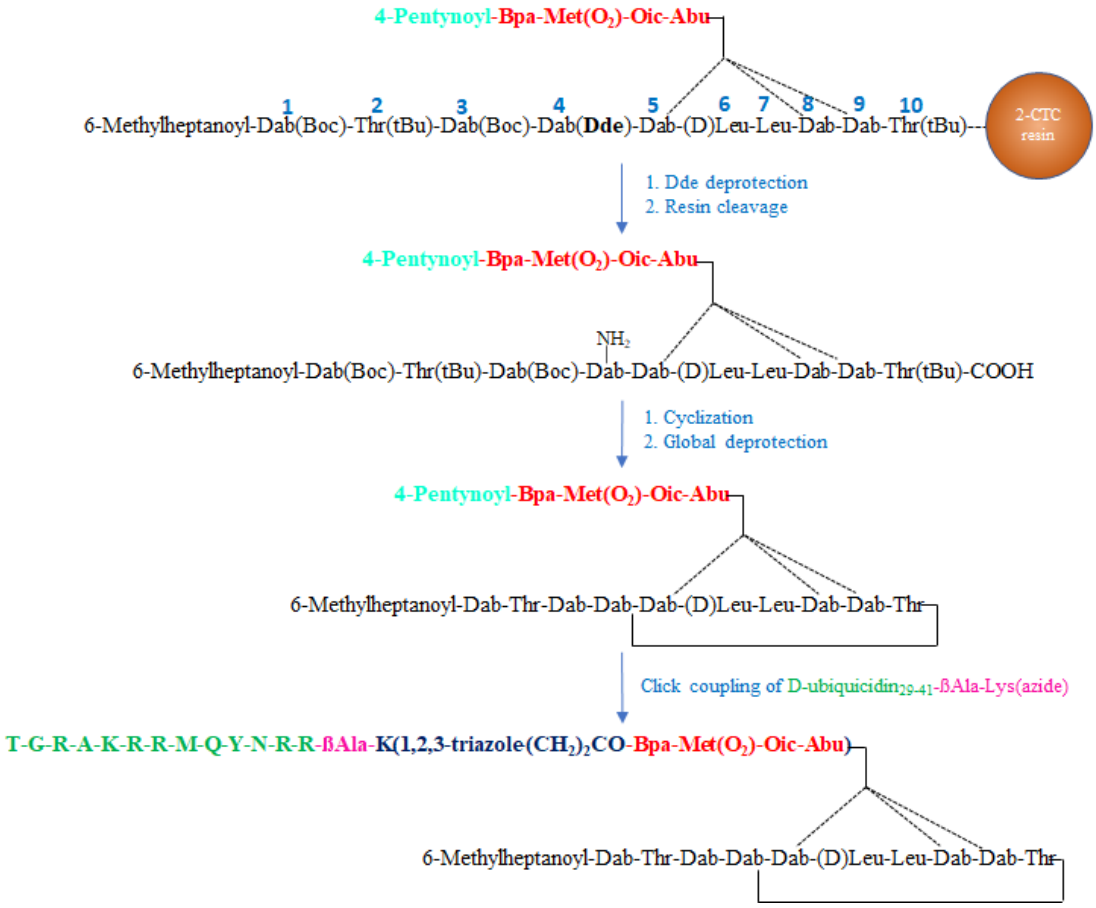

Figure 106. Synthetic strategy used for the total synthesis of colistin isomers assembled with the peptide construct on the side chain of the intracyclic Dab residues.

Concerning the synthesis of the other two isomers, having the peptide construct built on the side chain of the extracyclic Dab residues (1 and 3), the methodology shown in the Figure 107, was used.

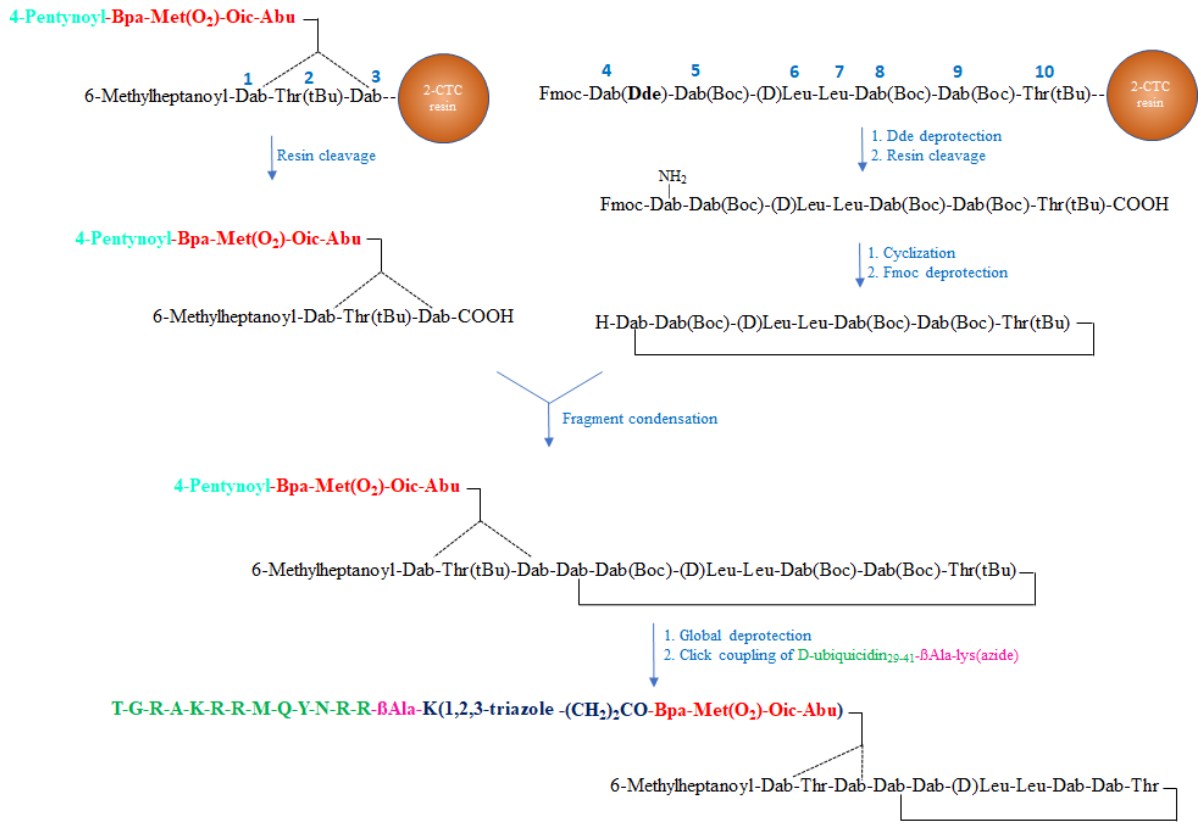

Figure 107. Synthetic strategy used for the total synthesis of colistin isomers assembled with the peptide construct on the side chain of the extracyclic Dab residues.

In fact, after assembling by solid phase the colistin sequence, bearing the Dab residue at position 1 or 3, the subsequent removal of the protecting Dde group from these residues in order to construct the elastase sequence, would result in the loss of the Dde protecting group on the γ-amino group of the Dab involved in cyclization in position 4.

So, the strategy relies on individual solid phase synthesis of two fragments for each of the two isomers and, then, a fragment condensation to get the final products.

More in detail, the synthetic approach started from the solid phase synthesis of the first fragment, by construction of the colistin residues from the fatty acid arm at the N-terminal until Dab in position 3, assembling the elastase substrate on the side chain of Dab in position 3 or 1, with the sequential deprotection/amidation methodology followed by eventual cleavage from the resin.

Accordingly, the solid phase synthesis of the other colistin construct fragment (synthetic scheme on the right side of the Figure 107), from the Dab residue in position 4 until the Thr in position 10, was carried out using the usual Fmoc deprotection and coupling sequence. Then, the removal of the side chain protecting group Dde from the 4-Dab residue was carried out, with the subsequent resin cleavage. In the event, this fragment was cyclized in solution and then underwent Fmoc deprotection.

This latter was then coupled with the previously obtained fragment having the elastase substrate in 3 or 1 position, leading to the two corresponding products, which were fully deprotected and linked to the ubiquicidin sequence by a click reaction to give separately the two isomers.

3.4 Synthesis and biological activity of the compounds

3.4.1 Synthesis of compounds 23, 24 and 25, having the elastase substrate attached to the γ-NH_2 of intracyclic Dab 9, 8 and 5.

The attachment of Fmoc-Thr(OtBu)-OH onto CTC resin in presence of DIPEA was the starting point of the synthetic pathway (Scheme 3).

Scheme 3. Attachment onto the CTC resin of Fmoc-Thr(OtBu)-OH, 1

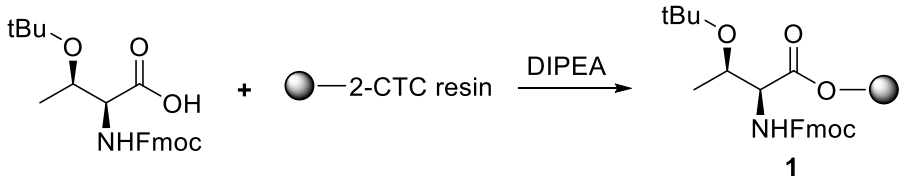

The Fmoc α-NH protecting group of the compound **1** attached to the resin was removed using 20% piperidine in DMF. Then amidation of Dde-L-Dab(Fmoc)-OH, having the α-NH protected as Dde and γ-NH as Fmoc, was performed using HCTU as activator and DIPEA as base in DMF, to give the intermediate **2** (

Scheme 4) which was starting material for the attachment of the elastase substrate at γ-NH of Dab in position 9. The above reported conditions were used for all the Fmoc

deprotection/coupling sequences in SPPS, except for a particular coupling that will be discussed later.

Scheme 4. Synthesis of the intermediate 2

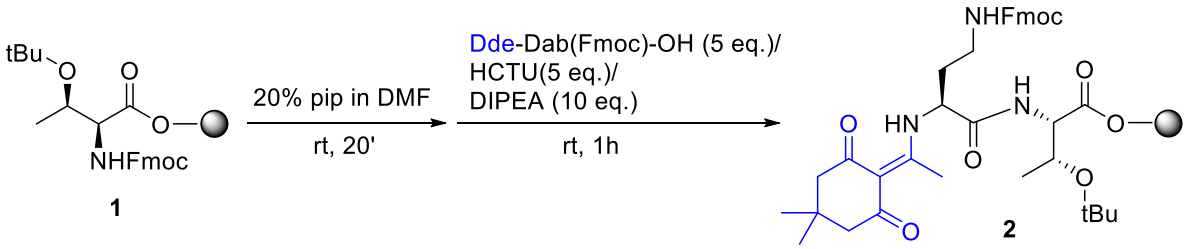

In the same way, both intermediates **3** and **4**, bearing at N-terminal Dde-L-Dab(Fmoc)-OH as well as **2,** were starting materials for the attachment of the elastase substrate at side chain of Dab in position 8 and 5 respectively, and were synthesized by sequential Fmoc deprotection followed by amidation with the appropriate amino acids (Scheme 5).

Scheme 5. Synthesis of the compounds 3 and 4[a]

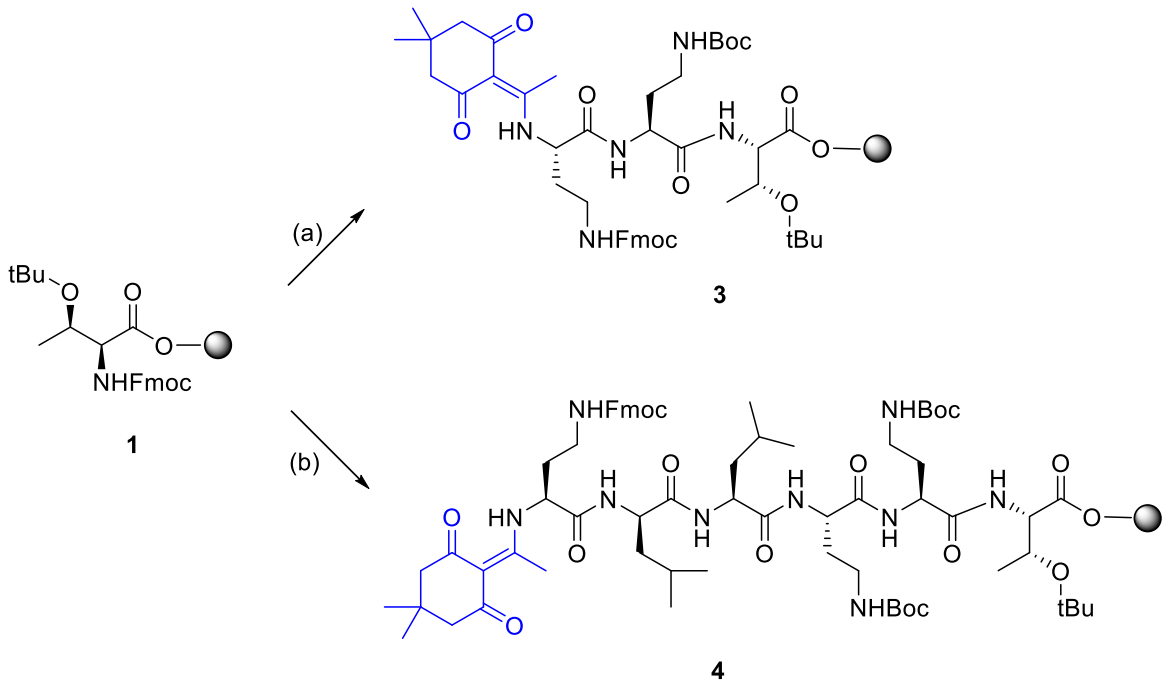

[a] Conditions: (a) sequential Fmoc deprotection (20% piperidine in DMF), rt, 20', followed by coupling (HCTU (5 eq.) and DIPEA (10 eq.)) with the following residues (5 eq.): Fmoc-Dab(Boc)-OH, Dde-Dab(Fmoc)-OH, in DMF, rt, 1h. (b) sequential Fmoc deprotection (20% piperidine in DMF), rt, 20', followed by coupling (HCTU (5 eq.) and DIPEA (10 eq.)) with the following residues (5 eq.): Fmoc-Dab(Boc)-OH, Fmoc-Dab(Boc)-OH, Fmoc-LLeu-OH, Fmoc-DLeu-OH, Dde-Dab(Fmoc)-OH in DMF, rt, 1h.

At this point, the assembling of the elastase substrate sequence (pentynoyc acid, Fmoc-L-Bpa-OH, Fmoc-L-Met(O_2)-OH, Fmoc-L-Oic-OH, Fmoc-L-Abu-OH) at γ-NH of Dde-L-Dab(Fmoc)-OH (Scheme 6) was performed in the same way for compounds **2**,**3** and **4**, using the sequential deprotection/coupling methodology above described. The only difference concerned the coupling of Fmoc-L-Bpa-OH, carried out twice with HATU as activator, that was proven to be a better activator than HCTU.

Scheme 6. Elastase substrate assembling (highlighted in red) giving the compounds 5, 6 and 7[a].

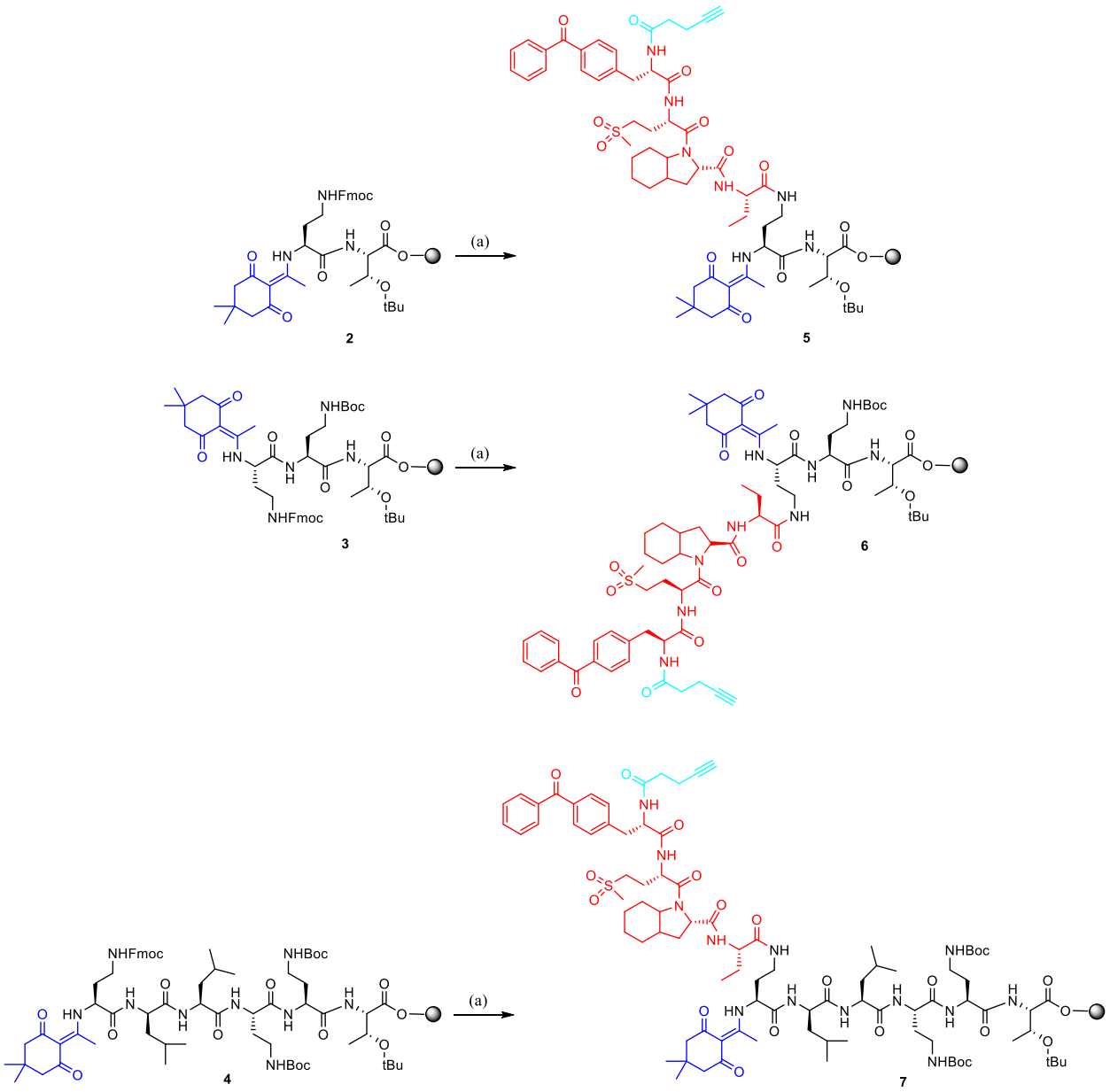

[a] Conditions: (a) sequential Fmoc deprotection (20% piperidine in DMF, rt, 20'), followed by coupling with the following residues (5 eq.): Fmoc-Abu-OH, Fmoc-Oic-OH, Fmoc-Met(O_2)-OH, Fmoc-Bpa-OH, 4-Pentynoic acid (with HCTU or HATU (5eq.), DIPEA (5 eq.), in DMF, rt, 1h).

To assemble the remaining colistin sequence, the Dde protecting group at the γ-amino position of Dab in **5**, **6** and **7** was removed with 2% hydrazine in DMF. The deprotection of Dde was monitored by analytical HPLC and ESI-MS, confirming the complete removal. The remaining colistin sequence was then properly assembled for all the three compounds by sequential Fmoc

deprotection followed by amidation. 6-Methyl-heptanoic acid was coupled as fatty acid arm at the N-terminus, leading to peptides **8**, **9** and **10** (Scheme 7).

Scheme 7. Dde cleavage and assembling of the rest of the colistin sequence to give the linear peptides 8, 9 and 10 [a]

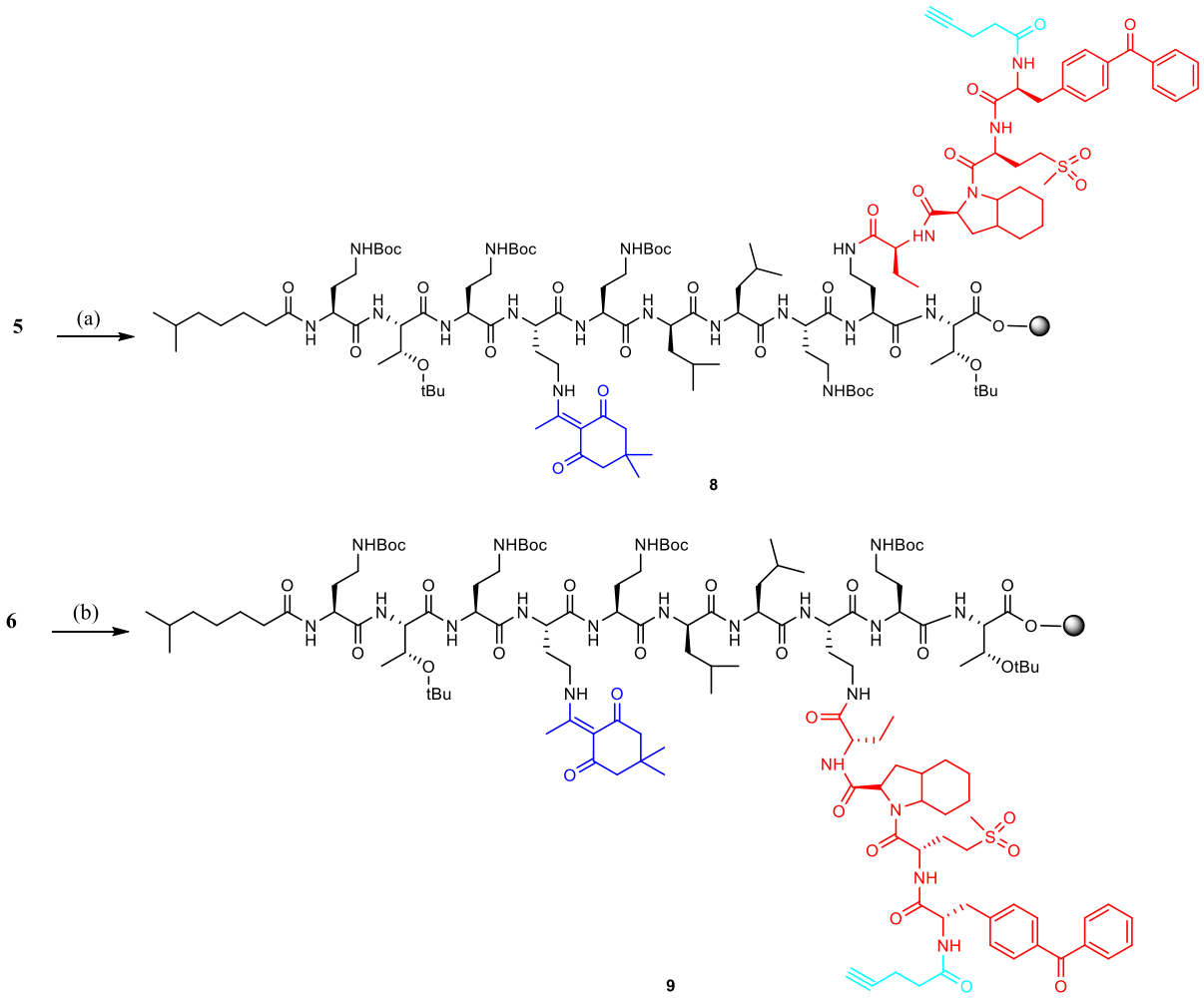

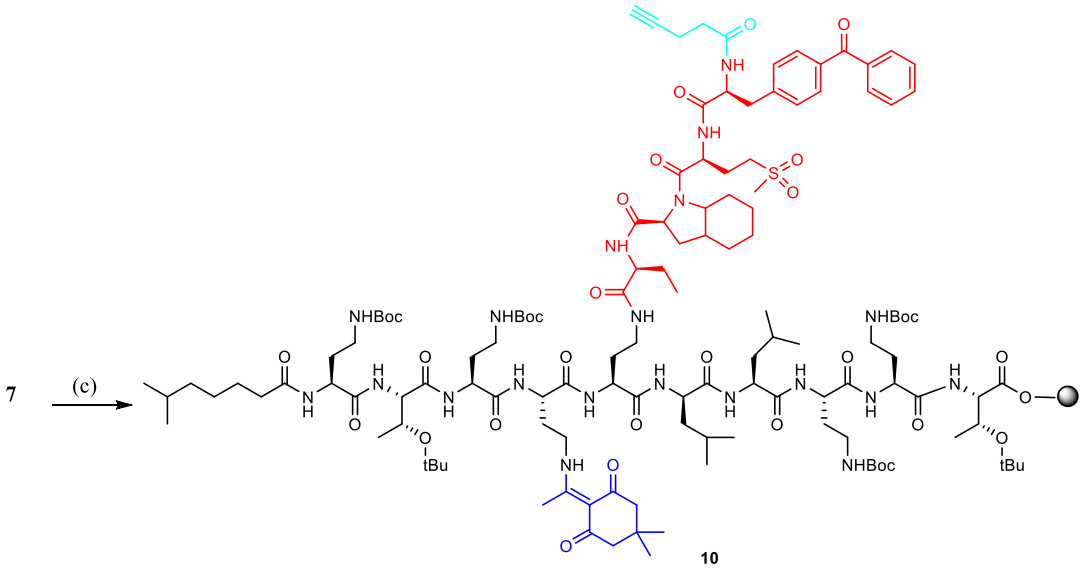

[a] Conditions: (a) (i) Dde cleavage using 2% hydrazine in DMF; (ii) sequential Fmoc deprotection (20% piperidine in DMF, rt, 20'), followed by coupling (Fmoc-AA-OH (5 eq.), HCTU (5 eq.), DIPEA (10 eq.), DMF, rt, 1h) with the following residues: Fmoc-Dab(Boc)-OH, Fmoc-Leu-OH-OH, Fmoc-D-Leu-OH, Fmoc-Dab(Boc)-OH, Fmoc-Dab(Dde)-OH, Fmoc-Dab(Boc)-OH, Fmoc-Thr(tBu)-OH, Fmoc-Dab(Boc)-OH, 4-pentynoic acid (with HCTU (5eq.), DIPEA (5 eq.), in DMF, rt, 1h); (b) (i) as before; (ii) sequential Fmoc deprotection followed by amidation with the following residues: Fmoc-Leu-OH-OH, Fmoc-Leu-OH, Fmoc-Dab(Boc)-OH, Fmoc-Dab(Dde)-OH, Fmoc-Dab(Boc)-OH, Fmoc-Thr(tBu)-OH, Fmoc-Dab(Boc)-OH, 4-pentynoic acid; (c) (i) as before; (ii) sequential Fmoc deprotection followed by amidation with the following residues: Fmoc-Dab(Dde)-OH, Fmoc-Dab(Boc)-OH, Fmoc-Thr(tBu)-OH, Fmoc-Dab(Boc)-OH, 4-pentynoic acid.

At this point, for the three compounds, **8**, **9** and **10**, the Dde group on γ-NH of the Dab involved in cyclization was removed using 2% hydrazine in DMF, as already reported, and subsequently the three peptides were cleaved from the resin using 1,1,1,3,3,3-hexafluoro-2-propanol: DCM in a 1:4 ratio, affording the corresponding peptides **11**, **12** and **13** (Scheme 8) whose structure was ascertained by HPLC and ESI-MS (see Experimental).

Scheme 8. Linear peptides 11, 12 and 13 cleaved from the resin, having free γ-NH Dab in position 4 [a]

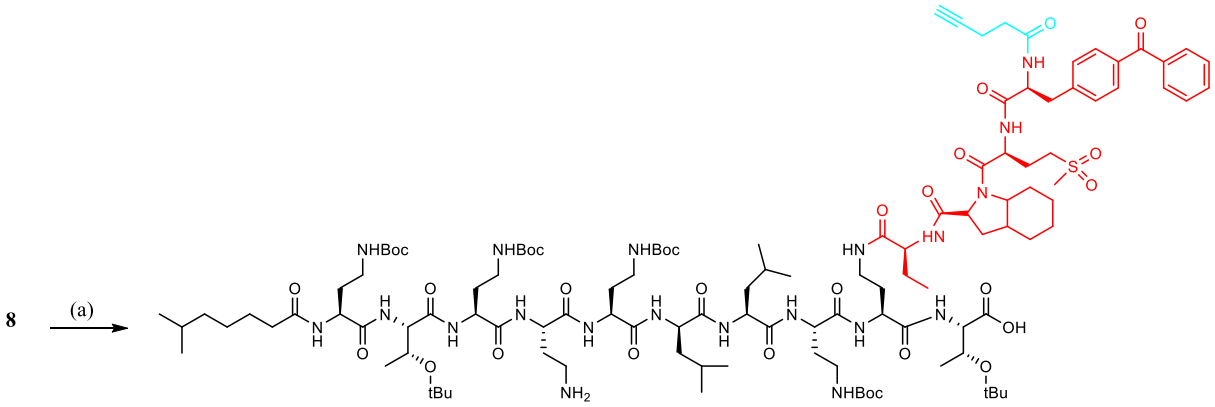

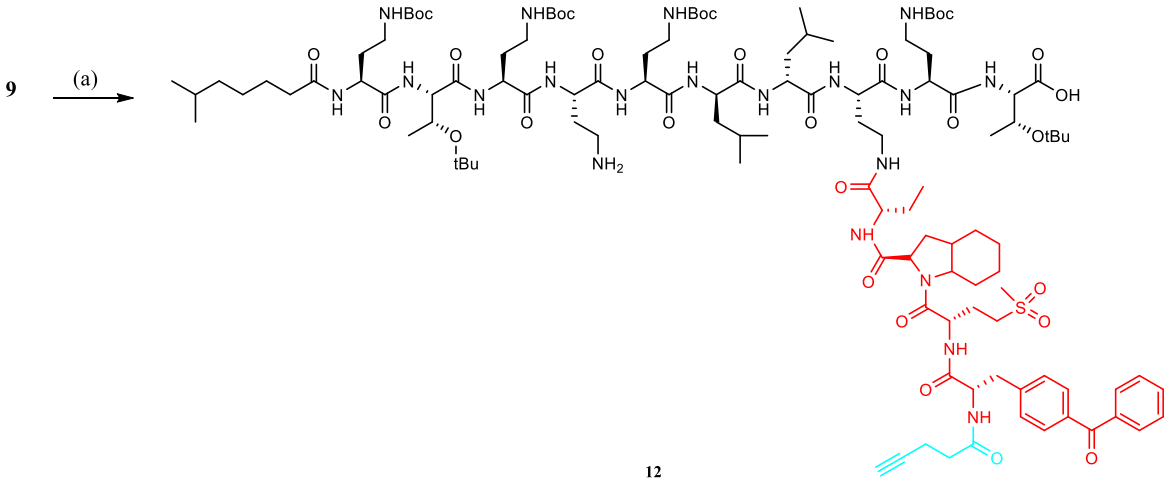

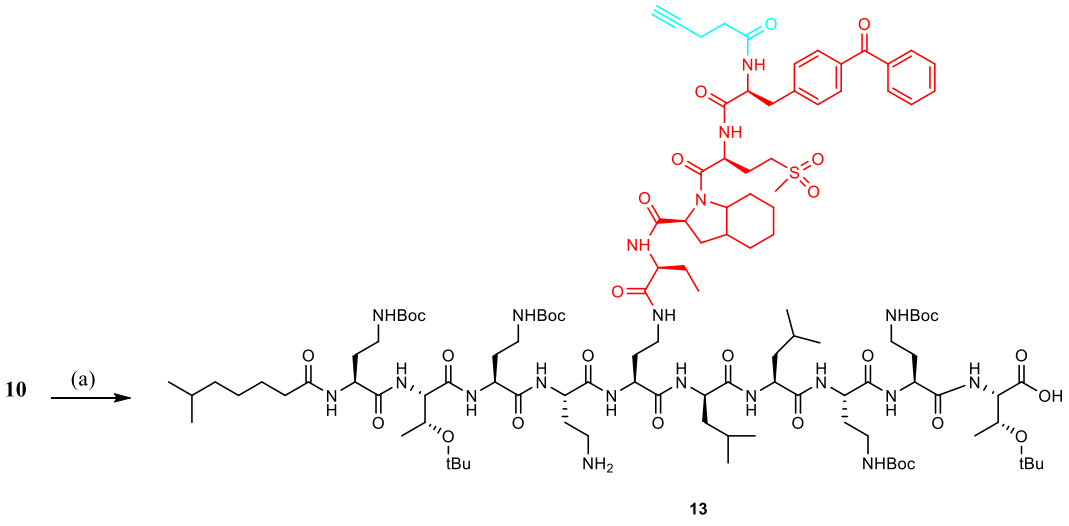

[a] Conditions: (a) (i) Dde cleavage using 2% hydrazine in DMF; (ii) 1,1,1,3,3,3-hexafluoro-2-propanol: DCM in a ratio 1:4 (resin cleavage).

Then, cyclization in solution between 10-Thr and 4-Dab was carried out exploiting different experimental conditions (Table 14), initially using only the compound **11** as trial, in order to find the appropriate cyclization conditions to be used also for the peptides **12** and **13** to give, in the event, the corresponding cyclized ones **14**, **15** and **16** (Table 14).

Table 14. Experimental conditions for cyclization reaction for obtaining peptides 14, 15 and 16.

Entry	Solvent (1 mg/ mL)	Activator (n°eq) Base (n°eq)	Temperature (T) and time (t)
a	DMF	HATU (2) DIPEA (4)	rt, overnight
b	DMF	HCTU (2) DIPEA (4)	rt, overnight
c	DMF	EDCI (2) DIPEA (4)	rt, overnight
d	DMF	T_3P (2) DIPEA (4)	rt, overnight
e	**DMF: DCM (1:50)**	**PyBOP/HOBt (3/3) DIPEA (6)**	**rt, overnight**

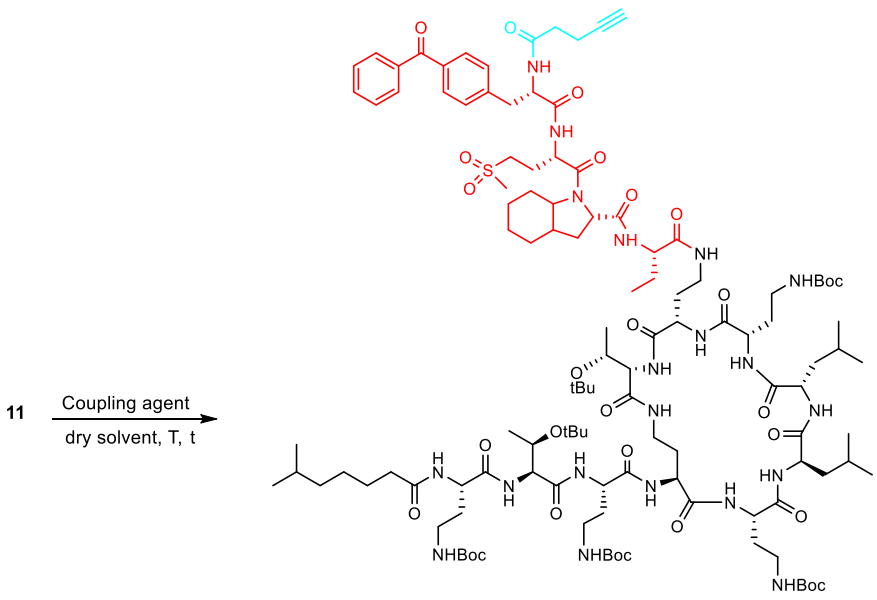

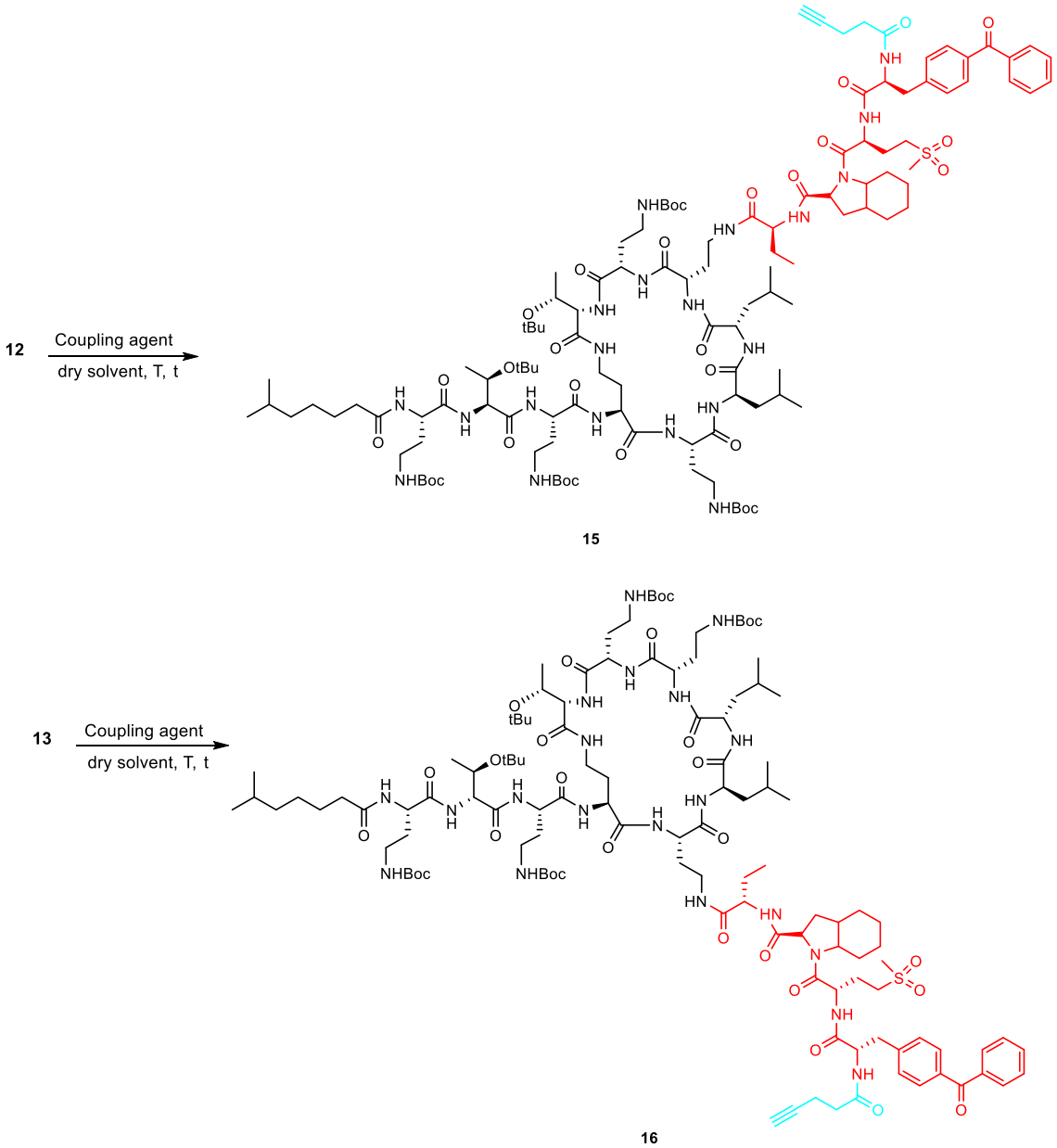

Indeed, it was reported in the literature that cyclization step can be the most challenging during the total synthesis of polymyxins in general.[159,160,161]

The experimental conditions tested differ each other mainly for the activator used, whereas the base (DIPEA), the temperature (rt), the concentration of the peptide (1 mg/mL) and solvent (DMF) remained unchanged (Table 14). This reaction was carried out in such diluted conditions in order to avoid side reactions, like oligo- or dimerization. Moreover, the outcome under the different reaction conditions was monitored by analytical HPLC (Figure 108 in HPLC analysis data, comparison of spectra **a**, **b**, **c, d** and **e**, referring to the different chemical conditions). However, due to the occurrence of major side reactions, the experimental

conditions highlighted in yellow in the Table 14, carried out following a reported procedure[161], revealed to be the best ones.

The three linear peptides **11**, **12** and **13** were dissolved in dry DCM, HOBt previously dissolved in anhydrous DMF was added, to give a final DMF: DCM ratio of 1:50, subsequently followed by PyBOP and DIPEA. The reaction was monitored by analytical HPLC and LC-MS, confirming the cyclization of the linear peptides to give the cyclized peptides **14**, **15** and **16** (Table 14).

Workup was easier when DCM was the main solvent of the reaction, owing to easy removal under reduced pressure. To the DMF residue, dioxane was added and the solution was lyophilized.

The *t*-butoxycarbonyl (Boc) and *t*-butoxy (tBu) group removal of the Dab and Thr side chain, respectively, was performed before exploiting different reaction condition (Table 15), monitored by analytical HPLC (see Figure 109 in HPLC analysis data and compare spectra **a**, **b** and **c**).

Table 15. Experimental conditions exploited for the global deprotection, giving the deprotected cyclized peptides 17, 18 and 19.

Entry	Concentration (µmoL/ mL)	Deprotection mixture	Temperature (T) and time (t)
a	20	TFA: H_2O 95: 5	rt, 90’
b	20	TFA: H_2O: IPr_3SiH 95:2.5:2.5	rt, 90’
c	20	TFA: anh. DCM 1:8	rt, 90’

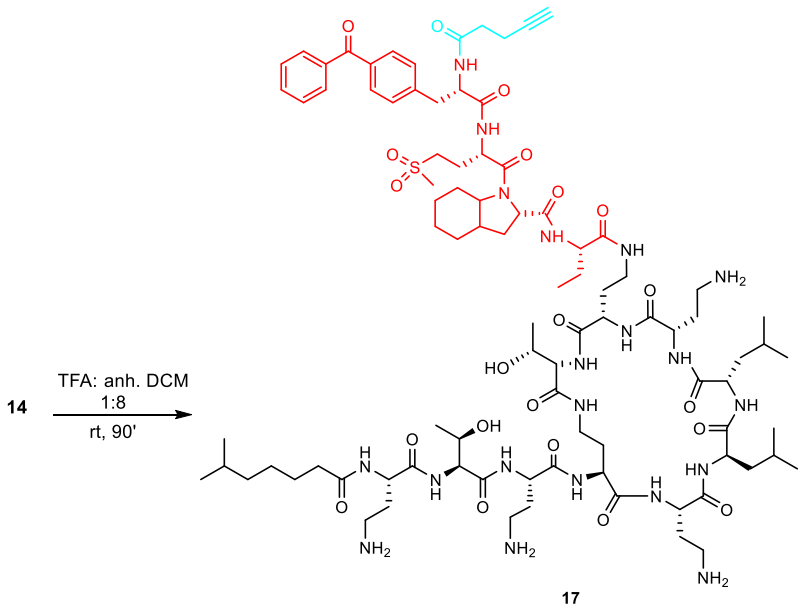
14
TFA: anh. DCM
1:8
rt, 90'

17

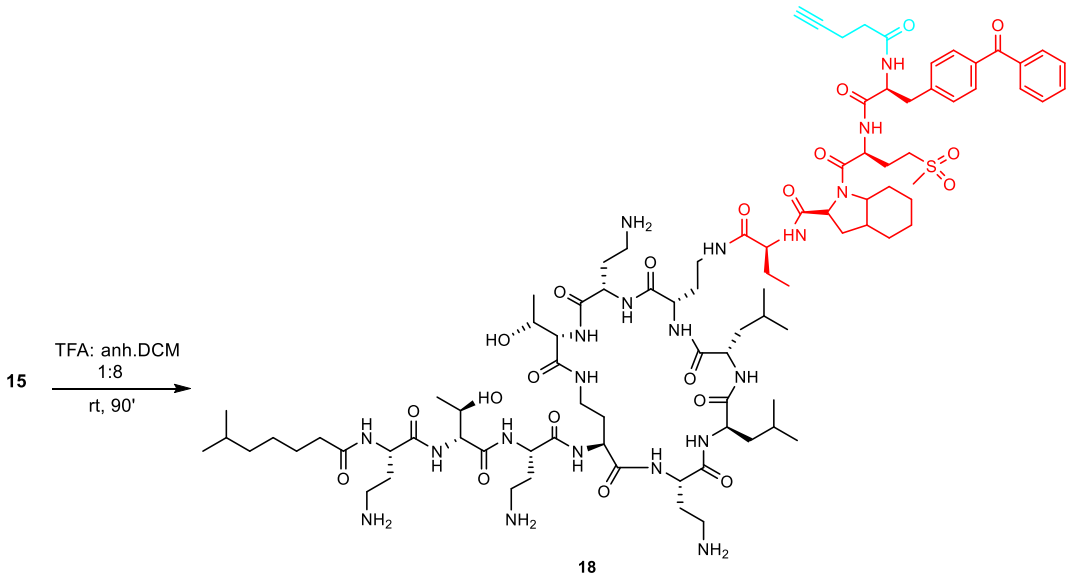
15
TFA: anh.DCM
1:8
rt, 90'

18

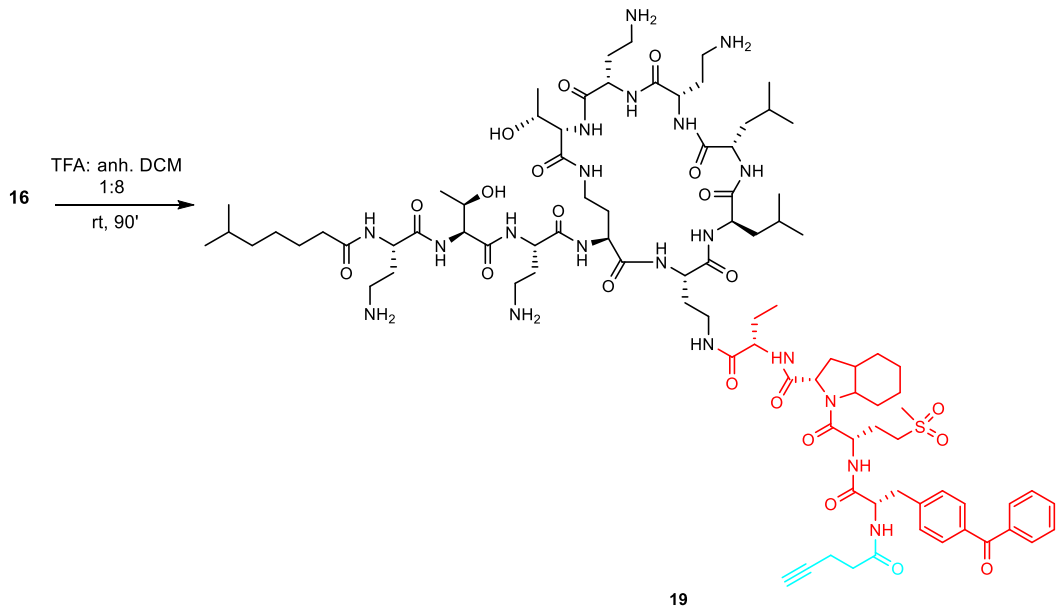
16
TFA: anh. DCM
1:8
rt, 90'

19

Using TFA: water in a 95:5 ratio (Entry **a**) or TFA: water: iPr_3SiH in a 95:2.5:2.5 ratio (Entry **b**) for 90 min., as reported in literature,[153] did not give the expected result, with major formation of by-products.

Instead, the use of TFA: anhydrous DCM used in this work, led to a much better and cleaner result, giving the deprotected cyclized peptides **17**, **18** and **19** (Table 15).

At this point, cold diethyl ether was added to the reaction that was centrifuged, in order to precipitate the deprotected peptides. Then, diethyl ether was removed, and the precipitates were lyophilized.

With the deprotected cyclized peptides in hands, the click coupling between each compound displaying the Ubi_{29-41} derivative **39** was performed. To the peptides 200 mM MOPS buffer at pH 7.0 was added until complete dissolution followed, from previously prepared solution stocks of THPTA 200 µM, by Na-ascorbate 2 mM and $CuSO_4$ 100 µM in a 95:2:2:1 ratio in volume, respectively, under argon atmosphere. After 2 hours at rt, formation of the final compounds **20**, **21** and **22** was confirmed by analytical HPLC and LC-MS (Scheme 9).

Scheme 9. Click coupling between deprotected cyclized peptides and Ubi_{29-41}, giving the compounds 20, 21 and 22

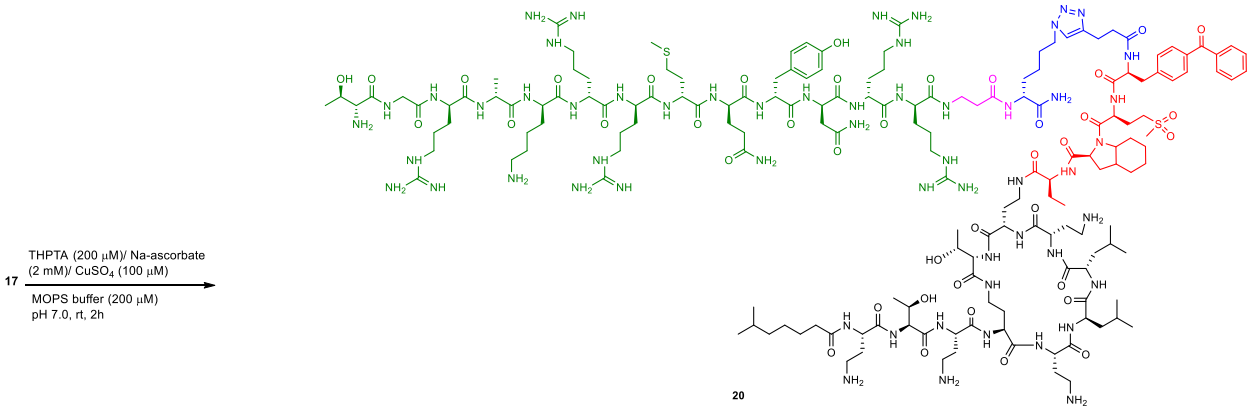

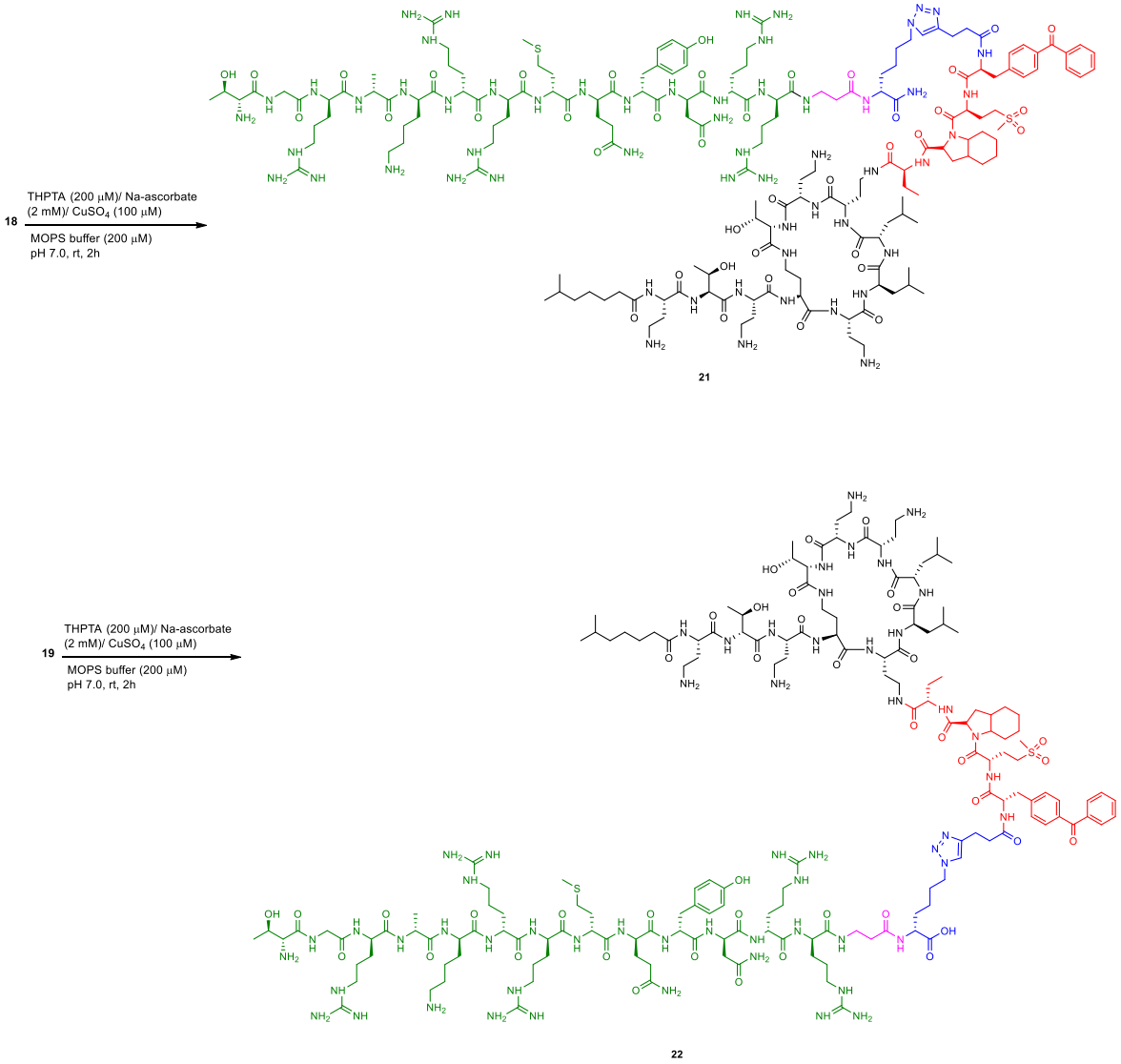

*3.4.2 Synthesis of compounds **37** and **38**, having the elastase substrate attached to the γ-NH_2 of extracyclic Dab 1 and 3.*

A different synthetic strategy was used for preparation of compounds **37** and **38**, having the elastase substrate attached to the γ-NH_2 of extracyclic Dab in position 1 and 3.

To synthesize the fragment of colistin, from 6-methylheptanoyl at the N-terminal until Dab residue in position 3, having attached the elastase substrate to the γ-amino side chain of the Dab in position 3, the attachment of Fmoc-Dab(Dde)-OH onto 2-CTC resin in the presence of DIPEA was the starting point, leading to **23** (Scheme 10).

Scheme 10. Attachment of Fmoc-Dab(Dde)-OH, 23, onto the CTC resin

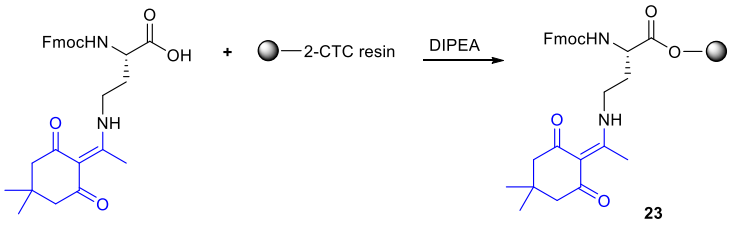

Then, repeated cycles of Fmoc deprotection - coupling with the appropriate amino acid until the last amidation with 6-methylheptanoic acid as fatty acid arm at the N-terminus, were employed to obtain **24** (

Scheme 11).

Scheme 11. Sequential cycle of Fmoc deprotection and amidation to obtain the compound 24[a]

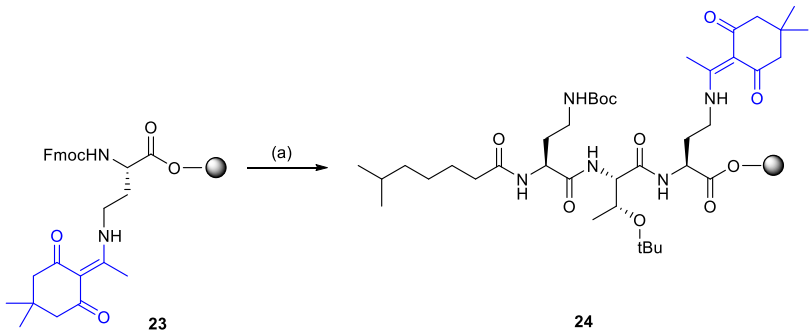

[a] Conditions: (a) sequential Fmoc deprotection (20% piperidine in DMF, rt, 20'), followed by coupling (HCTU (5 eq.), DIPEA (10 eq.), DMF, rt, 1h) with the following residues: Fmoc-Thr(tBu)-OH, Fmoc-Dab(Boc)-OH, 6-methylheptanoic acid.

The Dde protecting group of the γ-NH_2 of Dab in position 3 was removed by using the usual 2% v/v of hydrazine in DMF for 1h 30` for three times, washing with DMF. On the free γ-NH_2, the stepwise assembling of the elastase substrate was carried out according to the above-mentioned procedure (see Scheme 8), checking by analytical HPLC and LC-MS. Subsequently, the cleavage from the resin was performed obtaining compound **25** (Scheme 12), i.e the fragment having attached the elastase substrate at the amino side chain of Dab in position 3.

Scheme 12. Assembling of the elastase substrate after Dde removal and cleavage from the resin to obtain the fragment 25[a]

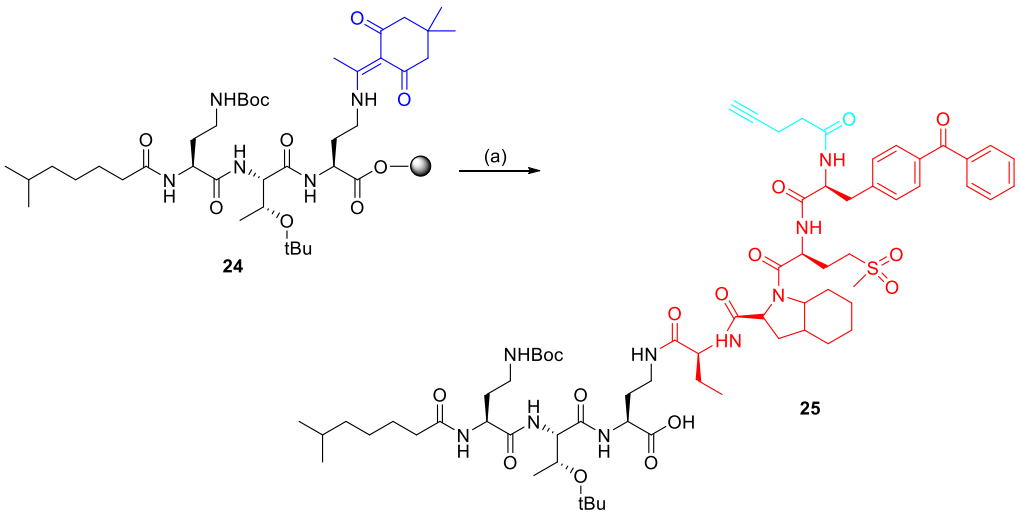

[a] Conditions: (a) (i) 2% hydrazine to remove Dde; (ii) sequential Fmoc deprotection (20% piperidine in DMF, rt, 20'), followed by coupling with the following residues (5 eq.): Fmoc-Abu-OH, Fmoc-Oic-OH, Fmoc-Met(O_2)-OH, Fmoc-Bpa-OH, 4-pentynoic acid (with HCTU or HATU (5eq.), DIPEA (5 eq.), in DMF, rt, 1h); (iii) 1,1,1,3,3,3-hexafluoro-2-propanol: DCM in a ratio 1:4 (resin cleavage).

The synthetic route used for obtaining the other fragment is almost identical to the previous one.

In fact, this time, the first step is the attachment of the Fmoc-Dab(Boc)-OH onto the 2-CTC resin to get the compound **26** (Scheme 13).

Scheme 13. Attachment of Fmoc-Dab(Boc)-OH, 26, onto the CTC resin

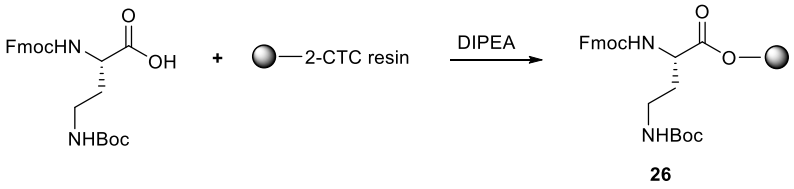

Thus, to obtain **26**, the compound **27**, having Dde-Dab(Fmoc)-OH at N-terminal was obtained with repeated cycles of Fmoc deprotection-coupling with the appropriate amino acid (Scheme 14).

Scheme 14. Sequential cycle of Fmoc deprotection and amidation to obtain 27[a].

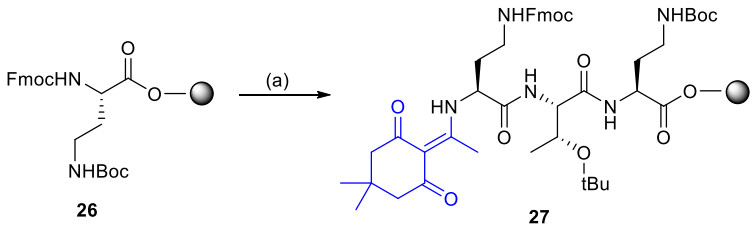

[a] Conditions: (a) sequential Fmoc deprotection (20% piperidine in DMF, rt, 20'), followed by coupling (HCTU (5 eq.), DIPEA (10 eq.), DMF, rt, 1h) with the following residues: Fmoc-Thr(tBu)-OH, Dde-Dab(Fmoc)-OH.

After removal of the Fmoc protecting group on the side chain of Dab, (corresponding to position 1), the assembling of the elastase substrate sequence was performed using the Fmoc removal and amidation sequence reported above, to get **28** (Scheme 15).

Scheme 15. Assembling of the elastase substrate sequence to obtain 28[a].

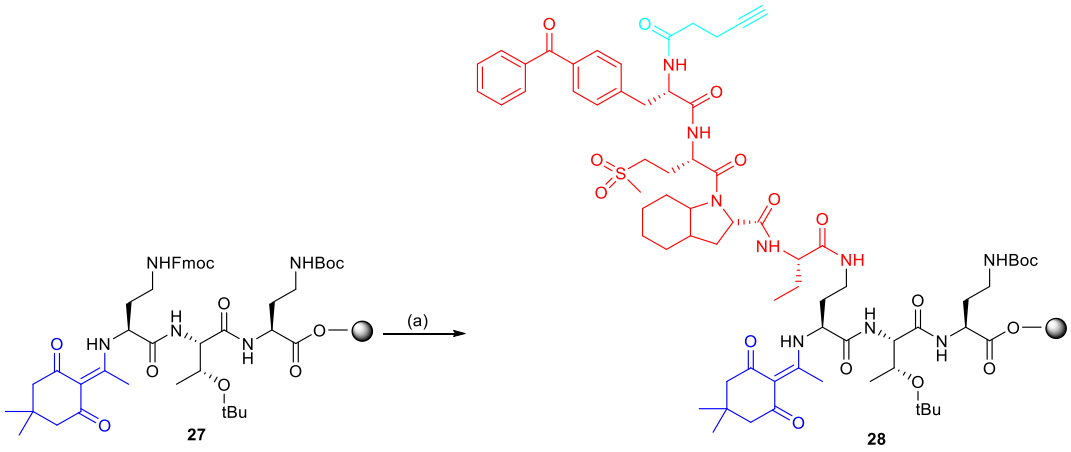

[a] Conditions: (a) sequential Fmoc deprotection (20% piperidine in DMF, rt, 20'), followed by coupling with the following residues (5 eq.): Fmoc-Abu-OH, Fmoc-Oic-OH, Fmoc-Met(O_2)-OH, Fmoc-Bpa-OH, 4-pentynoic acid (with HCTU or HATU (5eq.), DIPEA (5 eq.), in DMF, rt, 1h.

At this point, by using hydrazine, the amino side chain of the Dab in position 1 underwent removal of protecting group Dde, in order to perform the last coupling with 7-methylheptanoic acid at the N-terminus of the fragment. Cleavage from the resin led to fragment **29** (

Scheme 16).

Scheme 16. Dde removal from the amino side chain of the Dab in position 1, coupling with the fatty acid and cleavage from the resin, obtaining 29[a].

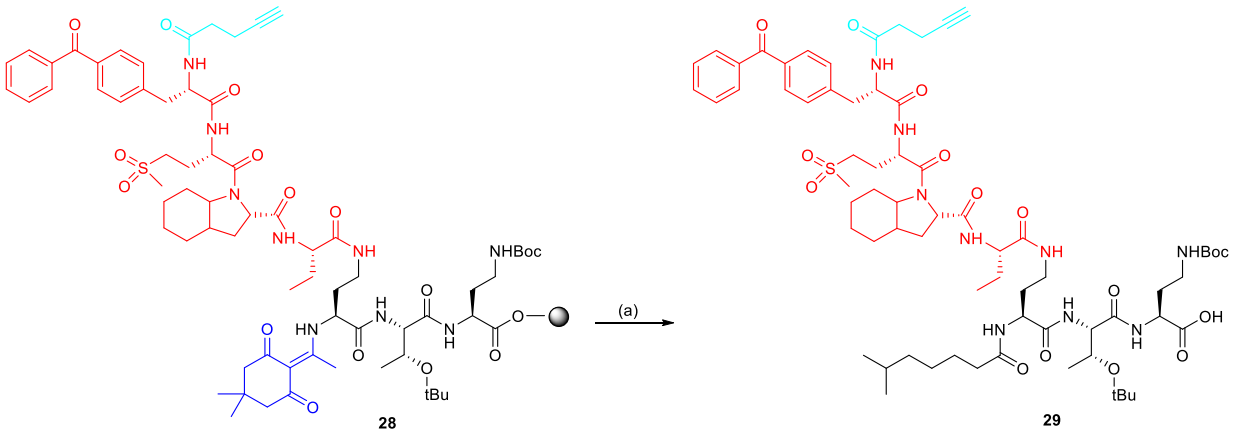

[a] Conditions: (a) (i) 2% hydrazine to remove Dde; (ii) coupling with 6-methylheptanoic acid (5 eq.), HCTU (5 eq.), DIPEA (10 eq.), in DMF, rt, 1h); (iii) 1,1,1,3,3,3-hexafluoro-2-propanol: DCM in a ratio 1:4 (resin cleavage).

According to the above reported synthetic pathway (Figure 107), the synthesis of the last fragment was performed as follows: starting from **1**, sequential cycles of Fmoc deprotection and amidation with the appropriate amino acid were carried out to give **30** (Scheme 17).

Scheme 17. Sequential Fmoc deprotection and coupling producing 30[a].

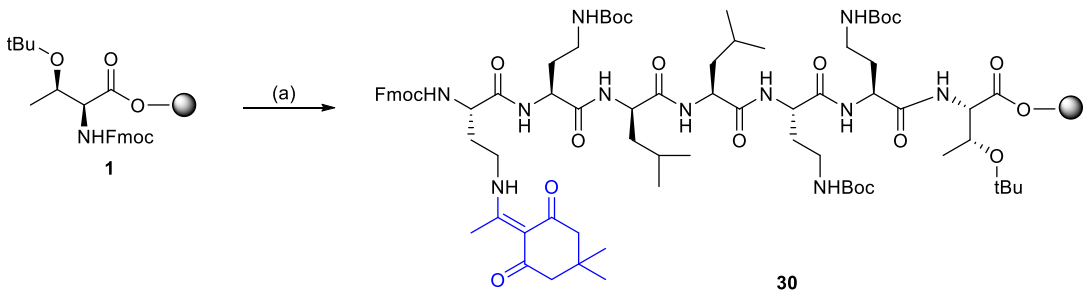

At this point, the removal of the Dde protecting group from the amino side chain of Dab in position 4 was performed by using different conditions with respect to the previous reactions, since treatment with hydrazine affects also the Fmoc protection from the α-amine of Dab 4.
Hydroxylamine hydrochloride in presence of imidazole in DCM: NMP (1:5) was added to the solid phase for 1h 30' and addition was repeated for three times, washing with NMP.[161] Hydroxylamine is indeed a nucleophile strong enough to remove Dde by *trans*-enamination reaction, but not a base strong enough to cleave Fmoc by basic elimination, which remained safely attached to the α-amine of Dab 4.
After verifying successful removal of Dde by analytical HPLC and LC-MS, the cleavage from the resin afforded compound **31** (Scheme 18).

Scheme 18. Dde removal and cleavage from the resin to obtain compound 31[a].

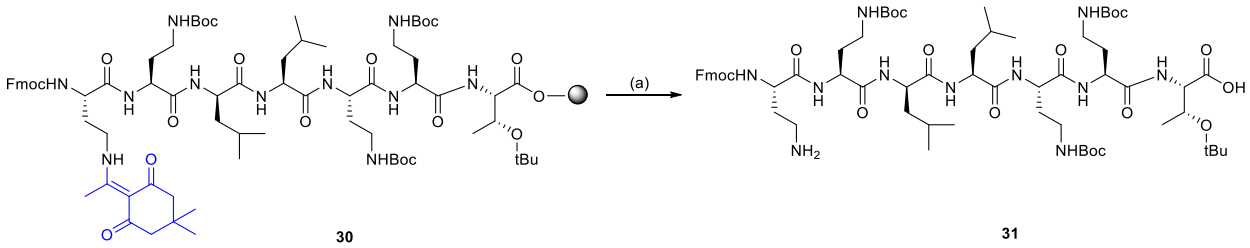

[a] Conditions: (a) (i) 2% hydrazine to remove the Dde; (ii) 1,1,1,3,3,3-Hexafluoruro-2-propanol: DCM in a ratio 1:4 (resin cleavage).

After removal of the solvents, dioxane was added to the residue and the solution was subsequently lyophilized.
The cyclization between the α-carboxyl of Thr corresponding to position 10 and the γ-amino side chain of the Dab in position 4, was performed in solution using the same condition as for the three previous colistin isomers (see Scheme 8).
The cyclization of **31** was again completed overnight and the result was checked by analytical HPLC and LC-MS. The DCM was removed under vacuum and to the DMF residual were added a few mL of a solution of 10% of piperidine in DMF in order to remove the Fmoc protecting group of the amino side chain of the Dab corresponding the position 4. After stirring for 2 h, the final fragment **33** was obtained (Scheme 19) after purification by preparative HPLC, and checked by HPLC and LC-MS (see Experimental).

Scheme 19. Cyclization and Fmoc removal of 31 to yield compound 32.

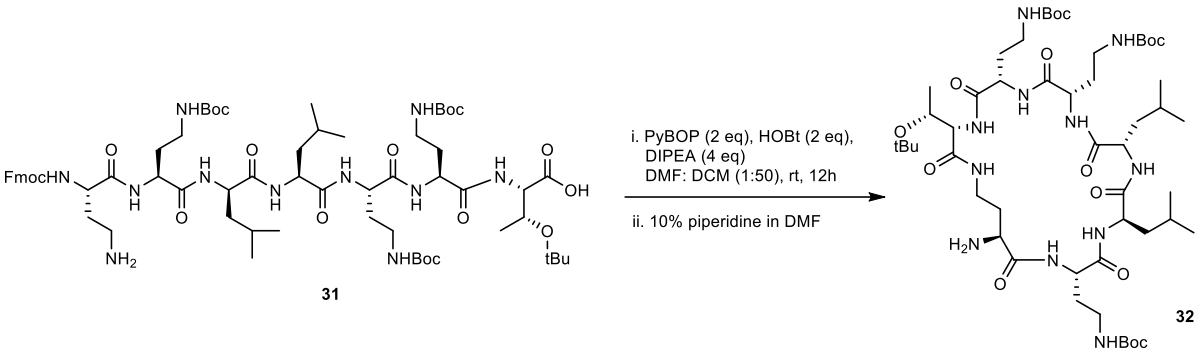

The next step was the coupling reaction between the free γ-NH_2 of fragment **32** and the carboxyl terminal of each of the two fragments **25** and **29**, to produce the final two colistin isomers. Starting from fragment **25**, the amidation reaction with fragment **32** was carried out by using the same activation as for the intracyclic reactions, but with different molar ratio (1.5, 1 and 3 eq. respectively for PyBOP, HOBt and DIPEA), the solvent being dry DMF at 0 °C. After 2h compound **33** with the elastase at position **3** was obtained (Scheme 20).

Scheme 20. Coupling between 25 and 32 to yield compound 33, corresponding to the colistin isomer having the elastase substrate attached to the γ-NH of Dab at 3 position.

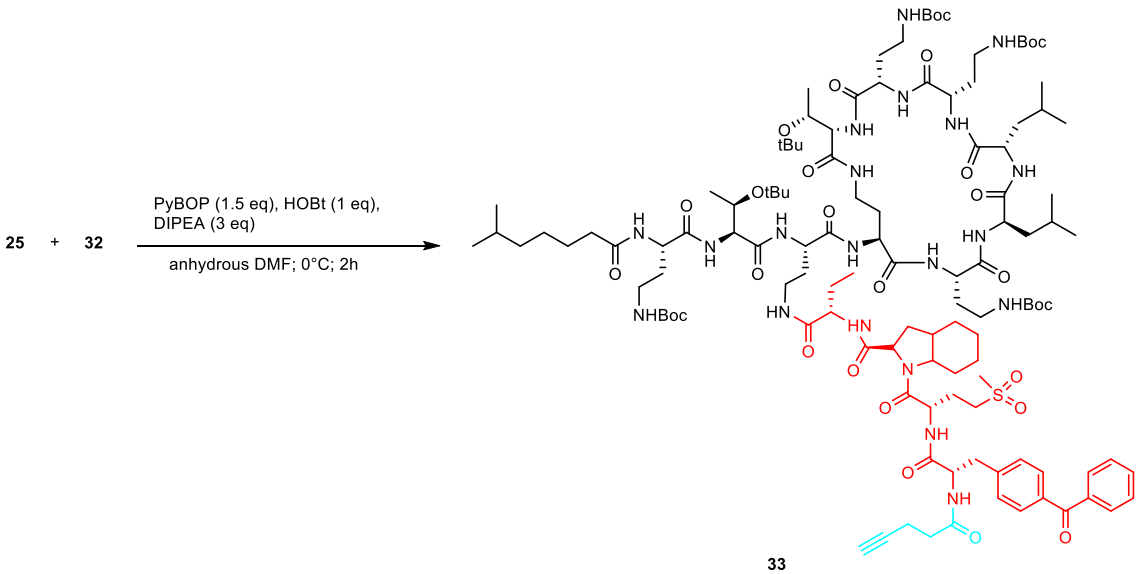

The coupling of fragment **32** with fragment **29** was carried out under the same experimental conditions, in order to obtain peptide **34** having elastase substrate attached at the amino side chain of Dab at position 1 (Scheme 21).

Scheme 21. Coupling between 29 and 32 to yield compound 34, corresponding to colistin isomer having the elastase substrate attached to the γ-NH of Dab at 1 position.

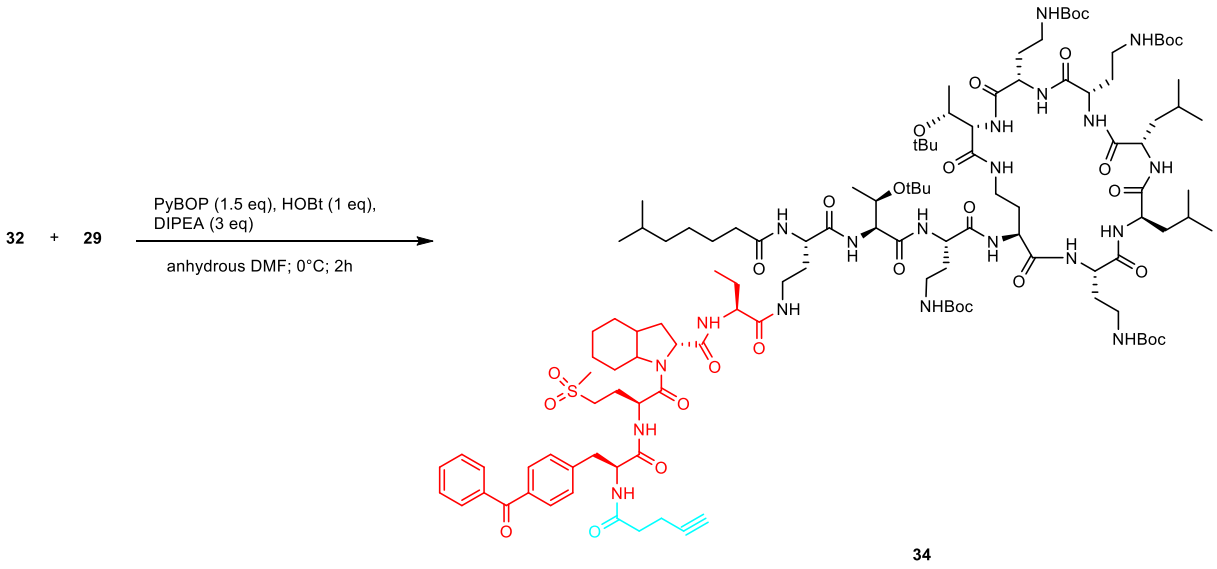

Having **33** and **34** in hands, the last two steps concerned the global deprotection and the click reaction of each with Ubi_{29-41}. Both the reactions were performed by using the experimental conditions already used for the previous three colistin isomers. Scheme 22 shows the global deprotection reaction for compound **33** (upper) and compound **34** (lower), leading to the deprotected peptides **35** and **36**, respectively.

Scheme 22. Global deprotection of 33 and 34 in order to obtain peptides 35 and 36, respectively.

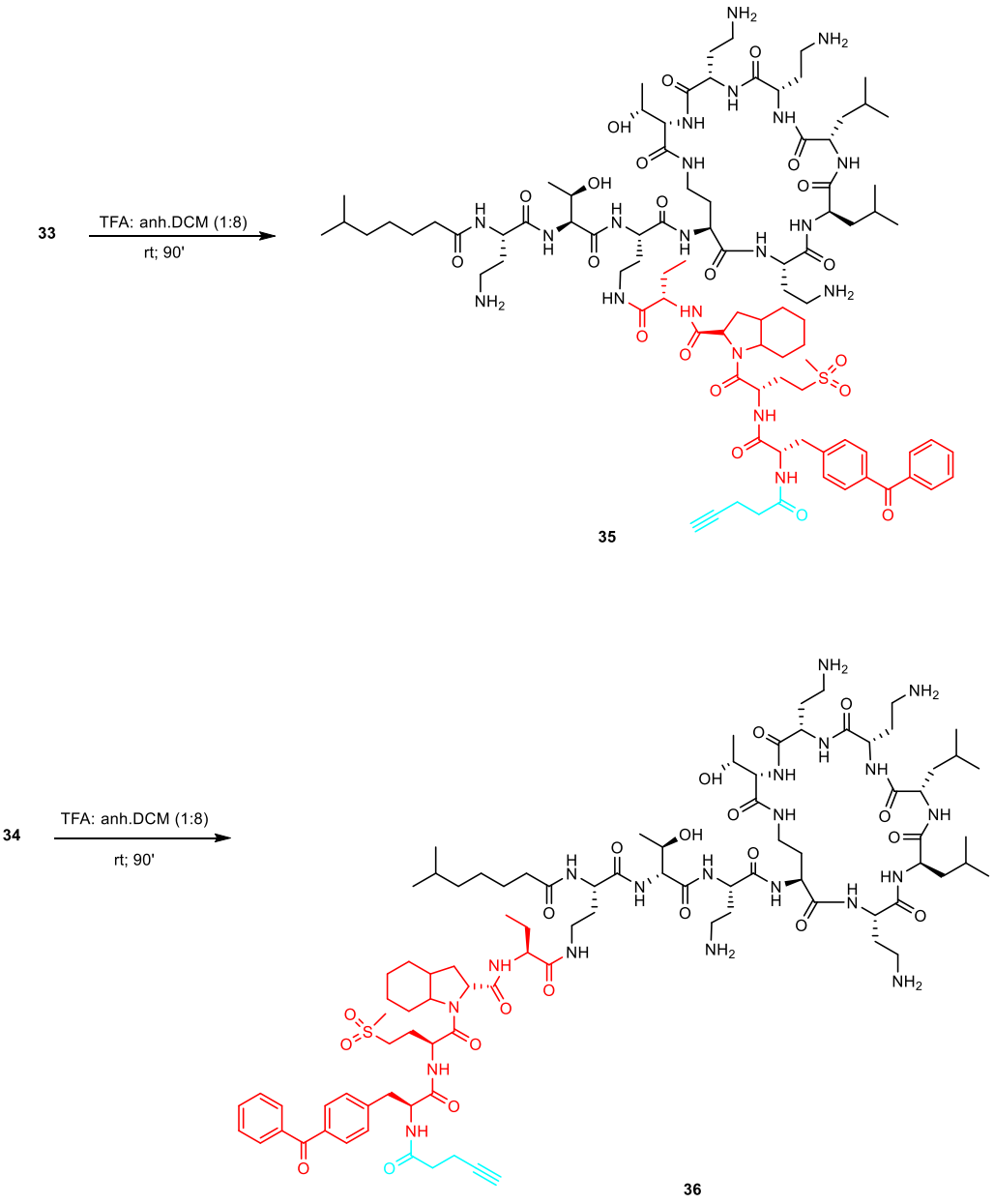

Eventually, Scheme 23 displays the click reaction of **35** and **36** with the Ubi_{29-41} in order to get the final peptides **37** and **38**, with elastase substrate on side chain of Dab at 3rd and at 1st position, respectively.

Scheme 23. Click reaction of 35 and 36 with Ubi_{29-41} in order to yield the final peptides 37 and 38, with elastase substrate in γ-NH of Dab at position 3 and 1, respectively.

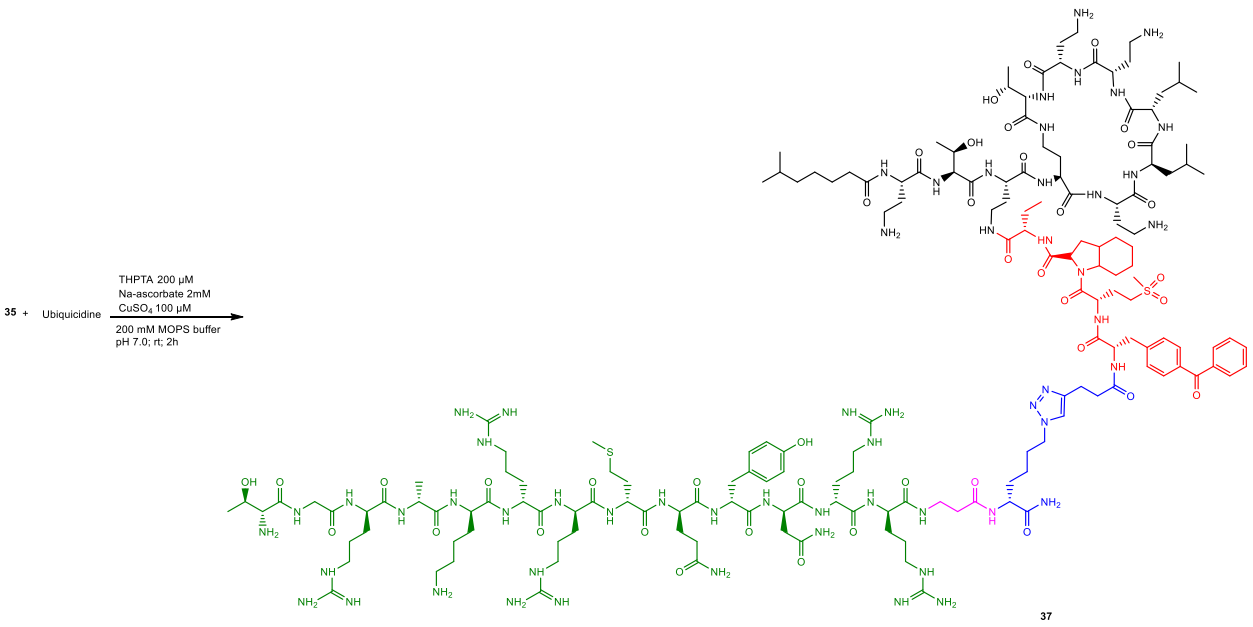

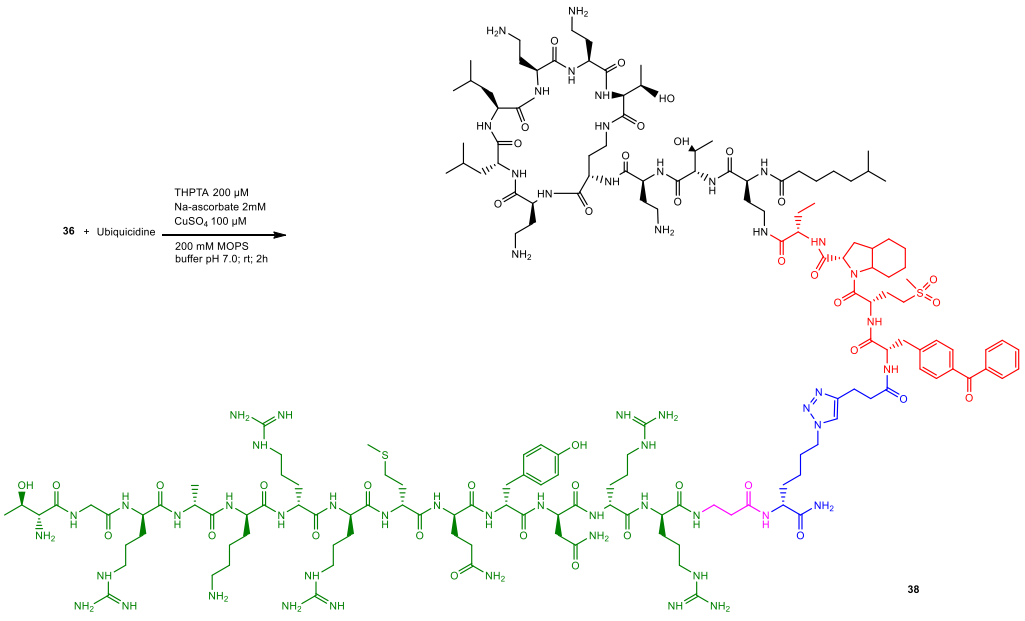

3.4.3 Antimicrobial activity of the five isomers

The antimicrobial activity of the five isomers was evaluated by determining the minimum inhibitory concentration (MIC) of the substance required to inhibit the growth of a given microorganism, against a strain of *E. coli* K12, according to the procedure[163] reported in the Experimental.

The results of MIC assay are provided by Table 16.

Table 16. Antibacterial assay of the 5 colistin isomers against E. coli K12

Compound	MIC without Elastase (μM)[a]	MIC with Elastase (μM)[a]
Colistin B	0.063	-
Peptide-colistin construct mixture	4	0.125
20	2	2
21	>32	>32
22	>32	2
37	4	0.25
38	4	1

[a] Conservative estimates of at least three independent trials.

The compound **37**, having the elastase substrate in position 3, was the colistin isomer having an almost similar antibacterial activity with respect to the peptide-colistin construct mixture, in presence of HNE.

Even the colistin regioisomer **38**, bearing elastase substrate in position 1, showed a quite good antibacterial activity when elastase was added, having a MIC value far three MIC potency.

Along cases **20** and **22**, bearing the elastase substrate in position 9 and 5 respectively, that showed an antimicrobial activity not so drastically high with respect to the mixture, the compound **21**, that have the HNE substrate in position 8, resulted as the worst of the regioisomers in terms of antibacterial activity.

On the other hand, considering the column of MIC values in the Table 16 when elastase was no added, the activity of the regioisomers was the same (**37**, **38** and almost **20**) or even worse (**21** and **22**) than the tested peptide-colistin isomers mixture.

Since in literature is well described as the amino side chains of the Dab residues in the intracycle part of the colistin are more important, in terms of antimicrobial activity, than the ones at Dab in extracyclic position (see the Introduction), this could possibly explain the no antibacterial activity observed for the compounds **21** and **22** (<32 μM), with respect to **20**, **37** and **38** when HNE is no added. Anyway, there are probably other reasons, since a similar result should be also observed for the isomer **20**, which showed a slightly better MIC value than the mixture and **37** and **38**, when HNE was no added.

The results when HNE was added, not only showed the regioisomer **37** as the most active against *E. coli* K12, but also highlighted somewhat differences in the fidelity and specific

activity of the individual isomers in presence of HNE, which cannot be safely discussed at the moment. Thus, these differences resulted in the lower (**38** and in particular **20**, **22**), or no antimicrobial activity (**21**).

3.5 Conclusion

With the aim to elucidate if there were differences of biological activities caused by specificity of the elastase activity for the isomers present in the peptide-colistin mixture, previously synthesised in HZI, the total synthesis of the individual regioisomers was carried out.
The antimicrobial activity against *E. coli* K12 showed the compound **37** as the one of the mixture mainly responsible for the activity and the most promising candidate to further studies. An investigation of the differences of HNE cleavage seems to be necessary in order to well explain these antibacterial differences among the colistin regioisomers.
In a view of a possible pharmaceutical application, toxicity tests are the immediately consequences after these preliminary results. Of course, further antibacterial assays against other Gram-negative pathogens (*A. baumanii*, *K. pneumoniae*, *P. aeruginosa*) and especially against the MDR ones, are necessary, in order to expand the spectrum activity of the promising compound(s).

3.6 Experimental

3.6.1 Materials and methods

The amino acids derivatives were purchased as follows. D- and L-Fmoc-azido lysine, Fmoc-L-Bpa-OH and Fmoc-L-Oic-OH were from Carbolution (St. Ingerbert, Germany); Fmoc-2-Abu-OH, Fmoc-L-Met(O_2)-OH, Fmoc-Dab(Boc)-OH, Fmoc-Dab(Dde)-OH, Dde-Dab(Fmoc)-OH, HATU, were from Iris Biotech (Marktredwitz, Germany).
The Rapp S RAM resin was from Rapp Polymere, Tübingen, Germany.
Standard Fmoc-amino acids were purchased from MultiSynTech (Witten, Germany). Side chain protections were as follows. Thr and Tyr: tBu, Arg: Pbf, Lys: Boc, Asn, Cys and Gln: Trt.
DIPEA was from Reagent Plus Grade, Sigma-Aldrich (Taufkirchen, Germany). DCM was from Baker analyzed, J.T. Baker (Gliwice, Poland). TFA for Peptide Synthesis >99.9% was from Roth (Karlsruhe, Germany). 1,1,1,3,3,3-hexafluoro-2-propanol 99.5% pure was from ACROS Organics (Geel, Belgium). PyBOP, HCTU were from Iris Pharmaceuticals. HOBt was from Gerhardt Inc. (Wolfhagen, Germany).

Colistin (sulfate) was obtained from Cayman Chemical (via distributor Biomol, Hamburg, Germany) and separated into the two major components, colistin A and colistin B by prep. HPLC on C-18 columns with gradients of water and acetonitrile containing 0.1% TFA.
Acetonitrile and water for HPLC (HPLC-grade) was from J.T. Baker; DMF (p.a. grade) was from Honeywell/Riedel-de-Haen.
The loading of the resin was measured by using the Pharmacia Ultrospec 2100 pro UV/Vis spectrometer.
The automated assembly of the ubiquicidine was performed by a Syro Multiple Peptide Synthesizer (MultiSynTech, Witten, Germany).
The analytical HPLC used for analyzing intermediate and final peptides was Merck-Hitachi LaChrom 7000 Series, column: Phenomenex Luna C18, 5µm, 2x50 mm; flow rate 0.7 ml/min, with gradients of acetonitrile in water containing 0.1% TFA.
All the purifications in the intermediate and final steps of peptide synthesis were performed by using preparative HPLC: Pump Knauer K-1800 with 100 mL head (low pressure gradient), Sykam S3250 UV/Vis detector, Teledyne FoxyR2 fraction collector, 2 different column sizes: Phenomenex Jupiter 4 µm Proteo 21.2 × 250 mm and 30 × 250 mm. Software: Clarity (DataApex).
MS data, after dissolving compounds in milliQ water, were collected on a Bruker Amazon SL LC-MS operating in the Apollo II electrospray mode. The chromatography system consisted of an Agilent 1200 with autosampler, binary high gradient pump and DAD-detector. The column used for the separation was Gemini NX 3µ C18 110A, 50 × 2 mm from Phenomenex. The binary pump operated at 400 µL/min of A: water with 0,1% formic acid and B: acetonitrile 0,1% formic acid. The used gradient was: 0 min 5% B, 17 min 80% B, 19 min 95% B, 21 min 95% B, in the overall run time of 25 min. Samples injections were typically 10 µL.

E. coli K12 was from Deutsche Sammlung für Mikroorganismen und Zellkulturen, Braunschweig, Germany; T-medium: 17 g/l LP 42 (Oxoid), LP44 (Oxoid) 3.0 g/l, Glucose 10.0 g/l, MOPS 10.47 g/l, NaCl 5.84 g/l, KCl 0.149 g/ml, CaCl2x 2 H2O 0.294 g/l, PH 7.4, sterile filtrated.
Neutrophil Elastase (human), affinity purified: USBiological (via distributor Biomol GmbH, Hamburg, Germany), catalogue No E2230-11.
Plate multiwell from Greiner Bio-One Microplate No. 675061, 96 well, half area, transparent, flat bottom (Greiner Bio-One, Frickenhausen, Germany).

Spectrophotometer for OD measurements for MIC: µQuant, BioTek (Bad Friedrichshall, Germany).

3.6.2 Synthetic procedures and characterizations

Fmoc-Thr(tBu)-2-CTC resin, 1

2-CTC resin with a loading of 1.55 mmol/g (1.0 g, 1.55 mmol) was suspended in anhydrous DCM (5 mL), after a previous sequentially washing with the same solvent (3 x 5 mL), in a 10 mL polypropylene syringe fitted with a polyethylene disc.
Fmoc-Dab(Boc)-OH (924.19 mg, 2.33 mmol) and DIPEA (1.62 mL, 9.32 mmol) were added to this suspension and the mixture was gently stirred at RT for 2h.
After coupling, the resin was sequentially washed with DCM (3 x 3 mL), DMF (3 x 3 mL) and lastly with DCM again (3 x 3 mL) and allowed to dry overnight.
The Fmoc of a small amount of the product resin was cleaved by a freshly made 20% piperidine in DMF (v/v), in order to determine the loading level of the resin which was calculated to be 0.396 mmol/g, via standard UV absorption method (Pharmacia Ultrospec 2100 pro UV/Vis spectrometer, wavelength 301 nm, molar extinction coefficient 7.800).

General coupling procedure for the SPPS synthesis.

All the couplings were performed on a scale of 50 µmol on 2-CTC resin (loading 0.396 mmol/g), by a sequential Fmoc deprotection/amidation methodology carried out as described below.
Fmoc-Thr(tBu)-2-CTC resin (126.3 mg, 50 µmol), **1**, was washed with DMF (3 x 2 mL) in a 5 mL polypropylene syringe fitted with a polyethylene disc; the solvent was removed by filtration.
To the resin, 20% piperidine in DMF (3 mL) was added and allowed to react at RT for 10 min. Then, the solution was filtered and the solid was washed with DMF (5 x 3 mL). The proper protected amino acids (250 µmol) and HCTU (103.4 mg, 250 µmol) both in fivefold excess, were dissolved in DMF (1 mL) and, to this, DIPEA (87.10 µL, 500 µmol), in tenfold excess was added. The activated amino-acid mixture was then added to the Fmoc-deprotected product resin and allowed to react at RT for 1h, gently stirred. Then, the solution was filtered and washed with DMF (8 x 3 mL).

Dde-Dab(Fmoc)-Thr(tBu)-2-CTC resin, 2

According to the general coupling procedure above reported, to Fmoc-Thr(tBu)-2-CTC resin (126.3 mg, 50 µmol) Dde-Dab(Fmoc)-OH (126.1 mg, 250 µmol) was coupled.

Dde-Dab(Fmoc)-Dab(Boc)-Thr(tBu)-2-CTC resin, 3

To Fmoc-Thr(tBu)-2-CTC resin (126.3 mg, 50 µmol), following the general coupling procedure,
the suitable protected amino acids were coupled as follows: Fmoc-Dab(Boc)-OH (110.1 mg, 250 µmol), Dde-Dab(Fmoc)-OH (126.1 mg, 250 µmol).

Dde-Dab(Fmoc)-DLeu-Leu-Dab(Boc)-Dab(Boc)-Thr(tBu)-2-CTC resin, 4

To Fmoc-Thr(tBu)-2-CTC resin (126.3 mg, 50 µmol), following the general coupling procedure,
the suitable protected amino acids were coupled as follows: Fmoc-Dab(Boc)-OH (110.1 mg, 250 µmol), Fmoc-Dab(Boc)-OH (110.12 mg, 250 µmol), Fmoc-Leu-OH (88.4 mg, 250 µmol), Fmoc-D-Leu-OH (88.35 mg, 250 µmol), Dde-Dab(Fmoc)-OH (126.1 mg, 250 µmol).

Dde-Dab(4-pentynoyl-Bpa-Met(O_2)-Oic-Abu)-Thr(tBu)-2-CTC Resin, 5

Dde-Dab(4-pentynoyl-Bpa-Met(O_2)-Oic-Abu)-Dab(Boc)-Thr(tBu)-2-CTC Resin, 6

Dde-Dab(4-pentynoyl-Bpa-Met(O_2)-Oic-Abu)-DLeu-Leu-Dab(Boc)-Dab(Boc)-Thr(tBu)-2-CTC Resin, 7

*The synthesis of compounds resin **5**, **6** and **7** was performed by the same chemical procedure as follows:*

Step 1: To Dde-Dab(Fmoc)-Thr(tBu)-2-CTC resin, **2**, Dde-Dab(Fmoc)-Dab(Boc)-Thr(tBu)-2-CTC resin, **3** and Dde-Dab(Fmoc)-DLeu-Leu-Dab(Boc)-Dab(Boc)-Thr(tBu)-2-CTC resin, **4**, following the general coupling procedure, the suitable protected amino acids was coupled, at the γ-amine of Dab at N-terminal of the resin product, as follows: Fmoc-Abu-OH (81.3 mg, 250 µmol), Fmoc-Oic-OH (97.9 mg, 250 µmol), Fmoc-Met(O_2)-OH (100.9 mg, 250 µmol).

Step 2: Fmoc-Bpa-OH (122.9 mg, 250 µmol) and HATU (95.0 mg, 250 µmol) were dissolved in DMF (1 mL) and, to this, DIPEA (87.1 µL, 500 µmol) was added. The activated aminoacid mixture, prepared in triplicated, was, then, each added to the Dde-Dab(H-Met(O_2)-Oic-Abu)-

Dab(Boc)-Thr(tBu)-2-CTC resin, Dde-Dab(H-Met(O_2)-Oic-Abu)-Dab(Boc)-Thr(tBu)-2-CTC resin, and Dde-Dab(H-Met(O_2)-Oic-Abu)-DLeu-Leu-Dab(Boc)-Dab(Boc)-Thr(tBu)-2-CTC resin, and allowed to react at RT for 1h, gently stirred; this coupling was repeated twice for each of the three product resins, filtering and washing with DMF (2 x 3 mL) in between.
Finally, the solutions were as usual filtered and washed with DMF (8 x 3 mL).
Step 3: To Dde-Dab(Fmoc-Bpa-Met(O_2)-Oic-Abu)-Dab(Boc)-Thr(tBu)-2-CTC resin, Dde-Dab(Fmoc-Bpa-Met(O_2)-Oic-Abu)-Dab(Boc)-Thr(tBu)-2-CTC resin and Dde-Dab(Fmoc-Bpa-Met(O_2)-Oic-Abu)-DLeu-Leu-Dab(Boc)-Dab(Boc)-Thr(tBu)-2-CTC resin, following the general coupling procedure, 4-pentynoic-OH (24.5 mg, 250 µmol) was coupled.

6-Methylheptanoyl-Dab(Boc)-Thr(tBu)-Dab(Boc)-Dab(Dde)-Dab(Boc)-DLeu-Leu-Dab(Boc)-Dab(4-pentynoyl-Bpa-Met(O_2)-Oic-Abu)-Thr(tBu)-2-CTC Resin, 8

Step 1: To the resin Dde-Dab(4-pentynoyl-Bpa-Met(O_2)-Oic-Abu)-Thr(tBu)-2-CTC, **5**, previously obtained, was added 2% hydrazine in DMF (2 mL).
The mixture was stirred at RT for 1h 30' for 3 times, filtering and washing with DMF in between.
Lastly, the product resin H-Dab(4-pentynoyl-Bpa-Met(O_2)-Oic-Abu)-Thr(tBu)-2-CTC was washed with DMF. The resulting product was cleaved from a small amount of resin (1 mg), by a solution of 1,1,1,3,3,3-hexafluoro-2-propanol: DCM in a ratio 1:4, in order to analyze the successful removal of Dde via analytical HPLC (Figure 110a) and LC-MS.
Gradient method: 0-95% solvent B over 23 min at flow rate of 0.700 mL/min (solvent A: 0.1% TFA in water; solvent B: 0.1% TFA in ACN). Major peak with retention time (t_R), at 11.85 min, by UV 220 nm (Figure 110a); Expected mass: 1005.49. **ESI-MS** found: (m/z) = 1006.5 $[M+H]^+$, 1028.5 $[M+Na]^+$;

Step 2: To H-Dab(4-Pentynoyl-Bpa-Met(O_2)-Oic-Abu)-Thr(tBu)-2-CTC previously obtained, following the general coupling procedure the suitable residues were coupled as follows: Fmoc-Dab(Boc)-OH (110.1 mg, 250 µmol); Fmoc-Leu-OH (88.4 mg, 250 µmol); Fmoc-DLeu-OH (88.4 mg, 250 µmol); Fmoc-Dab(Boc)-OH (110.1 mg, 250 µmol); Fmoc-Dab(Dde)-OH (126.1 mg, 250 µmol); Fmoc-Dab(Boc)-OH (110.1 mg, 250 µmol); Fmoc-Thr(tBu)-OH (99.4 mg, 250 µmol); Fmoc-Dab(Boc)-OH (110.1 mg, 250 µmol); 6-Methylheptanoic acid (36.0 mg, 250 µmol).

A small amount of resin (1 mg) was then cleaved by a solution of 1,1,1,3,3,3-hexafluoro-2-propanol: DCM in a ratio 1:4, in order to analyze the compound resin obtained, via analytical HPLC (Figure 110b) and LC-MS.

Gradient method: 0-95% solvent B over 23 min at flow rate of 0.700 mL/min (solvent A: 0.1% TFA in water; solvent B: 0.1% TFA in ACN). Major peak with retention time (t_R) at 19.95 min, by UV 220 nm; Expected mass: 2579.48. **ESI-MS** found: (m/z) = 1291.7 $[M+2H]^{2+}$, 1301.2 $[M+H+Na]^{2+}$.

6-Methylheptanoyl-Dab(Boc)-Thr(tBu)-Dab(Boc)-Dab(Dde)-Dab(Boc)-DLeu-Leu-Dab(4-pentynoyl-Bpa-Met(O_2)-Oic-Abu)-Dab(Boc)-Thr(tBu)-2-CTC resin, 9

Step 1: To the resin Dde-Dab(4-pentynoyl-Bpa-Met(O_2)-Oic-Abu)-Dab(Boc)-Thr(tBu)-2-CTC, previously obtained, was added 2% hydrazine in DMF (2 mL).
The mixture was stirred at RT for 1h 30' for 3 times, filtering and washing with DMF in between.
Lastly, the product resin was washed with DMF. The resulting product was cleaved from a small amount of resin (1 mg), by a solution of 1,1,1,3,3,3-hexafluoro-2-propanol: DCM in a ratio 1:4, in order to analyze the successful removal of Dde via analytical HPLC (Figure 111a) and LC-MS.
Gradient method: 0-95% solvent B over 23 min at flow rate of 0.700 mL/min (solvent A: 0.1% TFA in water; solvent B: 0.1% TFA in ACN). Major peak with retention time (t_R) at 12.71 min; Expected mass: 1205.60. **ESI-MS** found: (m/z) = 1206.6 $[M+H]^+$, 1228.6 $[M+Na]^+$;

Step 2: To H-Dab(4-pentynoyl-Bpa-Met(O_2)-Oic-Abu)-Dab(Boc)-Thr(tBu)-2-CTC obtained in step 1 and following the general coupling procedure, the suitable residues were coupled as follows: Fmoc-Leu-OH (88.4 mg, 250 µmol); Fmoc-DLeu-OH (88.4 mg, 250 µmol); Fmoc-Dab(Boc)-OH (110.1 mg, 250 µmol); Fmoc-Dab(Dde)-OH (126.1 mg, 250 µmol); Fmoc-Dab(Boc)-OH (110.1 mg, 250 µmol); Fmoc-Thr(tBu)-OH (99.4 mg, 250 µmol); Fmoc-Dab(Boc)-OH (110.1 mg, 250 µmol); 6-Methylheptanoic acid (36.0 mg, 250 µmol).

A small amount of resin (1 mg) was then cleaved by a solution of 1,1,1,3,3,3-hexafluoro-2-propanol: DCM in a ratio 1:4, in order to analyze the compound resin obtained, via analytical HPLC (Figure 111b) and LC-MS.

Gradient method: 0-95% solvent B over 23 min at flow rate of 0.700 mL/min (solvent A: 0.1% TFA in water; solvent B: 0.1% TFA in ACN). Major peak with retention time (t_R) at 19.75 min,

by 220 nm; Expected mass: 2581.48. **ESI-MS** found: (m/z) = 1291.7 $[M+2H]^{2+}$, 1301.2 $[M+H+Na]^{2+}$.

6-Methylheptanoyl-Dab(Boc)-Thr(tBu)-Dab(Boc)-Dab(Dde)-Dab(4-pentynoyl-Bpa-Met(O_2)-Oic-Abu)-DLeu-Leu-Dab(Boc)-Dab(Boc)-Thr(tBu)-2-CTC resin, 10

Step 1: To the resin Dde-Dab(4-Pentynoyl-Bpa-Met(O_2)-Oic-Abu)-DLeu-Leu-Dab(Boc)-Dab(Boc)-Thr(tBu)-2-CTC, previously obtained, was added 2% hydrazine in DMF (2 mL). The mixture was stirred at RT for 1h 30' for 3 times, filtering and washing with DMF in between.

Lastly, the product resin was washed with DMF. The resulting product was cleaved from a small amount of resin (1 mg), by a solution of 1,1,1,3,3,3-hexafluoro-2-propanol: DCM in a ratio 1:4, in order to analyze the successful removal of Dde via analytical HPLC (Figure 112a) and LC-MS.

Gradient method: 0-95% solvent B over 23 min at flow rate of 0.700 mL/min (solvent A: 0.1% TFA in water; solvent B: 0.1% TFA in ACN). Major peak with retention time (t_R) at 12.71 min. Expected mass: 1631.89. **ESI-MS** found: (m/z) = 1632.8 $[M+H]^+$, 1654.8 $[M+Na]^+$;

Step 2: To H-Dab(4-Pentynoyl-Bpa-Met(O_2)-Oic-Abu)-DLeu-Leu-Dab(Boc)-Dab(Boc)-Thr(tBu)-2-CTC obtained in step 1 and following the general coupling procedure, the suitable residues were coupled as follows: Fmoc-Dab(Dde)-OH (126.1 mg, 250 μmol); Fmoc-Dab(Boc)-OH (110.1 mg, 250 μmol); Fmoc-Thr(tBu)-OH (99.4 mg, 250 μmol); Fmoc-Dab(Boc)-OH (110.1 mg, 250 μmol); 6-Methylheptanoic acid (36.0 mg, 250 μmol).

A small amount of resin (1 mg) was cleaved by a solution of 1,1,1,3,3,3-hexafluoro-2-propanol: DCM in a ratio 1:4, in order to analyze the compound resin obtained, via analytical HPLC (Figure 112b) and LC-MS.

Gradient method: 0-95% solvent B over 23 min at flow rate of 0.700 mL/min (solvent A: 0.1% TFA in water; solvent B: 0.1% TFA in ACN). Major peak with retention time (t_R) at 19.75 min by 220 nm; Expected mass: 2579.48. **ESI-MS** found: (m/z) = 1291.7 $[M+2H]^{2+}$, 1301.2 $[M+H+Na]^{2+}$.

General procedure of Dde removal and resin cleavage to get the linear peptides 11, 12 and 13 and their characterization.

Note: representative procedure is referred to 50 μmol of starting compound used.

Step 1: Cleavage of Dde. To the resins **8**, **9** and **10**, previously obtained, were added, selectively to each of them, 2% hydrazine in DMF (2 mL).
The mixtures were stirred at RT for 1h 30' for 3 times, filtering and washing with DMF in between.
Lastly, the product resins were washed with DMF.

Step 2: Cleavage from the resin. Each of the three peptidyl resins, derivate from step 1, were then treated with 1,1,1,3,3,3-hexafluoro-2-propanol: DCM in a ratio 1:4 (40 mL x 1h for each product resin) and the filtrates were collected, solvents evaporated under vacuum, resuspended in dioxane and lyophilized, to have the compounds **11**, **12** and **13**, which were used in the next step without any further purification, previously analyzing them by HPLC (see Figure 113 in HPLC analysis data) and LC-MS.

6-Methylheptanoyl-Dab(Boc)-Thr(tBu)-Dab(Boc)-Dab(NH_2)-Dab(Boc)-DLeu-Leu-Dab(Boc)-Dab(4-pentynoyl-Bpa-Met(O_2)-Oic-Abu)-Thr(tBu)-OH, 11

Starting from the product resin **8** and following the general procedure, 80.0 mg of compound **11** was obtained as a white solid.

Analytical HPLC gradient method: 0-95% solvent B over 23 min at flow rate of 0.700 mL/min (solvent A: 0.1% TFA in water; solvent B: 0.1% TFA in ACN). Major peak, by UV 220 nm, with retention time (t_R), at 17.96 min (Figure 113a); Expected mass: 2415.40. **ESI-MS** found: (m/z) = 2416.4 $[M+H]^+$, 1209.2 $[M+2H]^{2+}$, 1220.2 $[M+Na+H]^{2+}$.

6-Methylheptanoyl-Dab(Boc)-Thr(tBu)-Dab(Boc)-Dab(NH_2)-Dab(Boc)-DLeu-Leu-Dab(4-pentynoyl-Bpa-Met(O_2)-Oic-Abu)-Dab(Boc)-Thr(tBu)-OH, 12

Starting from the resin **9** and following the general procedure, compound 84.8 mg of **12** was obtained as a white solid.

Analytical HPLC gradient method: 0-95% solvent B over 23 min at flow rate of 0.700 mL/min (solvent A: 0.1% TFA in water; solvent B: 0.1% TFA in ACN). Major peak, by UV 220 nm, with retention time (t_R), at 17.49 min (Figure 113b); Expected mass: 2415.40. **ESI-MS** found: (m/z) = 2416.4 $[M+H]^+$, 1209.2 $[M+2H]^{2+}$, 1220.2 $[M+Na+H]^{2+}$.

6-Methylheptanoyl-Dab(Boc)-Thr(tBu)-Dab(Boc)-Dab(NH_2)-Dab(4-pentynoyl-Bpa-Met(O_2)-Oic-Abu)-DLeu-Leu-Dab(Boc)-Dab(Boc)-Thr(tBu)-OH, 13

Starting from the resin **10** and following the general procedure, 73.4 mg of compound **13** were obtained as a white solid.

Analytical HPLC gradient method: 0-95% solvent B over 23 min at flow rate of 0.700 mL/min (solvent A: 0.1% TFA in water; solvent B: 0.1% TFA in ACN). Major peak, by UV 220 nm, with retention time (t_R), at 17.68 min (Figure 113c); Expected mass: 2415.40. **ESI-MS** found: (m/z) = 2416.4 $[M+H]^+$, 1209.2 $[M+2H]^{2+}$, 1220.2 $[M+Na+H]^{2+}$.

General procedure for the in solution-cyclization of the compounds 11, 12 and 13 to get 14, 15 and 16, respectively, and their characterization.

Note: representative procedure is referred to 50 µmol of starting compound used; the actual amounts of starting compounds used in the reactions are reported below.

Crude compounds **11**, **12** and **13** were individually dissolved in dry DMF: DCM in a ratio 1: 50 (2 mL: 98 mL) to make up a solution of the cleaved linear peptides in 0.5 µmol/mL concentration for each of them.
To each of the mixtures, PyBOP (78.1 mg, 150.0 µmol), HOBt (20.3 mg, 150 µmol) and DIPEA (52.3 µL, 300 µmol) were sequentially added under inert atmosphere and, the reactions were stirred at RT, to give the cyclic peptides **14**, **15** and **16**, after overnight. Then, DCM was removed under vacuum and the residual DMF was lyophilized using dioxane.
The crudes products so obtained were used in the next step without any further purification, after HPLC (see Figure 114 in HPLC analysis data) and LC-MS analysis.

6-Methylheptanoyl-Dab(Boc)-Thr(tBu)-Dab(Boc)-cyclo[Dab-Dab(Boc)-DLeu-Leu-Dab(Boc)-Dab(4-pentynoyl-Bpa-Met(O_2)-Oic-Abu)-Thr(tBu)], 14

Starting from the crude compound **11** (25 mg, assuming 10.35 µmol) and following the general procedure, 16.9 mg of cyclic peptide **14** was obtained as a light yellow waxy solid.

Analytical HPLC gradient method: 0-95% solvent B over 23 min at flow rate of 0.700 mL/min (solvent A: 0.1% TFA in water; solvent B: 0.1% TFA in ACN). Major peak with retention time (t_R) 19.99 min, bu UV 220 nm (Figure 114a); Expected mass: 2397.39. **ESI-MS** found: (m/z) = 1200.5 $[M+2H]^{2+}$; 1211.5 $[M+H+Na]^{2+}$; 1222.5 $[M+2Na]^{2+}$.

6-Methylheptanoyl-Dab(Boc)-Thr(tBu)-Dab(Boc)-cyclo[Dab-Dab(Boc)-DLeu-Leu-Dab(4-pentynoyl-Bpa-Met(O_2)-Oic-Abu)-Dab(Boc)-Thr(tBu)], 15

Starting from the crude compound **12** (30 mg, assuming 12.42 μmol) and following the general procedure, 19.7 mg of cyclic peptide **15** was obtained as a light yellow waxy solid.

Analytical HPLC gradient method: 0-95% solvent B over 23 min at flow rate of 0.700 mL/min (solvent A: 0.1% TFA in water; solvent B: 0.1% TFA in ACN). Major peak with retention time (t_R) 19.61 min, by UV 220 nm (Figure 114b); Expected mass: 2397.39. **ESI-MS** found: (m/z) = 1200.5 $[M+2H]^{2+}$; 1211.5 $[M+H+Na]^{2+}$; 1222.5 $[M+2Na]^{2+}$.

6-Methylheptanoyl-Dab(Boc)-Thr(tBu)-Dab(Boc)-cyclo[Dab-Dab(4-pentynoyl-Bpa-Met(O_2)-Oic-Abu)-DLeu-Leu-Dab(Boc)-Dab(Boc)-Thr(tBu)], 16

Starting from the crude compound **13** (35 mg, assuming 14.48 μmol) and following the general procedure, 24.3 mg of cyclic peptide **16** was obtained as a light yellow waxy solid.

Analytical HPLC gradient method: 0-95% solvent B over 23 min at flow rate of 0.700 mL/min (solvent A: 0.1% TFA in water; solvent B: 0.1% TFA in ACN). Major peak with retention time (t_R) 19.79 min, by UV 220 nm (Figure 114c); Expected mass: 2397.39. **ESI-MS** found: (m/z) = 1200.5 $[M+2H]^{2+}$; 1211.5 $[M+H+Na]^{2+}$; 1222.5 $[M+2Na]^{2+}$.

General procedure for global deprotection of the compounds 14, 15 and 16, to get the compounds 17, 18 and 19, respectively, and their characterization.
Note: representative procedure is referred to 50 μmol of starting compound used; the actual amounts of starting compounds used in the reactions are reported below.
Crude compounds **14**, **15** and **16** were individually dissolved in dry DCM (20 mL) and then TFA (2.5 mL) was added. The reactions were stirred at room temperature for 90 min. All the volatile species were removed under vacuum using water bath temperature not over than 30 °C. Next, cold diethyl ether was added to precipitate the peptide as light-yellow solid at the bottom and, the supernatant was then removed after centrifugation.
The crude peptide, dissolved in water, was then purified by preparative HPLC using the following gradient method: 10-55% solvent B over 60 min at flow rate of 20.00 mL/min (solvent A: 0.1% TFA in water; solvent B: 0.1% TFA in ACN).

The fractions containing the product, as TFA salt, were combined and lyophilized. The pure deprotected cyclic peptides were analyzed by analytical HPLC (see Figure 115 in HPLC analysis data) and LC-MS (see below).

6-Methylheptanoyl-Dab-Thr-Dab-cyclo[Dab-Dab-DLeu-Leu-Dab-Dab(4-pentynoyl-Bpa-Met(O_2)-Oic-Abu)-Thr], 17

Starting from compound **14** (20 mg, assuming 8.34 μmol) and following the general procedure, 3.77 mg (2.00 μmol) of the deprotected cyclic peptide **17** was obtained (assuming 24% yield) as a white solid.

Analytical HPLC gradient method: 0-95% solvent B over 23 min at flow rate of 0.700 mL/min (solvent A: 0.1% TFA in water; solvent B: 0.1% TFA in ACN). Major peak with retention time (t_R) 11.66 min, by UV 220 nm (Figure 115a); Expected mass: 1885.05. **ESI-MS** found (free amines): (m/z) = 1886.1 $[M+H]^+$; 943.7 $[M+2H]^{2+}$; 629.5 $[M+3H]^{3+}$; 472.5 $[M+4H]^{4+}$.

6-Methylheptanoyl-Dab-Thr-Dab-cyclo[Dab-Dab-DLeu-Leu-Dab(4-pentynoyl-Bpa-Met(O_2)-Oic-Abu)-Dab-Thr], 18

Starting from compound **15** (28 mg, assuming 11.67 μmol) and following the general procedure, 7.04 mg (3.73 μmol) of the deprotected cyclic peptide **18** was obtained (assuming 32% yield) as a white solid.

Analytical HPLC gradient method: 0-95% solvent B over 23 min at flow rate of 0.700 mL/min (solvent A: 0.1% TFA in water; solvent B: 0.1% TFA in ACN). Major peak with retention time (t_R) 11.85 min, by UV 220 nm (Figure 115b); Expected mass: 1885.05. **ESI-MS** found (free amines): (m/z) = 1886.1 $[M+H]^+$; 943.7 $[M+2H]^{2+}$; 629.5 $[M+3H]^{3+}$; 472.5 $[M+4H]^{4+}$.

6-Methylheptanoyl-Dab-Thr-Dab-cyclo[Dab-Dab(4-pentynoyl-Bpa-Met(O_2)-Oic-Abu)-DLeu-Leu-Dab-Dab-Thr], 19

Starting from cyclic peptide **16** (21 mg, 8.75 μmol) and following the general procedure, 4.13 mg (2.18 μmol) of deprotected cyclic peptide **19** was obtained in (assuming 25% yield) as a white solid.

Analytical HPLC gradient method: 0-95% solvent B over 23 min at flow rate of 0.700 mL/min (solvent A: 0.1% TFA in water; solvent B: 0.1% TFA in ACN). Major peak, , with retention

time (t_R) 11.77 min, by UV 220 nm (Figure 115c); Expected mass: 1885.05. **ESI-MS** found (free amines): (m/z) = 1886.1 $[M+H]^+$; 943.7 $[M+2H]^{2+}$; 629.5 $[M+3H]^{3+}$; 472.5 $[M+4H]^{4+}$.

General procedure for click reaction of Ubi$_{29-41}$ with the compounds 17, 18 and 19, to get final compounds 20, 21 and 22, respectively, and their characterization.

Note: representative procedure is referred to 50 µmol of starting compound used; the actual amounts of starting compounds used in the reactions are reported below.

Compounds **17**, **18** and **19** were individually dissolved in 200 mM MOMPS buffer solution at pH. 7.00 (4.75 mL) and, to each of them, Ubi$_{29-41}$ (115.09 mg, 60 µmol) was added.

To this, THPTA 200 µM (100 µL), Na-ascorbate 2 mM (100 µL) and $CuSO_4$ 100 µM (50 µL) were sequentially added and the mixture stirred at room temperature for 2h, under inert atmosphere.

After, the final products were purified by preparative HPLC using the following gradient method: 10-55% solvent B over 60 min at flow rate of 20.00 mL/min (solvent A: 0.1% TFA in water; solvent B: 0.1% TFA in ACN).

The fractions containing the product, as TFA salt, were combined and lyophilized. The pure final peptides (pure >95%) were analyzed by analytical HPLC (see Figure 116 in HPLC analysis data) and LC-MS (see below).

6-Methylheptanoyl-Dab-Thr-Dab-cyclo[Dab-Dab-DLeu-Leu-Dab-Dab(Ubi$_{29-41}$-βAla-Lys(1,2,3 triazol-butane-Bpa-Met(O_2)-Oic-Abu))-Thr], 20

Starting from deprotected cyclic peptide **17** (3.77 mg, 2.00 µmol) and following the general procedure, final peptide **20** was obtained in 54% yield (5.44 mg, 1.07 µmol) as white solid.

For the calculation of mole-based amounts of the peptide, eleven counter ions of trifluoroacetic acid (MW: 114) were taken into account (seven for each basic amino acid side chain and the free N-terminus of Ubi$_{29-41}$ and four for each of the amino side chain of colistin). MW: 5057.58.

Analytical HPLC gradient method: 0-95% solvent B over 23 min at flow rate of 0.700 mL/min (solvent A: 0.1% TFA in water; solvent B: 0.1% TFA in ACN). Major peak with retention time (t_R) 10.23 min, by UV 220 nm (Figure 116a).

Expected mass: 3801.11. **ESI-MS** found: (m/z) = 1268.6 $[M+3H]^{3+}$; 951.7 $[M+4H]^{4+}$; 761.5 $[M+5H]^{5+}$; 634.8 $[M+6H]^{6+}$; 544.2 $[M+7H]^{7+}$; 476.3 $[M+8H]^{8+}$; 423.5 $[M+9H]^{9+}$..

6-Methylheptanoyl-Dab-Thr-Dab-cyclo[Dab-Dab-DLeu-Leu-Dab(Ubi$_{29-41}$-βAla-Lys(1,2,3 triazol-butane-Bpa-Met(O$_2$)-Oic-Abu))-Dab-Thr], 21

Starting from deprotected cyclic peptide **18** (4.50 mg, 2.39 μmol) and following the general procedure, final peptide **21** was obtained in 57% yield (6.89 mg, 1.36 μmol) as white solid. For the calculation of mole-based amounts of the peptide, 11 counter ions of trifluoroacetic acid (MW: 114) were taken into account (seven for each basic amino acid side chain and the free N-terminus of Ubi$_{29-41}$ and four for each of the amino side chain of colistin). MW: 5057.58.

Analytical HPLC gradient method: 0-95% solvent B over 23 min at flow rate of 0.700 mL/min (solvent A: 0.1% TFA in water; solvent B: 0.1% TFA in ACN). Major peak, with retention time (t_R) 10.55 min, by UV 220 nm (Figure 116b); Expected mass: 3801.11. **ESI-MS** found: (m/z) = 1268.6 $[M+3H]^{3+}$; 951.7 $[M+4H]^{4+}$; 761.5 $[M+5H]^{5+}$; 634.8 $[M+6H]^{6+}$; 544.2 $[M+7H]^{7+}$; 476.3 $[M+8H]^{8+}$; 423.5 $[M+9H]^{9+}$.

6-Methylheptanoyl-Dab-Thr-Dab-cyclo[Dab-Dab(Ubi$_{29-41}$-βAla-Lys(1,2,3 triazol-butane-Bpa-Met(O$_2$)-Oic-Abu))-DLeu-Leu-Dab-Dab-Thr], 22

Starting from deprotected cyclic peptide **19** (3.80 mg, 2.01 μmol) and following the general procedure, final peptide **22** was obtained in 49% yield (4.96 mg, 0.98 μmol) as white solid. For the calculation of mole-based amounts of the peptide, 11 counter ions of trifluoroacetic acid (MW: 114) were taken into account (seven for each basic amino acid side chain and the free N-terminus of Ubi$_{29-41}$ and four for each of the amino side chain of colistin). MW: 5057.58.

Analytical HPLC gradient method: 0-95% solvent B over 23 min at flow rate of 0.700 mL/min (solvent A: 0.1% TFA in water; solvent B: 0.1% TFA in ACN). Major peak with retention time (t_R) 10.43 min, by UV 220 nm (Figure 116c); Expected mass: 3801.11. **ESI-MS** found: (m/z) = 1268.6 $[M+3H]^{3+}$; 951.7 $[M+4H]^{4+}$; 761.5 $[M+5H]^{5+}$; 634.8 $[M+6H]^{6+}$; 544.2 $[M+7H]^{7+}$; 476.3 $[M+8H]^{8+}$; 423.5 $[M+9H]^{9+}$.

Fmoc-Dab(Dde)-2-CTC Resin, 23

2-CTC resin of loading 1.55 mmol/g (1.0 g, 1.55 mmol) was suspended in anhydrous DCM (5 mL), after a previous sequentially washing with the same solvent (3 x 5 mL), in a 10 mL polypropylene syringe fitted with a polyethylene disc.
Fmoc-Dab(Dde)-OH (1.175 g, 2.33 mmol) and DIPEA (1.62 mL, 9.32 mmol) were added to this suspension and the mixture was gently stirred at RT for 2h.
After coupling, the resin was sequentially washed with DCM (3 x 3 mL), DMF (3 x 3 mL) and lastly with DCM again (3 x 3 mL) and allowed to dry overnight.
The Fmoc of small amount of the product resin was cleaved by a freshly made 20% piperidine in DMF (v/v), in order to determine the loading level of the resin which was calculated to be 0.277 mmol/g, via standard UV absorption method (Pharmacia Ultrospec 2100 pro UV/Vis spectrometer, wavelength 301 nm, molar extinction coefficient 7.800).

6-Methylheptanoyl-Dab(Boc)-Thr(tBu)-Dab(Dde)-2-CTC Resin, 24

Fmoc-Dab(Dde)-2-CTC resin (180.5 mg, 50 μmol) was washed with DMF (3 x 2 mL) in a 5 mL polypropylene syringe fitted with a polyethylene disc; the solvent was removed by filtration.
Then, following the general coupling procedure, the proper residues were coupled as follows: Fmoc-Thr(tBu)-OH (99.4 mg, 250 μmol); Fmoc-Dab(Boc)-OH (110.1 mg, 250 μmol); 6-Methylheptanoic acid (36.0 mg, 250 μmol).

6-Methylheptanoyl-Dab(Boc)-Thr(tBu)-Dab(4-pentynoyl-Bpa-Met(O_2)-Oic-Abu)-OH, 25

Step 1: Cleavage of Dde. To the product resin **24**, previously obtained, was added 2% hydrazine in DMF (2 mL).
The mixture was stirred at RT for 1h 30’ for 3 times, filtering and washing with DMF in between.
Lastly, the product resin so obtained, was washed with DMF.

Step2: According to the general coupling procedure the suitable residues were coupled, at the γ-amine of Dab at N-terminal of the resin product, as follows: Fmoc-Abu-OH (81.3 mg, 250 μmol); Fmoc-Oic-OH (97.9 mg, 250 μmol); Fmoc-Met(O_2)-OH (100.9 mg, 250 μmol).

Step 3: to 6-Methylheptanoyl-Dab(Boc)-Thr(tBu)-Dab(Fmoc-Met(O_2)-Oic-Abu)-2-CTC resin, obtained from step 2, 20% piperidine in DMF (3 mL) was added and allowed to react at RT for 10 min.

Then, the solution was filtered and the solid was washed with DMF (5 x 3 mL).

Fmoc-Bpa-OH (122.9 mg, 250 µmol) and HATU (95.0 mg, 250 µmol) were dissolved in DMF (1 mL) and, to this, DIPEA (87.1 µL, 500 µmol) was added. The activated aminoacid mixture was then added to 6-Methylheptanoyl-Dab(Boc)-Thr(tBu)-Dab(H-Met(O_2)-Oic-Abu)-2-CTC resin and allowed to react at RT for 1h, gently stirred; this coupling was repeated twice, filtering and washing with DMF (2 x 3 mL) in between.

Finally, the solution was as usual filtered and washed with DMF (8 x 3 mL).

Step 4: To 6-Methylheptanoyl-Dab(Boc)-Thr(tBu)-Dab(Fmoc-Bpa-Met(O_2)-Oic-Abu)-2-CTC resin, obtained from step 3, 4-pentynoic-OH (24.5 mg, 250 µmol) was coupled according the general coupling procedure.

Step 5: Cleavage from the resin.

The product resin, obtained from step 4, was then treated with 1,1,1,3,3,3-Hexafluoruro-2-propanol: DCM in a ratio 1:4 (40 mL x 1h for each product resin) and the filtrate was collected, solvents evaporated under vacuum, resuspended in Dioxane and lyophilized, to have the compound **25**, which was used in the next step without any further purification.

The crude product obtained was analyzed by analytical HPLC (see Figure 117 in HPLC analysis data) and LC-MS. The gradient method used for HPLC was: 0-95% solvent B over 23 min at flow rate of 0.700 mL/min (solvent A: 0.1% TFA in water; solvent B: 0.1% TFA in ACN). The major peak, corresponding to the compound **25**, was found to have a retention time (t_R) 15.73 min, by UV 220 nm (Figure 117); **ESI-MS**: (m/z)= 1332.7 $[M+H]^+$; 1354.7 $[M+Na]^+$.

Fmoc-Dab(Boc)-2-CTC Resin, 26

2-CTC resin of loading 1.55 mmol/g (1.0 g, 1.55 mmol) was suspended in anhydrous DCM (5 mL), after a previous sequentially washing with the same solvent (3 x 5 mL), in a 10 mL polypropylene syringe fitted with a polyethylene disc.

Fmoc-Dab(Boc)-OH (1.03 g, 2.33 mmol) and DIPEA (1.62 mL, 9.32 mmol) were added to this suspension and the mixture was gently stirred at RT for 2h.

After coupling, the resin was sequentially washed with DCM (3 x 3 mL), DMF (3 x 3 mL) and lastly with DCM again (3 x 3 mL) and allowed to dry overnight.

The Fmoc of small amount of the product resin was cleaved by a freshly made 20% piperidine in DMF (v/v), in order to determine the loading level of the resin which was calculated to be 0.268 mmol/g, via standard UV absorption method (Pharmacia Ultrospec 2100 pro UV/Vis spectrometer, wavelength 301 nm, molar extinction coefficient 7.800).

Dde-Dab(Fmoc)-Thr(tBu)-Dab(Boc)-2-CTC Resin, 27

Fmoc-Dab(Boc)-2-CTC resin (186.6 mg, 50 μmol) was washed with DMF (3 x 2 mL) in a 5 mL polypropylene syringe fitted with a polyethylene disc; the solvent was removed by filtration.
Then, according the general coupling procedure, the suitable residues were coupled as follows: Fmoc-Thr(tBu)-OH (99.4 mg, 250 μmol); Dde-Dab(Boc)-OH (126.1 mg, 250 μmol).

Dde-Dab(4-pentynoyl-Bpa-Met(O_2)-Oic-Abu)-Thr(tBu)-Dab(Boc)-2-CTC Resin, 28

Step 1: to Dde-Dab(Fmoc)-Thr(tBu)-Dab(Boc)-2-CTC resin, previously obtained, according to the general coupling procedure, the proper residues were coupled, at the γ-amine of Dab at N-terminal of the resin product, as follows: Fmoc-Abu-OH (81.3 mg, 250 μmol); Fmoc-Oic-OH (97.9 mg, 250 μmol); Fmoc-Met(O_2)-OH (100.9 mg, 250 μmol).

Step 2: to Dde-Dab(Fmoc-Met(O_2)-Oic-Abu)-Thr(tBu)-Dab(Boc)-2-CTC resin, obtained from step 1, 20% piperidine in DMF (3 mL) was added and allowed to react at RT for 10 min.
Then, the solution was filtered and the solid was washed with DMF (5 x 3 mL).
Fmoc-Bpa-OH (122.9 mg, 250 μmol) and HATU (95.0 mg, 250 μmol) were dissolved in DMF (1 mL) and, to this, DIPEA (87.1 μL, 500 μmol) was added. The activated aminoacid mixture was then added to Dde-Dab(H-Met(O_2)-Oic-Abu)-Thr(tBu)-Dab(Boc)-2-CTC resin and allowed to react at RT for 1h, gently stirred; this coupling was repeated twice, filtering and washing with DMF (2 x 3 mL) in between.
Finally, the solution was as usual filtered and washed with DMF (8 x 3 mL).

Step 3: To Dde-Dab(Fmoc-Bpa-Met(O_2)-Oic-Abu)-Thr(tBu)-Dab(Boc)-2-CTC resin, obtained from step 2, 4-pentynoic-OH (24.5 mg, 250 μmol) was coupled according the general coupling procedure.

7-Methylheptan-Dab(4-pentynoyl-Bpa-Met(O_2)-Oic-Abu)-Thr(tBu)-Dab(Boc)-OH, 29

Step 1: Cleavage of Dde.

To the product resin **28**, previously obtained, was added 2% hydrazine in DMF (2 mL). The mixture was stirred at RT for 1h 30' for 3 times, filtering and washing with DMF in between. Lastly, the product resin so obtained, H-Dab(4-pentynoyl-Bpa-Met(O_2)-Oic-Abu)-Thr(tBu)-Dab(Boc)-2-CTC resin, was washed with DMF (5 x 3 mL).

Step 2: 6-Methylheptanoyloic acid (36.0 mg, 250 μmol) was coupled following the general coupling procedure.

Step 3: Cleavage from the resin.
The product resin, obtained from step 4, was then treated with 1,1,1,3,3,3-hexafluoruo-2-propanol: DCM in a ratio 1:4 (40 mL x 1h for each product resin) and the filtrate was collected, solvents evaporated under vacuum, resuspended in dioxane and lyophilized, to have the compound **29**, which was used in the next step without any further purification.
The crude product obtained was analyzed by analytical HPLC (see Figure 118 in HPLC analysis data) and LC-MS. The gradient method used for HPLC was: 0-95% solvent B over 23 min at flow rate of 0.700 mL/min (solvent A: 0.1% TFA in water; solvent B: 0.1% TFA in ACN). The major peak, corresponding to the compound **29**, was found to have a retention time (t_R) 15.55 min, by UV 220 nm (Figure 118); Expected mass: 1331.71. **ESI-MS** (found): (m/z) = 1332.7 $[M+H]^+$; 1354.7 $[M+Na]^+$.

Fmoc-Dab(Dde)-Dab(Boc)-DLeu-Leu-Dab(Boc)-Dab(Boc)-Thr(tBu)-2-CTC Resin, 30

Step 1: Fmoc-Thr(tBu)-2-CTC resin (126.3 mg, 50 μmol), **2**, was washed with DMF (3 x 2 mL) in a 5 mL polypropylene syringe fitted with a polyethylene disc; the solvent was removed by filtration.
Then, following the general coupling procedure, the proper residue was coupled as follows: Fmoc-Dab(Boc)-OH (110.1 mg, 250 μmol); Fmoc-Dab(Boc)-OH (110.1 mg, 250 μmol); Fmoc-Leu-OH (88.4 mg, 250 μmol); Fmoc-D-Leu-OH (88.4 mg, 250 μmol); Fmoc-Dab(Dde)-OH (126.1 mg, 250 μmol).
The resulting product **30** was cleaved from a small amount of resin (1 mg), by a solution of 1,1,1,3,3,3-Hexafluoruro-2-propanol: DCM in a ratio 1:4, in order to analyze it via analytical HPLC (see Figure 119 in HPLC analysis data).
Gradient method: 0-95% solvent B over 23 min at flow rate of 0.700 mL/min (solvent A: 0.1% TFA in water; solvent B: 0.1% TFA in ACN). Major peak with retention time (t_R) 17.91 min,

by UV 220 nm, (Figure 119). Expected mass: 1487.85. **ESI-MS** (found): (m/z) = 1488.9 $[M+H]^+$; 744.9 $[M+2H]^{2+}$.

Fmoc-Dab(NH_2)-Dab(Boc)-DLeu-Leu-Dab(Boc)-Dab(Boc)-Thr(tBu)-OH, 31

Step 1: Cleavage of Dde. To the product resin, previously obtained (compound **30**), a solution of hydroxylamine*HCl in presence of imidazole as base in DCM: NMP (1:5) was added. The mixture was stirred for 1h 30' and repeated for three times, washing with NMP in between. Lastly, the product resin was washed with DMF (3 x 5 mL).

Step 2: Cleavage from the resin. The product resin, obtained from step 1, was then treated with 1,1,1,3,3,3-Hexafluoruro-2-propanol: DCM in a ratio 1:4 (40 mL x 1h) and the filtrate was collected, solvents evaporated under vacuum, resuspended in Dioxane and lyophilized, to have the compound **31**, which was used in the next step without any further purification.
The crude product obtained was analyzed by analytical HPLC (see Figure 120 in HPLC analysis data) and LC-MS. The gradient method used for HPLC was: 0-95% solvent B over 23 min at flow rate of 0.700 mL/min (solvent A: 0.1% TFA in water; solvent B: 0.1% TFA in ACN). The major peak, corresponding to the compound **31**, was found to have a retention time (t_R) 15.41 min, by UV 220 nm (Figure 120). Expected mass: 1323.77. **ESI-MS** (found): (m/z) = 1324.8 $[M+H]^+$; 662.9 $[M+2H]^{2+}$.

H-cyclo[Dab-Dab(Boc)-DLeu-Leu-Dab(Boc)-Dab(Boc)-Thr(tBu)], 32

Step 1: Crude compound **31** (50.8 mg, assuming 38.37 μmol) was dissolved in dry DMF: DCM in a ratio 1: 50 (0.9 mL: 49.1 mL) to make up a solution of the cleaved linear peptide in 0.8 μmol/mL concentration.
To the mixture, PyBOP (39.9 mg, 76.74 μmol), HOBt (10.4 mg, 76.74 μmol) and DIPEA (26.7 μL, 153.48 μmol) were sequentially added under inert atmosphere and the reaction was stirred at RT overnight, to give the derivate cyclic peptide.
Then, DCM was evaporated under vacuum using a bath temperature not high than 30°C.

Step 2: To Fmoc-cyclo[Dab-Dab(Boc)-DLeu-Leu-Dab(Boc)-Dab(Boc)-Thr(tBu)] in DMF residue, obtained from step 1, 10% piperidine in DMF (2 mL) was added. The mixture was stirred at RT for 1h.

After, the product was purified by preparative HPLC using the following gradient method: 30-80% solvent B over 60 min at flow rate of 20.00 mL/min (solvent A: 0.1% TFA in water; solvent B: 0.1% TFA in ACN).

The fractions containing the product, as TFA salt, were combined and lyophilized. 25.4 mg (23.41 μmol) of the pure peptide, compound **32** (purity >95%) was obtained (assuming 61% yield) as a white solid and analyzed by analytical HPLC (see Figure 121 in HPLC analysis data) and LC-MS. Major peak with retention time (t_R) 14.01 min, by UV 220 nm (Figure 121). Expected mass: 1083.69. **ESI-MS** (found): (m/z) = 1084.7 $[M+H]^+$; 2168.5 $[M+H]^+ \times 2$.

General procedure for the coupling reaction of the fragments 25 and 29, respectively with the fragment 32, to get the compounds 33 and 34.

Note: representative procedure is referred to 50 μmol of starting compound used; the actual amounts of starting compounds used in the reactions are reported below.

Crude fragments **25** and **29** were dissolved in anhydrous DMF and then PyBOP (39.0 mg, 75 μmol), HOBt (6.8 mg, 50 μmol) and DIPEA (26.1 μL, 150 μmol) were sequentially added. To this, fragment **32** (66.63 mg, 50 μmol) was slowly added and the mixture was stirred at 0°C for 2h, after adjusting to pH 8, by addition of more DIPEA.

Then, dioxane was added to the mixture and lyophilized.

The crude products were monitored by analytical HPLC (see Figure 122 in HPLC analysis data), using the following gradient method: 0-95% solvent B over 23 min at flow rate of 0.700 mL/min (solvent A: 0.1% TFA in water; solvent B: 0.1% TFA in ACN).

The products obtained were used in the next reaction without any further purification.

6-Methylheptanoyl-Dab(Boc)-Thr(tBu)-Dab(4-pentynoyl-Bpa-Met(O_2)-Oic-Abu)-cyclo[Dab-Dab(Boc)-DLeu-Leu-Dab(Boc)-Dab(Boc)-Thr(tBu)], 33

Starting from crude fragment **27** (13.1 mg, assuming 9.83 μmol) and following the general procedure, 21.2 mg of the compound **33** were obtained as a light yellow solid. Major peak with retention time (t_R) 19.44 min, by UV 220 nm (Figure 122a). Expected mass: 2397.39. **ESI-MS** found: (m/z) = 1200.5 $[M+2H]^{2+}$; 1211.5 $[M+H+Na]^{2+}$; 1222.5 $[M+2Na]^{2+}$.

6-Methylheptanoyl-Dab(4-pentynoyl-Bpa-Met(O_2)-Oic-Abu)-Thr(tBu)-Dab(Boc)-cyclo[Dab-Dab(Boc)-DLeu-Leu-Dab(Boc)-Dab(Boc)-Thr(tBu)], 34

Starting from crude fragment **29** (15.0 mg, assuming 11.26 μmol) and following the general procedure, 24.8 mg of the compound **34** were obtained as a light yellow solid. Major peak with retention time (t_R) 19.81 min, by UV 220 nm (Figure 122b). Expected mass: 2397.39. **ESI-MS** found: (m/z) = 1200.5 $[M+2H]^{2+}$; 1211.5 $[M+H+Na]^{2+}$; 1222.5 $[M+2Na]^{2+}$.

General procedure for global deprotection of the compounds 33 and 34, to get the compounds 35 and 36, respectively, and their characterization.

Note: representative procedure is referred to 50 μmol of starting compound used; the actual amounts of starting compounds used in the reactions are reported below.

Crude compounds **33** and **34** were individually dissolved in dry DCM (20 mL) and then TFA (2.5 mL) was added. The reactions were stirred at room temperature for 90 min. All the volatile species were removed under vacuum using water bath temperature not over than 30 °C. Next, cold diethyl ether was added to precipitate the peptide as light-yellow solid at the bottom and, the supernatant was then removed after centrifugation.
The crude peptide, dissolved in water, was then purified by preparative HPLC using the following gradient method: 10-55% solvent B over 60 min at flow rate of 20.00 mL/min (solvent A: 0.1% TFA in water; solvent B: 0.1% TFA in ACN).
The fractions containing the product, as TFA salt, were combined and lyophilized. The pure deprotected cyclic peptides were analyzed by analytical HPLC (see Figure 123 in HPLC analysis data) and LC-MS (see below).

6-Methylheptanoyl-Dab-Thr-Dab(4-pentynoyl-Bpa-Met(O_2)-Oic-Abu)-cyclo[Dab-Dab-DLeu-Leu-Dab-Dab-Thr], 35

Starting from crude compound **33** (21.2 mg, assuming 8.85 μmol) and following the general procedure, 4.01 mg (2.12 μmol) of deprotected peptide **35** were obtained in (assuming 24% yield). Major peak, by UV 220 nm, with retention time (t_R) 11.64 min (see Figure 123a).

Expected mass: 1885.05. **ESI-MS** found: (m/z) = 1886.1 $[M+H]^{+}$; 943.7 $[M+2H]^{2+}$; 629.5 $[M+3H]^{3+}$; 472.5 $[M+4H]^{4+}$.

6-Methylheptanoyl-Dab(4-pentynoyl-Bpa-Met(O_2)-Oic-Abu)-Thr-Dab-cyclo[Dab-Dab-DLeu-Leu-Dab-Dab-Thr], 36

Starting from crude compound **34** (24.8 mg, assuming 10.36 μmol) and following the general procedure for global deprotection, 3.90 mg (2.07 μmol) of deprotected peptide **36** were obtained (assuming 20% yield). Major peak with retention time (t_R) 12.01 min, by UV 220 nm (Figure 123b). Expected mass: 1885.05. **ESI-MS** found: (m/z) = 1886.1 $[M+H]^+$; 943.7 $[M+2H]^{2+}$; 629.5 $[M+3H]^{3+}$; 472.5 $[M+4H]^{4+}$.

General procedure for click reaction of Ubiquicidine with the compounds 17, 18 and 19, to get final compounds 20, 21 and 22, respectively, and their characterization.

Note: representative procedure is referred to 50 μmol of starting compound used; the actual amounts of starting compounds used in the reactions are reported below.

Compounds **35** and **36** were individually dissolved in 200 mM MOMPS buffer solution at pH. 7.00 (4.75 mL) and, to each of them, Ubiquicidine (115.0 mg, 60 μmol) was added.
To this, THPTA 200 μM (100 μL), Na-ascorbate 2 mM (100 μL) and $CuSO_4$ 100 μM (50 μL) were sequentially added and the mixture stirred at room temperature for 2h, under inert atmosphere.
After, the final products were purified by preparative HPLC using the following gradient method: 10-55% solvent B over 60 min at flow rate of 20.00 mL/min (solvent A: 0.1% TFA in water; solvent B: 0.1% TFA in ACN).
The fractions containing the product, as TFA salt, were combined and lyophilized. The pure final peptides (pure >95%) were analyzed by analytical HPLC (see Figure 124 in HPLC analysis data) and LC-MS (see below).

6-Methylheptanoyl-Dab-Thr-Dab(Ubi$_{29-41}$-βAla-Lys(1,2,3 triazol-butane-Bpa-Met(O_2)-Oic-Abu))-cyclo[Dab-Dab-DLeu-Leu-Dab-Dab-Thr], 37

Starting from the pure deprotected compound **35** (4.01 mg, 2.12 μmol) and following the general procedure for the click reaction, the final compound **37** was obtained in 70% yield (5.65 mg, 1.12 μmol) as white solid.
For the calculation of mole-based amounts of the peptide, 11 counter ions of trifluoroacetic acid (MW: 114) were taken into account (seven for each basic amino acid side chain and the free N-terminus of Ubi$_{29-41}$ and four for each of the amino side chain of colistin). MW: 5057.58.

Major peak, with retention time (t_R) 10.24 min, by UV 220 nm (Figure 124a); Expected mass: 3801.11. **ESI-MS** found: (m/z) = 1268.6 $[M+3H]^{3+}$; 951.7 $[M+4H]^{4+}$; 761.5 $[M+5H]^{5+}$; 634.8 $[M+6H]^{6+}$; 544.2 $[M+7H]^{7+}$; 476.3 $[M+8H]^{8+}$; 423.5 $[M+9H]^{9+}$.

6-Methylheptanoyl-Dab(Ubi$_{29-41}$-βAla-Lys(1,2,3 triazol-butane-Bpa-Met(O_2)-Oic-Abu))-Thr-Dab-cyclo[Dab-Dab-DLeu-Leu-Dab-Dab-Thr], 38

Starting from the pure deprotected compound **36** (4.01 mg, 2.12 µmol) and following the general procedure for the click reaction, the final compound **38** was obtained in 68% yield (5.48 mg, 1.08 µmol) as white solid.

For the calculation of mole-based amounts of the peptide, 11 counter ions of trifluoroacetic acid (MW: 114) were taken into account (seven for each basic amino acid side chain and the free N-terminus of Ubi$_{29-41}$ and four for each of the amino side chain of colistin). MW: 5057.58.

Major peak with retention time (t_R) 10.53 min, by UV 220 nm (Figure 124b);

Expected mass: 3801.11. **ESI-MS** found: (m/z) = 1268.6 $[M+3H]^{3+}$; 951.7 $[M+4H]^{4+}$; 761.5 $[M+5H]^{5+}$; 634.8 $[M+6H]^{6+}$; 544.2 $[M+7H]^{7+}$; 476.3 $[M+8H]^{8+}$; 423.5 $[M+9H]^{9+}$.

D-ubiquicidin$_{29-41}$-ßAla-Lys(N_3)-NH_2, 39

The all D-amino acid of peptide Thr-Gly-Arg-Ala-Lys-Arg-Arg-Met-Gln-Tyr-Asn-Arg-Arg-ßAla-Lys(azide)-amide was assembled on a scale of 100 µmole on Rapp S RAM resin (loading 220 µmole/g, Rapp Polymere, Tübingen, Germany) with a Syro Multiple Peptide Synthesizer (MultiSynTech, Witten, Germany). Fmoc chemistry with HCTU/diisopropylethyl amine activation with tenfold excess was employed for the coupling of the amino acids. Coupling time was 1 hour. Side chain protections were as follows: Arg: Pbf, Asn and Gln: Trt, Lys: Boc, Thr and Tyr: tBu. The crude peptide was cleaved from the resin and deprotected by a 3-hour treatment with TFA containing 3% triisopropylsilane and 2% water (10 ml/g resin). After precipitation with t-butylmethyl ether, the resulting crude peptide was purified by preparative HPLC with water/acetonitrile gradients (5-40% acetonitrile) containing 0.1% TFA. The final product was lyophilized from water and characterized by analytical HPLC and LC-MS.

Expected MW: 1916.07; **ESI-MS** found: (m/z) = 639.3 $[M+3H]^{3+}$; 480.2 $[M+4H]^{4+}$; 384,4 $[M+5H]^{5+}$; 320.5 $[M+6H]^{6+}$. For the calculation of mole-based amounts of the peptide, seven counter ions of trifluoroacetic acid (MW: 114) were taken into account (for each basic amino acid side chain and the free N-terminus). Yield: 28.5% (77.2 mg, 28.4 µmol).

3.6.3 General procedure for the antibacterial activity

All tested peptide-colistin constructs were dissolved in sterile water at 1 mM concentration (stock solution). *E. coli* K12 strain was grown overnight in T-Medium broth at 37 °C. The OD_{600} was adjusted to 1.0 (stock solution) and then diluted 1:1000. Stock solution of 2.6 U/mL of elastase in sterile water was diluted 5-times, with T-Medium broth, so getting a final concentration of 0.52 U/mL. In a sterile 96-well, flat-bottom polypropylene microtiter plate (Greiner-bio-one), 187.2 µL of T-Medium broth was added in column 1A-H, while 100 µL of it was added to the rest of the plate. 12.8 µL of each one of tested compounds (from 1 mM stock solution) was added in column 1A-H, getting a concentration of 64 µM and then, serial dilutions for each row (100 µL per well) were proceeded.

3.8 µL from the elastase solution of 0.52 U/mL were added in the rows, where MIC values in presence of elastase were calculated, in order to have a final concentration of 10 mU/mL. The added activities of HNE were obtained according to previous experiments performed at HZI.[164] Finally, 100 µL of diluted bacterial suspension were added into each well. The wells with bacteria alone were used as positive growth control wells. Colistin B alone was used as internal control, starting from 1 mM stock solution in sterile water. The plate was incubated at 37 °C for 20 hours in wet chamber. All tests were performed in triplicate. The calculated MICs (in µM), defined as the lowest concentrations of compounds inhibiting growth, were determined by measuring the absorbance at 600 nm with a Fusion universal microplate analyzer (Perkin-Elmer, MA).

3.7 HPLC analysis data

a

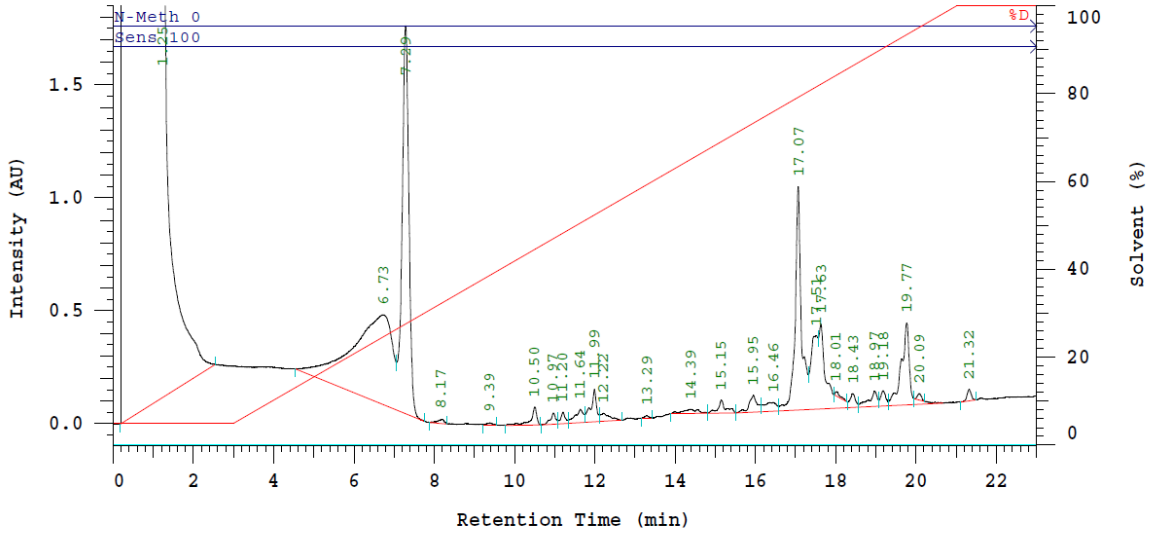

b

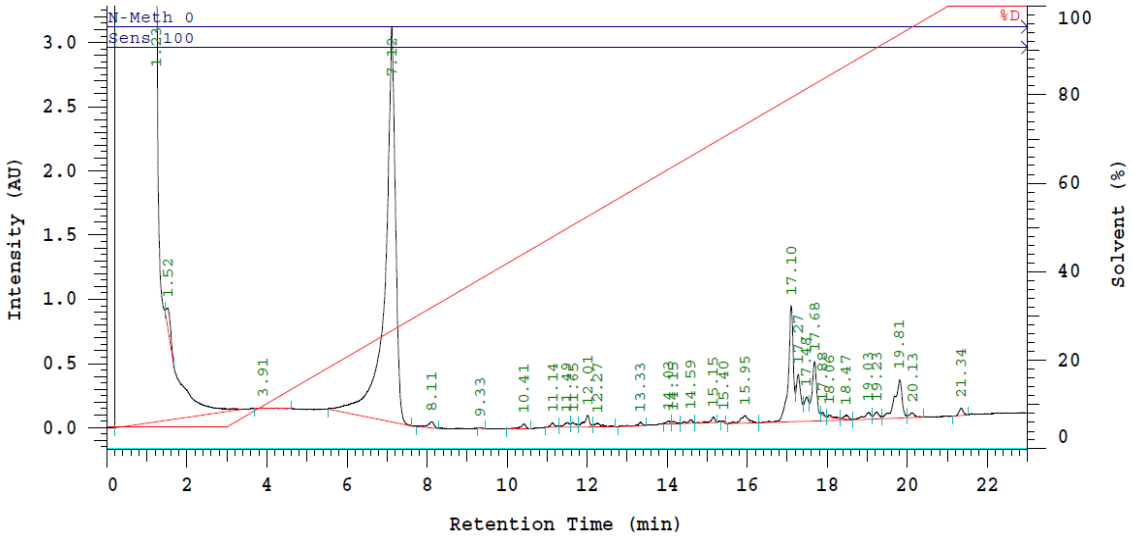
N-Meth 0
Sens 100
%D
Intensity (AU)
Solvent (%)
Retention Time (min)
1.52
3.91
7.12
8.11
9.33
10.41
11.14
11.85
12.27
13.33
14.59
15.15
15.40
15.95
17.10
17.27
17.48
17.68
17.88
18.47
19.03
19.81
20.13
21.34

c

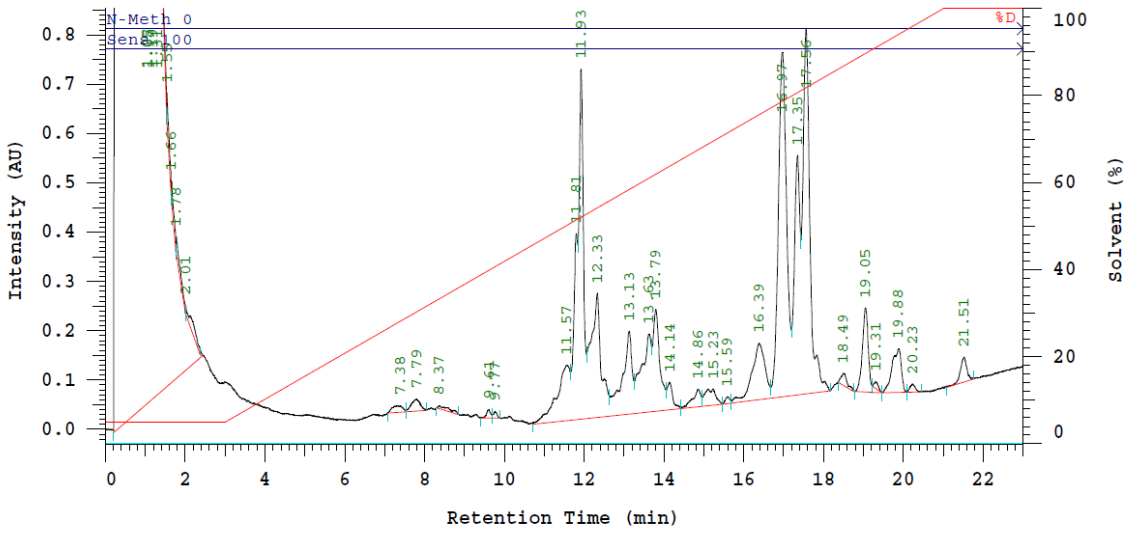
N-Meth 0
Sens 100
%D
Intensity (AU)
Solvent (%)
Retention Time (min)
1.66
1.78
2.01
7.38
7.79
8.37
9.61
9.77
11.57
11.81
11.93
12.33
13.13
13.63
13.79
14.14
14.86
15.23
15.59
16.39
16.97
17.35
17.56
18.49
19.05
19.31
19.88
20.23
21.51

d

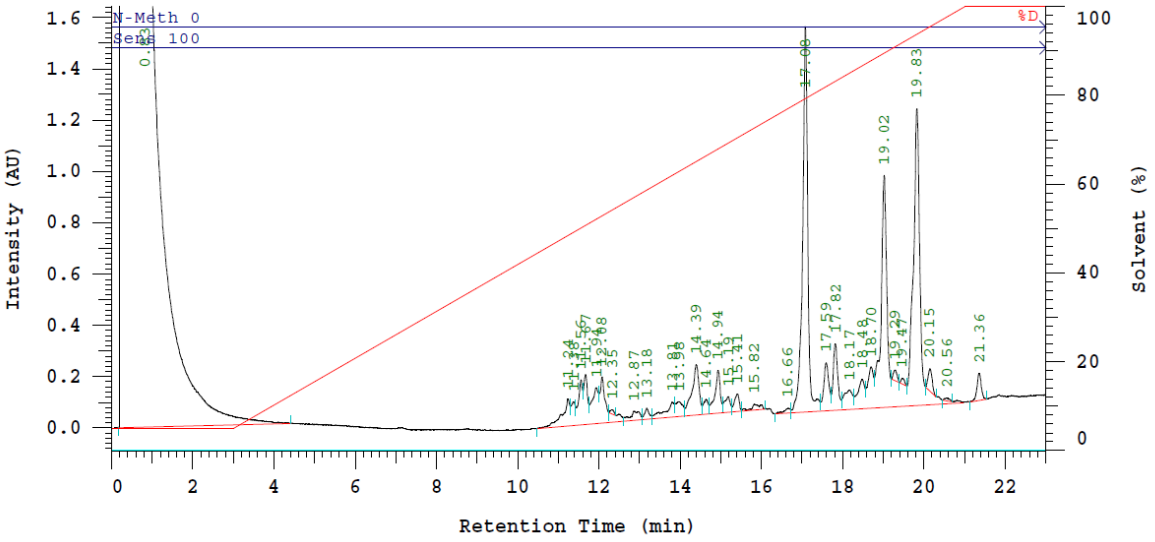

e

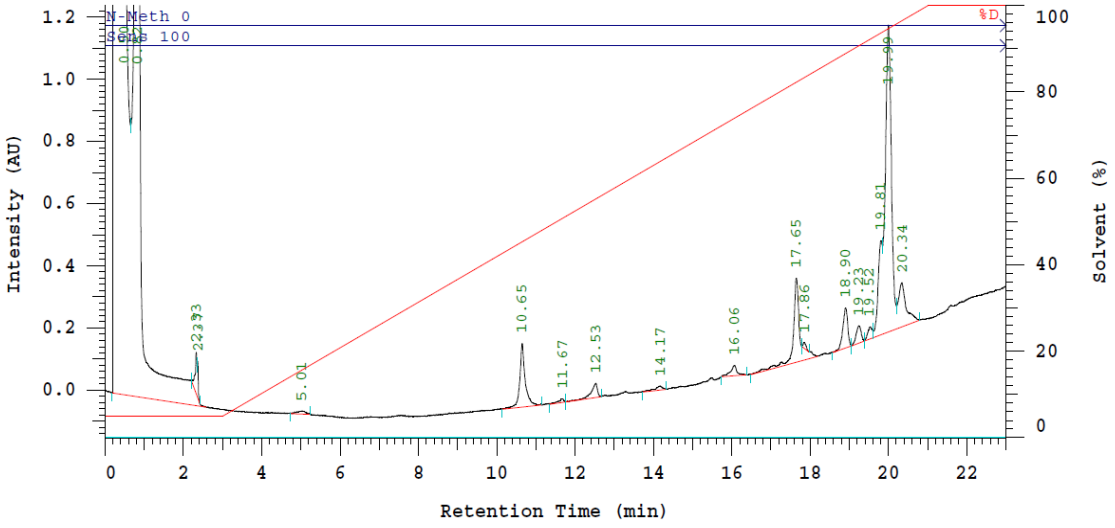

Figure 108. Analytical HPLC spectra for the different experimental conditions exploited for the cyclization reaction of 11.

a

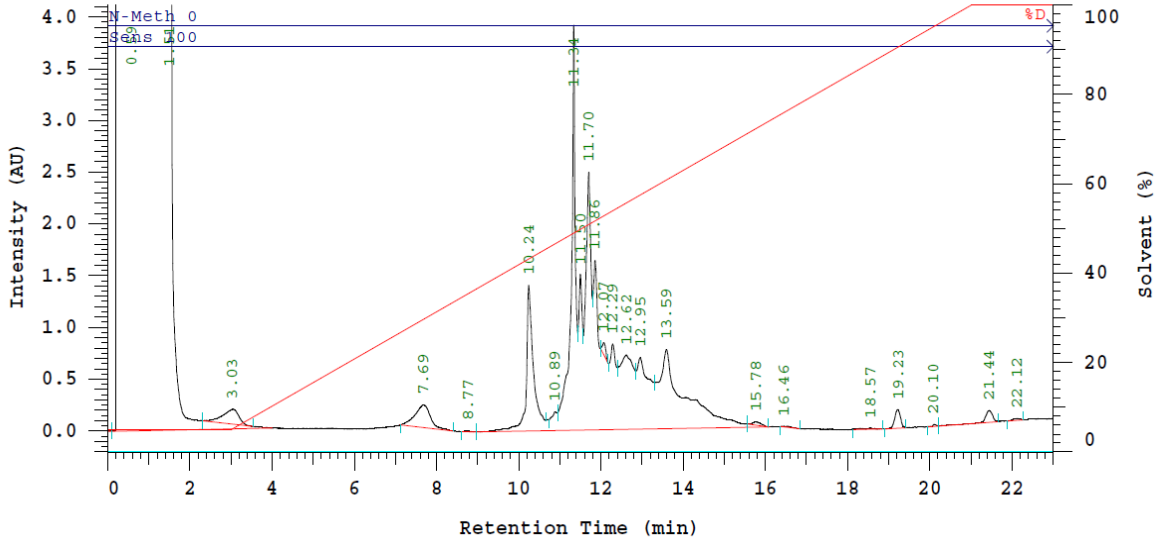
N-Meth 0
Sens 100
%D
Intensity (AU)
Solvent (%)
Retention Time (min)
0.89
1.51
3.03
7.69
8.77
10.24
10.89
11.34
11.70
11.86
12.62
12.95
13.59
15.78
16.46
18.57
19.23
20.10
21.44
22.12

b

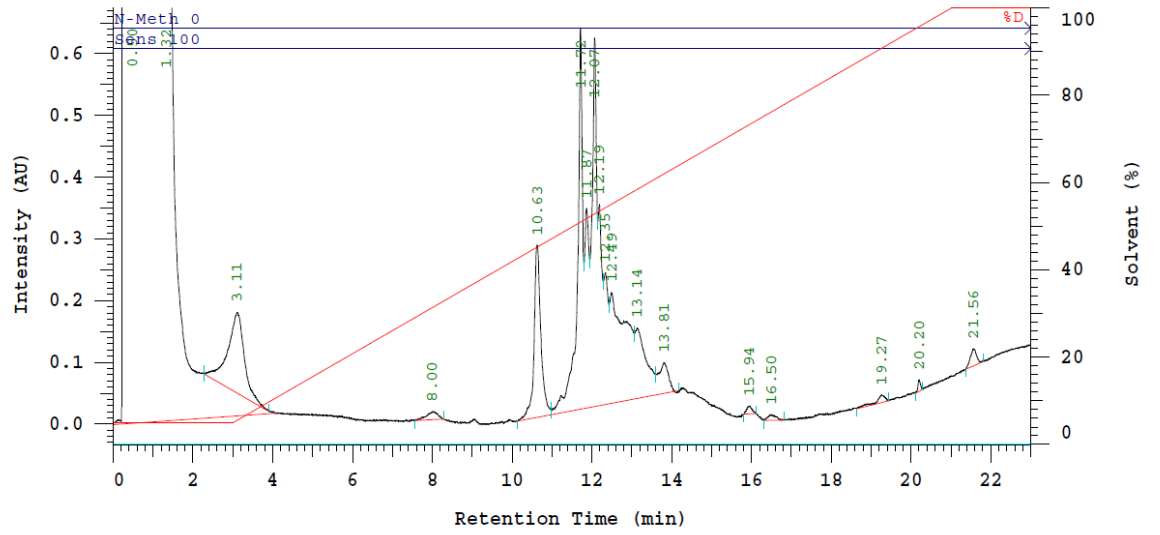
N-Meth 0
Sens 100
%D
Intensity (AU)
Solvent (%)
Retention Time (min)
0.90
1.32
3.11
8.00
10.63
11.78
12.07
12.19
13.14
13.81
15.94
16.50
19.27
20.20
21.56

c

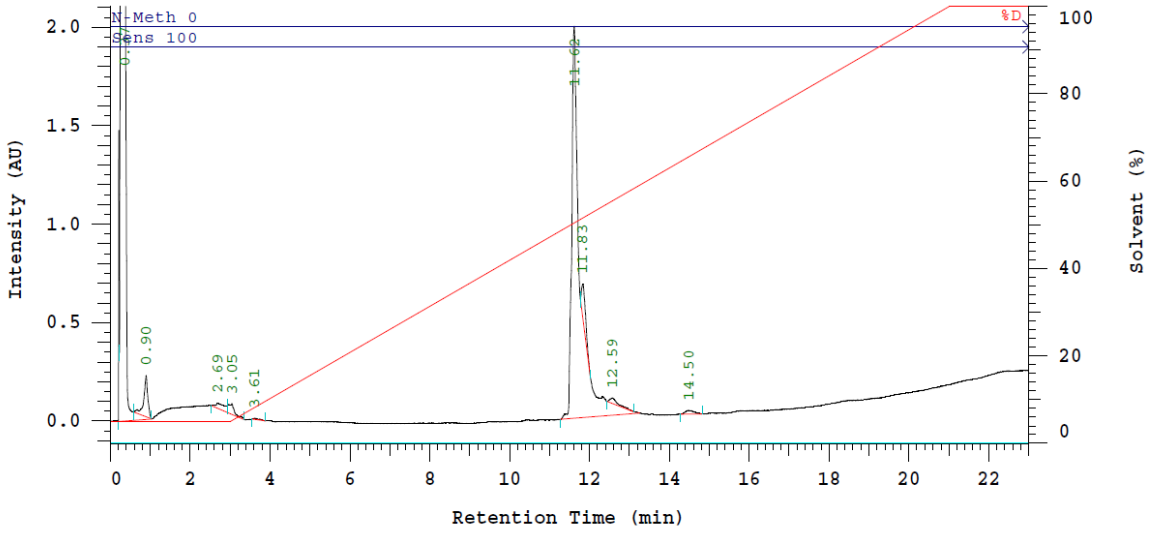
N-Meth 0
Sens 100
%D
Intensity (AU)
Solvent (%)
Retention Time (min)
0.90
2.69
3.05
3.61
11.62
11.83
12.59
14.50

Figure 109. Analytical HPLC spectra of the different experimental conditions tried for the global deprotection of 14.

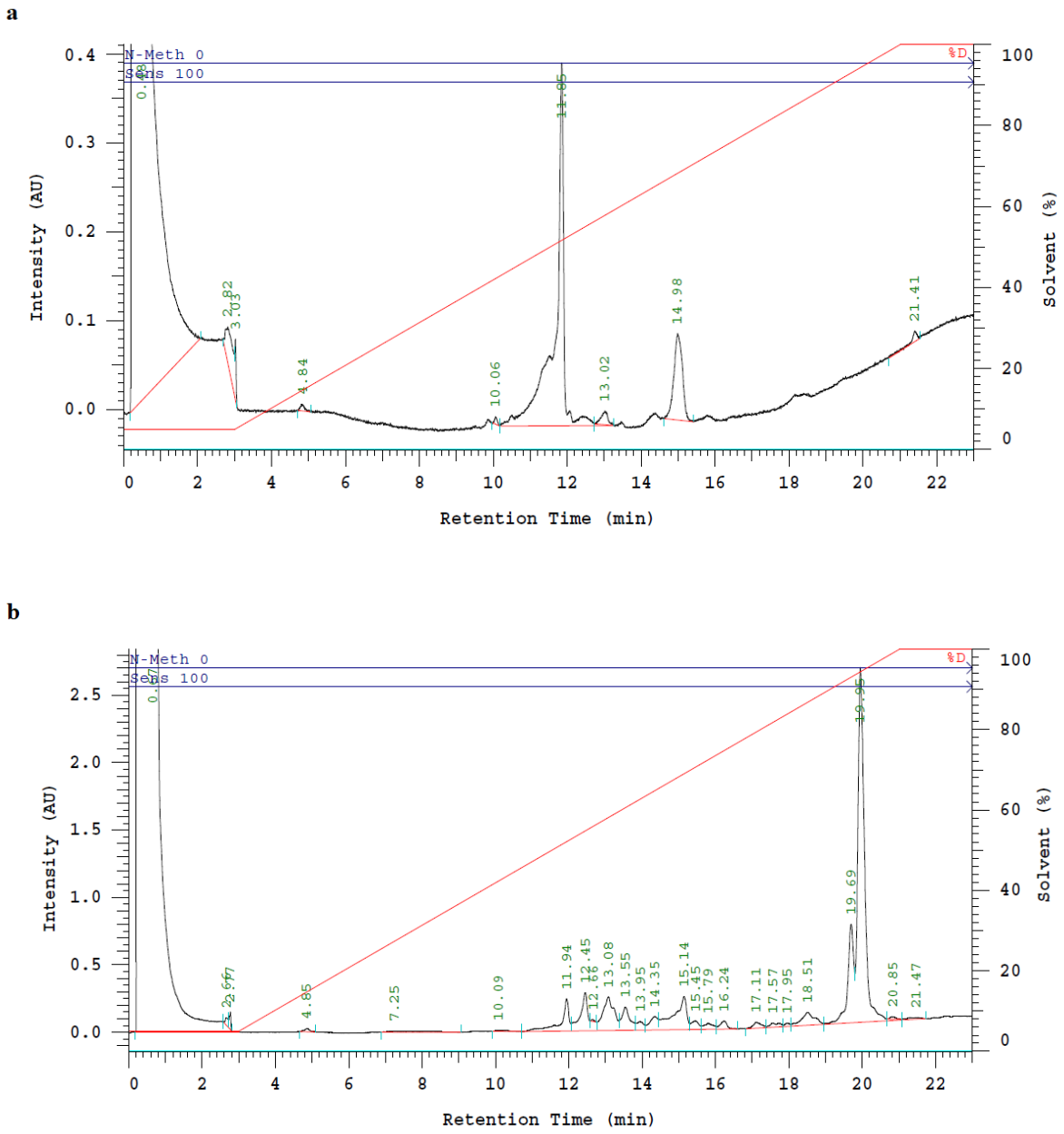

Figure 110. RP-HPLC performed for: (a) H-Dab(4-Pentynoyl-Bpa-Met(O_2)-Oic-Abu)-Thr(tBu)-OH; (b) 6-Methylheptanoyl-Dab(Boc)-Thr(tBu)-Dab(Boc)-Dab(Dde)-Dab(Boc)-DLeu-Leu-Dab(Boc)-Dab(4-Pentynoyl-Bpa-Met(O_2)-Oic-Abu)-Thr(tBu)-2-CTC Resin, 8.

a

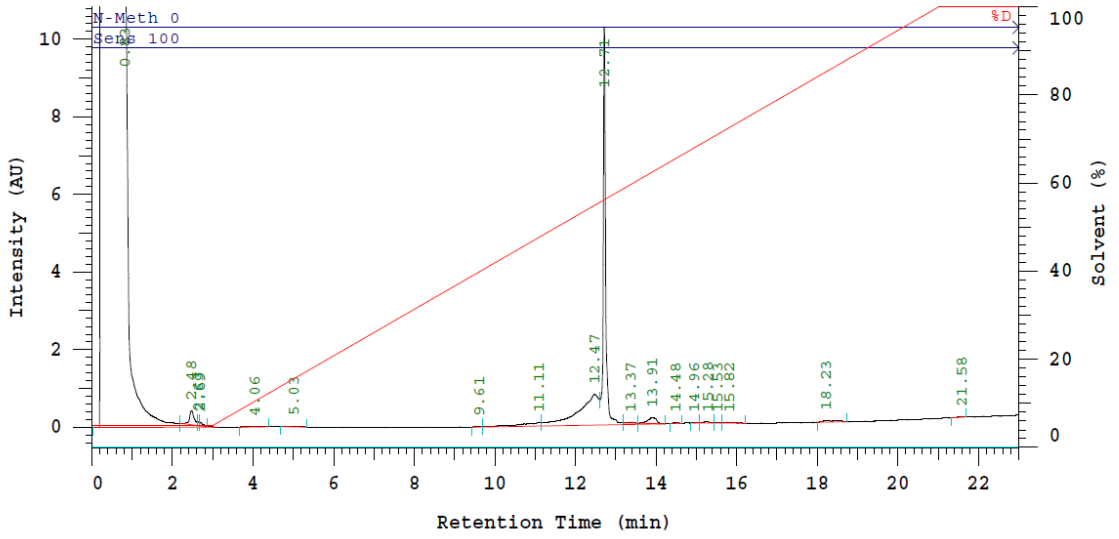

b

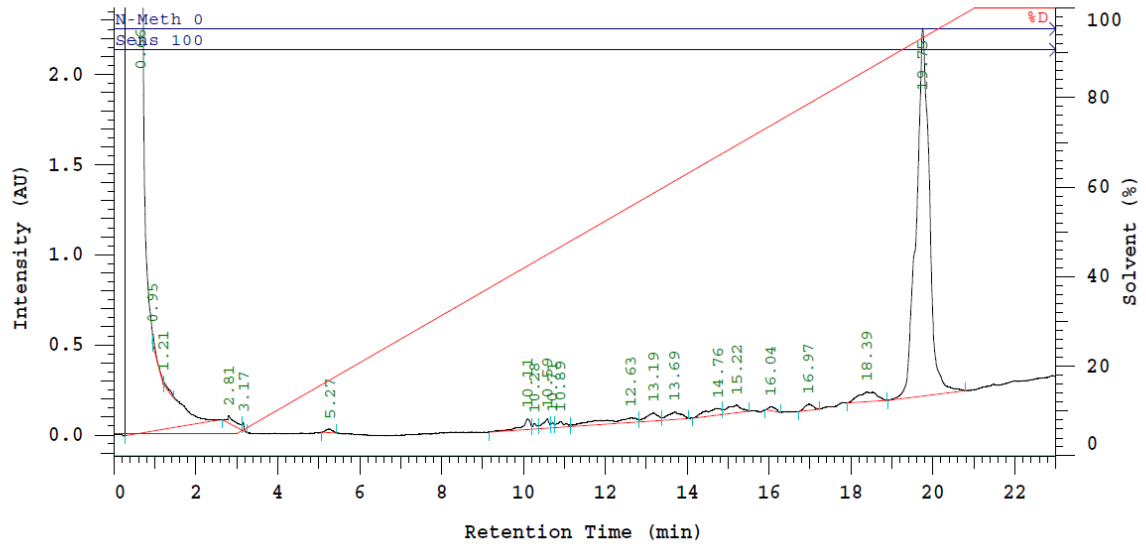

Figure 111. RP-HPLC performed for: (a) H-Dab(4-Pentynoyl-Bpa-Met(O_2)-Oic-Abu)-Dab(Boc)-Thr(tBu)-OH; (b) 6-Methylheptanoyl-Dab(Boc)-Thr(tBu)-Dab(Boc)-Dab(Dde)-Dab(Boc)-DLeu-Leu-Dab(4-Pentynoyl-Bpa-Met(O_2)-Oic-Abu)-Dab(Boc)-Thr(tBu)-2-CTC Resin, 9.

a

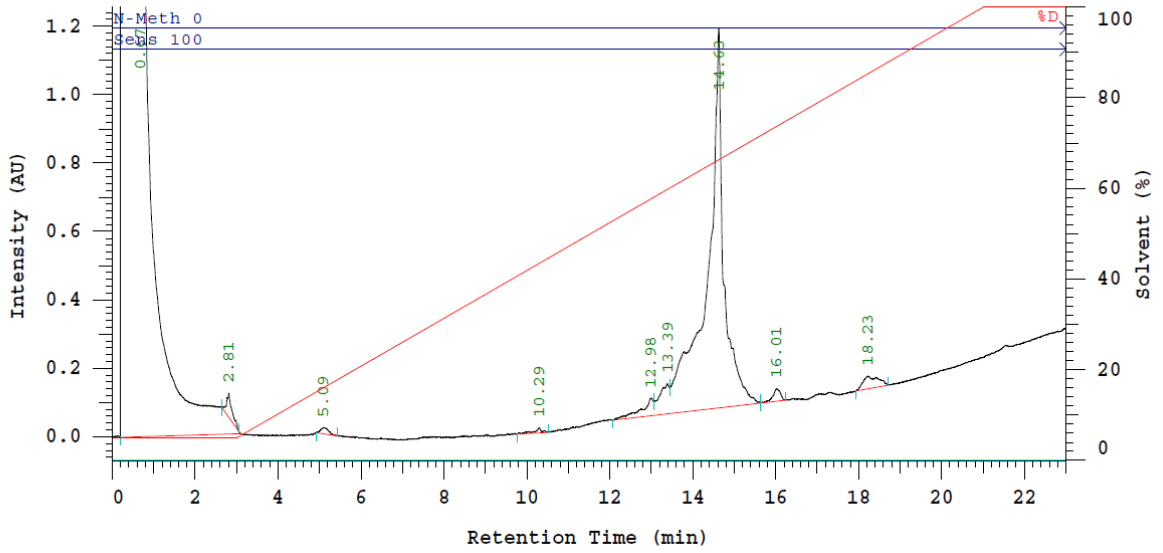

b

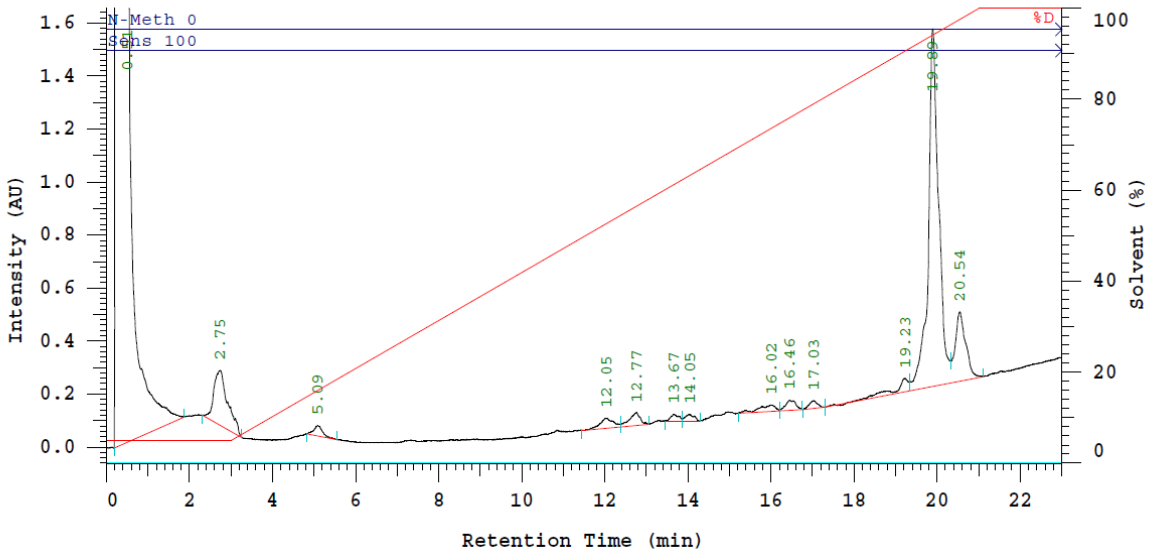

Figure 112. RP-HPLC performed for: (a) H-Dab(4-Pentynoyl-Bpa-Met(O_2)-Oic-Abu)-DLeu-Leu-Dab(Boc)-Dab(Boc)-Thr(tBu)-OH; (b) 6-Methylheptanoyl-Dab(Boc)-Thr(tBu)-Dab(Boc)-Dab(Dde)-Dab(4-Pentynoyl-Bpa-Met(O_2)-Oic-Abu)-DLeu-Leu-Dab(Boc)-Dab(Boc)-Thr(tBu)-2-CTC Resin, 10

a

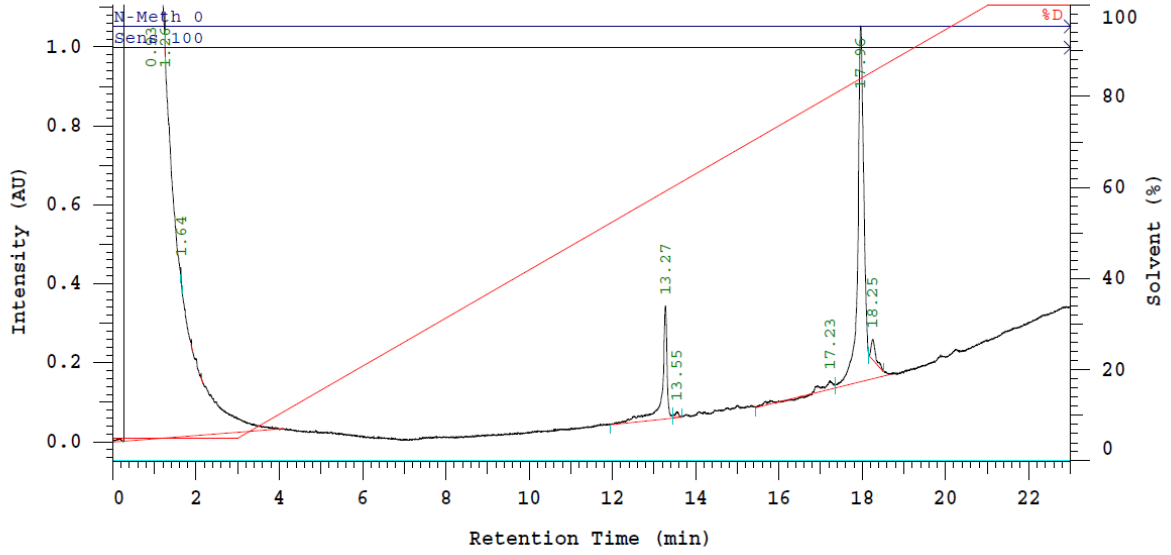
N-Meth 0
Sens 100
%D
Intensity (AU)
Solvent (%)
Retention Time (min)
1.64
13.27
13.55
17.23
17.96
18.25

b

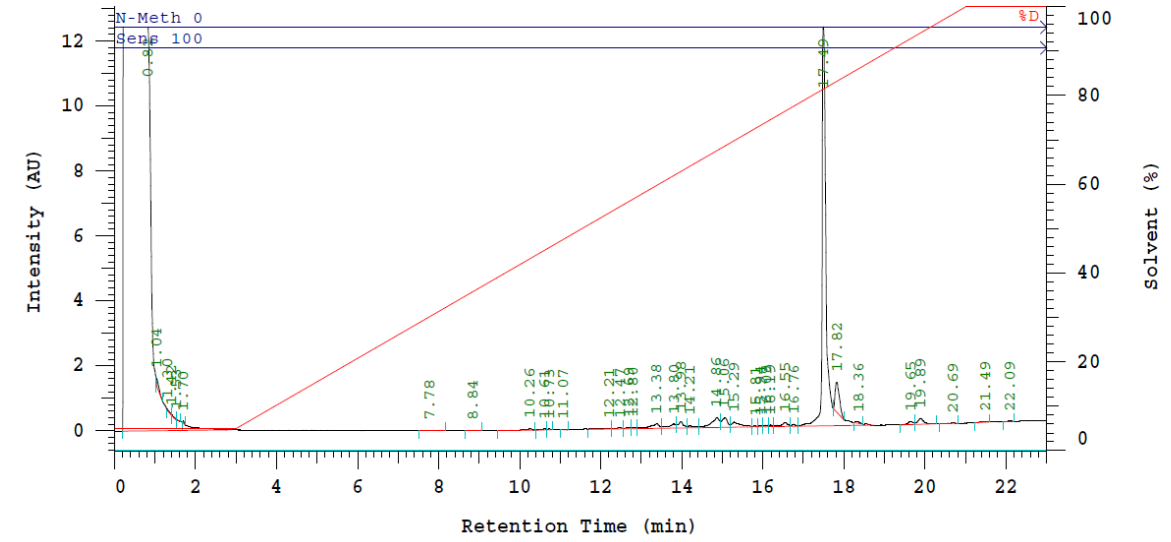
N-Meth 0
Sens 100
%D
Intensity (AU)
Solvent (%)
Retention Time (min)
7.78
8.84
10.26
11.07
13.38
14.21
17.49
17.82
18.36
19.65
19.89
20.69
21.49
22.09

c

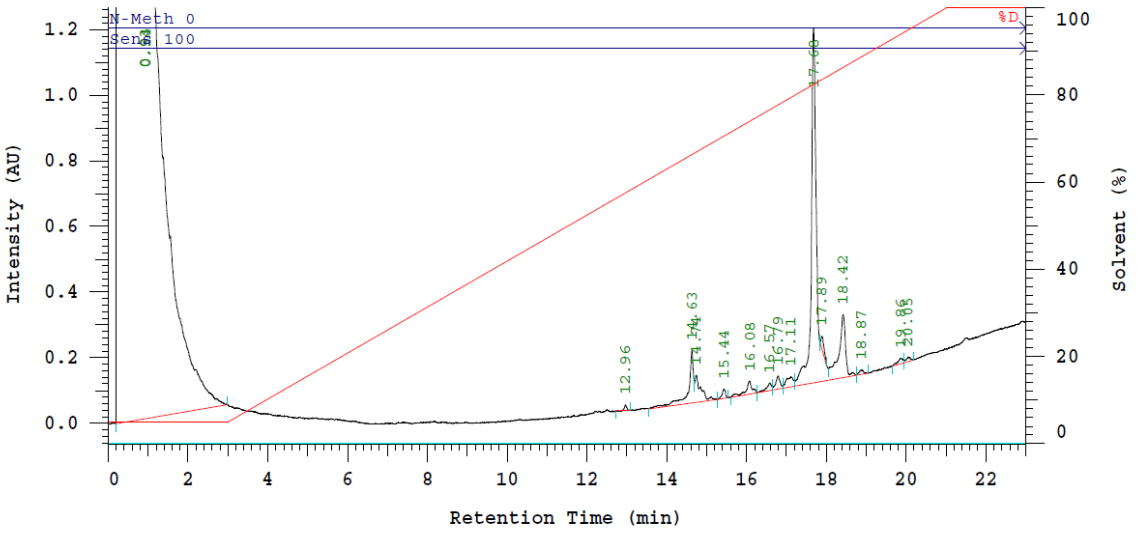

Figure 113. RP-HPLC performed for: (a) 6-Methylheptanoyl-Dab(Boc)-Thr(tBu)-Dab(Boc)-Dab(NH_2)-Dab(Boc)-DLeu-Leu-Dab(Boc)-Dab(4-Pentynoyl-Bpa-Met(O_2)-Oic-Abu)-Thr(tBu)-OH, 11; (b) 6-Methylheptanoyl-Dab(Boc)-Thr(tBu)-Dab(Boc)-Dab(NH_2)-Dab(Boc)-DLeu-Leu-Dab(4-Pentynoyl-Bpa-Met(O_2)-Oic-Abu)-Dab(Boc)-Thr(tBu)-OH, 12; (c) 6-Methylheptanoyl-Dab(Boc)-Thr(tBu)-Dab(Boc)-Dab(NH_2)-Dab(4-Pentynoyl-Bpa-Met(O_2)-Oic-Abu)-DLeu-Leu-Dab(Boc)-Dab(Boc)-Thr(tBu)-OH, 13.

a

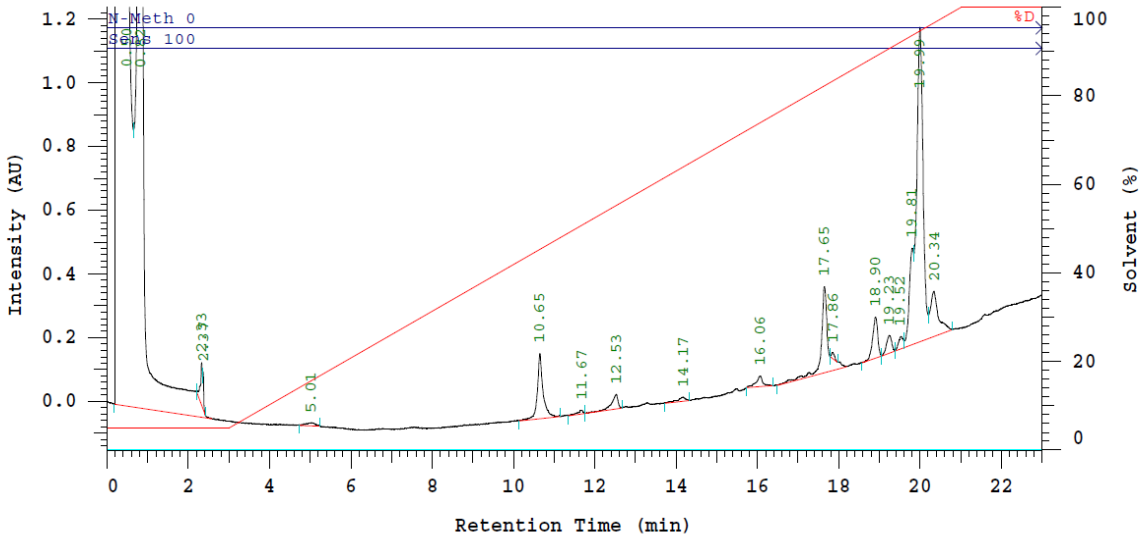

b

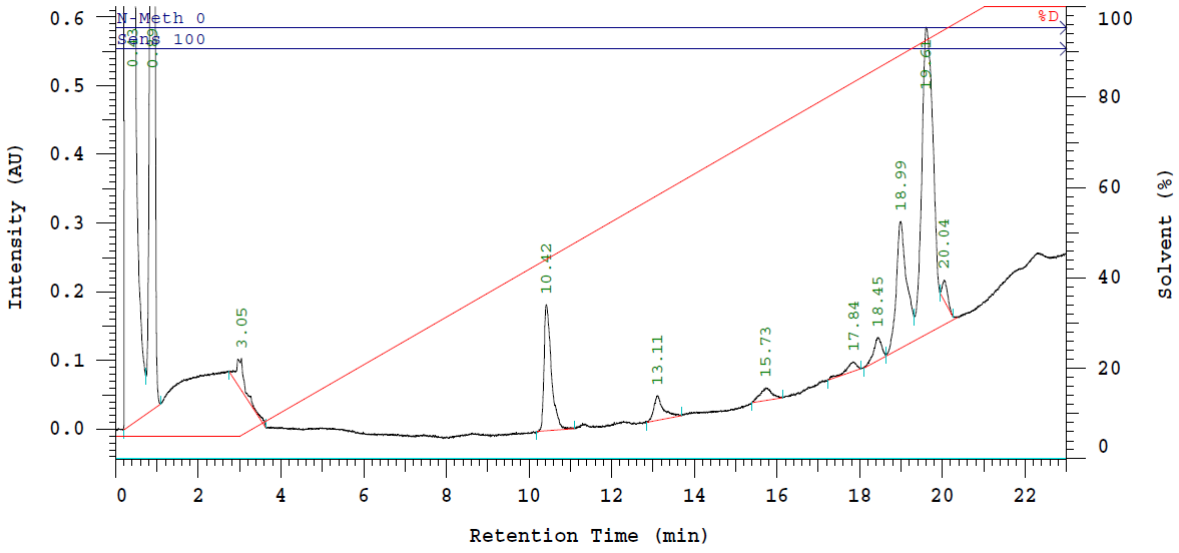

c

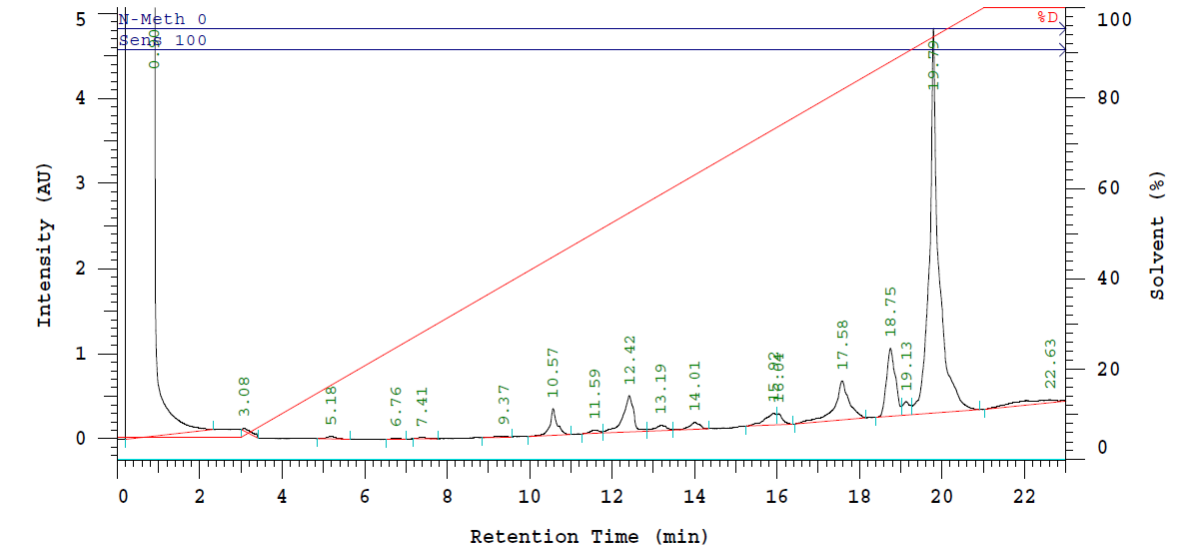

Figure 114. RP-HPLC of the cyclic peptides: (a) 6-Methylheptanoyl-Dab(Boc)-Thr(tBu)-Dab(Boc)-cyclo[Dab-Dab(Boc)-DLeu-Leu-Dab(Boc)-Dab(4-Pentynoyl-Bpa-Met(O_2)-Oic-Abu)-Thr(tBu)], 14; (b) 6-Methylheptanoyl-Dab(Boc)-Thr(tBu)-Dab(Boc)-cyclo[Dab-Dab(Boc)-DLeu-Leu-Dab(4-Pentynoyl-Bpa-Met(O_2)-Oic-Abu)-Dab(Boc)-Thr(tBu)], 15; (c) 6-Methylheptanoyl-Dab(Boc)-Thr(tBu)-Dab(Boc)-cyclo[Dab-Dab(4-Pentynoyl-Bpa-Met(O_2)-Oic-Abu)-DLeu-Leu-Dab(Boc)-Dab(Boc)-Thr(tBu)], 16.

a

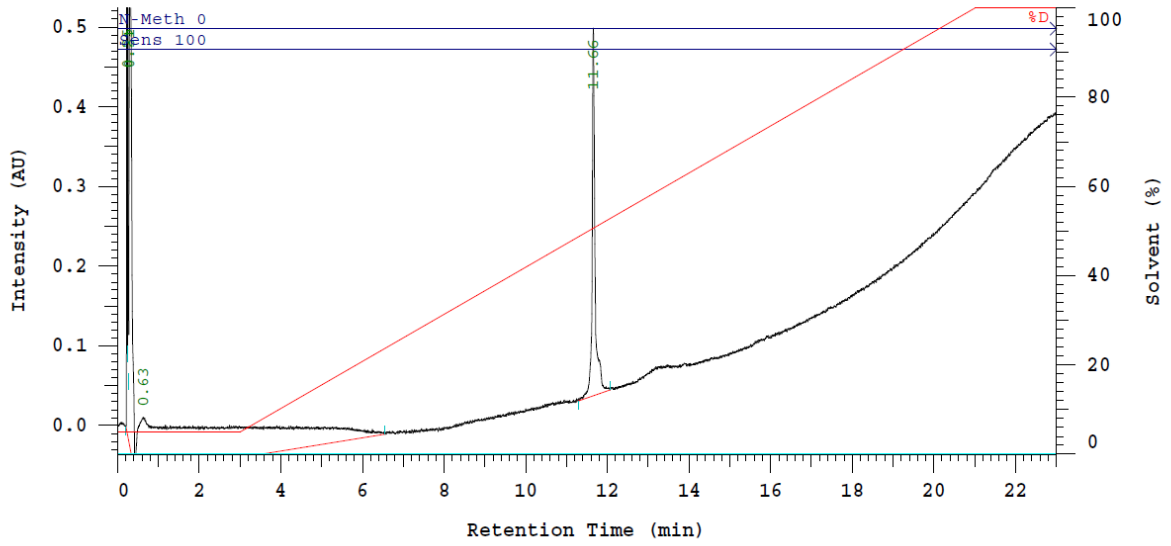
N-Meth 0
Gens 100
%D
11.66
0.63
Intensity (AU)
Solvent (%)
Retention Time (min)

b

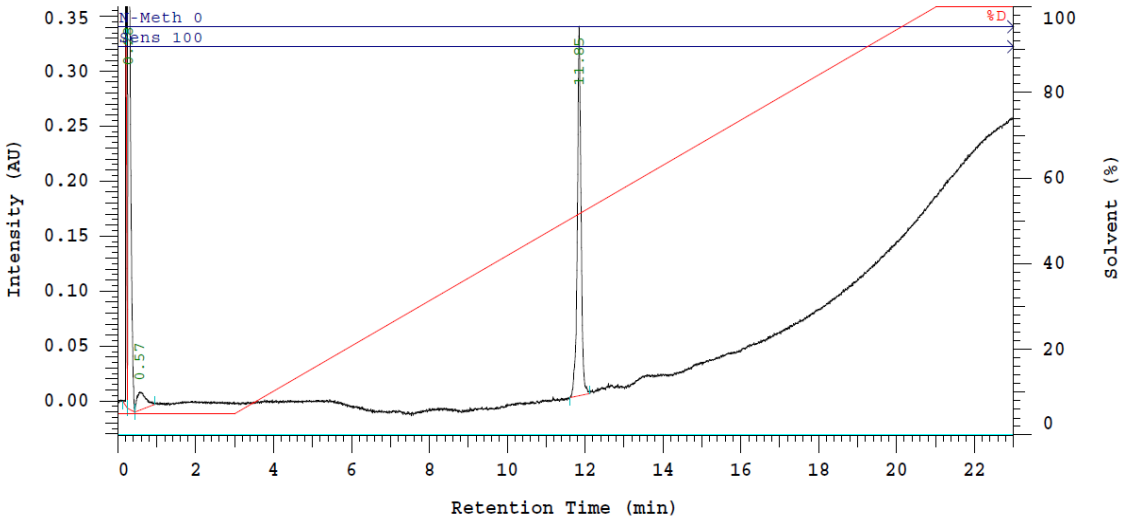
N-Meth 0
Gens 100
%D
11.95
0.57
Intensity (AU)
Solvent (%)
Retention Time (min)

c

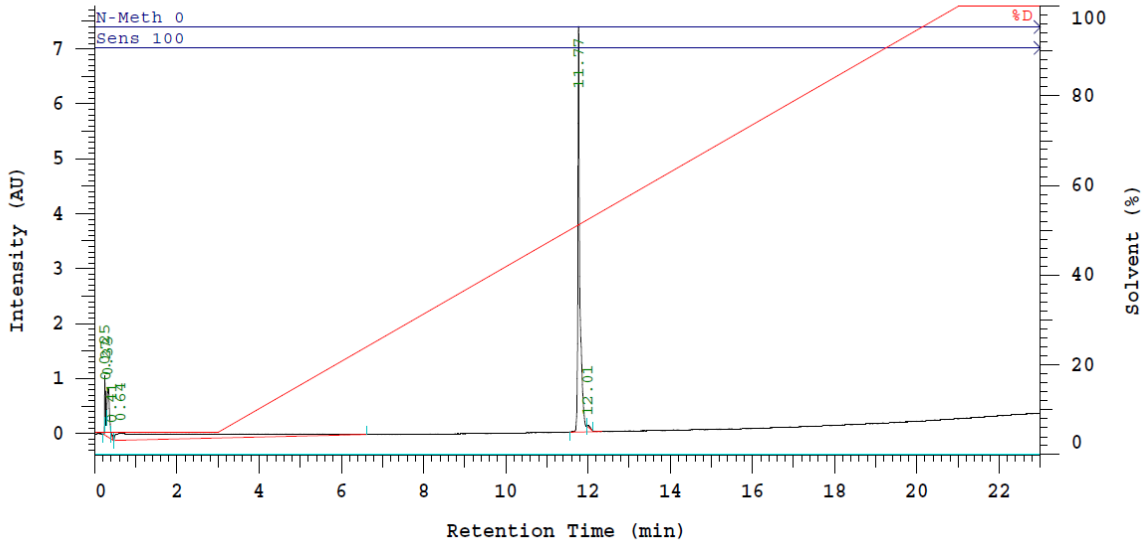

Figure 115. RP-HPLC of the deprotected cyclic peptides: (a) 6-Methylheptanoyl-Dab-Thr-Dab-cyclo[Dab-Dab-DLeu-Leu-Dab-Dab(4-Pentynoyl-Bpa-Met(O_2)-Oic-Abu)-Thr], 17; (b) 6-Methylheptan-Dab-Thr-Dab-cyclo[Dab-Dab-DLeu-Leu-Dab(4-Pentynoyl-Bpa-Met(O_2)-Oic-Abu)-Dab-Thr], 18; (c) 6-Methylheptanoyl-Dab-Thr-Dab-cyclo[Dab-Dab(4-Pentynoyl-Bpa-Met(O_2)-Oic-Abu)-DLeu-Leu-Dab-Dab-Thr], 19.

a

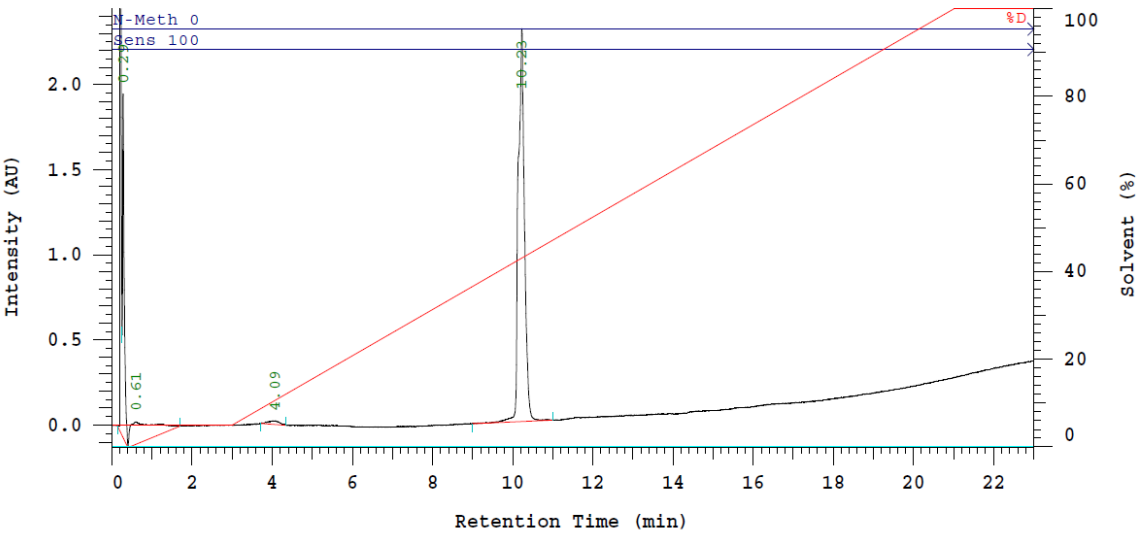

b

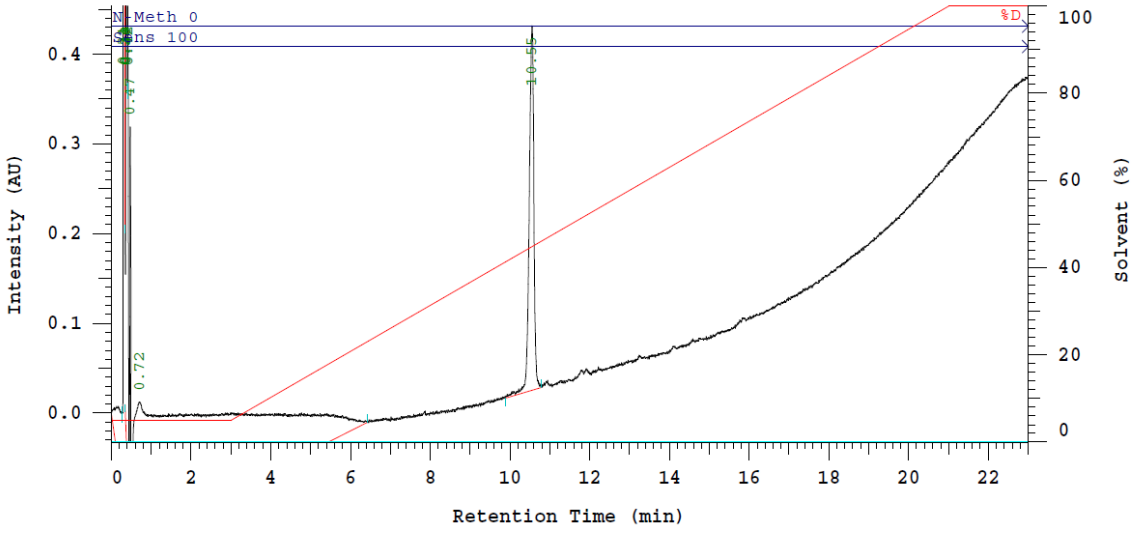

c

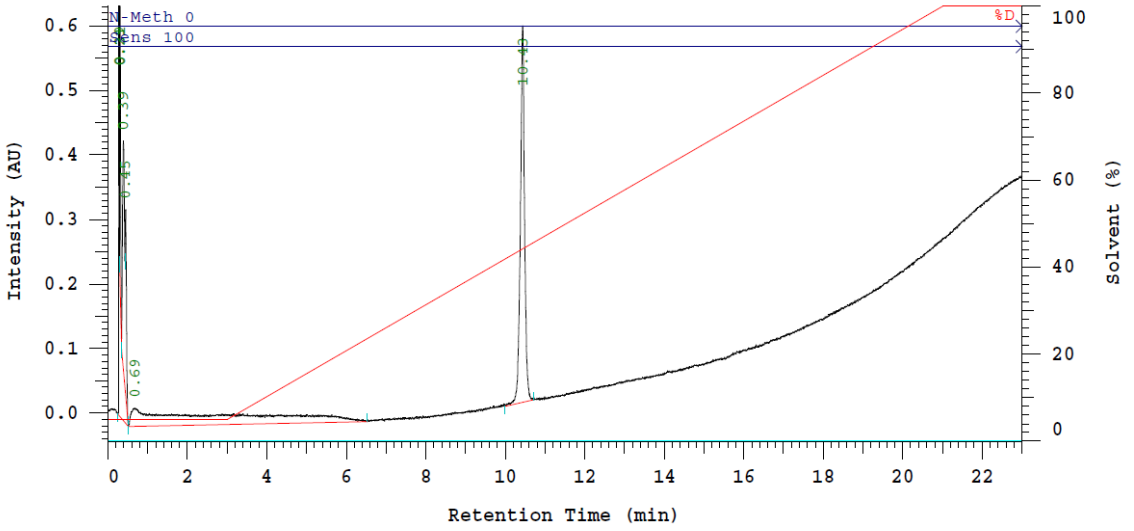

Figure 116. RP-HPLC for the final peptides: (a) 6-Methylheptanoyl-Dab-Thr-Dab-cyclo[Dab-Dab-DLeu-Leu-Dab-Dab(1,2,3 triazol-Ubiquicidine-Butan-Bpa-Met(O_2)-Oic-Abu)-Thr], 20; (b) 6-Methylheptanoyl-Dab-Thr-Dab-cyclo[Dab-Dab-DLeu-Leu-Dab(1,2,3 triazol-Ubiquicidine-Butan-Bpa-Met(O_2)-Oic-Abu)-Dab-Thr], 21; (c) 6-Methylheptanoyl-Dab-Thr-Dab-cyclo[Dab-Dab(1,2,3 triazol-Ubiquicidine-Butan-Bpa-Met(O_2)-Oic-Abu)-DLeu-Leu-Dab-Dab-Thr], 22.

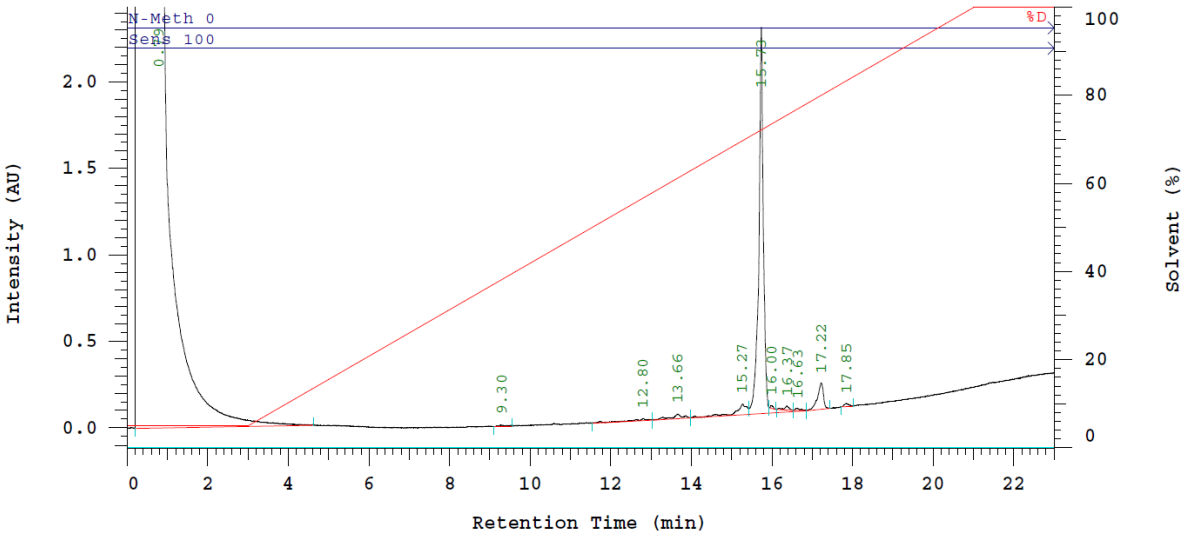

Figure 117. RP-HPLC for the crude 6-Methylheptanoyl-Dab(Boc)-Thr(tBu)-Dab(4-Pentynoyl-Bpa-Met(O_2)-Oic-Abu)-OH, 25

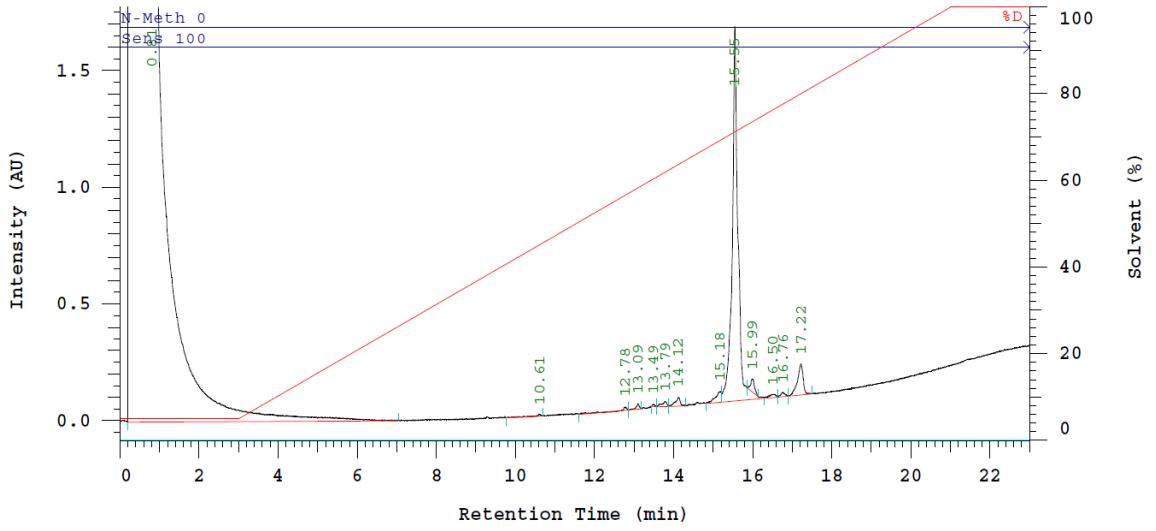

Figure 118. RP-HPLC for the crude 6-Methylheptanoyl-Dab(4-Pentynoyl-Bpa-Met(O_2)-Oic-Abu)-Thr(tBu)-Dab(Boc)-OH, 29

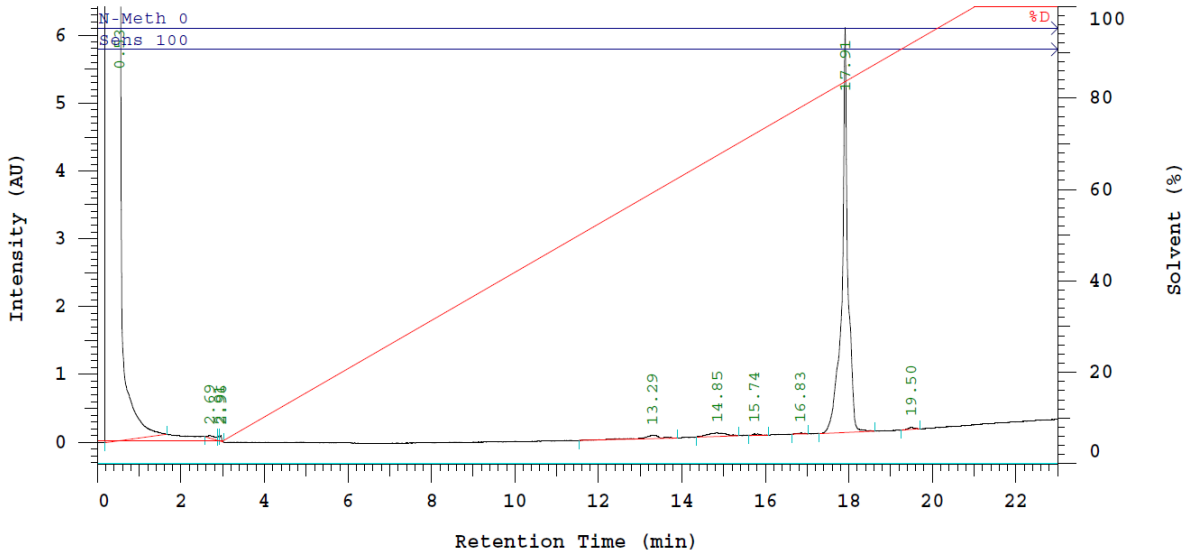

Figure 119. RP-HPLC of Fmoc-Dab(Dde)-Dab(Boc)-DLeu-Leu-Dab(Boc)-Dab(Boc)-Thr(tBu)-2-CTC resin, 30

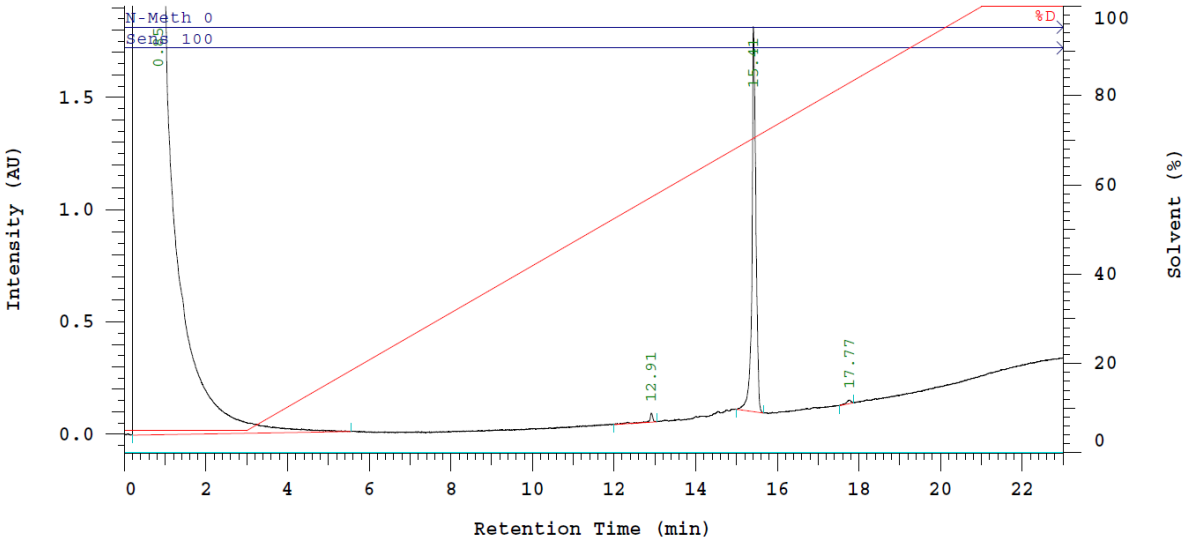

Figure 120. RP-HPLC of Fmoc-Dab(NH_2)-Dab(Boc)-DLeu-Leu-Dab(Boc)-Dab(Boc)-Thr(tBu)-OH, 31

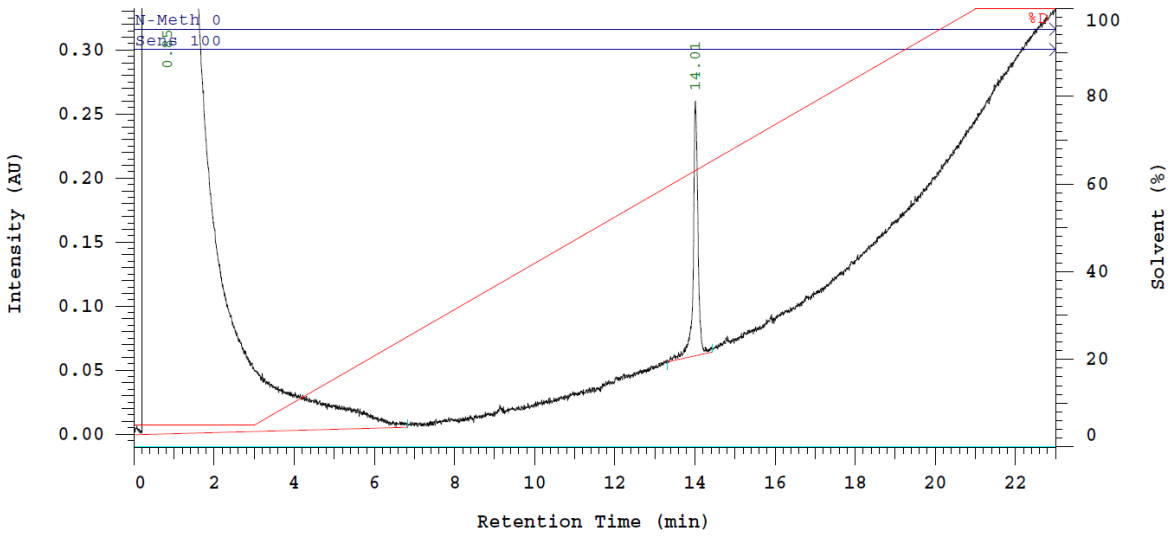

Figure 121. RP-HPLC of the pure H-cyclo[Dab-Dab(Boc)-DLeu-Leu-Dab(Boc)-Dab(Boc)-Thr(tBu)], 32

a

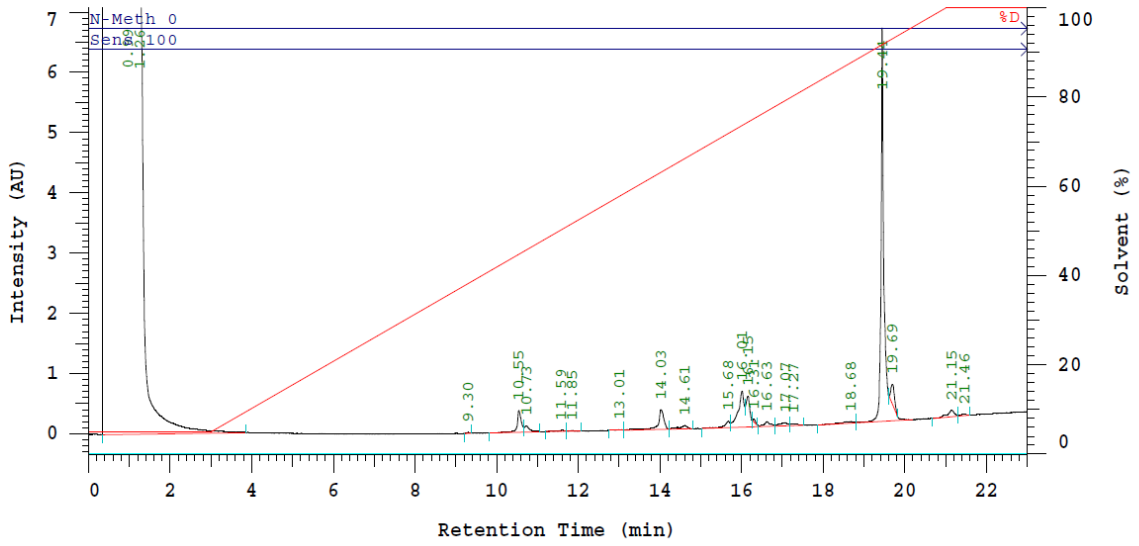

b

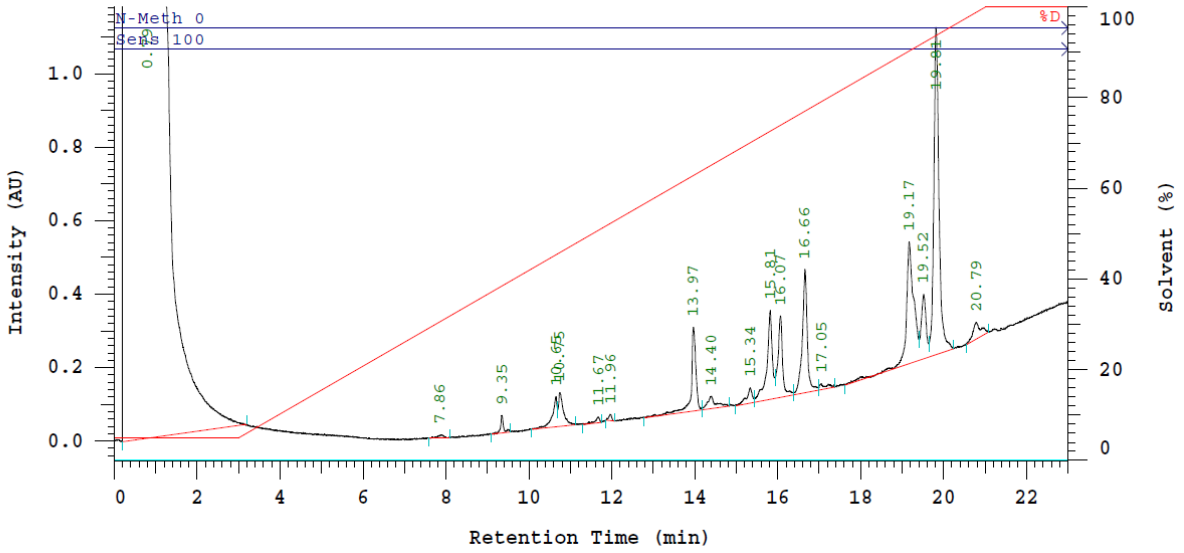

Figure 122. RP-HPLC of the coupling to get the compounds: (a) 6-Methylheptanoil-Dab(Boc)-Thr(tBu)-Dab(4-Pentynoyl-Bpa-Met(O_2)-Oic-Abu)-cyclo[Dab-Dab(Boc)-DLeu-Leu-Dab(Boc)-Dab(Boc)-Thr(tBu)], 33; (b) 6-Methylheptanoyl-Dab(4-Pentynoyl-Bpa-Met(O_2)-Oic-Abu)-Thr(tBu)-Dab(Boc)-cyclo[Dab-Dab(Boc)-DLeu-Leu-Dab(Boc)-Dab(Boc)-Thr(tBu)], 34

a

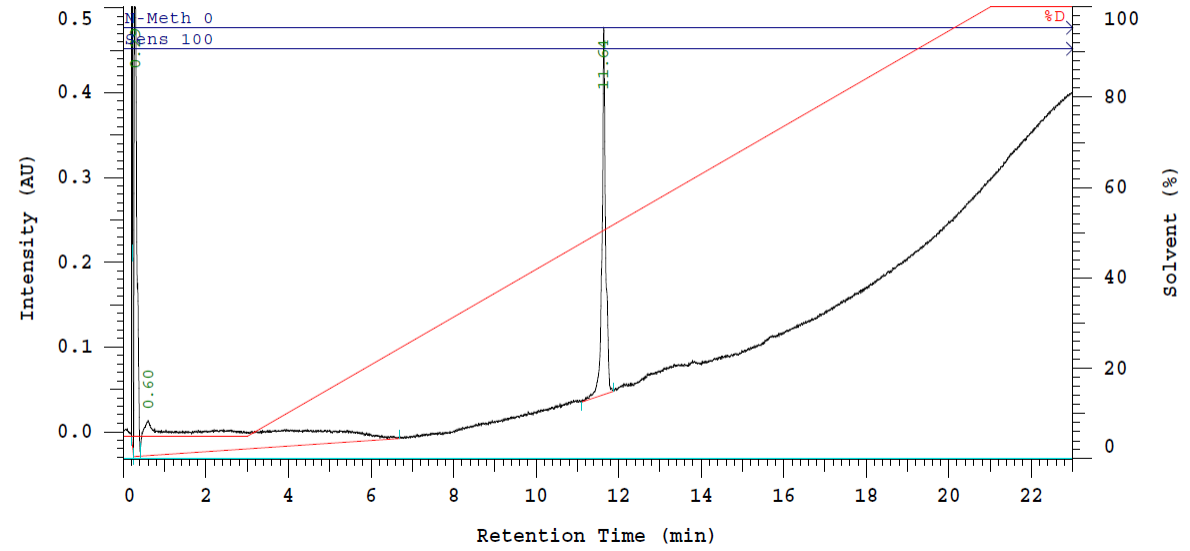

b

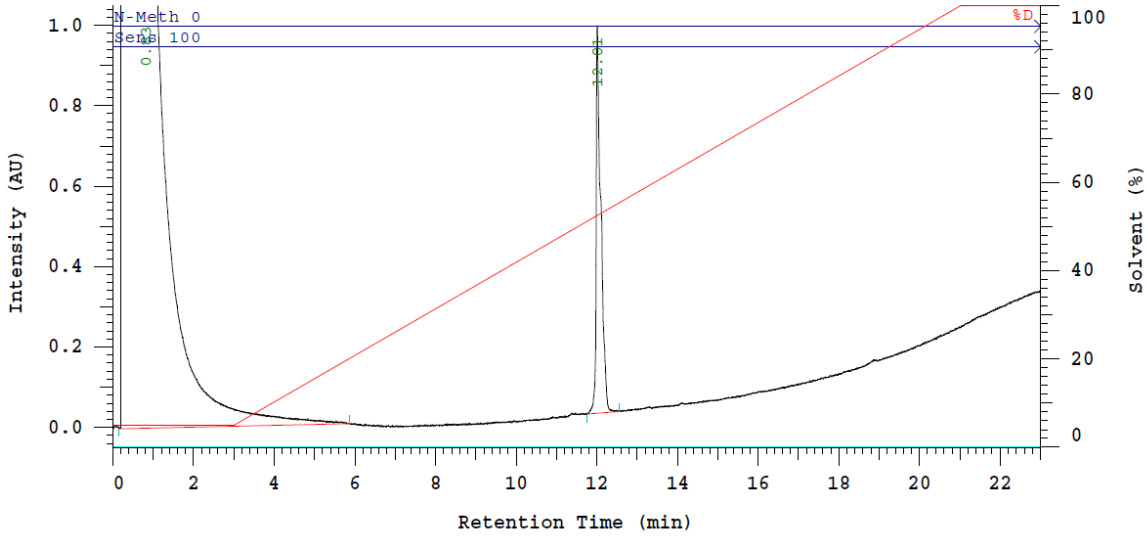

Figure 123. RP-HPLC for the deprotected cyclic peptides: (a) 6-Methylheptanoyl-Dab-Thr-Dab(4-Pentynoyl-Bpa-Met(O_2)-Oic-Abu)-cyclo[Dab-Dab-DLeu-Leu-Dab-Dab-Thr], 35; (b) 6-Methylheptanoyl-Dab(4-Pentynoyl-Bpa-Met(O_2)-Oic-Abu)-Thr-Dab-cyclo[Dab-Dab-DLeu-Leu-Dab-Dab-Thr], 36

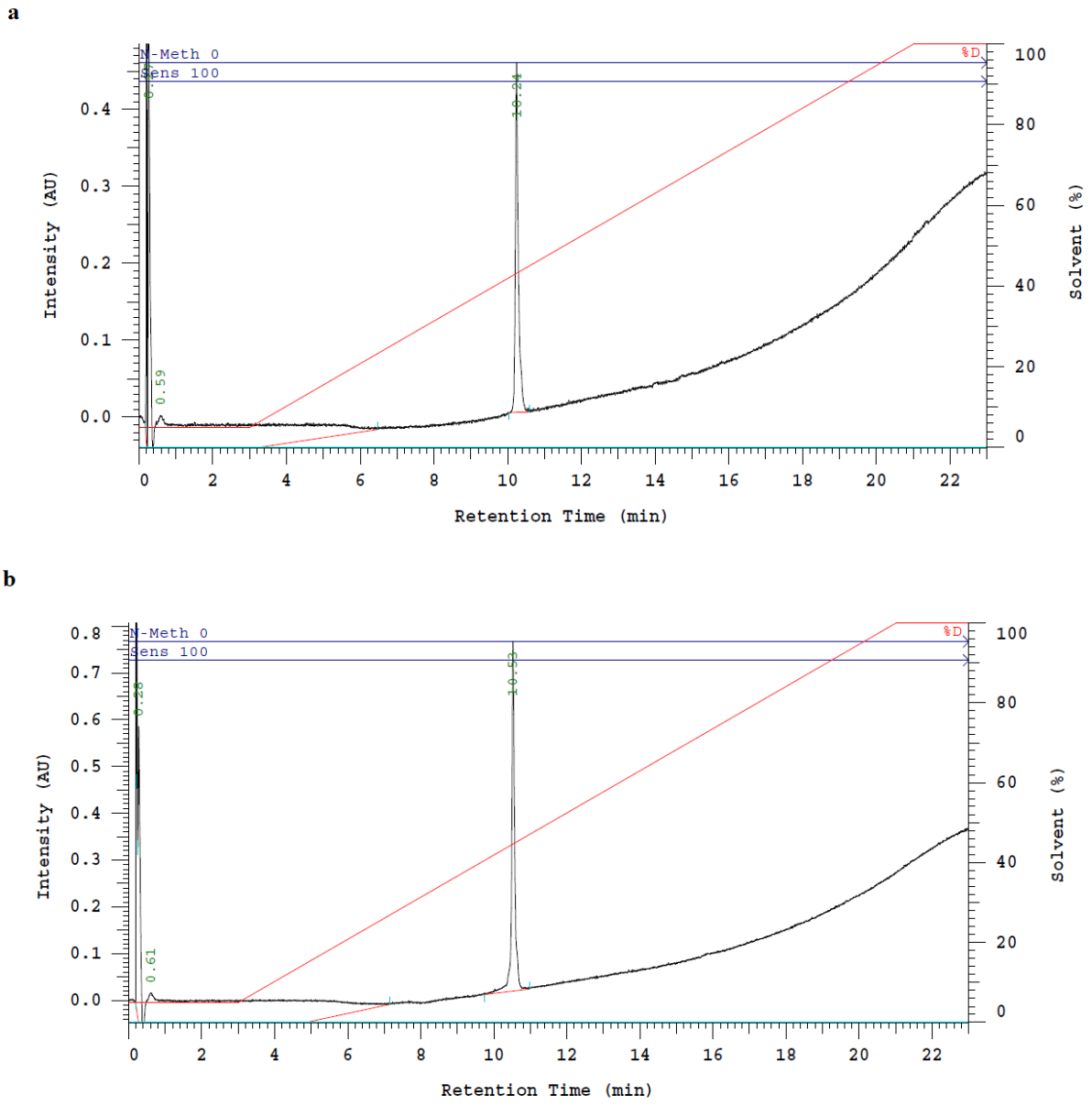

Figure 124. RP-HPLC for the final peptides: (a) 6-Methylheptanoyl-Dab-Thr-Dab(1,2,3 triazol-Ubiquicidine-Butan-Bpa-Met(O_2)-Oic-Abu)-cyclo[Dab-Dab-DLeu-Leu-Dab-Dab-Thr], 37; (b) 6-Methylheptanoyl-Dab(1,2,3 triazol-Ubiquicidine-Butan-Bpa-Met(O_2)-Oic-Abu)-Thr-Dab-cyclo[Dab-Dab-DLeu-Leu-Dab-Dab-Thr], 3

4. REFERENCES

[1] Landers, T. F.; Cohen, B.; Wittum, T. E.; Larson, E. L. A review of antibiotic use in food animals: perspective, policy, and potential. *Public Health Rep*. **2012**, *127*, 4-22.

[2] See, for example: a) https://www.who.int/antimicrobial-resistance/en/; b) https://www.cdc.gov/drugresistance; c) https://ecdc.europa.eu/en/antimicrobial-resistance/surveillance-and-disease-data/data-ecdc.

[3] Rossolini, G. M.; Arena, F.; Pecile, P.; Pollini, S. Update on the antibiotic resistance crisis. *Curr. Opin. Pharmacol*. **2014**, *18*, 56-60.

[4] Fjell, C. D.; Hiss, J. A.; Hancock, R. E.; Schneider, G. Designing antimicrobial peptides: form follows function. *Nat. Rev. Drug Disc.* **2012**, *11*, 37-51.

[5] Hancock, R. E. W.; Sahl, H. G. Antimicrobial and host-defense peptides as new anti-infective therapeutic strategies. *Nat. Biotechnol.* **2006**, *24*, 1551-1557.

[6] Jenssen, H. v.; Hamill, P.; Hancock, R. E. W. Peptide Antimicrobial Agents. *Clin. Microbiol. Rev*. **2006**, *19*, 491-511.

[7] Zasloff, M. Antimicrobial peptides of multicellular organisms. *Nature* **2002**, *415*, 389-395.

[8] Brogden, K. A. Antimicrobial peptides: pore formers or metabolic inhibitors in bacteria? *Nat. Rev. Microbiol.* **2005**, *3*, 238-250.

[9] Tew, G. N.; Scott, R. W.; Klein, M. L.; DeGrado, W. F. De novo design of antimicrobial polymers, foldamers, and small molecules: from discovery to practical applications. *Acc. Chem. Res.* **2009**, *43*, 30-39.

[10] Giuliani, A.; Rinaldi, A. Beyond natural antimicrobial peptides: multimeric peptides and other peptidomimetic approaches. *Cell. Mol. Life Sci.* **2011**, *68*, 2255-2266.

[11] Andersson, D. I.; Hughes, D.; Kubicek-Sutherland, J. Z. Mechanisms and consequences of bacterial resistance to antimicrobial peptides. *Drug Resist. Updat.* **2016**, *26*, 43-57.

[12] McPhee, J. B.; Hancock, R. E. W. Function and therapeutic potential of host defence peptides. *J. Pept. Sci.* **2005**, *11*, 677-687.

[13] Landman, D.; Georgescu, C.; Martin, D. A.; Quale, J. Polymyxins revisited. *Clin. Microbiol. Rev.* **2008**, *21*, 449-465.

[14] Falagas, M. E.; Kasiakou, S. K. Toxicity of polymyxins: a systematic review of the evidence from old and recent studies. *Crit. Care* **2006**, *10*, R27.

[15] Culf, A. S.; Ouellette, R. J. Solid-phase synthesis of *N*-substituted glycine oligomers (alpha-peptoids) and derivatives. *Molecules* **2010**, *15*, 5282-5335.

[16] Chen, Y. X.; Mant, C. T.; Farmer, S. W.; Hancock, R. E. W.; Vasil, M. L.; Hodges, R. S. Rational design of α-helical antimicrobial peptides with enhanced activities and specificity/therapeutic index. *J. Biol. Chem.* **2005**, *280*, 12316-12329.

[17] Won, H. S.; Jung, S. J.; Kim, H. E.; Seo, M. D.; Lee, B. J. Systematic peptide engineering and structural characterization to search for the shortest antimicrobial peptide analogue of gaegurin 5. *J. Biol. Chem.* **2004**, *279*, 14784-14791.

[18] Bruschi, M.; Pirri, G.; Giuliani, A.; Nicoletto, S. F.; Baster, I.; Scorciapino, M. A.; Casu, M.; Rinaldi, A. C. Synthesis, characterization, antimicrobial activity and LPS-interaction properties of SB041, a novel dendrimeric peptide with antimicrobial properties. *Peptides* **2010**, *31*, 1459-1467.

[19] Scorciapino, M. A.; Pirri, G.; Vargiu, A. V.; Ruggerone, P.; Giuliani, A.; Casu, M.; Bürck, J.; Wadhwani, P.; Ulrich, A. S.; Rinaldi, A. C. A novel dendrimeric peptide with antimicrobial properties: in vitro characterization of SB056. *Biophys. J.* **2012**, *102*, 1039-1048.

[20] Porter, E. A.; Wang, X.; Lee, H. S.; Weisblum, B.; Gellman, S. H. Non-haemolytic β-amino-acid oligomers. *Nature* **2000**, *404*, 565.

[21] Hamuro, Y.; Schneider, J. P.; DeGrado, W. F. De novo design of antibacterial β-peptides. *J. Am. Chem. Soc.* **1999**, *121*, 12200-12201.

[22] Dahui, L.; DeGrado, W. F. De novo design, synthesis, and characterization of antimicrobial β-peptides. *J. Am. Chem. Soc.* **2001**, *123*, 7553-7559.

[23] Porter, E. A.; Weisblum, B.; Gellman, S. H. Mimicry of host-defense peptides by unnatural oligomers: antimicrobial β-peptides. *J. Am. Chem. Soc.* **2002**, *124*, 7324-7330.

[24] Raguse, T. L.; Porter, E. A.; Weisblum, B.; Gellman, S. H. Structure-activity studies of 14-helical antimicrobial β-peptides: probing the relationship between conformational stability and antimicrobial potency. *J. Am. Chem. Soc.* **2002**, *124*, 12774-12785.

[25] Arvidsson, P. I.; Frackenpohl, J.; Ryder, N. S.; Liechty, B.; Petersen, F.; Zimmermann, H.; Camenisch, G. P.; Woessner, R.; Seebach, D. On the antimicrobial and hemolytic activities of amphiphilic β-peptides. *ChemBioChem* **2001**, *2*, 771-773.

[26] Violette, A.; Averlant-Petit, M. C.; Semetey, V.; Hemmerlin, C.; Casimir, R.; Graff, R.; Marraud, M.; Briand, J. P.; Rognan, D.; Guichard, G. *N,N'*-Linked oligoureas as foldamers: chain length requirements for helix formation in protic solvent investigated by circular dichroism, NMR spectroscopy, and molecular dynamics. *J. Am. Chem. Soc.* **2005**, *127*, 2156-2164.

[27] Violette, A.; Fournel, S.; Lamour, K.; Chaloin, O.; Frisch, B.; Briand, J.-P.; Monteil, H.; Guichard, G. Mimicking helical antibacterial peptides with nonpeptidic folding oligomers. *Chem. Biol.* **2006**, *13*, 531-38.

[28] Chongsiriwatana, N. P.; Patch, J. A.; Czyzewski, A. M.; Dohm, M. T.; Ivankin, A.; Gidalevitz, D.; Zuckermann, R. N.; Barron, A. E. Peptoids that mimic the structure, function, and mechanism of helical antimicrobial peptides. *Proc. Natl. Acad. Sci. U.S.A.* **2008**, *105*, 2794-2799.

[29] Chongsiriwatana, N. P.; Miller, T. M.; Wetzler, M.; Vakulenko, S.; Karlsson, A. J.; Palecek, S. P.; Mobashery, S.; Barron, A. E. Short alkylated peptoid mimics of antimicrobial lipopeptides. *Antimicrob. Agents Chemother.* **2011**, *55*, 417-420.

[30] Turkett, J. A.; Bicker, K. L. Evaluating the effect of peptoid lipophilicity on antimicrobial potency, cytotoxicity, and combinatorial library design. *ACS Comb. Sci.* **2017**, *19*, 229-233.

[31] Chongsiriwatana, N. P.; Wetzler, M.; Barron, A. E. Functional synergy between antimicrobial peptoids and peptides against Gram-negative bacteria. *Antimicrob. Agents Chemother.* **2011**, *55*, 5399-5402.

[32] Haug, B. E.; Stensen, W.; Kalaaji, M.; Rekdal, O.; Svendsen, J. S. Synthetic antimicrobial peptidomimetics with therapeutic potential. *J. Med. Chem.* **2008**, *51*, 4306-4314.

[33] Isaksson, J.; Brandsdal, B. O.; Engqvist, M.; Flaten, G. E.; Svendsen, J. S. M.; Stensen, W. A synthetic antimicrobial peptidomimetic (LTX 109): stereochemical impact on membrane disruption. *J. Med. Chem.* **2011**, *54*, 5786-5795.

[34] Liu, D. H.; Choi, S.; Chen, B.; Doerksen, R. J.; Clements, D. J.; Winkler, J. D.; Klein, M. L.; DeGrado, W. F. Nontoxic membrane-active antimicrobial arylamide oligomers. *Angew. Chem., Int. Ed.* **2004**, *43*, 1158-1162.

[35] Scott, R. W.; DeGrado, W. F.; Tew, G. N. De novo designed synthetic mimics of antimicrobial peptides. *Curr. Opin. Biotechnol*. **2008**, *19*, 620-627.

[36] Choi, S.; Isaacs, A.; Clements, D.; Liu, D. H.; Kim, H.; Scott, R. W.; Winkler, J. D.; DeGrado, W. F. De novo design and in vivo activity of conformationally restrained antimicrobial arylamide foldamers. *Proc. Natl. Acad. Sci. U.S.A.* **2009**, *106*, 6968-6973.

[37] Hall, K.; Aguilar, M.-I. Membrane interactions of antimicrobial β-peptides: the role of amphipathicity versus secondary structure induction. *Biopolymers (Peptide Science)* **2018**, *92*, 554-564.

[38] Savage, P. B.; Li, C.; Taotafa, U.; Ding, B.; Guan, Q. Antibacterial properties of cationic steroid antibiotics. *FEMS Microbiol. Lett.* **2002**, *217*, 1-7.

[39] Epand, R. F.; Savage, P. B.; Epand. R. M. Bacterial lipid composition and the antimicrobial efficacy of cationic steroid compounds (Ceragenins). *Biochim. Biophys. Acta* **2007**, *1768*, 2500-2509.

[40] Lai, X. Z.; Feng, Y.; Pollard, J.; Chin, J. N.; Rybak, M. J.; Bucki, R.; Epand, R. F.; Epand, R. M.; Savage, P. B. Ceragenins: cholic acid-based mimics of antimicrobial peptides. *Acc. Chem. Res.* **2008**, *41*, 1233-1240.

[41] Leszczyńska, K.; Namiot, A.; Fein, D. E.; Wen, Q.; Namiot, Z.; Savage, P. B.; Diamond, S.; Janmey, P. A.; Bucki, R. Bactericidal activities of the cationic steroid CSA-13 and the cathelicidin peptide LL-37 against *Helicobacter pylori* in simulated gastric juice. *BMC Microbiol.* **2009**, *9*, 187.

[42] Thaker, H. D.; Cankaya, A.; Scott, R. W.; Tew, G. N. Role of amphiphilicity in the design of synthetic mimics of antimicrobial peptides with Gram-negative activity. *ACS Med. Chem. Lett.* **2013**, *4*, 481-485.

[43] Falla, T. J.; Nedra Karunaratne, D.; Hancock, R. E. W. Mode of action of the antimicrobial peptide indolicidin. *J. Biol. Chem.* **1996**, *271*, 19298-19303.

[44] Ivankin, A.; Livne, L.; Mor, A.; Caputo, G. A.; DeGrado, W. F.; Meron, M.; Lin, B.; Gidalevitz, D. Role of the conformational rigidity in the design of biomimetic antimicrobial compounds. *Angew. Chem., Int. Ed.* **2010**, *49*, 8462 -8465.

[45] Padhee, S.; Hu, Y. G.; Niu, Y. H.; Bai, G.; Wu, H. F.; Costanza, F.; West, L.; Harrington, L.; Shaw, L. N.; Cao, C. H.; Cai, J. F. Nonhemolytic α-AApeptides as antimicrobial peptidomimetics. *Chem. Commun.* **2011**, *47*, 9729-9731.

[46] Radzishevsky, I. S.; Rotem, S.; Bourdetsky, D.; Navon-Venezia, S.; Carmeli, Y.; Mor, A. Improved antimicrobial peptides based on acyl-lysine oligomers. *Nat. Biotechnol.* **2007**, *25*, 657-659.

[47] Bremner, J.B.; Keller, P. A.; Pyne, S. G.; Boyle, T. P.; Brkic, Z.; David, D. M.; Garas, A.; Morgan, J.; Robertson, M.; Somphol, K.; Miller, M. H.; Howe, A. S.; Ambrose, P.; Bhavnani, S.; Fritsche, T. R.; Biedenbach, D. J.; Jones, R. N.; Buckheit, R. W., Jr.; Watson, K. M.; Baylis, D.; Coates, J. A.; Deadman, J.; Jeevarajah, D.; McCracken, A.; Rhodes, D. I. Binaphthyl-based dicationic peptoids with therapeutic potential. *Angew. Chem. Int. Ed.* **2010**, *49*, 537-540, and references cited therein.

[48] Haldar, J.; Kondaiah, P.; Bhattacharya, S. Synthesis and antibacterial properties of novel hydrolyzable cationic amphiphiles. Incorporation of multiple head groups leads to impressive antibacterial activity. *J. Med. Chem.* **2005**, *48*, 3823-3831.

[49] Hoque, J.; Akkapeddi, P.; Yarlagadda, V.; Uppu, D. S.; Kumar, P.; Haldar, J. Cleavable cationic antibacterial amphiphiles: synthesis, mechanism of action, and cytotoxicities. *Langmuir* **2012**, *28*, 12225-12234.

[50] Zhou, C.; Wang, F.; Chen, H.; Li, M.; Quiao, F.; Liu, Z.; Hou, Y.; Wu, C.; Fan, Y.; Liu, L.; Wang, S.; Wang, Y. Selective antimicrobial activities and action mechanism of micelles self-assembled by cationic oligomeric surfactants. *ACS Appl. Mater. Interfaces* **2016**, *8*, 4242-4249.

[51] Hansen, T.; Alst, T.; Havelkova, M.; Strom, M. B. Antimicrobial activity of small β-peptidomimetics based on the pharmacophore model of short cationic antimicrobial peptides. *J. Med. Chem.* **2010**, *53*, 595-606.

[52] Ghosh, C.; Manjunath, G. B.; Akkapeddi, P.; Yarlagadda, V.; Hoque, J.; Uppu, D. S. S. M.; Konai, M. M.; Haldar, J. Small molecular antibacterial peptoid mimics: the simpler the better! *J. Med. Chem.* **2014**, *57*, 1428-1436.

[53] Engler, A. C.; Wiradharma, N.; Ong, Z. Y.; Coady, D. J.; Hedrick, J. L.; Yang, Y. Y. Emerging trends in macromolecular antimicrobials to fight multi-drug-resistant infections. *Nano Today* **2012**, *7*, 201-222.

[54] Siedenbiedel, F.; Tiller, J. C. Antimicrobial polymers in solution and on surfaces: overview and functional principles. *Polymers* **2012**, *4*, 46-71.

[55] Huang, K.-S.; Yang, C.-H.; Huang, S.-L.; Chen, C.-Y.; Lu, Y.-Y.; Lin, Y.-S. Recent advances in antimicrobial polymers: a mini-review. *Int. J. Mol. Sci.* **2016**, 17, 1578.

[56] Amabili, P.; Calvaresi, M.; Martelli, G.; Orena, M.; Rinaldi, S.; Sgolastra, F. Imidazolidinone-tethered α-hydrazidopeptides – Synthesis and conformational investigation. *Eur. J. Org. Chem.* **2019**, 907-917.

[57] Kuroda, K.; DeGrado, W. F. Amphiphilic polymethacrylate derivatives as antimicrobial agents. *J. Am. Chem. Soc.* **2005***, 127*, 4128-4129.

[58] Ivanov, I.; Vemparala, S.; Pophristic, V.; Kuroda, K.; DeGrado, W. F.; McCammon, J. A.; Klein, M. L. Characterization of nonbiological antimicrobial polymers in aqueous solution and at water-lipid interfaces from all-atom molecular dynamics. *J. Am. Chem. Soc.* **2006***, 128*, 1778-1779.

[59] Amabili, P., Biavasco, F., Brenciani, A., Citterio, B., Corbisiero, D., Ferrazzano, L., Fioriti, S., Guerra, G., Orena, M., Rinaldi, S. Simple amphiphilic α-hydrazido acids: rational design, synthesis and in vitro bioactivity profile of a new class of potential antimicrobial compounds. *Eur. J. Med. Chem.* **2020**, *189*, 112072.

[60] Chai, J.-D.; Head-Gordon, M. Systematic optimization of long-range corrected hybrid density functionals. *J. Chem. Phys.* **2008**, *128*, 084106.

[61] Tomasi, J.; Mennucci, B.; Cammi, R. Quantum mechanical continuum solvation models. *Chem. Rev.* **2005**, *105*, 2999-3093.

[62] The NBO program in Gaussian 16 was used: NBO Version 3.1, Glendening, E. D.; Reed, A. E.; Carpenter, J. E.; Weinhold, F.

[63] Reed, A. E.; Curtiss, L. A.; Weinhold, F. Intermolecular interactions from a natural bond orbital, donor-acceptor viewpoint. *Chem. Rev.* **1988**, *88*, 899-926.

[64] AIMAll (Version 19.02.13), Keith, T. A., TK Gristmill Software, Overland Park KS, USA, 2019.

[65] Bader, R. F. W. A quantum theory of molecular structure and its applications. *Chem. Rev.* **1991**, *91*, 893-928.

[66] Singh, U. C.; Kollman, P. A. An approach to computing electrostatic charges for molecules. *J. Comput. Chem.* **1984**, *5*, 129-145.

[67] Besler, B. H.; Merz, K. M., Jr.; Kollman, P. A. Atomic charges derived from semiempirical methods. *J. Comput. Chem.* **1990**, 11, 431-439.

[68] Breneman, C. M.; Wiberg, K. B. Determining atom-centered monopoles from molecular electrostatic potentials-The need for high sampling density in formamide conformational analysis. *J. Comput. Chem.* **1990**, *11*, 361-373.

[69] Hu, H.; Lu, Z.; Yang, W. Fitting molecular electrostatic potentials from quantum mechanical calculations. *J. Chem. Theory Comput.* **2007**, *3*, 1004-1013.

[70] Lee, H.-S.; Syud, F. A.; Wang, X.; Gellman, S. H. Diversity in Short α-Peptide 12-Helices: High-Resolution Structural Analysis in Aqueous Solution of a Hexamer Containing Sulfonylated Pyrrolidine Residues. *J. Am. Chem. Soc.* **2001**, *123*, 7721-7722, and references cited therein.

[71] Patch, J. A.; Barron, A. E. Helical Peptoid Mimics of Magainin-2 Amide. *J. Am. Chem. Soc.* **2003**, *125*, 12092-12093.

[72] Methods for dilution antimicrobial susceptibility tests for bacteria that grow aerobically; Approved Standard-Tenth Edition (2017) Document M07-A10, Vol. 35, No 2. Clinical and Laboratory Standards Institute, Wayne, PA.

[73] Meroueh, S. O.; Bencze, K. Z.; Hesek, D.; Lee, M.; Fisher, J. F.; Stemmler, T. L.; Mobashery, S. Three-dimensional structure of the bacterial cell wall peptidoglycan. *Proc. Natl. Acad. Sci. U.S.A.* **2006**, *103*, 4404-4409.

[74] Li, J.; Koh, J.-J.; Liu, S.; Lakshminarayanan, R.; Verma, C. S.; Beuerman, R. W. Membrane active antimicrobial peptides: translating mechanistic insights to design. *Front. Neurosci.* **2017**, 11:73 doi: 10.3389/fnins.2017.00073.

[75] Som, A.; Tew, G. N. Influence of Lipid Composition on Membrane Activty of Antimicrobial Phenylene Ethynylene Oligomers. *J. Phys. Chem. B* **2008**, *112*, 3495-3502.

[76] Ilker, M. F.; Nüsslein, K.; Tew, G. N.; Coughlin, E. B. Tuning the hemolytic and antibacterial activities of amphiphilic polynorbornene derivatives. *J. Am. Chem. Soc.* **2004**, *126*, 15870-15875.

[77] Ge, Y. G.; MacDonald, D. L.; Holroyd, K. J.; Thornsberry, C.; Wexler, H.; Zasloff, M. In vitro antibacterial properties of pexiganan, an analog of magainin. *Antimicrob. Agents Chemother.* **1999**, *43*, 782-788.

[78] Uppu, D. S. S. M.; Akkapeddi, P.; Manjunath, G. B.; Yarlagadda, V.; Hoque, J.; Haldar, J. Polymers with tunable side-chain amphiphilicity as non-hemolytic antibacterial agents. *Chem. Commun.* **2013**, *49*, 9389-9391.

[79] Gabriel, G. J.; Madkour, A. E.; Dabkowski, J. M.; Nelson, C. F.; Nüsslein, K.; Tew, G. N. Synthetic mimic of antimicrobial peptide with nonmembrane-disrupting antibacterial properties. *Biomacromolecules* **2008**, *9*, 2980-2983.

[80] Munita, J. M.; Bayer, A. S.; Arias, C. A. Evolving resistance among Gram-positive pathogens. *Clinical Infect. Dis*. **2015**, *61*, 48-57.

[81] Long, K. S.; Vester, B. Resistance to linezolid caused by modifications at its binding site on the ribosome. *Antimicrob. Agents Chemother*. **2012**, *56*, 603-612.

[82] Sierra, J. M.; Ortega, M.; Tarragó, C.; Albet, C.; Vila, J.; Terencio, J.; Guglietta, A. Decreased linezolid uptake in an *in vitro*-selected linezolid-resistant *Staphylococcus epidermidis* mutant. *J. Antimicrob. Chemother.* **2009**, *64*, 990-992.

[83] Liu, Y.-Y.; Wang, Y.; Walsh, T. R.; Yi, L. X.; Zhang, R.; Spencer, J.; Doi, Y.; Tian, G.; Dong, B.; Huang, X.; Yu, L. F.; Gu, D.; Ren, H.; Chen, X.; Lv, L.; He, D.; Zhou, H.; Liang, Z.; Liu, J. H.; Shen, J. Emergence of plasmid-mediated colistin resistance mechanism MCR-1 in animals and human beings in China: a microbiological and molecular biological study. *Lancet Infect. Dis.* **2016**, *16*, 161-168.

[84] Gunn, J. S.; Ryan, S. S.; Van Velkinburgh, J. C.; Ernst, R. K.; Miller, S. I. Genetic and functional analysis of a PmrA-PmrB-regulated locus necessary for lipopolysaccharide modification, antimicrobial peptide resistance, and oral virulence of *Salmonella enterica* serovar typhimurium. *Infect. Immun.* **2000**, *68*, 6139-6146.

[85] Hill, A. V. The possible effects of the aggregation of the molecules of hæmoglobin on its dissociation curves. *J. Physiol.* **1910**, *40*, iv-vii.

[86] Weiss, J. N. The Hill equation revisited: uses and misuses. *FASEB J*. **1997**, *11*, 835-841.

[87] Colomer, A.; Pinazo, A.; Manresa, M. A.; Vinardell, M. P.; Mitjans, M.; Infante, M. R.; Pérez, L. Cationic Surfactants derived from lysine: effects of their structure and charge type on antimicrobial and hemolytic activities. *J. Med. Chem.* **2011**, *54*, 989-1002.

[88] Prenner, E. J.; Kiricsi, M.; Jelokhani-Niaraki, M.; Lewis, R. N. A. H.; Hodges, R. S. ; McElhaney, R. N. Structure-activity relationships of diastereomeric lysine ring size analogs of the antimicrobial peptide gramicidin S: mechanism of action and discrimination between bacterial and animal cell membranes. *J. Biol. Chem.* **2005**, *280*, 2002-2011.

[89] Vlieghe, P.; Lisowski, V.; Martinez, J.; Khrestchatisky, M. Synthetic therapeutic peptides: science and market. *Drug Disc. Today* **2010**, *15*, 40-56.

[90] Schmidt, N. W.; Mishra, A.; Lai, G. H.; Davis, M.; Sanders, L. K.; Tran, D.; Garcia, A.; Tai, K. P.; McCray, P. B.; Ouellette, A. J.; Selsted, M. E.; Wong, G. C. Criterion for amino acid composition of defensins and antimicrobial peptides based on geometry of membrane destabilization. *J. Am. Chem. Soc.* **2011**, *133*, 6720-6727.

[91] Zimmerberg, J.; Kozlov, M. M. How proteins produce cellular membrane curvature. *Nat. Rev. Mol. Cell Biol.* **2006**, *7*, 9-19.

[92] Simonetti, O.; Morroni, G.; Ghiselli, R.; Orlando, F.; Brenciani, A.; Xhuvelaj, L.; Provinciali, M.; Offidani, A.; Guerrieri, M.; Giacometti, A.; Cirioni, O. *In vitro* and *in vivo* activity of fosfomycin alone and in combination with rifampin and tigecycline against Gram-positive cocci isolated from surgical wound infections. *J. Med. Microbiol*. **2018**, *67*, 139-143.

[93] Chukwudi, C. U. rRNA binding sites and the molecular mechanism of action of the tetracyclines. *Antimicrob. Agents Chemother.* **2016**, *60*, 4433-4441.

[94] Delcour, A. H. Outer membrane permeability and antibiotic resistance. *Biochim. Biophys. Acta* **2009**, *1794*, 808-816.

[95] Antonelli, A.; D'Andrea, M. M.; Galano, A.; Borchi, B.; Brenciani, A.; Vaggelli, G.; Cavallo, A.; Bartoloni, A.; Giovanetti, E.; Rossolini, G. M. Linezolid-resistant *cfr*-positive MRSA, Italy. *J. Antimicrob. Chemother.* **2016**, *71*, 2349-2351.

[96] Simoni, S.; Morroni, G.; Brenciani, A.; Vincenzi, C.; Cirioni, O.; Castelletti, S.; Varaldo, P. E.; Giovanetti, E.; Mingoia, M. Spread of colistin resistance gene *mcr-1* in Italy: characterization of the *mcr-1.2* allelic variant in a colistin-resistant blood isolate of *Escherichia coli*. *Diagn. Microbiol. Infect. Dis.* **2018**, *91*, 66-68.

[97] Castanheira, M.; Davis, A. P.; Serio, A. W.; Krause K. M.; Mendes, R. E. *In vitro* activity of Plazomicin against *Enterobacteriaceae* isolates carrying genes encoding aminoglycoside-modifying enzymes most common in US Census divisions. *Diagn. Microbiol. Infect. Dis*. **2019**, *94*, 73-77.

[98] Poirel, L.; Jayol, A.; Nordmann, P. Polymyxins: antibacterial activity, susceptibility testing, and resistance mechanisms encoded by plasmids or chromosomes. *Clin. Microbiol. Rev.* **2017**, *30*, 557-596.

[99] Morroni, G.; Simonetti, O.; Brenciani, A.; Brescini, L.; Kamysz, W.; Kamysz, E.; Neubauer, D.; Caffarini, M.; Orciani, M.; Giovanetti, E.; Offidani, A.; Giacometti, A.; Cirioni, O. *In vitro* activity of Protegrin-1, alone and in combination with clinically useful antibiotics, against *Acinetobacter baumannii* strains isolated from surgical wounds. *Med. Microbiol. Immunol*. **2019**, doi: 10.1007/s00430-019-00624-7.

[100] Cirioni, O.; Simonetti, O.; Pierpaoli, E., Barucca, A.; Ghiselli, R.; Orlando, F., Pelloni, M.; Minardi, D., Cappelletti Trombettoni, M. M.; Guerrieri, M.; Offidani, A.; Giacometti, A.; Provinciali, M. Enhanced efficacy of combinations of pexiganan with colistin versus *Acinetobacter baumannii* in experimental sepsis. *Shock*. **2016**, *46*, 219-225.

[101] Fishovitz, J.; Hermoso, J. A.; Chang, M.; Mobashery, S. Penicillin-binding protein 2a of methicillin-resistant *Staphylococcus aureus*. *IUBMB Life* **2014**, *66*, 572-577.

[102] Hancock, R. E.; Farmer, S. W.; Li, Z. S.; Poole, K. Interaction of aminoglycosides with the outer membranes and purified lipopolysaccharide and OmpF porin of *Escherichia coli*. *Antimicrob. Agents Chemother.* **1991**, *35*, 1309-1314.

[103] Peterson, A. A.; Fesik, S. W.; McGroarty, E. J. Decreased binding of antibiotics to lipopolysaccharides from polymyxin-resistant strains of *Escherichia coli* and *Salmonella typhimurium*. *Antimicrob. Agents Chemother.* **1987**, *31*, 230-237.

[104] Berendsen, H. J. C.; van der Spoel, D.; van Drunen, R. GROMACS: A message-passing parallel molecular dynamics implementation. *Comput. Phys. Commun.* **1995**, *91*, 43-56.

[105] Wang, J.; Wolf, R. M.; Caldwell, J. W.; Kollman, P. A.; Case, D. A. Development and testing of a general AMBER force field. *J. Comput. Chem.* **2004**, *25*, 1157-1174.

[106] CHARMM General Force Field (CGenFF): A force field for drug-like molecules compatible with the CHARMM all-atom additive biological force fields. *J. Comput. Chem.* **2010**, *31*, 671-690.

[107] Reif, M. M.; Hünenberger, P. H.; Oostenbrink, C. New interaction parameters for charged amino acid side chains in the GROMOS force field. *J. Chem. Theory Comput.* **2012**, *8*, 3705-3723.

[108] Gaussian 16, Revision B.01, Frisch, M. J.; Trucks, G. W.; Schlegel, H. B.; Scuseria, G. E.; Robb, M. A.; Cheeseman, J. R.; Scalmani, G.; Barone, V.; Petersson, G. A.; Nakatsuji, H.; Li, X.; Caricato, M.; Marenich, A. V.; Bloino, J.; Janesko, B. G.; Gomperts, R.; Mennucci, B.; Hratchian, H. P.; Ortiz, J. V.; Izmaylov, A. F.; Sonnenberg, J. L.; Williams-Young, D.; Ding, F.; Lipparini, F.; Egidi, F.; Goings, J.; Peng, B.; Petrone, A.; Henderson, T.; Ranasinghe, D.; Zakrzewski, V. G.; Gao, J.; Rega, N.; Zheng, G.; Liang, W.; Hada, M.; Ehara, M.; Toyota, K.; Fukuda, R.; Hasegawa, J.; Ishida, M.; Nakajima, T.; Honda, Y.; Kitao, O.; Nakai, H.; Vreven, T.; Throssell, K.; Montgomery, J. A., Jr.; Peralta, J. E.; Ogliaro, F.; Bearpark, M. J.; Heyd, J. J.; Brothers, E. N.; Kudin, K. N.; Staroverov, V. N.; Keith, T. A.; Kobayashi, R.; Normand, J.; Raghavachari, K.; Rendell, A. P.; Burant, J. C.; Iyengar, S. S.; Tomasi, J.; Cossi, M.; Millam, J. M.; Klene, M.; Adamo, C.; Cammi, R.; Ochterski, J. W.; Martin, R. L.; Morokuma, K.; Farkas, O.; Foresman, J. B.; Fox, D. J. Gaussian, Inc., Wallingford CT, 2016.

[109] Becke, A. D. Density-functional thermochemistry. III. The role of exact exchange. *J. Chem. Phys.* **1993**, *98*, 5648-5652.

[110] Stephens, P. J.; Devlin, F. J.; Chabalowski, C. F.; Frisch, M. J. Ab initio calculation of vibrational absorption and circular dichroism spectra using density functional force fields. *J. Phys. Chem.* **1994**, *98*, 11623-11627.

[111] Goerigk, L.; Hansen, A.; Bauer, C.; Ehrlich, S.; Najibi, A.; Grimme, S. A look at the density functional theory zoo with the advanced GMTKN55 database for general main group thermochemistry, kinetics and noncovalent interactions. *Phys.Chem.Chem.Phys.* **2017**, *19*, 32184-32215.

[112] Lin, Y.-S.; Li, G.-D.; Mao, S.-P.; Chai, J.-D. Long-range corrected hybrid density functionals with improved dispersion corrections. *J. Chem. Theory Comput.* **2013**, *9*, 263-272.

[113] Grimme, S.; Antony, J.; Ehrlich, S.; Krieg, H. A consistent and accurate ab initio parametrization of density functional dispersion correction (DFT-D) for the 94 elements H-Pu. *J. Chem. Phys.* **2010**, *132*, 154104.

[114] Amabili, P.; Amici, A.; Campisi, G.; Guerra, G.; Monari, M.; Orena, M.; Piccinelli, F.; Rinaldi, S.; Tolomelli, A. Synthesis of enantiopure isosteres of amino acids containing a quaternary stereocenter: experimental and computational evaluation of a novel class of atropisomers. *Eur. J. Org. Chem.* **2018**, 6524-6536.

[115] The NBO program in Gaussian 16 was used: NBO Version 3.1, Glendening, E. D.; Reed, A. E.; Carpenter, J. E.; Weinhold, F..

[116] AIMAll (Version 19.02.13), Keith, T. A., TK Gristmill Software, Overland Park KS, USA, 2019.

[117] Gross, K. C.; Seybold, P. G.; Hadad, C. M. Comparison of different atomic charge schemes for predicting pKa variations in substituted anilines and phenols. *Int. J. Quantum Chem.* **2002**, *90*, 445-458.

[118] Choi, Y.; Kim, H.; Cho, K. W.; Paik, S. R.; Kim, H.-W.; Jeong, K.; Jung, S. Systematic probing of an atomic charge set of sialic acid disaccharides for the rational molecular modeling of avian influenza virus based on molecular dynamics simulations. *Carbohydr. Res*. **2009**, *344*, 541-544.

[119] Jacquemin, D.; le Bahers, T.; Adamo, C.; Ciofini, I. What is the "best" atomic charge model to describe through-space charge-transfer excitations? *Phys. Chem. Chem. Phys.* **2012**, *14*, 53835388.

[120] Jambeck, J. P. M.; Mocci, F.; Lyubartsev, A. P.; Laaksonen, A. Partial atomic charges and their impact on the free energy of solvation. *J. Comput. Chem.* **2013**, *34*, 187-197.

[121] Wang, B.; Li, S. L.; Truhlar, D. G. Modeling the partial atomic charges in inorganometallic molecules and solids and charge redistribution in lithium-ion cathodes. *J. Chem. Theory Comput.* **2014**, *10*, 5640-5650.

[122] Hamad, S.; Balestra, S. R. G.; Bueno-Perez, R.; Calero, S.; Ruiz-Salvador, A. R. Atomic charges for modeling metal-organic frameworks: Why and how. *J. Solid State Chem.* **2015**, *223*, 144-151.

[123] Taylor, R.; Kennard, O. Crystallographic evidence for the existence of CH···O, CH···N and CH···Cl hydrogen bonds. *J. Am. Chem. Soc.* **1982**, *104*, 5063-5070.

[124] Popelier, P. L. A. Characterization of a dihydrogen bond on the basis of the electron density. *J. Phys. Chem. A* **1998**, *102*, 1873-1878.

[125] Exner, M., Bhattacharya, S., Christiansen, B., Gebel, J., Goroncy-Bermes, P., Hartemann, P., Heeg, P., Ilschner, C., Kramer, A., Larson, E., Merkens, W., Mielke, M., Oltmanns, P., Ross, B., Rotter, M., Schmithausen, R., M., Sonntag, H. G., Trautmann, M. Antibiotic resistance: What is so special about multidrug-resistant Gram- negative bacteria? *GMS Hyg. Infect. Control* **12**, Doc05 (2017).

[126] Livermore, D. M. The need for new antibiotics. *Clin. Microbiol. Infect. Suppl.* **10**, 1–9 (2004).

[127] Nikaido, H. Multidrug resistance in bacteria (Author Manuscript). *Annu. Rev. Biochem.* 119–146 (2009).

[128] Cassir, N., Rolain, J. M. & Brouqui, P. A new strategy to fight antimicrobial resistance: The revival of old antibiotics. *Front. Microbiol.* **5**, 1–15 (2014).

[129] Gupta, S., Govil, D., Kakar, P. N., Prakash, O., Arora, D., Das, S., Govil, P., Malhotra, A. Colistin and polymyxin B: A re-emergence. *Indian J. Crit. Care Med.* **13**, 49–53 (2009).

[130] Velkov, T., Roberts, K. D., Nation, R. L., Thompson, P. E. & Li, J. Pharmacology of polymyxins: New insights into an 'old class of antibiotics. *Future Microbiol.* **8**, 711–724 (2013).

[131] Y. Koyama, A. Kurosasa, A. Tsuchiya & K. Takakuta, *J. Antibiot (Tokyo);* **3**, 457–458 (1950).

[132] Storm, D. R., Rosenthal, K. S. & Swanson, P. E. Polymyxin and Related Peptide Antibiotics. *Annu. Rev. Biochem.* **46**, 723–763 (1977).

[133] Bycroff, B.W., Chan, W. C., Chhabre, S. R., Hore, N. D. A novel lysine-protecting procedure for continuous flow solid phase synthesis of branched peptides. *J. Chem. Inf. Model.* **53**, 1689–1699 (2013).

[134] Biochein, J. & Komura, S. Partial purification and properties of L-2,4- diaminobutyrric acid activating enzyme from Polymyxin E producing organism. *J. Biochem.* **86**, 1013–1021 (1979).

[135] Orwa, J. A., Govaerts, C., Busson, R., Roets, E., Schepdael, A. V., Hoogmartens, J. Isolation and structural characterization of colistin components. *J. Antibiot. (Tokyo).* **54**, 595–599 (2001).

[136] Rhouma, M., Beaudry, F., Thériault, W., Letellier, A. & Allen, H. K. Colistin in Pig Production : Chemistry , Mechanism of Antibacterial Action , Microbial Resistance Emergence , and One Health Perspectives. **7**, 1–22 (2016).

[137] Falagas, M. E., Kasiakou, S. K. Colistin: The Revival of Polymyxins for the Management of Multidrug-Resistant Gram-Negative Bacterial Infections. *Pediatr. Infect. Dis. J.* **24**, 945 (2005).

[138] Li, J., Nation, R. L., Turnidge, J. D., Milne, R. W., Coulthard, K., Rayner, C. R., Paterson, D. Colistin: the re-emerging antibiotic for multidrug-resistant Gram-negative bacterial infections. *Lancet Infect. Dis.* **6**, 589–601 (2006).

[139] Velkov, T., Thompson, P. E., Nation, R. L. & Li, J. Structure-activity relationships of polymyxin antibiotics. *J. Med. Chem.* **53**, 1898–1916 (2010).

[140] Ordooei Javan, A., Shokouhi, S. & Sahraei, Z. A review on colistin nephrotoxicity. *Eur. J. Clin. Pharmacol.* **71**, 801–810 (2015).

[141] Falagas, M. E., Fragoulis, K. N., Kasiakou, S. K., Sermaidis, G. J. & Michalopoulos, A. Nephrotoxicity of intravenous colistin: A prospective evaluation. *Int. J. Antimicrob. Agents* **26**, 504–507 (2005).

[142] Grégoire, N., Aranzana-Climent, V., Magréault, S., Marchand, S. & Couet, W. Clinical Pharmacokinetics and Pharmacodynamics of Colistin. *Clin. Pharmacokinet.* **56**, 1441–1460 (2017).

[143] Mendes, C. A. C. & Burdmann, E. A. Polymyxins - review with emphasis on nephrotoxicity. *Rev. Assoc. Med. Bras.* **55**, 752–759 (2009).

[144] Falagas, M. E. & Kasiakou, S. K. Toxicity of polymyxins: A systematic review of the evidence from old and recent studies. *Crit. Care* **10**, (2006).

[145] Rabanal, F. & Cajal, Y. Recent advances and perspectives in the design and development of polymyxins. *Nat. Prod. Rep.* **34**, 886–908 (2017).

[146] Hindo, M. S. & Akura, N. S. Contribution of Each Amino Acid Residue in Polymyxin B 3 to Antimicrobial and Lipopolysaccharide Binding Activity. **57**, 240–244 (2009).

[147] Viljanen, P. and Vaara, M. Susceptibility of Gram-Negative Bacteria to Polymyxin B Nonapeptide. **25**, 701–705 (1984).

[148] Vaara, M., Siikanen, O., Apajalahti, J., Fox, J., Frimodt-Moller, N., He, H., Poudyal, A., Li, J., Nation, R. L., Vaara, T. A novel polymyxin derivative that lacks the fatty acid tail and carries only three positive charges has strong synergism with agents excluded by the intact outer membrane. *Antimicrob. Agents Chemother.* **54**, 3341–3346 (2010).

[149] Vaara, M. Polymyxin derivatives that sensitize Gram-negative bacteria to other antibiotics. *Molecules*. **24**, 249 (2019).

[150] Vaara, M. Novel derivatives of polymyxins. *J. Antimicrob. Chemother.* **68**, 1213–1218 (2013).

[151] Quale, J., Shah, N., Kelly, P., Babu, E., Backer, M., Rosas-Garcia, G., Salamera, J., George, A., Bratu, S., Landman, D. Activity of Polymyxin B and the Novel Polymyxin Analogue Pathogens in New York City. **18**, 132–136 (2012).

[152] Brown, P. & Dawson, M. J. Development of new polymyxin derivatives for multi-drug resistant Gram-negative infections. *J. Antibiot. (Tokyo).* **70**, 386–394 (2017).

[153] Magee, T. V *et al.* Discovery of Dap - 3 Polymyxin Analogues for the Treatment of Multidrug-Resistant Gram-Negative Nosocomial Infections. *J. Med. Chem.* **56**, 5079-5093 (2013).

[154] Kasperkiewicz, P., Pareba, M., Snipas, S. J., Parker, H., Winterbourn, C. C., Salvesen, G. S., Drag, M. Design of ultrasensitive probes for human neutrophil elastase through hybrid combinatorial substrate library profiling. *Proc. Natl. Acad. Sci. U. S. A.* **111**, 2518–2523 (2014).

[155] Hiemstra, P. S., Van Den Barselaar, M. T., Roest, M., Nibbering, P. H. & Van Furth, R. Ubiquicidin, a novel murine microbicidal protein present in the cytosolic fraction of macrophages. *J. Leukoc. Biol.* **66**, 423–428 (1999).

[156] Beiki, D., Yousefi, G., Fallahi, B., Tahmasebi, M. N., Gholamrezanezhad, A., Esfahani, A. F., Erfani, M., Eftekhari, M. 99mtc-Ubiquicidin [29-41], a promising radiopharmaceutical to differentiate orthopedic implant infections from sterile inflammation. *Iran. J. Pharm. Res.* **12**, 347–353 (2013).

[157] Welling, M. M., Hensbergen, A. W., Bunschoten, A., Velders, H., Smits, W. K., Roestenberg, M., Leeuwen, F. W. B. Fluorescent imaging of bacterial infections and recent advances made with multimodal radiopharmaceuticals. *Clin. Transl. Imaging* **7**, 125–138 (2019).

[158] Akram, A. R., Avlonitis, N., Lilienkampf, A., Perez-Lopez, A. M., McDonald, N., Chankeshwara, S. V., Scholefield, E., Haslett, C., Bradley, M., Dhaliwal, K. A labelled-ubiquicidin antimicrobial peptide for immediate in situ optical detection of live bacteria in human alveolar lung tissue. *Chem. Sci.* **6**, 6971–6979 (2015).

[159] Xu, W. L., Cui, A. L., Hu, X. X, You, X. F., Li, Z. R., Zheng, J. S. A new strategy for total solid-phase synthesis of polymyxins. *Tetrahedron Lett.* **56**, 4796–4799 (2015).

[160] Han, S. Y. & Kim, Y. A. Recent development of peptide coupling reagents in organic synthesis. *Tetrahedron* **60**, 2447–2467 (2004).

[161] Ramesh, S., Govender, T., Kruger, H. G., Albericio, F. & De La Torre, B. G. An improved and efficient strategy for the total synthesis of a colistin-like peptide. *Tetrahedron Lett.* **57**, 1885–1888 (2016).

[162] Díaz-Mochón, J. J., Bialy, L. & Bradley, M. Full orthogonality between Dde and Fmoc: The direct synthesis of PNA-peptide conjugates. *Org. Lett.* **6**, 1127–1129 (2004).

[163] Rohit, K., Sharma, Reddy, Ravi P., Tegge, W., Rahul, J., Discovery of Trp-His and His-Arg Analogues as new structural classes of short antimicrobial peptides. *J. Med. Chem.* **52**, 7421-7421 (2009).

[164] Höltke, A. Masterarbeit. Isolation of Human Neutrophil Granulocytes and Investigation of the Cleavage of Synthetic Peptide-Colistin Constructs by Neutrophil Elastase Eidesstattliche Erklärung.